Synthesis and conformational analysis of peptidomimetic foldamers containing diaza-peptide units : application in protein-protein interactions

Chenghui Shi

université PARIS-SACLAY

Synthesis and conformational analysis of peptidomimetic foldamers containing diaza-peptide units: application in protein–protein interactions

Synthèse et analyse conformationnelle de foldamères peptidomimétiques contenant des unités diaza-peptides: application aux interactions protéine-protéine

Thèse de doctorat de l'université Paris-Saclay

École doctorale n° 569 : Innovation thérapeutique : du fondamental à l'appliqué (ITFA)
Spécialité de doctorat : Chimie Thérapeutique
Graduate School : Santé et medicaments. Référent : Faculté de Pharmacie

Thèse préparée dans l'unité de recherche **BioCIS (Université Paris-Saclay, CNRS)**, sous la direction de **Sandrine Ongeri**, Professeur des Universités, et le co-encadrement de **Nicolo Tonali**, Maître de Conférence

Thèse soutenue à Paris-Saclay, le 02 décembre 2022, par

Chenghui SHI

Composition du Jury

David AITKEN Professeur, Université Paris-Saclay	Président
Celine DOUAT Chargée de recherche, HDR, Ludwig Maximilian University of Munich	Rapporteur & Examinatrice
Philippe KAROYAN Professeur, Sorbonne Université	Rapporteur
Muriel AMBLARD Directrice, Université de Montpellier	Examinatrice
David AITKEN Professeur, Université Paris-Saclay	Examinateur

THÈSE DE DOCTORAT

NNT : 2022UPASQ055

Acknowledgements

My deepest gratitude is first to my supervisor Prof. Sandrine Ongeri, not only for giving me the opportunity to work on this PhD project, but also for her continuous encouragement and support in my science research during the PhD study. She is so kind to me and so patient with me even when I had no confidence on the project.

I would also like to thank my co-supervisor Dr. Nicolo Tonali. He gave me many helps in scientific work. If no his instruction and work on CD, NMR and FTIR, the project would progress difficultly. He also helped me a lot in daily life. I still remember that my first day arriving Paris, he picked me up in the Robinson station and helped me to get into my residence.

I would like to thank everyone who worked in this PhD project:

Cordial thanks to Dr. Julia Kaffy for teaching me how to perform ThT assay and working a lot on that for the project. I am so happy to work with you.

Sincere thanks to Prof. Tâp Ha-Duong for his work on molecular MD simulation.

Thank to Prof. Olivier Lequin and Dr. Isabel Correia (Sorbonne Université) who worked on conformational studies of diaza-tripeptides.

Thank to Jean-François Gallard, Remi Franco and Jean Christophe for working on NMR experiment and Dr. Karine Leblanc for Mass spectroscopy.

I would also like to thank all the members of the Fluopepit team for always being available when I needed help: thank you Jean-Louis Soulier, Thierry Milcent and Benoît Crousse.

Of course, I would like to mention all my co-workers and friends in the university: thank you Davide, Nicolo, Maxence, Jacopo, José, Monika, Maud, Sondes, Léa, Lizeth, Anqi, Yaowei, Zhaojie, Yunxin and Yingmin. I am so happy to meet all of you.

Special thanks to my two best friends: Tingting and Ping, for the many wonderful moments passed all together during my PhD study.

In addition, thank to all the members of the jury who accepted to evaluate my research work.

Last but not least, I would like to give my greatest thanks to my parents and girlfriend Xueting. Although Covid-19 pandemic made it difficult for us to see each other, they always give me understanding, believe in me, and support me behind.

Curriculum Vitae

Education and Work

Oct.2019– Present	PhD student **BioCIS, Universite-Paris-Saclay**
Sept. 2017– Aug. 2019	Research assistant **Shanghai Institute of Materia Medica, University of Chinese Academy of Sciences**
Sept. 2014– June. 2017	Master of Science, major in Pharmacy **Shanghai Institute of Materia Medica, University of Chinese Academy of Sciences**
Sept. 2010– June. 2014	Bachelor of Science, major in Pharmacy **Zhengzhou University**

Research Experience

FLUOPEPIT, BioCIS –Synthesis, conformational studies and biophysical evaluation of peptidomimetic foldamers targeting Aβ aggregation for the treatment of Alzheimer's disease

Prof. Yushe Yang's Group –Design, synthesis and structure–activity relationship studies of novel bacterial type-II topoisomerase inhibitors.

Prof. Haiwei Xu's Group –Design, synthesis and structure–activity relationship studies of novel NS5B inhibitors as antiviral agents.

Publications

1. Shi, C.; Correia, I.; Tonali, N.; Ongeri, S.; Lequin, O. Two Consecutive Aza-Amino Acids in Peptides Promote Stable β-Turn Formation in Water. *Org. Biomol. Chem.* **2022**.
2. Ciccone, L., Shi, C., di Lorenzo, D., Van Baelen, A.-C.; Tonali, N. The Positive Side of the Alzheimer's Disease Amyloid Cross-Interactions: The Case of the Aβ 1-42 Peptide with Tau, TTR, CysC, and ApoA1. *Molecules*, **2020**, *25* (10), 2439.
3. Shi, C.; Zhang, Y.; Wang, T.; Lu, W.; Zhang, S.; Guo, B.; Chen, Q.; Luo, C.; Zhou, X.; Yang, Y. Design, Synthesis, and Biological Evaluation of Novel DNA Gyrase-Inhibiting Spiropyrimidinetriones as Potent Antibiotics for Treatment of Infections Caused by Multidrug-Resistant Gram-Positive Bacteria. *J. Med. Chem.* **2019**, *62* (6), 2950–2973.

Conferences

Oral communications: –BioCIS research day, Chatenay Malabry, France, 10th June 2021. "Exploring the effect of diazapeptide fragments on the secondary structure of the EF-helix TTP derived peptide sequence"

Posters: –GFPP22 –BPGM5 symposium, Port-Leucate, France, from 29th May to 3rd June. "Diaza-peptide motifs into a short TTR sequence induce helical structure, increase proteolytic stability and allow interaction with Amyloid β peptide"

–XXI Journée de l'ecole doctorale, Chatenay Malabry, France, 28th June 2022. "Diaza-peptide motifs into a short TTR sequence induce helical structure, increase proteolytic stability and allow interaction with Amyloid β peptide"

–ULLA Summer School, Uppsala, Sweden, 2-9th July 2022. "Diaza-peptide motifs in a short TTR sequence induce helical structure, increase proteolytic stability and interaction with Amyloid β peptide"

Table of Contents

List of abbreviations i

Abbreviations of 20 natural amino acids iv

Chapter 1 Introduction 1

1.1 Protein–protein interactions (PPIs) 1

1.1.1 Hot spots of PPIs 1

1.1.2 Different class of PPIs inhibitors 3

1.2 The specific case of PPIs: amyloidosis and amyloid proteins 5

1.2.1 Structure of amyloid fibrils 6

1.2.2 Mechanism and process of amyloid protein aggregation 7

1.2.3 Toxicity of amyloid aggregates 9

1.2.4 Amyloid cross-interactions 9

1.3 The most common amyloidosis: Alzheimer's disease (AD) 11

1.3.1 AD continuum and diagnostics 12

1.3.2 Pathophysiology of AD 14

Aβ 14

Tau 16

Apolipoprotein E (APOE) 17

Neuroinflammation 18

1.3.3 Treatment of AD 19

Acetylcholinesterase inhibitors 19

N-methyl-D-aspartate (NMDA) receptor antagonist 20

Anti-Aβ 21

Anti-Tau 25

1.3.4 Preclinical Aβ aggregation peptidic inhibitors 27

Peptides derived from Aβ sequences 27

Peptides not derived from Aβ sequence 34

1.3.5 Foldamers inhibiting Aβ aggregation 36

1.4 The Aβ chaperone: transthyretin (TTR) 36

1.4.1 The associations between TTR and Aβ 37

1.4.2 Aβ binding sites of TTR 39

1.4.3 Aβ aggregation inhibitors designed based on the Aβ–TTR interaction 41

1.5 Peptidomimetics 43

1.5.1 Peptidic foldamers 44

1.5.2 Peptidic foldamers mimicking helical structures 45

β-Peptides 45

γ-Peptides 48

Hybrid peptides (αβ, αγ, βγ and αβγ) 49

Peptoids 49

Oligoureas 50

Aminoxy acid oligomers 51

Azapeptides 53

1.5.3 Stapled peptides 54

1.6. Objective of the PhD thesis 55

References 58

Chapter 2 Design, synthesis and conformational studies of aqueous soluble diaza-tripeptides exhibiting β-turn structure 78

2.1 Design of diaza-tripeptides with improved aqueous solubility 78

2.2 Chemistry and synthetic strategies for diaza-tripeptides 80

2.3 Synthesis of diaza-tripeptides through the strategy A 83

2.3.1 Synthesis of the N-terminal fragment 83

2.3.2 Synthesis of the middle fragment A 86

2.3.3 Synthesis of the C-terminal fragment 87

2.3.4 Synthesis of the diaza-tripeptide 2.5 with azaGly as central residue 87

2.3.5 Synthesis of the diaza-tripeptides with azaAla (2.6) and azaLeu (2.7) as central residues 92

2.4 Synthesis of diaza-tripeptides through the strategy B 94

2.4.1 Synthesis of the middle fragment B 95

2.4.2 Synthesis of the aza-dipeptide fragment 96

2.4.3 Coupling the aza-dipeptide fragment with the N-terminal fragment 100

2.5 Conclusion about the synthesis of diaza-tripeptides 101

2.6 Conformational studies 103

2.6.1 Nuclear magnetic resonance (NMR) parameters 103

Vicinal $^{3}J_{HN\alpha}$ coupling constants 103

Chemical shift deviations (CSDs) 104

Temperature coefficients (ΔδNH/ΔT) 105

Nuclear Overhauser effect (NOE) 105

2.6.2 Conformational studies of the diaza-tripeptides 2.5, 2.6 and 2.7 by analysis of NMR parameters 106

2.7 Conclusion for chapter 2 107

References 109

Chapter 3 Synthesis and conformational analysis of aza-nonapeptides containing diaza-peptide units: application in protein–protein interactions 111

3.1 Design of novel aza-nonapeptides based on the sequence derived from the EF-helix of TTR 111

3.2 The strategy to synthesize long peptides containing one or more than one diaza-peptide units 114

3.3 Synthesis of building blocks 115

3.3.1 Synthesis of the building block A 115

3.3.2 Synthesis of the building block B 116

3.3.3 Synthesis of the building block C 119

3.4 Synthesis of long azapeptides or peptides using Fmoc based SPPS 120

3.4.1 Synthesis of peptides 1 and 8 120
3.4.2 Synthesis of peptide 2 123
3.4.3 Synthesis of peptide 3 125
3.4.4 Synthesis of peptide 4 126
3.4.5 Synthesis of peptide 5 127
3.4.6 Synthesis of peptide 6 128
3.4.7 Synthesis of peptide 7 129
3.4.8 Synthesis of peptides 9, 10 and 11 130

3.5 Conformational studies 132

3.5.1 Circular dichroism (CD) 133
3.5.2 NMR analysis 138
3.5.3 Fourier transform infrared radiation (FTIR) 151
3.5.4 Molecular dynamics simulation 154

3.6 Biophysical and biological evaluations 158

3.6.1 Thioflavin-T (ThT) assay 158
The activity of azapeptides against $A\beta_{42}$ aggregation in ThT assay 159
Screening condition of pretreatment of $A\beta_{42}$ protein 166
The activity of azapeptides against the new batch of $A\beta_{42}$ pretreated by HFIP . 174
ThT assay using oligomerization protocol in the preparation of $A\beta_{42}$ solution .. 179
Conclusion on ThT fluorescence assays for $A\beta_{42}$ aggregation 182
The activity of azapeptides against hIAPP aggregation in ThT assay 183
Analysis of the kinetic process of Aβ aggregation by AmyloFit 184
3.6.2 CD analysis of Aβ 185
CD analysis of $A\beta_{42}$ in the absence of inhibitors 185
CD analysis of $A\beta_{42}$ in the presence of peptide 10 or peptide 11 186
CD analysis of $A\beta_{1\text{-}28}$ in the absence or presence of peptides 187
3.6.3 Stability in human plasma 189
3.6.4 Membrane permeability 190
3.6.5 Cellular toxicity 191

3.7 Conclusion 192

References 196

Chapter 4 Synthesis and conformational studies of of aza-diketopiperazine (aza-DKP) based foldamers 201

4.1 Design of aza-DKPamers 202

4.2 Reported chemistry to synthesize aza-DKPs 205

4.3 Synthesis of 2,5-disubstituted aza-DKP monomer 209

4.3.1 Synthesis of aza-dipeptide (C-terminal amide) 4.7 209

4.3.2 Synthesis of aza-dipeptide (C-terminal ester) 4.8 210

4.3.3 Synthesis of aza-DKP monomer 4.1 211

4.4 Development of SPPS strategy for the synthesis of the aza-DKPamers 213

4.5 Conformational studies 217

4.5.1 Crystallization 217

4.5.2 CD 218

4.5.3 NMR 219

4.6 Conclusion 220

References 221

Conclusion and perspectives 223

Experimental part 226

Circular Dichroism Spectroscopy 226

FT-IR Spectroscopy 227

Fluorescence-Detected ThT Binding Assay ($A\beta_{42}$) 227

CD analysis of $A\beta_{42}$ with and without inhibitors 228

Human Plasmatic Stability Study 228

Blood-Brain Barrier (BBB) Permeability Measurement 229
Cell viability assay 229
Solid phase peptide Synthesis 230
Compounds in chapter 2 231
Compounds in chapter 3 266
Compounds in chapter 4 308

List of abbreviations

AA	Amino acid
Aβ	β Amyloid
Ac	Acetyl
AcOH	Acetic acid
ACN	Acetonitrile
AD	Alzheimer's disease
AFM	Atomic force microscopy
APOE	Apolipoprotein E
APP	Amyloid precursor protein
Ach	Acetylcholine
Aib	Aminoisobutyric acid
ABSMs	Amyloid β-sheet mimics
ACHC	2-Aminocyclohexanecarboxylic acid
ACBC	Aminocyclobutanecarboxylic acid
ACPC	2-Aminocyclopentanecarboxylic acid
ACHEC	2-Aminocyclohex-3-ene carboxylic acid
ABHC	2-Amino-6,6-dimethyl-bicyclo[3.1.1]-heptane-3-carboxylic acid
Alloc	Allyloxycarbonyl
APTS	*p*-Toluenesulfonic acid monohydrate
BSA	Buried surface area
BBB	Blood-brain barrier
BACE1	β-Secretase
Bu	Butyl
Bn	Benzyl
Boc	*tert*-Butyloxycarbonyl protecting group
Cbz	Benzyloxycarbonyl
cryo-EM	Cryo-electron microscopy
CSDs	Chemical shift deviations
CSF	Cerebrospinal fluid
CNS	Central nervous system
CHC	Central hydrophobic core
CD	Circular dichroism
COSY	Correlated Spectroscopy
DCM	Dichloromethane
DIBAL-H	Diisobutylaluminium hydride
DIC	N,N′-Diisopropylcarbodiimide
DIPEA	N,N′-Diisopropylethylamine
DKPs	Diketopiperazines
DMF	Dimethylformamide
DFT	Density function theory
ESI	Electrospray ionization
EDC	1-Ethyl-3-(3-dimethylaminopropyl)carbodiimide

EOAD	Early-onset AD
EGCG	Epigallocatechin-3-gallate
EtOH	Ethanol
Et_2O	Diethylether
EtOAc	Ethyl acetate
Fmoc	Fluorenylmethyloxycarbonyl
FDA	Food and Drug Administration
FAP	Familial amyloid polyneuropathy
FAC	Familial amyloid cardiomyopathy
FTIR	Fourier-transform infrared spectroscopy
GABA	γ-Aminobutyric acid
GSK-3β	Glycogen synthase kinase 3-beta
hIAPP	Human islet amyloid polypeptide
HCTU	2-(6-Chloro-1-H-benzotriazole-1-yl)-1,1,3,3-tetramethylaminium hexafluorophosphate
HFIP	Hexafluoroisopropanol
HPLC	High-performance liquid chromatography
HOBt	1-Hydroxybenzotriazole
HMBC	Heteronuclear Multiple Bond Correlation
HSQC	Heteronuclear Single Quantum Coherence
IAPP	Islet amyloid polypeptide
ISMs	Interaction surface mimics
K_2CO_3	Potassium carbonate
LC-MS	Liquid chromatography-mass spectrometry
LOAD	Late-onset AD
LMTM	Leuco-methylthioninium Bis(Hydromethanesulfonate)
MCI	Mild cognitive impairment
MD	Molecular dynamics
MeOH	Methanol
MM	Molecular mechanics
MRI	Magnetic resonance imaging
M-TTR	TTR monomer
NIA-AA	National Institute on Aging-Alzheimer's Association
NMM	N-Methylmorpholine
NFTs	Tau neurofibrillary tangles
NMDA	N-Methyl-D-aspartate
NMR	Nuclear magnetic resonance
NOEs	Nuclear overhauser effects
Oxyma	Ethyl cyanohydroxyiminoacetate
PB	Phosphate buffer
PD	Parkinson’s disease
PPIs	Protein–protein interactions
PET	Positron emission tomography
PED	Phosphodiesterase

PEG	Poly(ethylene glycol)
PPI	Polyproline type I helix
PPII	Polyproline type II helix
RBP	Retinol-binding protein
RCM	Ring-closing metathesis
ROESY	Rotational frame nuclear overhauser effect spectroscopy
ssNMR	Solid state nuclear magnetic resonance
SSA	Senile systemic amyloidosis
STD	Saturation transfer difference
Spe	*S*-1-Phenylethyl
SPPS	Solid phase peptide synthesis
s1npe	*S*-1-Naphthylethyl
sch	*S*-1-Cyclohexylethyl
TIPS	Triisopropyl silane
TTR	Transthyretin
TEA	Triethylamine
TBDMSCl	*tert*-Butyldimethylsilyl chloride
TEM	Transmission electron microscopy
TFA	Trifluoroacetic acid
THF	Tetrahydrofuran
ThT	Thioflavin-T
T2D	Type II diabetes
TNF	Tumor necrosis factor
T4	Thyroxine
Wt	Wild type
γ-Caas	*C*-Linked carbo-γ4-amino acids
ΔAla	α, β-Dehydroalanine
IL-1β	Interleukin 1 beta
TLR2	Toll-like receptor 2

Abbreviations of 20 natural amino acids

Amino acid	Three-letter code	One-letter code
Glycine	Gly	G
Alanine	Ala	A
Valine	Val	V
Leucine	Leu	L
Isoleucine	Ile	I
Phenylalanine	Phe	P
Tyrosine	Tyr	Y
Tryptophan	Trp	W
Methionine	Met	M
Cysteine	Cys	C
Serine	Ser	S
Threonine	Thr	T
Asparagine	Asn	N
Glutamine	Gln	Q
Aspartic acid	Asp	D
Glutamic acid	Glu	E
Arginine	Arg	R
Lysine	Lys	K
Histidine	His	H
Proline	Pro	P

Chapter 1

Introduction

1.1 Protein–protein interactions (PPIs)

Proteins as important biological macromolecules in organisms, usually play their roles by interacting with other molecules like DNAs, RNAs, other proteins or small chemical ligands. Protein–protein interactions (PPIs) could be physical contact directly between proteins, or just be functional correlations.[1] Once physical contacts occur between proteins, some dimers or multi-protein complexes will be formed transiently or permanently.[2] PPIs are deemed ubiquitously in biological processes, which implicate mitosis, apoptosis, metabolism, signal transduction, etc. Likewise, abnormal PPIs (misfolding of proteins, new undesired interactions, loss of special interactions and pathogen-host protein interactions) or stabilization of a protein complex at an inappropriate time and location can cause dysfunction of biological processes and result in various diseases in the end. Thanks to the technological advances in molecular biology, chemical biology and biophysics, more and more abnormal PPIs have been identified and their pathologies have been studied.[3–5] These aberrant PPIs provide us deep insights of pathological mechanism of diseases. To date, there are a lot of human diseases reported to relate with abnormal PPIs,[6] such as cancers (lymphocytic leukemia), neurodegenerative diseases (Alzheimer's disease, Parkinson's disease), infectious diseases (Trypanosoma parasites).[7] Thus, drug discovery based on PPIs has become an attractive method to find new therapeutic targets and molecules.

1.1.1 Hot spots of PPIs

It was estimated that there are 130,000-650,000 PPIs in human interactome netwoks.[8,9] To date, however, only limited PPIs interfaces have been well-defined. Only around 8100 structures of protein–protein complexes involving around 13 000 proteins have been reported in the Protein Data Bank. Interfaces of PPIs are different from traditional enzyme binding sites, which show much larger interfaces (1500-3000 $Å^2$) compared to traditional enzyme binding sites (300-500 $Å^2$).[10] Moreover, interfaces of PPIs are too flat and featureless to bind small molecules. These features

make PPIs as undruggable targets to design small molecules binding interfaces with high affinity and selectivity. Fortunately, Alanine scanning mutagenesis of PPI interfaces has revealed that several small segments, in some cases of PPIs, can contribute the majority of binding free energy.[11] Compared to the whole interface, these segments are composed of short continuous or discontinuous sequences which contain critical amino acid residues. These segments are called hot spots which are always near the center of the interfaces.[12,13] As shown in **Figure 1.1** [14], the hot spots on the interface of the complex between Ras and the Ras binding domain of RalGDP is a small red color region, which contains a few residues offering main Gibbs energy of protein–protein binding. Analysis of database of 2325 alanine mutations indicated that tryptophan, arginine and tyrosine are frequently found on the hot spots of PPIs.[12]

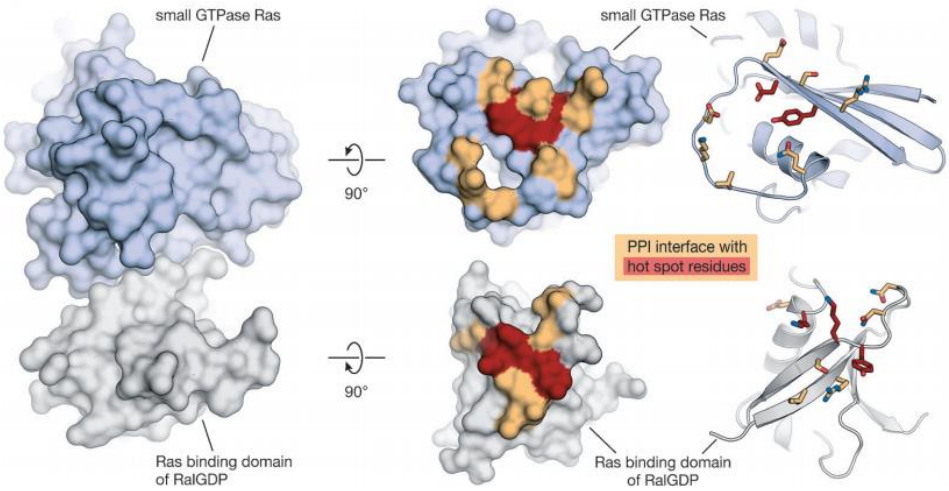

Figure 1.1: Left: Crystal structure in surface representation of the complex between Ras (light blue) and the Ras binding domain of RalGDP (gray, PDB: 1LFD); Right: The same proteins with their PPI interface (orange/red); hot spot residues are highlighted in red[14]

Hot spots usually locate on specific secondary structures (α-helix, β-sheet and β-turn) and these secondary structures decide the specificity and affinity of interaction.[15,16] One classical example of helical structure in PPIs is p53–MDM2. The interaction between p53 and MDM2 plays a critical role in cancer development and progression.[17] Phe19, Trp23 and Leu26, which are the three critical residues on the same face of the p53 helix, contribute to the huge binding energy to interact with MDM2 (**Figure 1.2**).[18,19] A molecule that mimics α-helix of p53 combining with these residues

analogues can bind to MDM2 with high affinity, thereby liberating p53 to inhibit tumor development.[20] β-sheet structures always exist in amyloid fibrils which involve the aggregation of proteins reported in many degenerative diseases and their β-sheet hot spots have been studied a lot.[21,22] Likewise, designing molecules mimicking β-sheet structure has become a popular approach to disturb PPIs involving β-sheet like interaction.[23] Several hot spots involving β-turn structure, such as the hot spots of the CD2-CD58 complex, were used to design novel peptides to modulate immune responses.[24] All these cases confirmed that hot spots and specific secondary structures provide a possibility to design molecules with high affinity and specificity to disrupt PPIs.

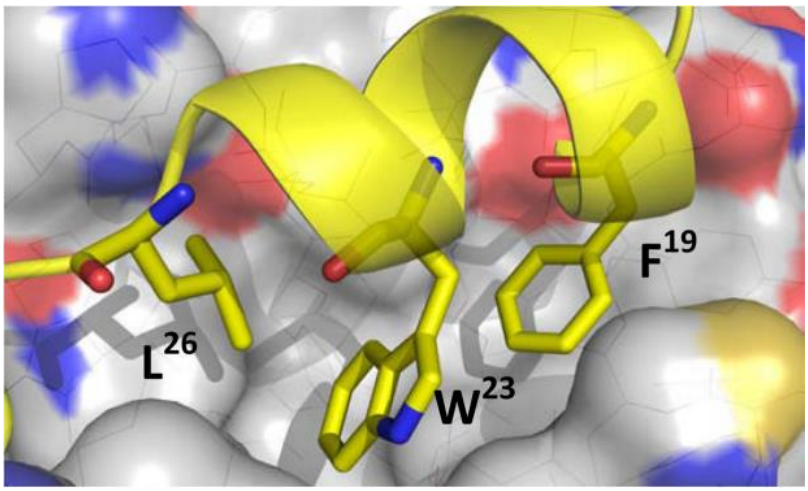

Figure 1.2: Key residues Phe19, Trp23 and Leu26 mounted on an α-helix of p53 (yellow) bound to MDM2 (grey)[19]

1.1.2 Different class of PPIs inhibitors

Molecules targeting PPIs can be divided into small molecules, peptides (or peptidomimetics) and antibodies. They have their own advantages and disadvantages. Small molecules usually show high permeability and stability as well as low costs. Many pharmaceutical companies and research institutions have put a lot of effort into the development of small molecules interfering with PPIs and made a great progress. The hallmark event is the approval in 2016 of Venetoclax, a Bcl-2 inhibitor[25,26], for the treatment of chronic lymphocytic leukemia. Even so, small molecules still have their limitations. Not all PPIs have hot spots on their interfaces. Only less than 10% of PPIs show hot spots on their interfaces.[13] Moreover, some hot spots are discontinuous and are still too large to

bind small molecules. For example, on the basis of the density of hot spot residues distributing on the helical interfaces of PPIs, the helical interfaces can be classified as cleft or extended structure (**Figure 1.3**).[27] Extended helical interfaces usually have larger hot spot regions that are not suitable for small molecules but suitable for larger molecules like peptides and peptidomimetics. In general, the bigger interfaces of PPIs give rise to the bigger areas of hot spots. Small molecules are more likely to block the PPIs with buried surface area (BSA) less than 2000 $Å^2$, but they usually show a low affinity to block PPIs with BSA larger than 2000 $Å^2$.[28] Peptides and peptidomimetics have moderate sizes between antibodies and small molecules, and thus are considered more suitable and easier to target PPIs with BSA larger than 2000 $Å^2$. Peptides show some advantages to interfere PPIs, such as high affinity, high specificity and safety. However, they suffer from poor metabolic stability and cell permeability that result in their fast *in vivo* elimination (short half-live) and low oral bioavailability. Moreover, short peptides usually lose their secondary structures which may play a critical role in the binding of the target proteins. Compared to peptides, peptidomimetics present many advantages such as an increased stability towards proteolysis, higher bioavailability for an oral administration and blood-brain barrier (BBB) permeability. They can offer more constrained conformations, which probably increase their binding affinity to target proteins. Thus, peptidomimetics have attracted a lot of interest in medicinal chemistry, especially for PPIs.[14,23,29] Monoclonal antibodies are considered as ideal molecules to block PPIs because of their high affinity and specificity as a result of large interfaces and special secondary structures. However, several problems of antibodies, including intracellular limitation, poor delivery, immunogenicity, very poor to no BBB permeability and high costs, cause their limitations in therapy.[30]

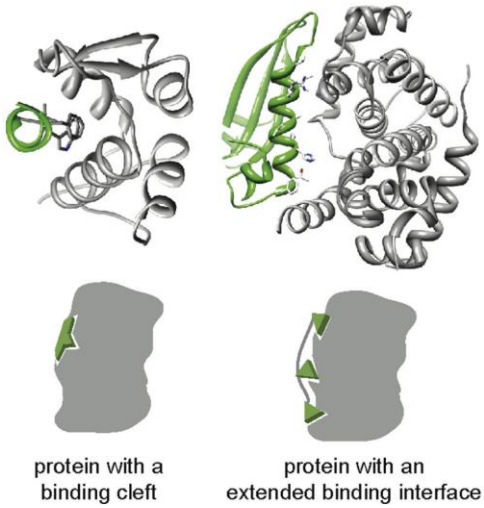

Figure 1.3: Two types of helical interface involved in PPIs[27]

1.2 The specific case of PPIs: amyloidosis and amyloid proteins

As we mentioned at the beginning, aberrant PPIs are able to result in various diseases. Among these aberrant PPIs, a specific type of PPIs, which involve protein misfolding to produce toxic oligomers and amyloid aggregates in tissue, give rise to a type of diseases called amyloidosis. Thus, amyloidosis has a character in which the deposition of amyloid proteins occurs in some organs, such as brain, heart, spleen and kidney. The proteins prone to aggregate into insoluble fibrils with cross-β-sheet structure are termed as amyloid proteins. Amyloid proteins can be divided in three categories, including i) structured native proteins undergoing a loss of their structure such as TTR, ii) intrinsically disordered proteins derived from endoproteolysis of a precursor such as Aβ and iii) full-length intrinsically disordered proteins such as Tau.[31,32] It has been suggested that almost all the proteins could aggregate into amyloid fibrils if the right conditions are provided.[33] Under physiological condition, amyloid proteins are in disordered structure or fold into specific structures and some of them play their corresponding biological functions. Under pathological condition, misfolding happens on these proteins resulting from the exposure of the hydrophobic residues, which drive the proteins aggregate together.

It should be noted that not all the amyloid aggregations could give rise to amyloidosis. In fact, some functional amyloid fibrils have been found in organisms. In mammal, some protein hormones in secretory granules of the endocrine system are stored in amyloid-like conformation but do not

show toxicity on cells.[34] In lower organisms such as bacteria and fungi, some amyloid fibrils have been reported to be involved in biofilm formation, host invasion and information transfer.[35] For example, curli, an extracellular amyloid fiber, is a major component of a complex extracellular matrix of *Escherichia coli* and *Salmonella spp*, which has been reported to be important in the early stage of biofilm formation.[36] However, in most cases, the aggregation of different amyloid proteins is able to induce corresponding diseases. To date, more than 30 amyloid proteins have been associated with specific diseases, including Aβ and Tau (Alzheimer's disease)[37], TTR (senile systemic amyloidosis)[38], hIAPP (type 2 diabetes)[39], α-synuclein (Parkinson's disease)[40], huntingtin protein (Huntington's disease)[41], etc.

1.2.1 Structure of amyloid fibrils

The structure of amyloid fibrils could be imaged by atomic force microscopy (AFM), transmission electron microscopy (TEM), solid state nuclear magnetic resonance (ssNMR), X-ray fiber diffraction and cryo-electron microscopy (cryo-EM). Although amyloid proteins show the diversity in amino acid sequence, the fibrils they form possess a common hallmark: cross-β-sheet structure. This cross-β-sheet structure shows a characteristic X-ray fiber diffraction pattern which has one diffraction signal around 4.7 Å arising from the distance of between hydrogen bonded β-strands and another diffraction signal around 10 Å arising from the spacing of several β-sheets (**Figure 1.4A**).[42] The cross-β-sheet structure also could be determined by several dyes, such as Congo red and thioflavin T, which makes the monitor of kinetics of amyloid aggregation easily.

In general, amyloid fibril is an unbranched structure with the width in the range from 6 nm to 12 nm and the length in several micrometers and it contains several protofilaments which often twist around each other. Each protofilament is built by stacking amyloid proteins in an order manner (cross-β): extended β-strand of each amyloid protein is perpendicular to the fiber axis and the hydrogen bonds between β-strands are parallel to the fiber axis. For example, the structure of an $A\beta_{42}$ fibrils resolved by cryo-EM revealed that two intertwined protofilaments composed of $A\beta_{42}$ monomers stacked in a parallel, in-register cross-β structure (**Figure 1.4B**).[43]

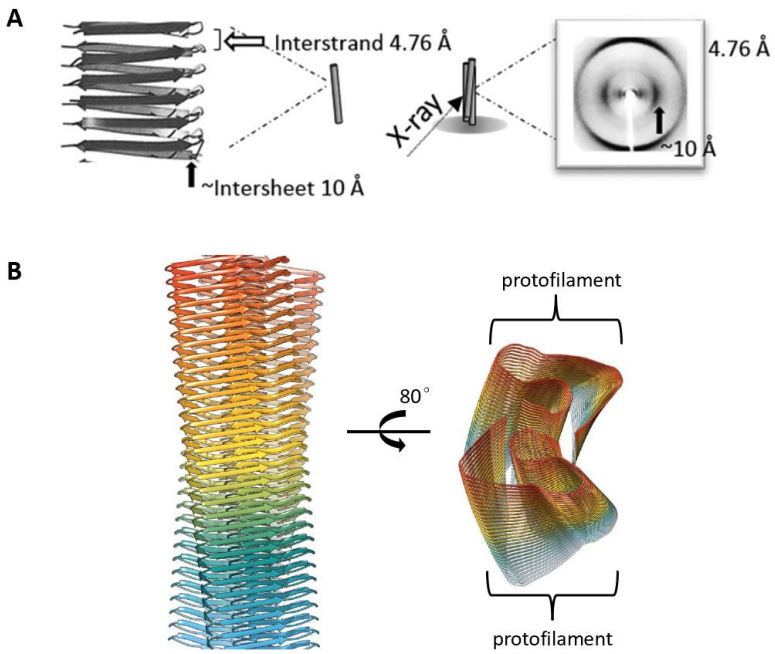

Figure 1.4: A) Characteristic X-ray fiber diffraction pattern of amyloid fibrils[42]; B) Atomic model of the $A\beta_{42}$ fibril composed of two intertwined protofilaments[43]

1.2.2 Mechanism and process of amyloid protein aggregation

The detailed mechanism of the aggregation of amyloid proteins is not yet completely understood. The conformational information of proteins (monomers) at the beginning of the aggregation (nucleation) is of particular importance for getting insight into the mechanism of the aggregation. Most amyloid proteins lack a stable three-dimensional structure, which thus are intrinsically disordered proteins (IDPs). It has been reported that there are helical intermediates formed transiently during the conformational change from disordered structure to β-sheet in Aβ aggregation and the transient helical structure seems to play a key role in the association between two monomers.[44–46] Some proteins with well-defined structures need an unfolding process of the proteins before their aggregation. [47,48] Once the proteins unfold, several hydrophobic residues and hydrogen bond donors or acceptors are exposed, which could drive and stabilize the aggregation of the proteins. For example, transthyretin (TTR) carries out its physiological functions in homotetrameric state while the dissociation of TTR result in the TTR monomer which has been proven as the culprit of TTR self-aggregation.[48]

The microscopic process of the formation of amyloid fibrils at least includes primary nucleation and elongation (**Figure 1.5**).[49] Generally, secondary nucleation and fragmentation are also involved in the amyloid aggregation and play key roles in the kinetic of amyloid aggregation (**Figure 1.5**). Primary nucleation is a spontaneous process at the very beginning of the aggregation. It is the rate-limiting step of the aggregation (**Figure 1.5a**). Then monomers accumulate to the nucleus resulting elongation (**Figure 1.5b**). Monomers also can form a new nucleus on the surface of existing fibrils easily, thereby accelerating the aggregation (**Figure 1.5c**). Sometimes fragmentation takes place to further speed up the aggregation (**Figure 1.5d**).

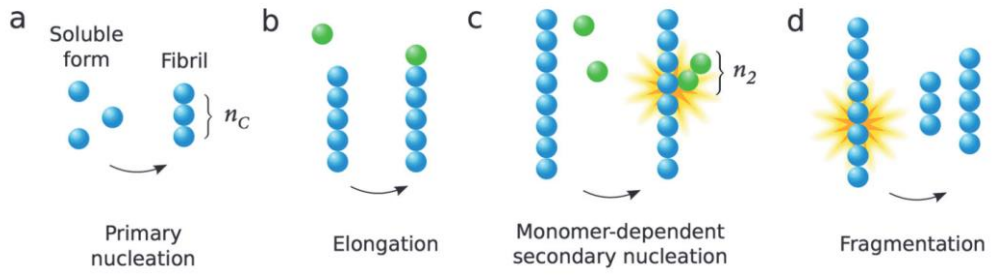

Figure 1.5: The proposed steps involved in amyloid aggregation[49]

At least three prominent models have been proposed to explain the thermodynamical process of amyloid aggregation, including nucleated polymerization, nucleated conformational conversion and downhill polymerization (**Figure 1.6**).[50] In the first model, the nucleus is the highest energy species in the whole process and is necessary for further self-assembly (**Figure 1.6a**). Once the nucleus is formed, the monomers could be added to nucleus easily and quickly to form fibrils. The process of nucleus formation could be bypass by adding seeds directly. In the second model, the nucleus is still required for the aggregation but it is not the highest energy species. The nucleus is converted from a structurally heterogeneous oligomers, and this conversion is the rate-limiting step of the aggregation (**Figure 1.6b**). The nucleus formation is not required for the third model. The process of the aggregation is regarded as a downhill process (**Figure 1.6c**). The addition of seeds doesn't accelerate the speed of the aggregation. It should be noted that these models just help us to understand the possible thermodynamical processes of the aggregation but are not the real processes because of more complex environment in living organisms.

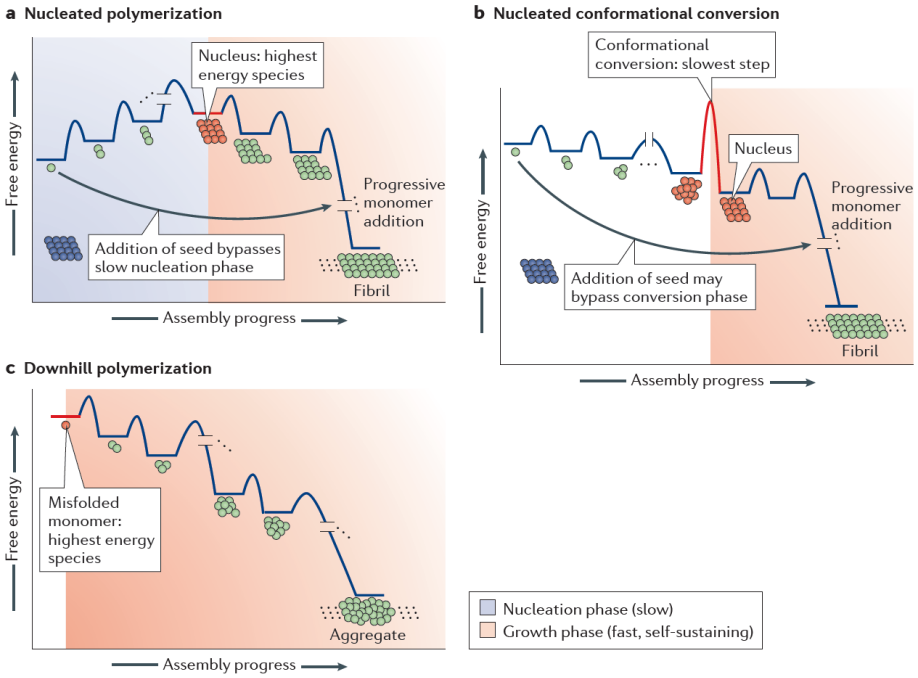

Figure 1.6: Three models proposed to explain the thermodynamical process of amyloid aggregation[50]

1.2.3 Toxicity of amyloid aggregates

Why amyloid aggregates could lead to diseases are still unclear. Tissue deposition of amyloid proteins appears to directly disrupt the structure and function of the tissue but maybe not the prominent causality of the toxicity. Fibrils can generate damaging redox activity, inflammation and promote the nucleation of toxic oligomer.[51,52] The aggregated intermediates, such as oligomers and protofibrils, have been proposed to be the main toxicants to cells.[42,49,53] It has been reported that small oligomers could destroy the membrane of cells, thereby resulting in calcium dysregulation. In addition, the calcium dysregulation also attributes to membrane receptors which could be activated by amyloid oligomers.[54] Intracellular oligomers can also give rise to dysfunctions of organelles, such as endoplasmic reticulum and mitochondria.[55,56]

1.2.4 Amyloid cross-interactions

Noteworthy, amyloid aggregates usually contain not only a single type of amyloid proteins, but also other type of proteins and thus amyloid aggregation involves complex homo or hetero PPIs. Some studies revealed that Aβ is just the major amyloid protein of the 488 proteins in AD related amyloid plaques.[57] In PD related Lewy's bodies, around 550 proteins have been detected, including α-synuclein, synphilin-1 and Tau.[58,59] This phenomenon can be rationally explained by the process of protein cross-seeding and co-assembly which has been considered as a fundamental event in biology.[60] Moreover, several amyloid proteins show the abilities to affect the kinetic of the aggregation of other amyloid proteins. For example, hIAPP has been reported to promote the α-synuclein amyloid formation, which can explain why T2D patients are susceptible to develop PD.[61] Some experiments suggested that Tau and α-synuclein can influence each other, accelerating their respective fibrillization processes and resulting in the formation of pathological inclusions in neurodegenerative diseases.[62] In addition, it has been reported that monomeric α-synuclein is able to inhibit amyloidogenesis of prion protein (PrP) *in vitro* through suppressing the nucleation step of the aggregation.[63] All these evidences indicate that some amyloid proteins show chaperone-like activity to other amyloid proteins and their amyloid cross-interactions play key roles in amyloid fibril formation.

We can divide the amyloid cross-interactions into two categories based on their effects to the progress of diseases. One is amyloid cross-interactions with positive effect, another one is amyloid cross-interactions with negative effect. The positive effects include inhibiting the formation of amyloid oligomers or amyloid fibrils, reducing the toxicity of aggregates, promoting the degradation of aggregates and promoting the dissociation of aggregates. In contrast, the negative effects include promoting the aggregation, increasing the toxicity of aggregates and inhibiting the degradation of aggregates. These effects are not mutually exclusive. Sometimes one amyloid protein which inhibits the amyloid fibril formation of another amyloid protein, simultaneously reduces the toxicity of the aggregate, like the effects that α-synuclein has on PrP[63] or TTR has on Aβ.[64] Thus, the amyloid proteins usually show complicated cross-interactions to each other.

To date, many amyloid cross-interactions have been investigated and the knowledge of them could help us to further understand the mechanisms of amyloid related diseases. In addition, amyloid cross-interactions provide a new strategy to design novel molecules capable of inhibiting amyloid

aggregation. For example, many studies have revealed that a lot of amyloid proteins can cross-interact with Aβ (**Figure 1.7**).[65] Some of these cross-interactions have been used in the design of novel peptides that inhibit Aβ aggregation, as reported in our recent review.[66] However, this strategy is still in its infancy. These novel peptides will be mentioned in detail in following section.

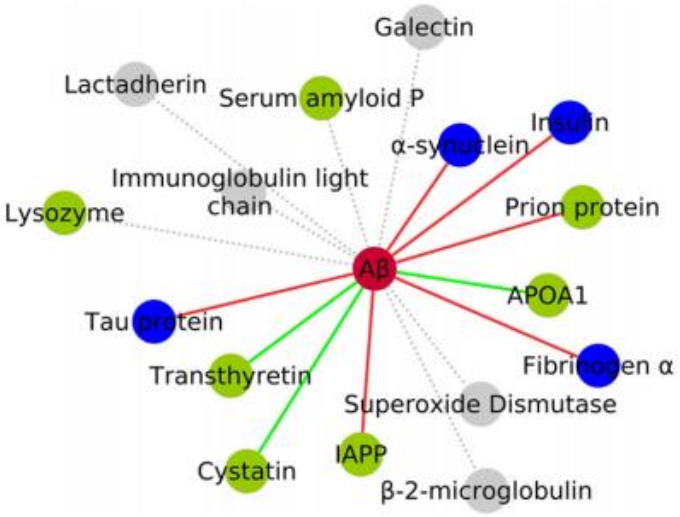

Figure 1.7: A cross-amyloid network for the Aβ peptide. Red lines: amyloid proteins that enhance the risk of AD (negative effect) *in vivo*. Green lines: amyloid proteins that decrease the progression of AD (positive effect) *in vivo*. Blue circles: amyloid proteins that promote Aβ fibrillation (negative effect) *in vitro*. Green circles: amyloid proteins that suppress Aβ fibrillation (positive effect) *in vitro*. Gray circles and lines: unknown[65]

1.3 The most common amyloidosis: Alzheimer's disease (AD)

Among amyloidosis, AD is the most common disease with high mortality. In 1906, Alois Alzheimer identified amyloid plaques in the brain of a woman who suffered from progressive dementia. This dementia now is named AD. Dementia cases were predicted to reach more than 152 million globally by 2050 with population growth and ageing, which nearly triple the cases in 2019. Therein, AD contributes the most of the cases and lead to heavy burden on health care and economy of society. The patients with the onset of AD after age 65 constitute the major cases of AD designated late-onset AD (LOAD), the rest of the relatively rare cases with the onset of AD before age 65 are termed early-onset AD (EOAD). AD patients would suffer from the difficulties in memory, thinking, language and even behavior, ultimately resulting in death. Although there are

enormous academies and pharmaceutical companies involving in the study of the disease, the exact mechanism of AD pathogenesis remains elusive and there are only a few drugs approved by the Food and Drug Administration (FDA) for treatment of the disease and most of them are not able to prevent the progression of the disease.

1.3.1 AD continuum and diagnostics

AD is an insidious and progressive disease in which the brain changes begin 15 years or more before symptoms onset. The progression of the disease is named Alzheimer's disease continuum which contains five phases including preclinical AD, mild cognitive impairment (MCI) due to AD, mild AD, moderate AD and severe AD (**Figure 1.8**).[67] In the phase of preclinical AD, patients show no symptoms but the pathological process of AD has started, such as the deposition of β amyloid (Aβ) protein, Tau pathology and synaptic dysfunction. The patients with MCI start to have very mild symptoms but they still can live or work normally without interference from the symptoms. The last three phases represent the severity of symptoms (memory loss, language problem, thinking problem, etc.) starting interfering with daily life, so these three phases are also called AD dementia.

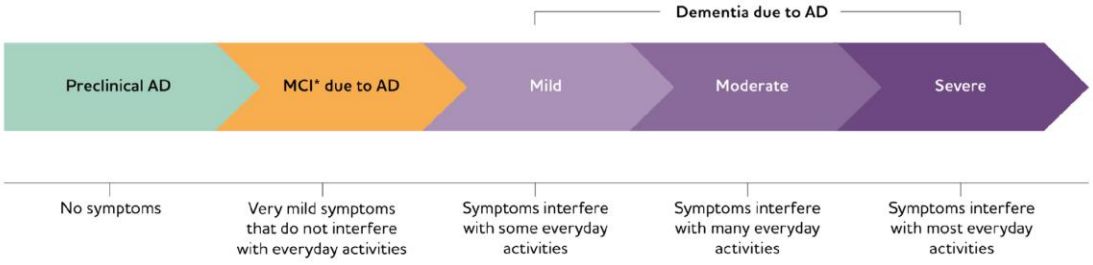

Figure1.8: AD continuum[67]

Different stages of AD have different diagnosis criteria. In 2011, the clinical diagnosis of AD dementia was revised by the National Institute on Aging-Alzheimer's Association (NIA-AA) based on the evaluation of symptoms of dementia incorporating the detection of related biomarkers[68]. In clinical practice, AD dementia is classified into two categories, including probable AD dementia and possible AD dementia. Firstly, patients diagnosed with AD dementia should meet the criteria of dementia. For probable AD dementia, the initial and most prominent cognitive deficits should be

associated with one of following syndromes, including amnestic syndrome manifested by the deficits of memory and non-amnestic syndrome manifested by impaired language functions, visuospatial abilities and executive functions. The onset of the symptoms usually is not sudden in few days but gradual over months to years in probable AD dementia. In addition, the patients should have no prominent features of other concomitant cerebrovascular diseases or dementias, such as the features of dementia with Lewy bodies. For the patients who meet the criteria of dementia but with a sudden onset of cognitive impairment and the presence of the features of other concomitant cerebrovascular diseases or dementias are defined as possible AD dementia. Whether patients are diagnosed as probable or possible AD dementia, when they show positive in AD biomarkers, the association of dementia with AD increases.

The clinical diagnosis of MCI also was reported by NIA-AA in 2011.[68] It is based on the assessment of cognitive impairment and AD biomarkers which are used to increase the certainty that MCI is due to AD.

Diagnosis of AD in preclinical phase is so far not feasible in clinical practice due to the lack of symptoms or cognitive impairments that could be used to assess and the insufficient accuracy and availability of AD biomarker tests.[68] Nevertheless, the diagnosis of AD which only depends on AD biomarkers is an urgent clinical need because of the long latent period and irreversible neuronal injury of AD. There are several AD biomarkers used in clinics. Aβ deposition in the brain, one of pathological hallmark of AD, gives rise to low concentration of $A\beta_{42}$ and increased $A\beta_{40}/A\beta_{42}$ ratio in cerebrospinal fluid (CSF). Analysis of the level of $A\beta_{42}$ in CSF provide useful information to assist the diagnosis of AD. However, the diagnoses based on the species in CSF require lumbar puncture to patients and corresponding laboratory facilities for performing fluid analysis, which limit their wide use. Aβ deposition in the brain also can be shown directly by positron emission tomography (PET) using several radioligands such as florbetapir, florbetaben and flutemetamol but PET imaging costs more than CSF analysis.[69–71] It should be noted that Aβ deposition also can be detected in disorders other than AD (e.g., Parkinson's disease and amyloid angiopathy) and some persons who have Aβ deposition in the brain do not develop dementia in their lifetime. Intracellular Tau neurofibrillary tangles (NFTs) is another pathological hallmark of AD and is more correlated with the progression of the disease, which can be used as an AD biomarker as well. Elevated level

of Tau (both Tau and phosphorylated Tau) in CSF and increased retention in Tau PET could indicate general injury of neuron and the possibility of AD but the tests have the same limitations in availability and cost. Moreover, elevated level Tau exists in other diseases such as prion disease, resulting in the reduced specificity for AD diagnosis. In the AD brain, glucose metabolism decreases as a result of the death of neurons. 18F-fluorodeoxyglucose (18F-FDG) uptake of brain could be monitored by PET, thereby making the trace of glucose metabolism in the brain possible but with low specificity and accuracy.[72] Magnetic resonance imaging (MRI) provides a visible image of cerebral atrophy, but it can only help the AD diagnosis after the impairment of brain.

Over the past decade, several criteria of AD diagnosis just based on AD biomarkers have been proposed for research purpose and more and more AD biomarkers as well as techniques have been investigated and developed for increasing their availability and accuracy.[73,74] For instance, analyses of Aβ and Tau in plasma instead of in CSF are possible and make the diagnoses more accessible although their reliabilities still need to be improved. New biomarkers, such as blood neurofilament light chain and neurogranin in CSF, have been used to help the diagnosis of AD for research purpose.[75,76] Further efforts are required to make for transferring them into clinical practice.

1.3.2 Pathophysiology of AD

Aβ

Despite the exact mechanism of AD pathogenesis remains elusive, the amyloid cascade is still the most widely accepted hypothesis.[37] Aβ is viewed as an initiator of this cascade by aggregation into oligomers and further into fibrils, which induces intracellular Tau neurofibrillary tangles, inflammatory responses, synaptic injury and neuronal loss, ultimately resulting in the dementia (**Figure 1.9**). It seems that Aβ aggregates in a concentration-dependent manner: the high concentration of Aβ causes Aβ aggregation.[77,78] The over-production of Aβ or the decrease of Aβ clearance in the brain were proposed to be the two reasons that initiate Aβ aggregation.[79] Age-related decrease in Aβ clearance has been reported.[80,81] This could explain why, although Aβ is produced in the brain of each person, the aggregation of Aβ generally is found in elders and elders have more risk to get AD than young people. Several genetic mutations which can destroy Aβ

homeostasis have been reported to support this hypothesis, including mutations in amyloid precursor protein (APP) or on presenilin (PEN) (increasing the production of Aβ and the ratio of $A\beta_{42}/A\beta_{40}$), mutations in APOE4 (influencing the clearance of Aβ) and trisomy 21 (Down's syndrome) (abundant production of Aβ).[37,82,83]

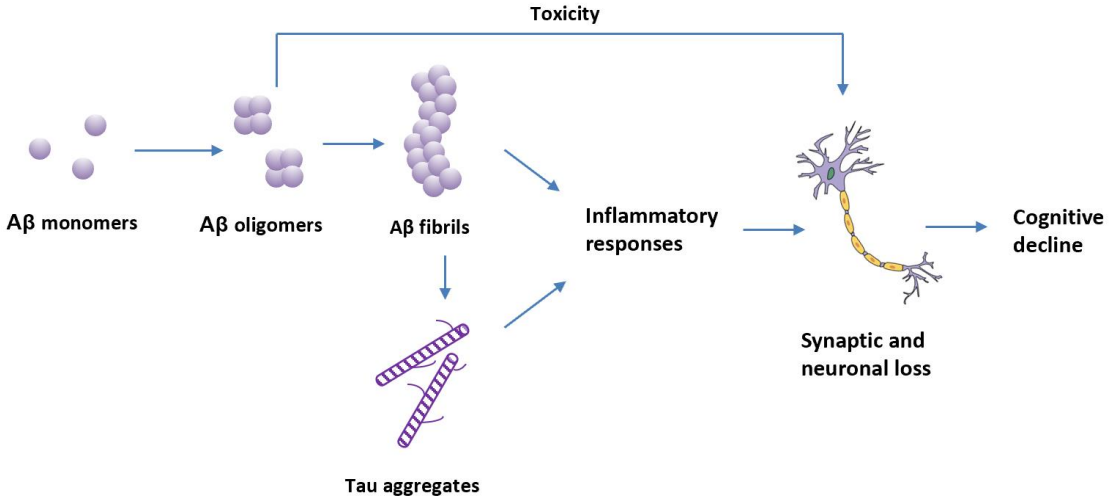

Figure 1.9: The illustration of amyloid cascade hypothesis

Aβ are 38- to 43-mer peptides produced from the sequential cleavage of amyloid precursor protein (APP) by β-secretase and γ-secretase in endosomes, which then are transferred and accumulate extracellularly (**Figure 1.10A**). $A\beta_{40}$ and $A\beta_{42}$ are the two most abundant alloforms of Aβ. $A\beta_{42}$ is more toxic than $A\beta_{40}$ because of its more aggregated propensity resulting from two more residues, Ile and Ala, at the C-terminus of $A\beta_{42}$ (**Figure 1.10B**). In a NMR study for visualizing Aβ aggregation, $A\beta_{42}$ seems to stimulate the aggregation of $A\beta_{40}$ whereas $A\beta_{40}$ delays the aggregation of $A\beta_{42}$ and the ratio of $A\beta_{42}/A\beta_{40}$ have an effect on the aggregation pathway and the dynamics of the oligomeric state.[84] The Aβ monomers show no toxicity on neurons but the toxicity appears once they aggregate into oligomers. The Aβ oligomers extracted from the AD brain, especially for Aβ dimers, can damage synaptic plasticity and disrupt memory in rodent models by perturbing glutamatergic synaptic transmission.[85] It was also reported that synthetic Aβ dimers $[A\beta S26C]_2$ are able to induce neuronal hyperactivation by the suppression of glutamate reuptake, resulting in a vicious cycle of hyperactivation.[86] Of course, not all soluble Aβ oligomers but only certain types of oligomers (small and diffusible oligomers) are able to impair synaptic plasticity. Another proposed

toxic mechanism underlying the toxicity of Aβ oligomers is destroying the integrity of membrane, thereby disrupting intracellular Ca^{2+} homeostasis. It was demonstrated that $A\beta_{42}$ oligomers rather than $A\beta_{40}$ oligomers, $A\beta_{42}$ monomers and fibrils show the ability to form voltage-independent, non-selective ion channels on the membrane excised from HEK293 cells of neuronal origin.[87] In addition to the formation of ion channel pores on membrane, Aβ oligomers can also disturb lipid bilayers by profound detergent-like effects whereas monomers and fibrils do not have the same effect.[88] Insoluble Aβ fibrils or plaques appear to be less toxic than Aβ oligomers but also play roles in the disease. Aβ plaques are proposed as reservoirs of Aβ oligomers and the dissociation of Aβ oligomers can be promoted by exposure to lipids.[89]

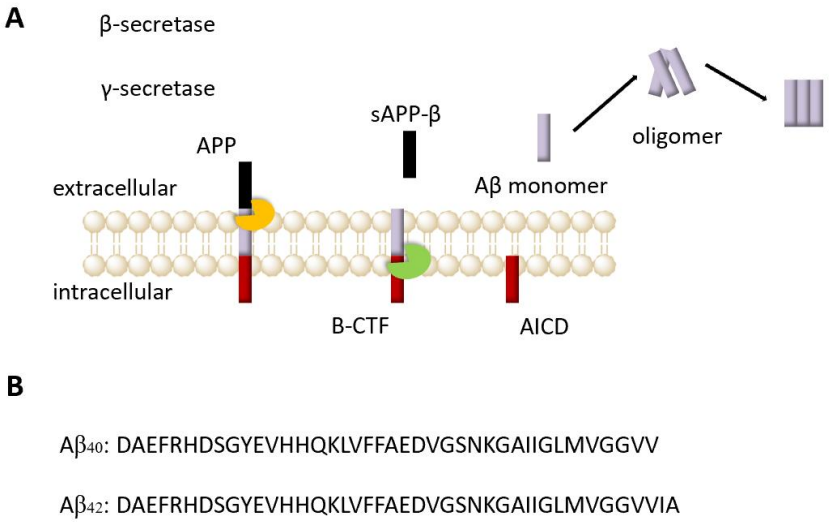

Figure 1.10: A) The illustration of the production of Aβ; B) The sequence of $A\beta_{40}$ and $A\beta_{42}$

Tau

Intracellular Tau NFTs are another pathological characteristic of AD. Tau proteins are microtubule binding proteins expressed mainly in neurons which play a role in the stabilization of microtubules. There are six Tau isoforms produced from alternative splicing and each of them has particular function and shows different expression during brain development. In physiological conditions, post-translational modifications of Tau are an important step for carrying out the biological functions of Tau. In pathological conditions, aberrant phosphorylation and acetylation of

Tau taking place in neurons lead to its dissociation from microtubules, ultimately resulting in the intracellular Tau NFTs and the dysfunction of microtubules. This process further induces axonal transport impairment and synaptic dysfunction, which causes cognitive decline. It was reported that Tau is able to bind a presynaptic vesicle-associated protein, synaptogyrin-3, which is significant for presynaptic vesicle mobility, thereby disturbing neurotransmitter release.[90] Recent studies showed that PHF-1 (one type of Tau phosphorylated at Ser396/404) prefer to accumulate in synaptic mitochondria to lead mitochondrial dysfunction, indicating one possible mechanism of synaptic impairment.[91] There are also other possible mechanisms of Tau causing synaptic dysfunction such as impairment of neuronal endocytosis and disruption of glutamate receptor trafficking.[92,93] The stimulus from Tau oligomers or fibrils can induce microglial morphological change which could affect neuroinflammation downstream.[94]

Compared to Aβ accumulation, the distribution and the burden of Tau accumulation was more correlated with cognitive decline.[95] The PET analyses of Aβ plaques and Tau NFTs suggest that the onset of Tau accumulation can be predicted by the progression of Aβ deposition whereas Tau-PET could be used to track cognitive impairment.[96] Taken together, Tau NFTs are viewed as a significant pathophysiology of AD and targeting Tau accumulation is another promising strategy to treat AD.

Apolipoprotein E (APOE)

APOE has three isoforms showing the similar sequences which only differ from each other at residue 112 and residue 158 (APOE2: cys112/cys158, APOE3: cys112/arg158, and APOE4: arg112/arg158). Through analyses of *APOE* genotype, the people with *APOE-ε4* allele have high risk at LOAD while *APOE-ε2* allele is able to decrease the AD risk, suggesting the *APOE* genotype is strongly correlated to AD risk.[97,98]

In the central nervous system (CNS), APOE serves as a transporter of apolipoprotein lipid and cholesterol and is mainly secreted by astrocytes. Multiple studies have indicated that the major linker of APOE to AD is its effect on Aβ deposition. Compared to APOE3 and APOE2, APOE4 has greater ability to increase Aβ oligomers and fibrils in the brain by accelerating the seeding process and the conversion of protofibrils to fibrils.[99–101] APOE does not influence the production of Aβ but involves the clearance of Aβ in the brain and APOE4 can reduce Aβ clearance compared to other

two isoforms.[102] It was reported that APOE regulates the clearance of Aβ by competitively binding to LDLR-related protein 1 which is on the surface of astrocyte, thereby blocking the Aβ uptake of astrocyte.[103] APOE4 seems to influence the progress of AD with Tau protein. Through the studies on P301S Tau transgenic mice with or without human *APOE* gene, it found that ApoE4 dramatically exacerbated Tau-mediated neurodegeneration.[104] In addition to the influence on Aβ, APOE4 could decrease blood-brain barrier (BBB) permeability, which may cause neurodegeneration because of the exposure to serum proteins.[105]

Neuroinflammation

The increased level of inflammatory markers in the brain of AD patient and high association between AD risk genes and innate immune functions implicate that neuroinflammation play critical roles in the progress of AD. Astrocytes and microglia are two main neuronal cells involving neuroinflammation. Astrocytes are able to clear Aβ plaques by uptake of Aβ with the aim of maintenance of the homeostasis in the early stage of AD. However, reactive astrocyte is likely to be detrimental to synapse and memory through excessive release of GABA which reduces spike probability of granule cells.[106] Microglia are the main innate immune cells in the CNS and involve Aβ clearance by phagocytosis and autophagy. The phagocytic function, however, is degenerated in the late-stage of AD, which may exacerbate the disease.[107] Amyloid cascade-inflammation hypothesis has been proposed to link microglial activation with the aggregation of Aβ and Tau.[108,109] Under the pathological stimulation like Aβ or Tau aggregation, sustaining activated microglia can impair neuronal functions. Aβ species can induce expression or up-regulation of some cytokines in microglia, such as IL-1β, TNF, by binding with TLR2 and scavenger receptors of microglia (**Figure 1.11**). Then the release of these cytokines causes synaptic dysfunction and neuronal death[110,111], or increases the production of β-secretase which further enhances the production of Aβ.[112] Additionally, it was demonstrated that microglia promote to seeding of Aβ aggregation by releasing apoptosis-associated speck-like protein which contains a C-terminal caspase recruitment domain (ASC) specks severing as binding cores for Aβ aggregation (**Figure 1.11**).[113]

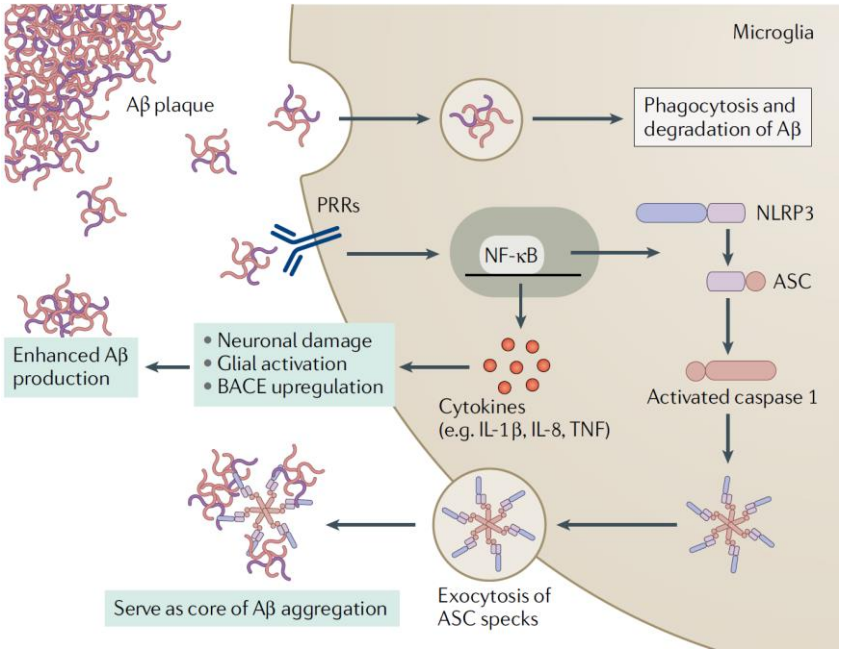

Figure 1.11: The illustration of microglial response to Aβ species[114]

Other factors including sleep impairment, brain infection and aging have also been implicated in the pathophysiology and development of AD, which has been reviewed well in literature.[115,116]

1.3.3 Treatment of AD

High medical and healthcare cost of AD not only impels governments to support more fundings on the fundamental research of AD in academy, but also attracts more and more pharmaceutical companies to discovery new drugs with novel targets or mechanisms. However, given the complicated mechanism of AD pathogenesis and the difficulty of BBB permeability for the drugs targeting CNS, so far there are only a few drugs approved by FDA for the treatment of AD and most of them are not able to prevent the progression of the disease. In this section, I would focus on introducing the drugs which have been approved by the FDA and on some molecules that were or are currently in the late stage of clinical trials which target Aβ and Tau proteins.[117]

Acetylcholinesterase inhibitors

In the brain of AD patient, synaptic dysfunction and neuronal loss lead the reduced synthesis of acetylcholine (ACh), an important neurotransmitter associated with memory and learning, which

is the fundamental of cholinergic hypothesis of AD. In order to keep the concentration of acetylcholine in the synaptic cleft, one most efficient way is inhibition of cholinesterases to reduce the proteolysis of ACh. Currently, there are three cholinesterase inhibitors in the markets, including donepezil, galantamine and rivastigmine (**Figure 1.12**). These three drugs can be used in the symptomatic treatment of mild to moderate AD. Donepezil is the most tolerated one with less side effects compared with the other two drugs and it's also the only one approved for severe AD[118]. Galantamine is a naturally occurring molecule isolated from the plant *Galanthus woronowii*. It's not only a selective, reversible acetylcholinesterase inhibitor but also an allosteric modulator of nicotinic cholinergic receptors, which is beneficial for the treatment of AD. Rivastigmine shows inhibition on both acetylcholinesterase and butyrylcholinesterase and is used in the treatment of Lewy bodies and Parkinson's disease dementia as well.

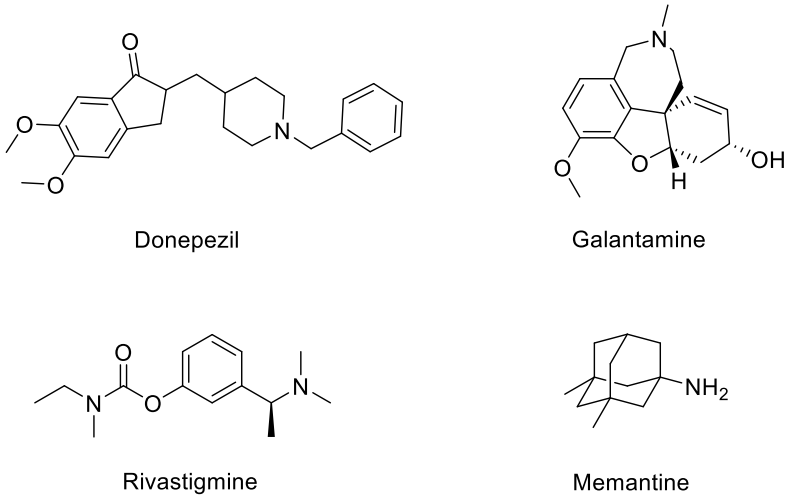

Figure 1.12: The structure of donepezil, galantamine, rivastigmine and memantine

N-methyl-D-aspartate (NMDA) receptor antagonist

Memantine is the only one NMDA receptor noncompetitive antagonist approved for the treatment of moderate to severe AD in 2003. The NMDA receptors are cationic channels responsible for transportation of Ca^{2+}, which are controlled by glutamate. In AD patients, the excessive glutamate activity induces the abundant of influx of Ca^{2+} in neurons, ultimately resulting in

excitotoxicity of the CNS. One possible mechanism of memantine for the treatment of AD is the noncompetitive antagonism of NMDA receptors thereby reducing the glutamate activity. Memantine can be used in combination with acetylcholinesterase inhibitors for the treatment of AD but could not prevent the progress of AD.

Anti-Aβ

On the basis of the amyloid cascade hypothesis, Aβ aggregation plays a key role in the trigger and progress of AD. Thus, the design and discovery of new molecules which can inhibit or decrease Aβ aggregation has been a promising strategy to prevent the progress of the disease over the past three decades. There are three ways proposed to decrease Aβ aggregation, including reduction of Aβ production, inhibition of Aβ aggregation and clearance of performed Aβ aggregation.

As mentioned before, the two key enzymes, β-secretase (BACE1) and γ-secretase, are responsible for the production of Aβ. Inhibiting these two enzymes is regarded as a direct way to block the production of Aβ. The cut of APP by BACE1 is a rate-limiting step of the production of Aβ. So far, there is no BACE1 inhibitor approved. Five BACE1 inhibitors reached to phase III clinical trials for the treatment of AD. Four of them led worse cognition to AD patients and the remaining one failed to describe clinical benefits (**Table 1.1**), while they all showed the ability to reduce the level of Aβ in CSF of AD patients.[119] It has been demonstrated that BACE1 inhibitors can reduce the synaptic activity at high doses.[120] Thus, currently a low dose of BACE1 inhibitors was suggested in clinical trials to keep the balance between the beneficial and detrimental effects of BACE1 inhibitors on the brain.

For γ-secretase inhibitors, semagacestat and avagacestat reached phase III trials and phase II trials, respectively, but both were terminated due to no clinical benefit and severe adverse events such as skin cancer. γ-Secretase was also proposed to play key roles in the function of Notch protein involving differentiation, maintenance and proliferation of cells.[121] That is a possible reason of the adverse events of γ-secretase inhibitors. Thus, γ-secretase modulator, tarenflurbil, was designed to avoid the adverse events but it showed insufficient efficacy in a phase III trial.

Drug	Company	Mechanism	Phase	Result
Verubecestat	Merck	BACE-1 inhibitor	III	cognitive worsening
Lanabecestat	AstraZeneca, Eli Lilly	BACE-1 inhibitor	III	cognitive worsening
Atabecestat	Janssen	BACE-1 inhibitor	III	cognitive worsening
Umibecestat	Amgen, Novartis	BACE-1 inhibitor	III	cognitive worsening
Elenbecestat	Eisai, Biogen	BACE-1 inhibitor	III	No clinical benefit
Semagacestat	Eli Lilly	γ-secretase inhibitor	III	No clinical benefit, severe adverse effect
Avagacestat	Bristol-Myers Squibb	γ-secretase inhibitor	II	No clinical benefit, severe adverse effect
Tarenflurbil	Myriad Genetics & Laboratories	γ-secretase modulator	III	No clinical benefit
EGCG	Charite University	Aβ aggregation inhibitor	II/III	No results
Resveratrol	ADCS	Aβ aggregation inhibitor	II	No results
Tramiprosate	Neurochem	Aβ aggregation inhibitor	III	No clinical benefit
ALZ-801	Alzheon	Aβ aggregation inhibitor	III	Ongoing
Scyllo-inositol	Elan	Aβ aggregation inhibitor	II	No clinical benefit
Aducanumab	Eisai, Biogen	Anti-Aβ antibody	IV	approved
Bapineuzumab	Janssen, Pfizer	Anti-Aβ antibody	III	No clinical benefit
Solanezumab	Eli Lilly	Anti-Aβ antibody	III	No clinical benefit
Crenezumab	AC Immune, Genentech	Anti-Aβ antibody	III	No clinical benefit
Gantenerumab	Hoffmann-La Roche	Anti-Aβ antibody	III	Ongoing
Lecanemab	Eisai, Biogen	Anti-Aβ antibody	III	Ongoing
Donanemab	Eli Lilly	Anti-Aβ antibody	III	Ongoing

Table 1.1: The drugs targeting Aβ in clinical trials

Aβ monomers can aggregate into oligomers firstly and further aggregate into fibrils which constitute Aβ plaque depositing in the brain. Oligomers are regarded as the most toxic species to neurons. The molecules capable of inhibiting Aβ aggregation or changing the pathway of aggregation which is less toxic to neurons are promising to prevent the progress of AD. Epigallocatechin-3-gallate (EGCG) (**Figure 1.13**) is a polyphenol compound mainly extracted from green tea leaves. It has been reported that EGCG is able to inhibit Aβ aggregation with other benefits to prevent pathology of AD, such as anti-inflammatory and antioxidant.[122] A phase II/III of EGCG was conducted by coadministration of donepezil or not but no result was posted. Resveratrol (**Figure 1.13**) is another polyphenol compound which has been extensively studied and could be extracted from many plants, such as grapes, mulberries and peanuts. It prevents the formation of Aβ plaques by promoting the formation of specific oligomers, off-pathway species, which could not further aggregate into fibrils. A phase II of resveratrol for determining if daily resveratrol therapy can delay or alter the deterioration of memory and daily functioning was started at 2012 but no result was posted. Tramiprosate (**Figure 1.13**) is a small aminosulfonate compound capable of binding to Aβ, thereby stabilizing Aβ in monomer and reducing the level of toxic oligomers and plaques in the brain. In a phase III trial for the treatment of mild to moderate AD, although tramiprosate failed to demonstrate a clinical benefit, statistically significant cognitive improvement was found in APOE4 carriers.[123] Due to high intersubject pharmacokinetic variability and side effects such as nausea, the prodrug of tramiprosate, ALZ-801(**Figure 1.13**), was designed and a phase III trial was started in May 2021.[124] Scyllo-inositol (**Figure 1.13**) is a small molecule founded in sharks and skates and it can inhibit Aβ aggregation. In clinical trials, scyllo-inositol shows high frequency of adverse effects in a high dose group. The lowest dose, 250 mg twice daily, is tolerated and further investigations in efficacy should be performed.[125]

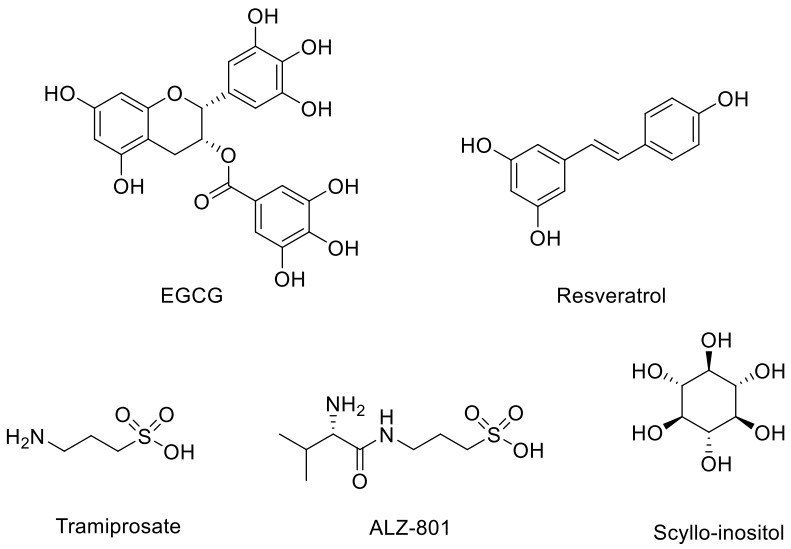

Figure 1.13: The structures of small molecule inhibitors against Aβ aggregation in clinical trials

The strategy to clear Aβ in the brain mainly relies on immunotherapy. Monoclonal antibody is the primary approach to recognize various Aβ species thereby promoting immune system to clear Aβ. Although several monoclonal antibodies failed in phase III trials because of no obvious efficacy or serious side effects (**Table 1.1**), the analyses of the clinical results and the mechanisms in which antibodies interact with Aβ give some insight into the correlation between antibodies and clinical benefits.[126] Bapineuzumab is a humanized form of murine monoclonal antibody that could bind the N-terminus of Aβ (residues 1-7) in a helical form.[127] It is able to recognize both monomers and fibrils. Solanezumab is preferential to recognize soluble monomers rather than fibrils and it binds the same epitope (midsection) of Aβ as crenezumab does, whereas crenezumab could recognize not only monomers but also oligomers and fibrils.[128] To date, the most successful antibody is aducanumab, which is thought to target the aggregates of Aβ including soluble oligomers and insoluble fibrils rather than Aβ monomers.[129] Although with the controversy in its efficacy, aducanumab was approved by the FDA in June 2021 and further clinical data in phase IV has been required by the FDA for confirming the efficacy.

Aducanumab was proposed to recognize the N-terminus of Aβ (residues 2-9) in a linear form, which is similar as gantenerumab (residues 1-11).[126] It seems that the epitopes of Aβ that antibodies bind make different clinical benefits of antibodies. Antibodies binding the midsection of Aβ displayed negative results in clinical trials while antibodies binding the N-terminus of Aβ have more

promising results. In addition, the conformations of the N-terminus of Aβ that antibodies bind also play a critical role in the efficacy. The antibodies (aducanumab and gantenerumab) recognizing epitopes of Aβ which is in extended conformation of the N-terminus prefer to bind and clear aggregated Aβ species, while bapineuzumab recognizing the N-terminus of Aβ in a helical form was proposed to bind both Aβ monomers and fibrils. This probably explains why aducanumab shows better clinical benefits than bapineuzumab. Despite of several failures of monoclonal antibodies targeting Aβ and the complicated mechanism that makes different antibodies have different clinical benefits, there are still several promising monoclonal antibodies, such as gantenerumab, lecanemab (BAN2401) and donanemab, in clinical trials. The clinical results from them will further help us understand more about the role of Aβ species in AD and how to design right antibodies for AD therapy.

Anti-Tau

Since the hyperphosphorylation of Tau is viewed as a crucial step of Tau aggregation, inhibition of the enzymes responsible for the phosphorylation of Tau is a rational way to block Tau pathology. Glycogen synthase kinase 3-beta (GSK-3β) is one of the significant kinases associated with the hyperphosphorylation of Tau and the subsequent neurodegeneration. A selective, irreversible GSK- 3β inhibitor, tideglusib (**Table 1.2**), did not reach primary endpoint and several secondary endpoints in a phase IIb trial for the treatment of mild to moderate AD.[130] The further trials were terminated. Another GSK-3β inhibitor widely studied in clinical trials is lithium (**Table 1.2**). It failed to prevent cognitive decline in mild or mild to moderate AD patients but it showed clinical benefits for prodromal AD patients.[131] The efficacy is waiting to be confirmed by further studies.

Molecules which can inhibit Tau aggregation directly are also promising candidates to treat AD. However, only a few molecules, including methylthioninium chloride (methylene blue) and its analogues, LMTM, reached to clinical trials and no one showed promising results so far.[132,133]

Immunotherapy to clear abnormal Tau species is an alternative to reduce Tau pathology and several antibodies entered phase II trials. Gosuranemab (**Table 1.2**) is able to bind the N-terminal fragments of Tau which is proposed to involve the spread of tauopathies. The development of

gosuranemab was halted because it showed no benefit on improvement of cognition and even on Tau-PET imaging in a clinical phase II trial.[134] Tilavonemab and semorinemab (**Table 1.2**) recognize pathological Tau through binding the N-terminus of Tau and they also failed to slow cognitive decline in phase II trials.[135,136] Zagotenemab, a humanized anti-Tau antibody recognizing specific pathological conformational epitope which involves the N-terminus of Tau, was abandoned since it missed its primary endpoint (**Table 1.2**).[137] It seems that antibodies binding the N-terminus of Tau could not prevent cognitive decline. An antibody targeting the microtubule-binding domain of Tau , bepranemab, become more promising to inhibit tauopathies and the clinical phase II trial for treatment of AD is planned to finish at 2025 (**Table 1.2**).[138] In addition, JNJ-63733657 binding to the central Tau phosphorylated epitope which is located at the microtubule-binding domain has just started a phase II trial (**Table 1.2**).[139] However, we doubt if the antibodies binding to the microtubule-binding domain of Tau can succeed in clinical trials because they might also prevent the interaction between microtubule and Tau, which is crucial to the stabilization of microtubules.

Drug	Company	Mechanism	Phase	Result
Tideglusib	Noscira	GSK-3β inhibitor	II	No clinical benefit
Lithium	University of Sao Paulo	GSK-3β inhibitor	II	No clinical benefit
Methylene blue	TauRx Therapeutics	Tau aggregation inhibitor	II	No clinical benefit
LMTM	TauRx Therapeutics	Tau aggregation inhibitor	II	No clinical benefit
Gosuranemab	Biogen, Bristol-Myers Squibb	Anti-Tau antibody	II	No clinical benefit
Tilavonemab	AbbVie, C2N Diagnostics	Anti-Tau antibody	II	No clinical benefit
Semorinemab	AC Immune, Genentech	Anti-Tau antibody	II	No clinical benefit
Zagotenemab	Eli Lilly	Anti-Tau antibody	II	No clinical benefit
Bepranemab	Hoffmann-La Roche, UCB	Anti-Tau antibody	II	Ongoing
JNJ-63733657	Janssen	Anti-Tau antibody	II	Ongoing

Table 1.2: The drugs targeting Tau in clinical phase II trials

Many molecules targeting Aβ or Tau, whether they are small molecules or antibodies, failed in clinical trials, making people start revisiting the amyloid cascade hypothesis. Molecules targeting CNS diseases always have problem on BBB permeability, which prevents the enough concentration in the brain. Especially for antibodies which have too big molecule weights to cross BBB by passive diffusion. This is probably a one reason to explain the failure on the clinical trials of some molecules. In addition, the pathological mechanism of AD is still under study. Aβ appears to aggregate in different pathways capable of generating various oligomers and fibrils, which may have different toxicities. More and more studies confirmed that Aβ oligomers are more toxic than Aβ fibrils,[85,86] indicating that removal of Aβ plaques in the brain may be not enough to reduce the toxicity because Aβ oligomers are more toxic. The biggest problem for AD therapies, in my opinion, is no availability to diagnose AD with high confidence in the early stage (before MCI) in clinic. As we mentioned above, AD can only be diagnosed in combination with the assessment of the symptoms of dementia. However, the damage of neurons is irreversible. Thus, it may be too late to treat AD by the inhibitors targeting Aβ aggregation when the symptoms have appeared.

1.3.4 Preclinical Aβ aggregation peptidic inhibitors

In the last section, some small molecules or antibodies treatments for AD in clinic or in clinical trials have been presented. In this section, peptides or peptidomimetics as Aβ aggregation inhibitors are presented. Peptides are viewed as more promising molecules to target PPIs because of their high selectivity and affinity as well as low toxicity in comparison with small molecules. In addition, peptides or peptidomimetics can present higher BBB permeability compared to antibodies (as we discussed in section 1.12). Thus, the discovery of peptides or peptidomimetics capable of interfering with the self-association of Aβ is a promising approach to obtain high selective, potent and low toxic drugs to treat AD. Here peptide or peptidomimetic inhibitors were divided into two categories: one is based on the peptide sequence derived from Aβ, the other one is based on the peptide sequence not derived from Aβ sequence.

Peptides derived from Aβ sequences

Tjernberg and coworkers found that the short peptide KLVFF, located at the central

hydrophobic core (CHC) of Aβ, is the most potent short fragment of Aβ which can binding full-length Aβ.[140] The key residues of the peptide interacting with full-length Aβ, Lys16, Leu17, and Phe20, were identified by alanine scanning. The peptide designed based on this sequence, Ac-QKLVFF-NH_2, showed the ability to prevent the fibril formation of $Aβ_{40}$, indicating that the CHC of Aβ actually contributes to the aggregation of Aβ and the peptides incorporating this sequence KLVFF can be used as Aβ aggregation inhibitors.

Afterward, a number of peptides containing this key sequence were investigated in different groups. Matsunaga and coworkers synthesized a series of octapeptides which are directly derived from Aβ and found peptides Aβ(15−22), Aβ(16−23) and Aβ(17−24) are able to inhibit the acid-induced aggregation of $Aβ_{42}$.[141] Through adding disrupting elements to the C-terminus of KLVFF, such as sequential Lys or Glu, the peptides KLVFFKKKK and KLVFFEEEE inhibited Aβ toxicity on cells by promoting the aggregation of Aβ.[142] This result implied that soluble Aβ oligomers are more toxic than insoluble Aβ fibrils. Through adding RG and GR to the N-terminus and C-terminus, respectively, of KLVFF, Austen and coworkers got two peptides, RGKLVFFGR and RGKLVFFGR-NH_2, which showed high aqueous solubility.[143] Both the peptides could inhibit Aβ aggregation but only RGKLVFFGR-NH_2 showed the inhibition of the formation of Aβ oligomers. Based on the sequence of Aβ15-25, Soto and coworkers synthesized a 11 amino acid peptide RDLPFFPVRID, called iAβ11, by substitution of several residues with prolines and charged amino acids to disrupt β-sheet structure and increase solubility. iAβ11 not only could inhibit Aβ accumulation but also partly disaggregate performed Aβ fibrils.[144] They further shortened iAβ11 to get LPFFD (iAβ5), which showed the similar activity as iAβ11 on Aβ aggregation. Another analogue, Ac-LPFFD-NH_2 (iAβ5p), was chronic intraperitoneal administrated in rodent model and showed the ability to reduce Aβ plaques and astrocytic response near the injection site.[145] Based on the peptide LPFFD, several new peptides, such as LPYFD-NH_2 and Ac-LPFFN-NH_2, were designed and all showed the potential to block Aβ aggregation as well. Liu and coworkers designed and synthesized a decapeptide Ac-RYYAAFFARR-NH_2 named RR based on the sequence of Aβ11−23. It inhibited the fibrillation of Aβ effectively by binding to the Aβ11-23 region of Aβ.[146] The hydrophobic C-terminus of Aβ also plays a key role in the self-aggregation of Aβ. Several sequences on the C-terminus were reported to show activity in the inhibition of Aβ aggregation such as

Aβ(31−42), Aβ(39−42) and Aβ(20−29).[147,148]

Based on the sequence derived from Aβ, a number of modified peptides were designed to increase the activity and selectivity or overcome the drawbacks of peptides such as proteolytic instability and bad membrane permeability (**Table 1.3**).

N-Methylation of amide can block the formation of hydrogen bond, thereby endowing peptides with the ability to destroy the pathway of aggregation. Hughes and coworkers reported *N*-methylated derivatives of Aβ(25−35) could prevent the fibrillogenesis of fragment Aβ(25−35) by blocking the formation of hydrogen bond on the outer edge of the assembling amyloid.[149] Gordon and coworkers reported that *N*-methyl amino acid containing peptide (Aβ16−22m) showed higher aqueous solubility, proteolytic stability and activity against Aβ fibrillogenesis compared to its nonmethylated congener.[150] They found that alternating *N*-methyl and nonmethylated amino acids in the sequence seems to be crucial for the activity. Further shortening Aβ16-22m gave Aβ16-20m, which not only retained the activity against Aβ aggregation but also were able to pass synthetic phospholipid bilayer vesicles and cell membranes.[151] Cruz and coworkers synthesized some peptides which have single point methylation at different residues. The peptides processing single methylation on Phe19 or Phe20 significantly inhibit the toxicity of $A\beta_{42}$ to rat pheochromocytoma cell (PC12).[152] Detailed influences of *N*-methylation on the solubility, membrane permeability, proteolytic stability and cell toxicity for peptides Aβ(16−21) and Aβ(32−37) were studied by Arvidsson and coworkers. It turned out that poly-*N*-methylation of peptides, especially for short peptides with six or less residues, make the proteolytic stability and aqueous solubility increased, whereas the membrane permeability of the peptides decreased.[153] Kokkoni and coworkers found a very potent peptide *D*-[(chGly)-(Tyr)-(chGly)-(chGly)-(mLeu)]-NH_2 (SEN304). In that case, the *D*-chirality, free N-terminus and amidated C-terminus are necessary for the good inhibition of Aβ aggregation, while the methylation is beneficial to the high solubility and nontoxicity of the peptide.[154]

Name	Sequence	Modification	Finding
NMeGly[33] NMeLeu[34]	Aβ(25−35), GSNKGAII(MeG)LM GSNKGAIIG(MeL)M	*N*-Methylation	No aggregation propensity, inhibit fibril assembly, alter fibril morphology and reduce the toxicity of prefolded amyloid
Aβ16−22m Aβ16−20m	K(MeL)V(MeF)F(MeA)E-NH_2 Ac-K(Me)LV(Me)FF-NH_2	*N*-Methylation	Inhibit $Aβ_{40}$ aggregation and disassemble $Aβ_{40}$ fibrils, higher aqueous solubility, proteolytic stability and membrane permeability
None	KKLV(MeF)FA-NH_2 KKLVF(MeF)A-NH_2	*N*-Methylation	Inhibit the toxicity of $Aβ_{42}$ to rat pheochromocytoma cell
SEN304	*D*-[(chG)-Y-(chG)-(chG)-(mL)]-NH_2	*N*-Methylation *D*-Amino acid	High solubility and nontoxicity
None	klvff	*D*-Amino acid	Higher proteolytic stability and activity
None	kklvffa	*D*-Amino acid	Improve survival in transgenic *caenorhabditis elegans* model
PPI-433 PPI-457	cholyl-lvffa cholyl-(lvffa)-NH_2	*D*-Amino acid	Stable in monkey cerebrospinal fluid
None	ffvlk	Retro-inverso peptide	Moderate affinity of binding artificial $Aβ_{40}$ fibrils
None	rGffvlkGr-NH_2	Retro-inverso peptide	Prevent the formation of Aβ oligomers
RI-OR2-TAT	Ac-rGffvlkGrrrrqrrkkrGy-NH_2	Retro-inverso peptide	BBB permeability
PPI-1019	(Me-l)vffl-NH_2	*N*-Methylation Retro-inverso peptide	Entered in Phase I and II clinical trials
None	cyclo17,21-[Lys17, Asp21]Aβ1-28	Cyclization	No self-association
None	cyclo-[klvf(β-Ph)f]	Cyclization *D*-Amino acid	Induce off-pathway of oligomeric species
None	klvfw-Aib	*D*-Amino acid Aib	Prevent primary nucleation of Aβ
AMY-1 AMY-2	Based on KLVFF	α, α-Disubstituted amino acid	Alter the pathway of Aβ aggregation to form nonfibrillar assemblies
P1	KLVFΔAIΔA	ΔA=α, β-Dehydroalanine	Increase proteolytic stability
None	Based on LVFFD-PEG	Fluorinated amino acids	Prevent Aβ aggregation
DDX3	KLVFF$(DDX)_3$	X=aminoethoxy ethoxy acetate	Inhibit cytotoxicity of Aβ aggregates to IMR-32 neuroblastoma cells
P4 P5	Thymine-(MeG)L(MeG)F(MeG)A-NH_2 Thymine-K(MeG)V(MeG)F(MeG)- NH_2	*N*-Methylation and thymine at N terminus	Rescue yeast cells from Aβ toxicity
ABSM 1a	Based on KLVFF	Cyclization “Hao” unit	High potent to inhibit Aβ aggregation
2a	Based on KLVFF	Diketopiperazine scaffold as β-turn inducer	β-Turn conformation is important for inhibiting Aβ aggregation
G1b G2b	Based on KLVFF, GLMVG, GVVIA	Piperidine–pyrrolidine as β-turn inducer	Highly efficient anti-aggregation activity to Aβ

Table 1.3: The modified peptidic inhibitors derived from Aβ sequence

Introduction of *D*-amino acid in peptides endows the peptides with the resistance to proteolysis. It was reported that the enantiomeric peptide of KLVFF, klvff, not only has higher proteolytic stability but also showed higher activity to prevent the β-sheet secondary structure of Aβ compared to KLVFF.[155] Several enantiomeric peptides based on CHC were synthesized and examined *in vitro* and *in vivo*, including pgklvya, kklvffarrrra, and kklvffa. Peptides kklvffarrrra and kklvffa showed the high inhibition of Aβ fibrillogenesis in ThT assays while pgklvya and kklvffa improved survival in transgenic *caenorhabditis elegans* model.[156] This strategy was also applied to increase the biochemical stability of peptide cholyl-LVFFA (PPI-368) showing potential polymerization inhibition. Both *D*-enantiomeric peptides, cholyl-lvffa (PPI-433) and cholyl-lvffa-NH_2 (PPI-457), retained the activity and were quite stable in monkey cerebrospinal fluid.[157] Zhang and coworkers reported that a retro-inverso peptide of KLVFF, ffvlk, could bind artificial $A\beta_{40}$ fibrils with a moderate affinity and resulted in lower fluorescence signal than KLVFF in thioflavin T assay with $A\beta_{40}$.[158] The conjugates of this peptide on a branched poly(ethylene glycol) (PEG) could increase the affinity to $A\beta_{40}$ fibrils and further reduce the fluorescence signal. On the basis of the retro-inverso sequence of KLVFF, Matharu and coworkers designed a peptide rGffvlkGr-NH_2 which increaseed the efficacy of inhibition of Aβ aggregation by preventing the formation of Aβ oligomers.[159] A similar work was performed by Taylor and coworkers at the same time to get peptide Ac-rGffvlkGr-NH_2 but with the problem on BBB permeability.[160] Further modification resulted in a BBB-penetrating peptide Ac-rGffvlkGrrrrqrrkkrGy-NH_2 (RI-OR2-TAT) which displayed better binding affinity to Aβ fibrils and reduction of Aβ plaques in transgenic mouse models.[161] Peptide (Me-l)vffl-NH_2 (PPI-1019) in which a methyl group is not on amide but on N-terminus[154], had been in Phase I and II clinical trials for the treatment of AD, but the result of trials is not posted.

Cyclization of linear peptides is an useful approach to maintain specific conformations of peptides as well as to increase their proteolytic stability. Kapurniotu and co-workers applied i, i+4 cyclic conformational constraint strategy on Aβ1-28 to get cyclo^{17,21}-[Lys^{17}, Asp^{21}]Aβ1-28 showing a more α-helical structure.[162] Compared to Aβ1-28 or [Lys^{17}, Asp^{21}]Aβ1-28, cyclo^{17,21}-[Lys^{17}, Asp^{21}]Aβ1-28 showed the ability to interfere with Aβ aggregation without the propensity of self-association. Arai and coworkers reported that some head-to-tail cyclic peptides, including cyclo-[KLVFF], cyclo-[klvff] and cyclo-[FFVLK], are all more potent than linear KLVFF to inhibit Aβ

aggregation in ThT assay. Through analysis of crucial pharmacophore motifs of the cyclic peptides, they successfully designed a series of non-peptidic Aβ inhibitors. In addition, they introduced an excess of phenyl group at the β-position of the Phe4 of cyclo-[KLVFF] to get a new peptide which is able to generate off-pathway oligomeric species.[163]

Adding unnatural amino acids or non peptidic motifs to peptides is proposed as a method to improve the proteolytic stability as well as activity of peptides. Geminally disubstituted aminobutyric acid (Aib) is regarded as a strong β sheet breaker, even stronger than proline. Horsley and coworkers designed and synthesized two Aib containing peptides with different chirality based on the sequence of KLVFF. The *D*-enantiomer showed a very strong activity against Aβ aggregation by preventing primary nucleation of Aβ.[164]

Etienne and coworkers designed two peptides, AMY1 and AMY2 (**Figure 1.14**), which have alternating α, α-disubstituted amino acid/*L*-amino acid in the CHC and these two peptides can alter the pathway of Aβ aggregation to form nonfibrillar assemblies.[165]

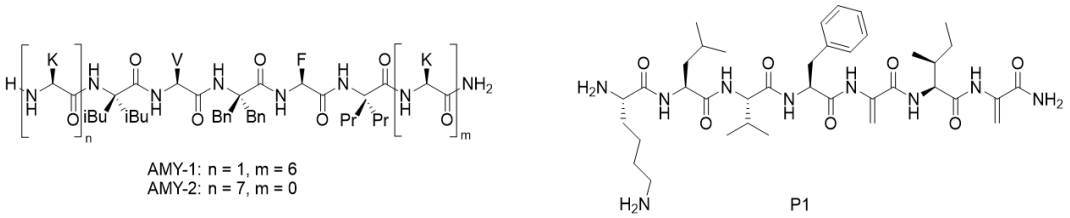

Figure 1.14: The structures of AMY-1, AMY-2 and P1

α, β-Dehydroalanine (ΔAla) was used to replace the residues in peptide KLVFF to get more proteolytic stable peptide P1 (KLVFΔAIΔA) which can inhibit Aβ aggregation (**Figure 1.14**).[166]

Loureiro and coworkers used fluorinated amino acids, such as 4,4,4-trifluorovaline, 4-fluoroproline and 3,4,5-trifluorophenylalanine, instead of natural amino acids in the synthesis of β-sheet breaker peptides based on the sequence LVFFD (**Figure 1.15**).[167] Among them, the peptides with the presence of fluorinated hydrophobic residues, 4,4,4-trifluorovaline and 3,4,5-trifluorophenylalanine were effective in preventing Aβ aggregation.

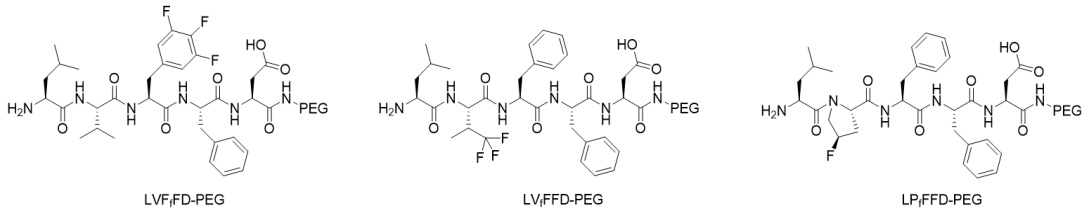

Figure 1.15: The structures of fluorinated peptides targeting Aβ aggregation

Several non peptidic motifs capable of disrupting β-sheet structure are useful to increase the inhibition of Aβ aggregation and decrease the propensity of self-association. Watanabe and coworkers incorporated a flexible hydrophilic disrupting element (aminoethoxy ethoxy acetate and aspartate) with KLVFF to give some compounds which inhibited the formation of Aβ aggregation and reduced the cytotoxicity of Aβ aggregates to IMR-32 neuroblastoma cells, especially for the most potent one, DDX3 (**Figure 1.16**).[168] Rajasekhar and coworkers developed several peptidomimetics based on the KLVFF to modulate Aβ toxicity. They introduced multiple hydrogen bond donor-acceptor moieties (thymine or barbiturate) at the N-terminus of the sequence to get P2 and P3 which showed increased inhibition efficiency (**Figure 1.16**). Further inserting of N-methylglycine alternatively into P2 gave P4, or into P3 gave P5 (**Figure 1.16**). Both showed improved blood serum stability and protective effect on yeast cells from $A\beta_{42}$ toxicity.[169] Nowick's group developed amyloid β-sheet mimics (ABSMs) to inhibit the aggregation of various amyloid proteins by introduction of various recognition segments in ABSMs.[170] ABSM is a 54-membered ring composed by one upper strand (a heptapeptide from amyloid protein as recognition region), one lower strand (Hao unit with flanked two dipeptides) and two δ-linked ornithine turns. One ABSM (**Figure 1.16**) possessing KLVFFAE as recognition segment in the upper strand showed the ability to bind β-structured oligomers and block Aβ nucleation, ultimately delaying Aβ aggregation. Our laboratory used diketopiperazine scaffold as a β-turn inducer to design several acyclic β-hairpin peptidomimetics based on the sequences of the C-terminus or CHC of Aβ (**Figure 1.16**).[171] The inhibitors with KLVF as recognition segment adopted stable β-hairpin mimic conformations and showed the activity against Aβ aggregation. Our laboratory also used another β-turn inducer, piperidine–pyrrolidine, to design several acyclic β-hairpin peptidomimetics capable of inhibiting Aβ aggregation (**Figure 1.16**).[172] In this study, all the acyclic β-hairpin peptidomimetics possessed

the same C-terminal arm, KLVFF-NH_2, as one of self-recognition elements but different N-terminal arms (second self-recognition element) which could be the sequences $G_{33}LMVG_{37}$ of $A\beta_{42}$ or $G_{38}VVIE_{42}$ (a mimic of the $G_{38}VVIA_{42}$ of $A\beta_{42}$). G1b and G2b, both without acetyl group at the N-terminus, showed very strong activities against Aβ aggregation and protective effect against $A\beta_{42}$ cellular toxicity.

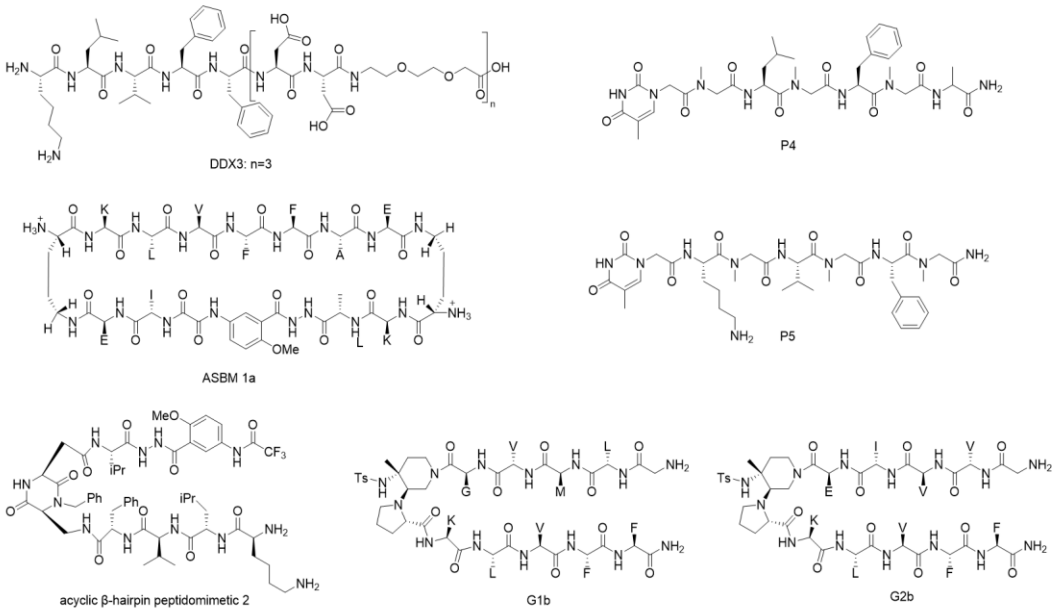

Figure 1.16: The structures of peptidic Aβ aggregation inhibitors with non peptidic motifs

Peptides not derived from Aβ sequence

This class of peptides can come from the screening of combinatorial libraries or the binding epitopes of proteins capable of interacting with Aβ.[173] Here we focus on the peptides derived from the epitopes of proteins capable of interacting with Aβ.

It was demonstrated that αA-crystallin, a small heat-shock protein, has chaperone-like activities and can capture aggregation-prone folding intermediates.[174] Santhoshkumar and Sharma reported that αA-crystallin showed potential to inhibit Aβ aggregation. Based on the chaperone region (melittin-binding sites) of αA-crystallin, they designed a peptide DFVIFLDVKHFSPEDLTVK, which showed the similar activity of αA-crystallin against Aβ

aggregation.[175]

It has been reported that type II diabetes (T2D) patients have a higher risk to develop AD than the persons without T2D and there is a cross-interaction between islet amyloid polypeptide (IAPP) and Aβ.[176,177] Based on the sequence of IAPP, Kapurniotu's group designed and synthesized a IAPP mimic in which a full length of IAPP was methylated on the amides of Gly24 and Ile26. The mimic was designated IAPP-GI. IAPP-GI could inhibit $A\beta_{40}$ fibrillogenesis and $A\beta_{40}$ toxicity by binding prefibrillar nontoxic $A\beta_{40}$ species to block their further aggregation into cytotoxic oligomers and fibrils. They further identified the hot segments of IAPP responsible for the interaction with Aβ, including IAPP(8-18) and IAPP(22-28).[178] Based on these two segments, peptides IAPP(8-18), IAPP(22-28)-GI and IAPP(8-28)-GI were synthesized but they did not have the activity as IAPP-GI has, indicating that the enough length of mimics is required for the activity.[179] Through introduction of various linkers to link IAPP(8-18) and IAPP(22-28)-GI, they got a series of IAPP cross-amyloid interaction surface mimics (ISMs) with structural preorganization. In this study, they found that the structure and activity of ISMs was determined by the nature of the linker and they got several nanomolar inhibitors of $A\beta_{40}$ cytotoxic self-assembly, such as R3-GI which has three arginine as a linker showed less β-sheet/β-turn contents and the higher activity to inhibit Aβ aggregation (**Figure 1.17**).[180] The further modification on R3-GI provided macrocyclic peptides with high proteolytic stability in human plasma and BBB crossing ability.[181] Peptides derived from TTR were also investigated to inhibit Aβ aggregation. Schwarzman and coworkers reported two sequences of TTR, TTR (37-43) and TTR (30-60) are able to inhibit Aβ deposition.[182] Murphy's lab did a lot of works on the design of peptides based on TTR capable of inhibiting Aβ aggregation. These works will be mentioned in detail in next section 1.4.

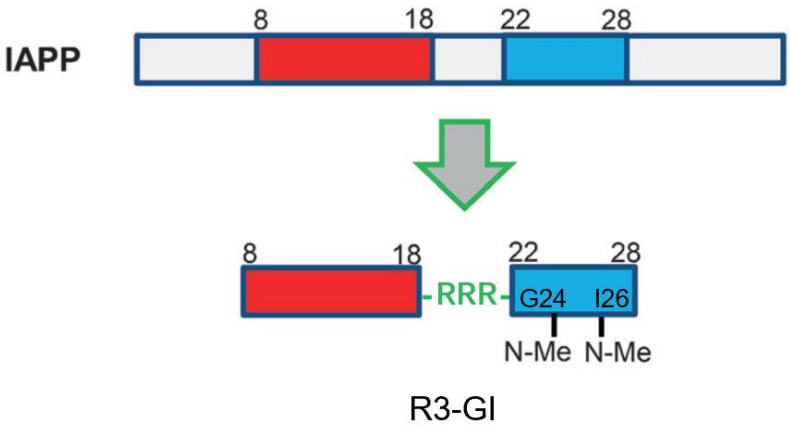

Figure 1.17: The design of the peptide R3-GI[180]

1.3.5 Foldamers inhibiting Aβ aggregation

Foldamers is one class of peptidomimetics and the detailed introduction of foldamers could be found in followed section 1.51. Foldamers normally have better proteolytic stability and bioavailability. The application of foldamers to mimic the secondary structures of Aβ or its chaperone proteins, thereby interfering Aβ aggregation, is of interest but there are only a few examples about it.

Some β-hairpin foldamers inhibiting Aβ aggregation have been reported by our group as we mentioned in the last section, including β-hairpin mimics containing a piperidine–pyrrolidine scaffold[172] and β-hairpin mimics containing a diketopiperazine scaffold[171] (**Figure 1.16**). Some helical foldamers were also reported to inhibit Aβ aggregation, including oligoquinoline-based foldamers[183], oligopyridylamide-based foldamers[184], β-peptide foldamers[185] and the foldamers composed by 4-amino(methyl)-1,3-thiazole-5-carboxylic acids (ATC) explored in our laboratory[186].

1.4 The Aβ chaperone: transthyretin (TTR)

Human transthyretin (TTR) is a 55kDa homotetramer which is mainly synthesized in the liver and choroid plexus and distributed in plasma and cerebrospinal fluid. Each subunit contains 127 amino acids which consists of two four-stranded β-sheets as well as a short α-helix and loop (**Figure**

1.18).[187] TTR is capable of carrying thyroxine (T4) through the hydrophobic channel at the center of TTR.[188] Moreover, it is also responsible for transportation of retinol through binding retinol-binding protein (RBP).[189] Self-assembly of wild type (wt) TTR in elderly individuals can form amyloid fibrils resulting in senile systemic amyloidosis (SSA).[38] Some TTR mutations can also lead familial amyloid polyneuropathy (FAP) and familial amyloid cardiomyopathy (FAC).[190–192] TTR amyloidosis is mainly attributed to the aggregation of monomeric TTR and dissociation of tetrameric TTR into monomers is considered to be the rate-limiting step in amyloid aggregation of TTR .[193,194]

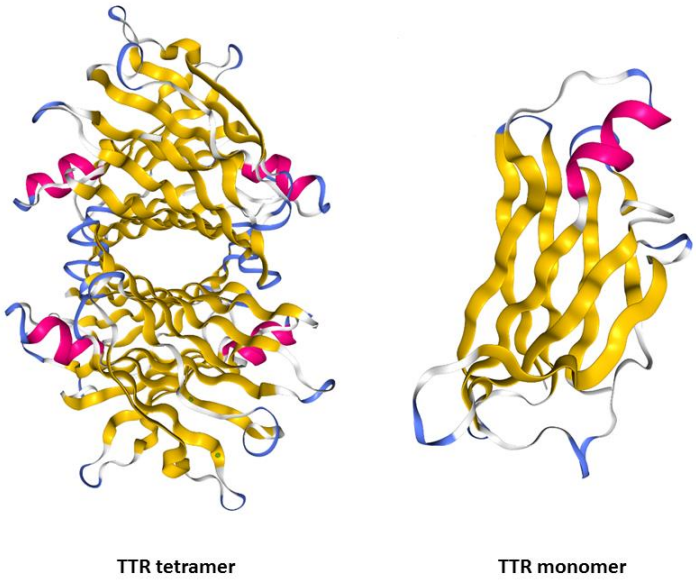

Figure 1.18: The structure of TTR (PDB: 5AKT): β-sheet structure is shown in yellow and α-helix is shown in purple

1.4.1 The associations between TTR and Aβ

In addition to the amyloidogensis involved, TTR shows a neuroprotection activity against Aβ toxicity. The correlation, the lower TTR level in CSF the more demented patient is, was reported in 1988 through the analysis of TTR levels in 31 patients.[195] In transgenic *caenorhabditis elegans* model, co-expression of TTR and Aβ prevented amyloid deposits, suggesting the positive functional

interaction between TTR and Aβ.[196] After that, a series of *in vivo* studies revealed the relationship between TTR and Aβ. Stein and Johnson suggested that the lack of neuronal cell loss in APPsw mice (high Aβ levels in the brain) may be attributed to the up-regulation of the biosynthesis of TTR.[197,198] Choi and coworkers found that the deletion of TTR gene can accelerate Aβ deposition in APPswe/PS1ΔE9 transgenic mice.[199] Buxbaum and coworkers found that the cognitive deficit associated with human AD is ameliorated in APP23 transgenic mice with the overexpression of wt human TTR transgene. Moreover, silencing the endogenous TTR gene in APP23 transgenic mice can increase the deposition of Aβ.[64] Many *in vitro* studies also revealed evidences and mechanisms of the interaction between TTR and Aβ. Schwarzman indicated that TTR is the major Aβ sequestering protein in CSF, which can prevent the formation of Aβ fibrils.[200] Buxbaum suggested that the protective effect of TTR is attributed to its capacity to bind toxic Aβ aggregates.[64] Murphy's group found that the incubation of Aβ with TTR reduces the size and length of the aggregates but not affects the linear morphology of the aggregates, suggesting that TTR can suppress the growth of the aggregates but not the initial assembly. Combining with the analysis of Aβ aggregation kinetics, they proposed that TTR prefers to bind to Aβ aggregates rather than monomeric Aβ to inhibit the growth of aggregates.[201] Moreover, they found that freshly prepared Aβ binds to a larger extent to TTR monomer (M-TTR) than to TTR tetramer, and pre-aggregated Aβ binds more to M-TTR than to freshly prepared Aβ.[202] In the further study, they proposed a supposed mechanism to explain the action TTR on Aβ: toxic Aβ oligomer binds to TTR tetramer and triggers the destabilization of TTR tetramer into TTR monomer, and then TTR monomer further captures toxic Aβ oligomer to inhibit the growth of Aβ aggregates.[203] Cardoso's group found the inverse correlation between the Aβ affinity of TTR and amyloidogenic potential of TTR by analyzing the Aβ affinity of different TTR variants.[204] They also found the improved interaction between Aβ and TTR when treating with some TTR stabilizers.[205,206] Moreover, they suggested that TTR participates in Aβ clearance by transporting Aβ from brain to liver as well as direct degradation of Aβ[207–209], but these functions were absent when TTR tetramer is destabilized. In addition, it was reported that Cu^{2+} can modulate the TTR conformation and stabilize TTR to enhance Aβ scavenging-activity.[210] Li and coworkers found that M-TTR prefers to bind to Aβ oligomer rather than Aβ monomer. TTR (TTR tetramer or M-TTR) inhibited the formation of Aβ fibrils through decreasing Aβ oligomer formation

and suppressing the conversion of large oligomers from small oligomers. Due to higher concentration of TTR tetramer, they suggested that the inhibition of Aβ fibrils formation is mainly mediated by TTR tetramer binding to Aβ monomer and oligomer, partially mediated by the TTR monomer binding to Aβ oligomer.[211] However, TTR monomer also plays a critical role in blocking the formation of Aβ deposits. Garai and coworkers found that monomeric TTR does not interact with monomeric Aβ but co-assembles with soluble Aβ aggregates to form amorphous precipitates, based on fluorescence correlation spectroscopy measurements.[212] More recently, the dissociation of TTR tetramer into monomers was reported necessary to inhibit the cellular toxicity of Aβ oligomers by analyzing the protection of nine TTR variants with different aggregation propensities.[213]

Although different groups and different methods gave some contradictory results, we still can make some conclusion. TTR tetramer and TTR monomer both inhibit the formation of Aβ fibrils but in different manners. It seems that TTR tetramer is more prone to sequester Aβ monomer than TTR monomer, whereas TTR monomer prefers to bind soluble aggregates of Aβ to form amorphous co-aggregates. TTR tetramer may play a main role in inhibiting the formation of Aβ fibrils due to higher concentration of TTR tetramer (0.25 - 0.5 μM) than TTR monomer (~25 nM) in CSF. In addition, TTR tetramer also exerts its neuron protective function through transportation of Aβ from brain to liver as well as direct degradation of Aβ.

1.4.2 Aβ binding sites of TTR

Many studies have confirmed that TTR can inhibit the aggregation of Aβ but there is still no detailed information on the binding mode between Aβ and TTR. The absence of co-crystal structure of TTR with Aβ results in that the binding site of TTR to Aβ is difficult to define. Even so, some progresses have been made by the utilization of some approaches like nuclear magnetic resonance (NMR) spectroscopy, cross-linking and tandem mass spectrometry, SPOT peptide array, alanine scanning mutagenesis and molecular modeling to predict the Aβ bind sites on TTR. Murphy's group employed cross-linking and tandem mass spectrometry technique to search the regions of TTR which interact with Aβ.[202] They used homobifunctional *N*-hydroxysuccinimide ester as cross-linked reagent to connect the lysine of TTR to the lysine of Aβ. The cross-linked product was isolated by gel electrophoresis. The isolated product was digested and analyzed by mass spectrometry. They

found three amino acids on TTR were able to cross-link with Aβ, including Lys9, Lys15 and Lys76. Lys 9 and Lys 15 were near or on the strand A (**Figure 1.19**), indicating that the strand A may interact with Aβ. As to Lys 76, it was near the EF-helix on TTR, suggesting that the EF-helix may take part in the interaction (**Figure 1.19**). After that, they employed SPOT technology to synthesize a series of peptides derived from TTR and tested the affinity of peptides to Aβ.[214] Two sequences showed interaction with Aβ. One was TIAALLSPYSYS, residues 106–117 of TTR, which was close to the strand G (**Figure 1.19**). The strand G was adjacent to the strand A and had no lysine, indicating that Aβ interacts with the strand G and lead itself cross-link with the lysine of the strand A. Another sequence was TTEEEFVEGIYKVEIDTKSYWKALG, residues 59–83 of TTR, which included the strand E as well as the EF-helix and loop. This result was consistent with the result from cross-linking and tandem mass spectrometry, which confirmed again the significance of the EF-helix in the interaction. They further mutated nine amino acids of TTR to alanine respectively and tested the binding of these TTR mutants to Aβ for confirming the results from cross-linking and tandem mass spectrometry and SPOT analysis.[214] These mutations included one residue on the strand A (L17A), two residues on the strand G (T106A and L110A), two residues on the strand E (I68A and I73A) and four residues K76A, L82A, I84A and S85A on the EF-helix/loop. The results showed L17A or S85A increased the binding of TTR to Aβ, whereas L82A or L110A reduced the binding of TTR to Aβ (**Figure 1.19**). All these four mutations showed no significant change on native fold of TTR except that S85A leaded TTR tetramer to be less stable than that of wt TTR. This result indicated S85A increased the binding of TTR to Aβ by influencing the stability of TTR tetramer. They presumed that L17A leads Aβ to be accessible to possible binding site L110 because of the decrease of steric hindrance from leucine to alanine, whereas L82A and L110A are likely to involve in hydrophobic interaction with Aβ.

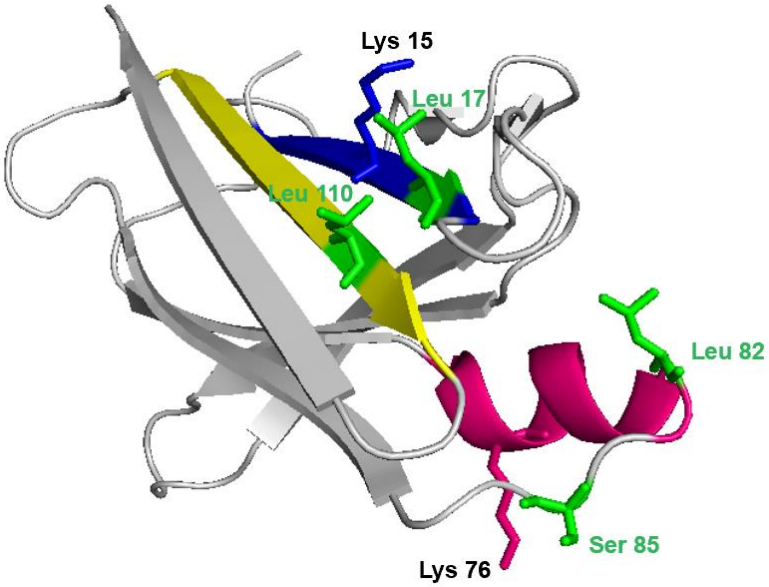

Figure 1.19: TTR monomer (PDB: 1DVQ), strand A (blue), strand G (yellow), EF-helix (hotpink). Four residues involved in the interaction with Aβ (green)

Li and coworkers recorded the two-dimensional ^{1}H-^{15}N HSQC NMR spectra of TTR in the absence and presence of Aβ and analyzed the different chemistry shifts.[211] They found the residues in or around the thyroxine (T4) binding site, the A-B loop and the EF-helix show great change in chemical shift during binding to Aβ, indicating that these three regions participate to the interaction with Aβ. The T4 binding site was considered a direct binding site to connect with Aβ, which is consistent with the report that residues L17, L110 and L82 are involved in binding with Aβ[214]. They presumed that the A-B loop and the EF-helix of TTR is not a direct binding site to interact with Aβ but acts as a conformational modulator to disturb the TTR structure.

Gimeno and coworkers also tried to search the Aβ binding site of TTR by saturation transfer difference (STD) NMR combining with molecular modeling.[215] They supposed that Aβ binds at the surface of TTR and the core region of the binding site is the RBP binding pocket, which involve the EF-helix of TTR. This was in agreement with the reports from Murphy's group indicating that the EF-helix is involved in the interaction with Aβ.[214]

1.4.3 Aβ aggregation inhibitors designed based on the Aβ–TTR interaction

Although the binding site of TTR to Aβ remains unclear, some peptides have been designed

based on the existing studies. As mentioned above, residues 106–117 of TTR participate in the interaction with Aβ.[214] Murphy's group employed SPOT technology to synthesize and test a series of peptides which are designed based on the sequence TIAALLSPYSYS.[216] After the analysis of the affinity of these peptides, they concluded that hydrophobic residues in the N-terminal domain (TIAALL) and aromatic groups in the C-terminal domain (SPYSYS) are two important sequences for the binding to Aβ. On the basis of these two sequences, they further designed and synthesized some new peptides. Among them, peptide G16 (**Figure 1.20**) was found to be able to specifically interact with Aβ to affect Aβ aggregation and inhibit Aβ toxicity. Since the EF-helix of TTR is also a potential bind site to Aβ, a peptide called Efh derived from the sequence of TTR on the EF-helix/loop (D_{74}TKSYWKALG_{83}) was synthesized and tested. However, this peptide did not increase the size of Aβ after cross-linking with Aβ, indicating no significant interaction with Aβ. In a protease protection assay, the incubation of Efh with Aβ could not prevent the degradation of Aβ, also suggesting the Efh has no strong interaction with Aβ to form Efh/Aβ complexes, thereby protecting Aβ from degradation. The lack of α-helical structure of Efh was proposed as a possible reason why Efh showed no strong interaction with Aβ.

Given that peptide G16 showed less effect of neuroprotection than TTR, Murphy's group tried to search more potent peptides based on G16. They thought that the lack of β-strand structure is the possible reason for the weak neuron protective effect of G16. Thus, they tried to transplant the G16 sequence onto a β-hairpin template. Two cyclic peptides, CG2 and CG3 (**Figure 1.20**), were designed to mimic the β-strand structure of binding site of TTR. CG3 showed stronger ability than G16 to suppress Aβ aggregation into fibrils as well as neuroprotection against Aβ toxicity *in vitro*.[217] However, CG3 was still not as effective as native TTR.

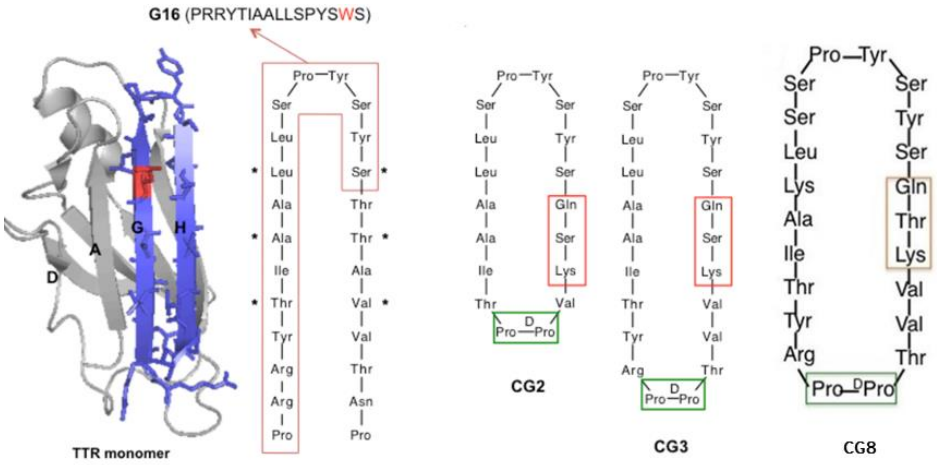

Figure 1.20: The peptides designed based on the binding site of TTR to Aβ[217,218]

In order to further maintain the antiparallel β-strand structure of CG3 and reduce its tendency to self-associate, the algorithm TANGO was employed to modify CG3 to block the tendency of self-association as well as maintain the β-strand structure. In the end, they found a new cyclic peptide CG8 which shows a more potent inhibition of Aβ fibrils formation (**Figure 1.20**). CG8 was likely to coalesce into Aβ aggregates to change the morphology of aggregates and inhibit further formation of Aβ fibrils. Meanwhile, CG8 was more stable against protease (pepsin) than CG3 and m-TTR.[218,219]

1.5 Peptidomimetics

As we showed in section 1.34, many peptides were designed to inhibit Aβ aggregation. The moderate size of peptides makes peptides interfere PPIs with high activity, enough selectivity and low immunogenicity. However, the poor metabolic stability and membrane permeability of peptides also prevent their development in medicinal chemistry.

Peptidomimetics are peptide analogs capable of mimicking the bioactive conformation of parent peptides. In addition to maintain the active conformation of peptides, peptidomimetics can also overcome the deficiencies of peptides in proteolytic stability and membrane permeability. On the basis of the degree of their similarity to the parent peptides, Grossmann et al. divided them into four classes (**Figure 1.21**).[220] Class A is most similar to its parent peptides and only presents a few modifications on the side chains or the backbone. This class of peptidomimetics retains substantial

peptide character and the backbones fold into active conformation of parent peptides, which are capable of orienting the side chains in the right direction to interact with targets. Class B still shows peptide character but less than class A. The major difference between class B and class A is the substantial alterations on the backbone, which could arise from the replacement of natural amino acids by non-natural amino acids in sequence. Peptidic foldamers are the major component of class B peptidomimetics. Class C shows no peptide character on the backbone but the key side chain functionalities on the backbone are aligned with the side chains of its parent peptides. The molecules in class D no longer need the same arrangement pattern of side chains as their parent peptides to maintain the interaction with targets. They just mimic the mode of action of peptides. This class of peptidomimetics could be derived from further modification on the peptidomimetics in class C or from the screening of compound libraries or virtual libraries.

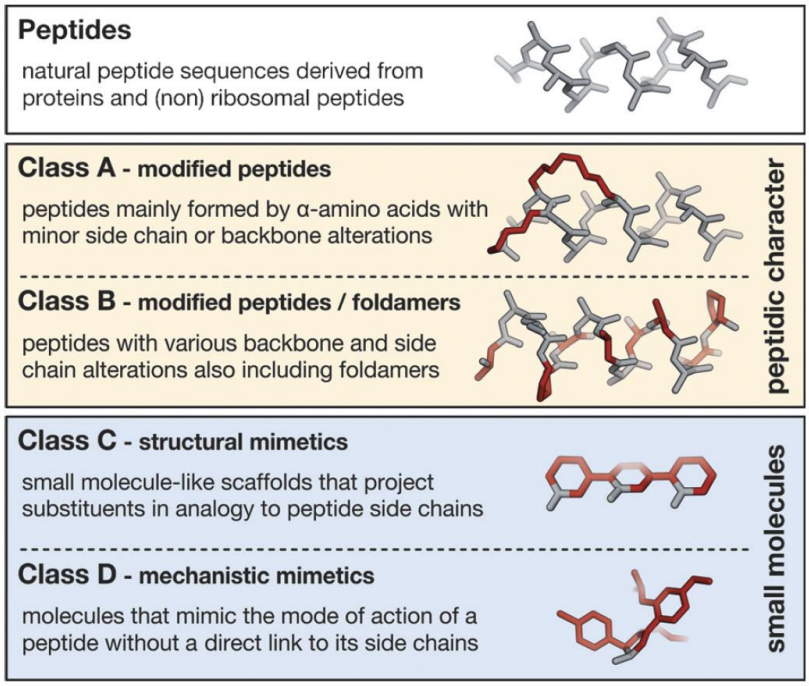

Figure 1.21: Classification of peptidomimetics[220]

1.5.1 Peptidic foldamers

The concept of foldamer was first proposed by Gellman.[221] Foldamer is a type of oligomer capable of displaying well-defined three-dimensional conformations and these conformations arise

from the inherent conformational preferences of the composite monomers rather than the constraint of covalent bond (cyclic peptide or stapled peptide). Therefore, the conformations of foldamers are induced and stabilized by a collective of noncovalent interaction. H-bonding interactions are considered as the main noncovalent interactions contributing to stabilize the well-defined conformations. Moreover, electrostatic interactions, pi stacking, van der Waals forces and solvation also play crucial roles in self-organization of foldamers.

Foldamers could be composed of only one type of monomer unit (homogeneous foldamers) or more than one type of monomer unit (heterogeneous foldamers). In addition, foldamers also could be classified based on backbone properties as peptidic and polyaromatic foldamers. Peptidic foldamers attract more attention from pharmaceutical industry than that of polyaromatic foldamers because that the high similarity of peptidic foldamers with natural peptides endows them with better drug-like nature.[222] There are numerous of peptidic foldamers has been reported that can fold into specific conformation to mimic the secondary structures of protein, such as α-helix, β-strand and β-hairpin. Here we will focus on peptidic foldamers mimicking helical structures because my PhD project is involved in the synthesis of peptidic foldamers capable of mimicking helical structures. It should be noted that although there are many helical peptidic foldamers, the use of these foldamers to interfere with PPIs is still in its infancy.

1.5.2 Peptidic foldamers mimicking helical structures

In natural proteins, α-helix is a common secondary structure and it is often located at the interfaces of PPIs. It has been reported that around 62% interfaces of PPIs possess α-helical structure, which means α-helix plays a key role in PPIs.[223] In addition, 3_{10}-helix and polyproline type II helix are also involved in part of PPIs. Thus, the design of foldamers which are able to mimic helical structures, thereby interfering corresponding aberrant PPIs, is a promising strategy to treat a lot of diseases associated with aberrant PPIs. Here several peptidic foldamers capable of folding into helical structures are concluded.

β-Peptides

β-Amino acids are the most extensively investigated monomers for the design and synthesis of

peptidic foldamers because of the ease of synthesis and the closest relatives of the natural α-amino acids. As compared with α-amino acids, additional methylene inserted between the amino group and the carboxylate group makes β-amino acids possess two positions for side chain arrangement. In accordance with the different substitution pattern on β-amino acids, they can be classified into β^2, β^3 and $\beta^{2,3}$ (**Figure 1.22**).

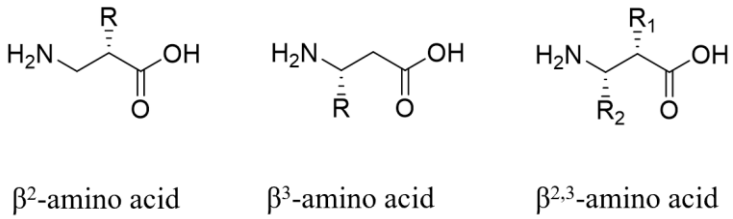

Figure 1.22: β-Amino acids

There are many literature demonstrating that β-peptides are able to fold into helical structures. For example, Seebach reported that a β-peptide composed by β^3-amino acids displays a left-handed helix in methanol, whereas a β-peptide composed by β^2-amino acids shows the mirror-image conformation: right-handed helix.[224–226] This finding suggested that the position of the side chains on β-amino acids plays an important role in the secondary structure control. Almost at the same time, Gellman's group reported that a hexamer composed by trans-2-aminocyclohexanecarboxylic acid (trans-ACHC) is able to self-organize into 14-helical structure which was corroborated by NMR and crystal structure, while a hexamer containing β-alanine showed fast NH/ND exchange behavior means no intramolecular H-bond.[227] This result indicated cyclic β-amino acids have more rigid conformation which can constrain the secondary structure of the foldamers of which they are composed. Afterward, several cyclic β-amino acids were all reported to construct β-peptide foldamers with helical structure, including ACBC, ACPC, ACHEC, ABHEC and ABHC (**Figure 1.23**).

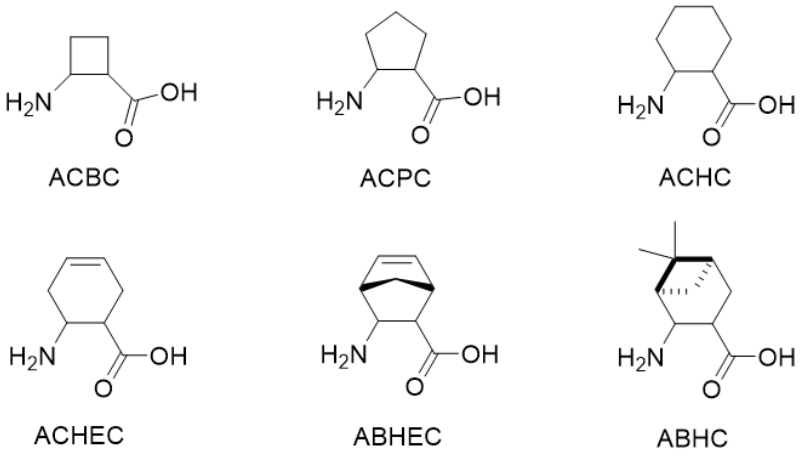

Figure 1.23: The structures of several cyclic β-amino acids

The ring size and stereochemistry of cyclic β-amino acids show great impacts on the torsional angle of backbone thereby affecting the secondary structure of the foldamers. For example, foldamers composed from trans-ACPC exhibit 12-helical structure (**Figure 1.24A**) by the analysis of the crystal structures of the hexamer and octamer[228] while the foldamers composed by trans-ACHC prefer to fold into 14-helical structure in NMR analysis.[227] When foldamers are constituted of *cis*-ACHC, 10/12-helix (**Figure 1.24B**) are observed in NMR analysis combined with theoretical calculation.[229]

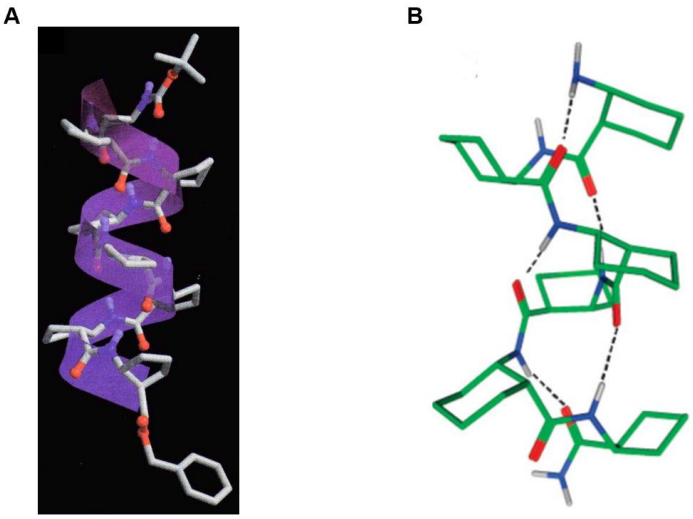

Figure 1.24: A) 12-Helix of the β-peptide constructed by trans-ACPC (from crystal structure)[228]; B) 10/12-Helix of the alternating cis-ACHC hexamer (from theoretical calculation)[229]

One example about β-peptide foldamers interfering PPIs involves β^3-peptides.[230] Based on a β^3-peptide showing 14-helix, three key residues on p53 involved in the interaction with MDM2 were introduced to the β^3-peptide, thereby mimicking the interaction with MDM2. The designed peptide showed good binding affinity to MDM2.

γ-Peptides

γ-Amino acid is another homologue of α-amino acid which has two extra methylene groups between the amino group and carboxylate group. The studies about the foldamers composed from γ-amino acids are not so many as β-peptides because of the difficulty of synthesis. The conformations of γ-peptides are controlled by several factors including substituent group, backbone substitution pattern and stereochemistry. The favourite structures of γ-amino acid oligomers predicted by theoretical calculation are 9-helical structure and 14-helical structure.[231] Hanessian reported several foldamers composed of γ^4-amino acids showing 14-helices in organic solvent (**Figure 1.25A**).[232] The introduction of a methyl group at the γ^2 position of γ^4-amino acids in *S*-configuration further stabilizes 14-helix whereas in *R*-configuration it destroys 14-helix. γ-Peptides constituted of gabapentin, a cyclic β, β-disubstituted γ^3-amino acid, are able to self-organize into 9-helices, which was confirmed by crystal structure (**Figure 1.25B**).[233] 9-Helical structure was also found in γ-peptides composed alternately by C-linked carbo-γ^4 -amino acids (γ-Caas) and γ-aminobutyric acids (GABAs).[234]

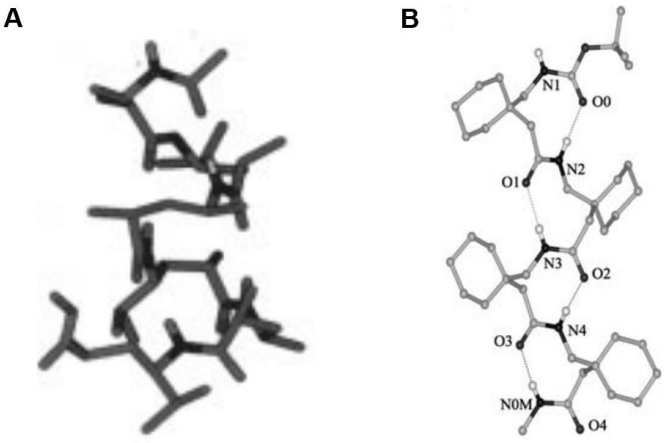

Figure 1.25: A) 14-Helix of γ-peptide[232]; B) 9-Helix of γ-peptide[233]

Hybrid peptides (αβ, αγ, βγ and αβγ)

The different combinations of α-amino acids, β-amino acids and γ-amino acids further lead the chemical diversity of foldamers. The combination of α-amino acids and β-amino acids were first reported to involve in hybrid peptidic foldamers. The early studies about αβ hybrid peptidic foldamers utilized the β-amino acids with cyclic side chains to promote heterogeneous oligomers self-organize into helical structure.[235,236] Subsequent works found that β-amino acids with acyclic side chains are usually harmful for helix-forming propensity.[237] Moreover, a number of researches indicated that the patterns, like ααβ, αββ or βαα in sequences also are capable of resulting in the helical structures of oligomers.[238,239] αγ- and βγ-hybrid peptides also show propensities to form helical structures based on the theoretical calculations.[240] Sharma synthesized novel αγ-hybrid peptides and βγ-hybrid peptides which are able to display 12/10- and 11/13-mixed helical structures, respectively.[241] βγ-Hybrid peptides were proposed to perfectly mimic α-helix in theory. Grison reported that an oligomer consisting of *trans*-ACBC and γ^4-amino acids in alternation can form 13-helix which has a nice topological superposition with α-helix.[242] αβγ-Hybrid peptides were also reported by Grison to show 12/13-mixed helices and these peptides were used to mimic α-helix of p53 to interfere with the PPI between p53 and hDM2.[243]

Peptoids

α-Peptoids and β-peptoids are special peptidomimetics as surrogates of α-peptides and β-peptides. The ease of synthesis of peptoids promotes their extensive studies in foldamers. In peptoids, the side chains on α-carbons of peptides are migrated to amides, thereby destructing the role of the amides as H-bond donors. Moreover, this migration leads tertiary amide bonds of peptoid from secondary amide bonds of peptide, which allows both *cis*- and *trans*-amide bonds in peptoids (amide bonds of residues in natural peptides prefer to be in *trans*-conformation except proline). Both these features make the backbones of peptoids more flexible than that of peptides. Therefore, the secondary structures of peptoids are mainly controlled by the side chains on the nitrogen.

Normally, bulky chiral side chains were used in peptoids to force the backbone in *cis*-amide helical structure. The influence of different *N*-alkyl side chain on this *cis*−trans equilibrium in α-

peptoids has been studied.[244,245] *R*-configuration of side chains makes left-handed helices whereas *S*-configuration of side chains gives right-handed helices. *S*-1-phenylethyl (spe) is a first type of bulky chiral side chains found to induce helical structures of α-peptoids.[246,247] Though introducing different substituent groups at the para position of phenyl of spe to increase chemical shift dispersion, ^{1}H and ^{13}C of the corresponding α-peptoids can be well assigned, thereby making the possibility to do the conformational analysis of the α-peptoids by NMR. The result showed the major conformation of the α-peptoids is right-handed helix.[247] Other types of bulky chiral side chain, such as *S*-1-naphthylethyl (s1npe) and *S*-1-cyclohexylethyl (sch), are also popular in the design of helical α-peptoids (**Figure 1.26A**).[248,249] Due to the similarity between α-helix and right-handed helix induced by α-peptoids, α-peptoids are promising α-helix mimics to inhibit PPIs, such as hDM2–p53 PPI.[250]

The effects of side chain on this *cis*−*trans* equilibrium in β-peptoids are similar to that of α-peptoids. Side chain s1npe shows best ability to induce the *cis*-conformation of amide bond in β-peptoids.[251] Several homomeric β-peptoid hexamers which have s1npe as side chains but different N-terminus were crystallized successfully and the crystal structures showed right-handed helical conformations with a helical pitch of 9.6–9.8 Å between turns (**Figure 1.26B**).[252]

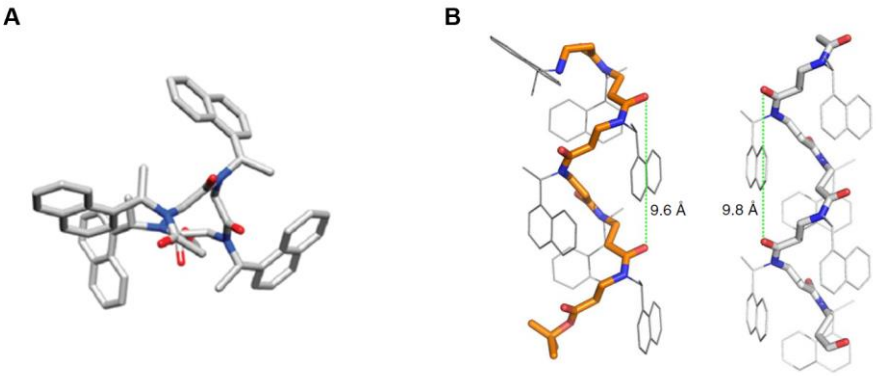

Figure 1.26: A) Polyproline type I helix generated from the α-peptoid which possess s1npe as side chains (X-ray crystal structure viewed parallel to the helical axis)[248]; B) X-ray crystal structure of homomeric β-peptoid hexamers which possess s1npe as side chains (orange one is a hexamer with free amine at the N-terminus, white one is a hexamer with acetyl group at the N-terminus)[252]

Oligoureas

Aliphatic *N*, *N'*-linked oligoureas were developed by Guichard's group.[253–255] This type of foldamers is consisted of γ-amino acid analogue in which α-carbon is replaced by nitrogen (**Figure 1.27A**). The replacement gives a urea structure as an amide bond surrogate in foldamers and the possibility to form three-centered H-bonding (**Figure 1.27B**). Homogeneous aliphatic oligoureas are able to fold into 2.5 helices (**Figure 1.27C**).[253,255] The propensity to fold into helical structure can be propagated from oligourea to α-peptide through the insertion of oligourea fragments in α-peptides. In these oligourea/peptide chimeras, the oligourea segments display 2.5- helical structure whereas the peptide segments show α- or 3_{10}-helical structures (**Figure 1.27D**).[256] These oligourea/peptide chimeras were also applied to mimic the α-helix of p53, interfering the PPI between MDM2 and p53.[257]

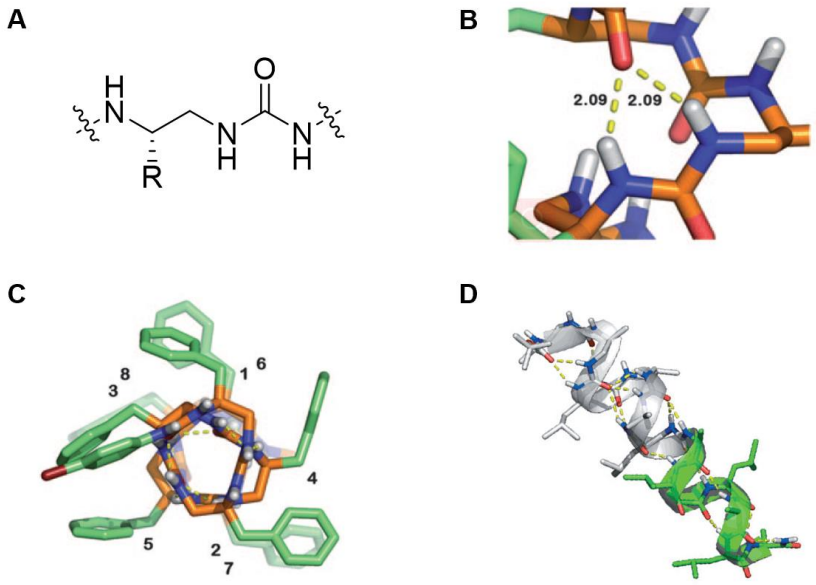

Figure 1.27: A) The structure of oligourea monomer; B) Three-centered H-bonding formed by oligourea[255]; C) Top view of homogeneous aliphatic oligoureas (2.5-helix)[255]; D) The helical structure formed in oligourea/peptide chimeras (oligourea segment in grey, peptide segment in green)[256]

Aminoxy acid oligomers

Replacement of carbon atom adjacent to nitrogen atom with oxygen atom in amino acid is a good way to change torsional characteristics of peptide backbone because of the extra hydrogen

bond formed on heteroatom or the repulsion between lone pairs of the two adjacent heteroatoms. Based on this idea, α-aminoxy acid, β-aminoxy acid and γ-aminoxy acid were designed and synthesized as analogues of β-amino acid, γ-amino acid and δ-amino acid, respectively (**Figure 1.28**). Comparing to amino acids, α-aminoxy acid, β-aminoxy and acid γ-aminoxy acid are preferential to form α N–O turn, β N–O turn and γ N–O turn (**Figure 1.28**), respectively.[258]

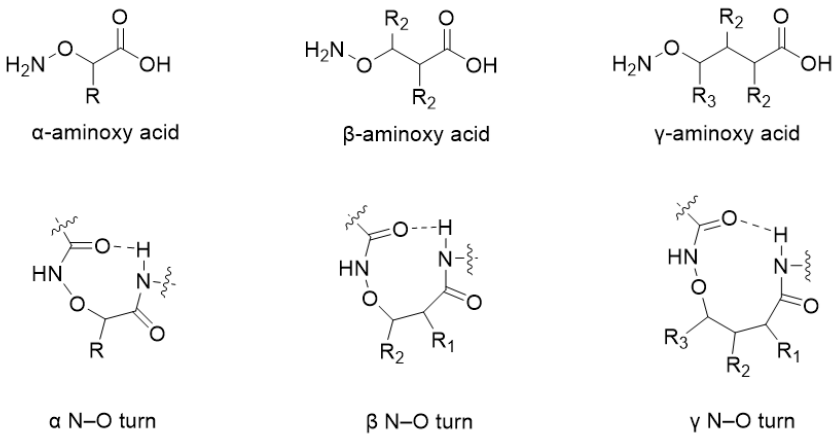

Figure 1.28: The structures of α-aminoxy acid, β-aminoxy acid and γ-aminoxy acid and the turns they form

Homogenous oligomers composed of α-aminoxy acid was reported to have propensity to induce consecutive α N–O turns, which ultimately construct helices called 1.8_8 helices (**Figure 1.29A**). Based on NMR, FT-IR and CD spectra and theoretical calculations, heterogenous oligomers composed of alternating α-aminoxy acids and alanine were proposed to form 7/8 helices which constructed by alternating a N–O turns and γ-turns (**Figure 1.29B**). So far there is no report about aminoxy acid foldamers interfering with PPIs.

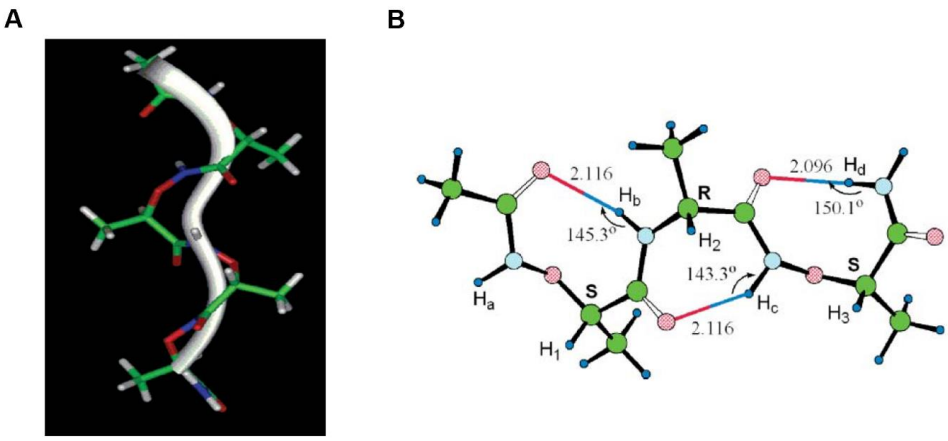

Figure 1.29: A) 1.8_8 Helix generated by homogenous α-aminoxy acid oligomer; B) Calculated most-stable conformation (7/8 helix) of one heterogenous oligomer composed of alternating α-aminoxy acids and alanines[258]

Azapeptides

Azapeptides are one type of pepdtidomimetics containing one or more of the aza-residues in sequences. Given the replacement of α-carbon atom by nitrogen atom, aza-residues do not show chirality that is present in natural residues (**Figure 1.30A**). The α-nitrogen could have more than one structure, including pyramids (sp3 character) which are able to inverse alternatively, and planer (sp2 character) attributed to the conjugation effect between α-nitrogen and amide bond. Moreover, the repulsion of lone pairs between two adjacent nitrogen atoms gives rise to an inherently twisted geometry of hydrazine structure. Thus, twisted hydrazine and planar urea are viewed as two key structural elements which determine the constrained conformation of azapeptides.[259,260]

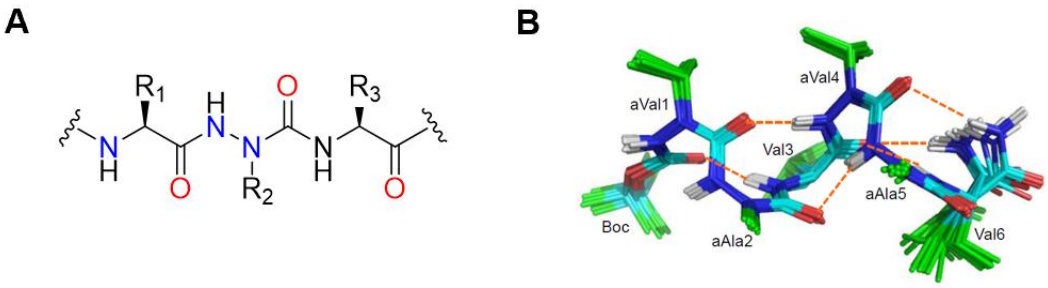

Figure 1.30: A) The structure of azapeptide; B) 3_{10}-Helix generated by azapeptide (Boc-azaVal-azaAla-Val-azaVal-azaAla-Val-NH_2)

The preferential dihedral angle values of aza-amino acid residue (ϕ, ψ) are close to (±90±30°, 0±30°) or (±90±30° or 180±30°), thereby endowing β-turn structure as preferential structure of azapeptides.[259,261–263] In addition to β-turn structure, aza-amino acids also have the potential to induce azapeptides in helical structures. Another ideal torsion angles (ϕ, ψ) of aza-amino acids fall in the region of polyproline type II helix, indicating the capacity to stabilize polyproline type II structure of peptides.[264] Triple helical collagen is a right-handed helix composed by three parallel, left-handed polyproline type II helices. The replacement of glycine by aza-glycine in triple helical collagen can improve the stability of the collagen. This stabilization is not only because of the extra hydrogen bond formed by the proton on α-nitrogen, but also because of the backbone preorganization from aza-glycine.[265,266] Recently, our lab found that the introduction of aza-amino acids, the isosteres of α-amino acid, in an aza/aza/α pattern, lead aza-peptides to mimic 3_{10}-helix (**Figure 1.30B**), but the specific structure is depended on side chains of the backbone.[267] To date, there is no report about using azapeptides as PPIs inhibitors.

1.5.3 Stapled peptides

Although stapled peptides do not completely fit with the definition of foldamers given by Gellman [221], they are used quite often to mimic α-helix. Stapled peptides could be obtained by the intra-cross-linking of side chains of peptides. Normally intra-cross-linking on side chains can induce peptides to fold into α-helical structure. Only small modifications on several side chains of peptides make stapled peptides ideal peptidomimetics to mimic α-helical structures, due to the same backbone composition (α-amino acid) and the ease of synthesis.

The anchoring residues, stapling chemistry and staple length of stapled peptides has been well reviewed.[268] For the stapled peptides composed of only natural amino acids, several combined pairs residues, including but not limited to Lys-Asp, Lys-Glu, Cys-Cys, Lys-Lys, are widely used to construct bridges. For example, coupling of the side chain of Lys with the carboxylic acid of Asp or Glu can form lactam bridge.[269] Introduction of nonnatural amino acids in peptides to do cross-linking is another strategy to obtain stapled peptides. The most common types of nonnatural amino acids used in stapled peptides are alkenyl nonnatural amino acids, which can be used in ruthenium-catalyzed ring-closing metathesis (RCM) (**Figure 1.31A**) or radical thiol-ene reaction to construct

bridges.[270,271] In addition, nonnatural amino acids possessing azide or alkyne functional group in side chains are also widely used as anchoring residues which are the substrates of "click" reaction (**Figure 1.31B**).

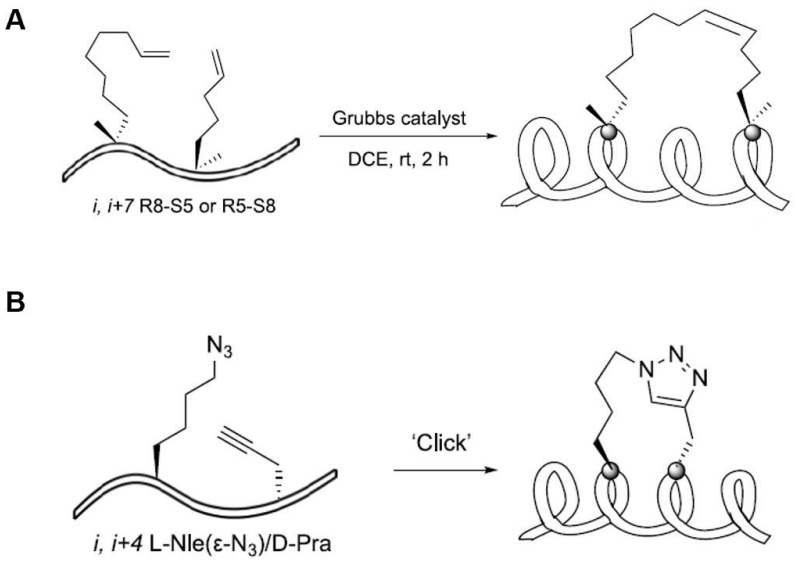

Figure 1.31: A) Stapled peptides constructed by RCM; B) Stapled peptides constructed by "click" reaction[268]

The relative position of two cross-linked residues is quite important for the formation of α-helical structure of peptides. Given the residues at position i, i+4, i+7, and i+11 are in the same face of α-helix, cross-linking of residues at i, i+4 or i, i+7 could give peptides with the strongest helicity.

One example about stapled peptides disrupting PPIs was reported by Amblard's group.[272] Based on the sequence of the C helix of CDK4, they designed and synthesized several i, i+4 stapled peptides by RCM to mimic α-helical structure of the C helix, thereby interfering with the interaction between CDK4 and cyclin D1.

1.6. Objective of the PhD thesis

As shown in the introduction, PPIs are linked to various diseases. Drug discovery based on PPIs is a promising strategy to treat these diseases and has been proven in some approvals of PPIs inhibitors. In amyloidosis, such as Alzheimer's disease (AD), PPIs involve self-amyloid interactions

and more recently discovered amyloid cross-interactions. Amyloid cross-interactions show different effects (positive or negative) on the corresponding amyloid aggregation. This phenomenon provides a new concept that designing short peptides based on the proteins showing chaperone-like activity to mimic the positive cross-interactions can afford efficient amyloid aggregation inhibitors. To date, only a few examples have been reported to bring enough proofs of concept to validate this strategy. TTR has been proposed as a chaperone-like protein of Aβ and it seems to play a positive role in the inhibition and the clearance of Aβ aggregates. Some peptides based on the strand G of TTR were reported to have activity on the inhibition of Aβ aggregation. However, the role of another binding site of Aβ on TTR, the EF-helix, has not yet been used to design peptide derivatives and evaluate them as small synthetic chaperons to inhibit Aβ aggregation.

In my PhD project, I was working on bringing different clues to answer four questions:

1. Do peptidic foldamers based on the small EF-helix of TTR capable of folding into helical structures have similar effects on Aβ as TRR shows? This proof of concept would bring additional data on this novel strategy aiming to mimic natural chaperon proteins to prevent amyloid proteins aggregation.
2. Although several peptidic foldamers have been reported to mimic helical structures and to inhibit PPIs, only few foldamers have been explored as inhibitors of amyloid protein aggregation. Do helical mimics could stabilize the helical conformation of amyloid proteins to prevent their further misfolding and aggregation in toxic and β-sheet rich structures?
3. Does the introduction of diaza-peptide units in a short TTR peptide sequence based on the EF-helix residues can mimic its helical structure and the orientation of its lateral chains? How many diaza-peptide units are necessary and in which position? Is this helical structure adopted in water?
4. Does this new class of peptidic foldamers containing diaza-peptide units are suitable to become drug candidates? Water solubility, proteolytic stability, membrane permeability in particular BBB permeability to reach the CNS? Can this new class of peptidic foldamers be used to target other PPIs?

In order to start answering to these questions, first we had to investigate the folding propensity

of short peptides containing diaza-peptide unit. Our laboratory has previously reported that aza-tripeptide containing one diaza-peptide unit could fold into repeat β-turns in organic solvent. Due to the necessity to use aqueous medium for evaluating biological activity and to consider an eventual *in vivo* activity, the further folding propensity of this type of diaza-tripeptides in water had to be investigated. This preliminary information will be presented in the chapter 2 of this manuscript. Based on the conformational results obtained on the diaza-tripeptides, we have then designed and synthesized several longer aza-nonapeptides containing diaza-peptide units based on the sequence of the EF-helix to study the effects of diaza-peptide units on the conformations. The activity of this new class of peptidic foldamers on Aβ aggregation have been then evaluated. Some preliminary drug-like properties have been tested on the most promising compound. All these data will be presented in the chapter 3 of this manuscript. Finally, in a last chapter 4, we will present how we demonstrated the possibility to exploit a side cyclization reaction observed during the synthesis of diaza-tripeptides (in the chapter 2) to synthesize 2,5-disubstituted aza-DKPs whose synthesis was not previously described. We developed the solid-phase synthesis of the trimers and tetramers of this aza-DKP monomer and their conformational analysis is in course.

References

(1) De Las Rivas, J.; de Luis, A. Interactome Data and Databases: Different Types of Protein Interaction. *Int. J. Genom.* **2004**, *5* (2), 173–178.

(2) Keskin, O.; Tuncbag, N.; Gursoy, A. Predicting Protein–Protein Interactions from the Molecular to the Proteome Level. *Chem. Rev.* **2016**, *116* (8), 4884–4909.

(3) Wang, Z.; Li, Z.; Ji, H. Direct Targeting of β-Catenin in the Wnt Signaling Pathway: Current Progress and Perspectives. *Med. Res. Rev.* **2021**, *41* (4), 2109–2129.

(4) Yoon, T.-Y.; Lee, H.-W. Shedding Light on Complexity of Protein–Protein Interactions in Cancer. *Curr. Opin. Chem. Biol.* **2019**, *53*, 75–81.

(5) Mattson, M. P.; Sherman, M. Perturbed Signal Transduction in Neurodegenerative Disorders Involving Aberrant Protein Aggregation. *Neuromol. Med.* **2003**, *4* (1), 109–131.

(6) Ryan, D.; Matthews, J. Protein–Protein Interactions in Human Disease. *Curr. Opin. Struct. Biol.* **2005**, *15* (4), 441–446.

(7) Dawidowski, M.; Emmanouilidis, L.; Kalel, V. C.; Tripsianes, K.; Schorpp, K.; Hadian, K.; Kaiser, M.; Mäser, P.; Kolonko, M.; Tanghe, S. Inhibitors of PEX14 Disrupt Protein Import into Glycosomes and Kill Trypanosoma Parasites. *Science* **2017**, *355* (6332), 1416–1420.

(8) Venkatesan, K.; Rual, J.-F.; Vazquez, A.; Stelzl, U.; Lemmens, I.; Hirozane-Kishikawa, T.; Hao, T.; Zenkner, M.; Xin, X.; Goh, K.-I.; Yildirim, M. A.; Simonis, N.; Heinzmann, K.; Gebreab, F.; Sahalie, J. M.; Cevik, S.; Simon, C.; de Smet, A.-S.; Dann, E.; Smolyar, A.; Vinayagam, A.; Yu, H.; Szeto, D.; Borick, H.; Dricot, A.; Klitgord, N.; Murray, R. R.; Lin, C.; Lalowski, M.; Timm, J.; Rau, K.; Boone, C.; Braun, P.; Cusick, M. E.; Roth, F. P.; Hill, D. E.; Tavernier, J.; Wanker, E. E.; Barabási, A.-L.; Vidal, M. An Empirical Framework for Binary Interactome Mapping. *Nat. Methods* **2009**, *6* (1), 83–90.

(9) Stumpf, M. P. H.; Thorne, T.; de Silva, E.; Stewart, R.; An, H. J.; Lappe, M.; Wiuf, C. Estimating the Size of the Human Interactome. *Proc. Natl. Acad. Sci. U.S.A.* **2008**, *105* (19), 6959–6964.

(10) Robertson, N.; Spring, D. Using Peptidomimetics and Constrained Peptides as Valuable Tools for Inhibiting Protein–Protein Interactions. *Molecules* **2018**, *23* (4), 959.

(11) Clackson, T.; Wells, J. A Hot Spot of Binding Energy in a Hormone-Receptor Interface. *Science* **1995**, *267* (5196), 383–386.

(12) Bogan, A. A.; Thorn, K. S. Anatomy of Hot Spots in Protein Interfaces. *J. Mol. Biol.* **1998**, *280* (1), 1–9.

(13) Moreira, I. S.; Fernandes, P. A.; Ramos, M. J. Hot Spots-A Review of the Protein-Protein Interface Determinant Amino-Acid Residues. *Proteins* **2007**, *68* (4), 803–812.

(14) Pelay-Gimeno, M.; Glas, A.; Koch, O.; Grossmann, T. N. Structure-Based Design of Inhibitors of Protein-Protein Interactions: Mimicking Peptide Binding Epitopes. *Angew. Chem. Int. Ed.* **2015**, *54* (31), 8896–8927.

(15) Jochim, A. L.; Arora, P. S. Systematic Analysis of Helical Protein Interfaces Reveals Targets for Synthetic Inhibitors. *ACS Chem. Biol.* **2010**, *5* (10), 919–923.

(16) Jesus Perez de Vega, M.; Martín-Martínez, M.; González-Muñiz, R. Modulation of Protein-Protein Interactions by Stabilizing/Mimicking Protein Secondary Structure

Elements. *Curr. Top. Med. Chem.* **2007**, *7* (1), 33–62.
(17) Picksley, S. M.; Lane, D. P. What the Papers Say: The P53-Mdm2 Autoregulatory Feedback Loop: A Paradigm for the Regulation of Growth Control by P53? *Bioessays* **1993**, *15* (10), 689–690.
(18) Murray, J. K.; Gellman, S. H. Targeting Protein–Protein Interactions: Lessons from P53/MDM2. *Pept. Sci.: Original Research on Biomolecules* **2007**, *88* (5), 657–686.
(19) Khoury, K.; Domling, A. P53 Mdm2 Inhibitors. *Curr. Pharm. Des.* **2012**, *18* (30), 4668–4678.
(20) Sang, P.; Shi, Y.; Lu, J.; Chen, L.; Yang, L.; Borcherds, W.; Abdulkadir, S.; Li, Q.; Daughdrill, G.; Chen, J.; Cai, J. α-Helix-Mimicking Sulfono-γ-AApeptide Inhibitors for P53–MDM2/MDMX Protein–Protein Interactions. *J. Med. Chem.* **2020**, *63* (3), 975–986.
(21) Mamone, S.; Glöggler, S.; Becker, S.; Rezaei-Ghaleh, N. Early Divergence in Misfolding Pathways of Amyloid-Beta Peptides. *ChemPhysChem* **2021**, *22* (21), 2158–2163.
(22) de Groot, N. S.; Pallarés, I.; Avilés, F. X.; Vendrell, J.; Ventura, S. Prediction of "Hot Spots" of Aggregation in Disease-Linked Polypeptides. *BMC Struct. Biol.* **2005**, *5*, 18.
(23) Laxio Arenas, J.; Kaffy, J.; Ongeri, S. Peptides and Peptidomimetics as Inhibitors of Protein–Protein Interactions Involving β-Sheet Secondary Structures. *Curr. Opin. Chem. Biol.* **2019**, *52*, 157–167.
(24) Liu, J.; Ying, J.; Chow, V. T. K.; Hruby, V. J.; Satyanarayanajois, S. D. Structure–Activity Studies of Peptides from the "Hot-Spot" Region of Human CD2 Protein: Development of Peptides for Immunomodulation. *J. Med. Chem.* **2005**, *48* (20), 6236–6249.
(25) Wendt, M. D.; Shen, W.; Kunzer, A.; McClellan, W. J.; Bruncko, M.; Oost, T. K.; Ding, H.; Joseph, M. K.; Zhang, H.; Nimmer, P. M. Discovery and Structure- Activity Relationship of Antagonists of B-Cell Lymphoma 2 Family Proteins with Chemopotentiation Activity in Vitro and in Vivo. *J. Med. Chem.* **2006**, *49* (3), 1165–1181.
(26) Gentile, M.; Petrungaro, A.; Uccello, G.; Vigna, E.; Recchia, A. G.; Caruso, N.; Bossio, S.; De Stefano, L.; Palummo, A.; Storino, F. Venetoclax for the Treatment of Chronic Lymphocytic Leukemia. *Expert Opin. Investig. Drugs* **2017**, *26* (11), 1307–1316.
(27) Raj, M.; Bullock, B. N.; Arora, P. S. Plucking the High Hanging Fruit: A Systematic Approach for Targeting Protein–Protein Interactions. *Bioorg. Med. Chem.* **2013**, *21* (14), 4051–4057.
(28) Ran, X.; Gestwicki, J. E. Inhibitors of Protein–Protein Interactions (PPIs): An Analysis of Scaffold Choices and Buried Surface Area. *Curr. Opin. Chem. Biol.* **2018**, *44*, 75–86.
(29) Cunningham, A. D.; Qvit, N.; Mochly-Rosen, D. Peptides and Peptidomimetics as Regulators of Protein–Protein Interactions. *Curr. Opin. Struct. Biol.* **2017**, *44*, 59–66.
(30) Bruzzoni-Giovanelli, H.; Alezra, V.; Wolff, N.; Dong, C.-Z.; Tuffery, P.; Rebollo, A. Interfering Peptides Targeting Protein–Protein Interactions: The next Generation of Drugs? *Drug Discov. Today* **2018**, *23* (2), 272–285.
(31) Fändrich, M. On the Structural Definition of Amyloid Fibrils and Other Polypeptide Aggregates. *Cell. Mol. Life Sci.* **2007**, *64* (16), 2066–2078.
(32) Eisele, Y. S.; Monteiro, C.; Fearns, C.; Encalada, S. E.; Wiseman, R. L.; Powers, E. T.; Kelly, J. W. Targeting Protein Aggregation for the Treatment of Degenerative Diseases. *Nat. Rev. Drug Discov.* **2015**, *14* (11), 759–780.
(33) Dobson, C. M.; Dobson, C. M. Protein Misfolding, Evolution and Disease. *Trends*

Biochem. Sci. **1999**, *24* (9), 329–332.

(34) Maji, S. K.; Perrin, M. H.; Sawaya, M. R.; Jessberger, S.; Vadodaria, K.; Rissman, R. A.; Singru, P. S.; Nilsson, K. P. R.; Simon, R.; Schubert, D.; Eisenberg, D.; Rivier, J.; Sawchenko, P.; Vale, W.; Riek, R. Functional Amyloids as Natural Storage of Peptide Hormones in Pituitary Secretory Granules. *Science* **2009**, *325* (5938), 328–332.

(35) Fowler, D. M.; Koulov, A. V.; Balch, W. E.; Kelly, J. W. Functional Amyloid – from Bacteria to Humans. *Trends Biochem. Sci.* **2007**, *32* (5), 217–224.

(36) Barnhart, M. M.; Chapman, M. R. Curli Biogenesis and Function. *Annu. Rev. Microbiol.* **2006**, *60*, 131–147.

(37) The Amyloid Hypothesis of Alzheimer's Disease at 25 Years. *EMBO Mol. Med.* **2016**, *8* (6), 595–608.

(38) Westermark, P.; Sletten, K.; Johansson, B.; Cornwell, G. G. Fibril in Senile Systemic Amyloidosis Is Derived from Normal Transthyretin. *Proc. Natl. Acad. Sci. U.S.A.* **1990**, *87* (7), 2843–2845.

(39) Bishoyi, A. K.; Roham, P. H.; Rachineni, K.; Save, S.; Hazari, M. A.; Sharma, S.; Kumar, A. Human Islet Amyloid Polypeptide (HIAPP) - a Curse in Type II Diabetes Mellitus: Insights from Structure and Toxicity Studies. *Biol. Chem.* **2021**, *402* (2), 133–153.

(40) Stefanis, L. α-Synuclein in Parkinson's Disease. *Cold Spring Harb. Perspect. Med.* **2012**, *2* (2), a009399.

(41) Wanker, E. E. Protein Aggregation and Pathogenesis of Huntingtons Disease: Mechanisms and Correlations. *Biol. Chem.* **2000**, *381* (9–10), 937–942.

(42) Ke, P. C.; Zhou, R.; Serpell, L. C.; Riek, R.; Knowles, T. P. J.; Lashuel, H. A.; Gazit, E.; Hamley, I. W.; Davis, T. P.; Fändrich, M.; Otzen, D. E.; Chapman, M. R.; Dobson, C. M.; Eisenberg, D. S.; Mezzenga, R. Half a Century of Amyloids: Past, Present and Future. *Chem. Soc. Rev.* **2020**, *49* (15), 5473–5509.

(43) Gremer, L.; Schölzel, D.; Schenk, C.; Reinartz, E.; Labahn, J.; Ravelli, R. B. G.; Tusche, M.; Lopez-Iglesias, C.; Hoyer, W.; Heise, H.; Willbold, D.; Schröder, G. F. Fibril Structure of Amyloid-β(1–42) by Cryo–Electron Microscopy. *Science* **2017**, *358* (6359), 116–119.

(44) Abedini, A.; Raleigh, D. P. A Critical Assessment of the Role of Helical Intermediates in Amyloid Formation by Natively Unfolded Proteins and Polypeptides. *Protein Eng. Des. Sel.* **2009**, *22* (8), 453–459.

(45) Broersen, K.; Rousseau, F.; Schymkowitz, J. The Culprit behind Amyloid Beta Peptide Related Neurotoxicity in Alzheimer's Disease: Oligomer Size or Conformation? *Alzheimer's Res. Ther.* **2010**, *2* (4), 12.

(46) Vivekanandan, S.; Brender, J. R.; Lee, S. Y.; Ramamoorthy, A. A Partially Folded Structure of Amyloid-Beta(1–40) in an Aqueous Environment. *Biochem. Biophys. Res. Commun.* **2011**, *411* (2), 312–316.

(47) Booth, D. R.; Sunde, M.; Bellotti, V.; Robinson, C. V.; Hutchinson, W. L.; Fraser, P. E.; Hawkins, P. N.; Dobson, C. M.; Radford, S. E.; Blake, C. C. F.; Pepys, M. B. Instability, Unfolding and Aggregation of Human Lysozyme Variants Underlying Amyloid Fibrillogenesis. *Nature* **1997**, *385* (6619), 787–793.

(48) Colon, W.; Kelly, J. W. Partial Denaturation of Transthyretin Is Sufficient for Amyloid Fibril Formation in Vitro. *Biochemistry* **1992**, *31* (36), 8654–8660.

(49) Arosio, P.; Knowles, T. P. J.; Linse, S. On the Lag Phase in Amyloid Fibril Formation. *Phys.*

Chem. Chem. Phys. **2015**, *17* (12), 7606–7618.

(50) Eisele, Y. S.; Monteiro, C.; Fearns, C.; Encalada, S. E.; Wiseman, R. L.; Powers, E. T.; Kelly, J. W. Targeting Protein Aggregation for the Treatment of Degenerative Diseases. *Nat. Rev. Drug. Discov.* **2015**, *14* (11), 759–780.

(51) Verma, M.; Vats, A.; Taneja, V. Toxic Species in Amyloid Disorders: Oligomers or Mature Fibrils. *Ann. Indian. Acad. Neurol.* **2015**, *18* (2), 138–145.

(52) Treusch, S.; Cyr, D. M.; Lindquist, S. Amyloid Deposits: Protection against Toxic Protein Species? *Cell Cycle* **2009**, *8* (11), 1668–1674.

(53) Ke, P. C.; Sani, M.-A.; Ding, F.; Kakinen, A.; Javed, I.; Separovic, F.; Davis, T. P.; Mezzenga, R. Implications of Peptide Assemblies in Amyloid Diseases. *Chem. Soc. Rev.* **2017**, *46* (21), 6492–6531.

(54) Shankar, G. M.; Bloodgood, B. L.; Townsend, M.; Walsh, D. M.; Selkoe, D. J.; Sabatini, B. L. Natural Oligomers of the Alzheimer Amyloid-β Protein Induce Reversible Synapse Loss by Modulating an NMDA-Type Glutamate Receptor-Dependent Signaling Pathway. *J. Neurosci.* **2007**, *27* (11), 2866–2875.

(55) Umeda, T.; Tomiyama, T.; Sakama, N.; Tanaka, S.; Lambert, M. P.; Klein, W. L.; Mori, H. Intraneuronal Amyloid β Oligomers Cause Cell Death via Endoplasmic Reticulum Stress, Endosomal/Lysosomal Leakage, and Mitochondrial Dysfunction in Vivo. *J. Neurosci. Res.* **2011**, *89* (7), 1031–1042.

(56) Cho, D.-H.; Nakamura, T.; Fang, J.; Cieplak, P.; Godzik, A.; Gu, Z.; Lipton, S. A. S-Nitrosylation of Drp1 Mediates β-Amyloid-Related Mitochondrial Fission and Neuronal Injury. *Science* **2009**, *324* (5923), 102–105.

(57) Liao, L.; Cheng, D.; Wang, J.; Duong, D. M.; Losik, T. G.; Gearing, M.; Rees, H. D.; Lah, J. J.; Levey, A. I.; Peng, J. Proteomic Characterization of Postmortem Amyloid Plaques Isolated by Laser Capture Microdissection. *J. Biol. Chem.* **2004**, *279* (35), 37061–37068.

(58) Wakabayashi, K.; Tanji, K.; Mori, F.; Takahashi, H. The Lewy Body in Parkinson's Disease: Molecules Implicated in the Formation and Degradation of α-Synuclein Aggregates: Molecular Components of Lewy Body. *Neuropathology* **2007**, *27* (5), 494–506.

(59) Xia, Q.; Liao, L.; Cheng, D.; Duong, D. M.; Gearing, M.; Lah, J. J.; Levey, A. I.; Peng, J. Proteomic Identification of Novel Proteins Associated with Lewy Bodies. *Front Biosci* **2008**, *13*(10), 3850–3856.

(60) Chaudhuri, P.; Prajapati, K. P.; Anand, B. G.; Dubey, K.; Kar, K. Amyloid Cross-Seeding Raises New Dimensions to Understanding of Amyloidogenesis Mechanism. *Ageing Res. Rev.* **2019**, *56*, 100937.

(61) Horvath, I.; Wittung-Stafshede, P. Cross-Talk between Amyloidogenic Proteins in Type-2 Diabetes and Parkinson's Disease. *Proc. Natl. Acad. Sci. U.S.A.* **2016**, *113* (44), 12473–12477.

(62) Giasson, B. I.; Forman, M. S.; Higuchi, M.; Golbe, L. I.; Graves, C. L.; Kotzbauer, P. T.; Trojanowski, J. Q.; Lee, V. M.-Y. Initiation and Synergistic Fibrillization of Tau and Alpha-Synuclein. *Science* **2003**, *300* (5619), 636–640.

(63) Shirasaka, M.; Kuwata, K.; Honda, R. α-Synuclein Chaperone Suppresses Nucleation and Amyloidogenesis of Prion Protein. *Biochem. Biophys. Res. Commun.* **2020**, *521* (1), 259–264.

(64) Buxbaum, J. N.; Ye, Z.; Reixach, N.; Friske, L.; Levy, C.; Das, P.; Golde, T.; Masliah, E.;

Roberts, A. R.; Bartfai, T. Transthyretin Protects Alzheimer's Mice from the Behavioral and Biochemical Effects of a Toxicity. *Proc. Natl. Acad. Sci. U.S.A.* **2008**, *105* (7), 2681–2686.

(65) Luo, J.; Wärmländer, S. K. T. S.; Gräslund, A.; Abrahams, J. P. Cross-Interactions between the Alzheimer Disease Amyloid-β Peptide and Other Amyloid Proteins: A Further Aspect of the Amyloid Cascade Hypothesis. *J. Biol. Chem.* **2016**, *291* (32), 16485–16493.

(66) Ciccone, L.; Shi, C.; di Lorenzo, D.; Van Baelen, A.-C.; Tonali, N. The Positive Side of the Alzheimer's Disease Amyloid Cross-Interactions: The Case of the Aβ 1-42 Peptide with Tau, TTR, CysC, and ApoA1. *Molecules* **2020**, *25* (10), 2439.

(67) 2020 Alzheimer's Disease Facts and Figures. *Alzheimer's & Dementia* **2020**, *16* (3), 391–460.

(68) Albert, M. S.; DeKosky, S. T.; Dickson, D.; Dubois, B.; Feldman, H. H.; Fox, N. C.; Gamst, A.; Holtzman, D. M.; Jagust, W. J.; Petersen, R. C.; Snyder, P. J.; Carrillo, M. C.; Thies, B.; Phelps, C. H. The Diagnosis of Mild Cognitive Impairment Due to Alzheimer's Disease: Recommendations from the National Institute on Aging-Alzheimer's Association Workgroups on Diagnostic Guidelines for Alzheimer's Disease. *Alzheimer's & Dementia* **2011**, *7* (3), 270–279.

(69) Sabri, O.; Seibyl, J.; Rowe, C.; Barthel, H. Beta-Amyloid Imaging with Florbetaben. *Clin. Transl. Imaging* **2015**, *3* (1), 13–26.

(70) Wong, D. F.; Rosenberg, P. B.; Zhou, Y.; Kumar, A.; Raymont, V.; Ravert, H. T.; Dannals, R. F.; Nandi, A.; Brašić, J. R.; Ye, W.; Hilton, J.; Lyketsos, C.; Kung, H. F.; Joshi, A. D.; Skovronsky, D. M.; Pontecorvo, M. J. In Vivo Imaging of Amyloid Deposition in Alzheimer's Disease Using the Novel Radioligand [18F]AV-45 (Florbetapir F 18). *J. Nucl. Med.* **2010**, *51* (6), 913–920.

(71) Martínez, G.; Vernooij, R. W.; Fuentes Padilla, P.; Zamora, J.; Flicker, L.; Bonfill Cosp, X. 18F PET with Flutemetamol for the Early Diagnosis of Alzheimer's Disease Dementia and Other Dementias in People with Mild Cognitive Impairment (MCI). *Cochrane Database Syst. Rev.* **2017**, *2017* (11), CD012884.

(72) Morbelli, S.; Bauckneht, M.; Arnaldi, D.; Picco, A.; Pardini, M.; Brugnolo, A.; Buschiazzo, A.; Pagani, M.; Girtler, N.; Nieri, A.; Chincarini, A.; De Carli, F.; Sambuceti, G.; Nobili, F. 18F–FDG PET Diagnostic and Prognostic Patterns Do Not Overlap in Alzheimer's Disease (AD) Patients at the Mild Cognitive Impairment (MCI) Stage. *Eur. J. Nucl. Med. Mol. Imaging* **2017**, *44* (12), 2073–2083.

(73) Dubois, B.; Hampel, H.; Feldman, H. H.; Scheltens, P.; Aisen, P.; Andrieu, S.; Bakardjian, H.; Benali, H.; Bertram, L.; Blennow, K.; Broich, K.; Cavedo, E.; Crutch, S.; Dartigues, J.-F.; Duyckaerts, C.; Epelbaum, S.; Frisoni, G. B.; Gauthier, S.; Genthon, R.; Gouw, A. A.; Habert, M.-O.; Holtzman, D. M.; Kivipelto, M.; Lista, S.; Molinuevo, J.-L.; O'Bryant, S. E.; Rabinovici, G. D.; Rowe, C.; Salloway, S.; Schneider, L. S.; Sperling, R.; Teichmann, M.; Carrillo, M. C.; Cummings, J.; Jack, C. R.; Proceedings of the Meeting of the International Working Group (IWG) and the American Alzheimer's Association on "The Preclinical State of AD"; July 23, 2015; Washington DC, USA. Preclinical Alzheimer's Disease: Definition, Natural History, and Diagnostic Criteria. *Alzheimer's & Dementia* **2016**, *12* (3), 292–323.

(74) Jack, C. R.; Bennett, D. A.; Blennow, K.; Carrillo, M. C.; Dunn, B.; Haeberlein, S. B.;

Holtzman, D. M.; Jagust, W.; Jessen, F.; Karlawish, J.; Liu, E.; Molinuevo, J. L.; Montine, T.; Phelps, C.; Rankin, K. P.; Rowe, C. C.; Scheltens, P.; Siemers, E.; Snyder, H. M.; Sperling, R.; Contributors. NIA-AA Research Framework: Toward a Biological Definition of Alzheimer's Disease. *Alzheimer's & Dementia* **2018**, *14* (4), 535–562.

(75) Zhou, W.; Zhang, J.; Ye, F.; Xu, G.; Su, H.; Su, Y.; Zhang, X.; Alzheimer's Disease Neuroimaging Initiative. Plasma Neurofilament Light Chain Levels in Alzheimer's Disease. *Neurosci. Lett.* **2017**, *650*, 60–64.

(76) Portelius, E.; Zetterberg, H.; Skillbäck, T.; Törnqvist, U.; Andreasson, U.; Trojanowski, J. Q.; Weiner, M. W.; Shaw, L. M.; Mattsson, N.; Blennow, K. Cerebrospinal Fluid Neurogranin: Relation to Cognition and Neurodegeneration in Alzheimer's Disease. *Brain* **2015**, *138* (11), 3373–3385.

(77) Meyer-Luehmann, M.; Coomaraswamy, J.; Bolmont, T.; Kaeser, S.; Schaefer, C.; Kilger, E.; Neuenschwander, A.; Abramowski, D.; Frey, P.; Jaton, A. L.; Vigouret, J.-M.; Paganetti, P.; Walsh, D. M.; Mathews, P. M.; Ghiso, J.; Staufenbiel, M.; Walker, L. C.; Jucker, M. Exogenous Induction of Cerebral Beta-Amyloidogenesis Is Governed by Agent and Host. *Science* **2006**, *313* (5794), 1781–1784.

(78) Bero, A. W.; Yan, P.; Roh, J. H.; Cirrito, J. R.; Stewart, F. R.; Raichle, M. E.; Lee, J.-M.; Holtzman, D. M. Neuronal Activity Regulates the Regional Vulnerability to Amyloid-β Deposition. *Nat. Neurosci.* **2011**, *14* (6), 750–756.

(79) Musiek, E. S.; Holtzman, D. M. Three Dimensions of the Amyloid Hypothesis: Time, Space and "Wingmen." *Nat. Neurosci.* **2015**, *18* (6), 800–806.

(80) Zhao, W.; Zhang, J.; Davis, E. G.; Rebeck, G. W. Aging Reduces Glial Uptake and Promotes Extracellular Accumulation of Aβ from a Lentiviral Vector. *Front. Aging Neurosci.* **2014**, *6*.

(81) Kress, B. T.; Iliff, J. J.; Xia, M.; Wang, M.; Wei, H. S.; Zeppenfeld, D.; Xie, L.; Kang, H.; Xu, Q.; Liew, J. A.; Plog, B. A.; Ding, F.; Deane, R.; Nedergaard, M. Impairment of Paravascular Clearance Pathways in the Aging Brain. *Ann. Neurol.* **2014**, *76* (6), 845–861.

(82) Tcw, J.; Goate, A. M. Genetics of β-Amyloid Precursor Protein in Alzheimer's Disease. *Cold Spring Harb. Perspect. Med.* **2017**, *7* (6), a024539.

(83) Bales, K. R.; Liu, F.; Wu, S.; Lin, S.; Koger, D.; DeLong, C.; Hansen, J. C.; Sullivan, P. M.; Paul, S. M. Human APOE Isoform-Dependent Effects on Brain β-Amyloid Levels in PDAPP Transgenic Mice. *J. Neurosci.* **2009**, *29* (21), 6771–6779.

(84) Pauwels, K.; Williams, T. L.; Morris, K. L.; Jonckheere, W.; Vandersteen, A.; Kelly, G.; Schymkowitz, J.; Rousseau, F.; Pastore, A.; Serpell, L. C.; Broersen, K. Structural Basis for Increased Toxicity of Pathological Aβ42:Aβ40 Ratios in Alzheimer Disease*. *J. Biol. Chem.* **2012**, *287* (8), 5650–5660.

(85) Shankar, G. M.; Li, S.; Mehta, T. H.; Garcia-Munoz, A.; Shepardson, N. E.; Smith, I.; Brett, F. M.; Farrell, M. A.; Rowan, M. J.; Lemere, C. A.; Regan, C. M.; Walsh, D. M.; Sabatini, B. L.; Selkoe, D. J. Amyloid-β Protein Dimers Isolated Directly from Alzheimer's Brains Impair Synaptic Plasticity and Memory. *Nat. Med.* **2008**, *14* (8), 837–842.

(86) Zott, B.; Simon, M. M.; Hong, W.; Unger, F.; Chen-Engerer, H.-J.; Frosch, M. P.; Sakmann, B.; Walsh, D. M.; Konnerth, A. A Vicious Cycle of β Amyloid-Dependent Neuronal Hyperactivation. *Science* **2019**, *365* (6453), 559–565.

(87) Bode, D. C.; Baker, M. D.; Viles, J. H. Ion Channel Formation by Amyloid-B42 Oligomers but Not Amyloid-B40 in Cellular Membranes. *J. Biol. Chem.* **2017**, *292* (4), 1404–1413.

(88) Bode, D. C.; Freeley, M.; Nield, J.; Palma, M.; Viles, J. H. Amyloid-β Oligomers Have a Profound Detergent-like Effect on Lipid Membrane Bilayers, Imaged by Atomic Force and Electron Microscopy. *J. Biol. Chem.* **2019**, *294* (19), 7566–7572.

(89) Lipids Revert Inert Aβ Amyloid Fibrils to Neurotoxic Protofibrils That Affect Learning in Mice. *The EMBO Journal* **2008**, *27* (1), 224–233.

(90) McInnes, J.; Wierda, K.; Snellinx, A.; Bounti, L.; Wang, Y.-C.; Stancu, I.-C.; Apóstolo, N.; Gevaert, K.; Dewachter, I.; Spires-Jones, T. L.; De Strooper, B.; De Wit, J.; Zhou, L.; Verstreken, P. Synaptogyrin-3 Mediates Presynaptic Dysfunction Induced by Tau. *Neuron* **2018**, *97* (4), 823-835.e8.

(91) Torres, A. K.; Rivera, B. I.; Polanco, C. M.; Jara, C.; Tapia-Rojas, C. Phosphorylated Tau as a Toxic Agent in Synaptic Mitochondria: Implications in Aging and Alzheimer's Disease. *Neural Regen. Res.* **2022**, *17* (8), 1645–1651.

(92) Hoover, B. R.; Reed, M. N.; Su, J.; Penrod, R. D.; Kotilinek, L. A.; Grant, M. K.; Pitstick, R.; Carlson, G. A.; Lanier, L. M.; Yuan, L.-L.; Ashe, K. H.; Liao, D. Tau Mislocalization to Dendritic Spines Mediates Synaptic Dysfunction Independently of Neurodegeneration. *Neuron* **2010**, *68* (6), 1067–1081.

(93) Xie, A.-J.; Hou, T.-Y.; Xiong, W.; Huang, H.-Z.; Zheng, J.; Li, K.; Man, H.-Y.; Hu, Y.-Z.; Han, Z.-T.; Zhang, H.-H.; Wei, N.; Wang, J.-Z.; Liu, D.; Lu, Y.; Zhu, L.-Q. Tau Overexpression Impairs Neuronal Endocytosis by Decreasing the GTPase Dynamin 1 through the MiR-132/MeCP2 Pathway. *Aging Cell* **2019**, *18* (3), e12929.

(94) Morales, I.; Jiménez, J. M.; Mancilla, M.; Maccioni, R. B. Tau Oligomers and Fibrils Induce Activation of Microglial Cells. *J. Alzheimer's Dis.* **2013**, *37* (4), 849–856.

(95) Nelson, P. T.; Alafuzoff, I.; Bigio, E. H.; Bouras, C.; Braak, H.; Cairns, N. J.; Castellani, R. J.; Crain, B. J.; Davies, P.; Tredici, K. D.; Duyckaerts, C.; Frosch, M. P.; Haroutunian, V.; Hof, P. R.; Hulette, C. M.; Hyman, B. T.; Iwatsubo, T.; Jellinger, K. A.; Jicha, G. A.; Kövari, E.; Kukull, W. A.; Leverenz, J. B.; Love, S.; Mackenzie, I. R.; Mann, D. M.; Masliah, E.; McKee, A. C.; Montine, T. J.; Morris, J. C.; Schneider, J. A.; Sonnen, J. A.; Thal, D. R.; Trojanowski, J. Q.; Troncoso, J. C.; Wisniewski, T.; Woltjer, R. L.; Beach, T. G. Correlation of Alzheimer Disease Neuropathologic Changes With Cognitive Status: A Review of the Literature. *J. Neuropathol. Exp. Neurol.* **2012**, *71* (5), 362–381.

(96) Hanseeuw, B. J.; Betensky, R. A.; Jacobs, H. I. L.; Schultz, A. P.; Sepulcre, J.; Becker, J. A.; Cosio, D. M. O.; Farrell, M.; Quiroz, Y. T.; Mormino, E. C.; Buckley, R. F.; Papp, K. V.; Amariglio, R. A.; Dewachter, I.; Ivanoiu, A.; Huijbers, W.; Hedden, T.; Marshall, G. A.; Chhatwal, J. P.; Rentz, D. M.; Sperling, R. A.; Johnson, K. Association of Amyloid and Tau With Cognition in Preclinical Alzheimer Disease: A Longitudinal Study. *JAMA Neurol* **2019**, *76* (8), 915–924.

(97) Corder, E. H.; Saunders, A. M.; Strittmatter, W. J.; Schmechel, D. E.; Gaskell, P. C.; Small, G. W.; Roses, A. D.; Haines, J. L.; Pericak-Vance, M. A. Gene Dose of Apolipoprotein E Type 4 Allele and the Risk of Alzheimer's Disease in Late Onset Families. *Science* **1993**, *261* (5123), 921–923.

(98) Reiman, E. M.; Arboleda-Velasquez, J. F.; Quiroz, Y. T.; Huentelman, M. J.; Beach, T. G.; Caselli, R. J.; Chen, Y.; Su, Y.; Myers, A. J.; Hardy, J.; Paul Vonsattel, J.; Younkin, S. G.;

Bennett, D. A.; De Jager, P. L.; Larson, E. B.; Crane, P. K.; Keene, C. D.; Kamboh, M. I.; Kofler, J. K.; Duque, L.; Gilbert, J. R.; Gwirtsman, H. E.; Buxbaum, J. D.; Dickson, D. W.; Frosch, M. P.; Ghetti, B. F.; Lunetta, K. L.; Wang, L.-S.; Hyman, B. T.; Kukull, W. A.; Foroud, T.; Haines, J. L.; Mayeux, R. P.; Pericak-Vance, M. A.; Schneider, J. A.; Trojanowski, J. Q.; Farrer, L. A.; Schellenberg, G. D.; Beecham, G. W.; Montine, T. J.; Jun, G. R. Exceptionally Low Likelihood of Alzheimer's Dementia in APOE2 Homozygotes from a 5,000-Person Neuropathological Study. *Nat. Commun.* **2020**, *11* (1), 667.

(99) Hori, Y.; Hashimoto, T.; Nomoto, H.; Hyman, B. T.; Iwatsubo, T. Role of Apolipoprotein E in β-Amyloidogenesis: ISOFORM-SPECIFIC EFFECTS ON PROTOFIBRIL TO FIBRIL CONVERSION OF Aβ IN VITRO AND BRAIN Aβ DEPOSITION IN VIVO*. *J. Biol. Chem.* **2015**, *290* (24), 15163–15174.

(100) Hashimoto, T.; Serrano-Pozo, A.; Hori, Y.; Adams, K. W.; Takeda, S.; Banerji, A. O.; Mitani, A.; Joyner, D.; Thyssen, D. H.; Bacskai, B. J.; Frosch, M. P.; Spires-Jones, T. L.; Finn, M. B.; Holtzman, D. M.; Hyman, B. T. Apolipoprotein E, Especially Apolipoprotein E4, Increases the Oligomerization of Amyloid β Peptide. *J. Neurosci.* **2012**, *32* (43), 15181–15192.

(101) Liu, C.-C.; Zhao, N.; Fu, Y.; Wang, N.; Linares, C.; Tsai, C.-W.; Bu, G. ApoE4 Accelerates Early Seeding of Amyloid Pathology. *Neuron* **2017**, *96* (5), 1024-1032.e3.

(102) Castellano, J. M.; Kim, J.; Stewart, F. R.; Jiang, H.; DeMattos, R. B.; Patterson, B. W.; Fagan, A. M.; Morris, J. C.; Mawuenyega, K. G.; Cruchaga, C.; Goate, A. M.; Bales, K. R.; Paul, S. M.; Bateman, R. J.; Holtzman, D. M. Human ApoE Isoforms Differentially Regulate Brain Amyloid-β Peptide Clearance. *Sci. Transl. Med.* **2011**, *3* (89), 89ra57-89ra57.

(103) Verghese, P. B.; Castellano, J. M.; Garai, K.; Wang, Y.; Jiang, H.; Shah, A.; Bu, G.; Frieden, C.; Holtzman, D. M. ApoE Influences Amyloid-β (Aβ) Clearance despite Minimal ApoE/Aβ Association in Physiological Conditions. *Proc. Natl. Acad. Sci. U.S.A.* **2013**, *110* (19), E1807–E1816.

(104) Shi, Y.; Yamada, K.; Liddelow, S. A.; Smith, S. T.; Zhao, L.; Luo, W.; Tsai, R. M.; Spina, S.; Grinberg, L. T.; Rojas, J. C.; Gallardo, G.; Wang, K.; Roh, J.; Robinson, G.; Finn, M. B.; Jiang, H.; Sullivan, P. M.; Baufeld, C.; Wood, M. W.; Sutphen, C.; McCue, L.; Xiong, C.; Del-Aguila, J. L.; Morris, J. C.; Cruchaga, C.; Fagan, A. M.; Miller, B. L.; Boxer, A. L.; Seeley, W. W.; Butovsky, O.; Barres, B. A.; Paul, S. M.; Holtzman, D. M. ApoE4 Markedly Exacerbates Tau-Mediated Neurodegeneration in a Mouse Model of Tauopathy. *Nature* **2017**, *549* (7673), 523–527.

(105) Bell, R. D.; Winkler, E. A.; Singh, I.; Sagare, A. P.; Deane, R.; Wu, Z.; Holtzman, D. M.; Betsholtz, C.; Armulik, A.; Sallstrom, J.; Berk, B. C.; Zlokovic, B. V. Apolipoprotein E Controls Cerebrovascular Integrity via Cyclophilin A. *Nature* **2012**, *485* (7399), 512–516.

(106) Jo, S.; Yarishkin, O.; Hwang, Y. J.; Chun, Y. E.; Park, M.; Woo, D. H.; Bae, J. Y.; Kim, T.; Lee, J.; Chun, H.; Park, H. J.; Lee, D. Y.; Hong, J.; Kim, H. Y.; Oh, S.-J.; Park, S. J.; Lee, H.; Yoon, B.-E.; Kim, Y.; Jeong, Y.; Shim, I.; Bae, Y. C.; Cho, J.; Kowall, N. W.; Ryu, H.; Hwang, E.; Kim, D.; Lee, C. J. GABA from Reactive Astrocytes Impairs Memory in Mouse Models of Alzheimer's Disease. *Nat. Med.* **2014**, *20* (8), 886–896.

(107) Navarro, V.; Sanchez-Mejias, E.; Jimenez, S.; Muñoz-Castro, C.; Sanchez-Varo, R.; Davila, J. C.; Vizuete, M.; Gutierrez, A.; Vitorica, J. Microglia in Alzheimer's Disease: Activated, Dysfunctional or Degenerative. *Front. Aging Neurosci.* **2018**, *10*.

(108) Hayes, A.; Thaker, U.; Iwatsubo, T.; Pickering-Brown, S. M.; Mann, D. M. A. Pathological Relationships between Microglial Cell Activity and Tau and Amyloid Beta Protein in Patients with Alzheimer's Disease. *Neurosci. Lett.* **2002**, *331* (3), 171–174.

(109) McGeer, P. L.; McGeer, E. G. The Amyloid Cascade-Inflammatory Hypothesis of Alzheimer Disease: Implications for Therapy. *Acta Neuropathol* **2013**, *126* (4), 479–497.

(110) Mishra, A.; Kim, H. J.; Shin, A. H.; Thayer, S. A. Synapse Loss Induced by Interleukin-1β Requires Pre- and Post-Synaptic Mechanisms. *J. Neuroimmune. Pharmacol.* **2012**, *7* (3), 571–578.

(111) Micheau, O.; Tschopp, J. Induction of TNF Receptor I-Mediated Apoptosis via Two Sequential Signaling Complexes. *Cell* **2003**, *114* (2), 181–190.

(112) Chen, C.-H.; Zhou, W.; Liu, S.; Deng, Y.; Cai, F.; Tone, M.; Tone, Y.; Tong, Y.; Song, W. Increased NF-KB Signalling up-Regulates BACE1 Expression and Its Therapeutic Potential in Alzheimer's Disease. *Int. J. Neuropsychopharmacol.* **2012**, *15* (1), 77–90.

(113) Venegas, C.; Kumar, S.; Franklin, B. S.; Dierkes, T.; Brinkschulte, R.; Tejera, D.; Vieira-Saecker, A.; Schwartz, S.; Santarelli, F.; Kummer, M. P.; Griep, A.; Gelpi, E.; Beilharz, M.; Riedel, D.; Golenbock, D. T.; Geyer, M.; Walter, J.; Latz, E.; Heneka, M. T. Microglia-Derived ASC Specks Cross-Seed Amyloid-β in Alzheimer's Disease. *Nature* **2017**, *552* (7685), 355–361.

(114) Leng, F.; Edison, P. Neuroinflammation and Microglial Activation in Alzheimer Disease: Where Do We Go from Here? *Nat. Rev. Neurol.* **2021**, *17* (3), 157–172.

(115) Ribarič, S. Peptides as Potential Therapeutics for Alzheimer's Disease. *Molecules* **2018**, *23* (2), 283.

(116) Long, J. M.; Holtzman, D. M. Alzheimer Disease: An Update on Pathobiology and Treatment Strategies. *Cell* **2019**, *179* (2), 312–339.

(117) Cummings, J.; Lee, G.; Ritter, A.; Sabbagh, M.; Zhong, K. Alzheimer's Disease Drug Development Pipeline: 2020. *Alzheimer's Dement.: Transl. Res. Clin. Interv.* **2020**, *6* (1), e12050.

(118) Seltzer, B. Donepezil: A Review. *Expert Opin. Drug Metab. Toxicol.* **2005**, *1* (3), 527–536.

(119) Vaz, M.; Silvestre, S. Alzheimer's Disease: Recent Treatment Strategies. *Eur. J. Pharmacol.* **2020**, *887*, 173554.

(120) Satir, T. M.; Agholme, L.; Karlsson, A.; Karlsson, M.; Karila, P.; Illes, S.; Bergström, P.; Zetterberg, H. Partial Reduction of Amyloid β Production by β-Secretase Inhibitors Does Not Decrease Synaptic Transmission. *Alzheimer's Res. Ther.* **2020**, *12* (1), 63.

(121) Gratton, R.; Tricarico, P. M.; Moltrasio, C.; Lima Estevão de Oliveira, A. S.; Brandão, L.; Marzano, A. V.; Zupin, L.; Crovella, S. Pleiotropic Role of Notch Signaling in Human Skin Diseases. *Int. J. Mol. Sci.* **2020**, *21* (12), 4214.

(122) Cascella, M.; Bimonte, S.; Muzio, M. R.; Schiavone, V.; Cuomo, A. The Efficacy of Epigallocatechin-3-Gallate (Green Tea) in the Treatment of Alzheimer's Disease: An Overview of Pre-Clinical Studies and Translational Perspectives in Clinical Practice. *Infect. Agent Cancer* **2017**, *12*, 36.

(123) Abushakra, S.; Porsteinsson, A.; Scheltens, P.; Sadowsky, C.; Vellas, B.; Cummings, J.; Gauthier, S.; Hey, J. A.; Power, A.; Wang, P.; L. Shen; Tolar, M. Clinical Effects of Tramiprosate in Apoe4/4 Homozygous Patients with Mild Alzheimer's Disease Suggest

Disease Modification Potential. *J. Prev. Alzheimer's Dis.* **2017**, *J Prev Alz Dis 20174* (3), 149–156.

(124) Hey, J. A.; Yu, J. Y.; Versavel, M.; Abushakra, S.; Kocis, P.; Power, A.; Kaplan, P. L.; Amedio, J.; Tolar, M. Clinical Pharmacokinetics and Safety of ALZ-801, a Novel Prodrug of Tramiprosate in Development for the Treatment of Alzheimer's Disease. *Clin. Pharmacokinet.* **2018**, *57* (3), 315–333.

(125) Rafii, M. S.; Skotko, B. G.; McDonough, M. E.; Pulsifer, M.; Evans, C.; Doran, E.; Muranevici, G.; Kesslak, P.; Abushakra, S.; Lott, I. T. A Randomized, Double-Blind, Placebo-Controlled, Phase 2 Study of Oral ELND005 (Scyllo-Inositol) in Young Adults with Down Syndrome without Dementia. *J. Alzheimers. Dis.* **2017**, *58* (2), 401–411.

(126) Crespi, G. A. N.; Hermans, S. J.; Parker, M. W.; Miles, L. A. Molecular Basis for Mid-Region Amyloid-β Capture by Leading Alzheimer's Disease Immunotherapies. *Sci. Rep.* **2015**, *5* (1), 9649.

(127) Feinberg, H.; Saldanha, J. W.; Diep, L.; Goel, A.; Widom, A.; Veldman, G. M.; Weis, W. I.; Schenk, D.; Basi, G. S. Crystal Structure Reveals Conservation of Amyloid-β Conformation Recognized by 3D6 Following Humanization to Bapineuzumab. *Alzheimers. Res. Ther.* **2014**, *6* (3), 31.

(128) Adolfsson, O.; Pihlgren, M.; Toni, N.; Varisco, Y.; Buccarello, A. L.; Antoniello, K.; Lohmann, S.; Piorkowska, K.; Gafner, V.; Atwal, J. K.; Maloney, J.; Chen, M.; Gogineni, A.; Weimer, R. M.; Mortensen, D. L.; Friesenhahn, M.; Ho, C.; Paul, R.; Pfeifer, A.; Muhs, A.; Watts, R. J. An Effector-Reduced Anti-β-Amyloid (Aβ) Antibody with Unique Aβ Binding Properties Promotes Neuroprotection and Glial Engulfment of Aβ. *J. Neurosci.* **2012**, *32* (28), 9677–9689.

(129) *Aduhelm (aducanumab-avwa) FDA Approval History*. Drugs.com. https://www.drugs.com/history/aduhelm.html (accessed 2022-10-17).

(130) Lovestone, S.; Boada, M.; Dubois, B.; Hüll, M.; Rinne, J. O.; Huppertz, H.-J.; Calero, M.; Andrés, M. V.; Gómez-Carrillo, B.; León, T.; del Ser, T.; Investigators, for the A. A Phase II Trial of Tideglusib in Alzheimer's Disease. *J. Alzheimer's Dis.* **2015**, *45* (1), 75–88.

(131) Forlenza, O. V.; Diniz, B. S.; Radanovic, M.; Santos, F. S.; Talib, L. L.; Gattaz, W. F. Disease-Modifying Properties of Long-Term Lithium Treatment for Amnestic Mild Cognitive Impairment: Randomised Controlled Trial. *Br. J. Psychiatry* **2011**, *198* (5), 351–356.

(132) Gauthier, S.; Feldman, H. H.; Schneider, L. S.; Wilcock, G. K.; Frisoni, G. B.; Hardlund, J. H.; Moebius, H. J.; Bentham, P.; Kook, K. A.; Wischik, D. J.; Schelter, B. O.; Davis, C. S.; Staff, R. T.; Bracoud, L.; Shamsi, K.; Storey, J. M. D.; Harrington, C. R.; Wischik, C. M. Efficacy and Safety of Tau-Aggregation Inhibitor Therapy in Patients with Mild or Moderate Alzheimer's Disease: A Randomised, Controlled, Double-Blind, Parallel-Arm, Phase 3 Trial. *The Lancet* **2016**, *388* (10062), 2873–2884.

(133) Wischik, C. M.; Staff, R. T.; Wischik, D. J.; Bentham, P.; Murray, A. D.; Storey, J. M. D.; Kook, K. A.; Harrington, C. R. Tau Aggregation Inhibitor Therapy: An Exploratory Phase 2 Study in Mild or Moderate Alzheimer's Disease. *J. Alzheimer's Dis.* **2015**, *44* (2), 705–720.

(134) *Gosuranemab | ALZFORUM*. https://www.alzforum.org/therapeutics/gosuranemab (accessed 2022-07-31).

(135) *Tilavonemab | ALZFORUM*. https://www.alzforum.org/therapeutics/tilavonemab

(accessed 2022-07-31).
(136) *Semorinemab | ALZFORUM*. https://www.alzforum.org/therapeutics/semorinemab (accessed 2022-07-31).
(137) *Zagotenemab | ALZFORUM*. https://www.alzforum.org/therapeutics/zagotenemab (accessed 2022-07-31).
(138) *Bepranemab | ALZFORUM*. https://www.alzforum.org/therapeutics/bepranemab (accessed 2022-07-31).
(139) Janssen Research & Development, LLC. *A Randomized, Double-Blind, Placebo-Controlled, Parallel-Group, Multicenter Study to Assess the Efficacy and Safety of JNJ-63733657, an Anti-Tau Monoclonal Antibody, in Participants with Early Alzheimer's Disease*; Clinical trial registration NCT04619420; clinicaltrials.gov, 2022.
(140) Tjernberg, L. O.; Näslund, J.; Lindqvist, F.; Johansson, J.; Karlström, A. R.; Thyberg, J.; Terenius, L.; Nordstedt, C. Arrest of -Amyloid Fibril Formation by a Pentapeptide Ligand (*). *J. Biol. Chem.* **1996**, *271* (15), 8545–8548.
(141) Matsunaga, Y.; Fujii, A.; Awasthi, A.; Yokotani, J.; Takakura, T.; Yamada, T. Eight-Residue Aβ Peptides Inhibit the Aggregation and Enzymatic Activity of Aβ42. *Regul. Pept.* **2004**, *120* (1), 227–236.
(142) Lowe, T. L.; Strzelec, A.; Kiessling, L. L.; Murphy, R. M. Structure–Function Relationships for Inhibitors of β-Amyloid Toxicity Containing the Recognition Sequence KLVFF. *Biochemistry* **2001**, *40* (26), 7882–7889.
(143) Austen, B. M.; Paleologou, K. E.; Ali, S. A. E.; Qureshi, M. M.; Allsop, D.; El-Agnaf, O. M. A. Designing Peptide Inhibitors for Oligomerization and Toxicity of Alzheimer's β-Amyloid Peptide. *Biochemistry* **2008**, *47* (7), 1984–1992.
(144) Soto, C.; Kindy, M. S.; Baumann, M.; Frangione, B. Inhibition of Alzheimer's Amyloidosis by Peptides That Prevent β-Sheet Conformation. *Biochem. Biophys. Res. Commun.* **1996**, *226* (3), 672–680.
(145) Chacón, M. A.; Barría, M. I.; Soto, C.; Inestrosa, N. C. β-Sheet Breaker Peptide Prevents Aβ-Induced Spatial Memory Impairments with Partial Reduction of Amyloid Deposits. *Mol. Psychiatry* **2004**, *9* (10), 953–961.
(146) Liu, J.; Wang, W.; Zhang, Q.; Zhang, S.; Yuan, Z. Study on the Efficiency and Interaction Mechanism of a Decapeptide Inhibitor of β-Amyloid Aggregation. *Biomacromolecules* **2014**, *15* (3), 931–939.
(147) Fradinger, E. A.; Monien, B. H.; Urbanc, B.; Lomakin, A.; Tan, M.; Li, H.; Spring, S. M.; Condron, M. M.; Cruz, L.; Xie, C.-W.; Benedek, G. B.; Bitan, G. C-Terminal Peptides Coassemble into Aβ42 Oligomers and Protect Neurons against Aβ42-Induced Neurotoxicity. *Proc. Natl. Acad. Sci. U.S.A.* **2008**, *105* (37), 14175–14180.
(148) Hao, J.; Zhang, W.; Zhang, P.; Liu, R.; Liu, L.; Lei, G.; Su, C.; Miao, J.; Li, Z. Aβ20–29 Peptide Blocking ApoE/Aβ Interaction Reduces Full-Length Aβ42/40 Fibril Formation and Cytotoxicity in Vitro. *Neuropeptides* **2010**, *44* (4), 305–313.
(149) Hughes, E.; Burke, R. M.; Doig, A. J. Inhibition of Toxicity in the β-Amyloid Peptide Fragment β-(25–35) Using N-Methylated Derivatives: A GENERAL STRATEGY TO PREVENT AMYLOID FORMATION*. *J. Biol. Chem.* **2000**, *275* (33), 25109–25115.
(150) Gordon, D. J.; Sciarretta, K. L.; Meredith, S. C. Inhibition of β-Amyloid(40) Fibrillogenesis and Disassembly of β-Amyloid(40) Fibrils by Short β-Amyloid Congeners Containing

N-Methyl Amino Acids at Alternate Residues. *Biochemistry* **2001**, *40* (28), 8237–8245.

(151) Gordon, D. j.; Tappe, R.; Meredith, S. c. Design and Characterization of a Membrane Permeable N-Methyl Amino Acid-Containing Peptide That Inhibits Aβ1–40 Fibrillogenesis. *J. Pept. Res.* **2002**, *60* (1), 37–55.

(152) Cruz, M.; Tusell, J. m.; Grillo-Bosch, D.; Albericio, F.; Serratosa, J.; Rabanal, F.; Giralt, E. Inhibition of β-Amyloid Toxicity by Short Peptides Containing N-Methyl Amino Acids. *J. Pept. Res.* **2004**, *63* (3), 324–328.

(153) Bose, P. P.; Chatterjee, U.; Hubatsch, I.; Artursson, P.; Govender, T.; Kruger, H. G.; Bergh, M.; Johansson, J.; Arvidsson, P. I. In Vitro ADMET and Physicochemical Investigations of Poly-N-Methylated Peptides Designed to Inhibit Aβ Aggregation. *Bioorg. Med. Chem.* **2010**, *18* (16), 5896–5902.

(154) Kokkoni, N.; Stott, K.; Amijee, H.; Mason, J. M.; Doig, A. J. N-Methylated Peptide Inhibitors of β-Amyloid Aggregation and Toxicity. Optimization of the Inhibitor Structure. *Biochemistry* **2006**, *45* (32), 9906–9918.

(155) Stereoselective Interactions of Peptide Inhibitors with the β-Amyloid Peptide. *J. Biol. Chem.* **2003**, *278* (37), 34874–34881.

(156) Jagota, S.; Rajadas, J. Synthesis of D-Amino Acid Peptides and Their Effect on Beta-Amyloid Aggregation and Toxicity in Transgenic Caenorhabditis Elegans. *Med. Chem. Res.* **2013**, *22* (8), 3991–4000.

(157) Findeis, M. A.; Musso, G. M.; Arico-Muendel, C. C.; Benjamin, H. W.; Hundal, A. M.; Lee, J.-J.; Chin, J.; Kelley, M.; Wakefield, J.; Hayward, N. J.; Molineaux, S. M. Modified-Peptide Inhibitors of Amyloid β-Peptide Polymerization. *Biochemistry* **1999**, *38* (21), 6791–6800.

(158) Zhang, G.; Leibowitz, M. J.; Sinko, P. J.; Stein, S. Multiple-Peptide Conjugates for Binding β-Amyloid Plaques of Alzheimer's Disease. *Bioconjugate Chem.* **2003**, *14* (1), 86–92.

(159) Matharu, B.; El-Agnaf, O.; Razvi, A.; Austen, B. M. Development of Retro-Inverso Peptides as Anti-Aggregation Drugs for β-Amyloid in Alzheimer's Disease. *Peptides* **2010**, *31* (10), 1866–1872.

(160) Taylor, M.; Moore, S.; Mayes, J.; Parkin, E.; Beeg, M.; Canovi, M.; Gobbi, M.; Mann, D. M. A.; Allsop, D. Development of a Proteolytically Stable Retro-Inverso Peptide Inhibitor of β-Amyloid Oligomerization as a Potential Novel Treatment for Alzheimer's Disease. *Biochemistry* **2010**, *49* (15), 3261–3272.

(161) Parthsarathy, V.; McClean, P. L.; Hölscher, C.; Taylor, M.; Tinker, C.; Jones, G.; Kolosov, O.; Salvati, E.; Gregori, M.; Masserini, M.; Allsop, D. A Novel Retro-Inverso Peptide Inhibitor Reduces Amyloid Deposition, Oxidation and Inflammation and Stimulates Neurogenesis in the APPswe/PS1ΔE9 Mouse Model of Alzheimer's Disease. *PLOS One* **2013**, *8* (1), e54769.

(162) Kapurniotu, A.; Buck, A.; Weber, M.; Schmauder, A.; Hirsch, T.; Bernhagen, J.; Tatarek-Nossol, M. Conformational Restriction via Cyclization in β-Amyloid Peptide Aβ(1-28) Leads to an Inhibitor of Aβ(1-28) Amyloidogenesis and Cytotoxicity. *Chem. Biol.* **2003**, *10* (2), 149–159.

(163) Arai, T.; Sasaki, D.; Araya, T.; Sato, T.; Sohma, Y.; Kanai, M. A Cyclic KLVFF-Derived Peptide Aggregation Inhibitor Induces the Formation of Less-Toxic Off-Pathway

Amyloid-β Oligomers. *ChemBioChem* **2014**, *15* (17), 2577–2583.

(164) Horsley, J. R.; Jovcevski, B.; Wegener, K. L.; Yu, J.; Pukala, T. L.; Abell, A. D. Rationally Designed Peptide-Based Inhibitor of Aβ42 Fibril Formation and Toxicity: A Potential Therapeutic Strategy for Alzheimer's Disease. *Biochem. J.* **2020**, *477* (11), 2039–2054.

(165) Etienne, M. A.; Aucoin, J. P.; Fu, Y.; McCarley, R. L.; Hammer, R. P. Stoichiometric Inhibition of Amyloid β-Protein Aggregation with Peptides Containing Alternating α,α-Disubstituted Amino Acids. *J. Am. Chem. Soc.* **2006**, *128* (11), 3522–3523.

(166) Rangachari, V.; Davey, Z. S.; Healy, B.; Moore, B. D.; Sonoda, L. K.; Cusack, B.; Maharvi, G. M.; Fauq, A. H.; Rosenberry, T. L. Rationally Designed Dehydroalanine (ΔAla)-Containing Peptides Inhibit Amyloid-β (Aβ) Peptide Aggregation. *Biopolymers* **2009**, *91* (6), 456–465.

(167) Loureiro, J. A.; Crespo, R.; Börner, H.; Martins, P. M.; Rocha, F. A.; Coelho, M.; Pereira, M. C.; Rocha, S. Fluorinated Beta-Sheet Breaker Peptides. *J. Mater. Chem. B* **2014**, *2* (16), 2259–2264.

(168) Watanabe, K.; Nakamura, K.; Akikusa, S.; Okada, T.; Kodaka, M.; Konakahara, T.; Okuno, H. Inhibitors of Fibril Formation and Cytotoxicity of β-Amyloid Peptide Composed of KLVFF Recognition Element and Flexible Hydrophilic Disrupting Element. *Biochem. Biophys. Res. Commun.* **2002**, *290* (1), 121–124.

(169) Rajasekhar, K.; Suresh, S. N.; Manjithaya, R.; Govindaraju, T. Rationally Designed Peptidomimetic Modulators of Aβ Toxicity in Alzheimer's Disease. *Sci. Rep.* **2015**, *5* (1), 8139.

(170) Cheng, P.-N.; Liu, C.; Zhao, M.; Eisenberg, D.; Nowick, J. S. Amyloid β-Sheet Mimics That Antagonize Protein Aggregation and Reduce Amyloid Toxicity. *Nature. Chem.* **2012**, *4* (11), 927–933.

(171) Vahdati, L.; Kaffy, J.; Brinet, D.; Bernadat, G.; Correia, I.; Panzeri, S.; Fanelli, R.; Lequin, O.; Taverna, M.; Ongeri, S.; Piarulli, U. Synthesis and Characterization of Hairpin Mimics That Modulate the Early Oligomerization and Fibrillization of Amyloid β-Peptide. *Eur. J. Org. Chem.* **2017**, *2017* (20), 2971–2980.

(172) Pellegrino, S.; Tonali, N.; Erba, E.; Kaffy, J.; Taverna, M.; Contini, A.; Taylor, M.; Allsop, D.; L. Gelmi, M.; Ongeri, S. β-Hairpin Mimics Containing a Piperidine–Pyrrolidine Scaffold Modulate the β-Amyloid Aggregation Process Preserving the Monomer Species. *Chem. Sci.* **2017**, *8* (2), 1295–1302.

(173) Goyal, D.; Shuaib, S.; Mann, S.; Goyal, B. Rationally Designed Peptides and Peptidomimetics as Inhibitors of Amyloid-β (Aβ) Aggregation: Potential Therapeutics of Alzheimer's Disease. *ACS Comb. Sci.* **2017**, *19* (2), 55–80.

(174) Das, K. P.; Surewicz, W. K. Temperature-Induced Exposure of Hydrophobic Surfaces and Its Effect on the Chaperone Activity of α-Crystallin. *FEBS Letters* **1995**, *369* (2), 321–325.

(175) Santhoshkumar, P.; Sharma, K. K. Inhibition of Amyloid Fibrillogenesis and Toxicity by a Peptide Chaperone. *Mol. Cell. Biochem.* **2004**, *267* (1), 147–155.

(176) Candeias, E.; Duarte, A. I.; Sebastião, I.; Fernandes, M. A.; Plácido, A. I.; Carvalho, C.; Correia, S.; Santos, R. X.; Seiça, R.; Santos, M. S.; Oliveira, C. R.; Moreira, P. I. Middle-Aged Diabetic Females and Males Present Distinct Susceptibility to Alzheimer Disease-like Pathology. *Mol. Neurobiol.* **2017**, *54* (8), 6471–6489.

(177) Yan, L.-M.; Velkova, A.; Tatarek-Nossol, M.; Andreetto, E.; Kapurniotu, A. IAPP Mimic Blocks Aβ Cytotoxic Self-Assembly: Cross-Suppression of Amyloid Toxicity of Aβ and IAPP Suggests a Molecular Link between Alzheimer's Disease and Type II Diabetes. *Angew. Chem. Int. Ed.* **2007**, *46* (8), 1246–1252.

(178) Andreetto, E.; Yan, L.-M.; Tatarek-Nossol, M.; Velkova, A.; Frank, R.; Kapurniotu, A. Identification of Hot Regions of the Aβ-IAPP Interaction Interface as High-Affinity Binding Sites in Both Cross- and Self-Association. *Angew. Chem. Int. Ed.* **2010**, *49* (17), 3081–3085.

(179) Andreetto, E.; Yan, L.-M.; Caporale, A.; Kapurniotu, A. Dissecting the Role of Single Regions of an IAPP Mimic and IAPP in Inhibition of Aβ40 Amyloid Formation and Cytotoxicity. *ChemBioChem* **2011**, *12* (9), 1313–1322.

(180) Andreetto, E.; Malideli, E.; Yan, L.-M.; Kracklauer, M.; Farbiarz, K.; Tatarek-Nossol, M.; Rammes, G.; Prade, E.; Neumüller, T.; Caporale, A.; Spanopoulou, A.; Bakou, M.; Reif, B.; Kapurniotu, A. A Hot-Segment-Based Approach for the Design of Cross-Amyloid Interaction Surface Mimics as Inhibitors of Amyloid Self-Assembly. *Angew. Chem. Int. Ed.* **2015**, *54* (44), 13095–13100.

(181) Spanopoulou, A.; Heidrich, L.; Chen, H.-R.; Frost, C.; Hrle, D.; Malideli, E.; Hille, K.; Grammatikopoulos, A.; Bernhagen, J.; Zacharias, M.; Rammes, G.; Kapurniotu, A. Designed Macrocyclic Peptides as Nanomolar Amyloid Inhibitors Based on Minimal Recognition Elements. *Angew. Chem. Int. Ed.* **2018**, *57* (44), 14503–14508.

(182) Schwarzman, A. L.; Tsiper, M.; Gregori, L.; Goldgaber, D.; Frakowiak, J.; Mazur-Kolecka, B.; Taraskina, A.; Pchelina, S.; Vitek, M. P. Selection of Peptides Binding to the Amyloid B-Protein Reveals Potential Inhibitors of Amyloid Formation. *Amyloid* **2005**, *12* (4), 199–209.

(183) Kumar, S.; Henning-Knechtel, A.; Chehade, I.; Magzoub, M.; Hamilton, A. D. Foldamer-Mediated Structural Rearrangement Attenuates Aβ Oligomerization and Cytotoxicity. *J. Am. Chem. Soc.* **2017**, *139* (47), 17098–17108.

(184) Kumar, S.; Hamilton, A. D. α-Helix Mimetics as Modulators of Aβ Self-Assembly. *J. Am. Chem. Soc.* **2017**, *139* (16), 5744–5755.

(185) Fülöp, L.; Mándity, I. M.; Juhász, G.; Szegedi, V.; Hetényi, A.; Wéber, E.; Bozsó, Z.; Simon, D.; Benkő, M.; Király, Z.; Martinek, T. A. A Foldamer-Dendrimer Conjugate Neutralizes Synaptotoxic β-Amyloid Oligomers. *PLOS One* **2012**, *7* (7), e39485.

(186) Kaffy, J.; Berardet, C.; Mathieu, L.; Legrand, B.; Taverna, M.; Halgand, F.; Van Der Rest, G.; Maillard, L. T.; Ongeri, S. Helical γ-Peptide Foldamers as Dual Inhibitors of Amyloid-β Peptide and Islet Amyloid Polypeptide Oligomerization and Fibrillization. *Eur. J. Chem.* **2020**, *26* (64), 14612–14622.

(187) Kanda, Y.; Goodman, D. S.; Canfield, R. E.; Morgan, F. J. The Amino Acid Sequence of Human Plasma Prealbumin. *J. Biol. Chem.* **1974**, *249* (21), 6796–6805.

(188) Chanoine, J.-P.; Alex, S.; Fang, S.-L.; Stone, S.; Leonard, J. L.; Körhle, J.; Braverman, L. E. Role of Transthyretin in the Transport of Thyroxine from the Blood to the Choroid Plexus, the Cerebrospinal Fluid, and the Brain. *Endocrinology* **1992**, *130* (2), 933–938.

(189) Monaco, H. L.; Rizzi, M.; Coda, A. Structure of a Complex of Two Plasma Proteins: Transthyretin and Retinol-Binding Protein. *Science* **1995**, *268* (5213), 1039–1041.

(190) Plante-Bordeneuve, V. Update in the Diagnosis and Management of Transthyretin

Familial Amyloid Polyneuropathy. *J. Neurol.* **2014**, *261* (6), 1227–1233.

(191) Planté-Bordeneuve, V.; Said, G. Familial Amyloid Polyneuropathy. *Lancet Neurol.* **2011**, *10* (12), 1086–1097.

(192) Jiang, X.; Buxbaum, J. N.; Kelly, J. W. The V122I Cardiomyopathy Variant of Transthyretin Increases the Velocity of Rate-Limiting Tetramer Dissociation, Resulting in Accelerated Amyloidosis. *Proc. Natl. Acad. Sci. U.S.A.* **2001**, *98* (26), 14943–14948.

(193) Reixach, N.; Deechongkit, S.; Jiang, X.; Kelly, J. W.; Buxbaum, J. N. Tissue Damage in the Amyloidoses: Transthyretin Monomers and Nonnative Oligomers Are the Major Cytotoxic Species in Tissue Culture. *Proc. Natl. Acad. Sci. U.S.A.* **2004**, *101* (9), 2817–2822.

(194) Quintas, A.; Vaz, D. C.; Cardoso, I.; Saraiva, M. J. M.; Brito, R. M. Tetramer Dissociation and Monomer Partial Unfolding Precedes Protofibril Formation in Amyloidogenic Transthyretin Variants. *J. Biol. Chem.* **2001**, *276* (29), 27207–27213.

(195) Riisøen, H. Reduced Prealbumin (Transthyretin) in CSF of Severely Demented Patients with Alzheimer's Disease. *Acta Neurol. Scand.* **1988**, *78* (6), 455–459.

(196) Link, C. D. Expression of Human Beta-Amyloid Peptide in Transgenic Caenorhabditis Elegans. *Proc. Natl. Acad. Sci. U.S.A.* **1995**, *92* (20), 9368–9372.

(197) Stein, T. D.; Johnson, J. A. Lack of Neurodegeneration in Transgenic Mice Overexpressing Mutant Amyloid Precursor Protein Is Associated with Increased Levels of Transthyretin and the Activation of Cell Survival Pathways. *J. Neurosci.* **2002**, *22* (17), 7380–7388.

(198) Stein, T. D.; Anders, N. J.; DeCarli, C.; Chan, S. L.; Mattson, M. P.; Johnson, J. A. Neutralization of Transthyretin Reverses the Neuroprotective Effects of Secreted Amyloid Precursor Protein (APP) in APPSW Mice Resulting in Tau Phosphorylation and Loss of Hippocampal Neurons: Support for the Amyloid Hypothesis. *J. Neurosci.* **2004**, *24* (35), 7707–7717.

(199) Choi, S. H.; Leight, S. N.; Lee, V. M.-Y.; Li, T.; Wong, P. C.; Johnson, J. A.; Saraiva, M. J.; Sisodia, S. S. Accelerated A Deposition in APPswe/PS1 E9 Mice with Hemizygous Deletions of TTR (Transthyretin). *J. Neurosci.* **2007**, *27* (26), 7006–7010.

(200) Schwarzman, A. L.; Gregori, L.; Vitek, M. P.; Lyubski, S.; Strittmatter, W. J.; Enghilde, J. J.; Bhasin, R.; Silverman, J.; Weisgraber, K. H.; Coyle, P. K. Transthyretin Sequesters Amyloid Beta Protein and Prevents Amyloid Formation. *Proc. Natl. Acad. Sci. U.S.A.* **1994**, *91* (18), 8368–8372.

(201) Liu, L.; Murphy, R. M. Kinetics of Inhibition of β-Amyloid Aggregation by Transthyretin. *Biochemistry* **2006**, *45* (51), 15702–15709.

(202) Du, J.; Murphy, R. M. Characterization of the Interaction of β-Amyloid with Transthyretin Monomers and Tetramers. *Biochemistry* **2010**, *49* (38), 8276–8289.

(203) Yang, D. T.; Joshi, G.; Cho, P. Y.; Johnson, J. A.; Murphy, R. M. Transthyretin as Both a Sensor and a Scavenger of β-Amyloid Oligomers. *Biochemistry* **2013**, *52* (17), 2849–2861.

(204) Costa, R.; Gonçalves, A.; Saraiva, M. J.; Cardoso, I. Transthyretin Binding to A-Beta Peptide - Impact on A-Beta Fibrillogenesis and Toxicity. *FEBS Letters* **2008**, *582* (6), 936–942.

(205) Ribeiro, C. A.; Saraiva, M. J.; Cardoso, I. Stability of the Transthyretin Molecule as a Key

Factor in the Interaction with A-Beta Peptide-Relevance in Alzheimer's Disease. *PLOS One* **2012**, *7* (9).

(206) Cotrina, E. Y.; Gimeno, A.; Llop, J.; Jiménez-Barbero, J.; Quintana, J.; Valencia, G.; Cardoso, I.; Prohens, R.; Arsequell, G. Calorimetric Studies of Binary and Ternary Molecular Interactions between Transthyretin, Aβ Peptides, and Small-Molecule Chaperones toward an Alternative Strategy for Alzheimer's Disease Drug Discovery. *J. Med. Chem.* **2020**, *63* (6), 3205–3214.

(207) Costa, R.; Ferreira-da-Silva, F.; Saraiva, M. J.; Cardoso, I. Transthyretin Protects against A-Beta Peptide Toxicity by Proteolytic Cleavage of the Peptide: A Mechanism Sensitive to the Kunitz Protease Inhibitor. *PLOS One* **2008**, *3* (8).

(208) Alemi, M.; Gaiteiro, C.; Ribeiro, C. A.; Santos, L. M.; Gomes, J. R.; Oliveira, S. M.; Couraud, P.-O.; Weksler, B.; Romero, I.; Saraiva, M. J. Transthyretin Participates in Beta-Amyloid Transport from the Brain to the Liver-Involvement of the Low-Density Lipoprotein Receptor-Related Protein 1? *Sci. rep.* **2016**, *6*, 20164.

(209) Alemi, M.; Silva, S. C.; Santana, I.; Cardoso, I. Transthyretin Stability Is Critical in Assisting Beta Amyloid Clearance–Relevance of Transthyretin Stabilization in Alzheimer's Disease. *CNS Neurosci. Ther.* **2017**, *23* (7), 605–619.

(210) Ciccone, L.; Fruchart-Gaillard, C.; Mourier, G.; Savko, M.; Nencetti, S.; Orlandini, E.; Servent, D.; Stura, E. A.; Shepard, W. Copper Mediated Amyloid-β Binding to Transthyretin. *Sci. Rep.* **2018**, *8* (1), 13744.

(211) Li, X.; Zhang, X.; Ladiwala, A. R. A.; Du, D.; Yadav, J. K.; Tessier, P. M.; Wright, P. E.; Kelly, J. W.; Buxbaum, J. N. Mechanisms of Transthyretin Inhibition of-Amyloid Aggregation In Vitro. *J. Neurosci.* **2013**, *33* (50), 19423–19433.

(212) Garai, K.; Posey, A. E.; Li, X.; Buxbaum, J. N.; Pappu, R. V. Inhibition of Amyloid Beta Fibril Formation by Monomeric Human Transthyretin. *Protein Sci.* **2018**, *27* (7), 1252–1261.

(213) Cao, Q.; Anderson, D. H.; Liang, W. Y.; Chou, J.; Saelices, L. The Inhibition of Cellular Toxicity of Amyloid-β by Dissociated Transthyretin. *J. Biol. Chem.* **2020**, *295* (41), 14015–14024.

(214) Du, J.; Cho, P. Y.; Yang, D. T.; Murphy, R. M. Identification of Beta-Amyloid-Binding Sites on Transthyretin. *Protein Eng. Des. Sel.* **2012**, *25* (7), 337–345.

(215) Gimeno, A.; Santos, L. M.; Alemi, M.; Rivas, J.; Blasi, D.; Cotrina, E. Y.; Llop, J.; Valencia, G.; Cardoso, I.; Quintana, J. Insights on the Interaction between Transthyretin and Aβ in Solution. a Saturation Transfer Difference (Std) Nmr Analysis of the Role of Iododiflunisal. *J. Med. Chem.* **2017**, *60* (13), 5749–5758.

(216) Cho, P. Y.; Joshi, G.; Johnson, J. A.; Murphy, R. M. Transthyretin-Derived Peptides as β-Amyloid Inhibitors. *ACS Chem. Neurosci.* **2014**, *5* (7), 542–551.

(217) Cho, P. Y.; Joshi, G.; Boersma, M. D.; Johnson, J. A.; Murphy, R. M. A Cyclic Peptide Mimic of the β-Amyloid Binding Domain on Transthyretin. *ACS Chem. Neurosci.* **2015**, *6* (5), 778–789.

(218) Lu, X.; Brickson, C. R.; Murphy, R. M. TANGO-Inspired Design of Anti-Amyloid Cyclic Peptides. *ACS Chem. Neurosci.* **2016**, *7* (9), 1264–1274.

(219) Pate, K. M.; Kim, B. J.; Shusta, E. V.; Murphy, R. M. Transthyretin Mimetics as Anti-β-Amyloid Agents: A Comparison of Peptide and Protein Approaches. *ChemMedChem*

2018, *13* (9), 968–979.

(220) Pelay-Gimeno, M.; Glas, A.; Koch, O.; Grossmann, T. N. Structure-Based Design of Inhibitors of Protein–Protein Interactions: Mimicking Peptide Binding Epitopes. *Angew. Chem. Int. Ed.* **2015**, *54* (31), 8896–8927.

(221) Gellman, S. H. Foldamers: A Manifesto. *Acc. Chem. Res.* **1998**, *31* (4), 173–180.

(222) Gopalakrishnan, R.; Frolov, A. I.; Knerr, L.; Drury, W. J.; Valeur, E. Therapeutic Potential of Foldamers: From Chemical Biology Tools to Drug Candidates? *J. Med. Chem.* **2016**, *59* (21), 9599–9621.

(223) Bullock, B. N.; Jochim, A. L.; Arora, P. S. Assessing Helical Protein Interfaces for Inhibitor Design. *J. Am. Chem. Soc.* **2011**, *133* (36), 14220–14223.

(224) Seebach, D.; Overhand, M.; Kühnle, F. N. M.; Martinoni, B.; Oberer, L.; Hommel, U.; Widmer, H. β-Peptides: Synthesis by Arndt-Eistert Homologation with Concomitant Peptide Coupling. Structure Determination by NMR and CD Spectroscopy and by X-Ray Crystallography. Helical Secondary Structure of a β-Hexapeptide in Solution and Its Stability towards Pepsin. *Helv. Chim. Acta* **1996**, *79* (4), 913–941.

(225) Seebach, D.; Ciceri, P. E.; Overhand, M.; Jaun, B.; Rigo, D.; Oberer, L.; Hommel, U.; Amstutz, R.; Widmer, H. Probing the Helical Secondary Structure of Short-Chain β-Peptides. *Helv. Chim. Acta* **1996**, *79* (8), 2043–2066.

(226) Hintermann, T.; Seebach, D. Synthesis of a β-Hexapeptide from (R)-2-Aminomethyl-Alkanoic Acids and Structural Investigations. *Synlett* **1997**, *1997* (Sup. I), 437–438.

(227) Appella, D. H.; Christianson, L. A.; Karle, I. L.; Powell, D. R.; Gellman, S. H. β-Peptide Foldamers: Robust Helix Formation in a New Family of β-Amino Acid Oligomers. *J. Am. Chem. Soc.* **1996**, *118* (51), 13071–13072.

(228) Appella, D. H.; Christianson, L. A.; Klein, D. A.; Powell, D. R.; Huang, X.; Barchi, J. J.; Gellman, S. H. Residue-Based Control of Helix Shape in β-Peptide Oligomers. *Nature* **1997**, *387* (6631), 381–384.

(229) Mándity, I. M.; Fülöp, L.; Vass, E.; Tóth, G. K.; Martinek, T. A.; Fülöp, F. Building β-Peptide H10/12 Foldamer Helices with Six-Membered Cyclic Side-Chains: Fine-Tuning of Folding and Self-Assembly. *Org. Lett.* **2010**, *12* (23), 5584–5587.

(230) Kritzer, J. A.; Stephens, O. M.; Guarracino, D. A.; Reznik, S. K.; Schepartz, A. β-Peptides as Inhibitors of Protein–Protein Interactions. *Bioorg. Med. Chem.* **2005**, *13* (1), 11–16.

(231) Baldauf, C.; Günther, R.; Hofmann, H.-J. Helix Formation and Folding in γ-Peptides and Their Vinylogues. *Helv. Chim. Acta* **2003**, *86* (7), 2573–2588.

(232) Hanessian, S.; Luo, X.; Schaum, R.; Michnick, S. Design of Secondary Structures in Unnatural Peptides: Stable Helical γ-Tetra-, Hexa-, and Octapeptides and Consequences of α-Substitution. *J. Am. Chem. Soc.* **1998**, *120* (33), 8569–8570.

(233) Vasudev, P. G.; Shamala, N.; Ananda, K.; Balaram, P. C9 Helices and Ribbons in γ-Peptides: Crystal Structures of Gabapentin Oligomers. *Angew. Chem. Int. Ed.* **2005**, *44* (31), 4972–4975.

(234) Sharma, G. V. M.; Jayaprakash, P.; Narsimulu, K.; Ravi Sankar, A.; Ravinder Reddy, K.; Radha Krishna, P.; Kunwar, A. C. A Left-Handed 9-Helix in γ-Peptides: Synthesis and Conformational Studies of Oligomers with Dipeptide Repeats of C-Linked Carbo-Γ4-Amino Acids and γ-Aminobutyric Acid. *Angew. Chem. Int. Ed.* **2006**, *45* (18), 2944–2947.

(235) De Pol, S.; Zorn, C.; Klein, C. D.; Zerbe, O.; Reiser, O. Surprisingly Stable Helical Conformations in α/β-Peptides by Incorporation of Cis-β-Aminocyclopropane Carboxylic Acids. *Angew. Chem. Int. Ed.* **2004**, *43* (4), 511–514.

(236) Hayen, A.; Schmitt, M. A.; Ngassa, F. N.; Thomasson, K. A.; Gellman, S. H. Two Helical Conformations from a Single Foldamer Backbone: "Split Personality" in Short α/β-Peptides. *Angew. Chem. Int. Ed.* **2004**, *43* (4), 505–510.

(237) Schmitt, M. A.; Choi, S. H.; Guzei, I. A.; Gellman, S. H. Residue Requirements for Helical Folding in Short α/β-Peptides: Crystallographic Characterization of the 11-Helix in an Optimized Sequence. *J. Am. Chem. Soc.* **2005**, *127* (38), 13130–13131.

(238) Schmitt, M. A.; Choi, S. H.; Guzei, I. A.; Gellman, S. H. New Helical Foldamers: Heterogeneous Backbones with 1:2 and 2:1 α:β-Amino Acid Residue Patterns. *J. Am. Chem. Soc.* **2006**, *128* (14), 4538–4539.

(239) Roy, R. S.; Karle, I. L.; Raghothama, S.; Balaram, P. α,β Hybrid Peptides: A Polypeptide Helix with a Central Segment Containing Two Consecutive β-Amino Acid Residues. *Proc. Natl. Acad. Sci. U.S.A.* **2004**, *101* (47), 16478–16482.

(240) Baldauf, C.; Günther, R.; Hofmann, H.-J. Helix Formation in α,γ- and β,γ-Hybrid Peptides: Theoretical Insights into Mimicry of α- and β-Peptides. *J. Org. Chem.* **2006**, *71* (3), 1200–1208.

(241) Sharma, G. V. M.; Jadhav, V. B.; Ramakrishna, K. V. S.; Jayaprakash, P.; Narsimulu, K.; Subash, V.; Kunwar, A. C. 12/10- and 11/13-Mixed Helices in α/γ- and β/γ-Hybrid Peptides Containing C-Linked Carbo-γ-Amino Acids with Alternating α- and β-Amino Acids. *J. Am. Chem. Soc.* **2006**, *128* (45), 14657–14668.

(242) Grison, C. M.; Robin, S.; Aitken, D. J. 13-Helix Folding of a β/γ-Peptide Manifold Designed from a "Minimal-Constraint" Blueprint. *Chem. Commun.* **2016**, *52*, 7802–7805.

(243) Grison, C. M.; Miles, J. A.; Robin, S.; Wilson, A. J.; Aitken, D. J. An α-Helix-Mimicking 12,13-Helix: Designed α/β/γ-Foldamers as Selective Inhibitors of Protein–Protein Interactions. *Angew. Chem. Int. Ed.* **2016**, *55* (37), 11096–11100.

(244) Sui, Q.; Borchardt, D.; Rabenstein, D. L. Kinetics and Equilibria of Cis/Trans Isomerization of Backbone Amide Bonds in Peptoids. *J. Am. Chem. Soc.* **2007**, *129* (39), 12042–12048.

(245) Gorske, B. C.; Bastian, B. L.; Geske, G. D.; Blackwell, H. E. Local and Tunable N→π* Interactions Regulate Amide Isomerism in the Peptoid Backbone. *J. Am. Chem. Soc.* **2007**, *129* (29), 8928–8929.

(246) Armand, P.; Kirshenbaum, K.; Falicov, A.; Dunbrack, R. L.; Dill, K. A.; Zuckermann, R. N.; Cohen, F. E. Chiral N-Substituted Glycines Can Form Stable Helical Conformations. *Fold Des.* **1997**, *2* (6), 369–375.

(247) Armand, P.; Kirshenbaum, K.; Goldsmith, R. A.; Farr-Jones, S.; Barron, A. E.; Truong, K. T. V.; Dill, K. A.; Mierke, D. F.; Cohen, F. E.; Zuckermann, R. N.; Bradley, E. K. NMR Determination of the Major Solution Conformation of a Peptoid Pentamer with Chiral Side Chains. *Proc. Natl. Acad. Sci. U.S.A.* **1998**, *95* (8), 4309–4314.

(248) Stringer, J. R.; Crapster, J. A.; Guzei, I. A.; Blackwell, H. E. Extraordinarily Robust Polyproline Type I Peptoid Helices Generated via the Incorporation of α-Chiral Aromatic N-1-Naphthylethyl Side Chains. *J. Am. Chem. Soc.* **2011**, *133* (39), 15559–

15567.

(249) Wu, C. W.; Kirshenbaum, K.; Sanborn, T. J.; Patch, J. A.; Huang, K.; Dill, K. A.; Zuckermann, R. N.; Barron, A. E. Structural and Spectroscopic Studies of Peptoid Oligomers with α-Chiral Aliphatic Side Chains. *J. Am. Chem. Soc.* **2003**, *125* (44), 13525–13530.

(250) Hara, T.; Durell, S. R.; Myers, M. C.; Appella, D. H. Probing the Structural Requirements of Peptoids That Inhibit HDM2–p53 Interactions. *J. Am. Chem. Soc.* **2006**, *128* (6), 1995–2004.

(251) Laursen, J. S.; Engel-Andreasen, J.; Fristrup, P.; Harris, P.; Olsen, C. A. Cis–Trans Amide Bond Rotamers in β-Peptoids and Peptoids: Evaluation of Stereoelectronic Effects in Backbone and Side Chains. *J. Am. Chem. Soc.* **2013**, *135* (7), 2835–2844.

(252) Laursen, J. S.; Harris, P.; Fristrup, P.; Olsen, C. A. Triangular Prism-Shaped β-Peptoid Helices as Unique Biomimetic Scaffolds. *Nat. Commun.* **2015**, *6* (1), 7013.

(253) Violette, A.; Averlant-Petit, M. C.; Semetey, V.; Hemmerlin, C.; Casimir, R.; Graff, R.; Marraud, M.; Briand, J.-P.; Rognan, D.; Guichard, G. N,N'-Linked Oligoureas as Foldamers: Chain Length Requirements for Helix Formation in Protic Solvent Investigated by Circular Dichroism, NMR Spectroscopy, and Molecular Dynamics. *J. Am. Chem. Soc.* **2005**, *127* (7), 2156–2164.

(254) Pendem, N.; Douat, C.; Claudon, P.; Laguerre, M.; Castano, S.; Desbat, B.; Cavagnat, D.; Ennifar, E.; Kauffmann, B.; Guichard, G. Helix-Forming Propensity of Aliphatic Urea Oligomers Incorporating Noncanonical Residue Substitution Patterns. *J. Am. Chem. Soc.* **2013**, *135* (12), 4884–4892.

(255) Fischer, L.; Claudon, P.; Pendem, N.; Miclet, E.; Didierjean, C.; Ennifar, E.; Guichard, G. The Canonical Helix of Urea Oligomers at Atomic Resolution: Insights into Folding-Induced Axial Organization. *Angew. Chem. Int. Ed.* **2010**, *49* (6), 1067–1070.

(256) Fremaux, J.; Mauran, L.; Pulka-Ziach, K.; Kauffmann, B.; Odaert, B.; Guichard, G. α-Peptide–Oligourea Chimeras: Stabilization of Short α-Helices by Non-Peptide Helical Foldamers. *Angew. Chem. Int. Ed.* **2015**, *54* (34), 9816–9820.

(257) Cussol, L.; Mauran-Ambrosino, L.; Buratto, J.; Belorusova, A. Y.; Neuville, M.; Osz, J.; Fribourg, S.; Fremaux, J.; Dolain, C.; Goudreau, S. R.; Rochel, N.; Guichard, G. Structural Basis for α-Helix Mimicry and Inhibition of Protein–Protein Interactions with Oligourea Foldamers. *Angew. Chem. Int. Ed.* **2021**, *60* (5), 2296–2303.

(258) Li, X.; Yang, D. Peptides of Aminoxy Acids as Foldamers. *Chem. Commun. (Camb)* **2006**, No. 32, 3367–3379.

(259) Thormann, M.; Hofmann, H.-J. Conformational Properties of Azapeptides. *J. Mol. Struct.: THEOCHEM* **1999**, *469* (1), 63–76.

(260) Reynolds, C. H.; Hormann, R. E. Theoretical Study of the Structure and Rotational Flexibility of Diacylhydrazines: Implications for the Structure of Nonsteroidal Ecdysone Agonists and Azapeptides. *J. Am. Chem. Soc.* **1996**, *118* (39), 9395–9401.

(261) Benatalah, Z.; Aubry, A.; Boussard, G.; Marraud, M. Evidence for a β-Turn in an Azadipeptide Sequence. *Int. J. Pept. Protein Res.* **1991**, *38* (6), 603–605.

(262) André, F.; Boussard, G.; Bayeul, D.; Didierjean, C.; Aubry, A.; Marraud, M. Aza-Peptides II. X-Ray Structures of Aza-Alanine and Aza-Asparagine-Containing Peptides. *J. Pept. Res.* **1997**, *49* (6), 556–562.

(263) André, F.; Vicherat, A.; Boussard, G.; Aubry, A.; Marraud, M. Aza-Peptides. III.

Experimental Structural Analysis of Aza-Alanme and Aza-Asparagine-Containing Peptides. *J. Pept. Res.* **1997**, *50* (5), 372–381.

(264) Lee, H.-J.; Song, J.-W.; Choi, Y.-S.; Park, H.-M.; Lee, K.-B. A Theoretical Study of Conformational Properties of N-Methyl Azapeptide Derivatives. *J. Am. Chem. Soc.* **2002**, *124* (40), 11881–11893.

(265) Zhang, Y.; Malamakal, R. M.; Chenoweth, D. M. Aza-Glycine Induces Collagen Hyperstability. *J. Am. Chem. Soc.* **2015**, *137* (39), 12422–12425.

(266) Harris, T.; Chenoweth, D. M. Sterics and Stereoelectronics in Aza-Glycine: Impact of Aza-Glycine Preorganization in Triple Helical Collagen. *J. Am. Chem. Soc.* **2019**, *141* (45), 18021–18029.

(267) Tonali, N.; Correia, I.; Lesma, J.; Bernadat, G.; Ongeri, S.; Lequin, O. Introducing Sequential Aza-Amino Acids Units Induces Repeated β-Turns and Helical Conformations in Peptides. *Org. Biomol. Chem.* **2020**, *18* (18), 3452–3458.

(268) Li, X.; Chen, S.; Zhang, W.-D.; Hu, H.-G. Stapled Helical Peptides Bearing Different Anchoring Residues. *Chem. Rev.* **2020**, *120* (18), 10079–10144.

(269) Taylor, J. W. The Synthesis and Study of Side-Chain Lactam-Bridged Peptides. *Pept. Sci.* **2002**, *66* (1), 49–75.

(270) Blackwell, H. E.; Grubbs, R. H. Highly Efficient Synthesis of Covalently Cross-Linked Peptide Helices by Ring-Closing Metathesis. *Angew. Chem. Int. Ed.* **1998**, *37* (23), 3281–3284.

(271) Hu, K.; Geng, H.; Zhang, Q.; Liu, Q.; Xie, M.; Sun, C.; Li, W.; Lin, H.; Jiang, F.; Wang, T.; Wu, Y.-D.; Li, Z. An In-Tether Chiral Center Modulates the Helicity, Cell Permeability, and Target Binding Affinity of a Peptide. *Angew. Chem. Int. Ed.* **2016**, *55* (28), 8013–8017.

(272) Bouclier, C.; Simon, M.; Laconde, G.; Pellerano, M.; Diot, S.; Lantuejoul, S.; Busser, B.; Vanwonterghem, L.; Vollaire, J.; Josserand, V.; Legrand, B.; Coll, J.-L.; Amblard, M.; Hurbin, A.; Morris, M. C. Stapled Peptide Targeting the CDK4/Cyclin D Interface Combined with Abemaciclib Inhibits KRAS Mutant Lung Cancer Growth. *Theranostics* **2020**, *10* (5), 2008–2028.

Chapter 2

Design, synthesis and conformational studies of aqueous soluble diaza-tripeptides exhibiting β-turn structure

Design and synthesis of peptidomimetics capable of mimicking the structures of the key recognition surfaces of proteins is a promising strategy to interfere with pathological PPIs. As we mentioned in section 1.5.2, azapeptides are good alternatives to natural peptides to stabilize some specific conformations. Previous studies in our laboratory have demonstrated that the tripeptides containing two consecutive aza-amino acids (diaza-peptide unit) are able to stabilize sequential β-turn structures, thus proving the interesting potentiality of diaza-peptide units in the design of peptidomimetic foldamers.[1] In this chapter, we would like to investigate the possibility of diaza-peptide units to maintain their folding properties even in water, which is more challenging due to the easy loss of hydrogen bonds. Three diaza-tripeptides with improved aqueous solubility were designed and synthesized. A conformational investigation through NMR analysis in water have been performed. The result is of particular importance for the future design of longer peptidomimetics with biological interest.

2.1 Design of diaza-tripeptides with improved aqueous solubility

As we mentioned in the chapter 1, due to the conformational constraint of aza-amino acids, the preferential structure of azapeptides is β-turn structure. Previously, our laboratory designed several tripeptides containing two consecutive aza-amino acids, which are termed as diaza-tripeptides (**Figure 2.1**).[1] The conformational studies, performed by a combination of NMR in CD_3OH, X-ray and MM/DFT calculation, demonstrated that, compared to the disordered structure of natural peptide **2.1**, diaza-tripeptide **2.2**, having side chain on α-nitrogen, shows two major conformers (**Figure 2.2A**): conformer A adopting a double β-turn structure stabilized by two 10-membered hydrogen bonds (the first one is formed between the carbonyl group of the Boc and the NH of the Val, the second one is formed between the carbonyl group of the azaVal and one carboxamide proton of the Val), whereas conformer B displaying only a single β-turn motif, due to the absence of the

second hydrogen bond. The twisted conformation around N-N bonds of aza-amino acids induce favored ϕ dihedral angles around ±90°. The ψ dihedral angles are restricted around 0° thanks to the presence of lateral chains (azaVal and azaAla). In conformer A, the two aza-residues have negative ϕ dihedral angles, which compatible with type I β-turn. Positive ϕ dihedral angles for the two aza-residues in conformer B are compatible with type I′ β-turn. The diaza-tripeptide **2.3** without side chains on aza-residues results in a more flexible and extended conformation. These results suggest that the introduction of two sequential N-substituted aza-amino acids into a peptide sequence can induce double β-turn structure or single β-turn structure. In addition, the conformational analysis of aza-hexapeptide **2.4** (**Figure 2.1**) comprising two diaza-tripeptide bricks showed the potentiality of aza/aza/α bricks to adopt hydrogen-bonded structures in longer peptides. This compound was proven to adopt repeated β-turns or fully helical structure, similar to a 3_{10}-helix (**Figure 2.2B**).

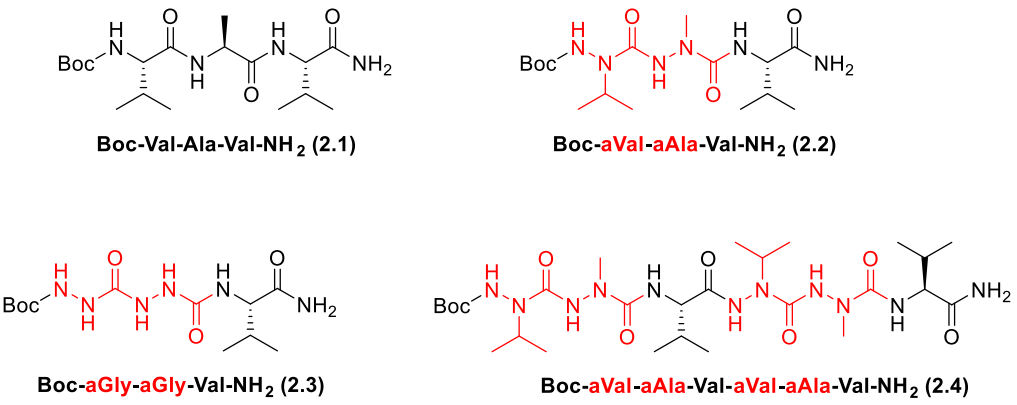

Figure 2.1: The diaza-tripeptides reported by our laboratory before

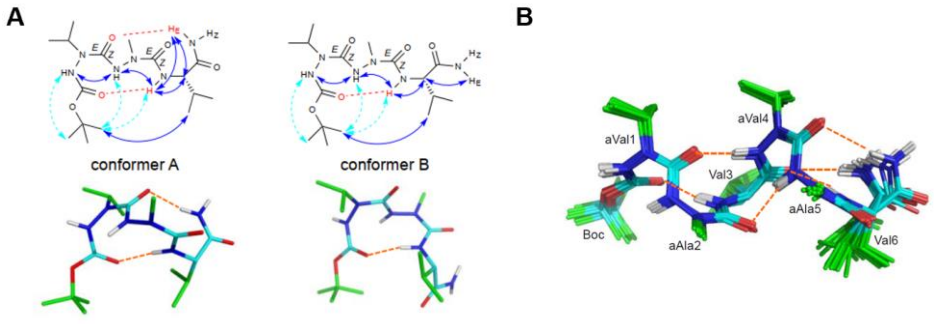

Figure 2.2: A) The two conformers of **2.2**, conformer A is a double β-turn structure whereas conformers B is a single β-turn structure; B) 3_{10}-Helix adopted by **2.4**

Because of the hydrophobic character of their side chains, these diaza-tripeptides have low aqueous solubility which prevented their NMR analysis in water. Conformational analysis in water is challenging but at the same time very interesting because it might be better to predict the conformations of peptides and peptidomimetics adopted in physiological conditions. Water is a major component in extracellular and intracellular media. In physiological conditions, most of the biomacromolecules and small drug entities carry out their biological function in aqueous medium. In general, drug candidates should have good aqueous solubility to get good ADMET properties (absorption, distribution, metabolism, elimination and toxicity) after administration in human bodies. Therefore, we sought to design and synthesize several aqueous soluble diaza-tripeptides and study their conformations in water by NMR to verify the stability of β-turn structures of diaza-tripeptides even in water. The conformations of these compounds will be also studied in methanol (protic solvent similar to water) for the comparison with previous studies.[1]

In order to improve the aqueous solubility of diaza-tripeptide **2.2**, we used more hydrophilic residues, acetylated azaLys and amidated serine, instead of Boc protected N-terminal azaVal and amidated C-terminal Val respectively. In the meanwhile, we placed different aza-residues in the central part of the tripeptides, including azaGly, azaAla and azaLeu **(Figure 2.3)**, to investigate the influence of the side chains of the central aza-residues on the conformation.

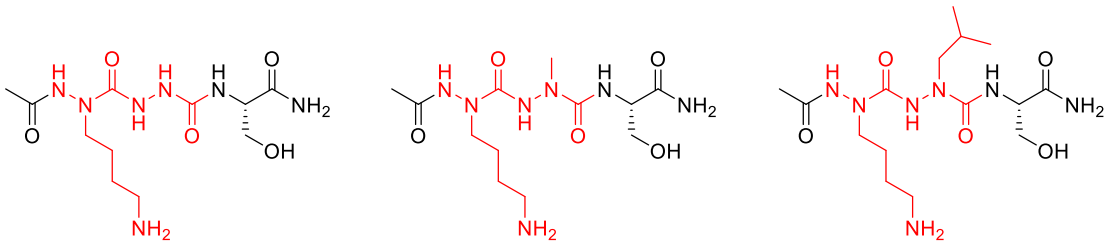

Figure 2.3: Structure of diaza-tripeptides designed to increase of aqueous solubility

2.2 Chemistry and synthetic strategies for diaza-tripeptides

The chemistry of azapeptides is mainly based on the synthesis of the corresponding protected-

1-alkylhydrazines or protected-2-alkylhydrazines and then coupling them to other protected hydrazines or natural amino acids. The main method to get the corresponding protected-2-alkylhydrazines is to performed a reductive amination from protected hydrazines with corresponding aldehydes or ketones, which has been reviewed and concluded very well in literature (**Figure 2.4**). [2–4]

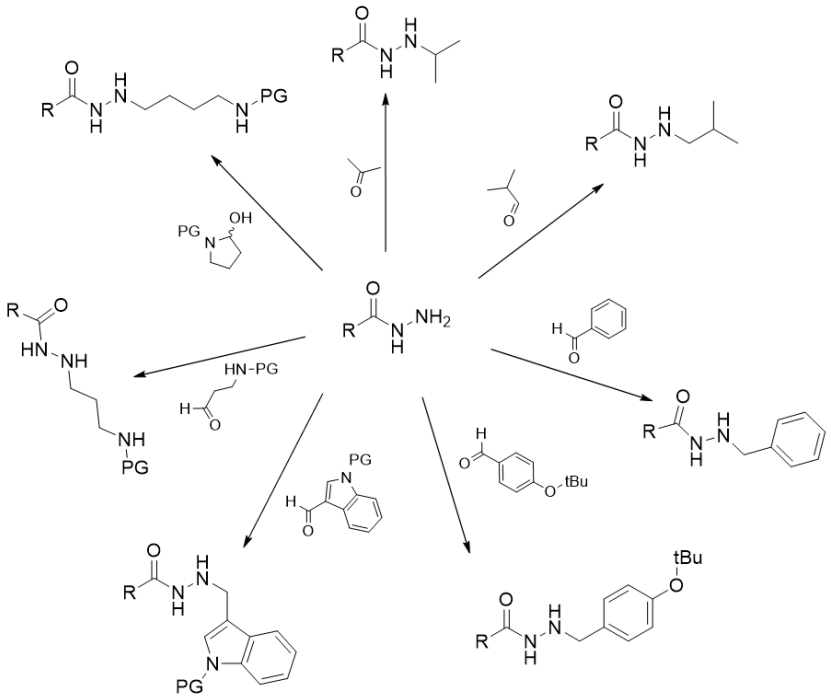

Figure 2.4: Reductive amination of protected hydrazines with different aldehydes or ketones provides various protected-2-alkylhydrazines

The coupling reactions can be divided into two classes: 1) coupling between two protected hydrazines; 2) coupling between protected hydrazines and natural amino acids (**Figure 2.5**). The coupling between two protected hydrazines need to activate one of protected hydrazines by carbonyl donors (phenyl chloroformate, 4-nitrophenyl chloroformate, phosgene, etc.) to obtain active carbamates or isocyanates, then using these active intermediates to react with another protected hydrazine. For the coupling between protected hydrazines and natural amino acids, the coupling will use different types of activating agents depending on the relative position of natural residues with aza-residues. When natural residues are at the C-terminus of aza-residues, the coupling between them need also carbonyl donors as activating reagents, whereas the peptide in which natural

residues are at the N-terminus of aza-residues, the natural amino acids should be activated by classical coupling reagents such as guanidinium and uronium salt (HCTU), carbodiimides (DCC or DIC). In our case, the diaza-tripeptides have natural residues at the C-terminus, so carbonyl donors were used as activating reagents.

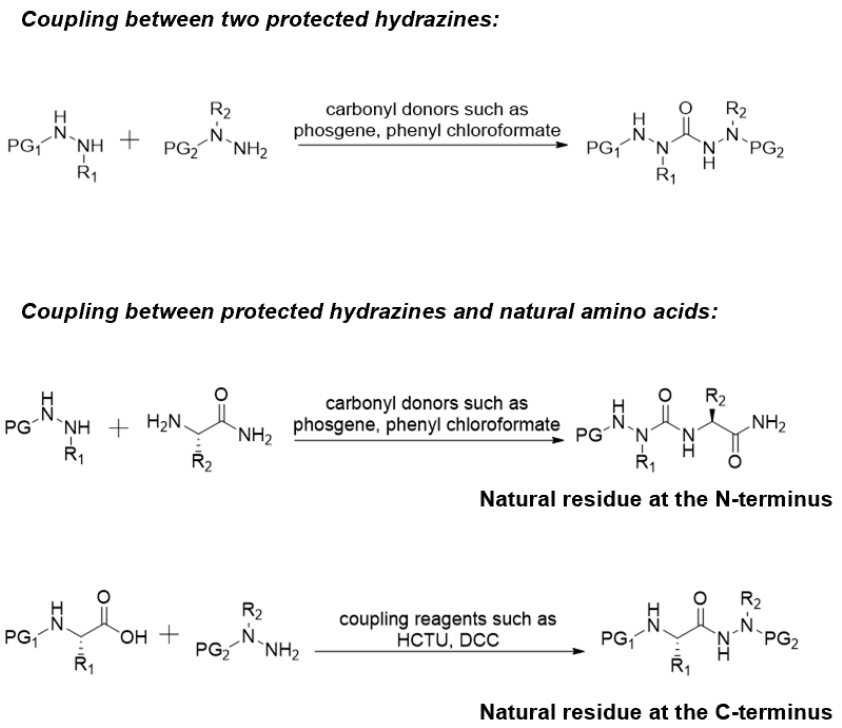

Figure 2.5: Two types of activating reagents used for coupling protected hydrazines

According to our previous result[5], there are two strategies to synthesize diaza-tripeptides (**Figure 2.6**). For strategy A in which the coupling starts from the N-terminus to the C-terminus, the first coupling between the N-terminal fragment and the middle fragment A gives diazapeptide fragment, which is used to couple with the C-terminal natural amino acid. Conversely, in strategy B (from the C-terminus to the N-terminus), the first coupling between the C-terminal natural amino acid and the middle fragment B provides the aza-dipeptide fragment to do the later coupling reaction with the N-terminal fragment. Here we first chose to synthesize the diaza-tripeptides using the strategy A because the strategy A has been proven with good yields in our laboratory.[5] We also tried to synthesize the diaza-tripeptides through the strategy B to evaluate the pros and cons between these two strategies. These two strategies use the same N-terminal fragment (acetyl azaLys precursor

in our case) and C-terminal fragment (amidated serine in our case) but different middle fragments (**Figure 2.6**).

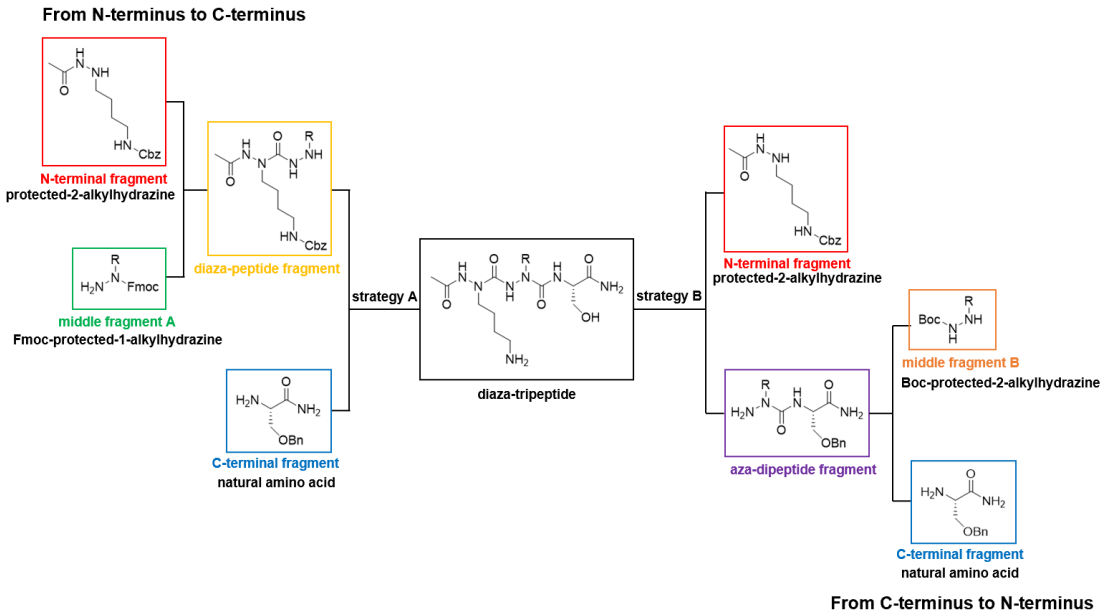

Figure 2.6: Two synthetic strategies to get the diaza-tripeptides **2.5**, **2.6** and **2.7**

2.3 Synthesis of diaza-tripeptides through the strategy A

2.3.1 Synthesis of the N-terminal fragment

Although there is no report about the synthesis of the N-terminal fragment **2.12b** (acetyl azaLys precursor), our laboratory has reported that Boc-protected azaLys precursor **2.12a** could be synthesized from the reductive amination of hemiacetal **2.9** with *t*-butyl carbazate in a moderate yield of 58% (**Figure 2.7A**).[5,6] The moderate yield of this reaction is ascribed to the lower reactivity of the hemiacetal compared to aldehydes or ketones. The use of hemiacetal **2.9** in this reaction is prefered due to an equilibrium between Cbz-protected 4-aminobutyraldehyde and hemiacetal **2.9** in acidic conditions which is used to transfer compound **2.8** to Cbz-protected 4-aminobutyraldehyde (**Figure 2.7B and Figure 2.8**). Cbz-protected 4-aminobutyraldehyde prefers to convert to hemiacetal **2.9** in acidic conditions. This always makes difficulty to get high yields of azaLys

precursor using reductive amination conditions. Nevertheless, we planned to synthesize acetyl azaLys precursor **2.12b** through the reductive amination of compound **2.9** with acetylhydrazide **2.11** (**Figure 2.8**).

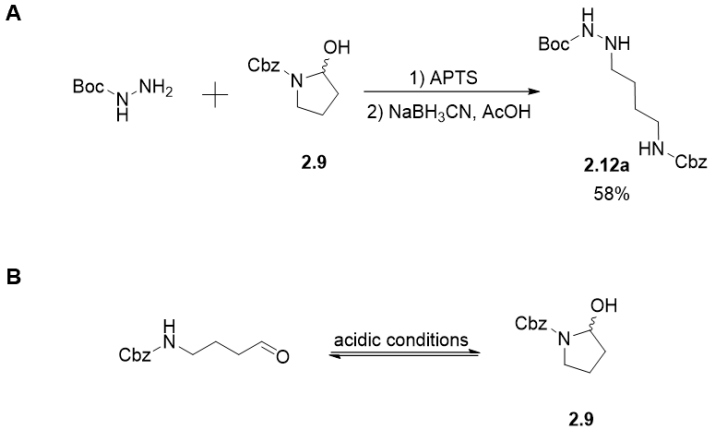

Figure 2.7: A) Synthesis of **2.12a** by reductive amination; B) Cbz-protected 4-aminobutyraldehyde have the propensity to convert to compound **2.9** in acidic conditions

The scheme of synthesis of **2.12b** is illustrated in **Figure 2.8**. The amino group of 4-aminobutyraldehyde diethylacetal was protected by Cbz group using benzyl chloroformate in the presence of TEA to provide compound **2.8** (Yield: 88%), which can be transformed to compound **2.9** in acidic conditions ($AcOH/H_2O$). In parallel, benzyl carbazate was acetylated using acetic anhydride and then the Cbz group was cleaved by catalytic hydrogenolysis to give **2.11**. Then the reductive amination reaction of compound **2.9** with compound **2.11** was performed firstly in THF using $NaBH_3CN$ as a reductive reagent and AcOH as an acidic catalyst but the target product was not obtained (**Table 2.1**, **Entry 1**). We hypothesized that the low acidity of AcOH for activating hemiacetal **2.9** prevents the reaction. Thus, a stronger acid, APTS, was tried in the reductive amination reaction. This time the reaction provided the target product but with only a 10% of yield (**Table 2.1**, **Entry 2**). Since the formation of imine (dehydration) in reductive amination reactions is reversable, the presence of water could make the equilibrium shifted to starting materials. To exclude the effect of water in the reaction, distilled THF was used but the yield was still very low (14%) (**Table 2.1**, **Entry 3**). Less APTS (0.25 eq) in the reaction made even lower the yield of the reaction (**Table 2.1**, **Entry 4**). We also tried MeOH instead of THF as solvent to increase the

solubility of $NaBH_3CN$ in the reactive solution, but the yield did not increase. (**Table 2.1**, **Entry 5**). We hypothesized that the lower yield of this reaction is probably attributed to the lower nucleophilicity of acetylhydrazide compared to *t*-butyl carbazate and the high aqueous solubility of the product **2.12b** which results in its partial loss during extraction.

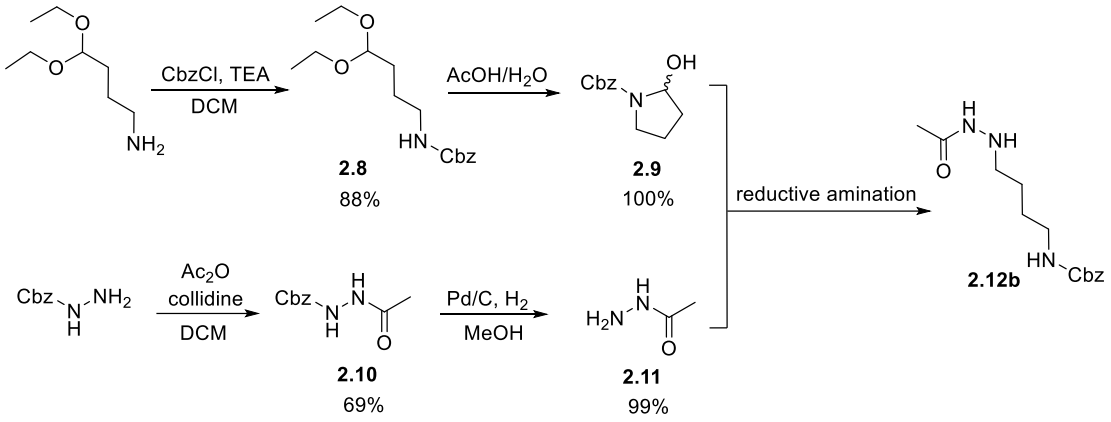

Figure 2.8: Scheme of the synthesis of **2.12b**

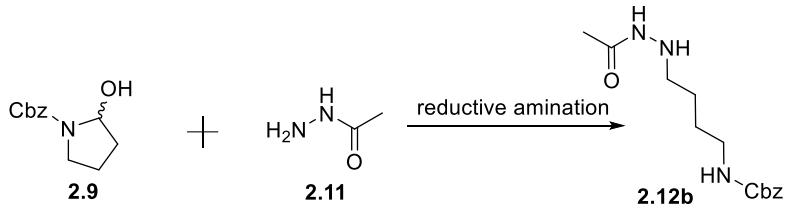

Entry	Catalyst	Solvent	Reductive reagent	Yield
1	0.9 eq AcOH	THF	$NaBH_3CN$	0%
2	0.9 eq APTS	THF	$NaBH_3CN$	10%
3	0.9 eq APTS	distilled THF	$NaBH_3CN$	14%
4	0.25 eq APTS	distilled THF	$NaBH_3CN$	8%
5	0.9 eq APTS	MeOH	$NaBH_3CN$	14%

Table 2.1: The tested conditions of reductive amination for the synthesis of compound **2.12b**

Due to the low yields of **2.12b** using the reductive amination of compound **2.9** with **2.11**, we decided to use the Boc-protected azaLys precursor **2.12a** instead of the acetyl azaLys precursor **2.12b** as the N-terminal fragment. The Boc group will be selectively removed at the end of the

synthesis of the diaza-tripeptides and then the afforded free amino group will be acetylated in the step before the removal of the Cbz group of azaLys and of the Bn group of serine. (**Figure 2.9**)

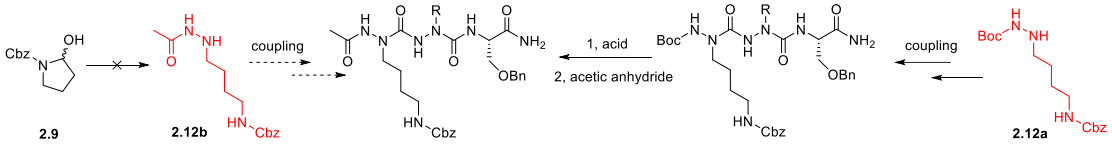

Figure 2.9: Scheme of the synthesis of diaza-tripeptides from **2.12a** instead of **2.12b**

2.3.2 Synthesis of the middle fragment A

Two different Fmoc-protected-1-alkyl hydrazines as middle fragment A were designed and prepared for the synthesis of the diaza-tripeptides **2.6** and **2.7**. One is Fmoc-protected-1-methylhydrazine (**2.13**) and the other one is Fmoc-protected-1-isobutylhydrazine (**2.16**). Here we chose Fmoc group as a protecting group in middle fragment A because it can be selectively cleaved in 20% piperidine/DMF after the coupling of the middle fragment A with the N-terminal fragment **2.12a** possessing Boc group and Cbz group as protecting groups.

Compound **2.13** could be obtained directly in a good yield (92%) through Fmoc protection of commercial methylhydrazine using Fmoc chloride (**Figure 2.10**).

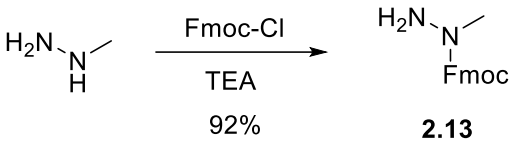

Figure 2.10: Synthesis of Fmoc-protected-1-methylhydrazine **2.13**

For the preparation of Fmoc-protected-1-isobutylhydrazine **2.16**, *t*-butyl carbazate was used in the reductive amination reaction with isobutyraldehyde using $NaBH_3CN$ in the presence of AcOH to provide compound **2.14** (Yield: 79%). Then Fmoc protection of **2.14** using Fmoc chloride in the presence of collidine gave compound **2.15** (Yield: 78%) which was subjected to the Boc cleavage using 4M HCl in dioxane to afford compound **2.16** as the hydrochloride salt in a satisfactory yield

of 94% (**Figure 2.11**).

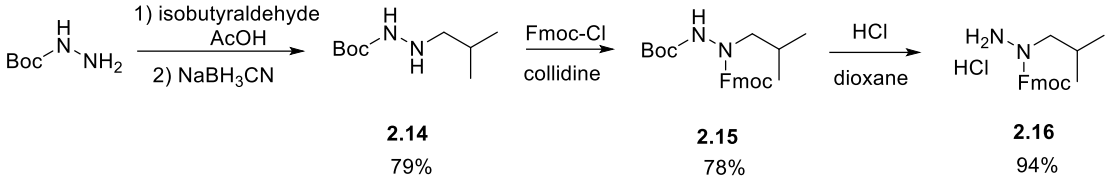

Figure 2.11: Synthesis of Fmoc-protected-1-isobutylhydrazine **2.16**

2.3.3 Synthesis of the C-terminal fragment

The C-terminal fragment, amidated serine **2.18**, was synthesized from Boc-Ser(Bn)-OH. The coupling reaction of Boc-Ser(Bn)-OH with ammonia using EDC and HOBT provided compound **2.17** with a yield of 78%. The Boc group was cleaved from compound **2.17** using 4M HCl in dioxane to give amidated serine **2.18** as the hydrochloride salt of the free amine (**Figure 2.12**).

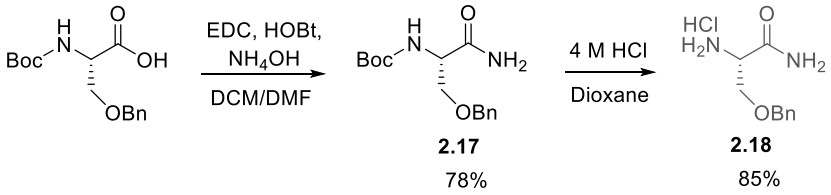

Figure 2.12: Scheme of the synthesis of **2.18**

2.3.4 Synthesis of the diaza-tripeptide 2.5 with azaGly as central residue

After getting all the fragments, we started synthesizing the designed diaza-tripeptides. Our laboratory has synthesized a diaza-tripeptide which has no substituent groups on the central aza-residue (azaGly) using the strategy A.[5] Here for the synthesis of diaza-tripeptide **2.5** we used the same procedure to do couplings[5] (**Figure 2.13**). Compound **2.12a** was activated by 4-nitrophenyl chloroformate to give compound **2.19** which could be purified by silica column (Yield: 74%). Compound **2.19** reacted with hydrazine hydrate to give compound **2.20** (Yield: 78%). Compound **2.20** was activated by phenyl chloroformate to give compound **2.21** (Yield: 98%), which was

coupled with compound **2.18** to provide compound **2.22** (Yield: 71%). The Boc group of **2.22** was removed by treating with HCl. The free amine was then acetylated by acetic anhydride in the presence of pyridine as a base to afford compound **2.23** in a yield of 75%. The last step consisted in deprotecting the Bn and Cbz groups of **2.23** by catalytic hydrogenolysis.

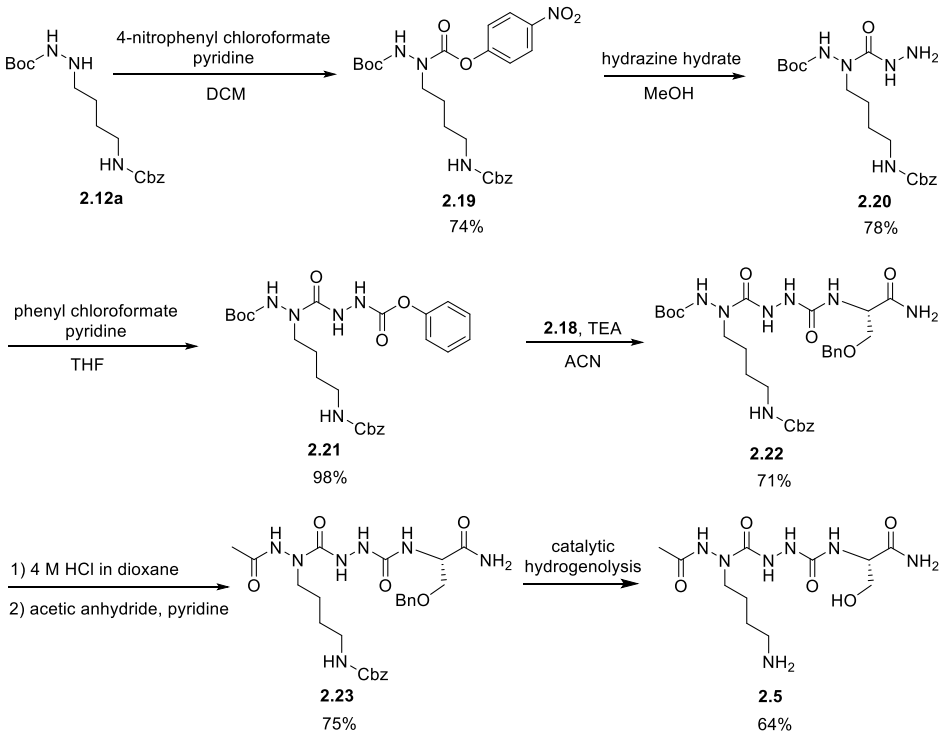

Figure 2.13: Scheme of the synthesis of Ac-aLys-aGly-Ser-NH_2 **2.5**

In the first trial of the catalytic hydrogenolysis, 10% Pd/C and MeOH were used as catalyst and solvent respectively, and the reaction was stirred at room temperature under hydrogen atmosphere overnight (**Table 2.2**, **Entry 1**). LC-MS analysis showed the reaction solution had one impurity (**2.24**) which shows molecular weight 14 larger than the target product, indicating a methylation side reaction (**Figure 2.14** and **2.15**). The similar polarity of **2.24** and **2.5** prevents their separation by HPLC. We speculated that the reason of methylation is the presence of formaldehyde in MeOH which causes the reductive amination with the free amine of the side chain of the azaLys. We used a new batch of dry and HPLC grade MeOH to perform the reaction again but the impurity could not be avoided. Catalytic transfer hydrogenolysis was tried using triethylsilane as in situ hydrogen source in MeOH[7] but the reaction showed the same result (**Table 2.2**, **Entry 2**). We

guessed that even the small trace of formaldehyde in MeOH could cause the methylation of the amine on the side chain of the azaLys because MeOH was used greatly in large excess compared to the small amount of compound **2.23**. The use of EtOH as solvent instead of MeOH in the same conditions of catalytic transfer hydrogenolysis led to the ethylation of the side chain of the azaLys (impurity **2.25**) (**Table 2.2**, **Entry 3**). All of these results suggest that the use of alcohols which have the possibility of the presence of aldehyde and ketone is not a good choice. Thus, we tried *t*-butanol as solvent, to avoid the possible presence of aldehyde or ketone byproducts which might react with the free amine of the azaLys in a reductive amination side reaction. After 24 h reaction in *t*-butanol at 40°C, the target product was not obtained but the starting material **2.23** was recovered (**Table 2.2**, **Entry 4**), thus demonstrating that tertiary alcohol are also not suitable for this reaction.

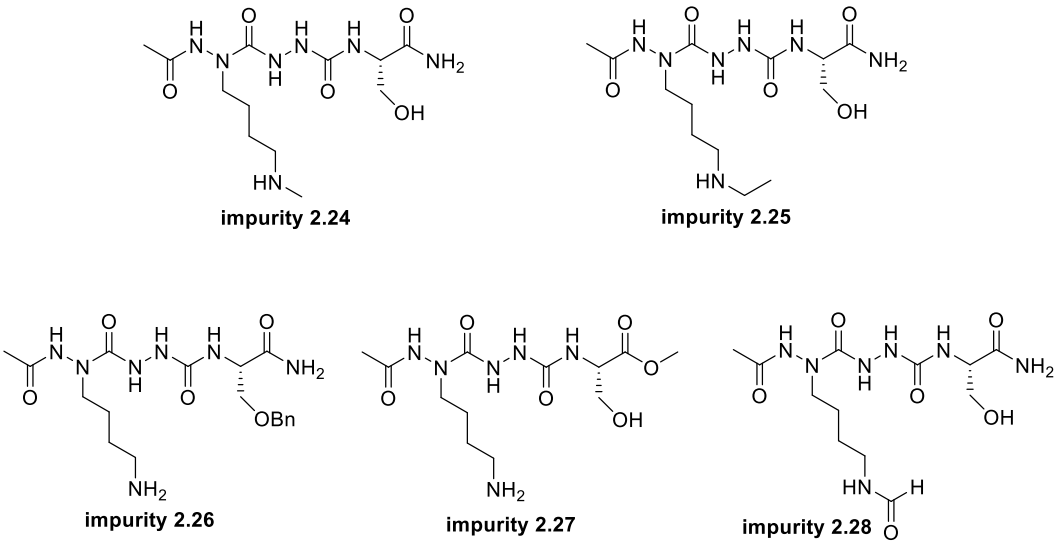

Figure 2.14: The impurities in the catalytic hydrogenolysis trials

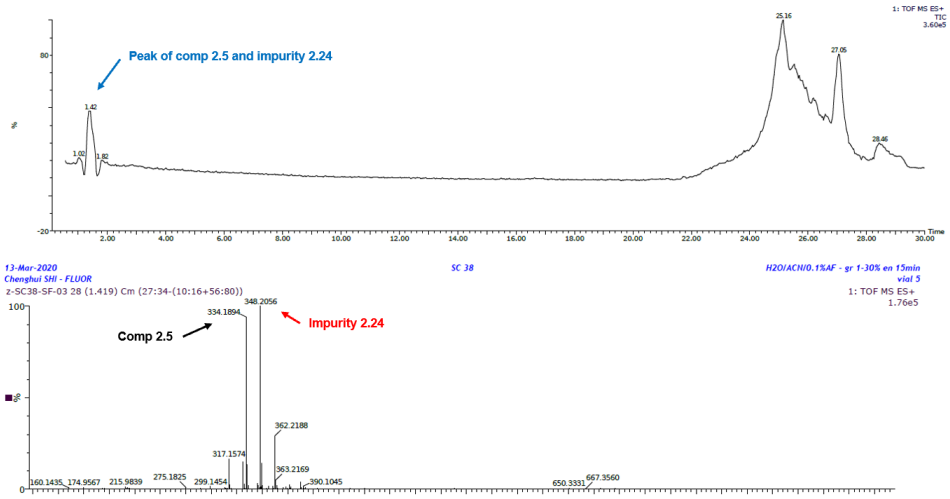

Figure 2.15: LC-MS spectrum of the reaction containing impurity **2.24**

We also tried several aprotic solvents, such as THF, EtOAc and DMF (**Table 2.2**, **Entry 5**, **6** and **7**). In these solvents, the starting material or the partially deprotected intermediate **2.26** were detected even after several hours of reaction. Using HFIP as solvent (**Table 2.2**, **Entry 8**), the starting material was successfully converted to intermediate **2.26** but the further deprotection of the Bn group was blocked. We thought that the further deprotection of the Bn group from **2.26** did not occur because of the low solubility of **2.26** in HFIP. The loss of Cbz group and the exposure of the free amine of the azaLys make **2.26** more polar than the starting material, thereby affecting the solubility of **2.26** in these solvents. Based on this speculation, we used mixed solvent of THF with H_2O to do catalytic hydrogenolysis. In the mixture of THF and H_2O with a ratio 3/1 (**Table 2.2**, **Entry 9**), no reaction occurred even after stirring at room temperature for 25 h. We reduced the proportion of H_2O in the mixed solvent to reach a ratio 10/1 but we did not find any product or starting material after 60 h of reaction (**Table 2.2**, **Entry 10**). We tried to add HCl in the catalytic hydrogenolysis and MeOH was used as solvent again because we hypothesized that acid also could protonate the free amine of the azaLys, thereby blocking the reductive amination with aldehyde. Unfortunately, although the Cbz group and Bn group were removed totally and there was no methylation on the azaLys, the amide of the serine was converted to methyl ester **2.27** in this condition (**Table 2.2**, **Entry 11**). For avoiding this side reaction and keep the enough polarity of solvent, we used a mixture of dioxane and H_2O as solvent but the reaction only showed a trace of the target product but with many degradants (**Table 2.2**, **Entry 12**). We also tried catalytic transfer

hydrogenolysis using cyclohexene as in situ hydrogen source in dioxane at 70°C in the presence of $Pd(OH)_2/C$ as a catalyst but only degradants could be found (**Table 2.2**, **Entry 13**).

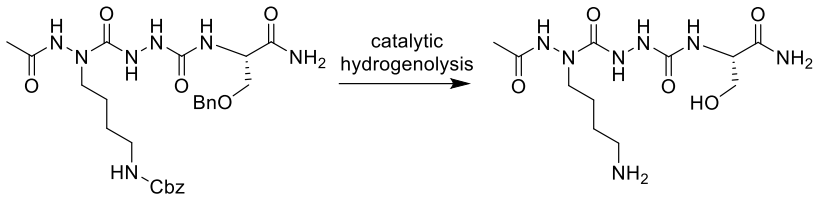

2.23 **2.5**

Entry	Catalyst	Solvent	Temperature	Hydrogen source	Time	Main product
1	10%Pd/C	MeOH	rt	H_2	overnight	Target product and impurity **2.24**
2	10%Pd/C	MeOH	rt	triethylsilane	24 h	Target product and impurity **2.24**
3	10%Pd/C	EtOH	rt	triethylsilane	9 h	Impurity **2.25**
4	10%Pd/C	*t*-butanol	40°C	H_2	24 h	Starting material
5	10%Pd/C	THF	rt	H_2	20 h	Starting material and **2.26**
6	10%Pd/C	EtOAc	rt	H_2	18 h	Starting material and **2.26**
7	10%Pd/C	DMF	rt	H_2	22 h	Starting material
8	10%Pd/C	HFIP	rt	H_2	18 h	Intermediate **2.26**
9	10%Pd/C	THF/H_2O (3/1)	rt	H_2	25 h	Starting material
10	10%Pd/C	THF/H_2O (10/1)	35	H_2	60 h	Degradation
11	10%Pd/C/ HCl	MeOH	rt	H_2	20 h	Impurity **2.27**
12	10%Pd/C/ HCl	Dioxane/H_2O (10/1)	rt	H_2	22 h	Degradation
13	20%$Pd(OH)_2/C$	dioxane	70°C	cyclohexene	22 h	Degradation
14	10%Pd/C	HCOOH/H_2O (1/2)	35°C	H_2	overnight	Target product and Impurity **2.28**
15	10%Pd/C	AcOH/H_2O (1/10)	rt	H_2	18 h	Target product

Table 2.2: The tested conditions for the catalytic hydrogenolysis have been tried

We then turned our attention back to the protic solvent because it seems only protic solvent have enough polarity to solubilize the intermediate **2.26** to allow further the removal of the Bn group. Formic acid was chosen firstly because it is very often used in catalytic transfer hydrogenolysis[8]. In

order to avoid the possibility of formylation of the aza-Lys, we did not use pure formic acid as solvent. We diluted it with water in a ratio (formic acid/H_2O) of 1/2, but the formylation (impurity **2.28**) took place in any case, while the deprotection was completely done in this condition (**Table 2.2**, **Entry 14**). We could not reduce the proportion of formic acid anymore due to the problem of the solubility of the starting material **2.23**. However, we found that a mixture of acetic acid and H_2O (1/10) allowed a moderate solubility of **2.23**. In this condition, we finally could deprotect the Cbz and Bn groups with a satisfactory yield and avoid any side reactions (**Table 2.2**, **Entry 15**). The target compound **2.5** was then purified by HPLC to get a product (Yield: 64%) pure enough to perform NMR experiments.

2.3.5 Synthesis of the diaza-tripeptides with azaAla (2.6) and azaLeu (2.7) as central residues

Previous studies in our laboratory found that compound **2.19** could not react with protected-1-alkylhydrazines to give diaza-peptides (**Figure 2.16A**),[5] whereas the diaza-peptides can be synthesized through coupling the N-terminus fragment with the active carbamate of protected-1-alkylhydrazine (**Figure 2.16B**). Comparing these two reactions, we observed that, for getting diaza-peptides, it is not efficient to activate protected-2-alkylhydrazines as active carbamates to react with protected-1-alkylhydrazines. The active carbamates of protected-2-alkylhydrazines are not reactive enough, making them only can react with hydrazine hydrate (without any substituent groups and protecting group). However, the active carbamates of protected-1-alkylhydrazines show good reactivity not only to hydrazine hydrate but also to protected-2-alkylhydrazines. Thus, the most efficient strategy to synthesize diaza-peptides is to prepare the active carbamates of protected-1-alkylhydrazines and then use these active carbamates to react with protected-2-alkylhydrazines. We speculated that the low reactivity of the active carbamates of protected-2-alkylhydrazines results from bigger steric hindrance because their side chains are closer to reactive site than that of the active carbamates of protected-1-alkylhydrazines. In addition, protected-2-alkylhydrazines are more nucleophilic than protected-1-alkylhydrazines due to the donor character of the alkyl chain. These factors suggest us that we probably can use stronger activating reagents with less steric hinderance to activate protected-2-alkylhydrazines, such as phosgene or triphosgene.

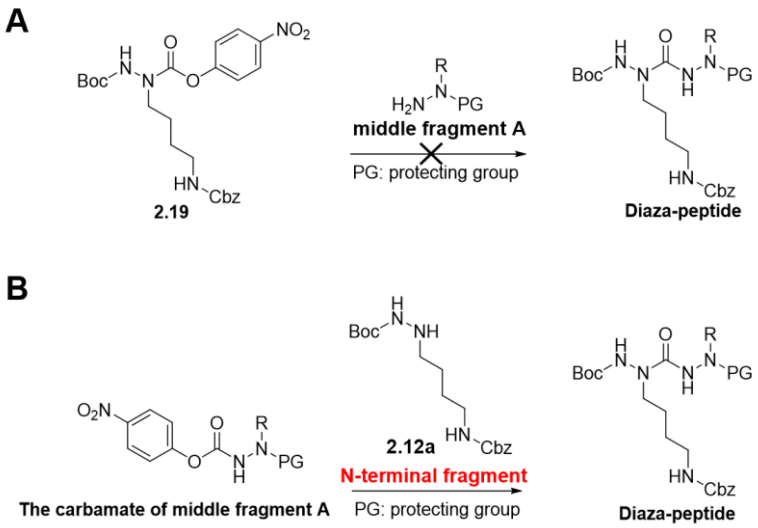

Figure 2.16: Two ways to synthesize diaza-peptides: A) activation of protected-2-alkylhydrazines; B) activation of protected-1-alkylhydrazines

The scheme for the synthesis of compounds **2.6** and **2.7** is illustrated in **Figure 2.17**. The azaAla and azaLeu precursors (**2.13** and **2.16**) were first activated using 4-nitrophenyl chloroformate to afford compounds **2.29a** and **2.29b** (Yields: 76% and 59%), which were reacted with **2.12a** (Boc-protected azaLys precursor) to give diaza-peptide moieties **2.30a** and **2.30b** (Yields: 79%). Fmoc groups were removed from **2.30a** and **2.30b** using 20% piperidine/DMF to provide **2.31a** and **2.31b** with good yields (91%). Afterwards, which activating reagent is used is very important for the coupling **2.31a** and **2.31b** with Ser(Bn)-NH_2 **2.18** because **2.31a** and **2.31b** could be viewed as protected-2-alkylhydrazines which are not good substrates to be activated. Instead of activating **2.31a** and **2.31b** using 4-nitrophenyl chloroformate, triphosgene was used as a carbonyl donor (**Figure 2.17**), which can form more reactive and less sterically hindered intermediates compared to their carbamate analogs. These activated intermediates could react very well followed by adding Ser(Bn)-NH_2 **2.18** and DIPEA. The only issue for this reaction is that, in the activating step, it is difficult to avoid the cyclization of the activated intermediates (giving **2.34** and **2.35** respectively in **Figure 2.18**), making total yields of **2.32a** and **2.32b** only moderate yields (46% and 54%). After that, the acetylated compounds **2.33a** and **2.33b** (Yields: 75% and 76%) were obtained by replacement of the N-terminal Boc protecting group of **2.32a** and **2.32b** by the acetyl group using

the same procedure that for the synthesis of **2.23** (Boc cleavage and acetylation in **Figure 2.13**). In the end, the target compounds **2.6** and **2.7** could be afforded by the cleavage of the Bn and Cbz groups using the same condition (Yields: 58% and 59%), catalytic hydrogenolysis in H_2O/acetic acid (10/1), previously developed for the synthesis of compound **2.5**.

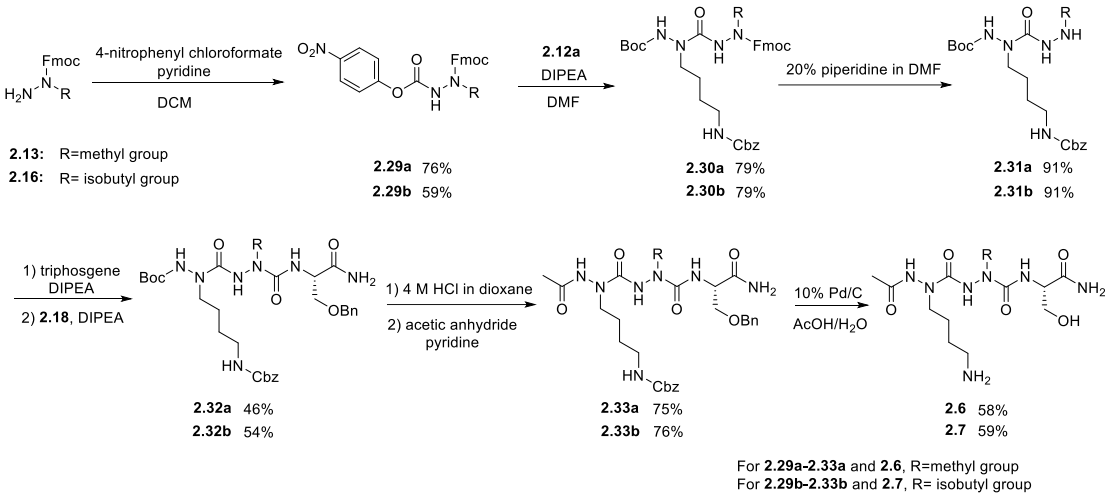

Figure 2.17: Synthesis of Ac-aLys-aAla-Ser-NH_2 **2.6** and Ac-aLys-aLeu-Ser-NH_2 **2.7**

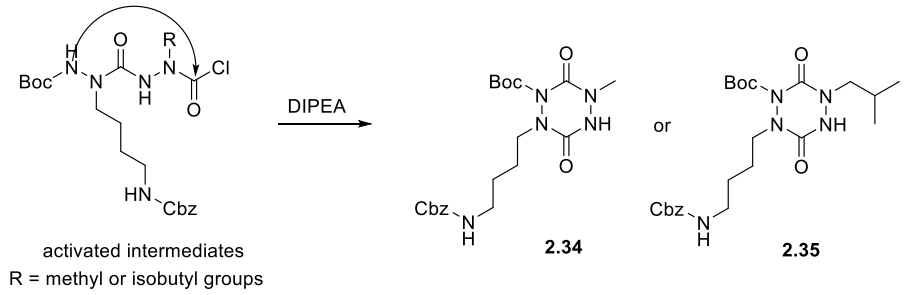

Figure 2.18: The impurities **2.34** and **2.35** formed when activating **2.31a** or **2.31b** using triphosgene

2.4 Synthesis of diaza-tripeptides through the strategy B

We also attempted to synthesize compounds **2.6** and **2.7** through the strategy B and compared the pros and cons between these two strategies. In the strategy B (**Figure 2.6** and **Figure 2.19**), the couplings start from the C-terminus to the N-terminus of the diaza-tripeptides. Instead of the middle

fragment A (Fmoc-protected-1-alkylhydrazines), the middle fragment B (Boc-protected-2-alkylhydrazines) is used to couple with the C-terminal fragment (natural amino acid) to provide the aza-dipeptide fragment. Then, the coupling between the aza-dipeptide fragment with the N-terminal fragment (Boc-protected-2-alkylhydrazines) gives diaza-tripeptides.

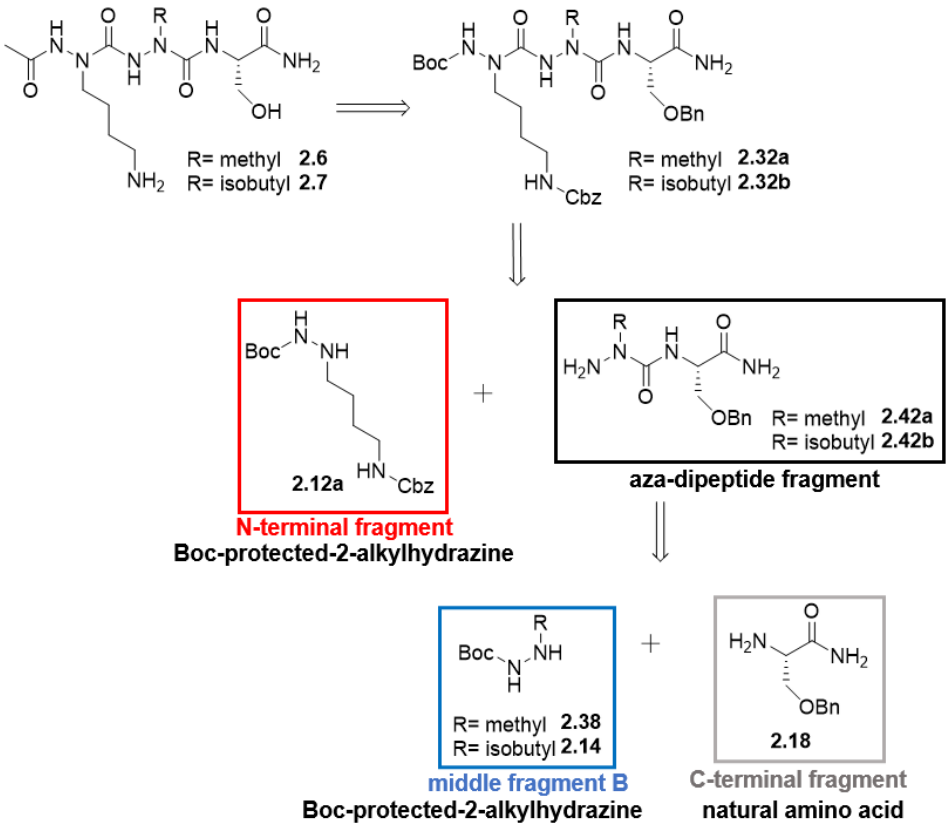

Figure 2.19: Retrosynthetic analysis (strategy B) for compounds **2.6** and **2.7**

2.4.1 Synthesis of the middle fragment B

As shown in the retrosynthetic analysis of compounds **2.6** and **2.7** in the strategy B (**Figure 2.19**), Boc-protected-2-methylhydrazine **2.38** and Boc-protected-2-isobutylhydrazine **2.14** were designed as the middle fragment B. Since **2.14** was already prepared when using the strategy A to synthesize **2.7**, we only needed to prepare **2.38**.

For the preparation of **2.38**, commercial methylhydrazine was used as a starting material (**Figure 2.20**). Due to higher nucleophilicity of the methylated nitrogen of methylhydrazine than its

non-methylated nitrogen, the methylated nitrogen should be first protected. A Cbz group was chosen here because it is easy to remove under catalytic hydrogenolysis. Methylhydrazine was protected with the Cbz group using benzyl chloroformate to give Cbz-protected-1-methylhydrazine **2.36** in a moderate yield of 39% (some product was lost when doing evaporation after chromatography purification because it has a low boiling point). Then the Boc group could be introduced in the non-methylated nitrogen of compound **2.36** using di-*tert*-butyl dicarbonate to give compound **2.37** (Yield: 89%). After that, the selective cleavage of the Cbz group from **2.37** using Pd/C and H_2 gave **2.38** (Yield: 85%).

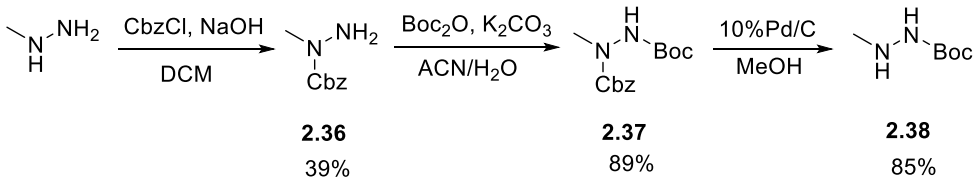

Figure 2.20: Synthesis of compound **2.38**

2.4.2 Synthesis of the aza-dipeptide fragment

For the preparation of **2.6**, the aza-dipeptide fragment **2.42a** should be first synthesized. There are two routes to couple the natural amino acid **2.18** with Boc-protected-2-methylhydrazine **2.38** to get **2.42a** (**Figure 2.21**). Route A consists in activating Boc-protected-2-methylhydrazine **2.38** and reacting it with the natural amino acid **2.18**. Route B, instead, involves first the activation of the natural amino acid **2.18** before coupling it with Boc-protected-2-methylhydrazine **2.38**. As we mentioned before, the carbamates of protected-2-alkylhydrazines always show low reactivity to nucleophiles. In our case, the active carbamate **2.39** actually could not react with the natural amino acid **2.18** in the presence of TEA as base. This result further confirmed our previous observation: the carbamates of protected-2-alkylhydrazines are not good active substrates to react with nucleophiles. Thus, instead of route A, route B was chosen to synthesize compound **2.42a**.

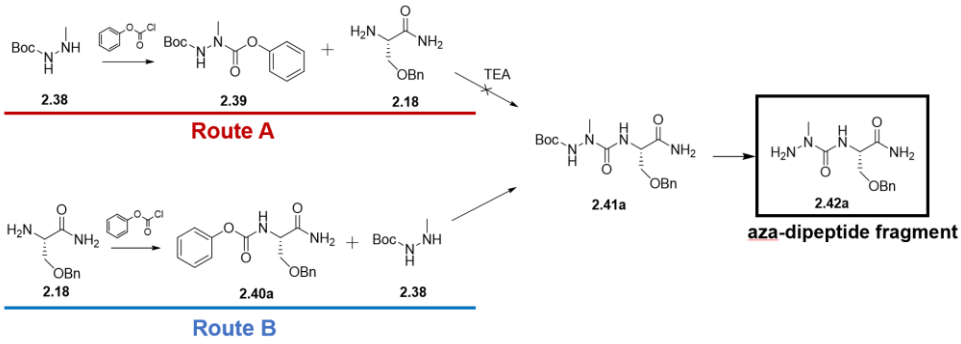

Figure 2.21: Two routes to synthesize aza-dipeptide **2.42a**

In route B (**Figures 2.21** and **2.22**), the natural amino acid **2.18** was activated by phenyl chloroformate to give the active carbamate **2.40a** (Yield: 71%). However, by using acetonitrile as solvent and TEA as base to perform the coupling reaction of **2.40a** with Boc-protected-2-methylhydrazine **2.38**, compound **2.41a** was obtained with only a 16% yield (**Table 2.3**, **Entry 1**). One reason for the low yield is the formation of the hydantoin side product **2.43** in the presence of TEA, suggesting that an intramolecular side reaction is favored rather than the coupling with Boc-protected-2-methylhydrazine **2.38** (**Figure 2.22**). We also tried to use 4-nitrophenyl chloroformate to activate **2.18** and successively engage this activated fragment **2.40b** to react with fragment **2.38** in DMF and TEA as base. The reaction did not afford **2.41a** with a good yield (Yield: 24%) but the impurity **2.43** was not detected in these conditions (**Table 2.3**, **Entry 2**). These results indicate that in the reaction the use of DMF as solvent can inhibit the impurity **2.43**. Thus, we tried to perform the coupling of the active carbamate **2.40a** with fragment **2.38** in DMF with TEA as base. Surprisingly, in this condition, the compound **2.41a** was obtained in a moderate but satisfactory yield (Yield: 53%) (**Table 2.3**, **Entry 3**). The Boc group was successively removed from compound **2.41a** to provide compound **2.42a**. It should be noted that the side product **2.44** (aza-diketopiperazine) (**Figure 2.22**), resulting from the intramolecular cyclization of the aza-dipeptide fragment **2.42a** was detected when the reaction time was stirred over 3 hours (long reaction time was required for the complete removal of Boc group).

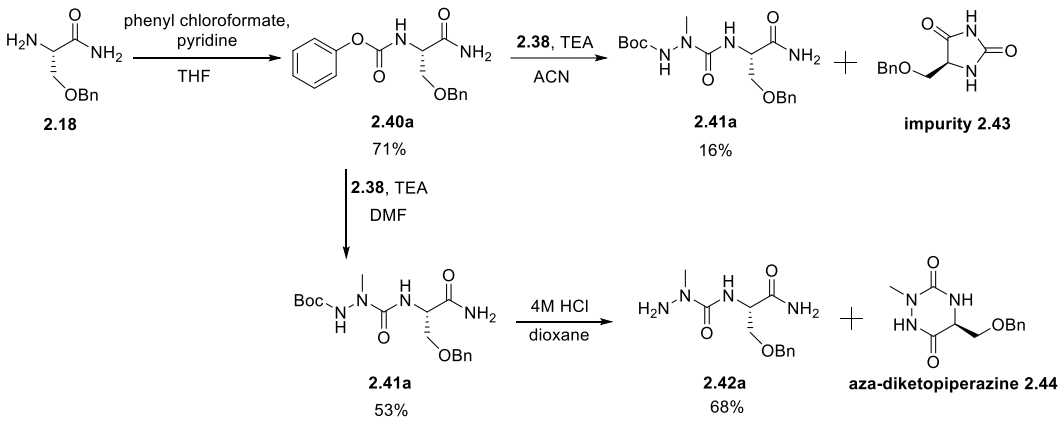

Figure 2.22: Synthesis of **2.42a**

Entry	R	Base	Temperature	Solvent	Yield
1	H	TEA	rt	ACN	16%
2	NO_2	TEA	rt	DMF	24%
3	H	TEA	rt	DMF	53%

Table 2.3: The conditions to synthesize compound **2.41a**

The synthesis of the other aza-dipeptide **2.42b**, which is required for the synthesis of **2.7**, was also tried using the same procedure as for the synthesis of **2.42a**. However, the coupling reaction between the active carbamate **2.40** and Boc-protected-2-isobutylhydrazine **2.14** did not take place (**Figure 2.23**) in the same condition (TEA as base and DMF as solvent) used for the synthesis of **2.41a**. It seems that the large isobutyl side chain hindered the coupling reaction.

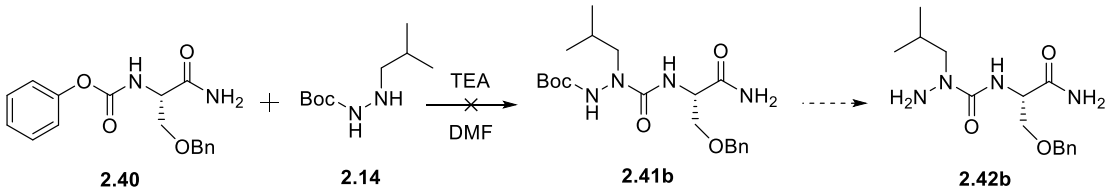

Figure 2.23: Synthesis of **2.42b** through route B

Route A was re-evaluated to synthesize the aza-dipeptide fragment **2.42b**. As we mentioned before, the carbamate (**2.39**) formed from Boc-protected-2-methylhydrazine **2.38**, could not react with the natural amino acid **2.18** to give the aza-dipeptide **2.41a** (**Figure 2.21**). However, we previously found that when triphosgene was used to activate the diaza-peptide fragments **2.31a** and **2.31b** (they could be viewed as protected-2-alkylhydrazines), the active intermediates have enough reactivity to couple with other nucleophiles, such as the natural amino acid **2.18** (**Figure 2.17**), while there is a risk of the cyclization of the activated intermediates, which makes low yields of the coupling reactions. Triphosgene was used as the carbonyl donor to activate **2.14** to give the activated intermediate **2.45**, which has no possibility to cyclize (**Figure 2.24**). As we expected, the active intermediate **2.45** could react with **2.18** to give compound **2.41b** in a moderate yield (57%) but with a side product **2.46** (resulting from the dimerization). Unfortunately, during the Boc cleavage of **2.41b** in a 4M HCl dioxane solution, it was observed that compound **2.42b** has higher propensity to cyclization compared to compound **2.42a**, which made difficult to get enough pure the aza-dipeptide fragment **2.42b** for further coupling reactions (**Figure 2.24**). We also tried to use TFA to remove the Boc group of **2.41b** but the result was even worse. The reaction showed only starting material **2.41b** and aza-diketopiperazine **2.47** after 1 h stirring at room temperature. This result suggests us that in the synthesis of the aza-dipeptide fragment, Boc group should be avoided as protecting group of hydrazine because it needs acidic conditions to be cleaved.

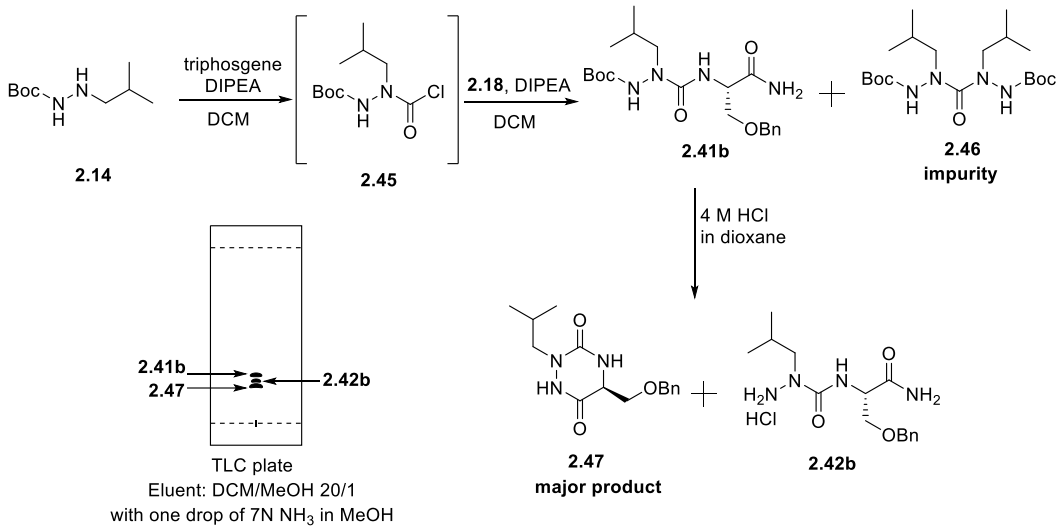

Figure 2.24: Synthesis of **2.42b** and the TLC detection after removing Boc group using 4M HCl dioxane solution

2.4.3 Coupling the aza-dipeptide fragment with the N-terminal fragment

Although we failed to get the aza-dipeptide fragment **2.42b**, the aza-dipeptide fragment **2.42a** was in our hands. Thus, the aza-dipeptide fragment **2.42a** was used to try its coupling with compound **2.12a** using different carbonyl donors (**Table 2.4**). Here we decided to activate the aza-dipeptide fragment **2.42a** because of two reasons: 1) previous work in our laboratory has succeed in the coupling of an aza-dipeptide fragment with Boc-protected-2-isobutylhydrazine **2.14** through activating the aza-dipeptide fragment (**Figure 2.25**)[5]; 2) we observed that activating the protected-1-alkylhydrazines to then react with protected-2-alkylhydrazines was the best strategy to do the couplings. Here aza-dipeptide fragment **2.42a** could be viewed as protected-1-alkylhydrazines.

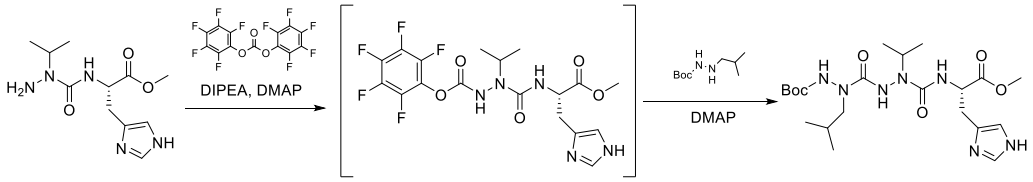

Figure 2.25: A successful example previously performed in our laboratory: activating an aza-dipeptide using bis(pentafluorophenyl) carbonate to react with Boc-protected-2-isobutylhydrazine **2.14**[5]

According to the previous work in our laboratory, bis(pentafluorophenyl) carbonate was used as the carbonyl donor, which can give a more reactive carbamate. However, the reaction showed no target product but mainly starting materials (**Figure 2.26**). It seems that no active intermediate was formed in the activating steps when using bis(pentafluorophenyl) carbonate as the carbonyl donors. We speculated the failure of the reaction probably due to the presence of water in the reaction, which destroys bis(pentafluorophenyl) carbonate or the active intermediate. Since we didn't have enough **2.42a**, the other carbonyl donors were not tried in this coupling. Combining the low yield and difficulty of the preparation of aza-dipeptide fragment and its risk to cyclize to aza-diketopiperazine in acidic conditions, we decided to stop the synthesis in the strategy B and suggested to synthesize the diaza-tripeptides from the N-terminus to the C-terminus (strategy A) (**Figure 2.18**).

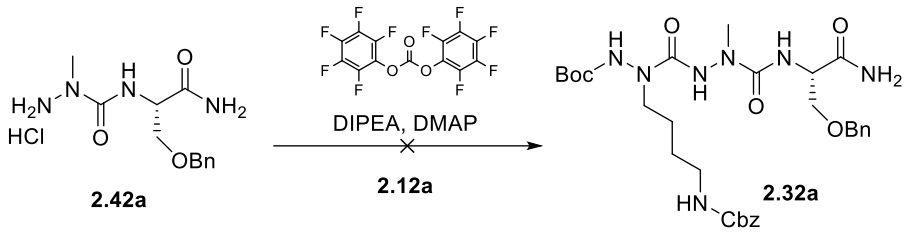

Figure 2.26: Failure of coupling **2.42a** to **2.12a** using bis (pentafluorophenyl) carbonate

2.5 Conclusion about the synthesis of diaza-tripeptides

Three diaza-tripeptides which have different side chains on the central aza-residue were synthesized through the strategy A (couplings start from the N-terminus to the C-terminus). Most of protected-2-alkylhydrazines can be obtained by reductive amination of protected hydrazines with corresponding aldehydes or ketones in good yields except for azaLys precursors. In our case, the acetyl azaLys precursor was even harder to prepare because of the lower nucleophilicity of acetylhydrazide and the high aqueous solubility of the acetyl azaLys precursor. Thus, we used Boc-protected azaLys precursor instead of the acetyl one as the N-terminal fragment to synthesize the diaza-tripeptides. The Boc group was selectively removed after all couplings and then the free amino group was acetylated using acetic anhydride.

After that, the removal of Cbz and Bn groups from the diaza-tripeptides in one pot reaction by catalytic hydrogenolysis indicated that when using alcohols as solvents, the presence of aldehydes leads to the alkylation of the amino group of the azaLys side chain in the diaza-tripeptides, whereas the use of aprotic solvents could not give the final product because of the low solubility of the intermediate (the intermediate possesses Bn group but no Cbz group). These results made us to try to use other protic solvents, such as formic acid or acetic acid, to make the reactions complete and to avoid the alkylation. In the end, we found that the target compounds could be obtained with no obvious side products when using a mixture of acetic acid and water (1/10) as solvent.

We also attempted to prepare diaza-tripeptides through the strategy B (couplings start from the C-terminus to the N-terminus). However, in the strategy B, the coupling between the C-terminal natural amino acid and the middle fragment B (protected-2-alkylhydrazines) is difficult and shows low yields. C-terminal natural amino acid is not a good substrate to be activated because of the risk

of the formation of the hydantoin, whereas the activation of protected-2-alkylhydrazines need triphosgene as the carbonyl donor, which lead to problems of dimerization. In addition, the aza-dipeptide fragment has propensity to cyclize to form an aza-diketopiperazine ring in acidic conditions. This suggests that it is better to not use Boc group as protecting group of hydrazine when using it in the synthesis of the aza-dipeptides. Taken together, we suggest to use the strategy A (From the N-terminus to the C- terminus) to prepare diaza-tripeptides.

For the coupling reactions involving in hydrazide, we try to give some rules to make the synthesis of diaza-peptides or aza-dipeptides more efficient (Figure **2.27**). There are two types of hydrazides which can form very different active carbamates. The first type is protected-2-alkylhydrazines. The carbamates formed form this type of hydrazides show low reactivity to nucleophiles except hydrazine hydrate. This might be due to the larger steric hindrance of the carbamates ascribed to the proximity between the side chains and the carbonyl group. However, it can be activated by phosgene of triphosgene as carbonyl chloride which has higher reactivity and less steric hindrance, to couple with natural amino acids. The second type is protected-1-alkylhydrazines, which can form the carbamates with high reactivity to nucleophiles. This might be due to the less steric hindrance of the carbamates ascribed to the distance between the side chains and the carbonyl group. Thus, when synthesizing diaza-peptides, it is better to activate protected-1-alkylhydrazines to then react with protected 2-alkylhydrazines.

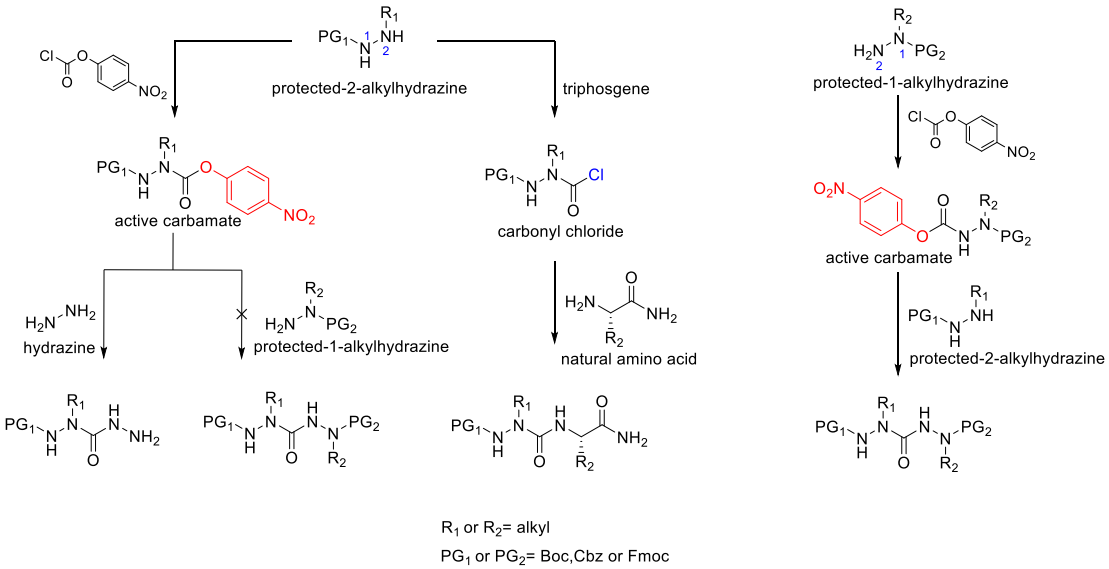

Figure 2.27: Conclusion about the coupling of hydrazides

2.6 Conformational studies

2.6.1 Nuclear magnetic resonance (NMR) parameters

NMR is a powerful technique not only capable to identify organic compounds but also to provide detailed information on the conformation of organic compounds, especially for polypeptides and proteins. The characterization of the conformation of polypeptides based on the analysis of specific NMR parameters has been reported in many papers and its accuracy has been proved by some crystallographic studies. These parameters include vicinal $^3J_{HN\alpha}$ coupling constants, chemical shift deviations (CSDs), temperature coefficients ($\Delta\delta NH/\Delta T$) and nuclear Overhauser effect (NOE).

Vicinal $^3J_{HN\alpha}$ coupling constants

Since the value of ^3J coupling constant is related to bond angle, the prediction of conformations of peptides by dihedral angle ϕ based on $^3J_{HN\alpha}$ coupling constant is possible. Using Karplus equation (**Figure 2.28A**), the torsion angles of each residue could be easily calculated by $^3J_{HN\alpha}$ coupling constants.[9] The statistical analysis of $^3J_{HN\alpha}$ coupling constants of numerous proteins which has been resolved by crystallography gives the mean value of $^3J_{HN\alpha}$ for different secondary structure.[10,11] For α-helix, 3_{10}-helix and β-strand, the mean values are 4.8, 5.6 and 8.5 Hz, respectively. Normally, the residues in α-helices show $^3J_{HN\alpha}$ coupling constants within the range 4-5 Hz (ϕ= -65±13°) and the residues in β-strands show $^3J_{HN\alpha}$ coupling constants within the range 8-10 Hz (ϕ= -112±40°) (**Figure 2.28B**). When $^3J_{HN\alpha}$ coupling constants fell within the range 6-8 Hz, it indicates the residues are in random coils or PPIIs.

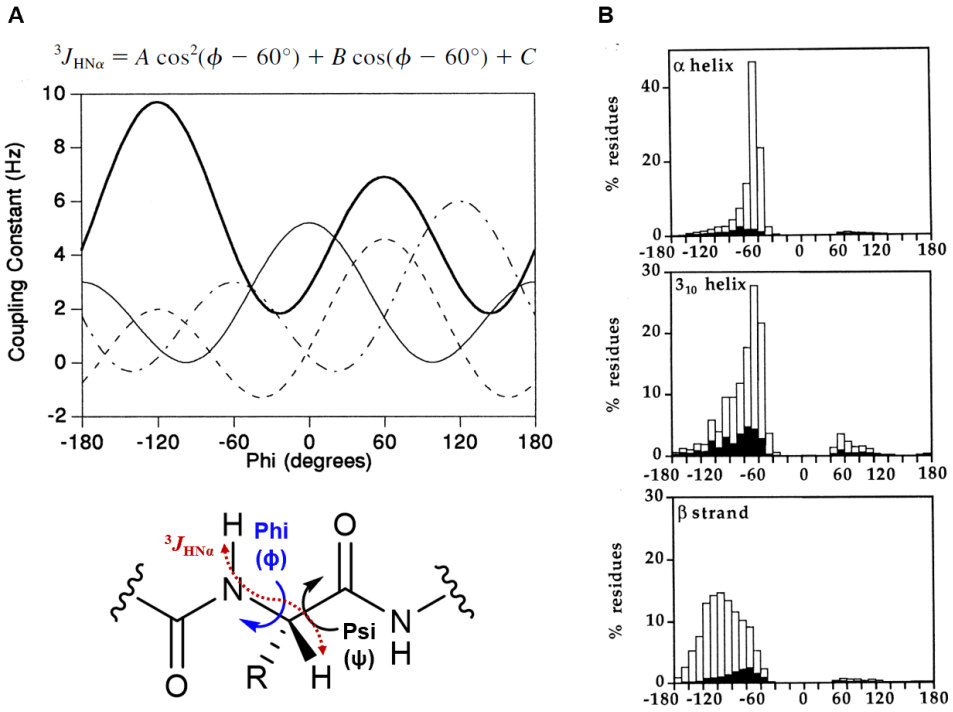

Figure 2.28: A) Karplus equation (for $^3J_{HN\alpha}$: A = 6.4, B = -1.4 and C = 1.9) and the Karplus curves for $^3J_{HN\alpha}$ (bold line);[9] B) Histograms showing the distribution of ϕ dihedral angles for residues in 85 high resolution structures (The values for terminal residues in the secondary structure regions are shown in black in the distributions)[11]

Chemical shift deviations (CSDs)

Chemical shifts of polypeptides are the most accessible parameters in NMR spectroscopy and are sensitive to the conformation of peptides. The deviations of the chemical shifts of tested peptides from the standard random coil value give very useful information on the conformation of the peptides. Specially, the chemical shifts of H^α, C^α and CO are quite sensitive to backbone torsion angles, which make them as good indicatives of the conformation of polypeptides.[12] For α-helix, the H^α is shifted upfield by an average of 0.38 ppm whereas the C^α and CO are shifted downfield by averages of 2.6 and 1.8 ppm, respectively. In contrast, for β-sheet, the H^α is shifted downfield by an average of 0.38 ppm whereas the C^α and CO are shifted upfield by averages of 1.1 ppm and 1.0 ppm, respectively. The summarized trends and criteria of CSDs for the determination of the secondary structure of peptides or proteins are shown in **Table 2.4**.[13]

Resonance	α-Helix	β-Sheet
H^{α}	-0.38 ppm	+0.38 ppm
H^{β}	0 ppm	-0.1 ppm
NH	-0.19 ppm	+0.29 ppm
C^{α}	+2.6 ppm	-1.1 ppm
C^{β}	-0.4 ppm	+2.2 ppm
CO	+1.8 ppm	-1.0 ppm
N	-1.7 ppm	+1.2 ppm

Table 2.4: The criteria of CSDs for different atoms of residues in α-helices and β-sheets

Temperature coefficients (ΔδNH/ΔT)

The temperature coefficients of amide protons are able to describe whether NHs are involved in intramolecular hydrogen bond or not. This parameter could be used to validate some secondary structures which contain intramolecular hydrogen bonds, such as α-helix and β-hairpin. The small absolute values of ΔδNH/ΔT represent strong hydrogen bonds present on NHs (> -4.6 ppb/K).[14] In contrast, the large values are indicative of the lack of hydrogen bonds.

Nuclear Overhauser effect (NOE)

NOE appears between two protons which are spatially close (< 5Å) so it gives the information about the relative spatially position between correlative protons. This NOE information could be collected and reflected on ^{1}H-^{1}H NOESY or ROESY spectra. Thus, the analysis of NOEs between protons is a powerful method to determine the conformation of polypeptides. Short-range NOEs such as NH_i/NH_{i+1} and H^{α}_i/NH_{i+1} NOEs between sequential residues provide the information on polypeptide backbone conformational preferences. Medium-range NOEs, such as H^{α}_i/NH_{i+3} and H^{α}_i/NH_{i+4}, are useful to identify specific secondary structure like α-helix. Long-range NOEs can be involved protons of the backbone and also protons of side chains. They can provide important information especially in the analysis of β-hairpin.

2.6.2 Conformational studies of the diaza-tripeptides 2.5, 2.6 and 2.7 by analysis of NMR parameters

Two NMR parameters were analysed, including the temperature coefficients of the amide protons and the ^{1}H-^{1}H ROE correlation, for compounds **2.5**, **2.6** and **2.7** in both water and methanol to compare the difference from compound **2.2**, previously described.[1] This work was performed by Isabelle Correia from LBM laboratory Sorbonne Université under the supervision of Prof. Olivier Lequin. The results first showed that the designed compounds have better solubility in water (more than 10 mM) than compound **2.2**, which makes available their NMR analysis in water. This confirmed that our design is successful to improve the aqueous solubility of diaza-tripeptides. The temperature coefficients of the amide protons of Ser for compounds **2.5**, **2.6** and **2.7** in water or methanol are all above -4.6 ppb/K and the ^{1}H-^{1}H ROE correlations between the methyl protons of the N-terminal acetyl group and the amide proton of Ser were observed in all these three compounds, indicating the first β-turn structures formed between the carbonyl group of the acetyl moiety and the NH of the residue Ser for these three compounds either in water or in methanol (**Figure 2.29**). Although NOEs between the Ser NH and carboxamide protons were observed, which is compatible with the second turn stabilized by a hydrogen bond involving the carboxamide protons of Ser and the carbonyl group of azaLys, the average temperature coefficients of carboxamide protons for these three compounds suggest the second β-turn structures are not as stable as shown in compound **2.2** (**Figure 2.2**). All these results confirmed that diaza-tripeptides bearing side chains prefer to fold into β-turn structures even in water, which is challenging for the formation of intramolecular hydrogen bond for small peptides. In addition, the side chain on the second aza-residue has an effect on conformational exchange. Compound **2.5** with azaGly shows fast exchange at room temperature while **2.6** (azaAla) and **2.7** (azaLeu) bearing a side chain on the second aza-residue exhibit slow exchange under the same conditions. It can be concluded that the presence of side chains reduces the conformational exchange. All the detailed results and conclusion have been published in the journal Organic & Biomolecular Chemistry[15], and the article can be found in annex of this manuscript.

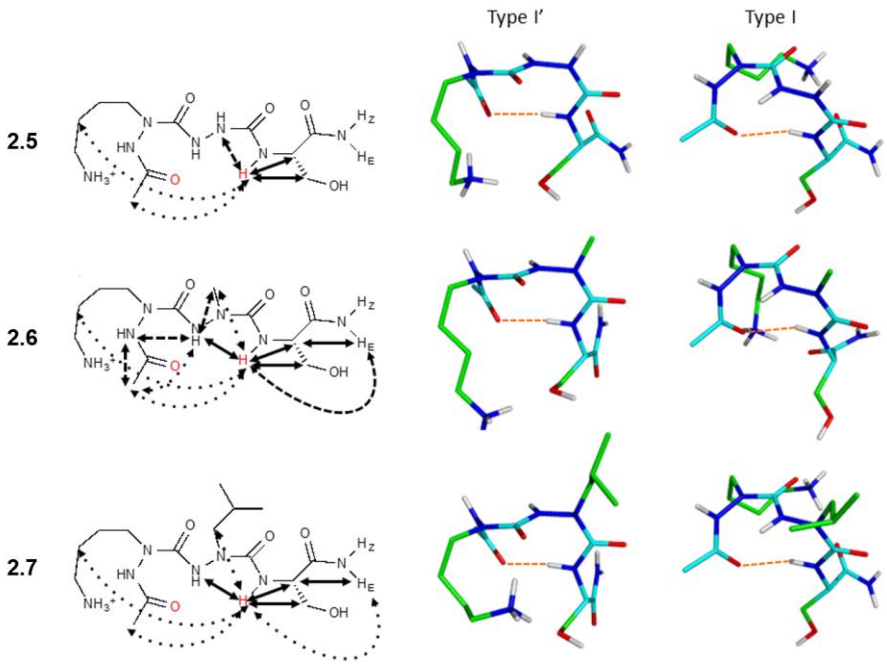

Figure 2.29: NMR structures of diaza-tripeptides **2.5**, **2.6**, and **2.7**. For each peptide, two low-energy NMR structures were selected to represent type I' and type I β-turn conformations. The diagram of ROE correlations is shown on the left. Strong, medium and weak ROE intensities are represented by solid, dashed and dotted lines, respectively

2.7 Conclusion for chapter 2

In this chapter, three new diaza-tripeptides (Ac-azaLys-azaAA-Ser-NH_2, AA = Gly, Ala and Leu) with improved aqueous solubility were designed and synthesized based on the previous work in our laboratory using the synthetic strategy A (from the N-terminus to the C-terminus). We also attempted to synthesize the diaza-tripeptides through the synthetic strategy B (from the C-terminus to the N-terminus) but we failed. Based on this work, the chemistry of diaza-tripeptides was concluded, which can give some instructions in the synthesis of diaza-tripetides.

1: For the preparation of the diaza-peptide fragment, the protected-1-alkylhydrazines should be activated rather than protected-2-alkylhydrazines because the carbamates of protected-1-alkylhydrazines are more reactive.

2: If it is necessary to activate protected-2-alkylhydrazines (in the case of the coupling of protected-2-alkylhydrazines to natural amino acids because activating natural acids has risk to get hydantoins), triphosgene can be used as the carbonyl donor.

3: Because the aza-dipeptide fragment has propensity to cyclized to aza-diketopiperazines in acidic conditions, it is better to avoid acidic conditions in the synthesis of the aza-dipeptide fragment.

4: Due to the low yield of the preparation of the aza-dipeptide fragment and its propensity to cyclized to aza-diketopiperazines in acidic conditions, we suggest the synthesis of diaza-tripeptides through the synthetic strategy A rather than the synthetic strategy B.

The conformational studies of the synthesized diaza-tripeptides were performed by our collaborators at the LBM through the analysis of NMR parameters of the diaza-tripeptides in water or methanol. The results show that the three new diaza-tripeptides have very similar conformational structures in both solvents. Type I and type I′ β-turn structures were observed in the diaza-peptides motifs (turn structures are stabilized by 10-membered hydrogen bond formed between the carbonyl group of the acetyl moiety and the amide proton of the Ser), which is of particular interest because type II β-turn structures were observed when only one aza-amino acid was inserted in peptides.[16,17] Type I and type I′ β-turn structures are more popular in protein structures than type II β-turn, which makes diaza-tripeptides having more potentiality to mimic PPIs.[18] The analysis of the influence of the side chain on the conformation of the diaza-tripeptides suggests that the presence of side chains on the first aza-residue is sufficient to keep β-turn structures of diaza-tripeptides. However, the presence or the absence of a side chain on the central aza-residue has an influence on the conformational exchange. The presence of a side chain reduces conformational exchange.

Overall, this work provides a proof that the introduction of diaza-peptide units is able to stabilize β-turn structures even in water, which is closer to physiological conditions than organic solvents. This means that diaza-peptide units could be regarded as a strong β-turn inducer and applied in peptidic foldamers. Since 3_{10}-helix was constructed by consecutive β-turns, this result encourages us to synthesize longer peptides containing more than one diaza-peptide units, which can probably fold into 3_{10}-helix.

Organic & Biomolecular Chemistry

ROYAL SOCIETY OF CHEMISTRY

PAPER

View Article Online
View Journal

Cite this: DOI: 10.1039/d2ob01225a

Two consecutive aza-amino acids in peptides promote stable β-turn formation in water†

Chenghui Shi,‡[a] Isabelle Correia,‡[b] Nicolo Tonali,[a] Sandrine Ongeri *[a] and Olivier Lequin *[b]

Received 8th July 2022,
Accepted 12th August 2022

DOI: 10.1039/d2ob01225a

rsc.li/obc

Studies on the synthetic methodologies and the structural propensity of peptides containing consecutive aza-amino acids are still in their infancy. Here, details of the synthesis and conformational analysis of tripeptides containing two consecutive aza-amino acids are provided. The demonstration that the type I β-turn folding is induced, even in aqueous media, by the introduction of one or two lateral chains on the diaza-peptide unit is of particular importance for the design of peptidomimetics of biological interest.

Introduction

Currently, more than 80 peptides have been approved as drugs for the treatment of various diseases, showing that peptide drugs have gained astounding interest in the pharmaceutical industry.[1–3] As one class of drug entities, peptides have medium molecular weights placing them between small molecules and antibodies as well as unique pharmacological properties, including high affinity, high selectivity and low immunogenicity. However, the lower proteolytic stability, membrane permeability and oral bioavailability of natural peptides still prevent their rapid development in drug discovery despite notable recent advances in peptide delivery technology.[1] Moreover, small peptides are rather flexible and only rarely adopt stable conformations, which may preclude their ability to interact with protein targets or to inhibit protein–protein interactions (PPIs), which involve generally well-defined secondary structures in the hot-spot sequences of interaction. Modified peptides and peptidomimetics represent alternative entities to avoid these limitations of peptides.[4] The field of peptide-based foldamers adopting stable conformations able to mimic secondary structures also represents recent promising therapeutic opportunities in particular to target PPIs.[5,6]

Azapeptides represent one type of peptidomimetics in which one or more of the residues are substituted by semicarbazide. It has been proved that azapeptides usually show higher selectivity and proteolytic stability than that of parent peptides.[7–9]

Given the repulsion between adjacent nitrogen lone pairs and the planar structure of the urea moiety, the preferential dihedral angle values of aza-amino acid residue (ϕ, ψ) are close to (±90 ± 30°, 0 ± 30°) or (±90 ± 30°, 180 ± 30°).[10,11] This narrow range of dihedral angle values explains why peptides containing a single aza-amino acid adopt a β-turn structure.[12–17] It has also been demonstrated that this non-extended structure can disrupt the β-hairpin conformation of peptides even when containing a D-Pro-Gly template in their sequence.[18] The few reported computational and experimental studies of peptides (mainly di- and tripeptides) containing one aza-amino acid residue have shown that this class usually adopts a type II β-turn conformation in their solid state or when in organic solvent ($CDCl_3$ or DMSO).[15,16,19,20] However, only non-classical azapeptides encompassing a *N*-amidothiourea moiety adopt a type II β-turn structure in water thanks to the enhanced H bond donor ability of the thioureido NH group.[21] To our knowledge, only one statement, made by us, on the more challenging synthesis and conformation study of azapeptides containing two sequential aza-amino acids has been reported so far.[22,23] In this conformational study, we observed that diaza-tripeptide **1** containing two aza-amino acids at its N-terminus (aza/aza/α pseudotripeptide, Fig. 1) is prone to adopt a single type I β-turn or two consecutive type I β-turn conformations in methanol,[23] whereas the corresponding natural tripeptide shows a highly disordered conformation. We exploited this property to synthesize the aza/aza/α/aza/aza/α pseudohexapeptide **2** composed of two diaza-tripeptide units (Fig. 1), which was shown to adopt highly folded conformations made of repeated β-turn conformations or even a full-length 3_{10}-helix structure. This suggests that the repeat mode aza/aza/α in longer peptide sequences has the propensity to induce helical construction in peptides.

[a]*Université Paris-Saclay, CNRS, BioCIS, 92290 Châtenay-Malabry, France. E-mail: sandrine.ongeri@universite-paris-saclay.fr*

[b]*Sorbonne Université, Ecole Normale Supérieure, PSL University, CNRS, Laboratoire des Biomolécules, 4 place Jussieu, 75252 Paris Cedex 05, France. E-mail: olivier.lequin@sorbonne-universite.fr*

†Electronic supplementary information (ESI) available: Experimental section and characterization, NMR data, LC-MS spectra. See DOI: https://doi.org/10.1039/d2ob01225a

‡These authors contributed equally to this work.

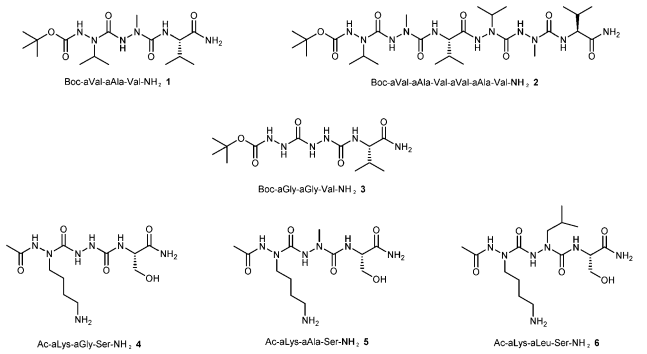

Fig. 1 Structure of the previously reported aza/aza/α pseudotripeptides and aza/aza/α/aza/aza/α pseudohexapeptide **1–3** [23] and of the newly synthesized aza/aza/α pseudotripeptides **4–6**. Aza-amino acids are designated with the letter "a" preceding their three-letter code.

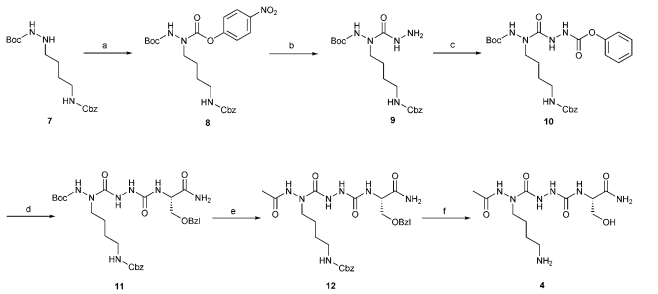

Scheme 1 Synthesis of diaza-tripeptide **4**. Reagents and conditions: (a) 4-nitrophenyl chloroformate, pyridine, DCM, r.t, overnight, 89%; (b) hydrazine monohydrate, MeOH, r.t, overnight, 68%; (c) phenyl chloroformate, pyridine, THF, r.t, 1 h, 98%; (d) Ser(Bzl)-NH_2, TEA, ACN, r.t, 24 h, 71%; (e) i: 4 M HCl in dioxane, r.t, 3 h; ii: acetic anhydride, pyridine, DCM, r.t, overnight, 75%; (f) H_2, Pd/C 10%, acetic acid/H_2O, r.t, overnight, 64%.

Notably, we found that the insertion of side chains on both aza-amino acids had a beneficial effect to stabilize the turn conformation of the diaza-tripeptides. Indeed, diaza-tripeptide **3** with two azaGly at its N-terminus (Fig. 1) showed higher conformational flexibility by NMR and MM/DFT calculations than diaza-tripeptide **1** bearing azaVal-azaAla, oscillating from a few helical populations to extended structures. On the basis of these findings, we have the aim of using these diaza-peptide units in peptidomimetic foldamers to target protein–protein interactions involving turn or helical secondary structures. For that purpose, we had to further investigate two new factors: (1) the ability of these units to retain their turn propensity in water, which is an even more challenging solvent than methanol for maintaining intramolecular hydrogen bonding and stable conformations, because solubility in water is mandatory for biological evaluations; and (2) the influence of the nature of the side chain of the aza-amino acid residues on the conformation.

Because of the low aqueous solubility of the diaza-tripeptides **1** and **2** mentioned above, their NMR analysis in water was not possible. Herein we propose introducing more hydrophilic aza- and natural amino acids in order to improve the aqueous solubility of the target diaza-tripeptides, thereby making possible their NMR analysis in water. Thus, azaLys was used instead of azaVal at the N-terminus while the natural amino acid Val was replaced by Ser at the C-terminus. The *N*-Boc protection was replaced by an acetyl group to further decrease the hydrophobic character and better mimic a neighboring amino acid residue. Meanwhile, we used three different aza-amino acids, including azaGly, azaAla and azaLeu as the central residue in diaza-tripeptides **4**, **5**, and **6**, respectively, in order to investigate the influence of the presence or not, and the nature of the side chain, on the conformation of diaza-tripeptides.

Results and discussion

For the synthesis of peptide **4** without a side chain on the central aza-amino acid, we used the same procedure as described in our previous work (Scheme 1).[22] Compound **7** was activated by 4-nitrophenyl chloroformate to give compound **8** (89% yield), which reacted with hydrazine monohydrate to give compound **9** with a yield of 68%. **9** was activated by phenyl chloroformate to give compound **10** (98% yield), which was coupled with Ser(Bzl)-NH_2 (synthesis described in the ESI†) to provide compound **11** in a satisfactory yield of 71%. The Boc group of **11** was removed using a solution of HCl in dioxane. The free amine was immediately acetylated using acetic anhydride in the presence of pyridine as base to afford compound **12** in a good yield of 75%. Finally, both Bzl and Cbz groups were simultaneously removed from **12** by catalytic hydrogenation using Pd/C as catalyst to obtain compound **4** with a yield of 64%.

As reported in our previous work,[22] the active carbamate of protected 2-alkyl-hydrazines could not couple with protected 1-alkyl-hydrazines but the active carbamate of protected 1-alkyl-hydrazine is able to react with protected 2-alkyl-hydrazine, so we changed the strategy to synthesize compounds **5** and **6**, which have side chains on their central aza-amino acid (Scheme 2). First, the activation of the protected 1-alkyl-hydrazines **13a** and **13b** using 4-nitrophenyl chloroformate afforded compounds **14a** and **14b** (76% and 59% yields, respectively), which reacted with **7** to give diaza-peptide moieties **15a** and **15b** with a good yield of 79%. Fmoc groups were cleaved from **15a** and **15b** using 20% piperidine/DMF to provide **16a** and **16b** in satisfactory yields (91%).

Given the bulkiness of alkyl groups on the nitrogen, which must be activated, active carbamates of **16a** and **16b** were less active to react with Ser(Bzl)-NH_2. Here, triphosgene was used to activate **16a** and **16b** to provide more active acyl chloride intermediates, followed by the addition of Ser(Bzl)-NH_2 to give tripeptides **17a** and **17b** in 46% and 54% yields, respectively. Compounds **18a** and **18b** were then obtained by the replacement of the Boc group by an acetyl group using the same operating protocol as that for the synthesis of **12** (75% and 76% yields, respectively). Finally, the target diaza-tripeptides **5** and **6** were afforded by the simultaneous cleavage of the Bzl and

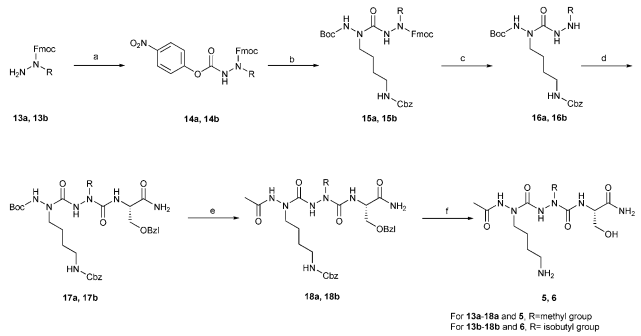

Scheme 2 Synthesis of diaza-tripeptides **5** and **6**. Reagents and conditions: (a) 4-nitrophenyl chloroformate, pyridine, DCM, r.t, overnight, 76% (**14a**) and 59% (**14b**); (b) compound **7**, DIPEA, ACN, r.t, 5 h, 79%; (c) 20% piperidine/DMF, r.t, 30 min, 91%; (d) i: triphosgene, DIPEA, DCM, r.t, 20 min; ii: Ser(Bzl)-NH_2, DIPEA, DCM, r.t, overnight, 46% (**17a**) and 54% (**17b**) for two steps; (e) i: 4 M HCl in dioxane, r.t, 3 h; ii: acetic anhydride, pyridine, DCM, r.t, overnight, 75% (**18a**) and 76% (**18b**) for two steps; (f) H_2, Pd/C 10%, acetic acid/H_2O, r.t, overnight, 58% (**5**) and 59% (**6**).

Cbz groups using catalytic hydrogenation (58% and 59% yields, respectively).

As expected, the three diaza-tripeptides **4–6** showed good solubility in aqueous solution (greater than 10 mM). We thus investigated their structures in water and compared them when in methanol solvent (Fig. 2), serving as a reference with respect to our previously published work.[23] Different NMR parameters were analysed to assess the hydrogen bonding and folding propensities of diaza-tripeptides, in particular the temperature dependency of the amide proton chemical shift (temperature coefficient $\Delta\delta_{HN}/\Delta T$) and the through-space dipolar ^1H–^1H ROE correlations.

Diaza-tripeptide Ac-aLys-aGly-Ser-NH_2 (**4**) shows evidence of intramolecular hydrogen bond formation in both methanol and water solvents. Indeed, the Ser amide proton chemical shift exhibits a low temperature dependency in comparison with other NH protons, the temperature coefficient being −1.4 ppb K^{-1} and −3.4 ppb K^{-1} in methanol and water, respectively (Table 1). These coefficients are well below the threshold value of −4.6 ppb K^{-1}, which is usually an indicator to consider hydrogen bond engagement.[24] In addition, a ROE correlation is observed in both solvents between the amide proton of Ser and the methyl protons of the N-terminal acetyl group (Fig. 3, S3 and S7†), supporting the formation of a β-turn folded structure, stabilized by an i, i + 3 hydrogen bond between the acetyl CO group and the Ser NH group. NMR structure calculations show that two turn conformations are compatible with the NMR data. Indeed, the diaza-peptide block can adopt either negative or positive ϕ angle values around ±90°, leading to type I or I′ β-turns, respectively (Fig. 4A). Such a conformational equilibrium between these two β turn types had been previously described for diaza-tripeptide **1** in methanol,[23] and was found to occur in a slow exchange regime on the NMR time-scale. Given that a single set of chemical shifts is observed for diaza-tripeptide **4** in both solvents at room temperature (Fig. 2), it is likely that the absence of a side chain in the azaGly residue enables faster rotation around the N–Nα bond, leading to a fast exchange regime on the NMR time-scale at room temperature. The appearance of slowly interconverting conformational isomers can only be detected for diaza-tripeptide **4** when cooling down to very low temperatures (228 K) in methanol (Fig. S5†).

Additional i, i + 2 ROEs were also observed between the Ser amide proton and the side chain methylenic protons (CH_2 γ, δ, ε) of azaLys (Fig. 3). These correlations can be accounted for a compact conformation in which azaLys side chain folds back onto Ser residue. The folding of aLys side chain is further suggested by the observation of a significant chemical shift

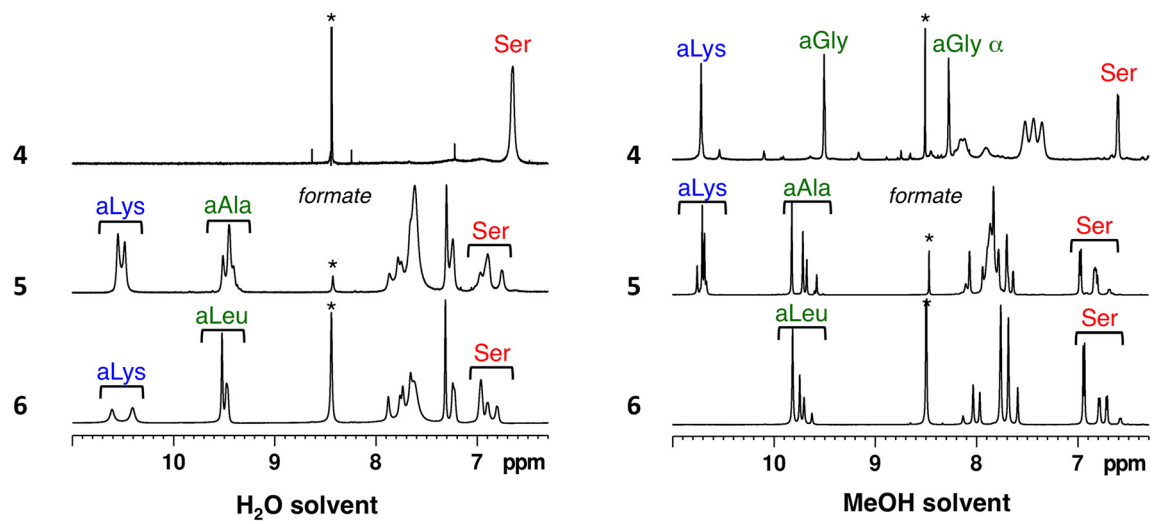

Fig. 2 1D ^1H NMR spectra of diaza-tripeptides **4–6** in water and in methanol, showing the region of HN resonances. Spectra were recorded at 278 K in water and at 228 K in methanol. The peak labelled with an asterisk corresponds to a formate impurity. Unlabelled peaks correspond to carboxamide NH_2, side-chain aLys NH_3^+ or impurities.

Table 1 HN proton temperature coefficient $\Delta\delta_{HN}/\Delta T$ (ppb K^{-1}) for compounds **4–6** in methanol and water. The range of temperature coefficients obtained for the different conformational isomers before signal coalescence is indicated in brackets

Compound	Solvent	T (K)	aLys1	aGly/aAla/aLeu2	Ser3	NH_2 Z	NH_2 E
4	MeOH	228–251	−5.8	−4.6, −7.9 (α)	−1.4	n.d.	n.d.
	H_2O	278–308	n.d.	n.d.	−3.4	n.d.	n.d.
5	MeOH	228–251	[−5.5, −4.8]	[−4.8, −4.0]	[−3.3, −2.2]	[−7.8, −6.8]	[−5.8, −4.9]
	H_2O	278–288	−7.3	−5.9	[−4.7, −3.2]	−5.5	—
6	MeOH	228–251	n.d.	[−5.0, −4.3]	[−2.9, −2.2]	[−7.4, −6.4]	[−5.3, −4.8]
	H_2O	278–298	[−8.8, −7.1]	−7.3	[−7.4, −4.3]	[−6.6, −5.8]	[−7.8, −4.0]

n.d., non-detected proton due to exchange.

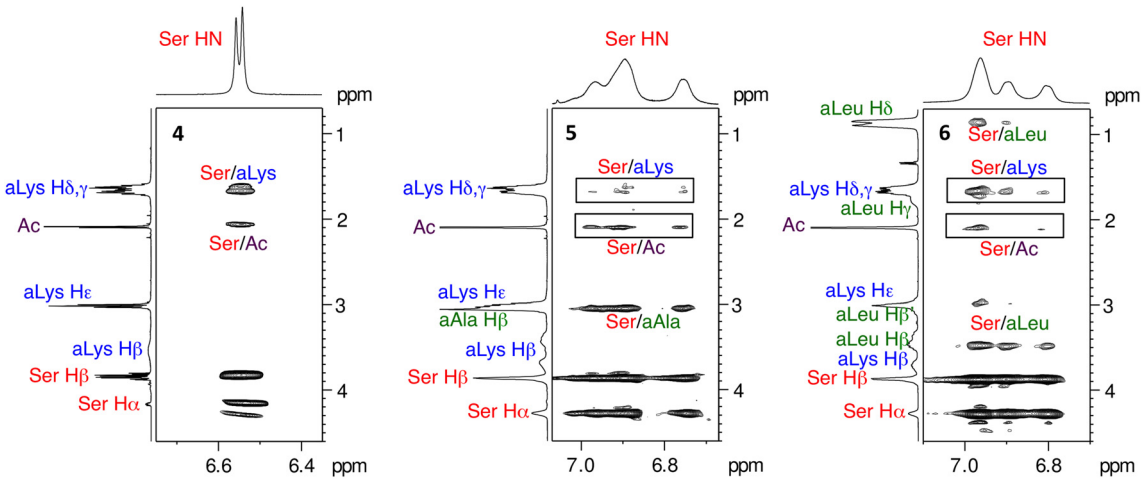

Fig. 3 2D ^1H–^1H ROESY spectra of diaza-tripeptides **4–6** in water showing the correlations of the Ser HN proton with side-chain aliphatic protons. Spectra were recorded at 308 K for **4**, and 278 K for **5** and **6**.

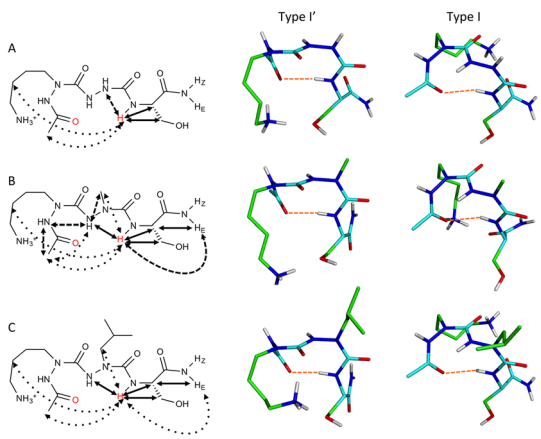

Fig. 4 NMR structures of diaza-tripeptides **4** (A), **5** (B) and **6** (C). For each peptide, two low-energy NMR structures were selected to represent type I' and type I β-turn conformations. The diagram of ROE correlations is shown on the left. Strong, medium and weak ROE intensities are represented by solid, dashed and dotted lines, respectively.

difference between the two diastereotopic CH_2 ε protons in methanol (0.08 ppm difference), which is usually not the case when a Lys side chain is fully exposed to solvent. Structure calculations indicate that this compact orientation could be stabilized by a hydrogen bond between the ammonium group of azaLys and either the hydroxyl or carbonyl group of Ser (Fig. 4A).

The NMR spectra of diaza-tripeptides Ac-aLys-aAla-Ser-NH_2 (**5**) and Ac-aLys-aLeu-Ser-NH_2 (**6**) displayed much higher complexity than diaza-tripeptide **4**, owing to the presence of chemical shift heterogeneity. As a matter of fact, different sets of resonances could be observed for the residues of **5** and **6**, in water and in methanol (Fig. 2), a situation reminiscent of that observed for diaza-tripeptide **1** in methanol. The NMR spectra of the previously studied diaza-tripeptide **1** in methanol showed two major conformational isomers at room temperature (~45% population) which were ascribed to sign inversion of the ϕ dihedral angle, as aforementioned. Two other minor isomers (~5% population) were ascribed to N-terminal Boc *cis*/*trans* isomerization. The situation differs in diaza-tripeptides **5** and **6**, in so far as four forms with closer populations could be evidenced. This prompted us to run temperature variation experiments to further investigate the origin of the chemical shift heterogeneity. Experiments in water at low temperature show that the different forms have close chemical shifts. The coalescence of proton signals arises around 298 K for diaza-tripeptide **5** (Fig. S12†) and above 308 K for diaza-tripeptide **6**

(Fig. S20†). Experiments in methanol enabled us to work at much lower temperatures, cooling down to 228 K. At this temperature, proton spectra exhibited much sharper and resolved peaks, providing better discrimination of the 4 forms. The peak integrations on 1D ^{1}H spectra yielded populations of 42%, 27%, 19% and 12% for diaza-peptide **5** (Fig. S13†) and 55%, 22%, 17% and 6% for diaza-peptide **6** (Fig. S21†). Exchange cross-peaks were observed on 2D ROESY spectra between the different forms (Fig. S15 and S23†), unambiguously proving that the four forms correspond to conformational isomers that interconvert during the mixing time of 2D experiments (250 ms). The chemical shifts of NH protons show linear temperature dependency over the 228–251 K temperature range and the amide protons of Ser residues in the 4 different isomers have the lowest temperature coefficients, between −2.2 and −3.3 ppb K^{-1}, supporting their engagement in intramolecular hydrogen bonds (Table 1). The temperature coefficients where much more difficult to measure in water owing to spectral overlap. Partial data could be obtained either after peak coalescence or for isolated HN peaks before coalescence. They indicate that Ser HN proton has the smallest temperature dependency in comparison with other HN protons.

The analysis of ROESY spectra in methanol at low temperature (Fig. S15 and S23†) shows diagnostic ROEs of β-turn folding, in particular the characteristic *i*, *i* + 3 correlation between Ser HN proton and acetyl protons. Strong sequential *i*, *i* + 1 HN–HN correlations also indicate that the aza-amino acids adopt (ϕ, ψ) angles values around (±90°, 0°). Finally, ROEs are observed between the Ser HN proton and aLys methylenic side-chain protons, as in diaza-tripeptide **4**. All these ROEs are also observed at a higher temperature, in both methanol and water (Fig. 3, S11 and S19†), where partial coalescence between the different forms occurred. Intriguingly, it was not possible to detect distinctive ROEs between the different forms at low temperatures that would provide clues about the nature of the conformational isomerism affecting the different conformers. Importantly, exchange peaks are observed even at the lowest temperature study in methanol. Therefore, magnetization transfers due to conformational exchange induce some contamination of the through-space dipolar ROE correlations, which may complicate the discrimination of distinctive conformational features. Of note, the sign inversion of ϕ angle between +90 and −90° in the aza-amino acids yields mirror-imaged backbone conformations within the diaza-amino acid unit and consequently gives rise to similar sets of ROEs.

Structure calculations based on NMR restraints show actually two possible turn conformations for diaza-tripeptides **5** and **6** (Fig. 4B and C) corresponding to types I and I′, as for diaza-tripeptides **1** [23] and **4** (Fig. 4A). However, we had previously shown for diaza-tripeptide **1** that a second 10-membered β-turn could be formed if the first turn adopts a type I conformation. This second turn was stabilized by a hydrogen bond involving the C-terminal primary amide group and the carbonyl group of the first aza-amino acid residue. Although this double turn conformation is compatible with the observed ROEs between Ser HN and carboxamide protons, the average temperature coefficient of carboxamide protons in the three diaza-tripeptides **4–6** suggests that this hydrogen bond is not as stable as the acetyl-Ser H-bond.

An unusual $N_{amide}\cdots H\text{–}N_{amide}$ hydrogen bond has been proposed to stabilize the backbone conformation of aza-amino acids with (ϕ, ψ) angles close to (±90 ± 30°, 0 ± 30°).[25,26] In the diaza-tripeptide β-turns, two $N_{amide}\cdots H\text{–}N_{amide}$ hydrogen bonds are formed between consecutive residues (N1···H–N2 and N2···H–N3), which could further contribute to the β-turn stabilization. It should be noted that these atypical hydrogen bonds do not seem to have a strong effect on amide proton temperature coefficients in methanol and water, in comparison with conventional C═O···H–N hydrogen bonds. This can be shown by comparing the temperature coefficients of HN2 and HN3 in the diaza-tripeptides **1** [23] and **4–6** (Table 1).

A particular feature of the studied diaza-tripeptides **5** and **6** is the presence of conformational isomerism that severely complicates NMR analyses, whatever the solvent. We show that the presence and the nature of the aza-amino acid side chain have an effect on the conformational exchange. Diaza-tripeptide **4** displays fast exchange at room temperature while diaza-tripeptides **5** and **6** bearing a side chain on the second aza-amino acid exhibit slow exchange under the same conditions. The bulkiness of the substituent (isobutyl *vs* methyl) also slows down the kinetics of interconversion, as indicated by differences in coalescence temperatures. One source of postulated conformational isomerism is the slow rotation around the N–Nα bond in substituted aza-amino acids (ϕ = ±90°), yielding 4 possible conformational isomers. Diaza-peptide units having opposite signs of their ϕ angles are not compatible with β-turn formation. As all conformational isomers show H-bonded β-turn features, this implies that the sign inversion of ϕ angle concerns both aza-amino acids simultaneously, yielding only two conformational isomers, *i.e.* (ϕ_1,ϕ_2) = (+90°, +90°) or (−90°,−90°). Another possibility of conformational exchange would be *E*/*Z* isomerism around amide bonds or the Nα–C′ bond (ψ angle). Indeed, we had previously suggested in the case of compound **1** that *E*/*Z* interconversion of Boc carbamate groups could be a source of conformational isomerism. In the case of N-terminal acetyl groups preceding aza-amino acids, *cis–trans* isomerism has also been reported for the Ac-azaGly amide bond.[25] Concerning the rotation around the Nα–C′ bond, sequential HN/HN ROEs are only compatible with conformations having ψ angles around 0°. Finally, the Nα atom in aza-amino acids has a small pyramidal character, offering the possibility of dynamically orienting the side chain in two opposite configurations. Lubell *et al.* have reported the adaptive chirality of the Nα center in aza-amino acids that could be achiral or exhibit either L or D-like chirality.[27] The X-ray structure and DFT analyses of diaza-tripeptide **1** revealed that the pyramidal character of the Nα atom is very weak.[23] Of note, a slow inversion of the Nα chiral center in peptides incorporating one aza-amino acid unit has not been observed by NMR analyses.[25,27,28] Nevertheless, it is possible that the situation may differ in peptides incorporating two consecutive aza-amino acids that are conformationally stabilized.

Conclusion

This work confirms our previous finding that unlike peptides containing exclusively α-amino acids, the conformational restriction conferred by the insertion of two consecutive aza-amino acids in aza/aza/α pseudotripeptides endows them with a strong tendency to adopt 10-membered type I β-turn conformations. The introduction of polar lateral chains on the N-terminus aza-amino acid (azaLys) and on the natural amino acid at the C-terminus (Ser), as well as the replacement of the N-Boc by an acetyl group, dramatically increased the solubility in water of compounds **4–6** compared to compound **1**. Although the NMR conformational studies of azapeptides **4–6** were hampered by conformational exchange, they did reveal striking similarities to the NMR spectra recorded in water and methanol conditions, in terms of HN chemical shifts, HN temperature coefficients, and sets of ROE correlations. Therefore, the conformational space of diaza-tripeptides is largely comparable in both solvents, indicating that stable turn conformations are populated even in the more challenging aqueous solvent. Diaza-tripeptides **4–6** have a strong propensity to adopt a 10-membered β-turn through an *i*, *i* + 3 hydrogen bond between the carbonyl group of the acetyl moiety and the amide proton of Ser. Two backbone conformations can be adopted in the diaza-amino acid segment corresponding to types I and I′ β-turns. This is of particular interest as the insertion of only one aza-amino acid induces a type II β-turn, which is less abundant in protein structures (19%) than the type I β-turn (46%),[29] and this conformation is stable only in the solid state or in an organic solvent but unstable in aqueous solution.[15,16,19,20]

However, the nature of the side chain of the aza-amino acid and amino acid residues has an influence on the stability of the double turn conformation. Our previous conformational study[23] of compound **3** containing two azaGly units had shown that the presence of side chains on both aza-amino acids had a beneficial effect in stabilizing the turn conformation of the diaza-tripeptides. This new report on Ac-aLys-aGly-SerCONH$_2$ **4**, which has similar β-turn propensity as diaza-tripeptides **5** and **6**, indicates that the presence of a single side chain on the first aza-amino acid residue is sufficient to promote turn stabilization.

The presence of conformational isomerism with provision of four conformers observed in the case of diaza-tripeptides **5** and **6** could be explained by the restricted pyramidal inversion of a nitrogen adopting a sp3 hybridization state, which could thus be a source of chirality producing two diastereomers. While this chirality has not been observed in previously reported NMR studies of peptides having one aza-amino acid,[25,27,28] two consecutive aza-amino acids could further constrain and slow down the nitrogen inversion. The presence of polar side chains allowing a hydrogen bond between the ammonium group of aLys and either the hydroxyl or carbonyl group of Ser could also further slow down the isomerization.

Overall, this work provides additional proof that foldamers based on diaza-amino acid units might resolve a major issue in the use of peptides as drugs, by stabilizing turns and promoting helical conformations, unlike in natural peptides, while having the ability to maintain the selectivity thanks to the lateral chains. The next exciting step will be to investigate the ability of longer peptides containing these diaza-amino acid units to target PPIs involving turn or helical secondary structures[30,31] or to stabilize the helical conformation of intrinsically disordered proteins (IDPs), such as amyloid proteins.[32,33] PPIs[34] and IDPs[35,36] represent two of the most challenging drug discovery targets nowadays. Furthermore, our demonstration of the folding propensity in water of peptides incorporating diaza-peptide units suggest the ability of these new peptidomimetic foldamers to be active in biologically compatible media.

Experimental section

General information

Usual solvents were purchased from commercial sources and DCM was dried and distilled over CaH_2. Thin-layer chromatography (TLC) analyses were performed on silica gel 60 F250 (0.26 mm thickness) plates. The plates were visualized with UV light (λ = 254 nm) or stained by a 4% solution of phosphomolybdic acid or ninhydrin in EtOH. NMR spectra were recorded on an Ultrafield Bruker AVANCE 300 (^{1}H, 300 MHz; ^{13}C, 75 MHz) or on a Bruker AVANCE 400 (^{1}H, 400 MHz; ^{13}C, 100 MHz). Chemical shifts δ are in ppm with the solvent resonance as the internal standard (^{1}H NMR, residual protiated solvent in $CDCl_3$: δ = 7.26 ppm, in CD_3OD and CD_3OH: δ = 3.31 ppm; ^{13}C NMR, $CDCl_3$: δ = 77.16 ppm, CD_3OD and CD_3OH: δ = 49.00 ppm), and the following abbreviations are used: singlet (s), doublet (d), doublet of doublet (dd), triplet (t), quintuplet (qt), multiplet (m), broad multiplet (bm), and broad singlet (brs). Mass spectra were obtained using a Bruker Esquire electrospray ionization apparatus. HRMS were obtained using a TOF LCT Premier apparatus (Waters) with an electrospray ionization source.

The purity of compounds was determined by HPLC-MS on an Agilent 1260 Infinity apparatus. Column: ATLANTIS T3 column (C18, 2.1 × 150mm–3μm); mobile phase: ACN/H_2O + 0.1% TFA (gradient 1–30% in 15 or 20 min). Preparative HPLC was performed on an Agilent 1260 Infinity II apparatus. Column: Pursuit (C18 10 × 250μm–5μm); mobile phase: ACN/H_2O + 0.1% formic acid.

Compounds **7**, **8**, **9**, **10** and **22** were prepared as reported in our previous literature[22] and **13a** was synthesized according to a published method.[37] The synthesis of **13b** and Ser(Bzl)-NH$_2$ are described in the ESI.† The protocols of synthesis and the characterization of intermediates **11** and **12**, **14a/b–18a/b** and of the final diaza-tripeptides **4–6** are detailed in the ESI.†

NMR conformational studies

NMR measurements conducted over a temperature range from 273 K to 308 K were acquired on a Bruker Avance 500 MHz NMR spectrometer equipped with a cryogenic TCI probe. ^{1}H

and ^{13}C resonance assignments were obtained from the analysis of 2D ^{1}H–^{1}H TOCSY (mixing time of 60 ms), 2D ^{1}H–^{1}H ROESY (mixing time of 250 ms), 2D ^{1}H–^{13}C HSQC, and 2D ^{1}H–^{13}C HMBC spectra. Low temperature NMR experiments (225–250 K) were conducted on a Bruker Avance 600 MHz NMR spectrometer equipped with a room temperature TBI probe. NMR data were processed with TopSpin 3.6 and analysed with either the TopSpin 3.6 or NMRFAM-SPARKY programs. For NMR studies in water, about 2.5 mg of compounds **4–6** was dissolved in 0.6 mL of H_2O/D_2O (90/10 v/v), pH = 5.5. DSS (sodium 4,4-dimethyl-4-silapentane-1-sulfonate, 0.1 mM) was used for chemical shift calibration. For NMR experiments in methanol, 4 to 6 mg of compounds **4–6** was dissolved in 0.6 mL of CD_3OH. ^{1}H and ^{13}C chemical shifts were referenced to the methanol solvent signal (residual protonated CHD_2OH at 3.31 ppm and deuterated $^{13}CD_3OH$ at 49.1 ppm, respectively). We checked that the pseudopeptides **4–6** did not self-assemble in aqueous solution or in methanol in this concentration range by assessing the absence of concentration dependency on chemical shifts upon a 10-fold dilution for samples in water or a 20-fold dilution for samples in methanol.

NMR structure calculations

Structures were calculated using the Amber14 program and ff14SB forcefield, as previously described.[23] Structures were refined using a GBSA solvation model. Aza-amino acid parametrization was made with Antechamber, using gaff forcefield atom types and partial charges were calculated with AM1-BCC. 2D ROESY cross-peaks were integrated using NMRFAM-SPARKY. Three classes of distance restraints were defined, corresponding to upper limit distances of 3.0, 3.8 and 5.0 Å.

Author contributions

C. Shi: conducting the research and investigation process in the chemical synthesis, specifically performing the experiments, and data collection; I. Correia: conducting the research and investigation process in the NMR conformational studies, specifically performing the experiments and data collection; N. Tonali: supervision and verification of the overall reproducibility of results and experiments in chemical synthesis; S. Ongeri: oversight and leadership responsibility for the research activity planning and execution; O. Lequin: formulation and evolution of overarching research goals and aims. Supervision and verification of the overall reproducibility of results and NMR structure calculation.

Conflicts of interest

There are no conflicts to declare.

Acknowledgements

The China Scholarship Council (CSC) is thanked for the PhD fellowship of C. Shi. Karine Leblanc (Service d'Analyses–HPLC-Masse BioCIS, Univ. Paris Saclay) is thanked for HPLC and HRMS analyses.

References

1 M. Muttenthaler, G. F. King, D. J. Adams and P. F. Alewood, *Nat. Rev. Drug Discovery*, 2021, **20**, 309–325.
2 A. F. B. Räder, M. Weinmüller, F. Reichart, A. Schumacher-Klinger, S. Merzbach, C. Gilon, A. Hoffman and H. Kessler, *Angew. Chem., Int. Ed.*, 2018, **57**, 14414–14438.
3 J. L. Lau and M. K. Dunn, *Bioorg. Med. Chem.*, 2018, **26**, 2700–2707.
4 E. Lenci and A. Trabocchi, *Chem. Soc. Rev.*, 2020, **49**, 3262–3277.
5 R. Gopalakrishnan, A. I. Frolov, L. Knerr, W. J. Drury and E. Valeur, *J. Med. Chem.*, 2016, **59**, 9599–9621.
6 I. M. Mándity and F. Fülöp, *Expert Opin. Drug Discovery*, 2015, **10**, 1163–1177.
7 M. Galibert, M. Wartenberg, F. Lecaille, A. Saidi, S. Mavel, A. Joulin-Giet, B. Korkmaz, D. Brömme, V. Aucagne, A. F. Delmas and G. Lalmanach, *Eur. J. Med. Chem.*, 2018, **144**, 201–210.
8 C. Proulx, D. Sabatino, R. Hopewell, J. Spiegel, Y. García Ramos and W. D. Lubell, *Future Med. Chem.*, 2011, **3**, 1139–1164.
9 Y. Tal-Gan, N. S. Freeman, S. Klein, A. Levitzki and C. Gilon, *Chem. Biol. Drug Des.*, 2011, **78**, 887–892.
10 H.-J. Lee, J.-W. Song, Y.-S. Choi, H.-M. Park and K.-B. Lee, *J. Am. Chem. Soc.*, 2002, **124**, 11881–11893.
11 M. Thormann and H.-J. Hofmann, *J. Mol. Struct.: THEOCHEM*, 1999, **469**, 63–76.
12 Z. Benatalah, A. Aubry, G. Boussard and M. Marraud, *Int. J. Pept. Protein Res.*, 1991, **38**, 603–605.
13 F. André, A. Vicherat, G. Boussard, A. Aubry and M. Marraud, *J. Pept. Res.*, 1997, **50**, 372–381.
14 F. André, G. Boussard, D. Bayeul, C. Didierjean, A. Aubry and M. Marraud, *J. Pept. Res.*, 1997, **49**, 556–562.
15 H.-J. Lee, K.-B. Lee, I.-A. Ahn, S. Ro, K.-H. Choi and Y.-S. Choi, *J. Pept. Res.*, 2000, **56**, 35–46.
16 H.-J. Lee, K.-H. Choi, I.-A. Ahn, S. Ro, H. G. Jang, Y.-S. Choi and K.-B. Lee, *J. Mol. Struct.*, 2001, **569**, 43–54.
17 S. Ro, H.-J. Lee, I.-A. Ahn, D.-K. Shin, K.-B. Lee, C.-J. Yoon and Y.-S. Choi, *Bioorg. Med. Chem.*, 2001, **9**, 1837–1841.
18 M. A. McMechen, E. L. Willis, P. C. Gourville and C. Proulx, *Molecules*, 2019, **24**, 1919.
19 H.-J. Lee, H.-M. Park and K.-B. Lee, *Biophys. Chem.*, 2007, **125**, 117–126.
20 C. Abbas, G. Pickaert, C. Didierjean, B. J. Grégoire and R. Vanderesse, *Tetrahedron Lett.*, 2009, **50**, 4158–4160.
21 X.-S. Yan, H. Luo, K.-S. Zou, J.-L. Cao, Z. Li and Y.-B. Jiang, *ACS Omega*, 2018, **3**, 4786–4790.

22 F. Bizet, N. Tonali, J.-L. Soulier, A. Oliva, J. Kaffy, B. Crousse and S. Ongeri, *New J. Chem.*, 2018, **42**, 17062–17072.
23 N. Tonali, I. Correia, J. Lesma, G. Bernadat, S. Ongeri and O. Lequin, *Org. Biomol. Chem.*, 2020, **18**, 3452–3458.
24 T. Cierpicki and J. Otlewski, *J. Biomol. NMR*, 2001, **21**, 249–261.
25 K. Baruah, B. Sahariah, S. S. Sakpal, J. K. R. Deka, A. K. Bar, S. Bagchi and B. K. Sarma, *Org. Lett.*, 2021, **23**, 4949–4954.
26 A. Lecoq, G. Boussard, M. Marraud and A. Aubry, *Biopolymers*, 1993, **33**, 1051–1059.
27 S. H. Bouayad-Gervais and W. D. Lubell, *Molecules*, 2013, **18**, 14739–14746.
28 P. A. Ottersbach, G. Schnakenburg and M. Gütschow, *Chem. Commun.*, 2012, **48**, 5772–5774.
29 N. Panasik Jr., P. J. Fleming and G. D. Rose, *Protein Sci.*, 2005, **14**, 2910–2914.
30 T. A. Edwards and A. J. Wilson, *Amino Acids*, 2011, **41**, 743–754.
31 X. Ran and J. E. Gestwicki, *Curr. Opin. Chem. Biol.*, 2018, **44**, 75–86.
32 S. Vivekanandan, J. R. Brender, S. Y. Lee and A. Ramamoorthy, *Biochem. Biophys. Res. Commun.*, 2011, **411**, 312–316.
33 Y. Bram, S. Peled, S. Brahmachari, M. Harlev and E. Gazit, *Sci. Rep.*, 2017, **7**, 14031.
34 H. Lu, Q. Zhou, J. He, Z. Jiang, C. Peng, R. Tong and J. Shi, *Signal Transduction Targeted Ther.*, 2020, **5**, 1–23.
35 J. Wang, Z. Cao, L. Zhao and S. Li, *Int. J. Mol. Sci.*, 2011, **12**, 3205–3219.
36 P. Joshi and M. Vendruscolo, in *Intrinsically Disordered Proteins Studied by NMR Spectroscopy*, ed. I. C. Felli and R. Pierattelli, Springer International Publishing, Cham, 2015, pp. 383–400.
37 C. Gibson, S. L. Goodman, D. Hahn, G. Hölzemann and H. Kessler, *J. Org. Chem.*, 1999, **64**, 7388–7394.

References

(1) Tonali, N.; Correia, I.; Lesma, J.; Bernadat, G.; Ongeri, S.; Lequin, O. Introducing Sequential Aza-Amino Acids Units Induces Repeated β-Turns and Helical Conformations in Peptides. *Org. Biomol. Chem.* **2020**, *18* (18), 3452–3458.

(2) Boeglin, D.; Lubell, W. D. Aza-Amino Acid Scanning of Secondary Structure Suited for Solid-Phase Peptide Synthesis with Fmoc Chemistry and Aza-Amino Acids with Heteroatomic Side Chains. *J. Comb. Chem.* **2005**, *7* (6), 864–878.

(3) Freeman, N. S.; Hurevich, M.; Gilon, C. Synthesis of N′-Substituted Ddz-Protected Hydrazines and Their Application in Solid Phase Synthesis of Aza-Peptides. *Tetrahedron* **2009**, *8* (65), 1737–1745.

(4) Proulx, C.; Sabatino, D.; Hopewell, R.; Spiegel, J.; García Ramos, Y.; Lubell, W. D. Azapeptides and Their Therapeutic Potential. *Future Med. Chem.* **2011**, *3* (9), 1139–1164.

(5) Bizet, F.; Tonali, N.; Soulier, J.-L.; Oliva, A.; Kaffy, J.; Crousse, B.; Ongeri, S. Towards a General Synthesis of Di-Aza-Amino Acids Containing Peptides. *New J. Chem.* **2018**, *42* (20), 17062–17072.

(6) Busnel, O.; Bi, L.; Baudy-Floc'h, M. Synthesis of Fmoc-Protected Aza-B3-Amino Acids via Reductive Amination of Glyoxylic Acid. *Tetrahedron Lett.* **2005**, *46* (41), 7073–7075.

(7) Mandal, P. K.; McMurray, J. S. Pd–C-Induced Catalytic Transfer Hydrogenation with Triethylsilane. *J. Org. Chem.* **2007**, *72* (17), 6599–6601.

(8) ElAmin, B.; Anantharamaiah, G. M.; Royer, G. P.; Means, G. E. Removal of Benzyl-Type Protecting Groups from Peptides by Catalytic Transfer Hydrogenation with Formic Acid. *J. Org. Chem.* **1979**, *44* (19), 3442–3444.

(9) Pardi, A.; Billeter, M.; Wüthrich, K. Calibration of the Angular Dependence of the Amide Proton-Cα Proton Coupling Constants, 3JHNα, in a Globular Protein: Use of 3JHNα for Identification of Helical Secondary Structure. *J. Mol. Biol.* **1984**, *180* (3), 741–751.

(10) Dyson, H. J.; Wright, P. E. Nuclear Magnetic Resonance Methods for Elucidation of Structure and Dynamics in Disordered States. *Methods Enzymol* **2001**, *339*, 258–270.

(11) Smith, L. J.; Bolin, K. A.; Schwalbe, H.; MacArthur, M. W.; Thornton, J. M.; Dobson, C. M. Analysis of Main Chain Torsion Angles in Proteins: Prediction of NMR Coupling Constants for Native and Random Coil Conformations. *J. Mol. Biol.* **1996**, *255* (3), 494–506.

(12) Wishart, D. S. Interpreting Protein Chemical Shift Data. *Prog. Nucl. Magn. Reson. Spectrosc.* **2011**, *58* (1), 62–87.

(13) Wishart, D. S.; Sykes, B. D.; Richards, F. M. Relationship between Nuclear Magnetic Resonance Chemical Shift and Protein Secondary Structure. *J. Mol. Biol.* **1991**, *222* (2), 311–333.

(14) Cierpicki, T.; Otlewski, J. Amide Proton Temperature Coefficients as Hydrogen Bond Indicators in Proteins. *J. Biomol. NMR* **2001**, *21* (3), 249–261.

(15) Shi, C.; Correia, I.; Tonali, N.; Ongeri, S.; Lequin, O. Two Consecutive Aza-Amino Acids in Peptides Promote Stable β-Turn Formation in Water. *Org. Biomol. Chem.* **2022**. https://doi.org/10.1039/D2OB01225A.

(16) Lee, H.-J.; Lee, K.-B.; Ahn, I.-A.; Ro, S.; Choi, K.-H.; Choi, Y.-S. Role of Azaamino Acid Residue in β-Turn Formation and Stability in Designed Peptide. *J. Pept. Res.* **2000**, *56* (1), 35–46.

(17) Lee, H.-J.; Choi, K.-H.; Ahn, I.-A.; Ro, S.; Jang, H. G.; Choi, Y.-S.; Lee, K.-B. The β-Turn Preferential Solution Conformation of a Tetrapeptide Containing an Azaamino Acid Residue. *J. Mol. Struct.* **2001**, *569* (1), 43–54.

(18) Panasik Jr., N.; Fleming, P. J.; Rose, G. D. Hydrogen-Bonded Turns in Proteins: The Case for a Recount. *Protein Sci.* **2005**, *14* (11), 2910–2914.

Chapter 3

Synthesis and conformational analysis of aza-nonapeptides containing diaza-peptide units: application in protein-protein interactions

In the previous chapter, we have established that diaza-peptide unit is able to induce β-turn structure of tripeptides in water when it is used to replace two consecutive natural amino acids at the N-terminus of the tripeptides. This property on the conformations of tripeptides has encouraged us to further investigate the impact of diaza-peptide unit on the conformations of longer peptides. Combining the questions we mentioned in the chapter 1, including

1) Do peptidic foldamers based on the small EF-helix of TTR capable of folding into helical structures have similar effects on Aβ as TRR shows?

2) Do helical mimics could stabilize the helical conformation of amyloid proteins to prevent their further misfolding and aggregation in toxic and β-sheet rich structures?

3) Does the introduction of diaza-peptide units in a short TTR peptide sequence based on the EF-helix residues can mimic its helical structures and the orientation of its lateral chains?

4) Does this new class of peptidic foldamers containing diaza-peptide units are suitable to become drug candidates?

in this chapter, several peptidic foldamers containing diaza-peptide units were designed based on the sequence of the EF-helix of TTR and synthesized on solid phase. The conformational studies of these peptidic foldamers were performed by CD, NMR, FTIR and MD simulation to give an insight into the possible conformations of the foldamers. Then two biophysical assays, including Thioflavin-T (ThT) assay and CD assay, were performed on these foldamers to evaluate their effects on Aβ folding and aggregation. In addition, several biological assays were also performed on the most active foldamer to test its proteolytic stability, BBB permeability and cellular toxicity, which give evidences that peptidic foldamers containing diaza-peptide units are druggable foldamers.

3.1 Design of novel aza-nonapeptides based on the sequence derived

from the EF-helix of TTR

It has been proved that TTR is associated with AD by the interaction with Aβ.[1–5] As we described in the chapter 1, two possible binding sites of TTR to Aβ have been proposed (**Figure 3.1**).[6] One is located at the strand G of TTR (residues 102–117), the other one is located at the EF-helix of TTR (residues 74–83). There are several peptides designed on the basis of the strand G, such as G16 and G8, that showed activity against Aβ aggregation (**Figure 3.1**).[7,8] However, a peptide (Efh) derived from the EF-helix had no effect on Aβ aggregates size and didn't show any strong interaction with Aβ (**Figure 3.1**).[8] It is likely that the lack of α-helical structure of the EF-helix derived peptide prevents its binding to Aβ.

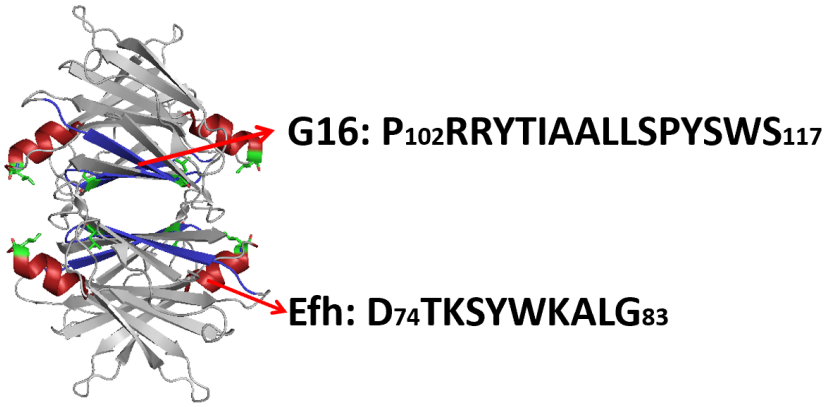

Figure 3.1: Two possible binding sites of TTR to Aβ, the strand G (blue) and the EF-helix (red) and the corresponding peptide sequences

As we mentioned in the first two chapters, azapeptides have a propensity to be in β-turn structures because of the inherent conformational property of aza-residues. It was also reported by our laboratory that two sequential aza-residues at the N-terminus of tripeptides could induce single β-turn structure or even double β-turn structure.[9] Moreover, repeat mode aza/aza/α in the hexapeptide **2.4** (chapter 2, **Figure 2.1**) showing a 3_{10}-helix type structure suggests that the mode aza/aza/α is a potential brick to induce helical structures by constructing repeated β-turn structure in long peptides. Although we have found the double β-turn structure does not always exist stably in diaza-tripeptides, the single β-turn structure of the diaza-tripeptides is quite stable even in water (the result we found in the chapter 2). We speculated that if we introduce one or more than one

diaza-peptide units into long peptides, the β-turn structure induced by diaza-tripeptide unit probably could promote the formation of helical structures. To verify this assumption, here we tried to design and synthesize several nonapeptides containing different numbers of diaza-peptide units at different positions based on the sequence derived from the EF-helix of TTR (residues 75–83).

We introduced one to three diaza-peptide units in different position of the sequence, including the N-terminus, the middle and the C-terminus (**Table 3.1**). In the first seven designed peptides (peptide **1** to peptide **7**), their N-termini were capped by acetyl group and their carboxylic acids of C-terminus were replaced by amides. Then based on the CD conformational studies and Thioflavin-T (ThT) assays of these peptides, we further designed three peptides **8**, **9** and **10** without acetyl groups at the N-terminus (analogues of peptides **1**, **3** and **6** respectively) to investigate the impact of N-terminal free amine on the conformation and activity. These designed peptides can shed light into the influence of the number and position of diaza-peptide units on the conformation of nonapeptides.

Peptide	Sequence
Peptide **1**	Ac-Thr-Lys-Ser-Tyr-Trp-Lys-azaAla-azaLeu-Gly-NH_2
Peptide **2**	Ac-Thr-Lys-Ser-azaTyr-azahomoTrp-Lys-Ala-Leu-Gly-NH_2
Peptide **3**	Ac-azahomoThr-azaLys-Ser-Tyr-Trp-Lys-Ala-Leu-Gly-NH_2
Peptide **4**	Ac-Thr-Lys-Ser-azaTyr-azahomoTrp-Lys-azaAla-azaLeu-Gly-NH_2
Peptide **5**	Ac-azahomoThr-azaLys-Ser-azaTyr-azahomoTrp-Lys-Ala-Leu-Gly-NH_2
Peptide **6**	Ac-azahomoThr-azaLys-Ser-Tyr-Trp-Lys-azaAla-azaLeu-Gly-NH_2
Peptide **7**	Ac-azahomoThr-azaLys-Ser-azaTyr-azahomoTrp-Lys-azaAla-azaLeu-Gly-NH_2
Peptide **8**	H-Thr-Lys-Ser-Tyr-Trp-Lys-azaAla-azaLeu-Gly-NH_2
Peptide **9**	H-azahomoThr-azaLys-Ser-Tyr-Trp-Lys-Ala-Leu-Gly-NH_2
Peptide **10**	H-azahomoThr-azaLys-Ser-Tyr-Trp-Lys-azaAla-azaLeu-Gly-NH_2
Peptide **11**	H-Thr-Lys-Ser-Tyr-Trp-Lys-Ala-Leu-Gly-NH_2

Table 3.1: Designed aza-nonapeptides based on the EF-helix

3.2 The strategy to synthesize long peptides containing one or more than one diaza-peptide units

The synthesis of diaza-tripeptides in solution shown in the chapter 2 has confirmed that the coupling of diaza-peptide fragments with a natural amino acid is feasible by using triphosgene as carbonyl donor. In order to synthesize long peptides containing diaza-peptide units, we decided to apply this chemistry to Fmoc based solid phase peptide synthesis (SPPS). Thus, we had to first synthesize diaza-peptide building blocks in solution (**Figure 3.2**).

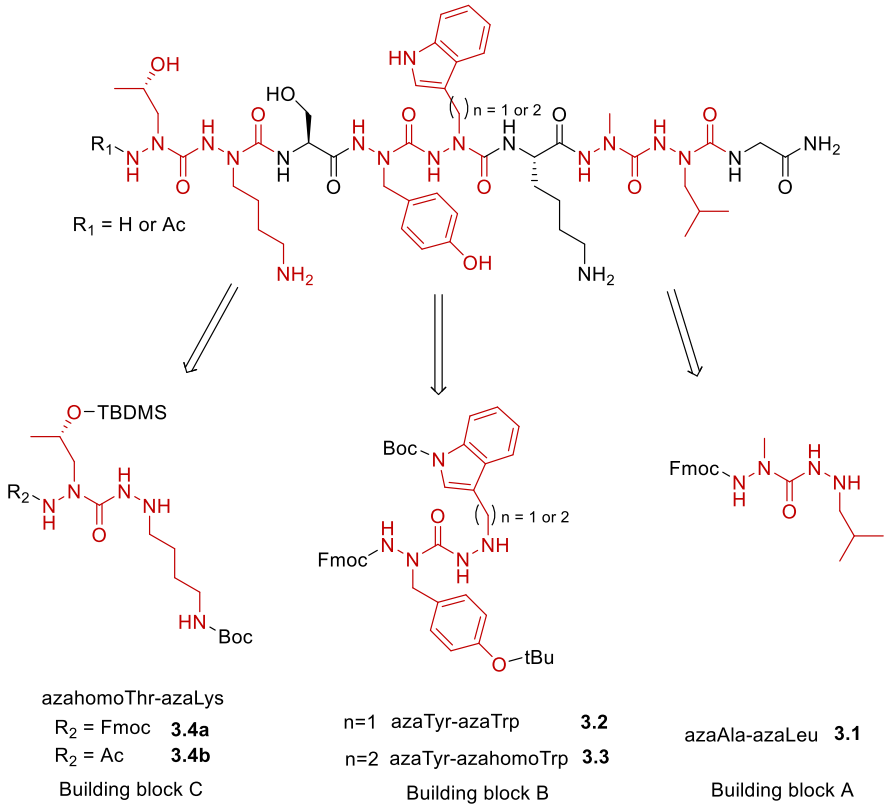

Figure 3.2: Design of building blocks

In the building block A (**3.1**), natural amino acids Ala and Leu were replaced by azaAla and azaLeu. In the building block B, Tyr was replaced by azaTyr. For the Trp, it has been reported that azaTrp residue was not stable in the acidic conditions used for the peptide cleavage from the Rink amide resin.[10] AzaTrp would lose the indolylmethyl moiety in acidic cleavage conditions (TFA) giving azaGly (**Figure 3.3**). Therefore, here we first synthesized building block B **3.2**, azaTyr-

azaTrp, to test its stability in acidic cleavage conditions. It was really unstable in acidic conditions. Thus, a new building block B (**3.3**), azaTyr-azahomoTrp, was used instead of azaTyr-azaTrp in the synthesis of aza-nonapeptides. In the building block C, since there is no report about the synthesis of azaThr precursor, probably because of synthetic issues and stability issues (similar to acetal structure unstable in acidic conditions), we used azahomoThr to replace azaThr. The synthesis of azahomoThr precursor was also not reported and thus was developed during my PhD.

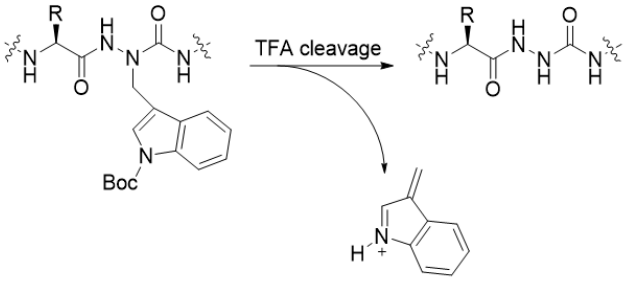

Figure 3.3: Instability of azaTrp under TFA cleavage condition

3.3 Synthesis of building blocks

3.3.1 Synthesis of the building block A

The synthesis of the building block A **3.1** was started from the reductive amination of benzyl carbazate with isobutyraldehyde using $NaBH_3CN$ as reductive reagent (**Figure 3.4**). After getting the Cbz-protected-2-isobutylhydrazine **3.5** (Yield: 94%), the Boc-protection of **3.5** using di-*tert*-butyl dicarbonate gave compound **3.6** (Yield: 82%). The Cbz-deprotection of compound **3.6** by catalytic hydrogenolysis provided Boc-protected-1-isobutylhydrazine **3.7** (Yield: 90%), which was activated by 4-nitrophenyl chloroformate to give compound **3.8** with 76% of yield. Treating **3.8** with **3.9** in the presence of DIPEA gave compound **3.10** in a yield of 82%. Removing the Boc group from **3.10** by treating it with 4M HCl in dioxane provided compound **3.1** as a hydrochloride salt (Yield: 90%).

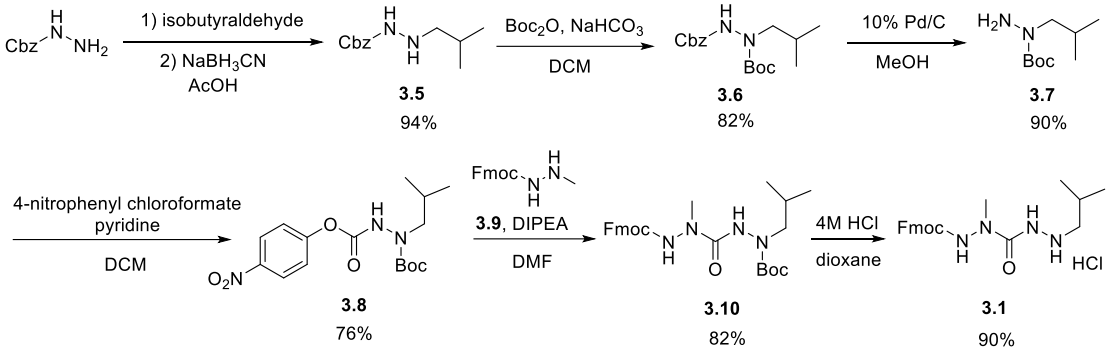

Figure 3.4: Synthesis of the building block A

The synthesis of compound **3.9** is illustrated in **Figure 3.5**. Methylhydrazine was protected with Boc group and Fmoc group consecutively and then the Boc group was removed using TFA to give compound **3.9** (Yield: 42%).

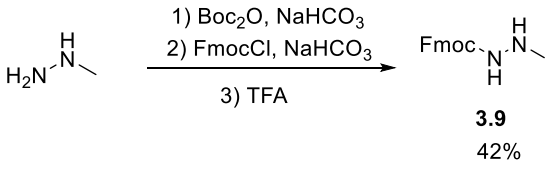

Figure 3.5: Synthesis of compound **3.9**

3.3.2 Synthesis of the building block B

For the synthesis of the building block B, at the beginning, we tried to synthesize azaTyr-azaTrp **3.2** and tested its stability in acidic conditions.

First, azaTyr precursor **3.13** (Yield: 86%) was synthesized through reductive amination of the commercially available compound **3.12** with Fmoc-hydrazine **3.11**. Likewise, azaTrp precursor **3.15** (Yield: 84%) was synthesized from reductive amination of the commercially available compound **3.14** with Fmoc-hydrazine **3.11** (**Figure 3.6**).

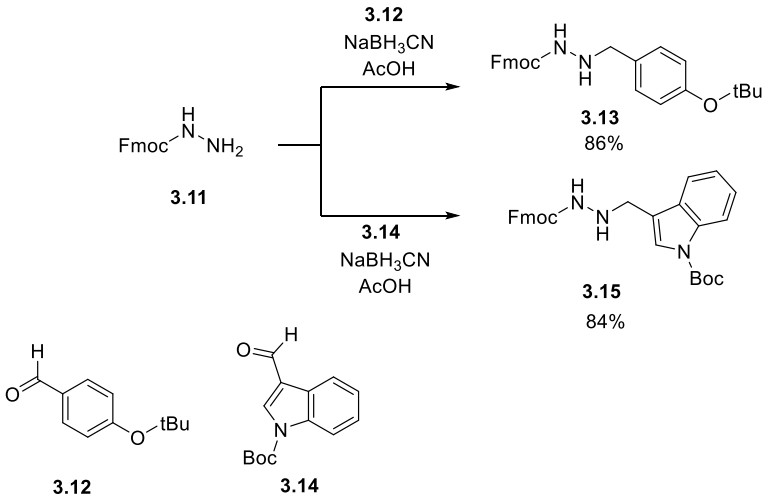

Figure 3.6: Synthesis of compounds **3.13** and **3.15**

Compound **3.15** was protected with Cbz group using CbzCl in the presence of collidine to give compound **3.16** (Yield: 78%). Compound **3.16** was treated with 20% piperidine/DMF to remove its Fmoc group to give compound **3.17** (Yield: 81%), which was activated by 4-nitrophenyl chloroformate to give compound **3.18** (Yield: 71%). Compound **3.18** reacted with compound **3.13** in the presence of DIPEA to give compound **3.19** in a low yield of 27%. Unfortunately, the cleavage of Cbz group from compound **3.19** did not give compound **3.2** because of the instability of Fmoc group under catalytic hydrogenolysis. (**Figure 3.7**)

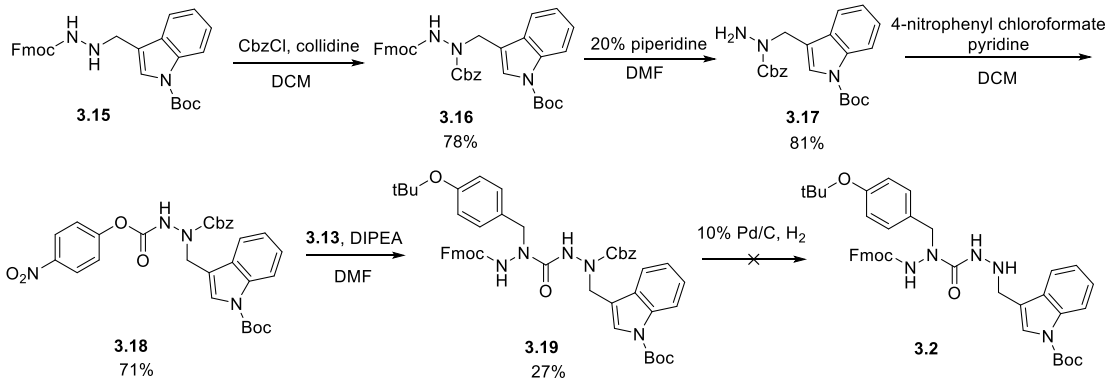

Figure 3.7: The first trial to synthesize compound **3.2**

Nevertheless, compound **3.19** was used to test the stability instead of **3.2**. Given that the deprotection of Boc group and *t*-Bu group and the cleavage of the peptides from the Rink amide

resin will be carried out in TFA/H_2O (95/5), compound **3.19** was treated by TFA/H_2O (95:5) for 1 h and the solution was checked by LC-MS. The result showed that **3.19** was actually unstable in this condition and the main product was azaTyr-azaGly **3.20b** (**Figure 3.8**), which was in line with the Lubell's report on azaTrp.[10]

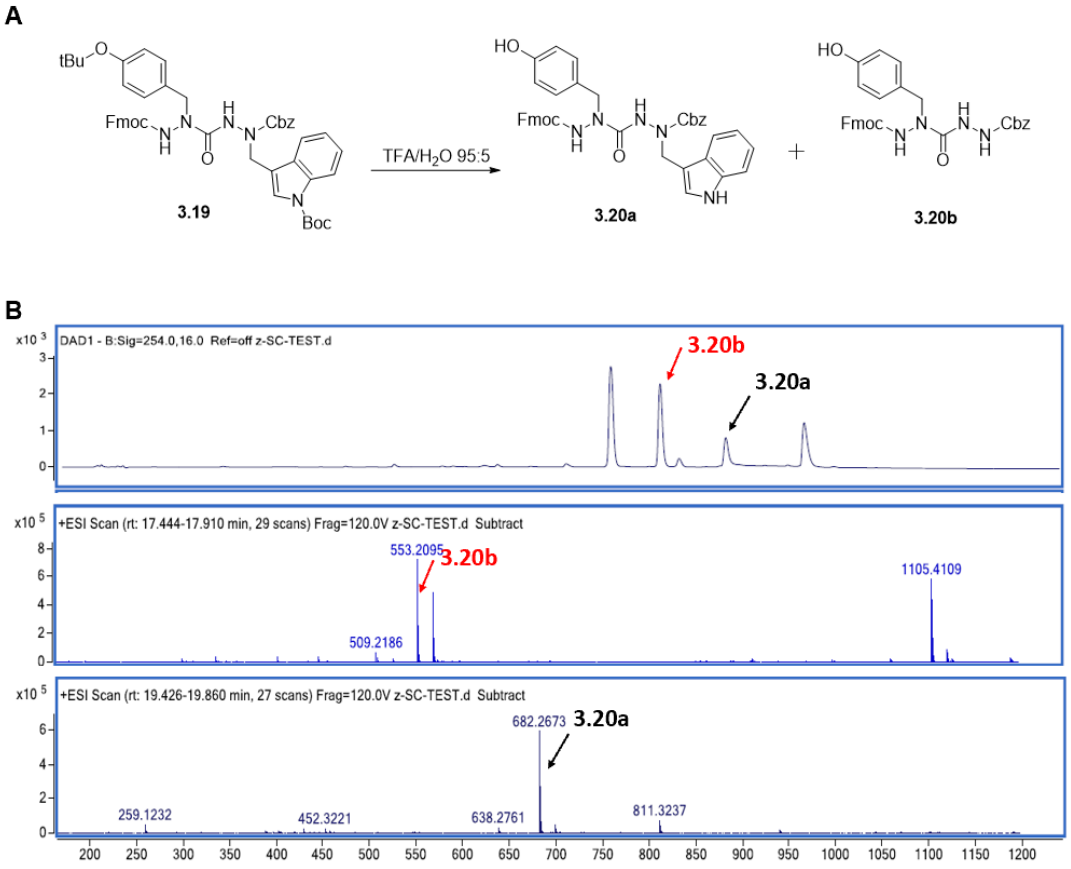

Figure 3.8: A) Side product when treating **3.19** with TFA/H_2O; B) LC-MS spectrum of the solution of **3.19** in TFA/H_2O (95/5) after 1 h incubation at room temperature

Thus, we decided to use azaTyr-azahomoTrp **3.3** instead of azaTyr-azaTrp **3.2** as building block B. The scheme of the synthesis of azaTyr-azahomoTrp **3.3** is illustrated in **Figure 3.9**. Indole-3-acetic acid was methylated using thionyl chloride in MeOH to give the ester, then the indole was protected using di-*tert*-butyl dicarbonate to give compound **3.21** (Yield: 95%). The ester of **3.21** was reduced to aldehyde **3.22** using DIBAL-H (Yield: 32%). The reductive amination of **3.22** with **3.11** provided compound **3.23** (Yield: 80%), which was protected with an Alloc group to give **3.24** (Yield: 90%). The Fmoc group of **3.24** was removed using 20% piperidine/DMF to give compound **3.25**

(Yield: 92%). The activation of the **3.25** using 4-nitrophenyl chloroformate gave compound **3.26** (Yield: 70%). Compound **3.26** reacted with compound **3.13** in the presence of DIPEA to provide compound **3.27** (Yield: 77%). In the end, the Alloc group was removed from **3.27** using Tetrakis-Pd reagent in the presence of N, N-dimethyl barbituric acid to give compound **3.3** in a yield of 74%.

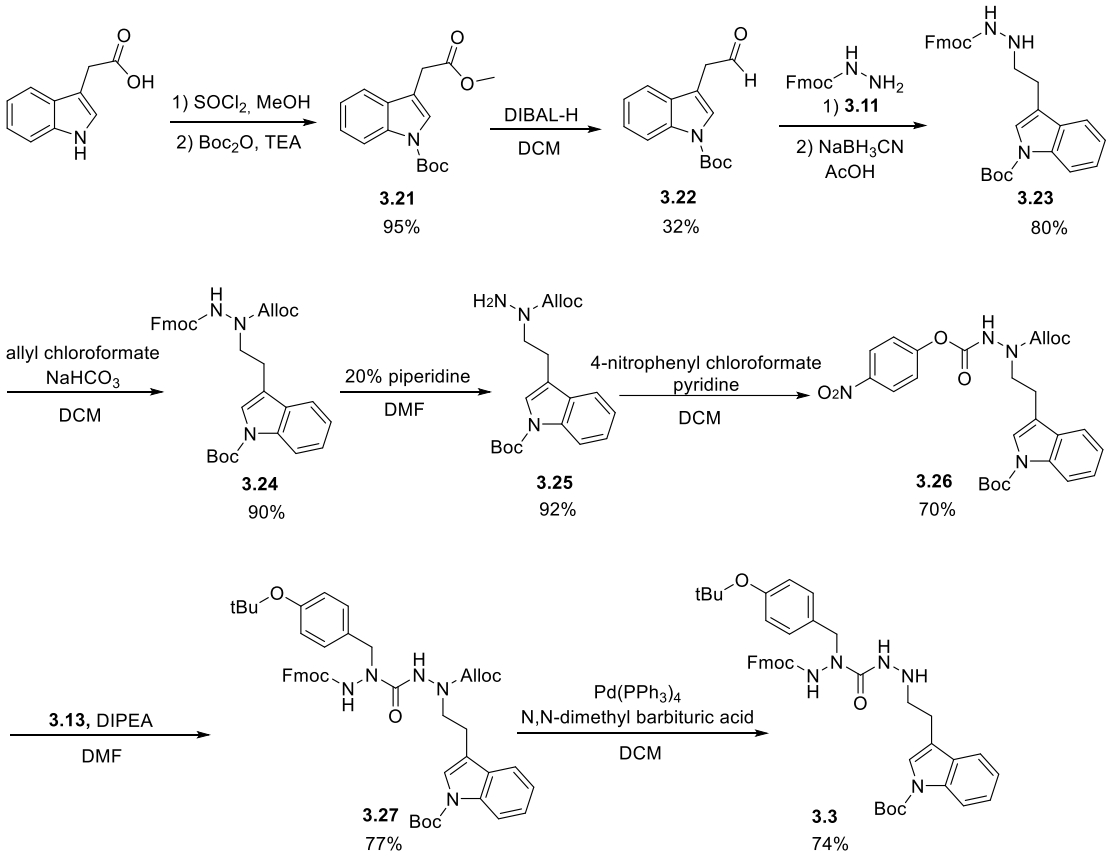

Figure 3.9: Synthesis of the building block B

3.3.3 Synthesis of the building block C

For the synthesis of the building block C (**Figure 3.10**), *S*-ethyl lactate was protected by TBDMSCl to give compound **3.28** in a satisfactory yield (99%). The ester of **3.28** was reduced to aldehyde **3.29** using DIBAL-H (Yield: 59%). Aldehyde **3.29** reacted with Fmoc-hydrazine **3.11** or acetyl hydrazide to give compounds **3.30a** (Yield: 53%) or **3.30b** (Yield: 90%) by reductive amination reaction. In parallel, the synthesis of azaLys part was started from the Boc protection of 4-aminobutyraldehyde diethylacetal using di-*tert*-butyl dicarbonate to give compound **3.31** in a

satisfactory yield (99%), which could be transformed to compound **3.32** in a mixture of acetic acid and water (2/1) at room temperature (Yield: 98%). The reductive amination of compound **3.32** with **3.11** gave compound **3.33** in a moderate yield of 39%. The protection of compound **3.33** using allyl chloroformate gave compound **3.34** (Yield: 86%) and then the removal of the Fmoc group from compound **3.34** was performed in 20% piperidine/DMF to give compound **3.35** (Yield: 84%). The activation of **3.35** using 4-nitrophenyl chloroformate gave compound **3.36** (Yield: 96%). Compound **3.36** reacted with **3.30a** or **3.30b** in the presence of DIPEA to give compound **3.37a** (Yield: 68%) or **3.37b** (Yield: 78%). The Alloc-deprotection of **3.38a** and **3.38b** afforded **3.4a** (Yield: 70%) and **3.4b** (Yield: 79%) using Tetrakis-Pd reagent in the presence of N, N-dimethyl barbituric acid.

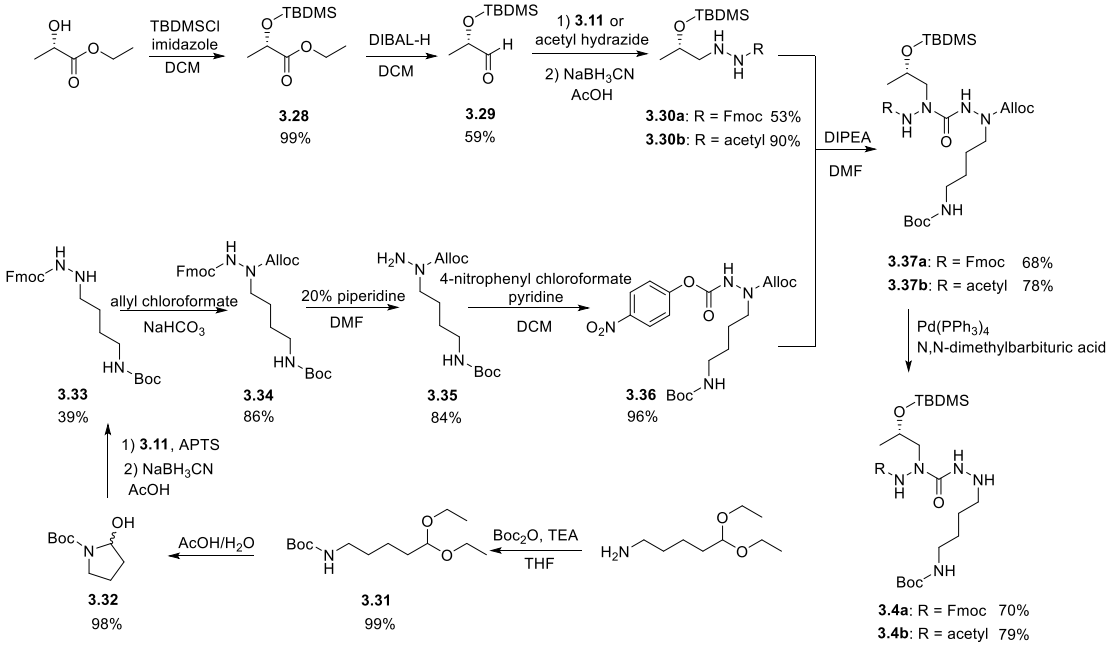

Figure 3.10: Synthesis of the building block C

3.4 Synthesis of long azapeptides or peptides using Fmoc based SPPS

3.4.1 Synthesis of peptides 1 and 8

The Rink amide MBHA resin (100-200 mesh) was chosen as insoluble polymer support in SPPS to get amide at the C-terminus of peptides. Peptide **1** was first synthesized (**Figure 3.11**)

because it is a sample one which has only one diaza-peptide unit at the C-terminus. Fmoc-Gly-OH was loaded to the resin using HCTU as a coupling reagent in the presence of 20% NMM in DMF to give resin **3.38**. The coupling was performed twice to ensure high yield (>85%). The yield was evaluated by the result from the Fmoc test.[11] Resin **3.38** was capped in the presence of NMM using acetic anhydride and then was treated with 20% piperidine in DMF to release the free amino group of Gly. To couple building block A with the Gly attached on the resin, a pre-activation of the building block A was first performed using triphosgene as a carbonyl donor and DIPEA as base in DCM. Then the reactive solution was transferred to the plastic syringe tube containing the resin and 1.5 eq DIPEA was added. The reaction was agitated on an automated shaker at room temperature for 5 h. After reaction, the resin was filtered, washed by organic solvents (DMF: 3 x 10 mL, MeOH: 3 x 10 mL, DCM: 3 x 10 mL) and dried under vacuum. The main product **3.39** of the reaction was verified by the LC-MS analysis of the solution from the cleavage of a resin aliquot. The Fmoc test also suggested a satisfactory yield of this step (74%). This means that the method we used for the synthesis of diaza-tripeptides in solution is applicable to the SPPS.

Next, resin **3.39** was treated with 20% piperidine in DMF to give the free amino group of the aza-residue at the N-terminus and then Fmoc-Lys(Boc)-OH was introduced using HCTU in the presence of NMM as base. After 1 h agitation in DMF, the Fmoc test showed only 27% yield. It seems that the less nucleophilic character of the amino group of aza-residue gives rise to the low yield of the coupling reaction. It was reported that Oxyma-based activators could lead to nearly complete aza-peptide bond formation.[12] Therefore, instead of using HCTU, a combination of DIC and Oxyma was used as coupling reagents in the coupling. In addition, collidine was used as base and the solvent was a mixture of DCM and DMF (1/2). After 5 h agitation at room temperature, the Fmoc test showed 55% yield. The reaction was performed again for 5 h to further increase the yield to 90% and the product **3.40** was confirmed by LC-MS.

The following natural amino acids were introduced sequentially by conventional protocol of SPPS using HCTU as a coupling reagent and NMM as base, to get resin **3.41**. The Fmoc group was removed from resin **3.41** using 20% piperidine in DMF and the acetylation was performed using 0.25 M acetic anhydride in DMF in the presence of NMM to give resin **3.42**. The peptide was cleaved from the resin **3.42** and the protecting groups (Boc and *t*Bu) were removed simultaneously

using a cocktail of TFA/H_2O/TIPS/thioanisole (90/5/2.5/2.5) to give the crude peptide **1** which was purified by semi-preparative HPLC (Total yield after purification: 15 %).

In parallel, peptide **8** without the acetyl group at the N-terminus could be obtained from resin **3.41** by the treatment with 20% piperidine in DMF and cleavage in TFA/H_2O/TIPS/thioanisole (90/5/2.5/2.5) (**Figure 3.11**). The crude was also purified by semi-preparative HPLC (Total yield after purification: 13 %).

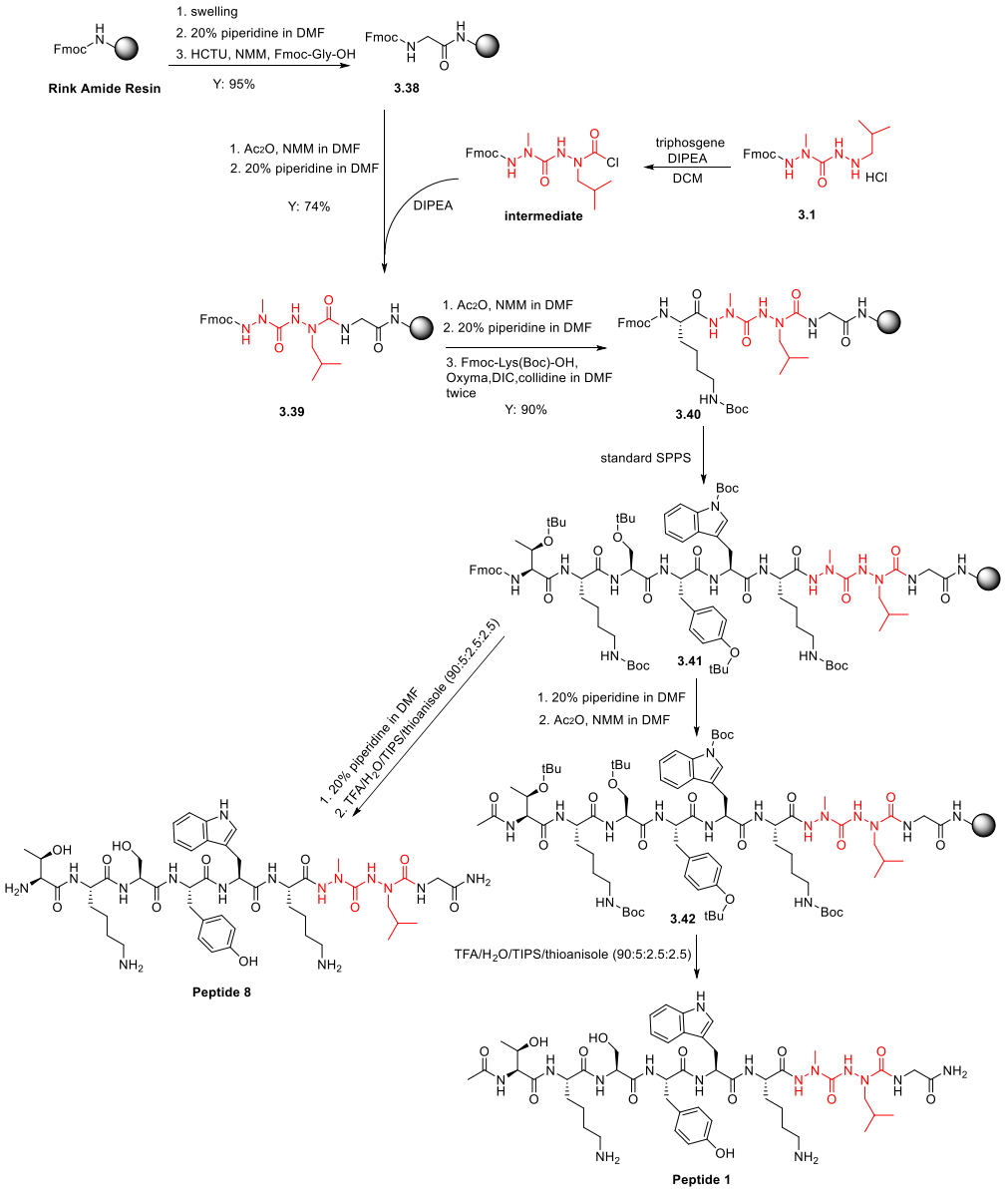

Figure 3.11: Synthesis of peptides **1** and **8** (The yields mentioned in the scheme are estimated yields using Fmoc test)

3.4.2 Synthesis of peptide 2

The synthesis of peptide **2** was started from four successive couplings of the corresponding protected-amino acids, Gly, Leu, Ala and Lys to the Rink amide resin, by conventional protocol of SPPS using HCTU as a coupling reagent and NMM as base to give resin **3.43** (**Figure 3.12**). Then the building block B **3.3** was introduced successfully using triphosgene as a carbonyl donor in DCM (5 h agitation at room temperature) to give resin **3.44** (Yield: 82%). After removing the Fmoc group from the resin **3.44** in 20% piperidine/DMF, we attempted to couple Fmoc-Ser(*t*Bu)-OH to the N-terminal aza-residue of resin **3.44** using the same conditions as we used for the synthesis of peptide **1**. However, the reaction only showed the low yields in the Fmoc test and LC-MS analysis (the conversion is less than 10%). The steric hindrance was considered as a main reason that blocks the reaction. In the synthesis of peptide **1**, the N-terminal aza-residue of resin **3.39** is azaAla with methyl group as a side chain whereas in the synthesis of peptide **2**, azaTyr is at the N-terminus of **3.44** whose more sterically hindered side chain might prevent the coupling reaction with the activated Fmoc-Ser(*t*Bu)-OH. In order to increase the yield of the reaction, the reaction temperature was increased to 40°C to overcome the steric hindrance. To our delight, resin **3.45** could be obtained in a good yield (85%) after coupling twice with Fmoc-Ser(*t*Bu)-OH at 40°C using DIC and Oxyma as coupling reagents. After that, Lys and Thr were introduced sequentially by conventional protocol of SPPS and the Fmoc group of **3.46** was replaced by an acetyl group to give resin **3.47** from which peptide **2** was cleaved and purified by semi-preparative HPLC. (Total yield after purification: 10 %).

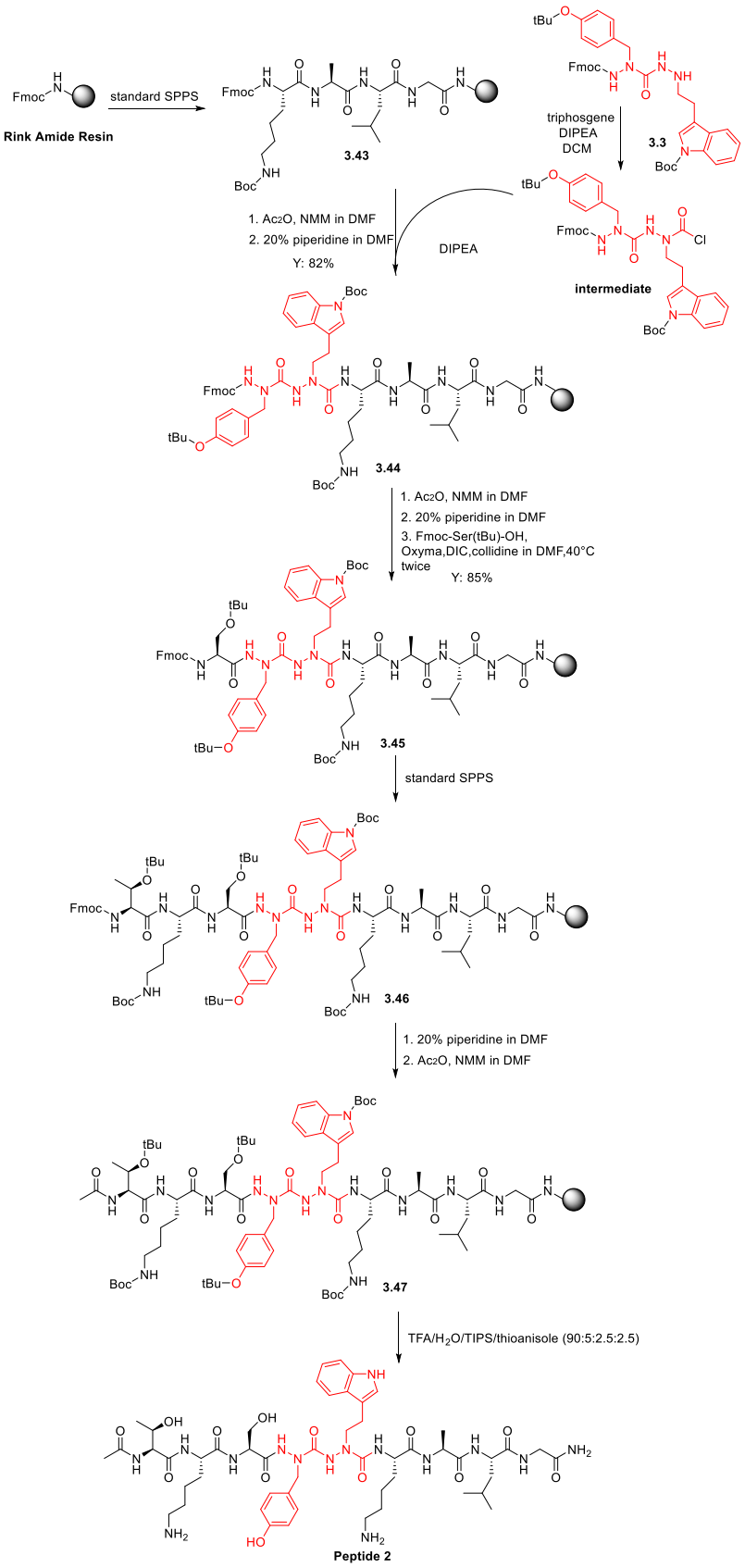

Figure 3.12: Synthesis of peptide **2** (The yields mentioned in the scheme are estimated yields using Fmoc test)

3.4.3 Synthesis of peptide 3

Peptide **3** was synthesized in a similar way (**Figure 3.13**). The first seven amino acids were introduced by conventional protocol of SPPS to give resin **3.48**. After removing the Fmoc group from resin **3.48**, the building block C **3.4b** was pre-activated by triphosgene in DCM to treat with the resin. The mixture was agitated at room temperature for 5 h to get resin **3.49** (Yield: 67%), from which peptide **3** was cleaved and purified by semi-preparative HPLC (Total yield after purification: 12 %).

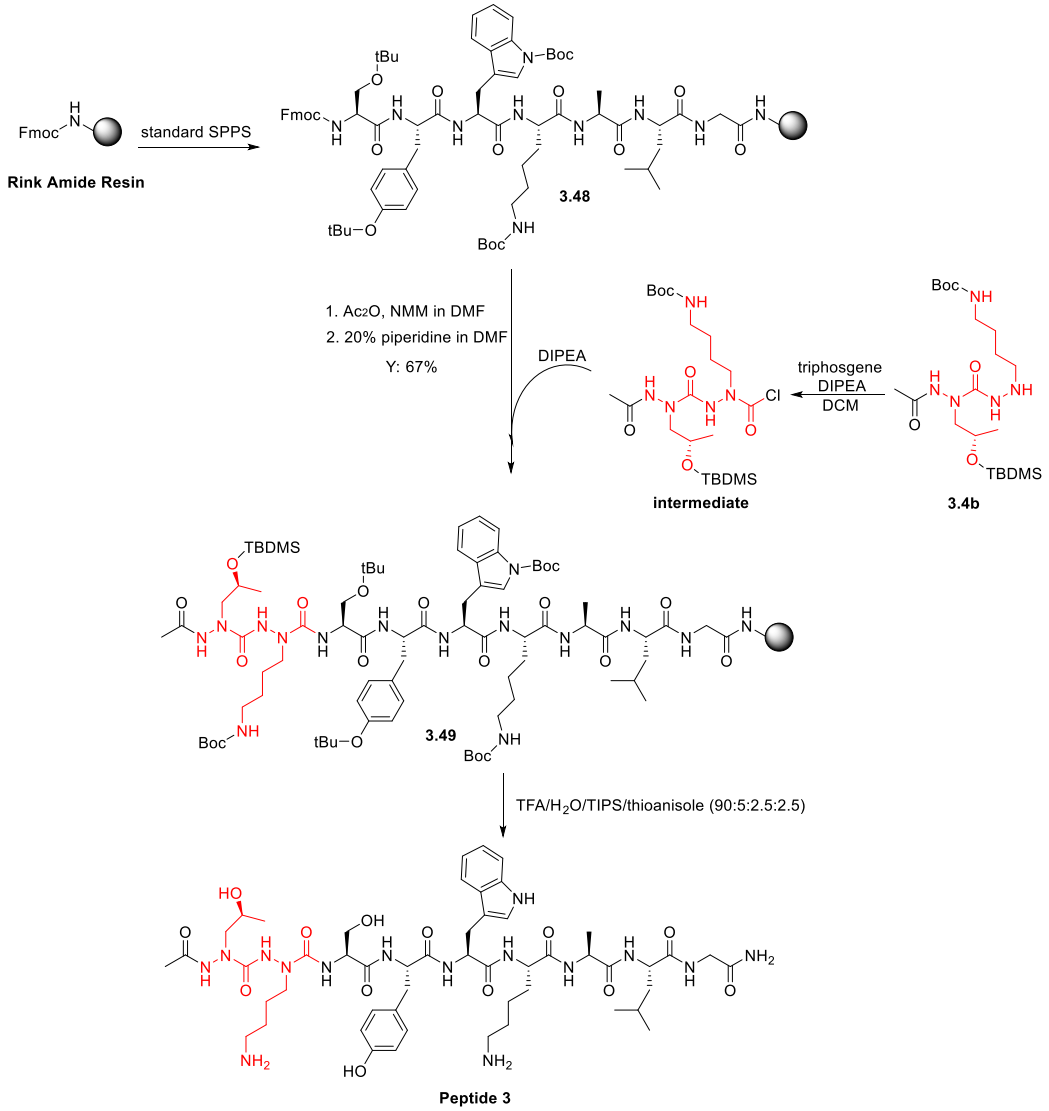

Figure 3.13: Synthesis of peptide **3** (The yield mentioned in the scheme is an estimated yield using Fmoc test)

3.4.4 Synthesis of peptide 4

On the basis of the chemistry we used for the syntheses of peptides **1**, **2** and **3**, peptides **4**, **5**, **6** and **7** could be synthesized easily.

Peptide **4** was prepared from the resin **3.40** (**Figure 3.14**). The resin **3.40** prepared previously (**Figure 3.11**) was first treated with 20% piperidine/DMF in a plastic syringe tube to release the free amino group. Then building block B **3.3** was preactivated using triphosgene in presence of DIPEA in DCM for 10 min. After that, the solution was transferred to the plastic syringe tube and the mixture was agitated at room temperature for 5 h to get resin **3.50**. Fmoc-Ser(*t*Bu)-OH was introduced using the same conditions used in the synthesis of **3.45** (**Figure 3.12**) to provide resin **3.51**, followed by standard SPPS procedure to give **3.52**. After replacement of the Fmoc group by an acetyl group, peptide **4** could be cleaved from resin **3.53** and purified by semi-preparative HPLC in a yield of 13 %.

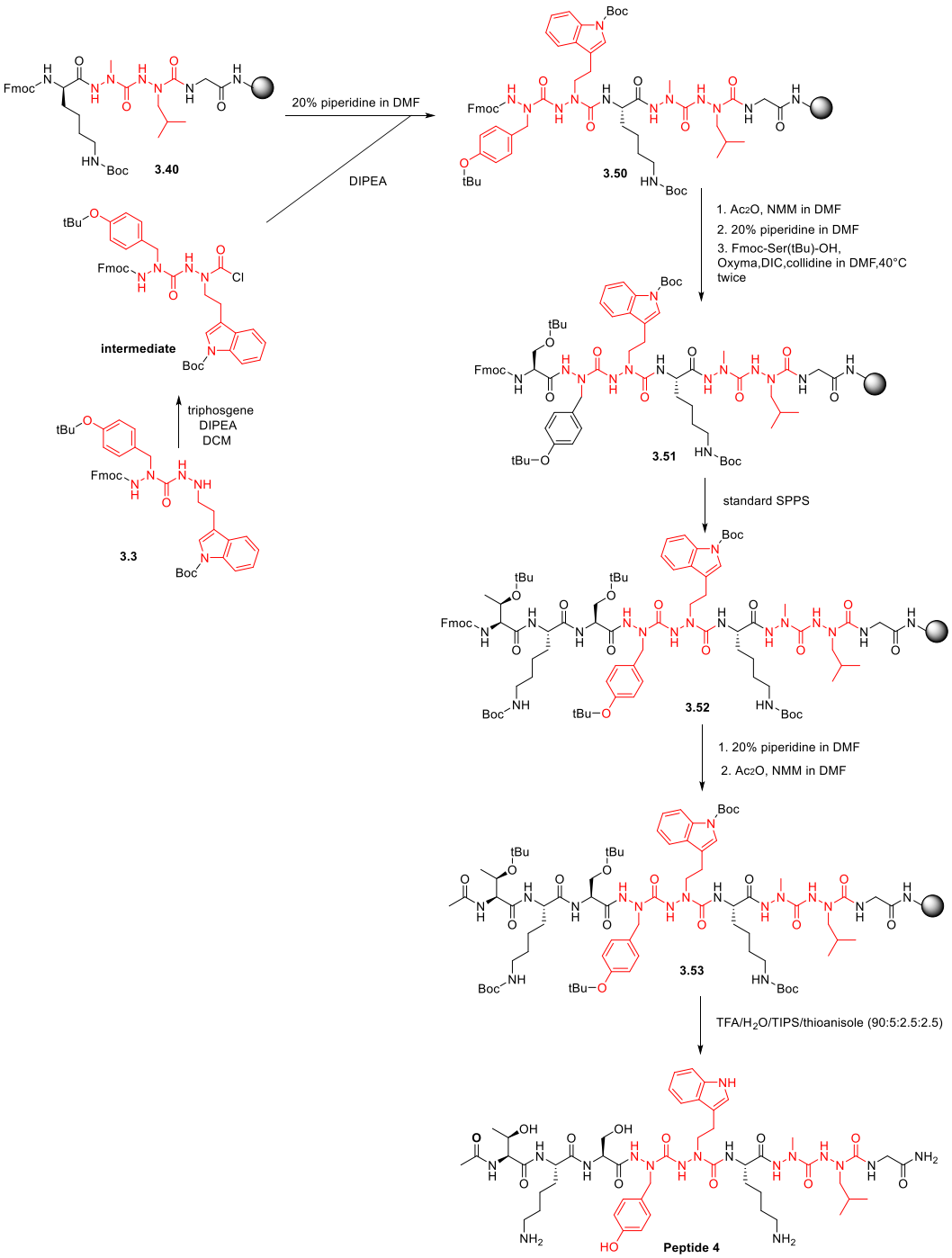

Figure 3.14: Synthesis of peptide **4**

3.4.5 Synthesis of peptide 5

Peptide **5** was prepared from the resin **3.45** (**Figure 3.15**). After removal of the Fmoc group from the resin **3.45**, the preactivated **3.4b** could react with the free amino group of the peptide to

provide resin **3.54**. Peptide **5** was cleaved from the resin **3.54** and purified by semi-preparative HPLC (Total yield after purification: 8 %).

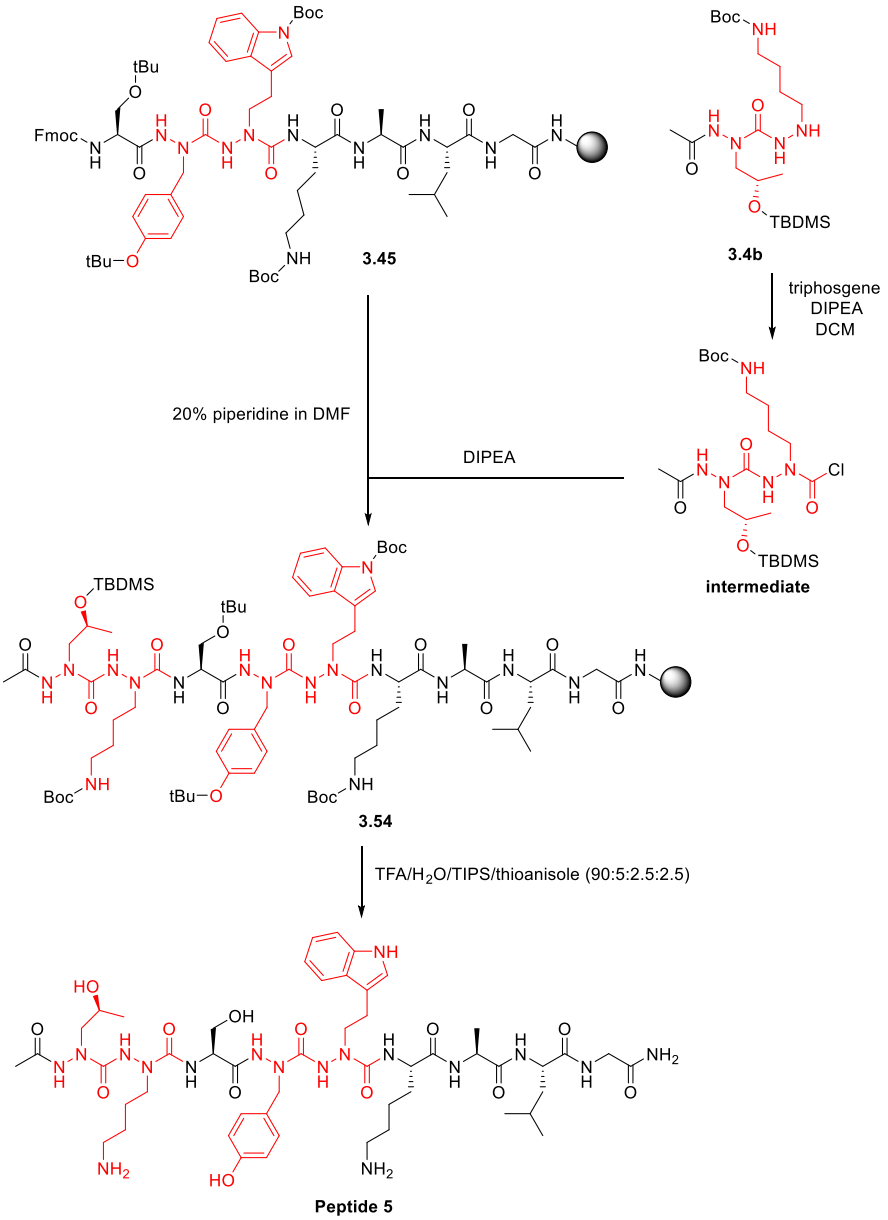

Figure 3.15: Synthesis of peptide **5**

3.4.6 Synthesis of peptide 6

Peptide **6** was prepared from the resin **3.40** prepared previously (**Figure 3.11**). The standard SPPS was performed on resin **3.40** to get resin **3.55** (**Figure 3.16**). Then the same procedure as the

one used for the synthesis of peptide **3** (see in **Figure 3.13**) was performed on the resin **3.55** to provide peptide **6** (Total yield after purification: 14 %).

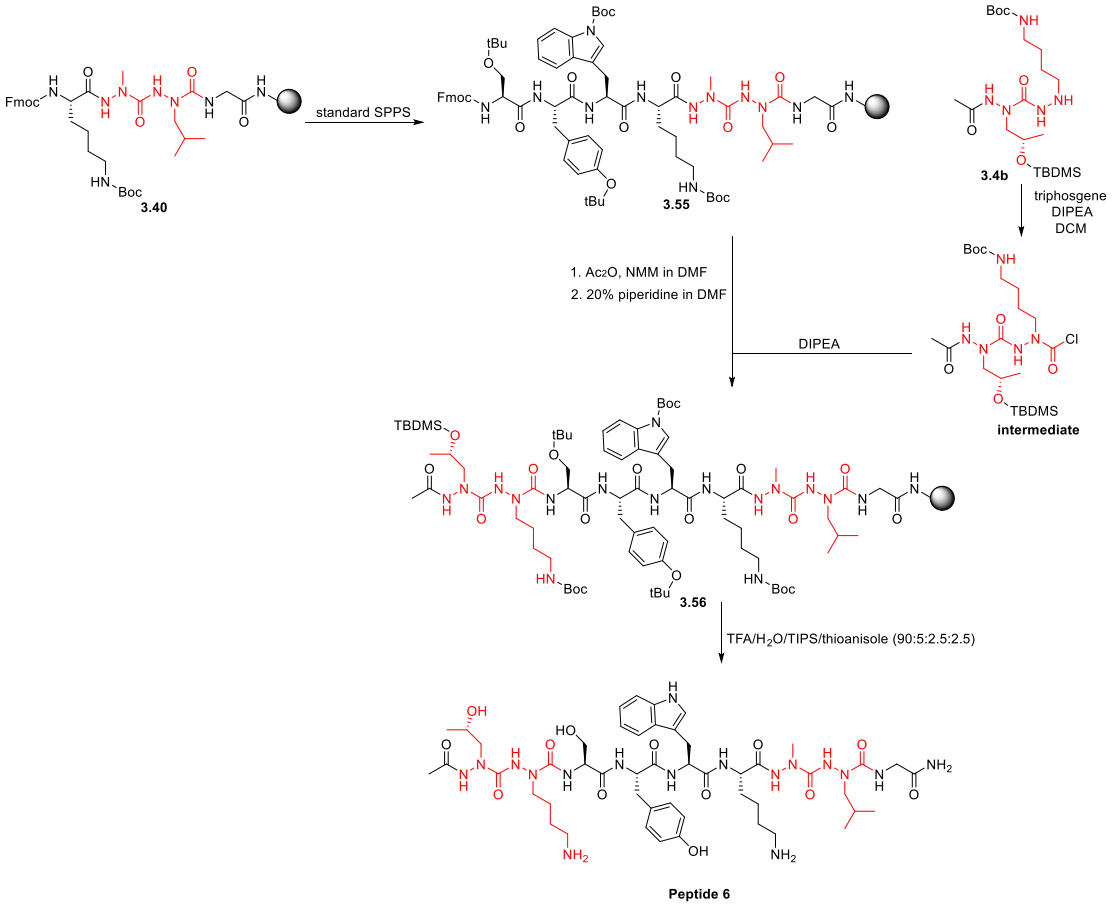

Figure 3.16: Synthesis of peptide **6**

3.4.7 Synthesis of peptide 7

Peptide **7** which contains three diaza-units could be synthesized from the resin **3.51** prepared previously (see in **Figure 3.14**). After removal of the Fmoc group from the resin **3.51**, the resin was treated with the activated intermediate of **3.4b** and DIPEA in a plastic syringe tube (**Figure 3.17**). The reaction was agitated on an automated shaker at room temperature for 5 h to give resin **3.57**. Peptide **7** was cleaved from the resin **3.57** and purified by semi-preparative HPLC (Total yield after purification: 10 %).

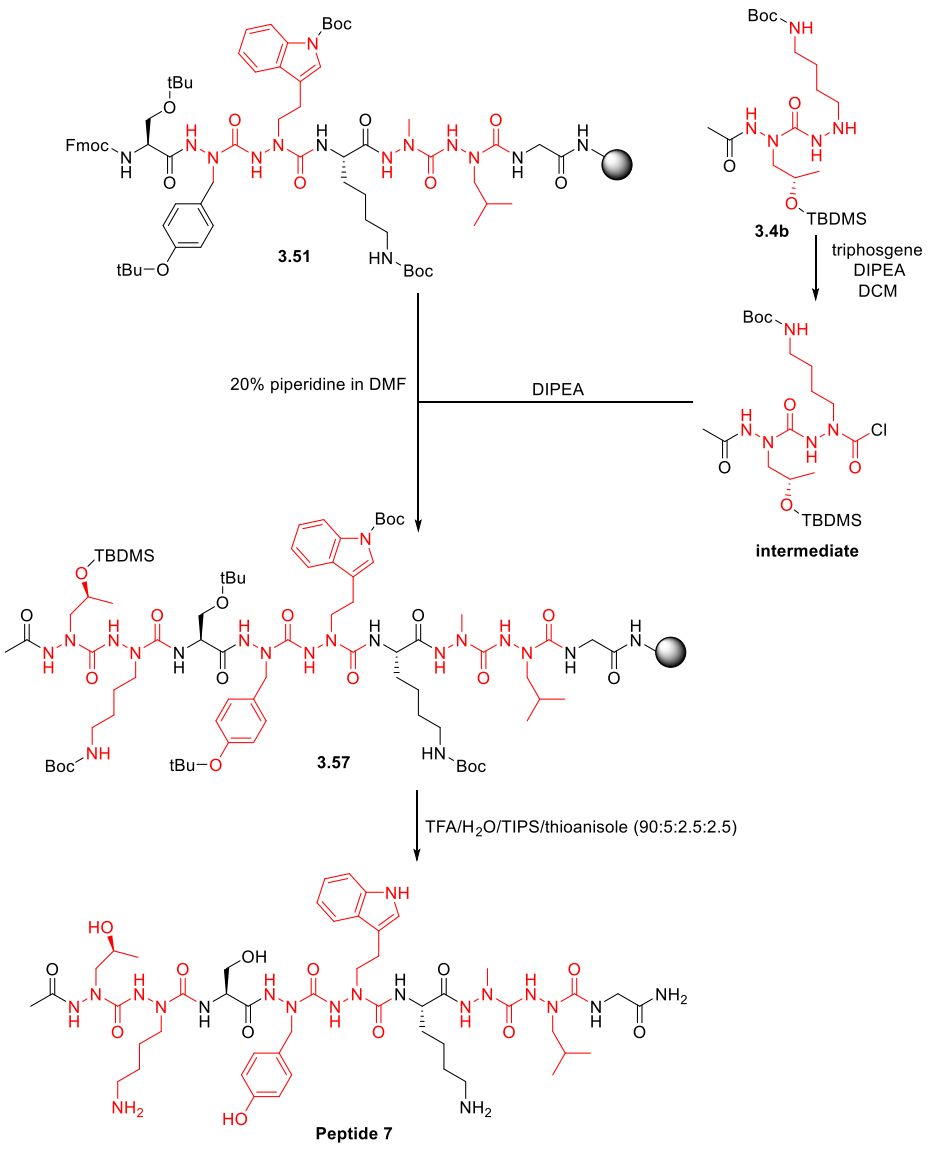

Figure 3.17: Synthesis of peptide **7**

3.4.8 Synthesis of peptides 9, 10 and 11

Peptides **9** and **10** (**Figure 3.18**) were prepared from resin **3.48** and resin **3.55**. After removal of the Fmoc group from **3.48** and **3.55**, the resins were treated with the activated building block C **3.4a** in the presence of DIPEA in DCM for 5 h to give resin **3.58** and resin **3.59**. Then the resin **3.58** and resin **3.59** were treated with 20% piperidine/DMF to remove the Fmoc group and then the cleavages were performed using TFA/H_2O/TIPS/thioanisole (90/5/2.5/2.5) for 1 h 30 min to provide crude peptides. Here the time of cleavage should be controlled because of the side reaction of the

azapeptides with free aza-residue at the N-terminus in acidic conditions (**Figure 3.19**). Although we did not find the peak of urazine structure by LC-MS analysis, the possible pathway to form the side products is proposed (**Figure 3.19A**) because the similar cyclization was found in the synthesis of diaza-tripeptides giving aza-diketopiperazines (in the chapter 2). The shorter the reaction time, the less side products were formed. The crudes were purified by semi-preparative HPLC (Total yield after purification: 14 % for peptide **9** and 7% for peptide **10**).

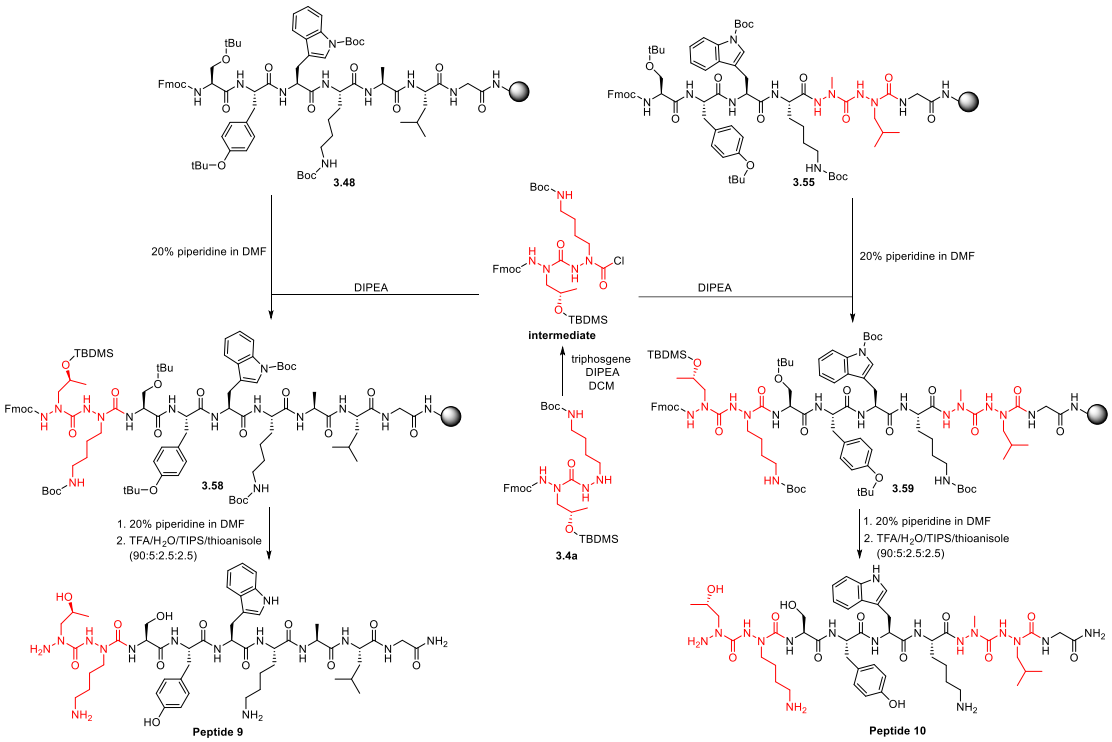

Figure 3.18: Synthesis of peptide **9** and peptide **10**

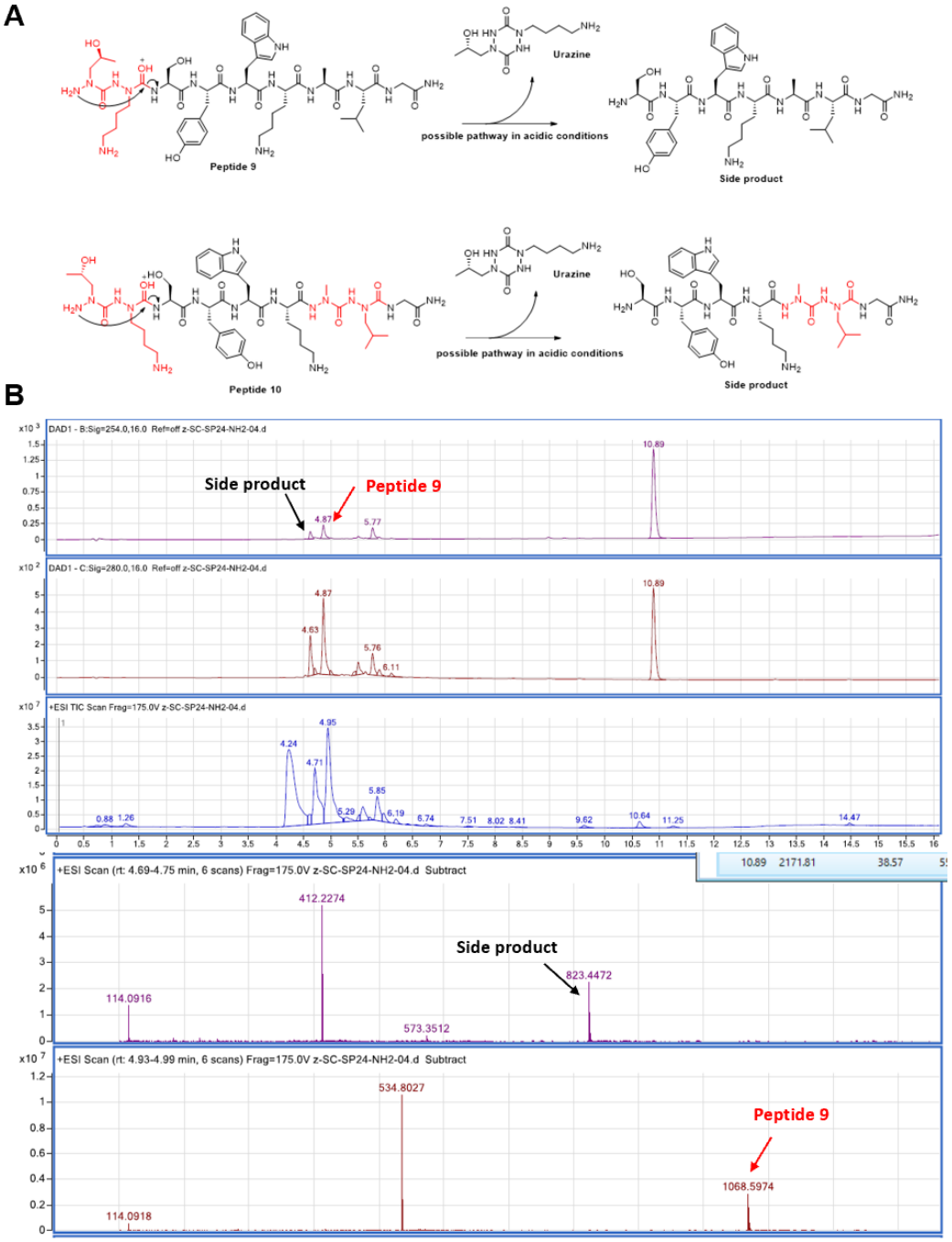

Figure 3.19: A) Possible pathway of side reaction from peptides **9** and **10** in acidic conditions; B) LC-MS spectrum of peptide **9** after cleavage from resin **3.58**

Peptide **11** containing only natural amino acids was prepared by conventional protocol of SPPS using HCTU as a coupling reagent and NMM as base and purified by semi-preparative HPLC.

3.5 Conformational studies

3.5.1 Circular dichroism (CD)

Plane polarized light could be viewed as two circularly polarized lights with equal intensity, which are right circularly polarized light and left circularly polarized light, respectively. CD is a classical spectroscopic method which is sensitive to the chirality of tested substance based on the different absorbances of chiral substance for right circularly polarized light and left circularly polarized light. Biomolecules, like proteins which are composed by chiral amino acids show several specific secondary structures, such as α-helix, β-sheet and random coil. Thanks to the ability of CD analyses to show quite different spectra for proteins depending on their secondary structures, CD has been extensively used for the determination of secondary structures of proteins or polypeptides. Given that in polypeptides or proteins, the most general chromophore is amide group which has two low energy electronic transition (**Figure 3.20**): n→π transition (near 220 nm) and π→π* transition (near 200 nm), the absorption spectra of polypeptides or proteins normally fall in the range of 190 nm and 260 nm.

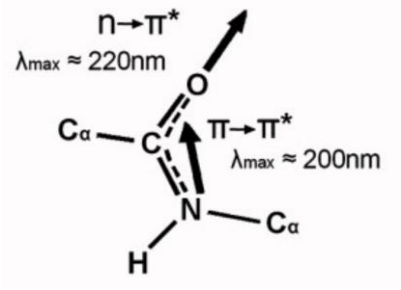

Figure 3.20: The illustration of two low energy electronic transition: n→π transition (near 220 nm) and π→π* transition (near 200 nm) in amide group[13]

α-Helix has a very distinct CD spectrum which shows a strong positive band around 190 nm and a negative band with two minima near 208 nm and 222 nm (**Figure 3.21**).[14] Normally, α-helix can be identified very well by CD with high confidence. β-Sheet shows less intense spectrum which has one positive band near 198 nm and one negative band near 215 nm (**Figure 3.21**).[14] Because of the diversity of β-sheet structure (parallel, antiparallel or mixed), the prediction of β-sheet in proteins shows less confidence.[15] In contrast of α-helix and β-sheet, the CD spectrum of random coil shows a negative band with a minimum between 190 nm and 200 nm and no obvious positive maximum between 210 nm and 230 nm.[14] In addition to these basic secondary structures,

polyproline structures also could be identified by CD. Polyproline type I usually exists in relatively nonpolar solvents like n-propanol and has one negative band with a minimum near 200 nm and one positive band with a maximum near 215 nm, whereas polyproline type II is favored in aqueous solution and has one negative band with a minimum near 205 nm and one weak positive band with a maximum near 226 nm (**Figure 3.22**).[16] For the polypeptides constituted by non-proline amino acids, blueshift happens around 10 nm on the spectrum of PPII because of the difference of transition between secondary and tertiary amides.

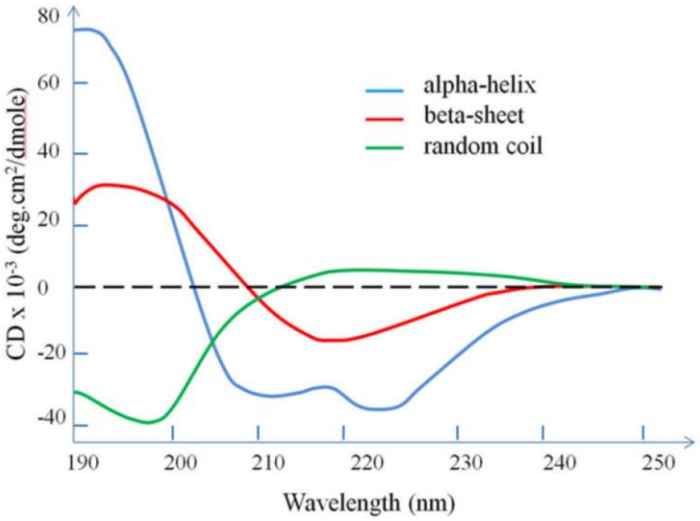

Figure 3.21: The standard CD spectra for α-helix, β-sheet and random coil[17]

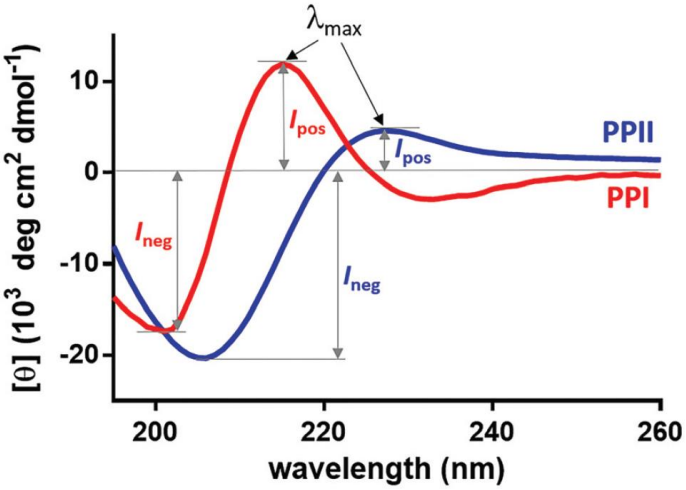

Figure 3.22: The standard CD spectra for PPI and PPII[18]

The conformations of our synthesized peptides were first analyzed by their CD spectra. The CD spectra of the peptides (125 μM) were measured in 20 mM phosphate buffer (PB) solution

(pH7.4) at 37°C. The natural peptide **11** showed typically random coil shape in its CD spectrum as we expected (**Figure 3.23A**). The peptides **1** and **3**, which have one diaza-peptide unit at the C-terminus and N-terminus respectively, showed similar shape of CD spectra with a strong negative band near 195 nm and a weak positive band near 225 nm (**Figure 3.23B**). For peptide **1**, the weaker positive band near 225 nm compared to peptide **3** indicates a less structured conformation. The peptide (**6**) which has two diaza-peptide units at the N-and C-termini respectively displayed an even stronger positive band at 225 nm in its CD spectrum (**Figure 3.23B**) compared to peptides **1** and **3**, but a less negative band near 195 nm. The spectra of peptides **1**, **3** and **6** indicate that diaza-peptide units at the N- or C-terminus of the nonapeptides have tendency to induce specific structure which has positive maximum around 225 nm. This positive band normally could be found in PPII but the CD spectra of PPII is generally accompanied by a negative signal near 205 nm. It was also reported, however, that some β/γ-peptides in 13-helix or Aib foldamers in 3_{10}-helix can display this positive band in CD spectra but they also show a negative band near 205 nm.[19–22] In addition, the proximity of two aromatic side chains in peptides also could create this positive band. [23–25] The similar CD spectrum with the spectrum of peptide **6** was also observed in peptide **10**, which has the same diaza-peptide units as peptide **6** but without acetyl group at the N-terminus (**Figure 3.23B**). This result suggests that acetyl group at the N-terminus has no obvious impact on the structural behavior of peptides in CD. When a diaza-peptide unit was placed in the central of the sequence (peptide **2**), the spectrum showed a negative minimum around 195 nm and a negative maximum near 212 nm (**Figure 3.23A**). The further introduction of one diaza-peptide unit at the N-terminus of peptide **2** to get peptide **5**, gave a weak negative minimum around 195 nm and a positive maximum near 212 nm (**Figure 3.23A**). For peptide **4**, which has two diaza-peptide units at the C-terminus and central part of the sequence respectively, although the spectrum showed the maximum near 212 nm, the minimum was in lower wavelength below 190 nm (**Figure 3.23A**). When three diaza-peptide units were introduced in the sequence (peptide **7**), the CD spectrum displayed one positive maximum between 190 nm and 200 nm and no negative band at tested wavelength (**Figure 3.23A**). We can see that the different numbers of diaza-peptide units at various positions of the sequence have different conformations based on the CD spectra, which suggests that diaza-peptide units have obvious impacts on the control of the peptide conformation.

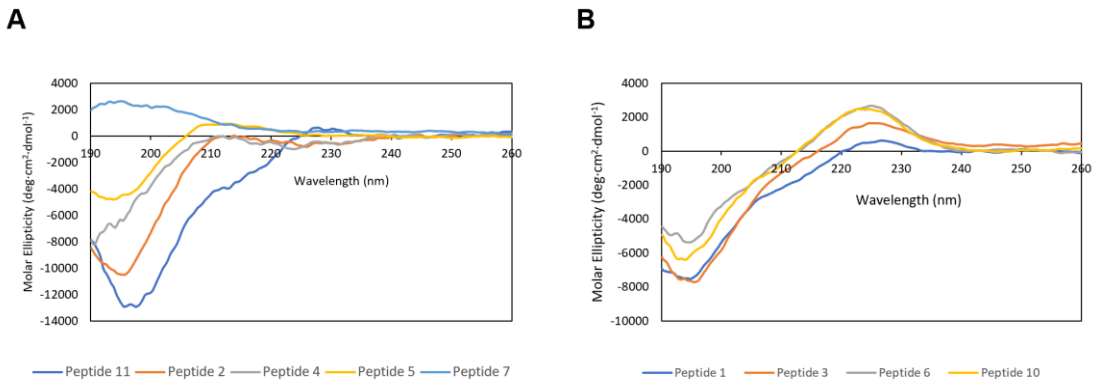

Figure 3.23: A) The CD spectra of peptides **2**, **4**, **5**, **7** and **11**; B) The CD spectra of peptides **1**, **3**, **6** and **10**; measured in 20 mM PB solution at 310 K (The concentration of peptides is 125 μM)

Given that the CD spectra of peptides **6** and **10** in PB solution showed strongest positive bands at 225 nm which could arise from PPII but also to 3_{10}-helix[21,22] or 13-helix[19,20] (see above), other CD assays on peptides **6** and **10** were performed to shed light into the property of the conformations. The spectra of peptide **10** in MeOH and ACN at the 37°C (310 K) were measured to investigate the influence of solvent on its conformation. Peptide **10** showed almost the same CD spectrum in MeOH compared it in PB solution but its spectrum in ACN showed small red shift on the negative minimum (from 196 nm to 200 nm), which make the CD spectrum more similar to the β/γ-peptides showing 13-helix or the Aib foldamer showing 3_{10}-helix[19–22] (**Figures 3.24A** and **3.24B**). The influences of temperature on the conformations of peptides **6** and **10** were studied by variable-temperature CD experiment. The intensities of the positive band around 225 nm and the negative band around 195 nm had small decreases for peptides **6** and **10** when the temperature was increased (**Figures 3.24C** and **3.24D**). As we known, PPII can be destroyed at high temperature.[26] The small decreases means that peptides **6** and **10** are relatively stable at high temperature, which is not compatible with PPII structure. Chaotropic agents, such as guanidine and urea, were reported to be able to bind backbone of polypeptides, thereby forcing polypeptides to be extended.[26,27] Thus, addition of urea will give rise to more rigid PPII structure, which could be reflected on the stronger positive band around 225 nm in CD spectra. The CD spectrum of peptide **6** was measured in 6 M urea aqueous solution and it actually showed stronger positive band around 225 nm (**Figure 3.24E**), which was in line with

PPII structure. It was reported that the presence of $CaCl_2$ in the solution of peptides can destroy PPII because $CaCl_2$ can disrupt the extended helix.[28,29] The CD spectrum of peptide **6** in 1 M $CaCl_2$ aqueous solution did not reduce the positive band around 225 nm (**Figure 3.24E**), which excluded the PPII of peptide **6**. The results from CD assays made difficult to attribute the positive band at 225 nm to a specific secondary structure. We could not exclude 3_{10}-helix which also show the same positive band. Moreover, in our case, there are two aromatic residues, Tyr and Trp, in the sequence and they are adjacent to each other. The introduction of diaza-peptide units at the N- and/or C-terminus probably brings these two aromatic side chains closer together in space, which also could generate this positive band. The CD analysis could not allow us to establish a defined conformation, so further conformational studies by other techniques such FTIR and NMR should be performed to provide more information about the conformation of the azapeptidic foldamers.

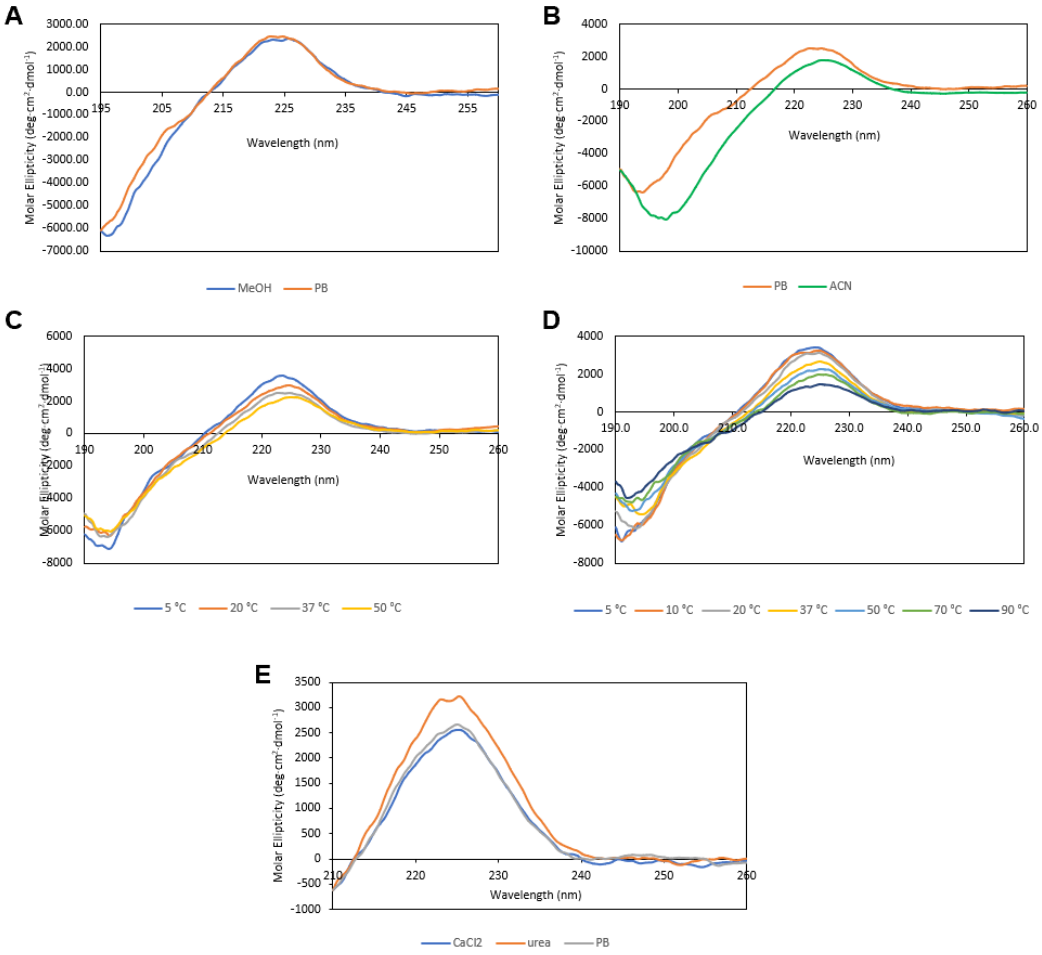

Figure 3.24: A) The CD spectrum of peptide **10** in MeOH; B) The CD spectrum of peptide **10** in ACN; C) The CD spectra of peptide **10** in PB solution at different temperature; D) The CD spectra of peptide **6** in PB solution at different temperature; E) The CD spectra of peptide **6** in 1 M $CaCl_2$ aqueous solution, 6 M urea aqueous solution or PB solution (concentration of peptide: 125 μM)

3.5.2 NMR analysis

To get more information about the conformations of peptides **6** and **10**, NMR spectroscopy studies were performed on peptides **6** and **10** in 90%H_2O/10%D_2O.

Peptide **6** only provided limited conformational information from NMR spectra. All amide ^1H resonances of peptide **6** could not be found at any temperature from 283 to 310 K, indicating the fast exchange of the amide protons with water. This result suggests that no intramolecular hydrogen bond could be formed on peptide **6** in water. The absence of the signals of amide ^1H resonances

prevented the calculation of $^{3}J_{HN\alpha}$ coupling constants and amide proton temperature coefficients ΔδNH/ΔT. Only H^{α}-CSDs could be calculated (**Table 3.2**). All the values of H^{α}-CSDs we calculated were negative but above -0.38 ppm (for α-helix, the values normally are smaller than -0.38 ppm, for β-sheet, the values normally are larger than +0.38 ppm), which means the corresponding residues are neither in α-conformation nor in β-conformation. No indicative ROEs were found between the protons on the backbone because of the absence of signal of amide protons. Some long-range proton ROEs between side chain protons of residues i and i+2 were observed but could not be sure (azaLys^{2}/Tyr^{4} and Tyr^{4}/Lys^{6}) because of the failure to distinguish the side chain protons between aza-Lys^{2} and Lys^{6} (**Figure 3.25**). Several long-range proton ROEs between side chain protons or α-protons of residue i and side chain protons or α-protons of residues i+1 (Ser^{3}/Tyr^{4}, Trp^{5}/Lys^{6}, Lys^{6}/azaAla^{7}), as well as a ROE between side chain protons of residues i and i+3 (Trp^{5}/aLeu^{8}) were observed (**Figures 3.25**, **3.26** and **3.27**), suggesting folded structures of peptide **6** in water.

Residue	δ H^{α} (ppm)	H^{α}-CSD (ppm)
Ser	4.20	-0.27
Tyr	4.40	-0.15
Trp	4.57	-0.09
Lys	4.11	-0.21
Gly	3.77	-0.19

Table 3.2: The H^{α}-CSD of peptide **6** measured in 90%H_2O/10%D_2O at 298 K

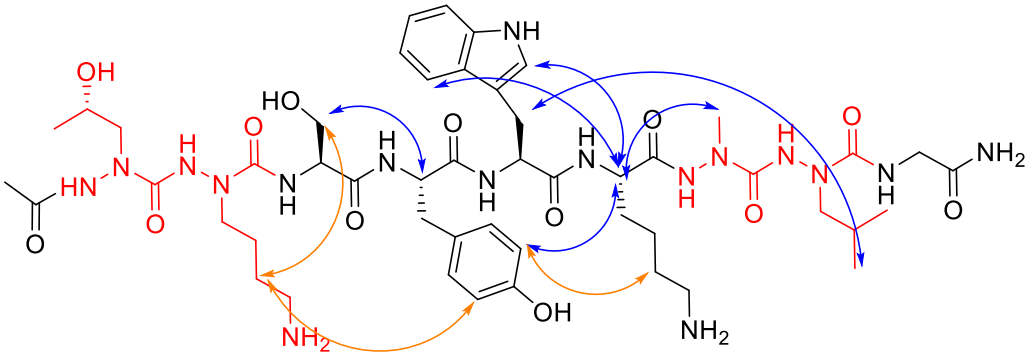

Figure 3.25: Long-range ROEs between side chains of peptide **6** in water (310 K): unambiguous ROEs are in blue (Ser^3/Tyr^4, Trp^5/Lys^6, Lys^6/azaAla^7), ambiguous ROEs are in orange.

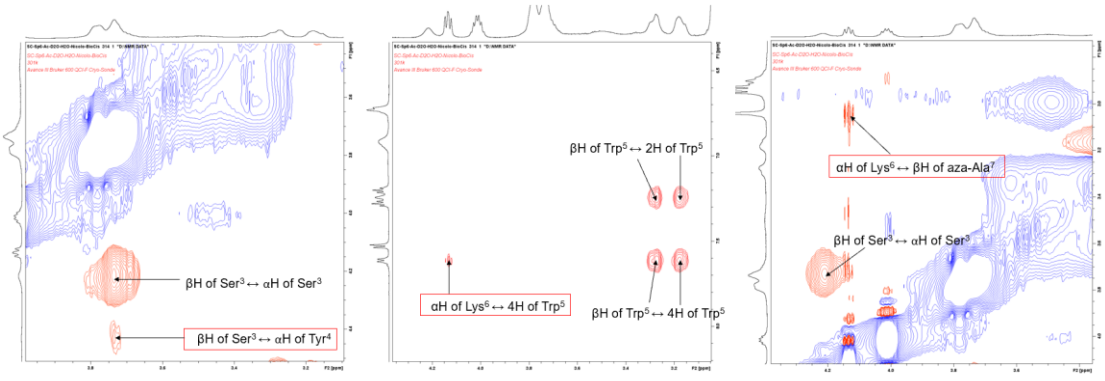

Figure 3.26: The ROE signals Ser^3/Tyr^4, Trp^5/Lys^6 and Lys^6/azaAla^7 (peptide **6** in water, 310 K)

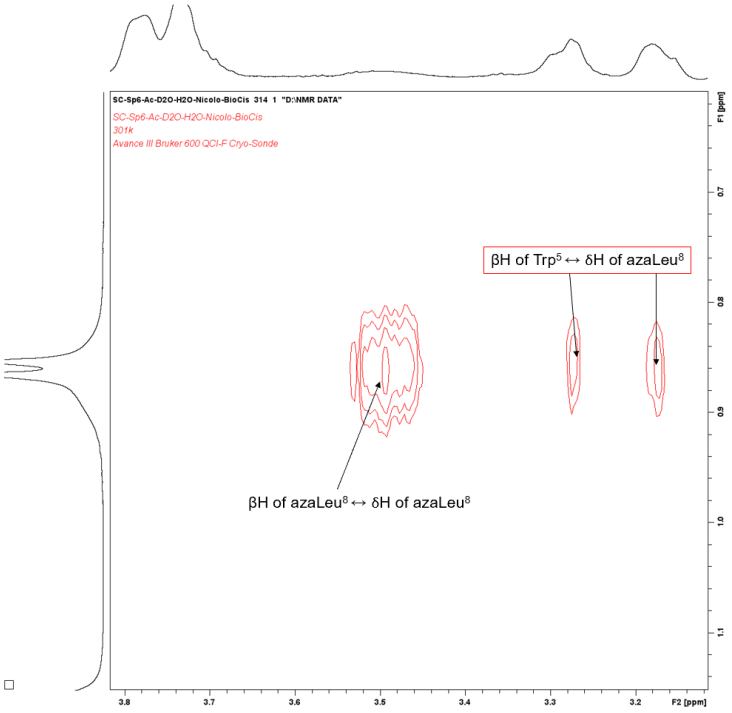

Figure 3.27: The ROE signals Trp^5/azaLeu^4 (peptide **6** in water, 310 K)

For peptide **10**, all amide ^{1}H resonances of natural residues could be found and assigned from temperature 280 to 310 K. It is difficult, however, to assign the amide ^{1}H resonances for aza-residues because there is no α-protons on aza-residues to make correlation with the amide protons. Thanks to ^{1}H-^{1}H COSY, ^{1}H-^{13}C HSQC and ^{1}H-^{13}C HMBC and ^{1}H-^{1}H DIPSI experiments, all the other ^{1}H resonances pertinent for conformational analysis could be assigned except some ^{1}H resonances on side chains. That made us focus on the analysis of NMR parameters of natural residues in the sequence. Four $^3J_{HN\alpha}$ coupling constants (Ser^3, Tyr^4, Trp^5, Lys^6) we could calculate and the average value was 5.7± 0,21 Hz (**Table 3.3**), indicating preferred ϕ angle values were in the range between -60° and -90°, which were compatible with a 3_{10}-helix (for α-helix: around 4.8 Hz, for 3_{10}-helix: around 5.6 Hz).[30] We turned to calculate amide proton temperature coefficients ΔδNH/ΔT and H^{α}-CSDs (**Table 3.3**). Here we only got the amide proton temperature coefficients of residues Tyr^4, Trp^5 and Lys^6 because the serious overlap of the amide ^{1}H resonances of Gly^9 and Ser^3 with aromatic protons below 310 K made the impossibility to get precise chemical shifts. None of them was above -4.6 ppb/K indicating there was no stable intramolecular hydrogen bond. We guessed that due to the high solvation level of water solvent, it is difficult to form stable intramolecular hydrogen bond for

the aza-nonapeptides in water. The H^{α}-CSDs of for natural residues of peptide **10** (**Table 3.3**) showed similar values with peptide **6** on H^{α}-CSDs, indicating the probable similar conformations between peptide **6** and peptide **10**. In the spectrum of ^{1}H-^{1}H ROSEY, sequential ROE correlations between side chain protons or α-protons of residue i and side chain protons or α-protons of residue i+1 were found from Ser to azaAla (Ser^{3}/Tyr^{4}, Tyr^{4}/ Trp^{5}, Trp^{5}/Lys^{6}, Lys^{6}/$azaAla^{7}$) suggested folded structures (**Figures 3.28** and **3.29**). A ROE between side chains of residues i and i+3 (Trp^{5}/$azaLeu^{8}$) was also found in peptide **10** (**Figures 3.28** and **3.29**). However, an additional ROE between the side chain protons of Tyr^{4} and the side chain protons of Trp^{5} suggest a slightly different folded structures compared to peptide **6**. It should be noticed also the presence of a weak d_{NN} (i, i+1) NOE between Ser^{3} and Tyr^{4} (**Figures 3.28**) indicates that Ser^{3} was in helical conformation. The intensity ratios of short-range ROEs Nα (i, i) / αN (i-1, i), which is sensitive to the value of the ψ angle of residue i-1, were calculated **(Table 3.4)**. When this intensity ratio is larger than 0.5, it means a shift to an increased population of helical backbone angles compared to random coil. The average of the ratios for peptide **10** measured in water was 0.71 ± 0.39, which was an indicative of non-extended structure.[31,32] Here we could not give precise conformations for peptides **6** and **10** in water just by the analysis of the NMR parameters we got.

Residue	δ H^{α} (ppm)	δ NH (ppm)	$^{3}J_{HN\alpha}$ (Hz)	ΔδNH/ΔT (ppb/K)	H^{α}-CSD (ppm)
Ser	4.23	6.92	5.6	/	-0.24
Tyr	4.44	8.08	6.5	-6.0	-0.11
Trp	4.55	7.89	5.3	-5.2	-0.11
Lys	4.15	8.02	5.3	-5.4	-0.17
Gly	3.79	6.98/7.42	/	/	-0.17

Table 3.3: The NMR parameters of peptide **10** measured in 90%H_2O/10%D_2O at 310 K

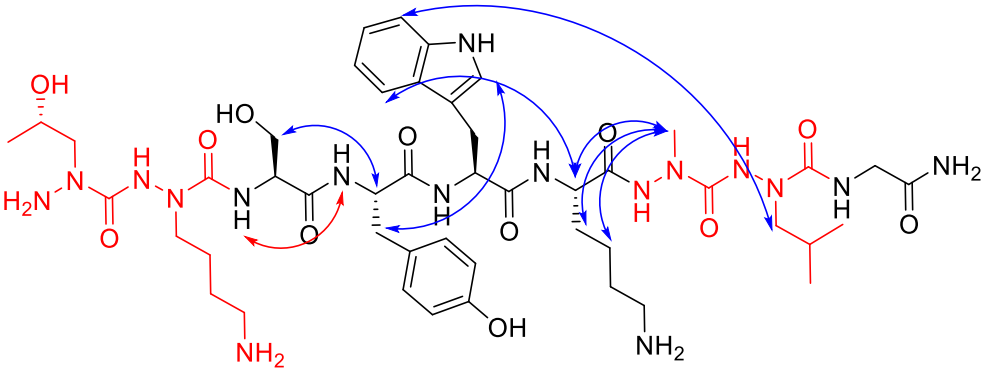

Figure 3.28: The ROEs were displayed in peptide **10** by arrows, the ROE d_{NN} (i, i+1) between Ser^3 and Tyr^4 is in red, other long-range ROEs involving side chains are in blue. (water, 310 K)

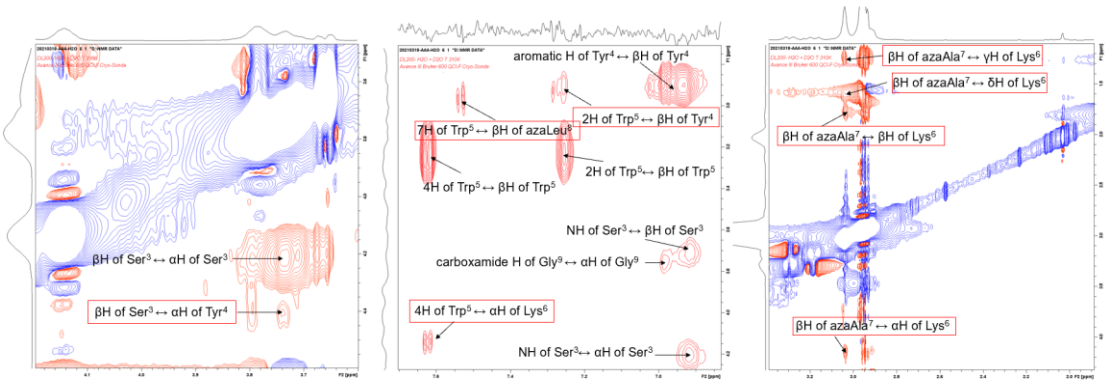

Figure 3.29: The ROE signals Ser^3/Tyr^4, Trp^5/Lys^6, Tyr^4/ Trp^5, Trp^5/Lys^6, Lys^6/azaAla^7 and Trp^5/azaLeu^8 (peptide **10** in water, 310 K)

$d_{\alpha N}$ (i, i) / $d_{\alpha N}$ (i-1, i)	peptide **10** in water (313 K)	peptide **10** in DMF (333 K)
Ser^3/Tyr^4	0.39	0.79
Tyr^4/Trp^5	0.24	1.71
Trp^5/Lys^6	1.49	1.51
Average	0.71 ± 0.39	1.34 ± 0.21

Table 3.4: ROEs intensity ratios for the peptide **10** in water or DMF

The fact that no intramolecular hydrogen bond was observed for peptide **10** in water might arise from the difficulty for peptide **10** to maintain its intramolecular hydrogen bonds in water, due to the high solvation level. We tried to do the NMR analysis of peptide **10** in CD_3OH but the signals of NHs of peptide **10** were in low dispersion. In the end, we decided to use deuterated DMF as

solvent to perform NMR studies for peptide **10**. NMR spectra of peptide **10** were measured in deuterated DMF from 298 to 343 K to investigate the influence between polar protic and aprotic solvents on its conformation. Peptide **10** showed resonance broadening of ^{1}H at low temperature and no sharp signals were obtained until the temperature reach to 333 K. Therefore, the NMR parameters of peptide **10** in deuterated DMF were calculated at 333 K (**Table 3.5**). The average value of $^{3}J_{HN\alpha}$ coupling constants from residues Ser^{3} to Lys^{6} was calculated precisely (6.3±0.34 Hz), indicating that this region is in helical folding. Amide proton temperature coefficients ΔδNH/ΔT of natural residues could be precisely calculated and most amide protons of natural residues were involved in intramolecular hydrogen bonds except the one from Ser^{3} and one carboxamide proton (**Table 3.5**). This result is different from the result we got the spectrum in water, which proves that peptide **10** preferentially forms intramolecular hydrogen bonds in DMF rather than in water and this even at high temperature (333 K). Similar proton ROEs were found for peptide **10** in DMF as those found in water and two additional long-range proton ROEs between residues i and i+3 ($ahThr^{1}$/Tyr^{4} and Ser^{3}/Lys^{6}) and one additional long-range proton ROE between residues i and i+5 (Ser^{3}/$azaLeu^{8}$) suggest more folded structures of **10** in DMF (**Figures 3.30**, **3.31** and **3.32**). This is also supported by the ROE intensity ratios calculated for peptide **10** in DMF (**Table 3.4**). Peptide **10** in DMF showed Nα (i, i) / αN (i-1, i) ratios (average value is 1.34 ± 0.21) superior to the ratios (average value is 0.71 ± 0.39) in water, which suggests a shift to an increased population of helical backbone angles compared to these ratios in water.[31,32]

Residue	$^{3}J_{HN\alpha}$ (Hz)	ΔδNH/ΔT (ppb/K)
Ser	5.3	-5.0
Tyr	6.4	-3.8
Trp	6.6	-3.2
Lys	6.8	-3.5
Gly	/	-4.0
Amide A	/	-1.9
Amide B	/	-8.0

Table 3.5: The NMR parameters of peptide **10** measured in deuterated DMF at 333 K

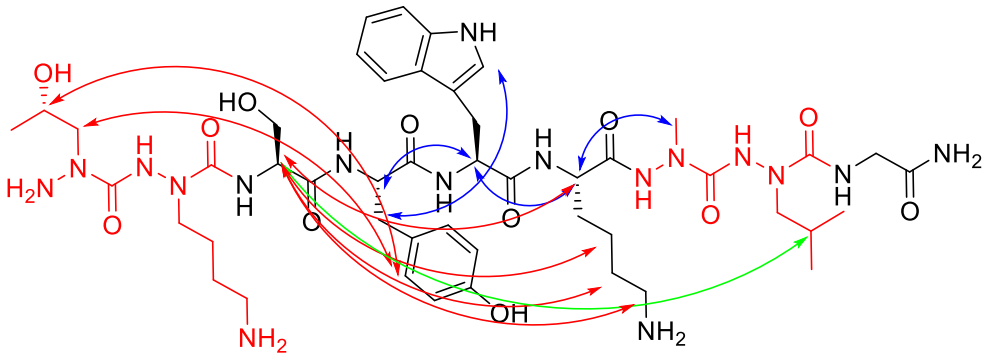

Figure 3.30: The ROEs were displayed in peptide **10** by arrows: NOEs between residues i and i+1 are in blue, NOEs between residues i and i+3 are in red, NOEs between residues i and i+5 are in green (in DMF, 333 K)

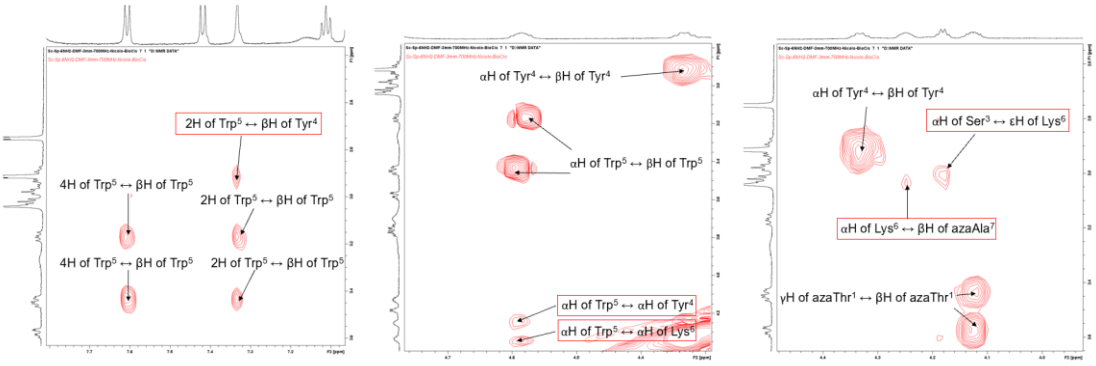

Figure 3.31: The ROE signals Tyr^4/Trp^5, Trp^5/Lys^6, Lys^6/azaAla^7 and Ser^3/Lys^6 (peptide **10** in DMF, 333 K)

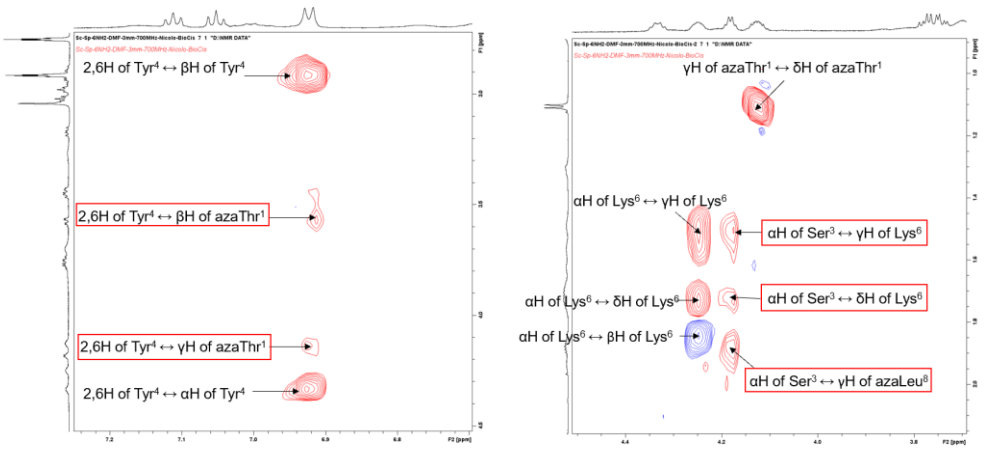

Figure 3.32: The ROE signals azaThr^1/Tyr^4, Ser^3/Lys^6 and Ser^3/azaLeu^8 (peptide **10** in DMF, 333 K)

The difficulty of assignment of amide protons on the diaza-peptide units in peptides **6** and **10** let us turn attention on NMR analysis of peptide **9**, which has only one diaza-peptide unit at its N-terminus. The NMR experiments of peptide **9** was performed in CD_3OH from 258 to 298 K but NMR parameters were calculated and collected at 258 K because the signals of NH and H^{α} were in good dispersion and split in this condition, which made the calculation of $^3J_{HN\alpha}$ coupling constant possible. At 258 K, a new major conformer appeared with the conformer (minor conformer) we found at 298 K. The ratio of two conformer was about 3:1 at 258 K. The conformers showed different chemical shifts on α-protons of Trp^5 and Lys^6, NH proton of Gly^9 and side chain protons of several residues, including $azaThr^1$, Tyr^4 and Leu^8, so the secondary structure of their backbones have difference. We first focused on the analysis of the major conformer, and then tried to describe the minor conformer which was the conformer displayed at 298 K.

As shown in **Table 3.6**, all of the $^3J_{HN\alpha}$ coupling constants fell within the range between 5.5 and 7.5 Hz, which means no extended structure of the major conformer for peptide **9**. In contrast with the peptide **10** measured in water, the amide proton temperature coefficients ΔδNH/ΔT of all the residues in peptide **9** were above -4.6 ppb/K except $azaLys^2$, Lys^6 and Ala^7, indicating that the NHs of Ser^3, Tyr^4, Trp^5, Leu^8, Gly^9 and carboxamide were involved in stable intramolecular hydrogen bonds. Sequential short-range NOEs d_{NN} (i, i+1) from $azaLys^2$ to Lys^6 and Ala^7 to Gly^9 (**Figures 3.33** and **3.34**) were found. The failure to find NOE d_{NN} (i, i+1) from Lys^6 to Ala^7 might be ascribed to too close chemical shift on NH protons for these two residues (8.09 ppm for Lys^6 and 8.11 ppm for Ala^7). This result suggests that a helical structure of peptide **9** was displayed in methanol. Several medium-range NOEs $d_{\alpha N}$ (i, i+2) were observed but only Tyr^4/Lys^6 could be sure (the others were ambiguous because of peaks overlap) (**Figures 3.33** and **3.35**). Medium-range NOEs $d_{\alpha N}$ (i, i+3) were also ambiguous due to peaks overlap. However, the unambiguous and obvious NOEs $d_{\alpha\beta}$ (i, i+3) were observed on Ser^3/Lys^6, Tyr^4/Ala^7 and Trp^5/Leu^8 (**Figures 3.33** and **3.36**), which further supports a helical structure for peptide **9**. Moreover, there was a weak NOEs $d_{\alpha N}$ (i, i+4) on Lys^6/carboxamide (**Figures 3.33** and **3.35**). We speculated a 3_{10}-helix of the peptide because of the β-turn conformational inductivity of diaza-peptide unit as we mentioned in the chapter 2, more compatible $^3J_{HN\alpha}$ coupling constants (**Table 3.6**) to 3_{10}-helix for the residues ($^3J_{HN\alpha}$ coupling constants of α-helix is around 4.8 Hz whereas $^3J_{HN\alpha}$ coupling constants of 3_{10}-helix is

around 5.6 Hz) and the strong and ambiguous ROEs $d_{\alpha N}$ (i, i+2) on Tyr[4]/Lys[6].[33,34]

Residue	$^{3}J_{HN\alpha}$ (Hz)	ΔδNH/ΔT (ppb/K)
azaLys[2]	/	-4.7
Ser[3]	6.3	-0.5
Tyr[4]	6.5	-2.8
Trp[5]	5.5	-3.3
Lys[6]	5.6	-5.8
Ala[7]	5.6	-4.8
Leu[8]	7.1	-3.0
Gly[9]	6.7	-3.3/-5.5 (minor)
carboxamide Ha	/	-3.0
carboxamide Hb	/	-3.9

Table 3.6: The NMR parameters of peptide **9** (CD_3OH, 258 K)

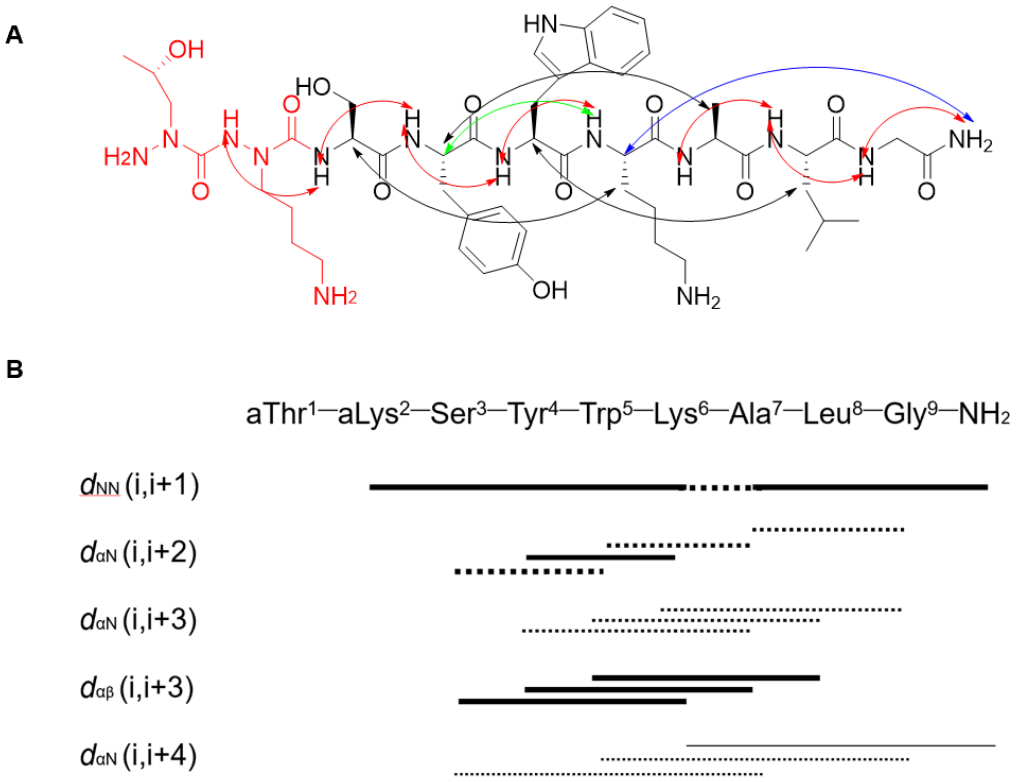

Figure: 3.33: A) The unambiguous NOEs of peptide **9** observed in CD_3OH at 258K are displayed by arrows: NOEs d_{NN} (i, i+1) are in red, NOEs $d_{\alpha N}$ (i, i+2) are in green, NOEs $d_{\alpha\beta}$ (i, i+3) are in black, NOEs $d_{\alpha N}$ (i, i+4) are in blue; B) Summary of the indicative NOE correlations observed in the NOESY spectrum of peptide **9** in CD_3OH at 258 K: the NOE intensities are reflected by the thickness of the lines, the unambiguous NOEs are drawn with solid lines whereas ambiguous NOEs (due to peaks overlap) are drawn with dashed lines

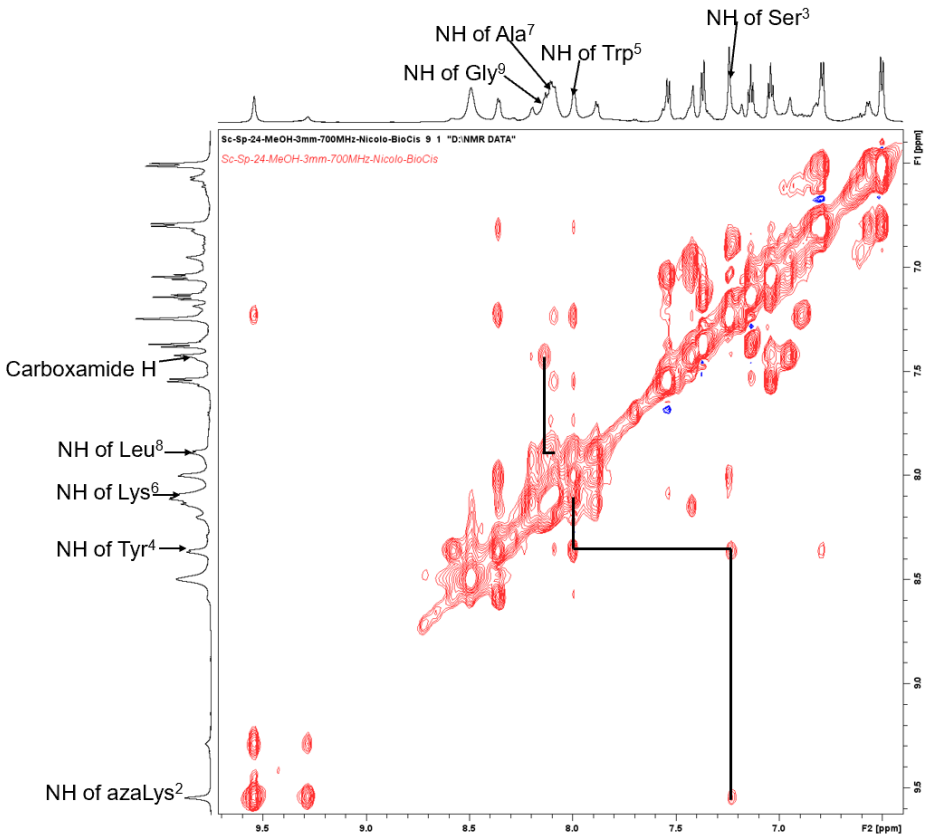

Figure 3.34: The ^{1}H-^{1}H NOESY spectrum showing sequential NOEs d_{NN} (i, i+1) of peptide **9** in CD_3OH at 258 K

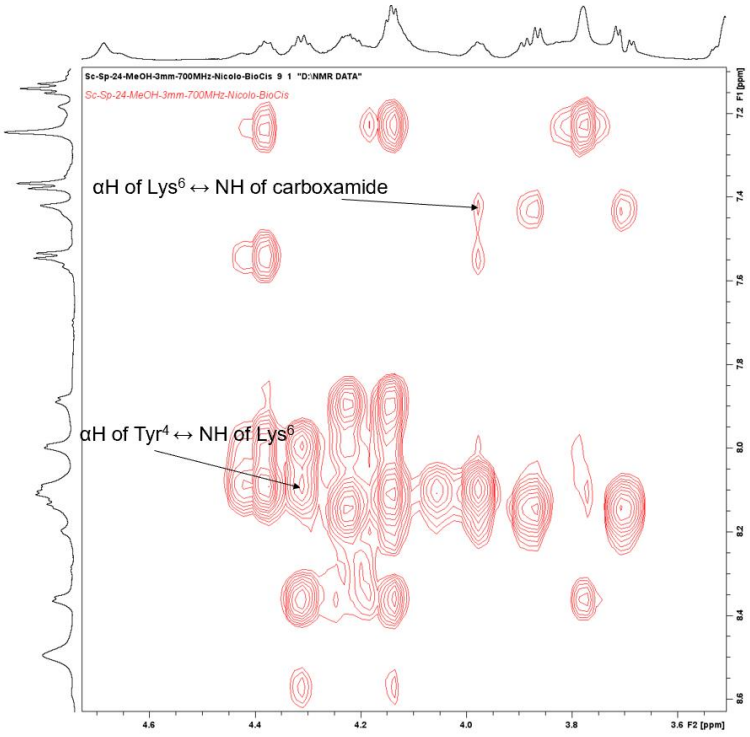

Figure 3.35: The ^{1}H-^{1}H NOESY spectrum showing medium-range NOE $d_{\alpha N}$ (i, i+2) of Tyr^{4}/Lys^{6} and NOE $d_{\alpha N}$ (i, i+4) of Lys^{6}/carboxamide (peptide **9** in CD_3OH at 258 K)

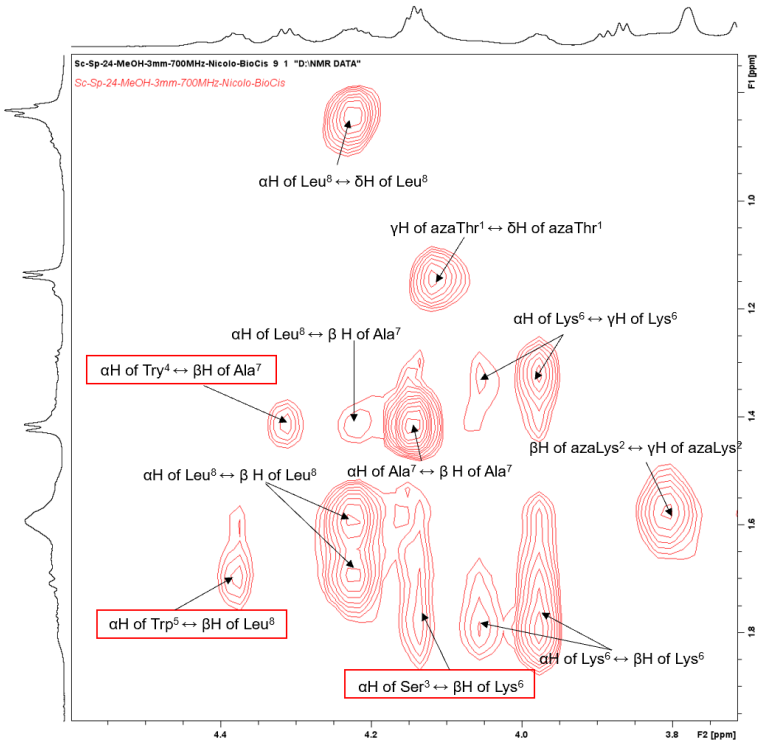

Figure 3.36: The ^{1}H-^{1}H NOESY spectrum showing medium-range NOEs $d_{\alpha\beta}$ (i, i+3) of peptide **9** in CD_3OH at 258 K

The difference between the major conformer and the minor conformer was also tried to demonstrate by NMR parameters. The most informative clues are the difference of chemical shifts of α-proton of Trp^5 and Lys^6 and the difference on the NH proton of Gly^9. The minor conformer showed the more downfield chemical shifts of α-proton of Trp^5 (4.43 ppm) and Lys^6 (4.05 ppm) than that of the major conformer (4.38 ppm for Trp^5 and 3.98 ppm for Lys^6), which means more extended conformation for the Trp^5 and Lys^6 in the minor conformer. In combination with the relatively small amide proton temperature coefficients ΔδNH/ΔT of Lys^6 (-5.8 ppb/K) and Ala^7 (-4.8 ppb/K), we speculated the minor conformer does not have an intact helical structure as the major conformer shows. It seems that the helical structure of the minor conformer is disrupted into two segments by Trp^5 and Lys^6. In addition, the proton temperature coefficient ΔδNH/ΔT of Gly^9 in the minor conformer was below -4.6 ppb/K, which means no stable intramolecular hydrogen bond was involved. This result suggests that the minor conformer has different arrangement of the residues Leu^8 and Gly^9 in space, which distorts partially a helical structure of the minor conformer at the C-terminus (the fraying of helical structure at the C-terminus). Thus, we hypothesized that, in the minor conformer, the first segment from $azaThr^1$ to Tyr^4 is in a 3_{10}-helical structure but the second segment from Trp^5 to Gly^9 is in a helical structure with partial distortions.

Overall, we can give insight into the conformation of peptide **9** in methanol based on the results from NMR analysis. At 258 K, there are two conformers of peptide **9**. The major one displays an intact 3_{10}-helix whereas the minor one only shows a 3_{10}-helical structure on the first segment from $azaThr^1$ to Tyr^4. The helical structure of the minor conformer is disrupted by relatively extended Trp^5 and Lys^6. The second segment from Trp^5 to Gly^9 is in a helical structure with partial distortions. Moreover, the minor conformer shown in methanol at 258 K is the conformer of peptide **9** at 298 K. This means that the intact helical structure is stable at a lower temperature (258 K) whereas the helical structure was distorted at the C-terminus at room temperature (298 K). This supports that the N-terminal diaza-peptide unit has a propensity to induce helical structures. However, the inductive effect does not propagate very far from the N-terminal diaza-peptide unit.

3.5.3 Fourier transform infrared radiation (FTIR)

Given that vibrational frequencies of amide groups are influenced by intermolecular and

intramolecular effects, FTIR, a spectroscopy providing the vibrational frequencies of molecules, is able to give insight into conformational preference of polypeptides or proteins. Amide I band (1600-1700 cm^{-1}) is a major band for conformational analysis of polypeptides. This band comprises mainly of the peptide backbone CO stretching vibrations, but usually has a broad contour that is composed of several overlapping bands due to various protein segments with different secondary structures.[35] Deconvolution of the amide I band makes it possible to distinguish between the individual component types.[36]

FTIR experiments were performed on peptides **6** and **10** in MeOH or H_2O to get the information of amide I band. The FTIR spectrum of amide I band of peptide **6** dissolved in MeOH consists of dominant β-turn/ β-sheet bands, representing the most populated secondary structures with 65% of the total relative area (**Figure 3.37**, **A** and **C**), together. A small contribution (17%) is associated to aggregated strands (1609 and 1625 cm^{-1}). A lower content of helices is observed (18%) with a single peak at 1654 cm^{-1}, corresponding to the characteristic α-helix wavenumber. For peptide **10**, the FTIR spectrum of the compound, dissolved in MeOH, shows a similar trend with a global 64% of β-turn/β-sheet conformations, with a less extent of aggregated strands (11%, 1606 cm^{-1}) and an increase in α-helix content (26%, 1651 cm^{-1}) (**Figure 3.37**, **B** and **D**).

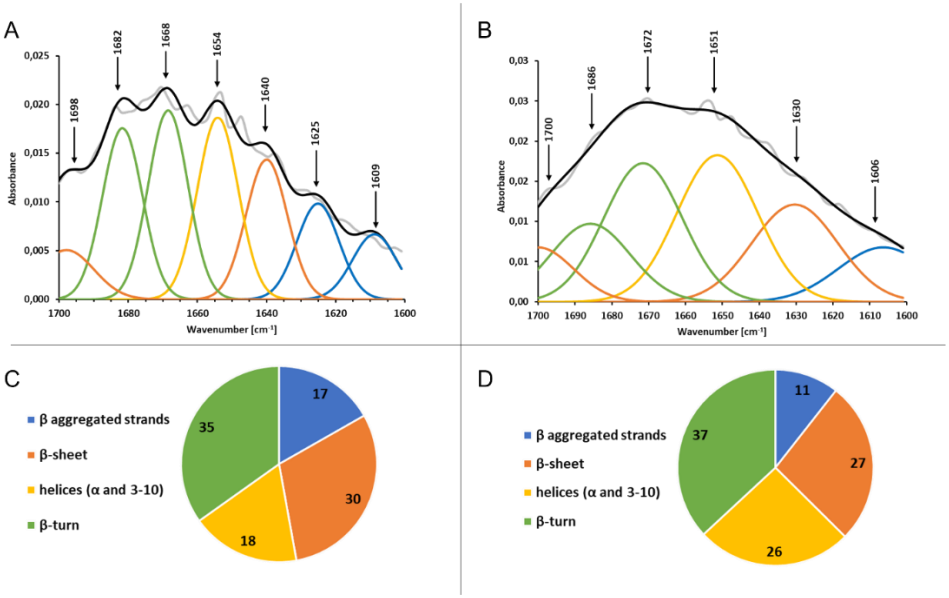

Figure 3.37: ATR-FTIR spectra of peptide **6** (A) and peptide **10** (B) dissolved in MeOH (2 mM) and their corresponding deconvolution (C, D) for secondary structure quantification. Gray line: experimental curve; Black line: model curve after deconvolution. Averaged standard deviations: 6.46 for peptide **6** and 10.26 for peptide **10**

Interestingly, the FTIR spectrum amide I band of peptide **6** dissolved in H_2O shows obvious decreases on β-turn and β-sheet conformations (21% and 14%) as well as an increase of aggregated strands (32%, 1615 cm $^{-1}$) but a quite constant helices content (16%) compared to peptide **6** dissolved in MeOH (**Figure 3.38 A** and **C**). In water, α-helix (1656 cm $^{-1}$) and 3_{10}-helix (1664 cm $^{-1}$) of the peptide are possible to distinguish by deconvolution. It should be noted that random coil structure (17%) appears for peptide **6** in H_2O. The more aggregated strands and the presence of random coil for peptide **6** in H_2O indicate that compared to peptide **6** in MeOH, peptide **6** in H_2O is more aggregated and tends to lose its structure. For peptide **10** dissolved in H_2O, the FTIR spectrum shows a similar trend with a global 62% of β-turn/β-sheet conformations, a quite constant aggregated strands (14%, 1606 cm $^{-1}$) and helices content (24%) as it is dissolved in MeOH (**Figure 3.38 B** and **D**). For the helix band, the deconvolution also shows two different wavenumbers, one associated with α-helix (13%, 1650 cm $^{-1}$) and the other with 3_{10}-helix (12%, 1661 cm $^{-1}$).

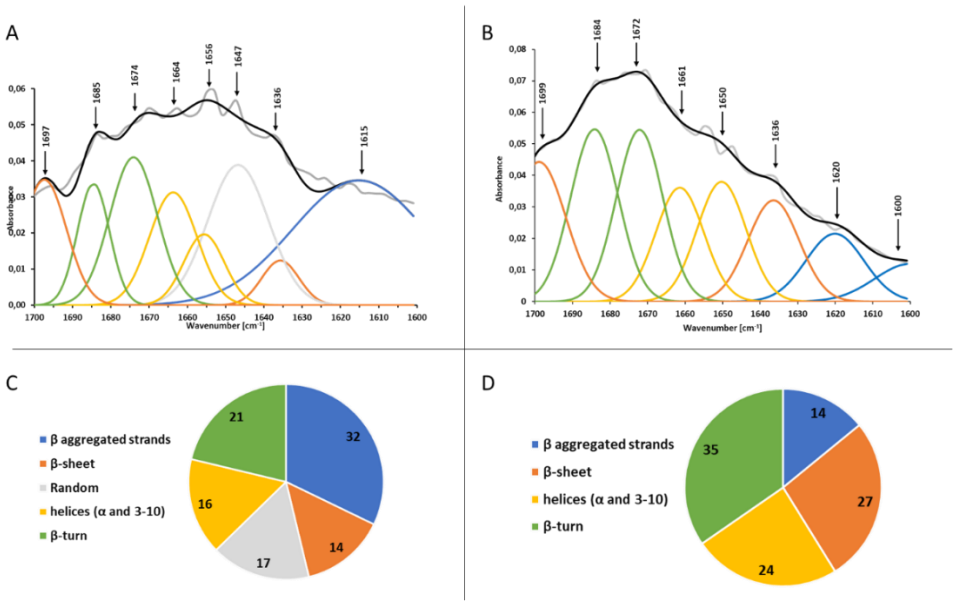

Figure 3.38: ATR-FTIR spectra of peptide **6** (A) and peptide **10** (B) dissolved in H_2O (2 mM) and their corresponding deconvolution (C, D) for secondary structure quantification. Gray line: experimental curve; Black line: model curve after deconvolution. Averaged standard deviations: 7.25 for peptide **6** and 7.09 for peptide **10**

All these data allow to confirm the quite similar secondary structures of peptide **10** both in MeOH and in H_2O, as already assessed by CD. The FTIR spectra of peptides **6** and **10** could demonstrate that the absence of the N-terminal acetyl group has an influence on the helices content despite peptides **6** and **10** have comparable spectra in CD experiments. In fact, the deconvolution of peptide **10** FTIR spectrum shows a clear increase in the helices content (24%) compared to peptide **6** (16%), with the possibility to stabilize a helical conformation in between α- and 3_{10}-helix in H_2O. For peptide **6**, 3_{10}-helix attributes the main content of its helical structure in H_2O, whereas peptide **10** shows nearly equal α-helix and 3_{10}-helix contents. The high β-turn content is in perfect agreement with our previous results, which demonstrated that the sequential introduction of aza-amino acids induces repeated β-turns conformations, which could interconvert with a fully helical structure, mimicking a 3_{10}-helix.[9]

3.5.4 Molecular dynamics simulation

In order to get more insights about the difference of peptides **6** and **10**, and their ability to

mimic the EF-helix of TTR, molecular dynamics (MD) analysis and superimposition of the preferred structures of peptides **6** and **10** with the EF-helix of TTR were conducted. This work was performed by Prof. Tâp HA-DUONG and here the results is presented.

MD simulations were performed using the GROMACS 2019.1 package[37] with the Generalized AMBER Force Field (GAFF)[38]. Time evolutions of their root-mean-square deviation (RMSD) relative to their initial conformations show that both peptides **6** and **10** sampled many times several preferential conformations without being trapped in a particular potential energy minimum (**Figure 3.39A**). This suggests that both simulated solutes converged to a dynamical equilibrium characterized by similar radius of gyration, independently of the N-terminal chemical state (**Figure 3.39B**). Theoretical and experimental conformational ensembles of peptide **10** were compared by using the vicinal $^{3}J_{HN\alpha}$ coupling constants of its central natural amino acid segment Ser^{3}-Lys^{6}. The values calculated from its MD simulation are fairly close to those measured by NMR, with averaged values around 5.4-5.7 Hz, indicating that the backbone of the peptide central region has rather compact local conformations ($\phi \sim -70°$) in both experiments and simulations. This is confirmed by the computed Ramachandran plots of the two peptides where it can see that the backbone dihedral angles (ϕ, ψ) of the central residues Ser^{3} to Lys^{6} predominantly have values of helical conformations (**Figure 3.40A**). The high propensity of both peptides **6** and **10** to form helical conformations during their MD simulations is illustrated in **Figure 3.41**. As indicated by the RMSD values lower than or around 3 Å, the two most populated clusters of the two foldamers can be well superimposed on the α-helical segment 75-83 of TTR. In addition, the orientations of the side chains in the most popular cluster of peptide **10** are the same as those in the crystallographic structure of TRR helix 75-83. Nevertheless, the helical conformations of simulated peptides **6** and **10** look more like 3_{10} helices than α-helices, as suggested by the distributions of backbone CO-HN hydrogen bond lengths computed from MD simulations (**Figure 3.40B**).

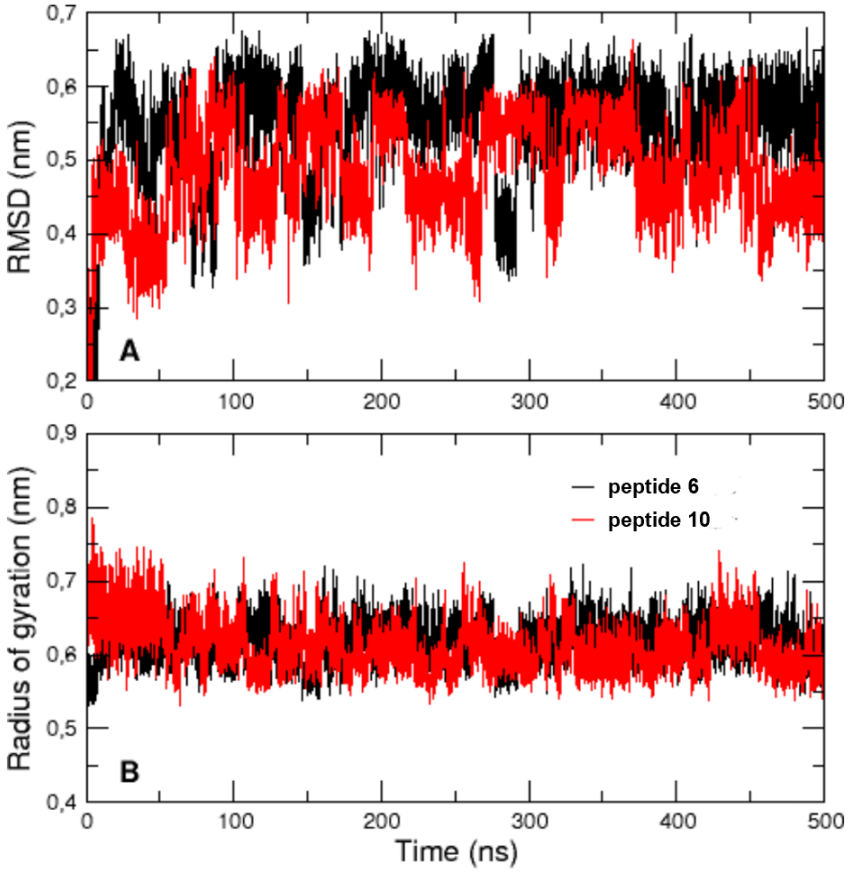

Figure 3.39: A) Time evolutions of the root-mean-square deviation (RMSD) relative to the initial conformations of peptides **6** (black lines) and **10** (red lines); B) the radius of gyration of peptides **6** (black lines) and **10** (red lines)

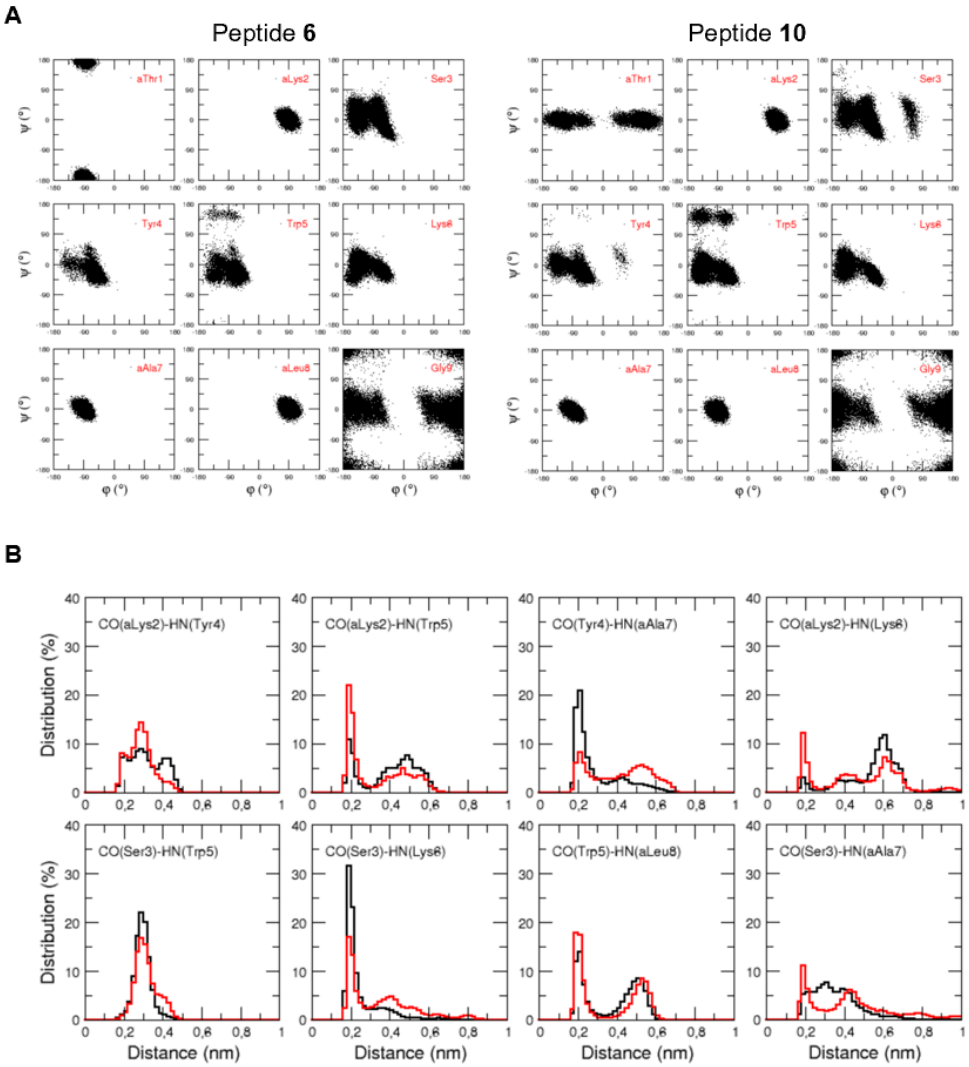

Figure 3.40: A) Ramachandran plots of peptides **6** and **11** computed from their MD simulations; B) Distributions of backbone CO-HN hydrogen bond lengths in MD conformational ensembles of peptides **6** (black lines) and **10** (red lines)

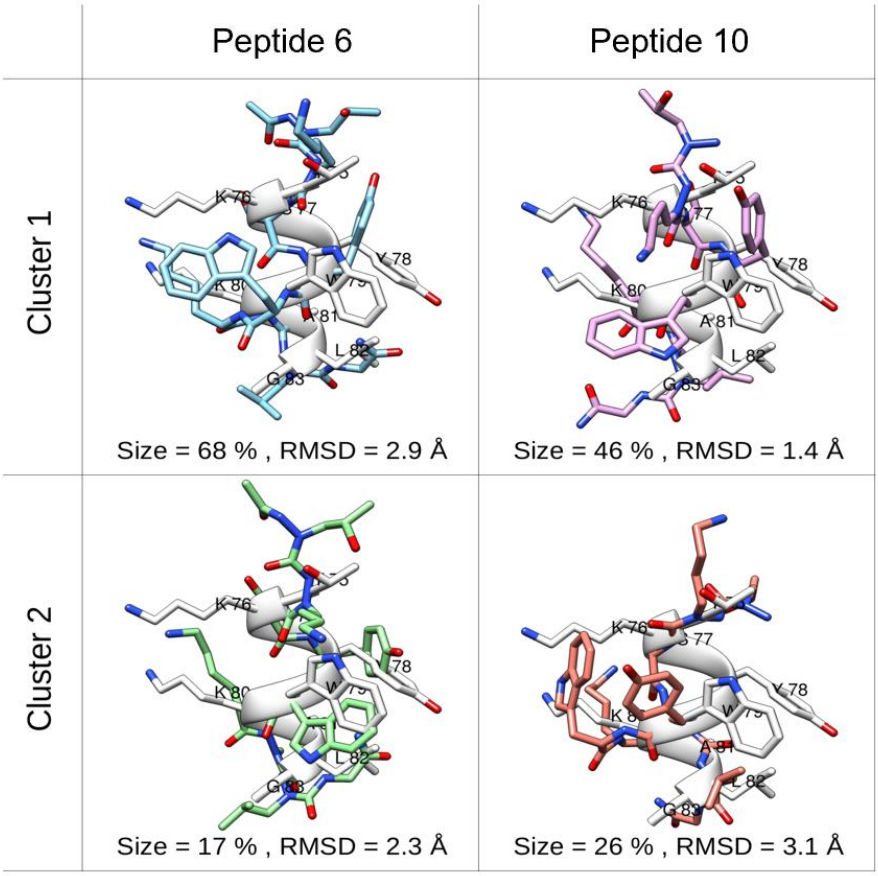

Figure 3.41: Representative structures of the two most populated clusters of peptides **6** (left) and **10** (right) superimposed on EF-helix (residues 75-83) of TRR PDB structure 5N7C (white). The size of each cluster is indicated as percentages of the MD trajectories. The RMSD are calculated over the Cα (or Nα) of the peptidomimetics.

3.6 Biophysical and biological evaluations

3.6.1 Thioflavin-T (ThT) assay

Thioflavin-T (ThT) is a dye which strongly fluoresces at specific range of wavelengths (near 485 nm) upon binding to β-sheet rich structures when excited at 450 nm.[39,40] In solution, the benzylamine and benzothiazole rings of ThT could rotate freely to quench excited states (**Figure 3.42A**), resulting in low fluorescence emission. Once ThT binds to amyloid fibrils, the free rotation is blocked to preserve the excited states, causing the fluorescence enhancement of ThT.[41] This specific property of ThT to bind to amyloid fibrils (β-sheet rich structures) makes ThT extensively

used for monitoring the kinetics of amyloid proteins aggregation, such as Aβ aggregation.[42]

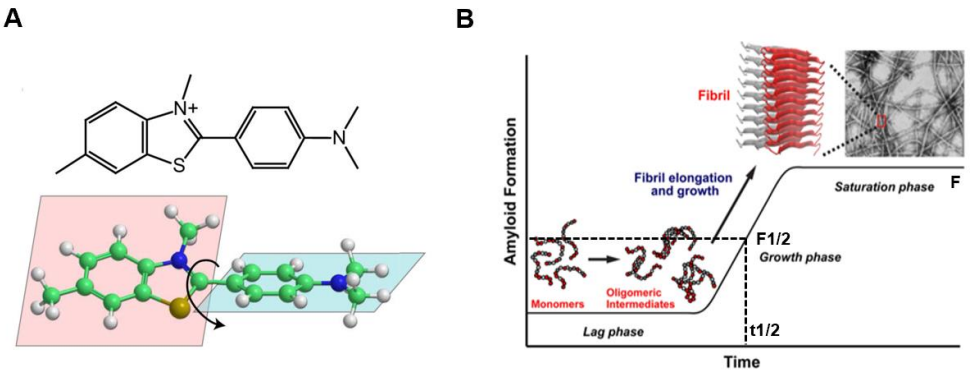

Figure 3.42: A) The structure of ThT and illustration of the rotation between benzylamine and benzathiozole ring;[41] B) Aggregation curve in ThT assays

The activity of azapeptides against $A\beta_{42}$ aggregation in ThT assay

The ThT fluorescence assay was used to test the activity of our aza-nonapeptides on $A\beta_{42}$ aggregation. $A\beta_{42}$ solution was prepared with a batch of $A\beta_{42}$ bought from Bachem (Batch 1, selected for its high aggregation quality) and using our standard fibrillization protocol ($A\beta_{42}$ was dissolved in a 1% ammonia aqueous solution to a concentration of 1 mM and then was diluted to 0.2 mM with Tris buffer just before filling the plate).[43,44] Several experiments were performed to ensure the relevance of our results and each experiment was performed in triplicate. Resveratrol and TTR were used as positive controls. The concentration of $A\beta_{42}$ in the assay is 10 µM and two different inhibitor/amyloid peptide ratios: 10/1 and 1/1 were tested. Two parameters: $t_{1/2}$ (the time when reaching the half value of maximal fluorescence) and F (fluorescence intensity at plateau) (**Figure 3.42B**) were calculated from the fluorescence curves to describe the kinetics and the final extent of fluorescence of the fibrillization process. Relative extension/reduction of $t_{1/2}$ ($\Delta t_{1/2}$) is defined as the experimental $t_{1/2}$ in the presence of the tested inhibitor relative to the one obtained without the inhibitor. The relative extension/reduction of F (ΔF) is defined as the intensity of experimental fluorescence plateau observed with the tested inhibitor relative to the value obtained without the inhibitor.

The parameters $\Delta t_{1/2}$ and ΔF for the first experiment are shown in **Table 3.7** for peptides **1**-**7**, **10**, **11**, resveratrol and TTR and mean fluorescence curves for the most active peptides **1**, **3**, **6**, **10**, **11**, resveratrol and TTR are represented in **Figure 3.43** to **Figure 3.45**.

Resveratrol, as a positive control, showed strong activity to decrease the fluorescence intensity at the plateau **(Figure 3.43)** not only at the high molar ratio (ΔF = -72%) but also at the low molar ratio (ΔF = -60%), comparable to values described in the literature (-90% and -60% respectively).[45] However, as observed on curves from the literature, its ability to delay the aggregation kinetics is more modest ($\Delta t_{1/2}$ = +42%, +8 % for respectively ratios 10/1 and 1/1).[45,46] TTR showed very strong activity (no aggregation of $A\beta_{42}$) even at the low molar ratio of 1/1. It should be specified that this 1/1 ratio corresponds to TTR tetramer/$A\beta_{42}$ monomer: it becomes 4/1 if we consider TTR monomer/$A\beta_{42}$ monomer. Generally, in the literature, it is the concentration of the tetramer of TTR which is used since it is the stable and active form of TTR. At the high molar ratio (10/1), the natural peptide **11** derived from the EF-helix of TTR delayed significantly $A\beta_{42}$ aggregation with $\Delta t_{1/2}$ = +245% and reduced the fluorescence plateau with ΔF = -44%. However, it had no obvious effect on $A\beta_{42}$ aggregation at the low molar ratio (1/1), indicating that the natural peptide retains part of the activity of TTR against $A\beta_{42}$ aggregation. The aza-nonapeptides bearing an acetyl group at the N-terminus (peptide **1** to peptide **7**), at the molar ratio of 10/1, showed lower activity on $A\beta_{42}$ fibrillization compared to the natural peptide **11** (the natural peptide has a free amine at the N-terminus) with +68% < $\Delta t_{1/2}$ < +196% and -27% < ΔF < -43%. Nevertheless, peptides with different numbers of diaza-peptide units at different positions of the sequence showed different effects on $A\beta_{42}$ aggregation, which means the association between conformation and activity of these peptides. The aza-nonapeptides possessing one diaza-peptide unit at the C- or N-terminus (peptides **1** and **3**) displayed longer $t_{1/2}$ ($\Delta t_{1/2}$ = +196 and +193%) compared to other N-acetylated aza-nonapeptides and close to the value of the natural peptide ($\Delta t_{1/2}$ = +245%). However, peptide **1** appeared to be less effective on the fluorescence plateau (ΔF = -27%). The introduction of one diaza-peptide unit in the central part of the sequence (peptide **2**) had a reduced effect on delaying the aggregation ($\Delta t_{1/2}$ = +137%) compared to the natural peptide ($\Delta t_{1/2}$ = +245%) and the further introduction of another diaza-peptide unit at the C-terminus (peptide **4**) showed the even lower activity on delaying the aggregation ($\Delta t_{1/2}$ =+79%). Peptide **5** (one diaza-peptide unit in the central part of the sequence and

the other one at the N-terminus) and peptide **7** (three diaza-peptide units at three different positions) displayed strong effects on F at 10/1 ratio (and even at the molar ratio of 1/1 for **7**) comparable to the natural peptide **11** (ΔF = -40, -43, -44% for respectively **5**, **7** and **11**). Unlike the result observed for the fluorescence plateau, the activity of **5** and **7** on $A\beta_{42}$ aggregation kinetics is weaker than for **11** ($\Delta t_{1/2}$ = +110% and +68% compared to +245%). Peptide **6** which has two diaza-peptide units at the C- and N-termini respectively, showed a modest effect on $A\beta_{42}$ aggregation ($\Delta t_{1/2}$ = +87% and ΔF = -30%). To our surprise, peptide **10**, the non-acetylated analogue of peptide **6**, showed the strongest activity at the molar ratio of 10/1 compared to the natural peptide ($\Delta t_{1/2}$ = +363 *vs* +245% and ΔF = -62% *vs* -44% for **10** *vs* **11**) (**Figure 3.45**). This promising result suggests that the presence of two diaza-peptide units positioned at the N- and C-termini combined with a free amine at the N-terminus are probably crucial for the inhibition of $A\beta_{42}$ aggregation.

Compound	Molar ratio compound/ $A\beta_{42}$	$\Delta t_{1/2}$ Increase (%)	ΔF Decrease (%)
Peptide **1**	10/1	+196±19	-27±9
	1/1	+30±8	NE
Peptide **2**	10/1	+137±19	-38±1
	1/1	+29±2	NE
Peptide **3**	10/1	+193±12	-35±11
	1/1	+35±4	NE
Peptide **4**	10/1	+79±8	-38±7
	1/1	+21±8	NE
Peptide **5**	10/1	+110±27	-40±4
	1/1	+24±2	-19±1
Peptide **6**	10/1	+87±16	-30±6
	1/1	+12±4	NE
Peptide **7**	10/1	+68±8	-43±10
	1/1	+21±6	-23±4
Peptide **10**	10/1	+363±11	-62±6
	1/1	+54±22	NE
Peptide **11**	10/1	+245±18	-44±6
	1/1	+23±3	NE
Resveratrol	10/1	+42±27	-72±3
	1/1	+8±7	-60±5
TTR	1/1	NA	NA

Table 3.7: Parameters $\Delta t_{1/2}$ and ΔF of tested inhibitors in the first ThT experiment, parameters are expressed as mean±SD; NE = no effect; NA = no aggregation

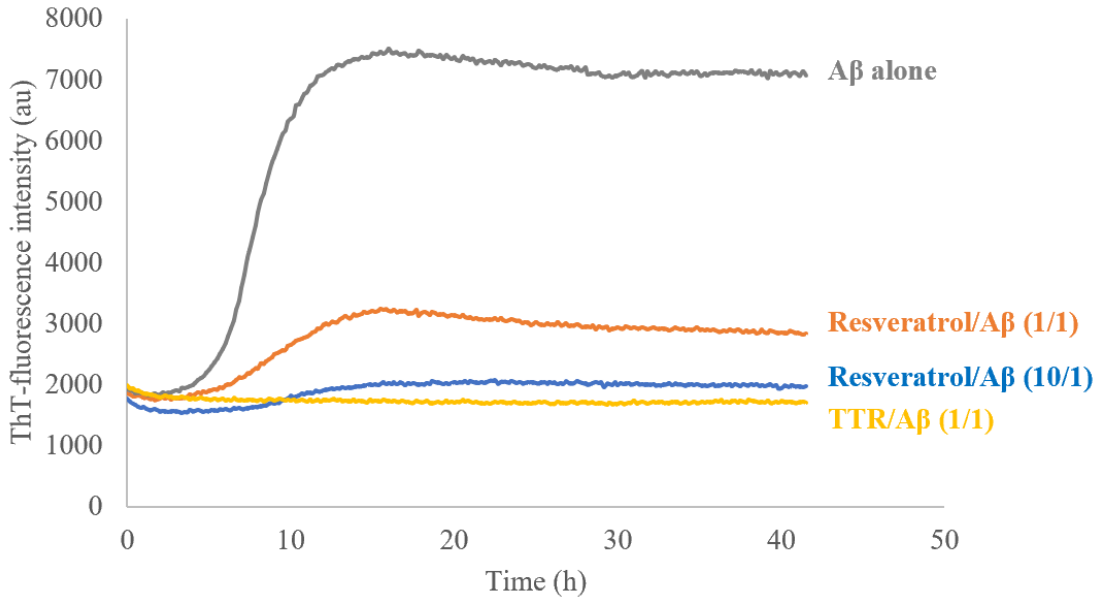

Figure 3.43: Mean ThT curves of $A\beta_{42}$ aggregation in the presence of resveratrol or TTR

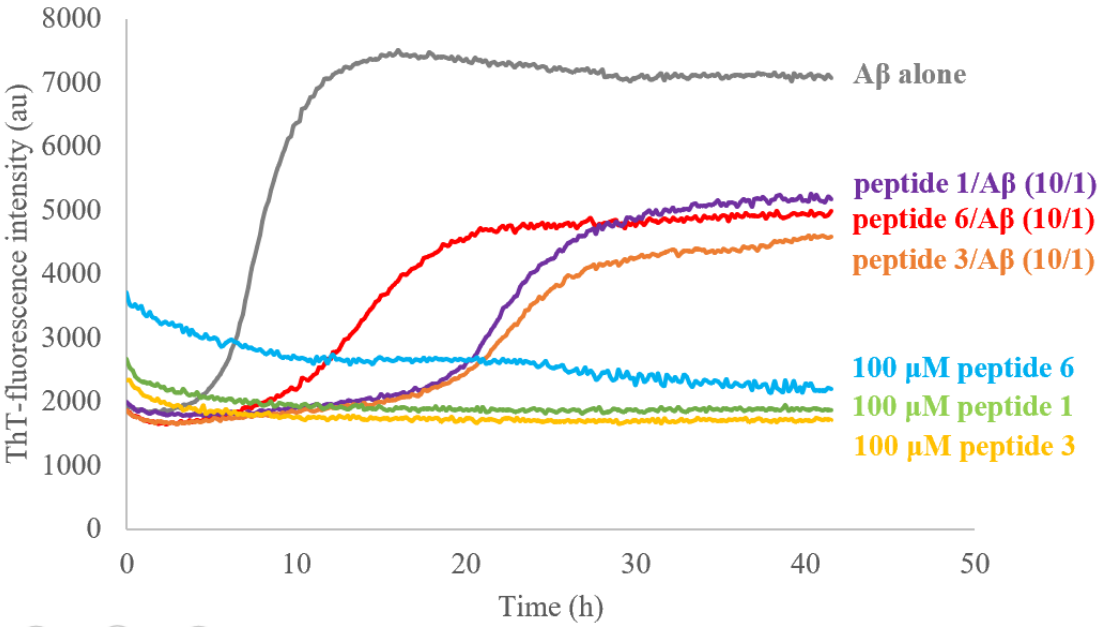

Figure 3.44: Mean ThT curves of $A\beta_{42}$ aggregation in the presence of peptide **1**, peptide **3** or peptide **6**

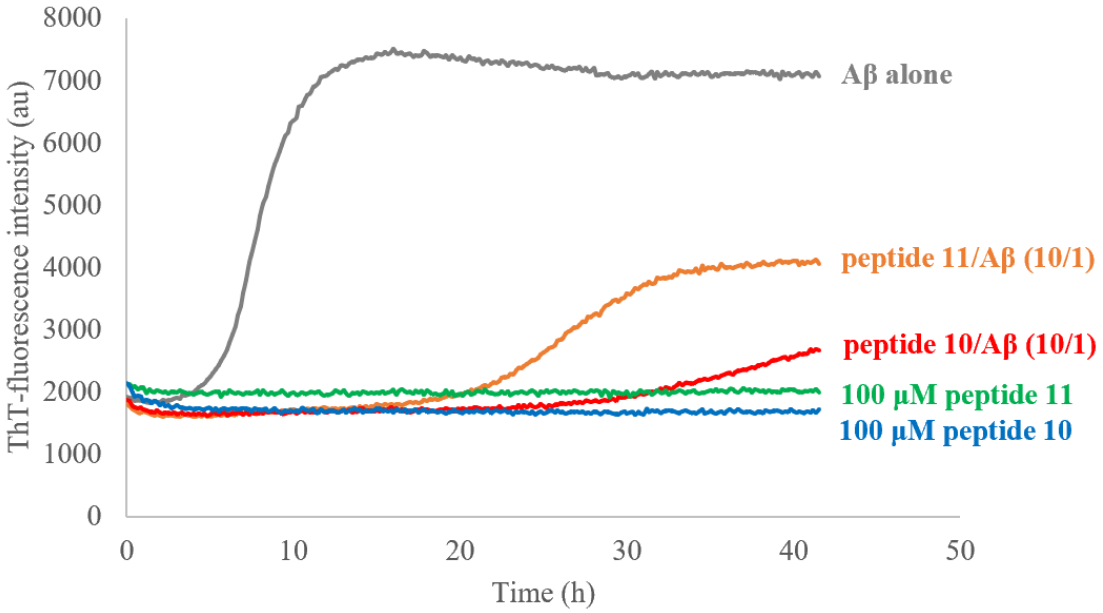

Figure 3.45: Mean ThT curves of $A\beta_{42}$ aggregation in the presence of peptide **10** or peptide **11**

Based on the results of the first ThT experiment, we found that the free amine at the N-terminus of the peptides is likely to play a key role in the interaction with $A\beta_{42}$. Thus, we designed and synthesized two new aza-nonapeptides with a free amine at the N-terminus (peptides **8** and **9**) based on peptides **1** and **3**, which showed the strongest effect on delaying $A\beta_{42}$ aggregation among the N-acetylated aza-nonapeptides in the first ThT experiment. The second ThT experiment was performed for all the synthesized peptides using the same protocol (fibrillization protocol) and the same commercial batch of $A\beta_{42}$ from Bachem (Batch 1) but bought later and received in another flask.

Although this time all the tested inhibitors showed a slight weaker effect on $A\beta_{42}$ aggregation compared to the results obtained from the first ThT experiment, all the inhibitors showed the similar ranking of effects on $A\beta_{42}$ aggregation (**Table 3.8**). The reproducibility of amyloid aggregation kinetics is an issue. Being a process generating metastable species, amyloid aggregation is sensitive to the experimental conditions (temperature, time, buffers …). At the low molar ratio (1/1), all the tested inhibitors did not show obvious effects on $A\beta_{42}$ aggregation except for TTR ($\Delta t_{1/2}$ = +305%, ΔF = -71%). Thus, we focused on the comparison of the activity of peptides at the molar ratio of 10/1. Peptide **10** was still the strongest inhibitor among the tested peptides ($\Delta t_{1/2}$ = +260%, ΔF = -55%). The aza-nonapeptides having an acetyl group at the N-terminus were still less potent than the natural peptide **11** ($\Delta t_{1/2}$ = +214%, ΔF = -55%). Among them, aza-nonapeptide **3** still showed the

strongest effect on delaying $A\beta_{42}$ aggregation ($\Delta t_{1/2}$ = +106%) compared to the other acetylated aza-nonapeptides. Aza-nonapeptides **5** and **7** also kept a strong effect on the decrease of F (ΔF = -58% for **5** and -56% for **7**) and a weak effect on delaying the aggregation ($\Delta t_{1/2}$ = +79% for **5** and +45% for **7**). These results were in accordance with the results from the first ThT experiment. However, the aza-nonapeptide possessing one diaza-peptide unit at the C-terminus (**1**) seems to loss potency in this experiment regarding the delay of the kinetics ($\Delta t_{1/2}$ = +63%, ΔF = -27%). It was less potent to delay the aggregation than aza-nonapeptides **2** ($\Delta t_{1/2}$ = +105%, ΔF = -52%) and **5** ($\Delta t_{1/2}$ = +79%) in this experiment whereas it was more potent than **2** and **5** in the first experiment. Regarding the two new aza-nonapeptides without acetyl group at the N-terminus, we found that the free amine of N-terminus has different effects on the activity depending on the peptide. Aza-nonapeptide **8** showed no improvement on delaying $A\beta_{42}$ aggregation ($\Delta t_{1/2}$ = +38%, ΔF = -34%) compared to its acetylated counterpart (peptide **1**) (**Figure 3.46**), whereas aza-nonapeptide **9** showed a stronger activity to delay $A\beta_{42}$ aggregation ($\Delta t_{1/2}$ = +202%, ΔF = -50%) compared to its counterpart peptide **3** ($\Delta t_{1/2}$ = +106%, ΔF = -32%) (**Figure 3.47**). The different change in activity from acetylated aza-nonapeptides to non-acetylated aza-nonapeptides indicates that the free amine is just beneficial for the activity of some aza-nonapeptides rather than all the aza-nonapeptides.

Compound	Molar ratio compound/ $A\beta_{42}$	$\Delta t_{1/2}$ Increase (%)	ΔF Decrease (%)
Peptide **1**	10/1	+63±5	-27±8
	1/1	NE	NE
Peptide **2**	10/1	+105±11	-52±11
	1/1	+5±3	33±8
Peptide **3**	10/1	+106	-32±14
	1/1	+8+1	NE
Peptide **4**	10/1	+36±4	-52±6
	1/1	+4±2	-24±6
Peptide **5**	10/1	+79±25	-58±9
	1/1	+8±1	-34±11
Peptide **6**	10/1	+32±6	-37±7
	1/1	+5±2	-24±3
Peptide **7**	10/1	+45±3	-56±5
	1/1	NE	-33±13
Peptide **8**	10/1	+38±8	-34±6
	1/1	NE	NE
Peptide **9**	10/1	+202±25	-50±5
	1/1	+16±3	14±9
Peptide **10**	10/1	+260±88	-55±2
	1/1	+27±3	NE
Peptide **11**	10/1	+214±66	-55±8
	1/1	+16±3	-20±3
TTR	1/1	+305±11	-71±2
	1/4	+76	-38

Table 3.8: Parameters $\Delta t_{1/2}$ and ΔF of tested inhibitors in the second ThT experiment, parameters are expressed as mean±SD; NE = no effect; NA = no aggregation

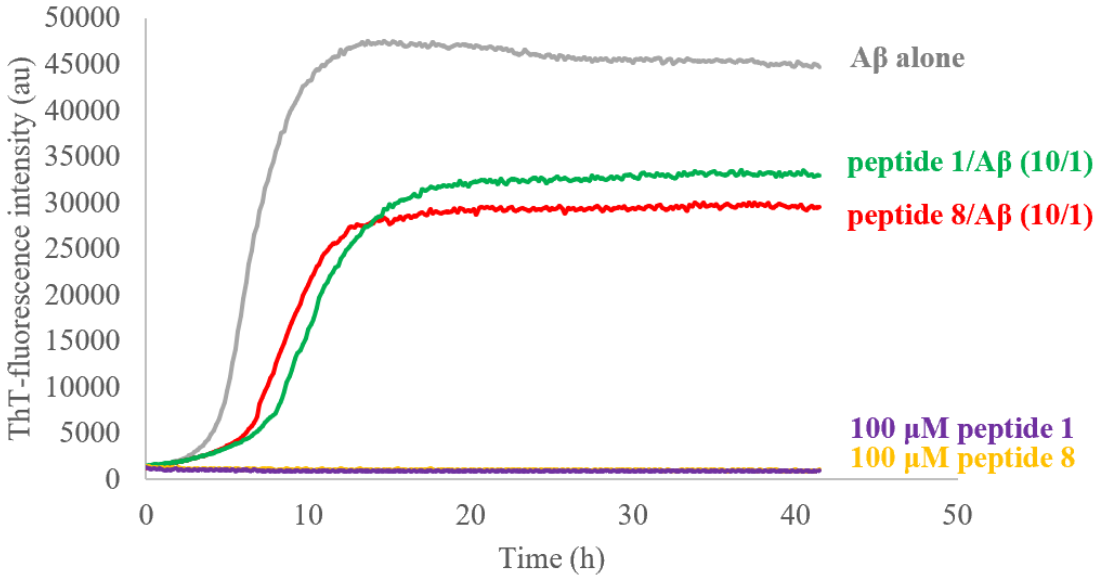

Figure 3.46: Mean ThT curves of $A\beta_{42}$ aggregation in the presence of peptide **1** or peptide **8** in second ThT experiment

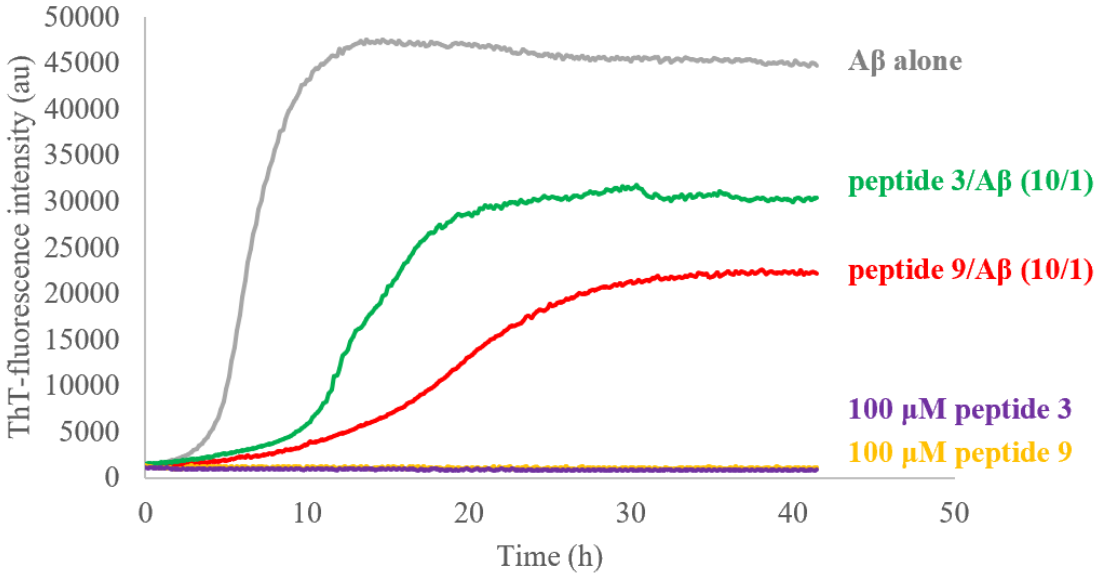

Figure 3.47: Mean ThT curves of $A\beta_{42}$ aggregation in the presence of peptide **3** or peptide **9** in second ThT experiment

Screening condition of pretreatment of $A\beta_{42}$ protein

All the synthesized peptides must be tested at least twice in triplicated to confirm their activity.

Due to the run out of $A\beta_{42}$ peptide, a new batch of $A\beta_{42}$ peptide was purchased and kinetics of aggregation of the new $A\beta_{42}$ peptide was monitored by ThT assays. However, the curves of $A\beta_{42}$ aggregation from this new batch of peptide showed the absence of lag phase at the beginning of aggregation. It has been reported that different Aβ sources give various aggregation propensity and morphology of Aβ peptide, which ultimately give rise to unreproducible results.[47] In order to find a batch of $A\beta_{42}$ peptide of good quality with nice aggregation curve, we purchased several new batches of $A\beta_{42}$ from different companies and checked their aggregation curves by ThT assay. Unfortunately, all the commercial sources of $A\beta_{42}$ peptides we bought showed unsuitable ThT curves: some of them had already aggregated or just showed a very weak propensity to aggregate into fibrils (**Figures 3.48 D** and **E**) and some were able to aggregated into fibrils but just showed short or no lag phase (**Figures 3.48 A**, **B** and **C**). Thus, none of them were suitable for testing the activity of peptides against $A\beta_{42}$ aggregation.

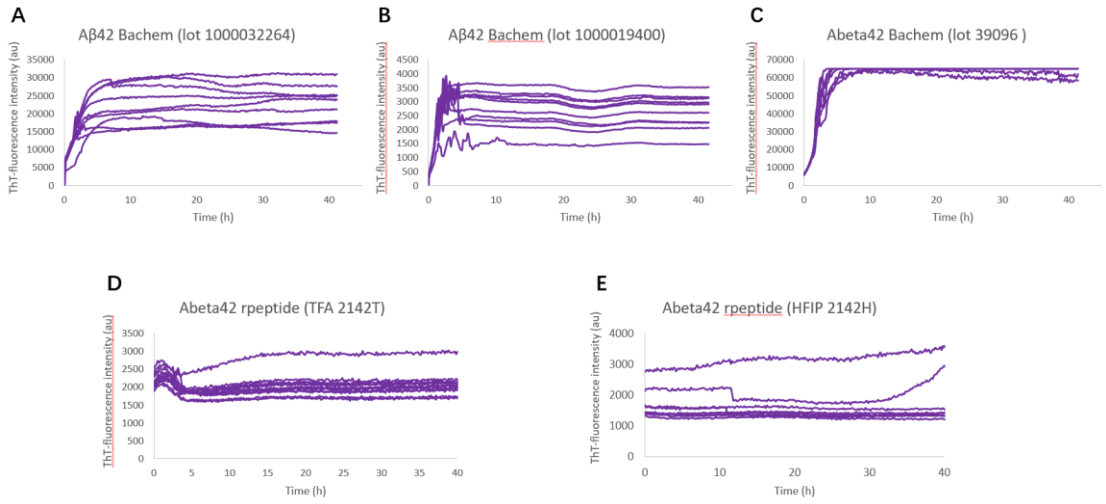

Figure 3.48: Aggregation curves of different batches of $A\beta_{42}$ in ThT experiment

The short lag phase could arise from the presence of amyloid nuclei or seeds at the beginning of the assay. This suggests that there are already some $A\beta_{42}$ aggregates (oligomers or small fibrils) formed as nuclei in these $A\beta_{42}$ peptides, thereby accelerating the process of the aggregation. Therefore, disaggregating existed nuclei in $A\beta_{42}$ peptides is a way to extend or recover a long lag phase of the aggregation in order to start the kinetics from monomeric amyloid peptides exclusively.

Herein, the batch of $A\beta_{42}$ peptide bought from Bachem (**Figure 3.48B**), which showed quite

short lag phase (less than 1 h) in the ThT assay was chosen to perform a pretreatment to destroy the existed nuclei. We will name this batch, batch 2.

The pretreatment of $A\beta_{42}$ with ammonia or HFIP has been reported in the literature.[48,49] $A\beta_{42}$ normally has TFA as counterion because of the gradient elution with TFA during HPLC purification. Thus, the pretreatment of $A\beta_{42}$ with ammonia can avoid the pH of the $A\beta_{42}$ solution from reaching the isoelectric point (pH= 5.5) of $A\beta_{42}$, at which $A\beta_{42}$ aggregation propensity is maximal, during solubilization.[50] HFIP is thought to induce α-helical structure of peptides, thereby disaggregating existed oligomers of the peptides. Here we used 1% ammonia aqueous solution or 10% ammonia aqueous solution or HFIP to pretreat $A\beta_{42}$ at the concentration of 1 mg/mL. The screening also concerned the time of pretreatment and the influence of sonication. Thus, three conditions were tested in each pretreatment reagent (**Table 3.9**), including condition 1 (1 h without sonication), condition 2 (5 min with sonication) and condition 3 (5 min without sonication). After these pretreatments, we used two different protocols, protocol A or protocol B (**Table 3.10**), to prepare $A\beta_{42}$ solution in the ThT assay to test the influence of the solvent medium on the kinetics of aggregation. Protocol A used Tris buffer to dissolve $A\beta_{42}$ to a concentration of 0.2 mM directly. Protocol B used 1% ammonia aqueous solution to dissolve $A\beta_{42}$ to a concentration of 1 mM and then dilute it to 0.2 mM with Tris buffer (fibrillization protocol). The aim of this optimization work was to find the best conditions to observe an $A\beta_{42}$ aggregation kinetics showing a long lag phase starting from low fluorescence values combined with high fluorescence plateau as observed with $A\beta_{42}$ (batch 1) in the control grey curves of **Figure 3.43** to **Figure 3.47**.

Condition	Sonication	Time
Condition 1	no	1 h
Condition 2	yes	5 min
Condition 3	no	5 min

Table 3.9: Three conditions used to pretreat $A\beta_{42}$ with 1% ammonia aqueous solution or 10% ammonia aqueous solution or HFIP (the concentration is 1 mg/mL)

Solubilization protocol	Solvent medium
Protocol A	Tris buffer
Protocol B	1% ammonia aq + Tris buffer

Table 3.10: Two protocols used to solubilize $A\beta_{42}$ in ThT assays

Table 3.11 summarizes the parameters $t_{1/2}$ and F for the pretreatment with 1% ammonia aqueous solution and curves are presented in **Figure 3.49**. We can see that in the case of $A\beta_{42}$ without pretreatment, the lag phase was very short whatever the protocol used to dissolve $A\beta_{42}$. However, different protocols had impact on the fluorescence plateau. Protocol B displayed higher fluorescence plateau than protocol A and this phenomenon was also visible in the case of $A\beta_{42}$ with pretreatments (conditions 1, 2 or 3). $A\beta_{42}$ with no pretreatment in protocol B also showed higher fluorescence at the beginning of the aggregation process than with protocol A. The difference on fluorescence at the beginning of aggregation and plateau indicated respectively different starting aggregate states of $A\beta_{42}$ and final morphologies of $A\beta_{42}$ fibrils. This suggests that different protocols using in the preparation of $A\beta_{42}$ solution maybe change the pathway of the aggregation.

Using 1% ammonia aqueous solution to pretreat $A\beta_{42}$ (1 mg/1 mL) still showed short lag phase of $A\beta_{42}$ aggregation as the $A\beta_{42}$ without pretreatment whatever the conditions and protocols used (**Table 3.11** and **Figure 3.49**). However, for all the pretreatment conditions, the aggregation of $A\beta_{42}$ had longer growth phases in protocol A than in protocol B (**Table 3.11** and **Figure 3.49**). The longer growth phases reflect a slower elongation during the aggregation in protocol A. Moreover, $A\beta_{42}$ pretreated by 1% ammonia aqueous solution in these three conditions also showed an important difference on the fluorescence at the beginning of aggregation as well as the plateau between the two different protocols; higher for protocols B (red curves in **Figure 3.49**) and lower for protocols A (green curves in **Figure 3.49**) as we observed with the $A\beta_{42}$ without pretreatment. This phenomenon indicates that $A\beta_{42}$ pretreated with 1% ammonia aqueous solution also displays different starting states between protocol A and protocol B. Taken together, these results indicate that $A\beta_{42}$ pretreated by 1% ammonia aqueous solution takes different pathways of aggregation when solubilized with the different protocols. The pretreatment of $A\beta_{42}$ with 1% ammonia aqueous

solution didn't lead to satisfactory aggregation curves.

1% ammonia (1mg/1mL) Pretreatment condition	Protocol	$t_{1/2}$ (h)	F (au)
No pretreatment	A	1.0±0.09	1450±367
	B	1.4±0.31	3622±835
Condition 1	A	8.0±1.87	4476±1138
	B	1.7±0.24	8008±1114
Condition 2	A	7.4±1.20	5518±1114
	B	1.3±0.15	8847±1357
Condition 3	A	10.0±3.74	3114±520
	B	1.7±0.23	8366±1263

Table 3.11: Parameters $t_{1/2}$ and F of $A\beta_{42}$ which was pretreated by 1% ammonia aqueous solution, parameters are expressed as mean±SD

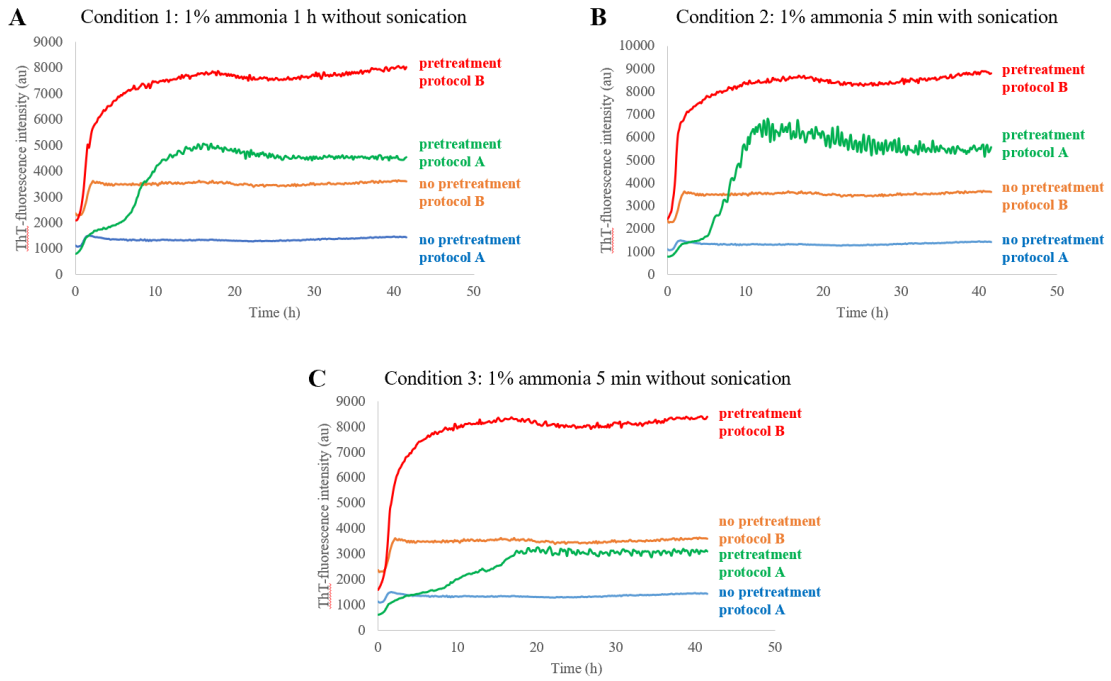

Figure 3.49: Mean ThT curves of $A\beta_{42}$ aggregation. A) pretreated by 1% ammonia aqueous solution for 1 h without sonication (condition 1); B) pretreated by 1% ammonia aqueous solution for 5 min with sonication (condition 2); C) pretreated by 1% ammonia aqueous solution for 5 min without sonication (condition 3)

Similar to pretreatment with 1% ammonia aqueous solution, pretreatment with 10% ammonia

aqueous solution also showed long growth phase but short lag phase in protocol A which results in medium $t_{1/2}$ (1.0 h < $t_{1/2}$ < 8.4 h) (**Table 3.12 and Figure 3.50**). In protocol B, all the conditions show shorter $t_{1/2}$ ($t_{1/2}$ < 1.9 h) because of the short growth phase. Moreover, in conditions 1 and 2, we could see the difference on the starting state of $A\beta_{42}$ between the two protocols (**Figure 3.50A** and **Figure 3.50B,** green *vs* red curves at t0). However, in condition 3, it seems that the aggregation starts from the same state of $A\beta_{42}$ even using different protocols (there is no big gap between the fluorescence at the beginning of the aggregation) (**Figure 3.50C,** green *vs* red curves at t0). Overall, 10% ammonia aqueous solution pretreatment also did not make $A\beta_{42}$ showing suitable aggregation curves no matter which protocol was used to solubilize $A\beta_{42}$ essentially because of the short to medium lag phases.

10% ammonia (1mg/1mL) Pretreatment condition	Protocol	$t_{1/2}$ (h)	F
No pretreatment	A	1.0±0.09	1450±367
	B	1.4±0.31	3622±835
Condition 1	A	7.4±0.40	5012±915
	B	1.6±0.41	7273±1197
Condition 2	A	8.4±1.42	4484±533
	B	1.4±0.56	5293±1100
Condition 3	A	7.6±1.38	5249±535
	B	1.9±0.51	5298±592

Table 3.12: Parameters $t_{1/2}$ and F of $A\beta_{42}$ which was pretreated by 10% ammonia aqueous solution, parameters are expressed as mean±SD

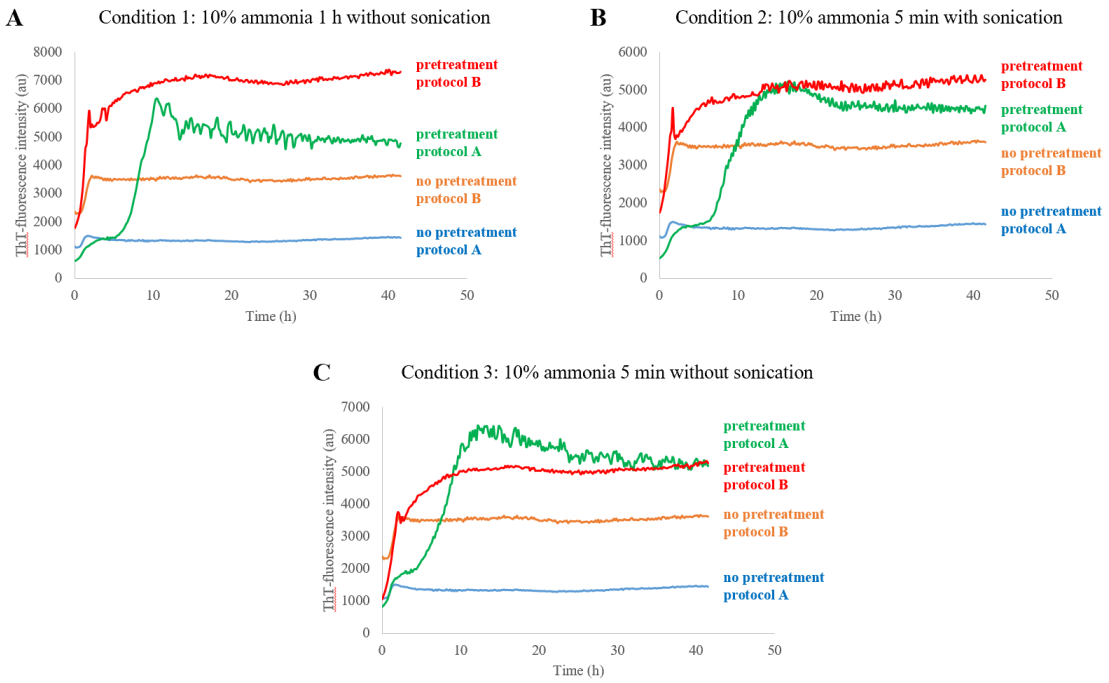

Figure 3.50: The mean ThT curves of $A\beta_{42}$ aggregation. A) pretreated by 10% ammonia aqueous solution for 1 h without sonication (condition 1); B) pretreated by 10% ammonia aqueous solution for 5 min with sonication (condition 2); C) pretreated by 10% ammonia aqueous solution for 5 min without sonication (condition 3)

HFIP pretreatment (1 mg/1mL) whatever the conditions, 1, 2 or 3 let to increase the $t_{1/2}$ and the F compared to $A\beta_{42}$ without pretreatment (**Table 3.13** and **Figure 3.51**). The longer lag phase confirmed that HFIP actually could disaggregate the existing aggregates of $A\beta_{42}$ in batch 2. The different conditions didn't give rise to obvious difference on $t_{1/2}$ and F whereas the different protocols have impacts on $t_{1/2}$ and F. In Protocol B, $A\beta_{42}$ aggregation always showed even more noticeably a longer $t_{1/2}$ and higher F than protocol A. For the condition 1, protocol B increased not only fluorescence plateau but also the fluorescence during the lag phase compared to protocol A (**Figure 3.51A**). This means that $A\beta_{42}$ pretreated in this condition also shows different state at the beginning of aggregation when using different protocols. It seems that condition 3 combined with protocol B is the more optimal treatment to get a long $t_{1/2}$ and the highest F, and to reproduce the aggregation kinetics observed previously with batch 1 in the first two ThT assays (grey curves in **Figure 3.43** to **Figure 3.47**).

HFIP (1mg/1mL) Pretreatment condition	Protocol	$t_{1/2}$ (h)	F (au)
No pretreatment	A	1.0±0.09	1450±367
	B	1.4±0.31	3622±835
Condition 1	A	11.1±0.82	3547±192
	B	16.6±0.70	5991±542
Condition 2	A	10.7±1.81	3711±986
	B	14.2±0.56	5021±850
Condition 3	A	9.9±1.57	2936±505
	B	12.0±0.25	6521±772

Table 3.13: Parameters $t_{1/2}$ and F of $A\beta_{42}$ which was pretreated by HFIP, parameters are expressed as mean±SD

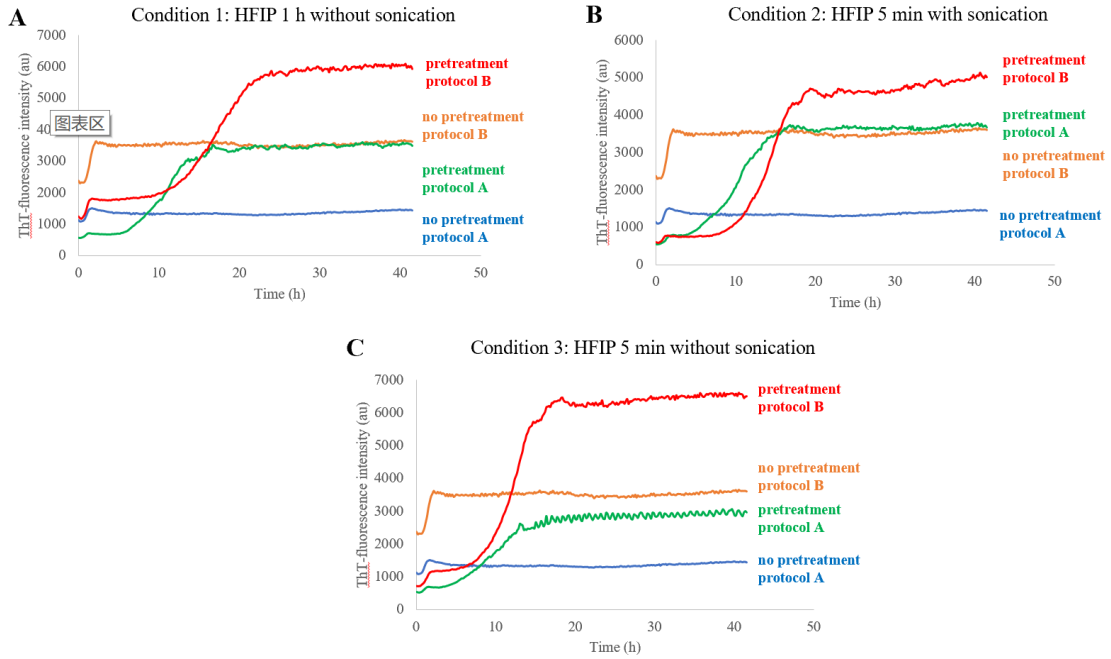

Figure 3.51: Mean ThT curves of $A\beta_{42}$ aggregation. A) pretreated by HFIP for 1 h without sonication (condition 1); B) pretreated by HFIP for 5 min with sonication (condition 2); C) pretreated by HFIP for 5 min without sonication (condition 3)

Through investigating the conditions of pretreatment of $A\beta_{42}$ and the protocols to dissolve $A\beta_{42}$, we can say that $A\beta_{42}$ aggregation is really a complex process which is affected by various factors. Given that the exact mechanism of amyloid aggregation is still elusive (amyloid proteins can aggregate in different pathways, have various morphologies of aggregates that are metastable

species), it is hard to give an explanation why the different conditions give rise to different kinetics of the aggregation. As we know, the $A\beta_{42}$ from different suppliers or different batches of $A\beta_{42}$ usually have different ways to prepare (chemical synthesis or biosynthesis) and various protocols to purify. These all can affect the purity and state of $A\beta_{42}$, thereby changing the pathway of the aggregation. That explains why it is difficult to have reproducible *in vitro* kinetics of $A\beta_{42}$ aggregation. Considering that the aim of this optimization work is to recover an $A\beta_{42}$ aggregation control kinetics showing a long lag phase combined with a high fluorescence plateau, we selected the following conditions: pretreatment with HFIP (1mg/mL) by conditions 3 (5 min without sonication) and solubilization by protocol B (solubilized by 1% ammonia aqueous solution to 1mM, then diluted by tris buffer to 0.2 mM) (**Table 3.13**, **Figure 3.51C** red curve).

The activity of azapeptides against the new batch of $A\beta_{42}$ pretreated by HFIP

$A\beta_{42}$ (Batch 2) pretreated by HFIP in condition 3 was chosen to perform ThT assay for testing the activity of several our inhibitors. $A\beta_{42}$ solution was prepared using fibrillization protocol (protocol B). All the inhibitors we tested showed a weaker activity or even lost the activity to delay the aggregation except resveratrol (**Table 3.14** and **Figure 3.52**). The natural peptide **11** and peptide **9** which showed potent aggregation activity using the Batch 1 of $A\beta_{42}$, had just weaker activity to delay the aggregation ($\Delta t_{1/2}$ = +35% for **11** and $\Delta t_{1/2}$ = +16% for **9**) and to reduce the fluorescence plateau (ΔF = -20% for **11** and ΔF = -33% for **9**) at the molar ratio of 10/1 with this batch of $A\beta_{42}$ (**Figure 3.53** and **Figure 3.54**). Several tested compounds lost their activity to delay the aggregation even at the molar ratio of 10/1, such as **2**, **5** and **8**. Even for peptide **10**, the most potent compound against $A\beta_{42}$ aggregation before, just showed no effect on delaying the aggregation (**Figure 3.55**). Likewise, TTR showed also less activity on the extension of $t_{1/2}$ ($\Delta t_{1/2}$ = +100% *vs* > +305 % with batch 1). Although most compounds could reduce fluorescence plateau, the decrease was not as obvious as before except for **5** (ΔF = -48%), suggesting **5** has potent activity to change the morphology of $A\beta_{42}$ fibrils even using the new batch of $A\beta_{42}$ peptide which probably have a different aggregate state at the beginning. Only for peptide **6** the activity remained ($\Delta t_{1/2}$ = 60%, ΔF = -29%) but this compound was not a strong inhibitor in the three ThT experiments.

All these results indicated that TTR and the peptides derived from TTR are not strong inhibitors

when tested with this batch of $A\beta_{42}$. It should be noted that for this batch of $A\beta_{42}$ (pretreated by HFIP), the fluorescence of control curves (incubation of inhibitors in the absence of $A\beta_{42}$) is obvious lower than fluorescence of the curves in the presence of $A\beta_{42}$ at t0 whereas in the experiments using the batch 1 of $A\beta_{42}$, there is no obvious difference on the fluorescence at t0 between the presence or absence of $A\beta_{42}$. This indicates that even $A\beta_{42}$ is pretreated by HFIP, there is still some small aggregated species at the beginning of the aggregation that increase the initial fluorescence. Their presence engages the amyloid peptide into a different pathway of aggregation, for which our peptides and TTR seem to be less sensitive and therefore less active. Nevertheless, resveratrol, which is described as a strong and non-selective amyloid aggregation inhibitor which even can destroy existed aggregates still showed excellent activity for this new batch of $A\beta_{42}$, which highlights the different mechanism of action between resveratrol and our peptides.

Compound	Molar ratio compound/ $A\beta_{42}$	$\Delta t_{1/2}$ Increase (%)	ΔF Decrease (%)
Peptide **1**	10/1	+36±19	NE
	1/1	-7	-25±12
Peptide **2**	10/1	NE	-36±6
	1/1	NE	-10±6
Peptide **3**	10/1	+21±7	-21±5
	1/1	NE	-27±12
Peptide **5**	10/1	NE	-48±2
	1/1	NE	-19±2
Peptide **6**	10/1	+60±4	-29±6
	1/1	+13±8	NE
Peptide **8**	10/1	NE	-15±11
	1/1	NE	-26±4
Peptide **9**	10/1	+16±3	-33±2
	1/1	NE	-8±4
Peptide **10** *	10/1	NE	-17±4
	1/1	NE	-13±7
Peptide **11** *	10/1	+35±7	-20±9
	1/1	+23±15	NE
Resveratrol	10/1	NA	-87±1
	1/1	NE	-61±2
TTR	1/1	+100±47	+22

Table 3.14: Parameters $\Delta t_{1/2}$ and ΔF of tested inhibitors on the $A\beta_{42}$ pretreated by HFIP in condition 3 (fibrillation protocol), parameters are expressed as mean±SD; NE = no effect; NA = no aggregation; Asterisk means that peptides were purified by semi-preparative HPLC using ACN/H_2O + 0.1% TFA

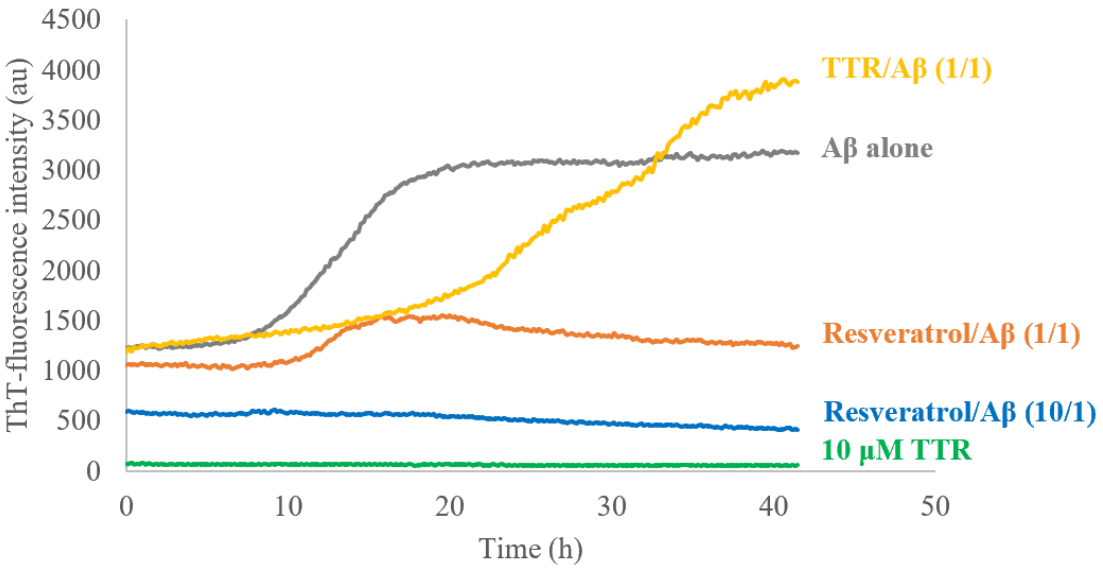

Figure 3.52: Mean ThT curves of $A\beta_{42}$ (pretreated by HFIP for 5min without sonication) aggregation in the presence of resveratrol or TTR

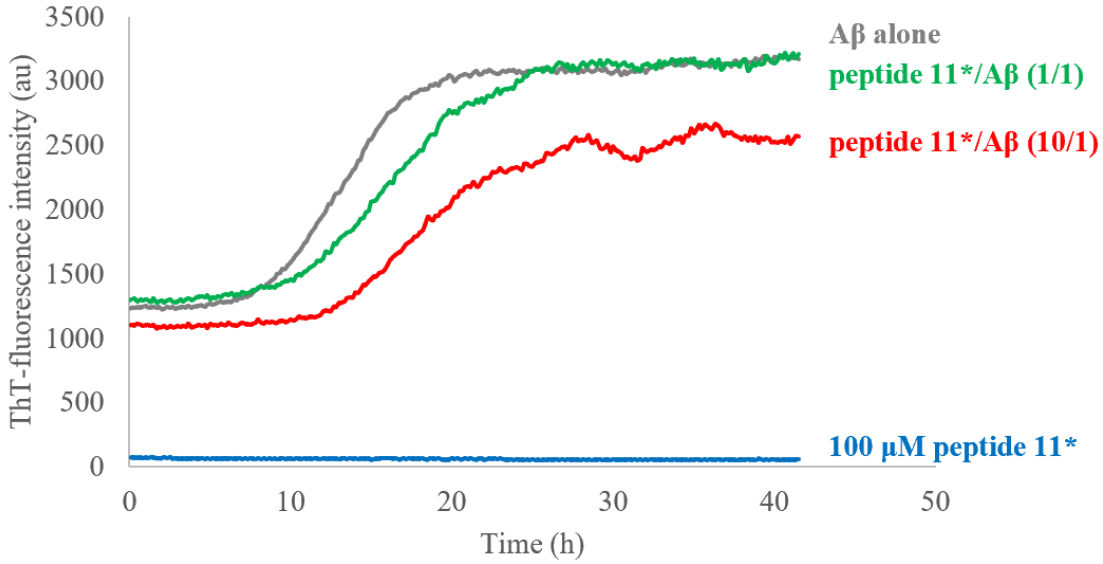

Figure 3.53: Mean ThT curves of $A\beta_{42}$ (pretreated by HFIP for 5min without sonication) aggregation in the presence of the natural peptide **11**; Asterisk means that the peptide was purified by semi-preparative HPLC using ACN/H_2O + 0.1% TFA

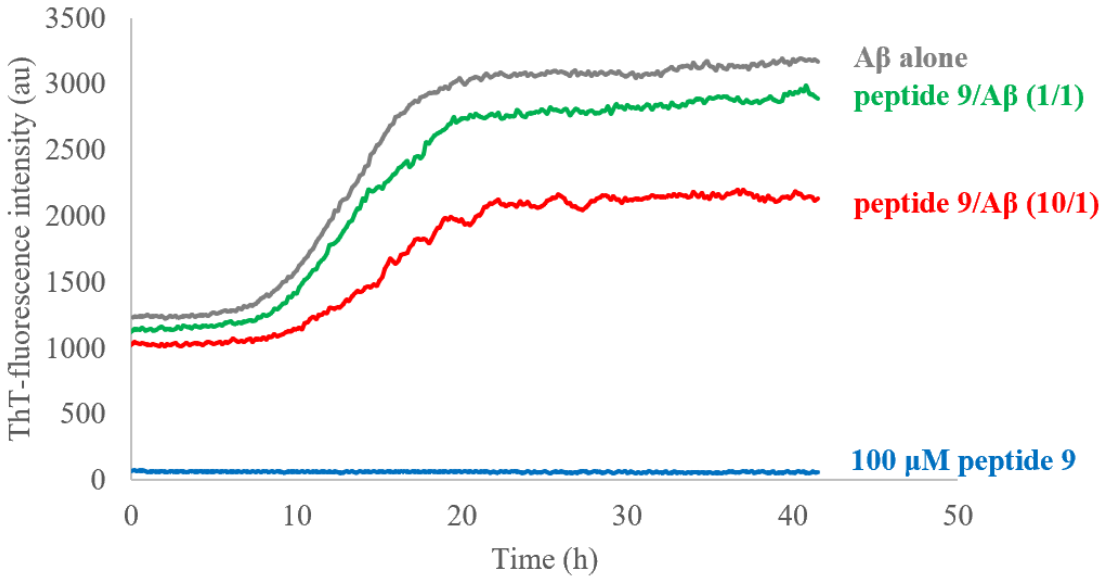

Figure 3.54: Mean ThT curves of $A\beta_{42}$ (pretreated by HFIP for 5min without sonication) aggregation in the presence of peptide **9**.

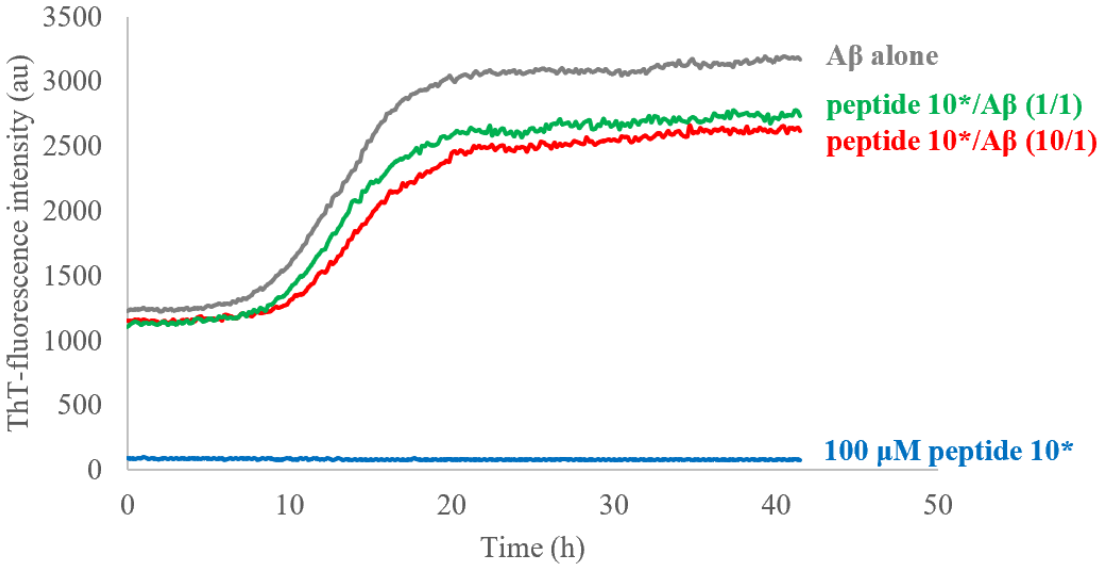

Figure 3.55: Mean ThT curves of $A\beta_{42}$ (pretreated by HFIP for 5min without sonication) aggregation in the presence of peptide **10**; Asterisk means that the peptide was purified by semi-preparative HPLC using ACN/H_2O + 0.1% TFA

It should be also noted that in this experiment, we also used new batch of peptides **10** and **11**, which probably have slight difference on the counterion compared to the peptides used in the last two ThT tests because this time peptides **10** and **11** were purified by semi-preparative HPLC using

ACN/H_2O + 0.1% TFA instead of ACN/H_2O + 0.1% formic acid as eluent. To rule out the impact of the counterions of peptides, we used the old batch of **10** and **11** (purified by semi-preparative HPLC using ACN/H_2O + 0.1% formic acid) that were used at the beginning, to do ThT assay again on this new batch of $A\beta_{42}$. The result showed that even for the **10** and **11** purified by semi-preparative HPLC using ACN/H_2O + 0.1% formic acid, the activity against the aggregation of this new batch of $A\beta_{42}$ was still lost. We speculated that the pretreatment of Aβ with HFIP did not disaggregate all the oligomers of $A\beta_{42}$. Therefore, it suggests that our peptides probably rather target the $A\beta_{42}$ monomer or less aggregated states of $A\beta_{42}$ to prevent the first nucleation rather than more aggregated $A\beta_{42}$ oligomers or fibrils to prevent secondary nucleation and elongation. This is in accordance with our design to target rather the primary helical conformation of Aβ to prevent its misfolding in β-sheet rich structure. Our peptides are not able to target β-sheet rich structure of Aβ.

ThT assay using oligomerization protocol in the preparation of $A\beta_{42}$ solution

Due to the loss activity of our peptides on the aggregation of $A\beta_{42}$ pretreated by HFIP when using fibrillization protocol in ThT assay, we also wanted to test another protocol to prepare $A\beta_{42}$ solution; in particular a protocol established to stabilize oligomers during the aggregation pathway that was developed in the laboratory and named oligomerization protocol.[51] Instead of fibrillization protocol (dissolving $A\beta_{42}$ in a 1% aqueous ammonia to a concentration of 1 mM then diluting the solution to 0.2 mM with Tris buffer) that we used before, in the oligomerization protocol, $A\beta_{42}$ was dissolved in a 1% aqueous ammonia to a concentration of 1mg/mL directly. The results are shown in **Table 3.15**. Although most tested peptides were still not so active to delay the aggregation of the $A\beta_{42}$ which was pretreated by HFIP (condition 3), most of them were more potent than in fibrilization protocol. Moreover, most compounds showed stronger effect on the decrease of fluorescence plateau. Peptides **3** and **9** were, with the oligomerization protocol, the two most active peptides on delaying the aggregation (**Table 3.15** and **Figure 3.56**). For peptide **10**, the TFA salt still showed no activity on inhibition of $A\beta_{42}$ aggregation, but the formic acid salt showed moderated activity (**Table 3.15** and **Figure 3.57**) although this activity was still not as strong as when using the batch 1 of $A\beta_{42}$. For peptide **11**, both salts showed similar activity on inhibition of $A\beta_{42}$ aggregation in oligomerization protocol (**Figure 3.58**). This means that **10** is more sensitive to the change of the

counterion in oligomerization protocol. All these results with this protocol suggest that the 2 different protocols of $A\beta_{42}$ preparation (fibrillization *vs* oligomerization protocol) have a crucial impact on the activity of our peptides. It seems that our peptides are more potent in oligomerization protocol in which oligomers aggregate to fibrils slowly. Given that it should be different pathways of $A\beta_{42}$ aggregation in these two protocols, we hypothesized that our peptides have more influence on the $A\beta_{42}$ species which are formed in the pathway from the oligomerization protocol.

Compound	Molar ratio compound/ $A\beta_{42}$	$\Delta t_{1/2}$ Increase (%)	ΔF Decrease (%)
Peptide **1**	10/1	NE	-75±3
Peptide **3**	10/1	+142±15	-86±2
Peptide **6**	10/1	NE	NE
Peptide **8**	10/1	NE	-50±28
Peptide **9**	10/1	+110±5	-82±6
Peptide **10**	10/1	+71±29	-73±7
Peptide **10** *	10/1	NE	NE
Peptide **11**	10/1	+68±39	-74±5
Peptide **11** *	10/1	+30±15	-80±1

Table 3.15: Parameters $\Delta t_{1/2}$ and ΔF of tested inhibitors on the aggregation of $A\beta_{42}$ pretreated by HFIP in condition 3 (oligomerization protocol), parameters are expressed as mean±SD; NE = no effect; Asterisk means that peptides were purified by semi-preparative HPLC using ACN/H_2O + 0.1% TFA

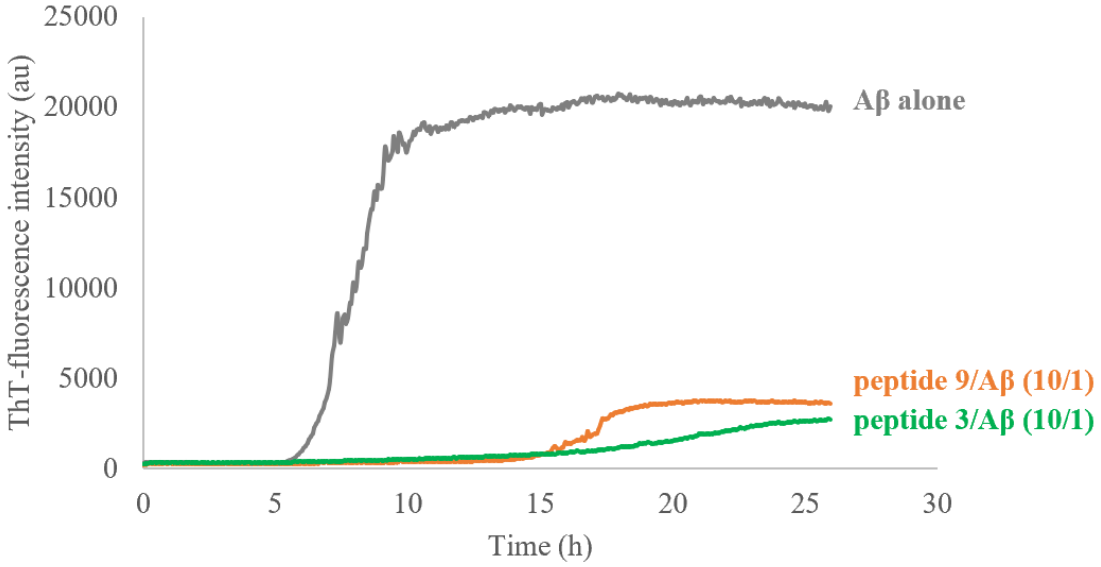

Figure 3.56: Mean ThT curves of $A\beta_{42}$ (pretreated by HFIP for 5min without sonication) aggregation (oligomerization protocol) in the presence of peptide **3** or peptide **9**

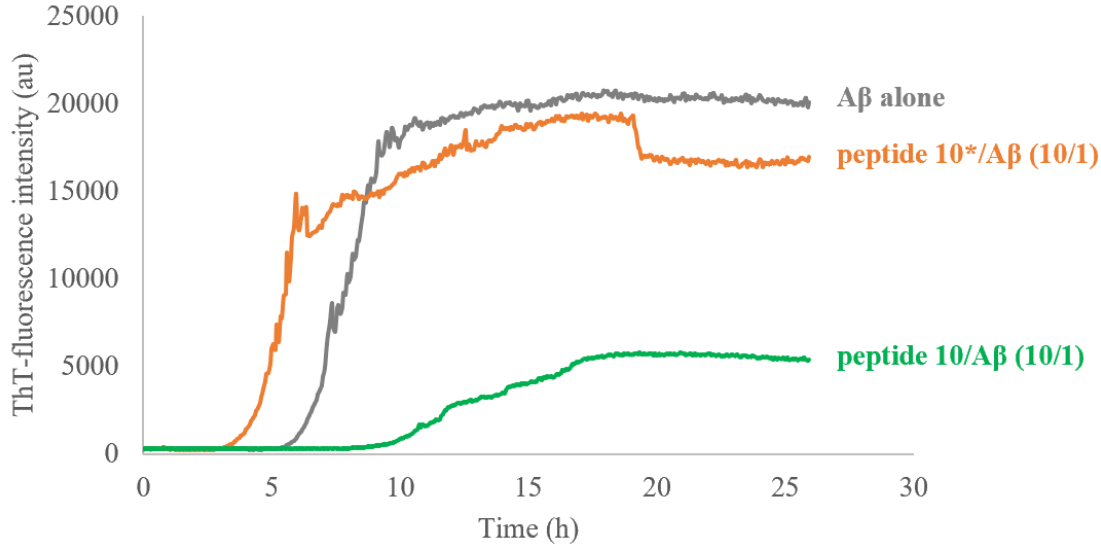

Figure 3.57: Mean ThT curves of $A\beta_{42}$ (pretreated by HFIP for 5min without sonication) aggregation (oligomerization protocol) in the presence of peptide **10**; Asterisk means that the peptide was purified by semi-preparative HPLC using ACN/H_2O + 0.1% TFA

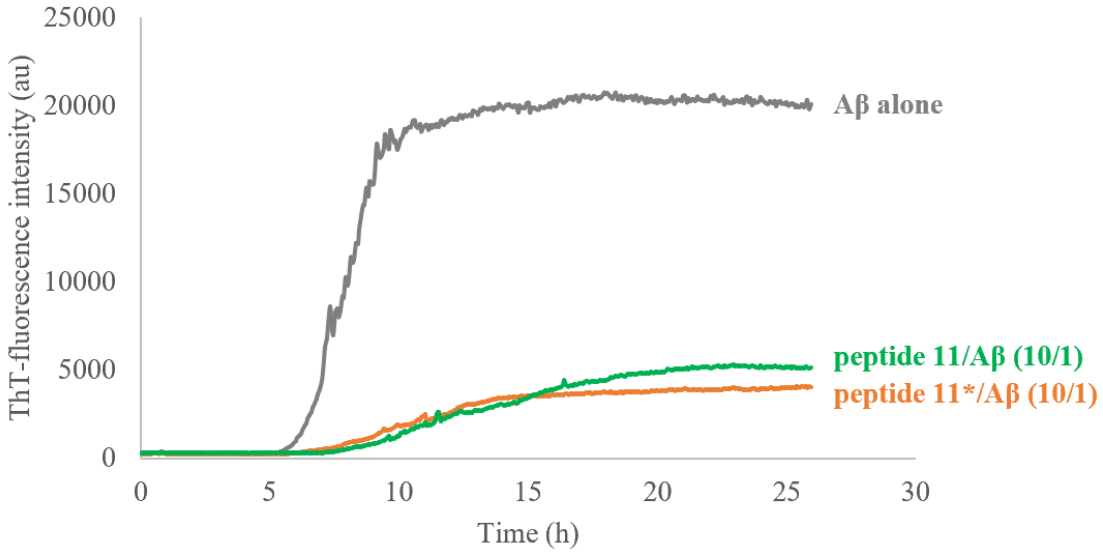

Figure 3.58: Mean ThT curves of $A\beta_{42}$ (pretreated by HFIP for 5min without sonication) aggregation (oligomerization protocol) in the presence of the natural peptide **11**; Asterisk means that the peptide was purified by semi-preparative HPLC using ACN/H_2O + 0.1% TFA

Conclusion on ThT fluorescence assays for $A\beta_{42}$ aggregation

The introduction of diaza-peptide units into the EF-helix sequence turned out to be a relevant strategy to disrupt the aggregation pathway of amyloid peptide $A\beta_{42}$. Indeed, among the ten aza-nonapeptides designed, synthesized and tested, peptide **10** possessing two diaza-peptide units at the N- and C-termini respectively and no acetylation at the N-terminus, was proved to be even more active than their natural analogue **11** on $A\beta_{42}$ aggregation. In the conformation studies we discussed in section 3.5, peptide **10** displayed a folded structure (helical structure) which can project its side chains in the same direction as the EF-helix of TTR does. This means that the conformation of the peptides which can mimic the EF-helix actually increases the activity against $A\beta_{42}$ aggregation. The free N-terminal amine of **10** also plays a key role in the inhibition of $A\beta_{42}$ aggregation, because the acetylated counterpart of **6** showed only a weak activity. Indeed, the presence of the free amine at the N-terminus induce a better interaction with $A\beta_{42}$, supporting our previous observations on the importance of establishing ionic interactions with acidic residues of $A\beta_{42}$ ($E_{3\text{-}11\text{-}22}$, $D_{1\text{-}7\text{-}23}$ or C-terminus of $A\beta_{42}$). This rule, however, is not compatible with all the peptides. For example, peptide **8** which has also a free amine at the N-terminus and a diaza-peptide unit at the C-terminus only

showed the similar activity compared to its acetylated counterpart **1**. The difference activity between peptides **6** and **10** might also be attributed to the slight difference between the conformations of peptides **6** and **10**, as we mentioned in section 3.5.

Moreover, we observed that our inhibitors displayed different results when using different batches of $A\beta_{42}$ or solubilization protocols of $A\beta_{42}$. This suggests that it is challenging to reproduce the outcome for some inhibitors in ThT assay when using different batch of $A\beta_{42}$ or different protocols to prepare $A\beta_{42}$ solution because of the different mechanism of inhibitors. We speculated that our peptides are more sensitive to $A\beta_{42}$ monomers or the less aggregated states whereas different batches of $A\beta_{42}$ or different protocols to prepare $A\beta_{42}$ solution may produce different starting states of $A\beta_{42}$, which gives the different and non-reproducible activities of our peptides against $A\beta_{42}$ aggregation. Moreover, these results indicate that our peptides rather target helical structure conformation of Aβ before the misfolding in β-sheet rich structure. Further investigations should be performed to find suitable pretreatment conditions to well disaggregate oligomers or fibrils. To characterize the $A\beta_{42}$ species formed after the different pretreatments, several techniques, such as Capillary Electrophoresis[44] and Western Blot, probably could be used to help us to have an idea of the states of $A\beta_{42}$. This work will be performed in the future.

The activity of azapeptides against hIAPP aggregation in ThT assay

As we mentioned in the chapter 1, there is a cross-interaction between Aβ and hIAPP and they show 25% identical residues in the sequences.[52] It has been proposed that TTR can also interfere with the formation of hIAPP fibrils.[53] Moreover, several Aβ aggregation inhibitors such as resveratrol and EGCG, also show activity to inhibit IAPP aggregation. Thus, the activities on the inhibition of hIAPP aggregation for peptides **9**, **10**, and **11** were evaluated by ThT fluorescence assay to determine the selectivity between $A\beta_{42}$ and hIAPP. As shown in **Figure 3.59**, all the tested peptides showed no obvious inhibitory activities on hIAPP aggregation at the molar ratio of 10/1. However, all the tested compounds seem to be able to slightly decrease the fluorescence plateau at a lower molar ratio (4/1) but could not delay the aggregation. Thus, we can say at the molar ratio of 10/1, our peptides can selectively inhibit $A\beta_{42}$ aggregation. According to these results, the EF-helix of TTR might not be involved in TTR–hIAPP interaction.

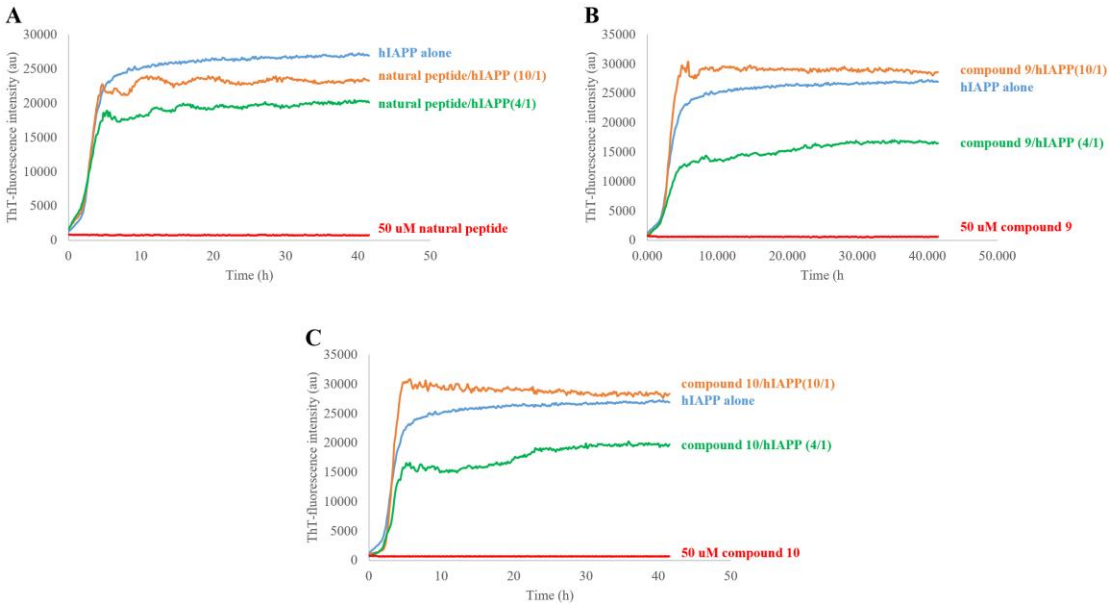

Figure 3.59: Mean ThT curves of hIAPP aggregation in the presence of the natural peptide **11** (A), peptide **9** (B), or peptide **10** (C).

Analysis of the kinetic process of Aβ aggregation by AmyloFit

To get insight into molecular mechanisms underlying the inhibition of the process of Aβ aggregation by aza-nonapeptide **10** and the natural peptide **11**, we used the experimental data from the ThT assays to run a kinetic analysis on AmyloFit[54], an online platform for the processing and analysis of experimental protein aggregation kinetic data.

Under our conditions, $A\beta_{42}$ alone follows a molecular model in which the mechanism dominating the kinetics of aggregation is the secondary nucleation. The experimental data for TTR are consistent with predictions made by altering the rate constants of secondary nucleation (k_2) or elongation (k_+). The secondary nucleation pathway is specifically perturbed. In particular, the k_+k_2 value in the presence of TTR was found to decrease by a factor of approximately 100 and 10 with 10 μM and 2.5 μM TTR concentration, respectively (**Table 3.16**). The same effect is observed for peptide **11**, with the k_+k_2 value decreased by a factor of 100 at 100 μM concentration (no effect observed at 1:1 ratio) (**Table 3.16**). Conversely, the experimental data for aza-nonapeptide **10** are consistent with predictions made by altering the product of the rate constants of elongation and

primary nucleation (k_+k_n), thus demonstrating that the primary nucleation pathway is specifically perturbed, by a factor of 100 at 100 μM (ratio 10:1), and 10 at 10 μM (ratio 1:1) (**Table 3.16**). This analysis showed a different mechanism of inhibition of our aza-nonapeptide **10** compared to TTR and EF-helix derived peptide **11**.

	$A\beta_{42}$	$A\beta_{42}$/TTR		$A\beta_{42}$/**10**		$A\beta_{42}$/**11**	
	none	2.5 μM	10 μM	10 μM	100 μM	10 μM	100 μM
k_+k_n	$1.24e^4$	$1.24e^4$	$1.24e^4$	$1.59e^3$	$9.61e^{-6}$	$1.24e^4$	$1.24e^4$
k_+k_2	$2.05e^{15}$	$4.68e^{14}$	$3.68e^{13}$	$2.05e^{15}$	$2.05e^{15}$	$1.35e^{15}$	$9.22e^{13}$
Mean residual error	0.000607	0.00605		0.000881		0.00120	

Table 3.16: The kinetic parameters obtained from the analysis of experimental data on AmyloFit (The concentration of $A\beta_{42}$ is 10 μM)

3.6.2 CD analysis of Aβ

CD analysis of $A\beta_{42}$ or $A\beta_{1\text{-}28}$ with and without inhibitors was used to evaluated the effects of inhibitors on Aβ conformation and aggregation.

CD analysis of $A\beta_{42}$ in the absence of inhibitors

Time-dependent CD experiments of $A\beta_{42}$, at 25 μM in PB solution (10 mM) at pH 7.4, showed the slow transition from unordered to ordered structure of $A\beta_{42}$ after 5 h incubation (**Figure 3.60A**), as evidenced by the slow increase of the negative minimum at λ≈215 nm and the positive maximum at λ=195 nm. An isodichroic point was observed at λ=208 nm, which suggested a two-state transition from random coil to β-sheet conformation (**Figure 3.60A**). The data were consistent with our previous results.[51] At this condition, $A\beta_{42}$ reached the characteristic shape of β-sheet conformation after 5 h incubation.

The CD deconvolution with the algorithm BeStSel[15] revealed the presence of an α-helix at the very beginning of the kinetics, together with a predominantly random coil conformation (**Figure 3.60B**). A stable antiparallel β-sheet structure was also present, probably due to the self-folding of $A\beta_{42}$ into a β-hairpin manner (**Figure 3.60B**). During time, the disappearance of the α-helix content,

the increase in the content of parallel β-sheet and the decrease in the content of random coil were observed, suggesting that, proceeding with the aggregation process, each monomer of $A\beta_{42}$, in β-hairpin conformation, interacts with another monomer, forming parallel β-sheet rich aggregates. The β-sheet content increased by 193% in 5 h, with an antiparallel β-sheet conformation remaining stable overtime and a high ratio between parallel and antiparallel (**Figure 3.62**).

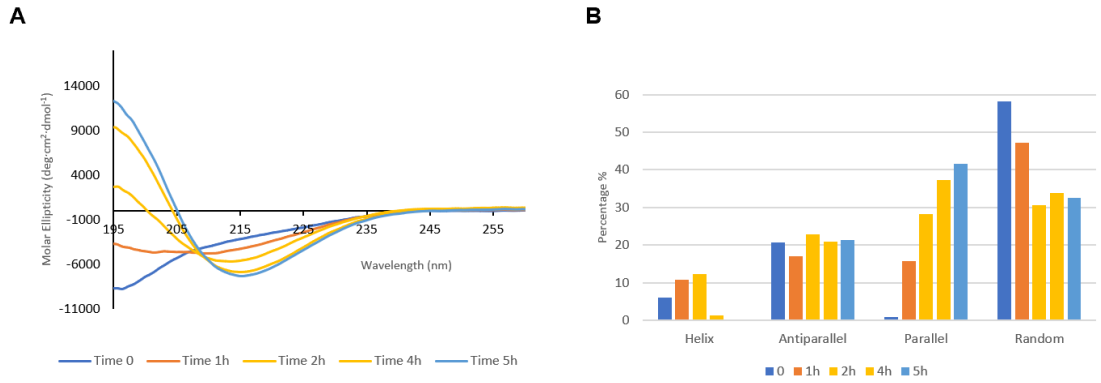

Figure 3.60: A) CD spectra of $A\beta_{42}$ monitored at different incubation time; B) Estimated content of secondary structures of $A\beta_{42}$

CD analysis of $A\beta_{42}$ in the presence of peptide 10 or peptide 11

CD spectra of $A\beta_{42}$ (25 μM) in the presence of peptide **10** or peptide **11** (125 μM) after 5 h incubations (**Figures 3.61A** and **3.61B**) showed the negative minimum of $A\beta_{42}$ around 215 nm were slightly shifted to low wavelength (around 212 nm). The change in the minimum suggested a possible perturbation in the global secondary structure at the end of the kinetics. This change could be appreciated thanks to the deconvolution (**Figure 3.61C** and **3.61D**), which clearly showed that both peptides were able to remarkably decrease the parallel β-sheet content, accordingly to their ability to inhibit the aggregation process. Moreover, the α-helix, which was observed at the beginning of the kinetics, was maintained stable until 5 h, suggesting a possible stabilization of $A\beta_{42}$ in its monomeric state, at a conformation which is not able to aggregate.

The β-sheet content only increased in 5 h by 36% in the presence of peptide **11** and by 95% in the presence peptide **10**, with lower ratios between parallel and antiparallel β sheets compared to the one of $A\beta_{42}$ alone (**Figure 3.62**).

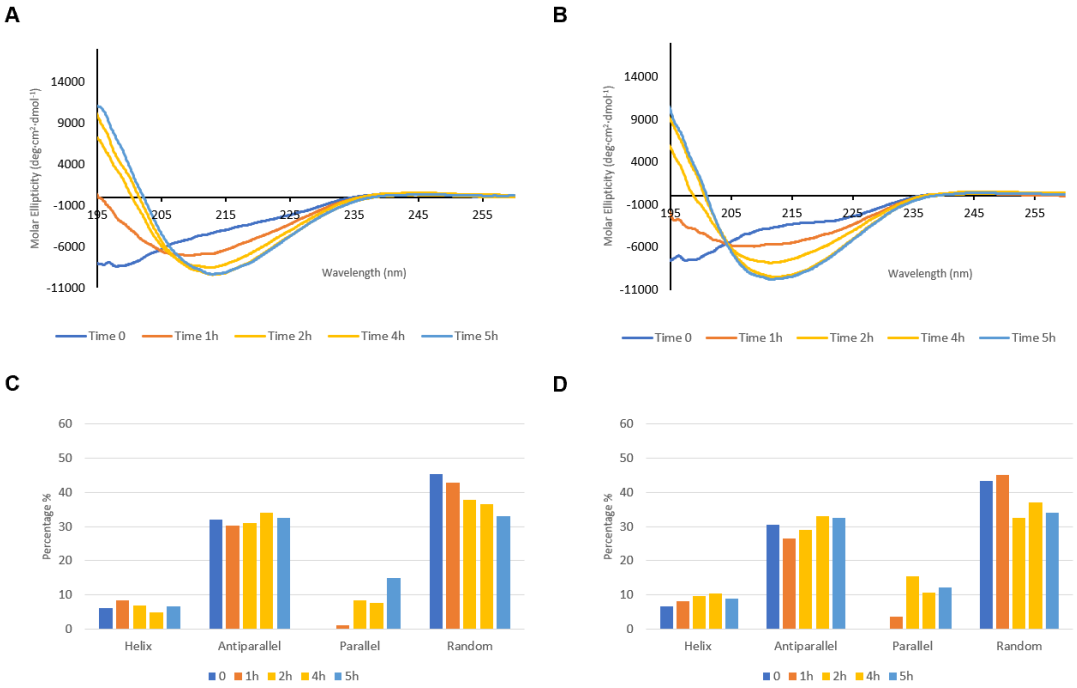

Figure 3.61: A) CD spectra of $A\beta_{42}$ in the presence of peptide **10** (A) or peptide **11** (B) monitored at different incubation time; Estimated content of secondary structures of $A\beta_{42}$ in the presence of peptide **10** (C) or peptide **11** (D)

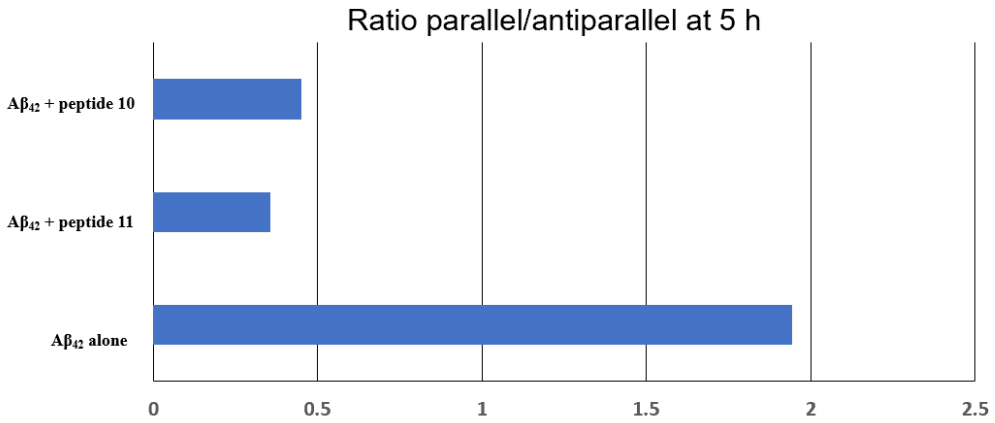

Figure 3.62 The ratio of parallel/antiparallel of $A\beta_{42}$ after 5 h incubation

CD analysis of $A\beta_{1-28}$ in the absence or presence of peptides

The same CD experiments were also performed on the $A\beta_{1-28}$ to investigate conformational changes of $A\beta_{1-28}$ in the absence or presence of peptides.

$A\beta_{1-28}$ alone showed the very low content of α-helix at the beginning or after 3 h incubation (less than 10%) (**Figure 3.63A**). The low content of β-strand of $A\beta_{1-28}$ even after 3 h incubation indicated a lower aggregated propensity of $A\beta_{1-28}$ compared to $A\beta_{42}$. When $A\beta_{1-28}$ was incubated with peptide **10**, the content of α-helix was increased and this α-helical content could be mostly retained after 3 h incubation (**Figure 3.63A**), which means peptide **10** could stabilize the α-helical content of $A\beta_{1-28}$. The very low content of β-strand (less than 10%) of $A\beta_{1-28}$ in the presence of peptide **10** confirmed the ability of peptide **10** against Aβ aggregation. The natural peptide **11** also showed the ability to increase the α-helical content of $A\beta_{1-28}$ but less potent to decrease β-strand after 3 h incubation (**Figure 3.63A**). We can clearly see in **Figure 3.63B** that, $A\beta_{1-28}$ showed the highest ratio of between α-helical content and β-strand content after 3 h incubation in the presence of peptide **10**.

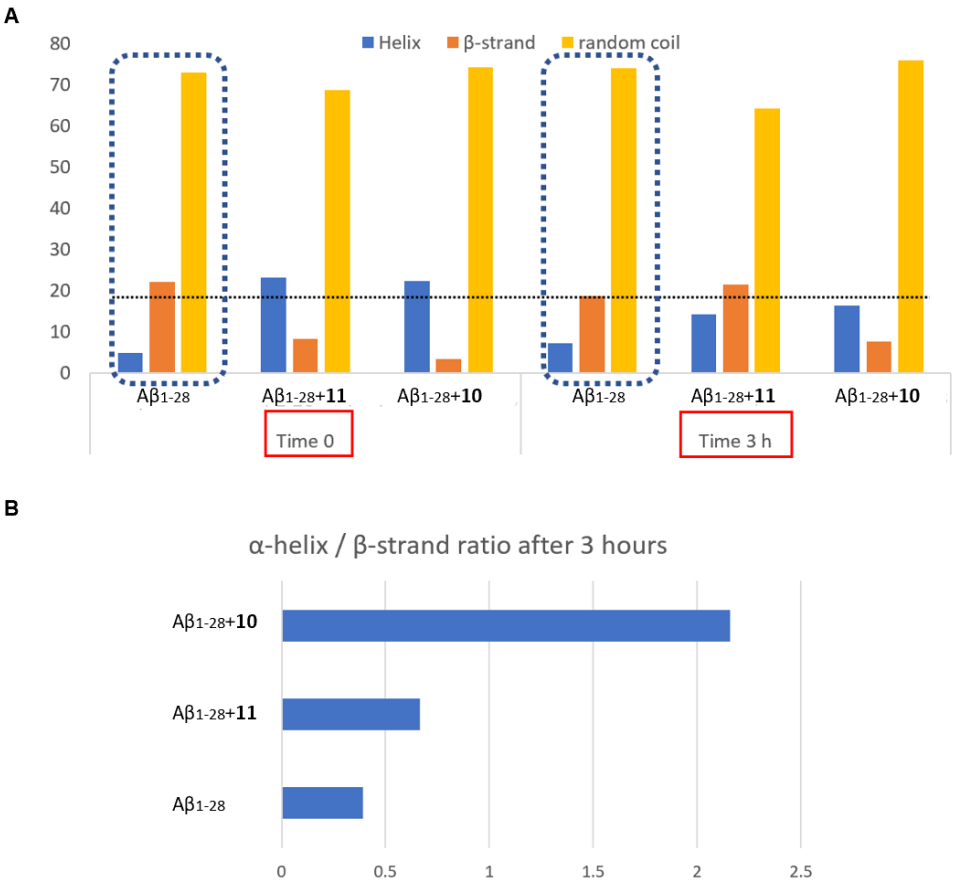

Figure 3.63: A) Estimated content of secondary structures of $A\beta_{1\text{-}28}$ (25 µM) in the absence or presence of peptide **10** or **11** (125 µM); B) The ratio of α-helix/β-strand of $A\beta_{1\text{-}28}$ after 3 h incubation

All these results suggest that peptide **10** is able to interact at the early steps of the kinetics (helical structure of Aβ), with the preliminary folding of Aβ before its misfolding in pathological β-sheet structures prone to aggregation. This also indicates that **10** interacts with the N-terminal part of $A\beta_{42}$ ($A\beta_{1\text{-}28}$) as reported for TTR.[55]

3.6.3 Stability in human plasma

In general, azapeptides show higher proteolytic stability than natural peptides.[56] The stability of the azapeptides **10** and natural peptide **11** were tested in human plasma to compare their proteolytic stability with two controls (Enalapril and Procaine). The experiments were performed by the platform SMArt-MS (Dr. Alain Pruvost, CEA/DRF/JOLIOT). After two hours incubation in

human plasma at 37°C, only 6% of the aza-nonapeptide **10** was degraded whereas 99% of the natural peptide **11** was degraded (**Table 3.17**). This result indicates that the aza-nonapeptide **10** which contains two diaza-peptide units at the N-terminus and C-terminus, respectively, has excellent stability in human plasma. This also confirms our hypothesis that the introduction of diaza-peptide units into natural peptides really is able to improve the proteolytic stability of natural peptides.

Compounds	Percentage (%) of degradation at 30 min	Percentage (%) of degradation at 120 min	$t_{1/2}$ (min)
Peptide **10**	15.0	6.0	5.24
Peptide **11**	98.1	99.1	NA
Enalapril	2.5	2.6	NA
Procaine	100	100	1.1

NA: not available

Table 3.17: *In vitro* human plasma stability of peptides **10** and **11** at 37°C

3.6.4 Membrane permeability

As we mentioned before, peptides normally have a limited membrane permeability. Only cell-penetrating peptides possessing cationic, amphiphilic or hydrophobic properties can show membrane permeability. For peptides targeting proteins in CNS, they have to cross the BBB to interact with the target proteins. The BBB is the barrier between the cerebral capillary blood and the extracellular fluid of the brain and is mainly composed of endothelial cells of the cerebral capillaries by tight junctions. The BBB permeability is the major obstacle of CNS drugs to exert their biological activity. Here the BBB permeability of the aza-nonapeptide **10** was tested using *in vitro* rat BBB model by the group of Dr. Aloïse Mabondzo (CEA, Université Paris Saclay).[57]

The experimental results (**Table 3.18**) show that the apparent permeability (Papp) values of peptide **10** at 10 μM and 5 μM (6.77×10^{-7} cm/s and 8.39×10^{-7} cm/s, respectively) are lower than the one of Lucifer yellow, a reference compound (3.13×10^{-6} cm/s), indicating a limited passage across the *in vitro* rat BBB model for peptide **10**. The ratio between the apparent permeability value from the basal to apical compartment (1.6) and from the apical to basal compartment (2.6) suggests that peptide **10** is a potential substrate of the efflux transporters located at the rat BBB. This is a reason why peptide **10** displays limited passage across the rat BBB model. Thus, the limited BBB

permeability could be improved by further structural modification on peptide **10** to reduce the affinity of efflux transporters. However, this permeability is comparable with the one of cell penetrating peptides[58] and much higher than biologics such as anti-Aβ antibodies.

Concentration (μM)	10 μM		5 μM	
Permeability determination	Apical to Basal	Basal to Apical	Apical to Basal	Basal to Apical
Papp (cm/s)	$6.77x10^{-7}$	$1.07x10^{-6}$	$8.39x10^{-7}$	$2.14x10^{-6}$
Papp ratio BA/AB	1.6		2.6	

Table 3.18: BBB permeability of peptide **10**

3.6.5 Cellular toxicity

The toxicity of peptide **10** was also tested by performing MTT (3-(4,5-dimethylthiazol-z-yl)-2,5-diphenyl-tetrazotium bromide) assay. After one hour exposure of rat brain endothelial cells with peptide **10** at different concentrations (from 1 μg/mL to 100 μg/mL), the viability of the cells showed no obvious decrease compared to the cells without any treatment or with DMSO (0.2 or 1%) (**Figure 3.64**). As a positive control, less than 10% of the cells were viable after one hour exposure to a 100% DMSO. These results indicate that peptide **10** has no obvious toxicity to cells even at the concentration of 100 μg/mL.

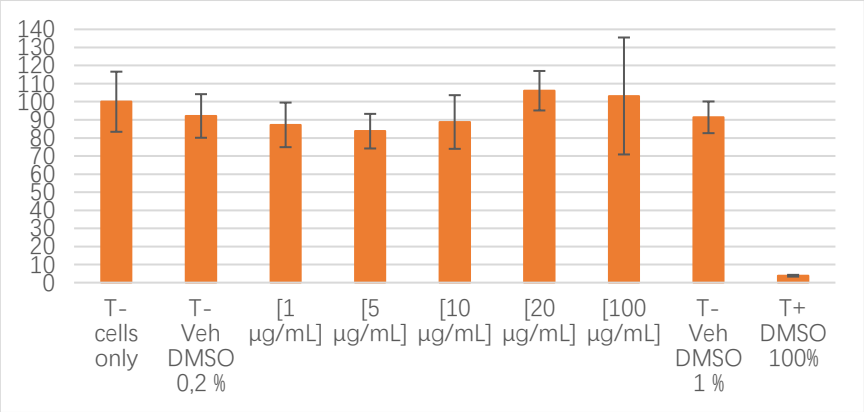

Figure 3.64: Cell viability after 1 hour of exposure to peptide **10**.

3.7 Conclusion

In this chapter, based on the previous work in our laboratory, the results we got from the chapter 2 and questions we wanted to answer in this project (see the objective of the thesis, chapter 1), we designed and synthesized ten aza-nonapeptides which have different numbers of diaza-peptide units at different positions of the EF-helix sequence (N-terminus, central region and C-terminus). The Fmoc-based solid phase synthesis for these long azapeptides was developed. First, the different Fmoc-protected diaza-peptide units were synthesized in solution (the synthesis of diaza-peptides has been discussed in the chapter 2). Then we used triphosgene as a carbon donor to couple diaza-peptide units to the N-terminus of peptides attached on resin. For coupling natural amino acids to the N-terminus of aza-residues, DIC/Oxyma were used as coupling reagent to improve the coupling yields. In some cases, due to big steric hindrance of lateral chains on both aza-residues and natural residues, this coupling should be performed at 40°C.

CD experiment on these peptides showed that they have different conformations based on the number and position of diaza-peptide units in the sequence. The diaza-peptide units at the N-terminus or C-terminus of the sequence could induce specific structures which have positive band around 225 nm and negative band around 196 nm.

Peptides **6** and **10** with strong positive bands around 225 nm were further chosen to study their conformation in water by NMR experiments. The fast exchange of amide NHs of peptide **6** with water made it impossible to calculate $^{3}J_{HN\alpha}$ and temperature coefficients $\Delta\delta NH/\Delta T$ of its residues. However, ROEs found in peptide **6** suggest folded structures in water. For peptide **10**, folded structures with slight difference with peptide **6** could be proposed based on a few different ROEs. The conformation of peptide **10** in DMF was also studied for the comparison with peptide **10** in water. The NMR parameters ($^{3}J_{HN\alpha}$, temperature coefficients $\Delta\delta NH/\Delta T$ and ROEs) of peptide **10** in DMF demonstrated more folded structures than in water. FTIR spectra of peptides **6** and **10** indicate that they have different conformations in water. Peptide **10** is more structured and less aggregated than peptide **6** in water. The MD simulation of peptide **10** provides its most populated cluster, which can mimic the EF-helix well as demonstrated by low RMSD values and a similar orientation of its side chains. The conformation of peptide **9** possessing one diaza-peptide unit at the N-terminus was

also studied by NMR in CD_3OH. The NMR parameters at 258 K described two conformers of peptide **9**. The major one was an intact 3_{10}-helix structure but the other one showed two different segments at the N-terminus and C-terminus, respectively. The N-terminal segment showed 3_{10}-helix structure but the C-terminus segment showed a helical structure with fraying. At 298 K, peptide **9** just showed only one conformer which was the minor conformer at 258 K. These results indicate diaza-peptide unit at the N-terminus actually has the ability to induce helical structures of the peptides but the inductive effect propagate not so far. It seems that the introduction of one diaza-peptide unit at the C-terminus has less this helically inductive effect (less positive band around 225 nm in CD spectra). On the contrary, introducing diaza-peptide units in the central region has no this helically inductive effect or even disrupt this effect (based on the different CD spectra). The similar effect was also observed by Guichard's group.[59] In their oligourea/peptide chimeras, when oligourea segments were placed at the N- or C-terminus of the chimeras, oligourea segments could serve as helical nucleation templates to induce helices of the chimeras. This N-terminal inductive effect has also been reported by Aitken's group.[60] They found that the 12-helices of the *trans*-2-aminocyclobutanecarboxylic acid (*t*ACBC) foldamers could be transformed to 8-helices by introducing a N-aminoazetidine-2-carboxylic acid (AAzC) at the N-terminus of the foldamers. However, this effect only works in their foldamers with the length up to six residues.

Then we tested the activity of the synthesized peptides against Aβ aggregation by ThT assay. We found that peptides **9** and **10** without acetyl group at the N-terminus exhibited stronger activity than other azapeptides. This result suggests that the activity of the peptides against Aβ aggregation is correlated with the conformation of the peptides but in some case the free amine group at the N-terminus is important for the activity. This highlights that the presence of the free hydrazine at the N-terminus can induce a ionic interaction with $A\beta_{1\text{-}42}$, supporting our previous observations on the importance of establishing ionic interactions between cationic groups of ligands with acidic residues of $A\beta_{42}$ ($E_{3\text{-}11\text{-}22}$, $D_{1\text{-}7\text{-}23}$ or C-term of $A\beta_{42}$).[43,44,61,62] Peptide **10** showed the best activity which was even better than the natural peptide **11**, that also possess a N-free amine but a random coil conformation in water (we cannot exclude however that the natural peptide can adopt an helical structure when it is interacting with $A\beta_{42}$). Kinetic analysis of the curves from ThT assay by

AmyloFit demonstrated that peptide **10** targets the step of primary nucleation, which is different with TTR and the natural peptide **11** that target the secondary nucleation step.

The activity of peptide **10** was also confirmed by the CD analysis of the solution of $A\beta_{42}$ with peptide **10**. Peptide **10** showed the ability to maintain the helix of $A\beta_{42}$ (monomeric state) and reduce its parallel β-sheet structure. In addition, the CD analysis of the solution of $A\beta_{1\text{-}28}$ in the presence of **10** also demonstrated our peptide **10** inhibit Aβ aggregation through stabilizing the helical structure of the N-terminus of Aβ. To our knowledge, several inhibitors which can stabilize α-helical structures of Aβ monomer have been reported as a promising strategy to reduce the Aβ aggregation.[63]

In addition, peptide **10** showed high proteolytic stability in human plasma on the contrary of the natural peptide **11** which was immediately degraded. Furthermore, no obvious toxicity to rat brain endothelial cells and a limited BBB permeability (comparable with a reported CPP and superior to antibodies) were observed.

As we had to face to many problems of reproducibility of the *in vitro* aggregation assays, we also tried to pretreat $A\beta_{42}$ by several conditions to find a good aggregation curve in ThT assay (long lag phase and high fluorescence plateau) for testing compounds against $A\beta_{42}$ aggregation. Our results highlighted again the difficulties to obtain reproducible *in vitro* aggregation kinetics because of different suppliers, batches, pretreatments and solubilization protocols. Thus, care should be taken when comparing the ThT results from different groups. Further work on it needs to be performed in the future to get reproducible ThT curves of $A\beta_{42}$. However, our difficulties to get good inhibition with our helical mimics when $A\beta_{42}$ is not mainly in its monomeric state further indicates that our helical foldamers preferentially target the helical monomeric forms of $A\beta_{42}$.

In the end, we can try to answer the questions we mentioned at the beginning of this chapter based on the results we have got. Peptide **10** with two diaza-peptide units at the N-terminus and C-terminus of the EF-helix sequence, respectively, can mimic the helical structure of the EF-helix. This helical conformation seems to play a key role in stabilizing the helical structure of the N-terminus of Aβ and actually makes peptide **10** showing a stronger activity against Aβ aggregation than other synthesized peptides. Although it is not active as TTR protein, the mechanism of peptide **10** seems to be different from the one of TTR: peptide **10** targets the primary nucleation of the

aggregation whereas TTR targets the secondary nucleation. In addition, peptide **10** shows very good proteolytic stability and low toxicity. However, the low BBB permeability of peptide **10** (potential substrate of efflux transporters) indicates that further modification should be performed in the future. A manuscript of the work in this chapter for publication is in preparation.

References

(1) Buxbaum, J. N.; Ye, Z.; Reixach, N.; Friske, L.; Levy, C.; Das, P.; Golde, T.; Masliah, E.; Roberts, A. R.; Bartfai, T. Transthyretin Protects Alzheimer's Mice from the Behavioral and Biochemical Effects of Aβ Toxicity. *Proc. Natl. Acad. Sci. U.S.A.* **2008**, *105* (7), 2681–2686.

(2) Link, C. D. Expression of Human Beta-Amyloid Peptide in Transgenic Caenorhabditis Elegans. *Proc. Natl. Acad. Sci. U.S.A.* **1995**, *92* (20), 9368–9372.

(3) Stein, T. D.; Johnson, J. A. Lack of Neurodegeneration in Transgenic Mice Overexpressing Mutant Amyloid Precursor Protein Is Associated with Increased Levels of Transthyretin and the Activation of Cell Survival Pathways. *J. Neurosci.* **2002**, *22* (17), 7380–7388.

(4) Stein, T. D.; Anders, N. J.; DeCarli, C.; Chan, S. L.; Mattson, M. P.; Johnson, J. A. Neutralization of Transthyretin Reverses the Neuroprotective Effects of Secreted Amyloid Precursor Protein (APP) in APPSW Mice Resulting in Tau Phosphorylation and Loss of Hippocampal Neurons: Support for the Amyloid Hypothesis. *J. Neurosci.* **2004**, *24* (35), 7707–7717.

(5) Choi, S. H.; Leight, S. N.; Lee, V. M.-Y.; Li, T.; Wong, P. C.; Johnson, J. A.; Saraiva, M. J.; Sisodia, S. S. Accelerated Aβ Deposition in APPswe/PS1ΔE9 Mice with Hemizygous Deletions of TTR (Transthyretin). *J. Neurosci.* **2007**, *27* (26), 7006–7010.

(6) Du, J.; Cho, P. Y.; Yang, D. T.; Murphy, R. M. Identification of Beta-Amyloid-Binding Sites on Transthyretin. *Protein Eng. Des. Sel.* **2012**, *25* (7), 337–345.

(7) Pate, K. M.; Kim, B. J.; Shusta, E. V.; Murphy, R. M. Transthyretin Mimetics as Anti-β-Amyloid Agents: A Comparison of Peptide and Protein Approaches. *ChemMedChem* **2018**, *13* (9), 968–979.

(8) Cho, P. Y.; Joshi, G.; Johnson, J. A.; Murphy, R. M. Transthyretin-Derived Peptides as β-Amyloid Inhibitors. *ACS Chem. Neurosci.* **2014**, *5* (7), 542–551.

(9) Tonali, N.; Correia, I.; Lesma, J.; Bernadat, G.; Ongeri, S.; Lequin, O. Introducing Sequential Aza-Amino Acids Units Induces Repeated β-Turns and Helical Conformations in Peptides. *Org. Biomol. Chem.* **2020**, *18* (18), 3452–3458.

(10) Proulx, C.; Lubell, W. D. Copper-Catalyzed N-Arylation of Semicarbazones for the Synthesis of Aza-Arylglycine-Containing Aza-Peptides. *Org. Lett.* **2010**, *12* (13), 2916–2919.

(11) Amblard, M.; Fehrentz, J.-A.; Martinez, J.; Subra, G. Methods and Protocols of Modern Solid Phase Peptide Synthesis. *Mol. Biotechnol.* **2006**, *33* (3), 239–254.

(12) Arujõe, M.; Ploom, A.; Mastitski, A.; Järv, J. Comparison of Various Coupling Reagents in Solid-Phase Aza-Peptide Synthesis. *Tetrahedron Lett.* **2017**, *58* (35), 3421–3425.

(13) Whitmore, L.; Wallace, B. A. Protein Secondary Structure Analyses from Circular Dichroism Spectroscopy: Methods and Reference Databases. *Biopolymers* **2008**, *89* (5), 392–400.

(14) Wei, Y.; Thyparambil, A. A.; Latour, R. A. Protein Helical Structure Determination Using CD Spectroscopy for Solutions with Strong Background Absorbance from 190-230 Nm. *Biochim. Biophys. Acta* **2014**, *1844* (12), 2331–2337.

(15) Micsonai, A.; Wien, F.; Kernya, L.; Lee, Y.-H.; Goto, Y.; Réfrégiers, M.; Kardos, J. Accurate Secondary Structure Prediction and Fold Recognition for Circular Dichroism Spectroscopy. *Proc. Natl. Acad. Sci. U.S.A.* **2015**, *112* (24), E3095–E3103.

(16) Kakinoki, S.; Hirano, Y.; Oka, M. On the Stability of Polyproline-I and II Structures of Proline Oligopeptides. *Polym. Bull.* **2005**, *53* (2), 109–115.

(17) Correcirc, D. H. A.; a; Ramos, C. H. I. The Use of Circular Dichroism Spectroscopy to Study Protein Folding, Form and Function. *Afr. J. Biochem. Res.* **2009**, *3* (5), 164–173.

(18) Tsai, C.-L.; Wu, S.-Y.; Hsu, H.-K.; Huang, S.-B.; Lin, C.-H.; Chan, Y.-T.; Wang, S.-K. Preparation and Conformational Analysis of Polyproline Tri-Helix Macrocycle Nanoscaffolds of Varied Sizes. *Nanoscale* **2021**, *13* (8), 4592–4601.

(19) Aitken, D.; Grison, C.; Robin, S. 13-Helix Folding of a β/γ-Peptide Manifold Designed from a "Minimal-Constraint" Blueprint. *Chem. Commun.* **2016**, *52*.

(20) Grison, C. M.; Miles, J. A.; Robin, S.; Wilson, A. J.; Aitken, D. J. An α-Helix-Mimicking 12,13-Helix: Designed α/β/γ-Foldamers as Selective Inhibitors of Protein–Protein Interactions. *Angew. Chem. Int. Ed.* **2016**, *55* (37), 11096–11100.

(21) Bodero, L.; Guitot, K.; Lensen, N.; Lequin, O.; Brigaud, T.; Ongeri, S.; Chaume, G. Introducing the Chiral Constrained α-Trifluoromethylalanine in Aib Foldamers to Control, Quantify and Assign the Helical Screw-Sense**. *Chem. Eur. J.* **2022**, *28* (8), e202103887.

(22) Toniolo, C.; Polese, A.; Formaggio, F.; Crisma, M.; Kamphuis, J. Circular Dichroism Spectrum of a Peptide 310-Helix. *J. Am. Chem. Soc.* **1996**, *118* (11), 2744–2745.

(23) Cochran, A. G.; Skelton, N. J.; Starovasnik, M. A. Tryptophan Zippers: Stable, Monomeric β-Hairpins. *Proc. Natl. Acad. Sci. U.S.A.* **2001**, *98* (10), 5578–5583.

(24) Mahalakshmi, R.; Raghothama, S.; Balaram, P. NMR Analysis of Aromatic Interactions in Designed Peptide β-Hairpins. *J. Am. Chem. Soc.* **2006**, *128* (4), 1125–1138.

(245) Wu, L.; McElheny, D.; Takekiyo, T.; Keiderling, T. A. Geometry and Efficacy of Cross-Strand Trp/Trp, Trp/Tyr, and Tyr/Tyr Aromatic Interaction in a β-Hairpin Peptide. *Biochemistry* **2010**, *49* (22), 4705–4714.

(26) Kelly, M. A.; Chellgren, B. W.; Rucker, A. L.; Troutman, J. M.; Fried, M. G.; Miller, A.-F.; Creamer, T. P. Host–Guest Study of Left-Handed Polyproline II Helix Formation. *Biochemistry* **2001**, *40* (48), 14376–14383.

(27) Parrot, I.; Huang, P. C.; Khosla, C. Circular Dichroism and Nuclear Magnetic Resonance Spectroscopic Analysis of Immunogenic Gluten Peptides and Their Analogs *. *J. Biol. Chem.* **2002**, *277* (47), 45572–45578.

(28) Dalcol, I.; Pons, M.; Ludevid, M.-D.; Giralt, E. Convergent Synthesis of Repeating Peptides (Val-X-Leu-Pro-Pro-Pro)8 Adopting a Polyproline II Conformation. *J. Org. Chem.* **1996**, *61* (20), 6775–6782.

(29) Kapitán, J.; Gallo, D.; Goasdoué, N.; Nicaise, M.; Desmadril, M.; Hecht, L.; Leclercq, G.; Barron, L. D.; Jacquot, Y. Identification of a Human Estrogen Receptor α-Derived Antiestrogenic Peptide That Adopts a Polyproline II Conformation. *J. Pept. Sci.* **2009**, *15* (7), 455–464.

(30) Smith, L. J.; Bolin, K. A.; Schwalbe, H.; MacArthur, M. W.; Thornton, J. M.; Dobson, C. M. Analysis of Main Chain Torsion Angles in Proteins: Prediction of NMR Coupling Constants for Native and Random Coil Conformations. *J. Mol. Biol.* **1996**, *255* (3), 494–

506.

(31) Gagné, S. M.; Tsuda, S.; Li, M. X.; Chandra, M.; Smillie, L. B.; Sykes, B. D. Quantification of the Calcium-Induced Secondary Structural Changes in the Regulatory Domain of Troponin-C. *Protein Sci.* **1994**, *3* (11), 1961–1974.

(32) Maltsev, A. S.; Grishaev, A.; Bax, A. Monomeric α-Synuclein Binds Congo Red Micelles in a Disordered Manner. *Biochemistry* **2012**, *51* (2), 631–642.

(33) Lancelot, N.; Elbayed, K.; Raya, J.; Piotto, M.; Briand, J.-P.; Formaggio, F.; Toniolo, C.; Bianco, A. Characterization of the 310-Helix in Model Peptides by HRMAS NMR Spectroscopy. *Chem. Eur. J.* **2003**, *9* (6), 1317–1323.

(34) Kumazawa, S.; Kanda, M.; Aoyama, H.; Utagawa, M.; Ohtani, H.; Chiga, I.; Mikawa, T.; Hayase, T.; Hino, T. Nuclear Magnetic Resonance Study and Secondary Structure Determination of the Antibiotic Peptide, Aibellin. *Biosci. Biotechnol. Biochem.* **1994**, *58* (12), 2188–2192.

(35) Surewicz, W. K.; Mantsch, H. H.; Chapman, D. Determination of Protein Secondary Structure by Fourier Transform Infrared Spectroscopy: A Critical Assessment. *Biochemistry* **1993**, *32* (2), 389–394.

(36) Byler, D. M.; Susi, H. Examination of the Secondary Structure of Proteins by Deconvolved FTIR Spectra. *Biopolymers* **1986**, *25* (3), 469–487.

(37) Abraham, M. J.; Murtola, T.; Schulz, R.; Páll, S.; Smith, J. C.; Hess, B.; Lindahl, E. GROMACS: High Performance Molecular Simulations through Multi-Level Parallelism from Laptops to Supercomputers. *SoftwareX* **2015**, *1–2*, 19–25.

(38) Wang, J.; Wolf, R. M.; Caldwell, J. W.; Kollman, P. A.; Case, D. A. Development and Testing of a General Amber Force Field. *J. Comput. Chem.* **2004**, *25* (9), 1157–1174.

(39) Levine III, H. Thioflavine T Interaction with Synthetic Alzheimer's Disease β-Amyloid Peptides: Detection of Amyloid Aggregation in Solution. *Protein Sci.* **1993**, *2* (3), 404–410.

(40) LeVine, H. [18] Quantification of β-Sheet Amyloid Fibril Structures with Thioflavin T. In *Methods in Enzymology*; Amyloid, Prions, and Other Protein Aggregates; Academic Press, 1999; Vol. 309, pp 274–284.

(41) Biancalana, M.; Koide, S. Molecular Mechanism of Thioflavin-T Binding to Amyloid Fibrils. Biochim. Biophys. Acta - *Proteins Proteom.* **2010**, *1804* (7), 1405–1412.

(42) Gade Malmos, K.; Blancas-Mejia, L. M.; Weber, B.; Buchner, J.; Ramirez-Alvarado, M.; Naiki, H.; Otzen, D. ThT 101: A Primer on the Use of Thioflavin T to Investigate Amyloid Formation. *Amyloid* **2017**, *24* (1), 1–16.

(43) Kaffy, J.; Berardet, C.; Mathieu, L.; Legrand, B.; Taverna, M.; Halgand, F.; Van Der Rest, G.; Maillard, L. T.; Ongeri, S. Helical γ-Peptide Foldamers as Dual Inhibitors of Amyloid-β Peptide and Islet Amyloid Polypeptide Oligomerization and Fibrillization. *Chem. Eur. J.* **2020**, *26* (64), 14612–14622.

(44) Pellegrino, S.; Tonali, N.; Erba, E.; Kaffy, J.; Taverna, M.; Contini, A.; Taylor, M.; Allsop, D.; L. Gelmi, M.; Ongeri, S. β-Hairpin Mimics Containing a Piperidine–Pyrrolidine Scaffold Modulate the β-Amyloid Aggregation Process Preserving the Monomer Species. *Chem. Sci.* **2017**, *8* (2), 1295–1302. https://doi.org/10.1039/C6SC03176E.

(45) Feng, Y.; Wang, X.; Yang, S.; Wang, Y.; Zhang, X.; Du, X.; Sun, X.; Zhao, M.; Huang, L.; Liu, R. Resveratrol Inhibits Beta-Amyloid Oligomeric Cytotoxicity but Does Not Prevent

Oligomer Formation. *Neurotoxicology* **2009**, *30* (6), 986–995.

(46) Chan, S.; Kantham, S.; Rao, V. M.; Palanivelu, M. K.; Pham, H. L.; Shaw, P. N.; McGeary, R. P.; Ross, B. P. Metal Chelation, Radical Scavenging and Inhibition of Aβ42 Fibrillation by Food Constituents in Relation to Alzheimer's Disease. *Food Chem.* **2016**, *199*, 185–194.

(47) Foley, A. R.; Raskatov, J. A. Assessing Reproducibility in Amyloid β Research: Impact of Aβ Sources on Experimental Outcomes. *ChemBioChem* **2020**, *21* (17), 2425–2430.

(48) Ryan, T. M.; Caine, J.; Mertens, H. D. T.; Kirby, N.; Nigro, J.; Breheney, K.; Waddington, L. J.; Streltsov, V. A.; Curtain, C.; Masters, C. L.; Roberts, B. R. Ammonium Hydroxide Treatment of Aβ Produces an Aggregate Free Solution Suitable for Biophysical and Cell Culture Characterization. *PeerJ* **2013**, *1*, e73.

(49) Teplow, D. B. Preparation of Amyloid B-Protein for Structural and Functional Studies. In *Methods in Enzymology*; Amyloid, Prions, and Other Protein Aggregates, Part C; Academic Press, 2006; Vol. 413, pp 20–33.

(50) Jäkel, L.; Biemans, E. A. L. M.; Klijn, C. J. M.; Kuiperij, H. B.; Verbeek, M. M. Reduced Influence of ApoE on Aβ43 Aggregation and Reduced Vascular Aβ43 Toxicity as Compared with Aβ40 and Aβ42. *Mol. Neurobiol.* **2020**, *57* (4), 2131–2141.

(51) Tonali, N.; Dodero, V. I.; Kaffy, J.; Hericks, L.; Ongeri, S.; Sewald, N. Real-Time BODIPY-Binding Assay To Screen Inhibitors of the Early Oligomerization Process of Aβ1–42 Peptide. *ChemBioChem* **2020**, *21* (8), 1129–1135.

(52) Yan, L.-M.; Velkova, A.; Tatarek-Nossol, M.; Andreetto, E.; Kapurniotu, A. IAPP Mimic Blocks Aβ Cytotoxic Self-Assembly: Cross-Suppression of Amyloid Toxicity of Aβ and IAPP Suggests a Molecular Link between Alzheimer's Disease and Type II Diabetes. *Angew. Chem. Int. Ed.* **2007**, *46* (8), 1246–1252.

(53) Wasana Jayaweera, S.; Surano, S.; Pettersson, N.; Oskarsson, E.; Lettius, L.; Gharibyan, A. L.; Anan, I.; Olofsson, A. Mechanisms of Transthyretin Inhibition of IAPP Amyloid Formation. *Biomolecules* **2021**, *11* (3), 411.

(54) Meisl, G.; Kirkegaard, J. B.; Arosio, P.; Michaels, T. C. T.; Vendruscolo, M.; Dobson, C. M.; Linse, S.; Knowles, T. P. J. Molecular Mechanisms of Protein Aggregation from Global Fitting of Kinetic Models. *Nat. Protoc.* **2016**, *11* (2), 252–272.

(55) Ciccone, L.; Fruchart-Gaillard, C.; Mourier, G.; Savko, M.; Nencetti, S.; Orlandini, E.; Servent, D.; Stura, E. A.; Shepard, W. Copper Mediated Amyloid-β Binding to Transthyretin. *Sci. Rep.* **2018**, *8* (1), 13744.

(56) Tarchoun, K.; Yousef, M.; Bánóczi, Z. Azapeptides as an Efficient Tool to Improve the Activity of Biologically Effective Peptides. *Future Pharmacol.* **2022**, *2* (3), 293–305.

(57) Lacombe, O.; Videau, O.; Chevillon, D.; Guyot, A.-C.; Contreras, C.; Blondel, S.; Nicolas, L.; Ghettas, A.; Bénech, H.; Thevenot, E.; Pruvost, A.; Bolze, S.; Krzaczkowski, L.; Prévost, C.; Mabondzo, A. In Vitro Primary Human and Animal Cell-Based Blood–Brain Barrier Models as a Screening Tool in Drug Discovery. *Mol. Pharm.* **2011**, *8* (3), 651–663.

(58) Majerova, P.; Hanes, J.; Olesova, D.; Sinsky, J.; Pilipcinec, E.; Kovac, A. Novel Blood–Brain Barrier Shuttle Peptides Discovered through the Phage Display Method. *Molecules* **2020**, *25* (4), 874.

(59) Mauran, L.; Kauffmann, B.; Odaert, B.; Guichard, G. Stabilization of an α-Helix by Short Adjacent Accessory Foldamers. *C. R. Chim.* **2016**, *19* (1), 123–131.

(60) Altmayer-Henzien, A.; Declerck, V.; Farjon, J.; Merlet, D.; Guillot, R.; Aitken, D. J. Fine Tuning of β-Peptide Foldamers: A Single Atom Replacement Holds Back the Switch from an 8-Helix to a 12-Helix. *Angew. Chem. Int. Ed.* **2015**, *127* (37), 10957–10960.

(61) Kaffy, J.; Brinet, D.; Soulier, J.-L.; Correia, I.; Tonali, N.; Fera, K. F.; Iacone, Y.; Hoffmann, A. R. F.; Khemtémourian, L.; Crousse, B.; Taylor, M.; Allsop, D.; Taverna, M.; Lequin, O.; Ongeri, S. Designed Glycopeptidomimetics Disrupt Protein–Protein Interactions Mediating Amyloid β-Peptide Aggregation and Restore Neuroblastoma Cell Viability. *J. Med. Chem.* **2016**, *59* (5), 2025–2040.

(62) Vahdati, L.; Kaffy, J.; Brinet, D.; Bernadat, G.; Correia, I.; Panzeri, S.; Fanelli, R.; Lequin, O.; Taverna, M.; Ongeri, S.; Piarulli, U. Synthesis and Characterization of Hairpin Mimics That Modulate the Early Oligomerization and Fibrillization of Amyloid β-Peptide. *Eur. J. Org. Chem.* **2017**, *2017* (20), 2971–2980.

(63) Nerelius, C.; Sandegren, A.; Sargsyan, H.; Raunak, R.; Leijonmarck, H.; Chatterjee, U.; Fisahn, A.; Imarisio, S.; Lomas, D. A.; Crowther, D. C.; Strömberg, R.; Johansson, J. α-Helix Targeting Reduces Amyloid-β Peptide Toxicity. *Proc. Natl. Acad. Sci. U.S.A.* **2009**, *106* (23), 9191–9196.

Chapter 4

Synthesis and conformational studies of aza-diketopiperazine (aza-DKP) based foldamers

As mentioned in the chapter 2, during the synthesis of the aza-dipeptide fragment, interesting aza-diketopiperazines (aza-DKPs) (**2.44** and **2.47**) have been isolated during the Boc cleavage in acidic conditions (**Figure 4.1A**). These aza-DKPs are analogues of 2,5-diketopiperazines (2,5-DKPs) (**Figure 4.1B**) but have three nitrogen atoms in the ring system.

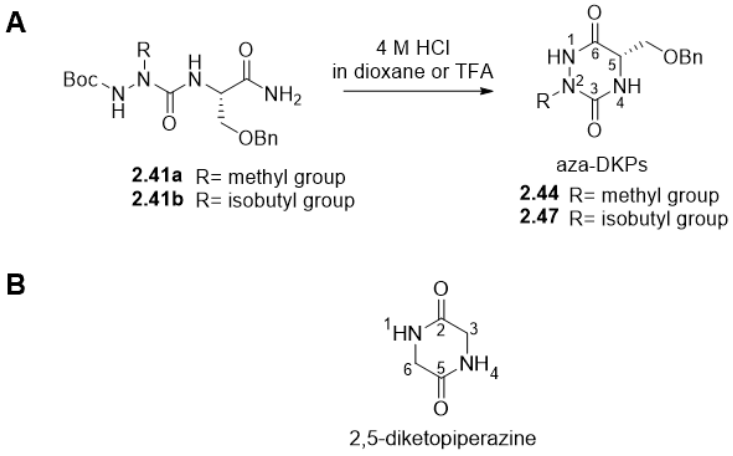

Figure 4.1: A) The aza-DKP side products from Boc cleavage of aza-dipeptides observed in the chapter 2; B) Structure of 2,5-diketopiperazine

2,5-DKPs are cyclodipeptides which are widely produced from bacteria, fungi, plants, and mammals. They have various biological activities associated with different targets such as phosphodiesterase 5 (PED 5) and oxytocin receptors.[1] Thus, 2,5-DKPs have attracted great attention in the medicinal chemistry field. Comparing to 2,5 DKPs, aza-DKPs are underprivileged because to our knowledge they are not present in nature and because of their relatively complicated synthesis.[2] However, aza-DKPs show higher aqueous solubility and metabolic stability compared to 2,5-DKPs, which provides aza-DKPs opportunities to mimic 2,5 DKPs but with improved physicochemical and pharmacokinetic properties.[2,3] Furthermore, aza-DKPs show similar

propensity and conformation as 2,5-DKPs by X-ray crystallography. As shown in **Figure 4.2**, the substituent groups on the aza-DKP are in similar directions as the corresponding substituent groups on the 2,5-DKP except the methyl group.[3] The methyl group deviated from the N2−N1−C1 plane with an angle of 27.1° in the aza-DKP whereas in the 2,5-DKP, the methyl group has deviation from C1−C2−N1 plane with an angle of 48.1°. This means the N1 nitrogen of the aza-DKP is in a partial sp3 hybridization. These all make aza-DKP a very interesting scaffold for future applications in foldamer and medicinal chemistry fields. Here we tried to use aza-DKPs as building block to design several foldamers. The design and synthesis of these foldamers (we termed them aza-DKPamers) are presented in this chapter.

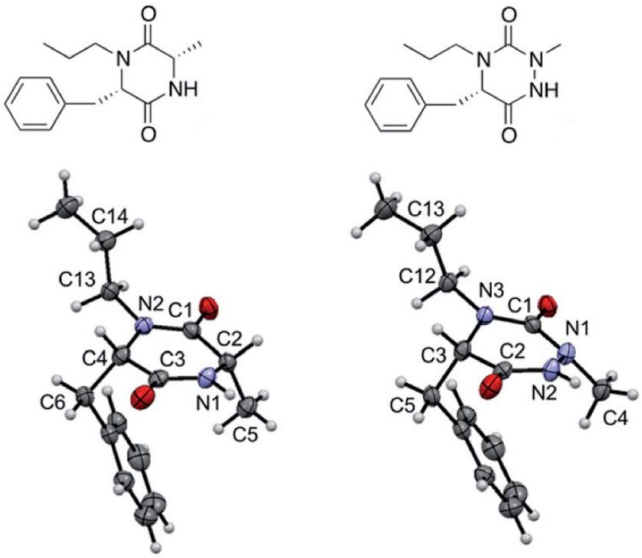

Figure 4.2: The crystal structures show the similar conformation of DKP scaffold and aza-DKP scaffold[3]

4.1 Design of aza-DKPamers

Piarulli's group reported two novel foldamers constituted of bifunctional DKPs.[4] In these foldamers, each monomer is a DKP possessing one amine functional group and one carboxylic acid functional group, which can be viewed as a dipeptide constituted of one β^2-amino acid and one β^3-amino acid (**Figure 4.3A**). 10-Membered hydrogen bond is formed between the amine group of β^2-

amino acid and the carbonyl group of β[3]-amino acid, constructing a reverse turn structure of this DKP. The NMR conformational analysis (in CD_3OH and DMSO-d_6) and stochastic dynamics (SD) simulation revealed that four sequential DKP monomers connected by amide bonds resulted in repeated reverse turns looking like a β-bend ribbon structure (a particular type of 3_{10}-helix) (**Figure 4.3B**).

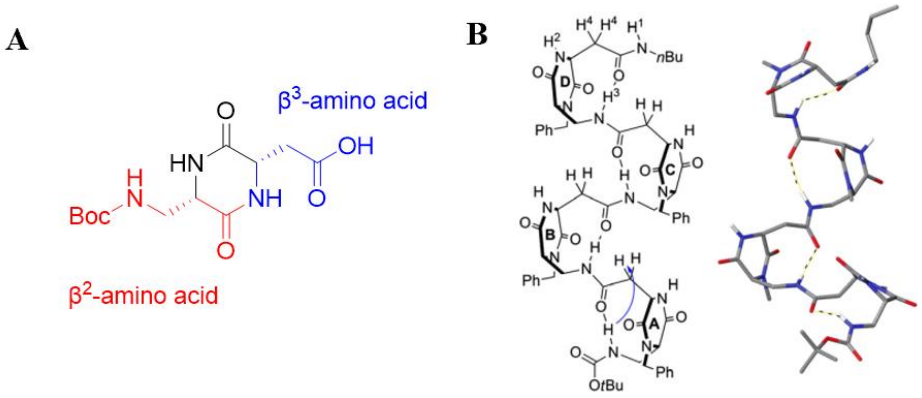

Figure 4.3: A) Structure of the DKP monomers reported by Piarulli's group; B) β-Bend ribbon structure formed by reverse turn of the DKP[4]

The aza-DKPs we found in the chapter 2 have the same substituted mode as the DKP monomer used in the design of the DKP based foldamer. Inspired by the DKP based foldamer, we decided to design bifunctional aza-DKP monomer and use it to design and synthesize several aza-DKP based foldamers (aza-DKPamers). The aza-DKP monomer **4.1** we designed can be viewed as a dipeptide constituted of one aza-γ[2]-amino acid and one β[3]-amino acid (**Figure 4.4A**). There are two reasons why we used aza-γ[2]-amino acid to construct the aza-DKP monomer rather used aza-β[2]-amino acid, which is closer structure with the β[2]-amino acid used in the DKP monomer that Piarulli's laboratory designed. One is the synthetic issue that aza-β[2]-amino acids should be unstable in acidic conditions because of the similar chemical structure to acetal. The second reason, as we mentioned before, is that the nitrogen which replaces α-carbon in aza-DKPs only has partial sp^3 property, making the substituent groups on this nitrogen less out of plane constituted by this nitrogen and its neighbor atoms (N1–N2–C3 plane). The additional carbon atom inserted in aza-γ[2]-amino acids compared to aza-β[2]-amino acids can form 11-membered hydrogen bond, which probably has less ring tension

than 10-membered hydrogen bond (**Figure 4.4B**). Because of the adaptive chirality of the nitrogen, another conformation of the aza-DKP monomer, an open conformation, also should be noted (**Figure 4.4B**).

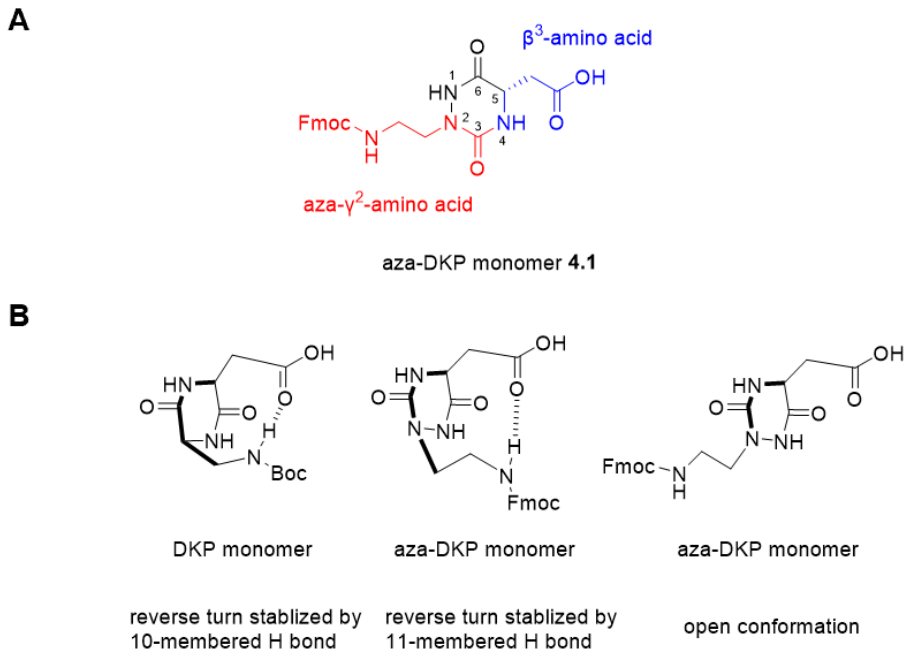

Figure 4.4: A) Structure of the designed aza-DKP monomers **4.1**; B) 10-membered hydrogen bond in DKP and two possible conformations in aza-DKP

The foldamers (aza-DKPamers) composed by this aza-DKP monomer could be viewed as β/γ peptides. It has been reported that β/γ peptides have propensities to fold into 13 helix or 11/13 mixed helix.[5,6] Compared to the linear-dipeptides composed by β-amino acid and γ-amino acid, the aza-DKP monomer showing more constrained conformation might give more stable helical structures to aza-DKPamers or on the contrary, the constraint will prevent the helical folding of aza-DKPamers. The objective of this project is to investigate the conformation of these foldamers. Moreover, the replacement of the DKP monomer by the aza-DKP monomer also provides the possibility to increase aqueous solubility of the foldamers, putatively allowing their application in drug discovery.

Four aza-DKPamers were designed, including three trimers **4.2**, **4.3** and **4.4** and one tetramer **4.5 (Figure 4.5)**. **4.3** Ac-(aza-DKP)$_3$-NH$_2$ and **4.5** Ac-(aza-DKP)$_4$-NH$_2$ were designed to explore the impact of the length on the conformation and stabilization of intramolecular hydrogen bond. H-(aza-DKP)$_3$-NH$_2$ **4.2** with a free amine group at the N-terminus was designed to evaluate the effect

of the free amine group on the conformation versus Ac-(aza-DKP)$_3$-NH$_2$ **4.3** with an acetyl group. 4-Br-benzoyl-(aza-DKP)$_3$-NH$_2$ **4.4** with a 4-bromobenzoyl group at the N-terminus was designed to facilitate to the crystallization of this type of foldamers.[7]

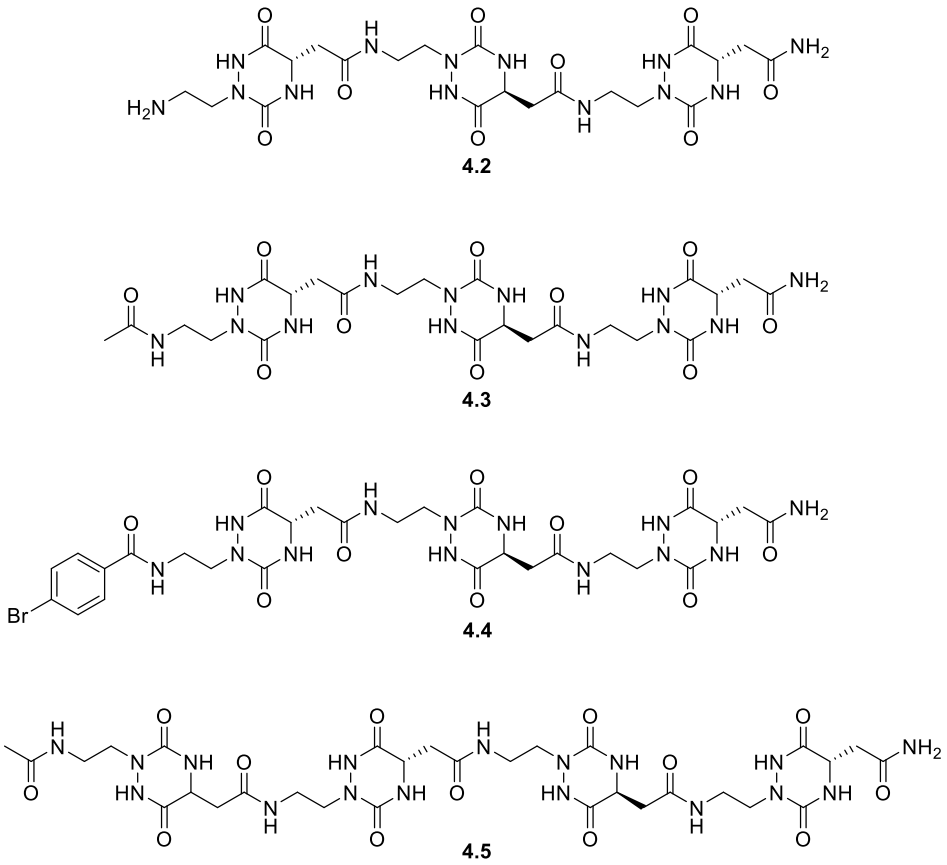

Figure 4.5: Structures of four aza-DKPamers

4.2 Reported chemistry to synthesize aza-DKPs

In literature, some examples reporting the synthesis of aza-DKPs could be found, and most of them show the preparation of aza-DKPs through cyclization of aza-dipeptides: the N-terminal hydrazine attacks to the C-terminal ester (aminolysis). Pinnen *et al.* reported a synthesis of cyclo-(azaPhe-Pro), treating Boc-azaPhe-Pro-OMe with HCl.[8] After that, the conversion of other cyclo-(azaAA-Pro) compounds from the corresponding aza-dipeptides Boc-azaAA-Pro-OR using HCl was also reported (**Figure 4.6**).[9,10]

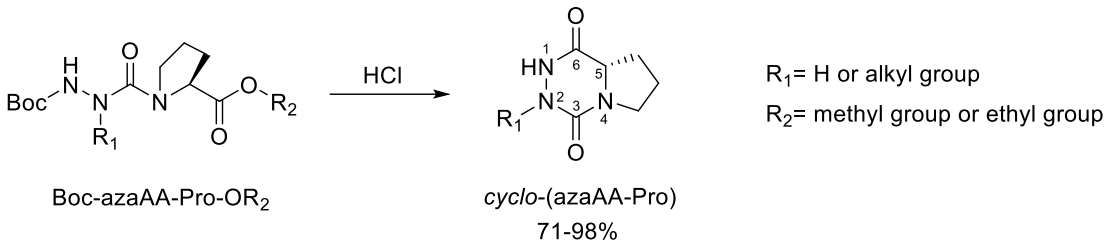

Figure 4.6: Aza-dipeptides Boc-azaAA-Pro-OR can be transformed to aza-DKPs cyclo-(azaAA-Pro) by treating with HCl

Bonnet's group reported the synthesis of aza-DKPs from Boc-protected aza-dipeptides (Boc-azaAA-alkylAA-OR) by treating them with *p*-TsOH or Amberlyst 15 resin (polymer-supported *p*-TSOH) in solution (**Figure 4.7A**).[11] Based on the result from the solution phase synthesis, they further developed the solid phase synthesis of aza-DKPs from Boc-protected aza-dipeptides by treating with TFA. The synthesis allowed to give 2,4,5-trisubstituted aza-DKPs in moderate yields (**Figure 4.7B**) but a very low yield (3%) for 2,5-disubstituted aza-DKPs, indicating that the N-substituted natural amino acid (R2 group) in the aza-dipeptides is very important for the cyclization of the aza-dipeptides. They also developed a methodology to synthesize novel bicyclic aza-DKP scaffolds incorporating six- or seven-membered rings.[12]

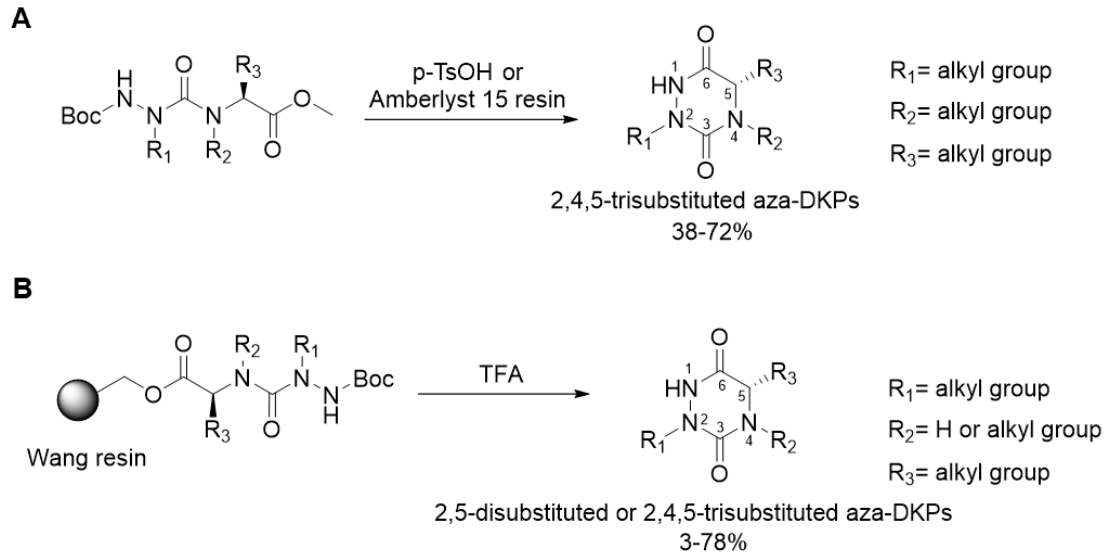

Figure 4.7: A) The synthesis of 2,4,5-trisubstituted aza-DKPs in solution; B) The synthesis of 2,5-disubstituted or 2,4,5-trisubstituted aza-DKPs on solid phase

Aza-DKPs cyclo-(azaAA-Gly) could also be obtained by treating the corresponding aza-depeptides (azaAA-alkylGly-OCH_2CH_3) in basic conditions using NaH as base (**Figure 4.8**). This reaction could provide 2,4-disubstituted or 1,2,4-trisubstituted aza-DKPs.[13]

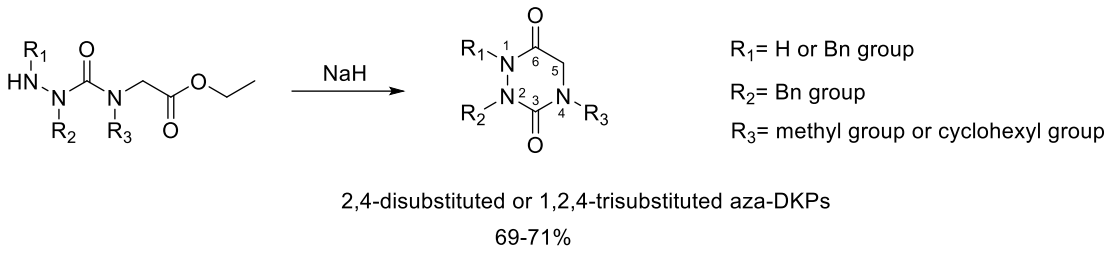

Figure 4.8: The synthesis of 2,4-disubstituted or 1,2,4-trisubstituted aza-DKPs

Hamuro *et al.* reported another solid phase approach for the synthesis of aza-DKPs on phoxime resin (phosgenated *p*-nitrophenyl(polystyrene)ketoxime). The peptides synthesized on this resin could be cleaved by thermolysis without any acids or bases. However, the cyclization of aza-dipeptides would happen when it is performed in the presence of DIPEA (**Figure 4.9**) at 80°C. The reaction could give 1,5-disubstituted or 1,2,5-trisubstituted aza-DKPs in moderate yields.[14]

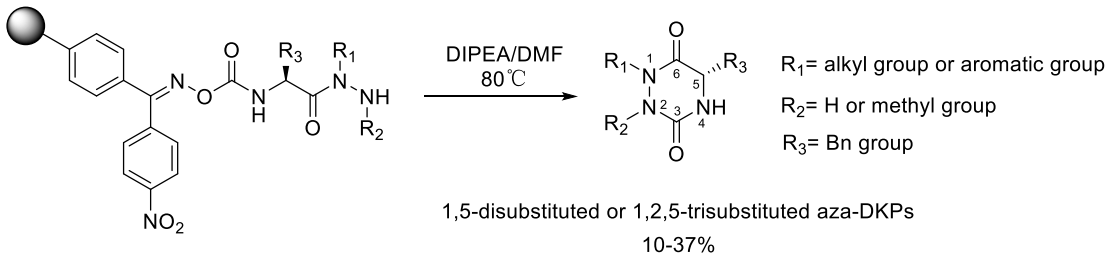

Figure 4.9: The synthesis of 1,5-disubstituted or 1,2,5-trisubstituted aza-DKPs

In addition to the cyclization of aza-dipeptides, aza-DKPs also can be obtained by one-pot synthesis using the corresponding carbazates, primary amines and chloroacetyl chlorides (**Figure 4.10**).[15] This method provides 1,4-disubstituted aza-DKPs.

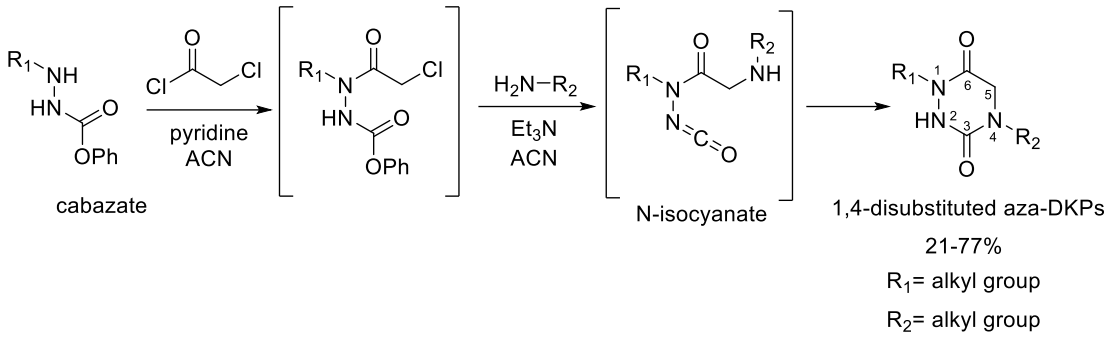

Figure 4.10: One pot reaction gives 1,4-disubstituted aza-DKPs

From literature, it is possible to notice that aza-DKP are always obtained from their corresponding aza-dipeptides with methyl or ethyl ester at the C-terminus. This is rational to make easier cyclization because of methoxyl or ethyoxyl groups are better leaving groups compared to hydroxy group and amino group. In our case, however, we could observe that the cyclization can easily occur in acidic conditions even with an amide group at the C-terminus of aza-dipeptides (**Figure 4.1**). In addition, the presence of substituent groups on the nitrogen of the natural amino acid in aza-dipeptide is likely to play a key role in the cyclization of the aza-dipeptide especially for the reactions carried out in acidic conditions. We speculated that the substituent group can constrain a conformation of the aza-dipeptides, which can promote the cyclization. While the presence of substituent groups on the β-nitrogen of aza-residues (aza-peptoid) seems to have less effects on the cyclization. Moreover, to our surprise, although all reported aza-DKPs show various substituted modes on the ring (**Figure 4.11**), the reported synthesis of 2,5-disubstituted aza-DKPs only shows a very low yield (3%). This makes very attractive our protocol to cyclize aza-dipeptide with C-terminal amide to obtain 2,5-disubstituted aza-DKPs.

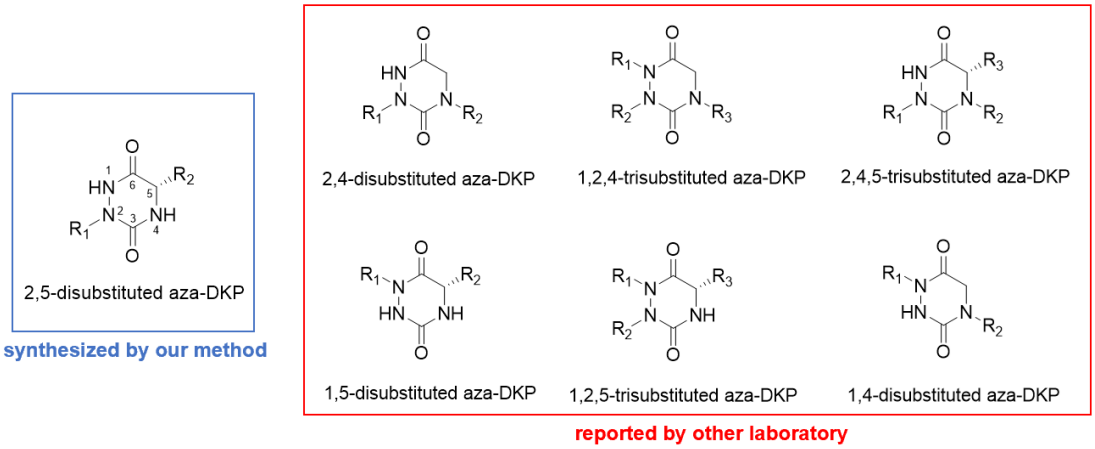

Figure 4.11: aza-DKPs with different substituted mode

4.3 Synthesis of 2,5-disubstituted aza-DKP monomer

As we mentioned before, the reported synthesis of 2,5-disubstituted aza-DKPs from aza-dipeptides with ester at the C-terminus just showed a quite low yield (3%)[11], whereas we could easily obtain 2,5-disubstituted aza-DKPs from aza-dipeptides with a less reactive C-terminal carboxamide. This interesting result prompted us to compare the reactivity of these two different C-termini in the synthesis of our designed 2,5-disubstituted aza-DKPs. Thus, we decided to synthesize compound **4.6** from two different aza-dipeptides **4.7** and **4.8** having a C-terminal amide or methyl ester, respectively (**Figure 4.12**).

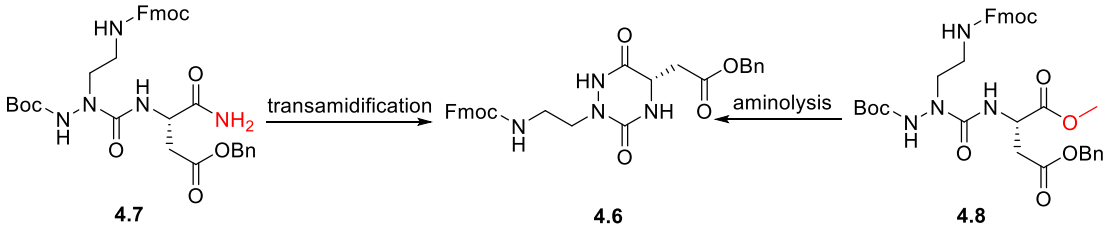

Figure 4.12: Two pathways for the synthesis of the 2,5-disubstituted aza-DKP **4.6**

4.3.1 Synthesis of aza-dipeptide (C-terminal amide) 4.7

Compound **4.7** was obtained by coupling compound **4.11** with Asp(OBn)-NH_2 **4.13** (**Figure 4.13**). Compound **4.11** was synthesized from commercially available ethanolamine. Ethanolamine was protected by a Fmoc group using Fmoc-Cl in the presence of $NaHCO_3$ to give compound **4.9** (Yield: 92%), which was oxidated to aldehyde **4.10** by Dess-Martin oxidation (Yield: 65%). Reductive amination of aldehyde **4.10** with *t*-butyl carbazate provided compound **4.11** with a good yield (91%). The synthesis of the Asp(OBn)-NH_2 **4.13** from Boc-Asp(OBn)-OH required two steps. First, the amidation of Boc-Asp(OBn)-OH with ammonia using EDC and HOBt as coupling reagents gave compound **4.12** (Yield: 94%). Secondly, the Boc cleavage of compound **4.12** treating with HCl 4M in dioxane gave compound **4.13** as a hydrochloride salt. After getting **4.11** and **4.13**, **4.11** was activated by triphosgene in the presence of DIPEA in DCM, followed by the coupling with **4.13** gave compound **4.7** in a moderate yield of 61%.

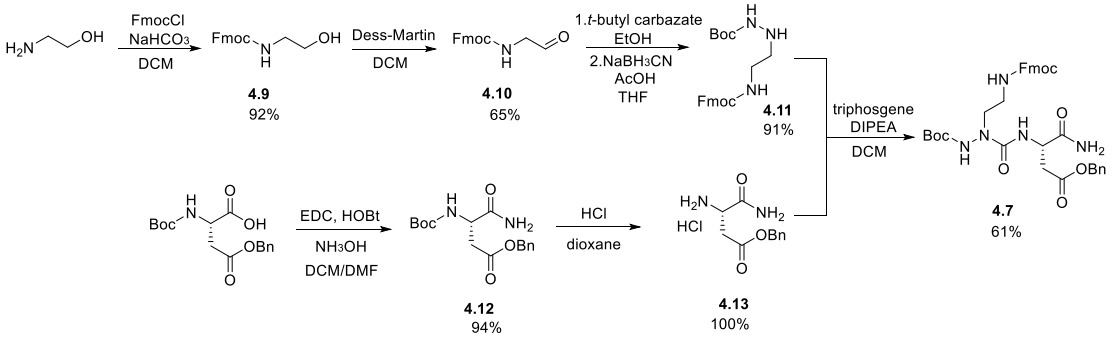

Figure 4.13: Synthesis of **4.7**

4.3.2 Synthesis of aza-dipeptide (C-terminal ester) 4.8

For the synthesis of compound **4.8** with the C-terminal ester, a similar approach as for **4.7** has been used. The synthesis required the obtention of the intermediate Asp(OBn)-OMe **4.15** (**Figure 4.14**). In a first attempt, we tried to perform the esterification of Fmoc-Asp(OBn)-OH by reacting with methanol in the presence of thionyl chloride at reflux. Fmoc-protecting group was chosen here because it is stable in acidic conditions and could be selectively removed in basic conditions. However, the reaction showed the transesterification of the Bn ester of the side chain into a methyl ester **4.14b**. To avoid this side transesterification reaction occurring in acidic conditions,

iodomethane was chosen as methylated reagent. Instead of Fmoc-Asp(OBn)-OH, Boc-Asp(OBn)-OH was used to reacted with iodomethane in the presence of K_2CO_3 providing compound **4.16** with an excellent yield (100%). The Boc group of **4.16** was then cleaved using 4M HCl in dioxane to afford compound **4.15** (98%). Compound **4.15** was activated by treating with triphosgene and then reacted with aza-amino acid precursor **4.11** to give compound **4.8** in a low yield (31%).

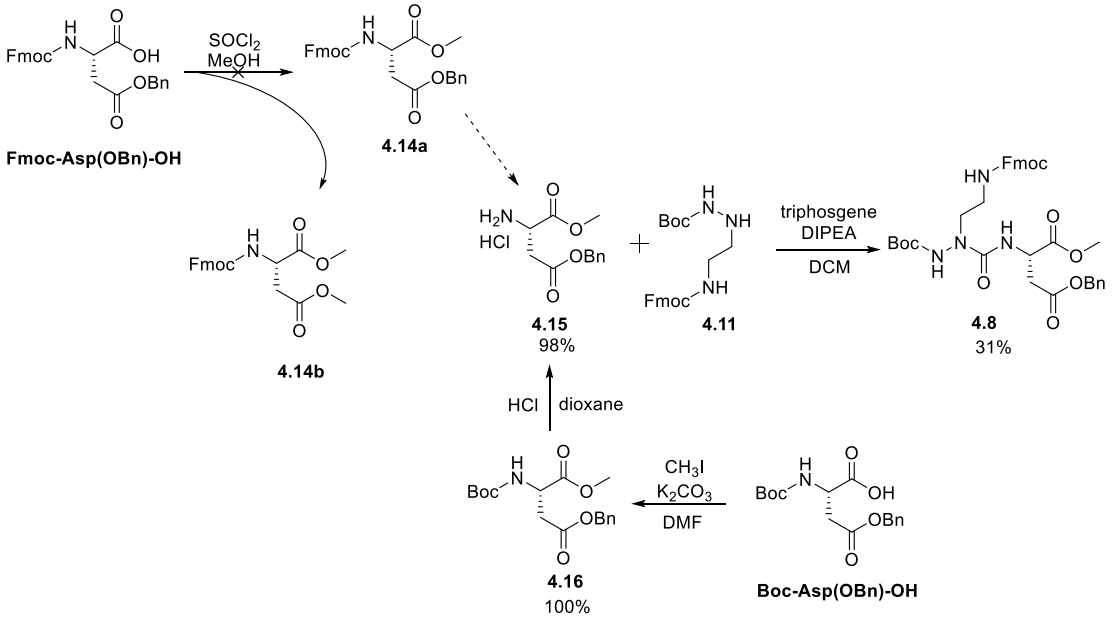

Figure 4.14: Synthesis of **4.8**

4.3.3 Synthesis of aza-DKP monomer 4.1

In the chapter 2, we found that TFA was better to promote the cyclization of aza-dipeptide fragments than HCl. Thus, both compounds **4.7** and **4.8** were subjected to the cyclization to give compound **4.1** by treating them with TFA in DCM (2:1) (**Figure 4.15**). Compound **4.7** with the C-terminal carboxamide could be easily converted to the free amine intermediate and successively to its cyclized form **4.6** as previously observed for the aza-dipeptides **2.41a** and **2.41b** (chapter 2, Figure **2.22** and **2.24**). However, for compound **4.8** having a methyl ester at the C-terminus, TFA could not allow to obtain **4.6**. Only Boc-deprotected product **4.17** was found during the reaction (**Figure 4.15**). The temperature was increased up to 50°C but the cyclization still did not occur. This means that Boc-deprotected product **4.17** from compound **4.8** is quite difficult to be cyclized to **4.6**

in acidic conditions, whereas the Boc-deprotected intermediate of **4.7** is easily cyclized to **4.6**. In theory, amide is less reactive than ester because of less electronegativity of nitrogen atom compared to oxygen atom. Less electronegativity of nitrogen atom results less positive character of carbonyl carbon which makes less reactivity the amide. In our case, the result is reversed.

After getting **4.6**, the benzyl group of **4.6** was removed selectively by catalytic transfer hydrogenolysis using triethylsilane as a hydride donor to afford the target compound **4.1**, suitable for a solid phase synthetic approach. Here the reaction time (30 min) and the amount of triethylsilane (6 eq) should be control to avoid the cleavage of Fmoc group.

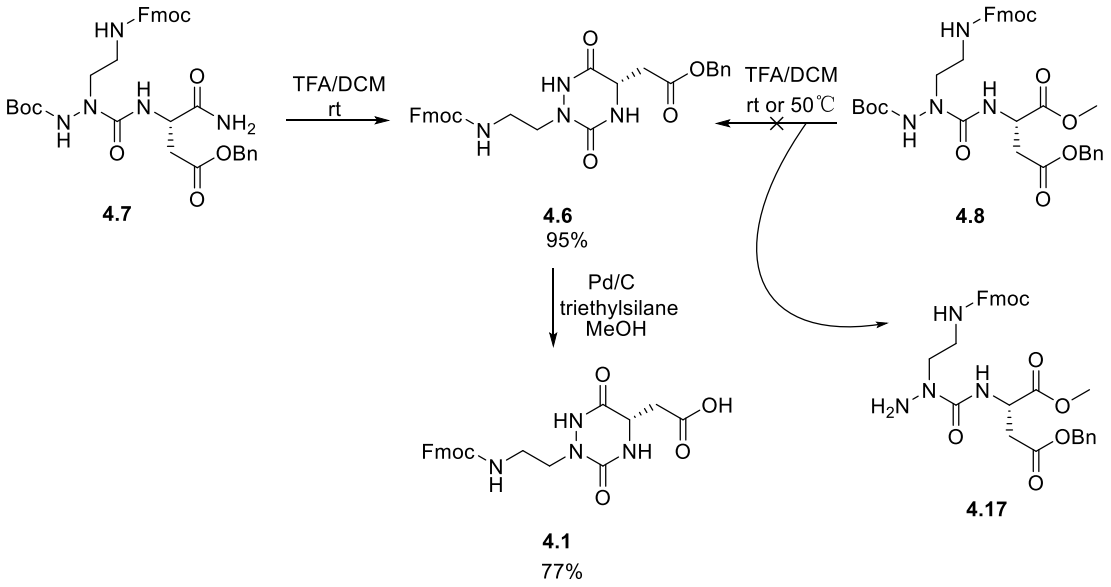

Figure 4.15: Synthesis of aza-DKP monomer **4.1**

The result demonstrated that aza-dipeptides with an ester as a C-terminus are not suitable to synthesize 2,5-disubstituted aza-DKPs in acidic conditions although they have been used to synthesized other aza-DKPs with different substituted mode as we mentioned before (Section 4.2, **Figure 4.7**). In the cases reported from literature[11], 2,4,5-trisubstituted aza-DKPs could be synthesized with moderate yields in acidic conditions (TFA) from aza-dipeptides with an ester as C-terminus (ester link to Wang resin). However, in the same condition, aza-dipeptides with an ester as C-terminus only give 2,5-disubstituted aza-DKPs in a very low yield (3%). In our case, the aza-dipeptide with ester as C-terminus could not give the 2,5-disubstituted aza-DKP in the mixture of

TFA and DCM. These two cases suggest that for the aza-dipeptides with an ester as C-terminus, the presence of substituent groups on the nitrogen of the natural amino acids is necessary to facilitate its aminolysis in acidic conditions, to allow its cyclization. This N-substitution might induce a specific constraint/conformation favoring the cyclization. For the aza-dipeptides with an amide as C-terminus, the presence of substituent groups on the nitrogen of the natural amino acids is not necessary for the cyclization.

4.4 Development of SPPS strategy for the synthesis of the aza-DKPamers

In order to synthesize foldamers with an amide at the C-terminus, Rink amide resin was used as polymer support for the SPPS. As shown in **Figure 4.16**, Fmoc cleavage was performed using 20% piperidine in DMF at room temperature for 20 min twice. The coupling of the first monomer **4.1** (2 eq) was performed by using DIC (2 eq) and Oxyma (3.3 eq) as coupling reagents and collidine (15 eq) as base. The base is necessary for the high coupling yield of the reaction and the reaction was agitated in plastic syringe tubes at room temperature for 8 h. After that, a capping was performed using acetic anhydride and NMM to avoid possible deleted byproducts. Then the next coupling was performed using the same procedure and coupling reagents as the first one. This cycle was repeated three or four rounds, depending on the length of the designed trimeric or tetrameric foldamers.

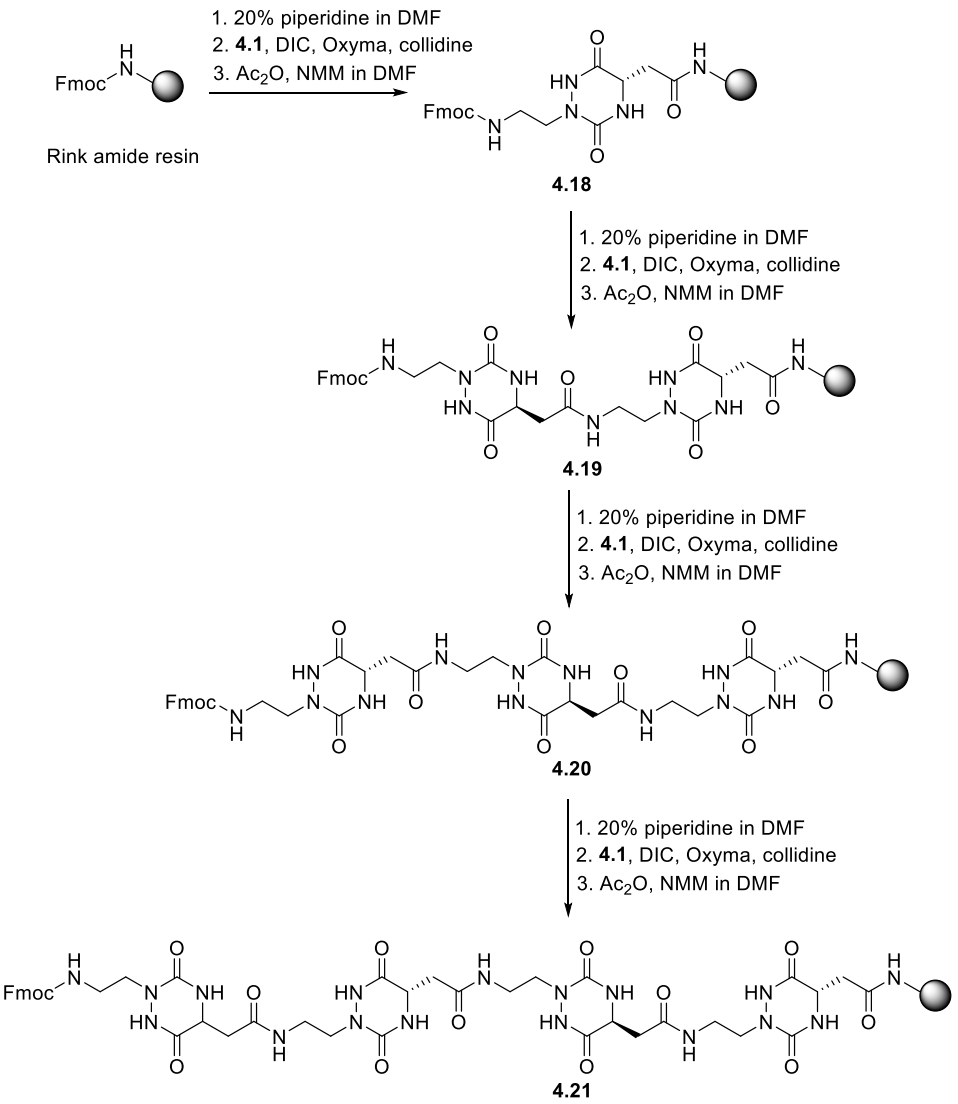

Figure 4.16: Synthesis of resins **4.20** and **4.21**

To get the trimer H-(aza-DKP)$_3$-NH$_2$ **4.2** which has a free amine group at the N-terminus, the Fmoc-protected intermediate **4.20** was treated with 20% piperidine in DMF to remove the Fmoc group, and successively the final H-(aza-DKP)$_3$-NH$_2$ **4.2** was cleaved from the resin **4.22** through a solution of TFA and H_2O (95:5) at room temperature for 2 h (**Figure 4.17**). The crude was purified by semi-preparative HPLC (Total yield: 49%).

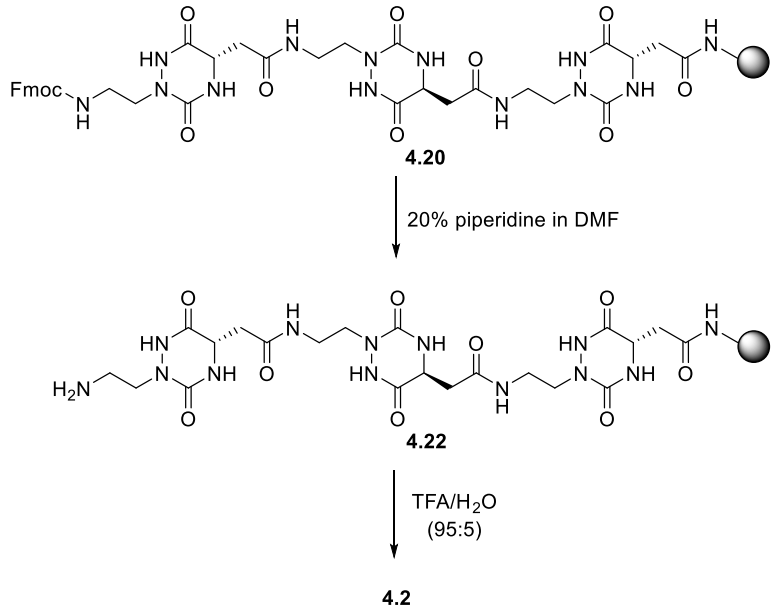

Figure 4.17: Synthesis of H-(aza-DKP)$_3$-NH$_2$ **4.2**

For the trimer Ac-(aza-DKP)$_3$-NH$_2$ **4.3** and the tetramer Ac-(aza-DKP)$_4$-NH$_2$ **4.5** having an acetyl group at the N-terminus (**Figure 4.18** and **Figure 4.19**), after removal of the Fmoc group from intermediates **4.20** and **4.21** in 20% piperidine/DMF, acetylation was performed at room temperature using acetic anhydride (5 eq) in the presence of pyridine (10 eq) in DMF to provide intermediates **4.23** and **4.24**, which were cleaved from resins using TFA/H_2O (95:5). The crudes were purified by semi-preparative HPLC to provide pure **4.3** and **4.5** (Total yields: 34% and 27%).

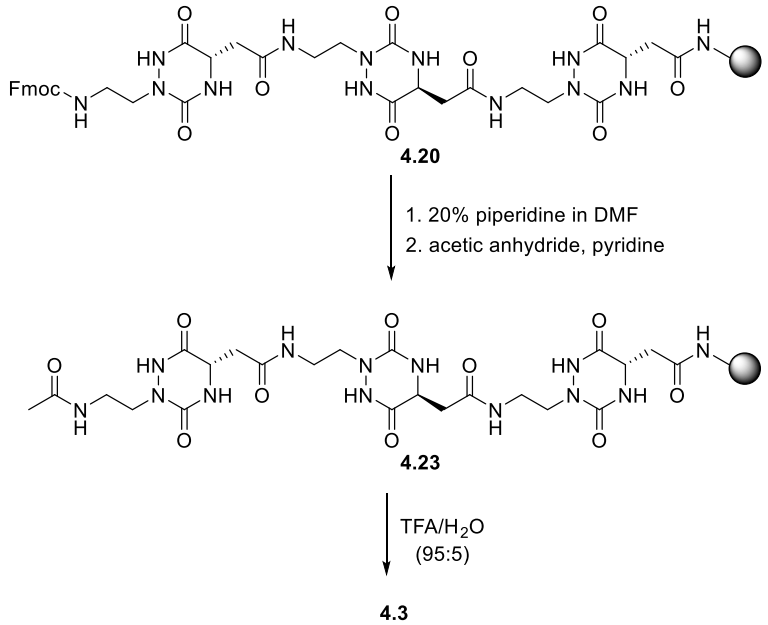

Figure 4.18: Synthesis of Ac-(aza-DKP)$_3$-NH$_2$ **4.3**

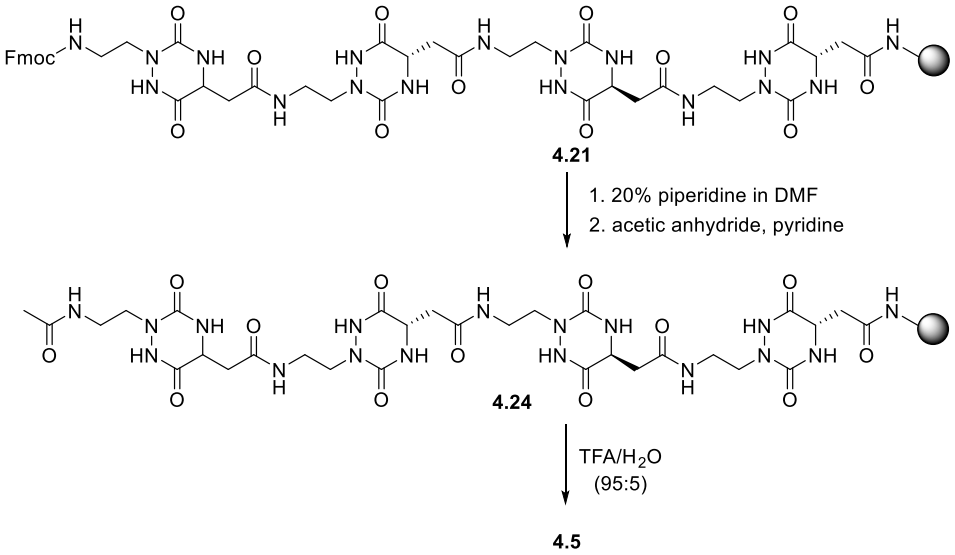

Figure 4.19: Synthesis of Ac-(aza-DKP)$_4$-NH$_2$ **4.5**

For the trimer 4-Br-benzoyl-(aza-DKP)$_3$-NH$_2$ **4.4** having a 4-bromobenzoyl group at its N-terminus (**Figure 4.20**), the intermediate **4.20** was first treated in 20% piperidine in DMF to remove the Fmoc group, then the free amine group was benzoylated by treating with 4-bromobenzoyl chloride (3 eq) in the presence of collidine (5 eq) in DMF at room temperature for 2 h. Although we could find the designed product **4.4** during the LC-MS analysis of the crude, an impurity bearing two 4-bromobenzoyl groups was detected (the ratio of **4.4**/impurity detected by HPLC is around 1/1), which means that the benzoyl chloride is too reactive and can afford multiple benzoylation on the aza-DKPamers. It is difficult to know where the additional 4-bromobenzoyl group in the impurity. Thus, we reduced the equivalent of 4-bromobenzoyl chloride (1.2 eq) and collidine (1.5 eq). However, this time the reaction showed a large amount of remaining starting material. We hypothesized that the problem was the presence of water in the solvent (DMF) which can consume some 4-bromobenzoyl chloride. To make the reaction as complete as possible, we repeated the reaction in the same conditions three rounds to get a satisfactory conversion. Then **4.4** was cleaved from the resin using TFA/H_2O (95:5). The crude was precipitated in Et_2O and the solid was washed by a mixture of ACN and H_2O (1:1) to get the pure foldamer **4.4** (Total yield: 19%).

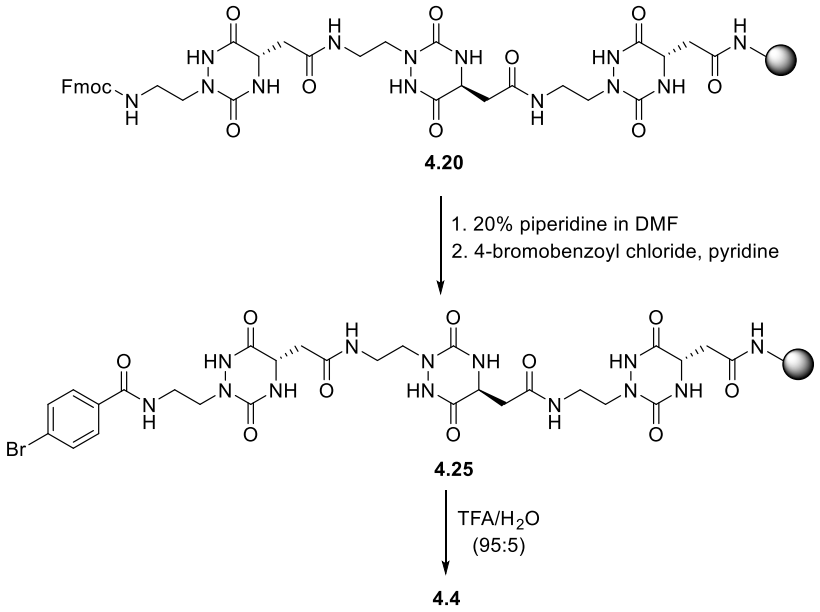

Figure 4.20: Synthesis of 4-Br-benzoyl-(aza-DKP)$_3$-NH$_2$ **4.4**

4.5 Conformational studies

4.5.1 Crystallization

Single-crystal X-ray diffraction is a powerful technique to provide the conformations of compounds in solid state. In order to know the preferential conformation adopted by the synthesized compounds in solid state, we attempted to crystallize Ac-(aza-DKP)$_3$-NH$_2$ **4.3** and Ac-(aza-DKP)$_4$-NH$_2$ **4.5** at the beginning. Unfortunately, compounds **4.3** and **4.5** showed very low solubility (less than 0.25 mg/mL) in all solvents we tried except water. It seems that **4.3** and **4.5** are too hydrophilic to solubilize in organic solvent. Thus, we synthesized 4-Br-benzoyl-(aza-DKP)$_3$-NH$_2$ **4.4** having 4-bromobenzoyl group at the N-terminus. 4-Bromophenyl group is known in literature to promote crystal formation and phasing as shown in Baptiste Legrand and Muriel Amblard's work.[7] The aromatic group we introduced at the N-terminus could improve the hydrophobicity of **4.4**, but not enough to be able to solubilize it in organic solvents, whereas its solubility in water decreased a lot. Due to the low solubility of the foldamers and in order to improve the crystallization conditions, we sent these foldamers to Dr. Baptiste Legrand who is an expert in crystallization and conformational studies of foldamers (Université de Montpellier).

4.5.2 CD

CD can give preliminary information about secondary structure of foldamers. CD experiments were performed on Ac-(aza-DKP)$_3$-NH$_2$ **4.3** (trimer) and Ac-(aza-DKP)$_4$-NH$_2$ **4.5** (tetramer) in PB solution (125 μM). They showed very similar CD spectra with a negative minimum around 200 nm but **4.3** showed more negative Cotton effect around this wavelength (**Figure 4.21A**) than compound **4.5**. The similar CD spectra indicate a similar folding state for both the trimer and tetramer. Although the negative band around 200 nm is a characteristic in random coil peptides, our compounds are far from peptides to make a comparison. We compared these CD spectra with the CD spectra of the DKP based foldamers from Piarulli's group. The DKP based foldamers designed by Piarulli's group showed different CD spectrum (0.2 mM in MeOH) depending on the length of the DKP based foldamers (**Figure 4.21B**).[4] For the DKP based trimer, its spectrum showed a very weak negative minimum at 198 nm and two strong negative minima at 208 and 220 nm, whereas for the DKP based tetramer, it showed a rather strong negative minimum at 200 nm and a weaker negative minimum at 225 nm with a negative maximum at 215 nm. The authors indicated that the spectrum of the DKP based tetramer was similar to oligopeptides having a central DKP unit and also to other peptidomimetics adopting β-bend ribbon conformation. In the spectra of peptidomimetics adopting β-bend ribbon conformation, as shown in literature, there are a positive band at 195 nm and a negative minimum near 205 nm followed by a negative shoulder near 220 nm (**Figure 4.21C**).[16,17] In our case, the minimum was near 200 nm and no positive band and negative shoulder were near 195 nm and 220 nm, respectively. Thus, the CD spectra of DKP based oligomers or other peptidomimetics adopting β-bend ribbon conformation are different with the CD spectra of our aza-DKP trimer and tetramer. Nevertheless, we could not exclude β-bend ribbon conformation of our aza-DKPamers because in our CD analysis, the solvent was PB aqueous solution, which was different from the solvent (MeOH) used in CD analysis for peptidomimetics adopting β-bend ribbon conformation. Due to lack of time, we have not tried to explore the conformation at MeOH or other organic solvent such as TFE.

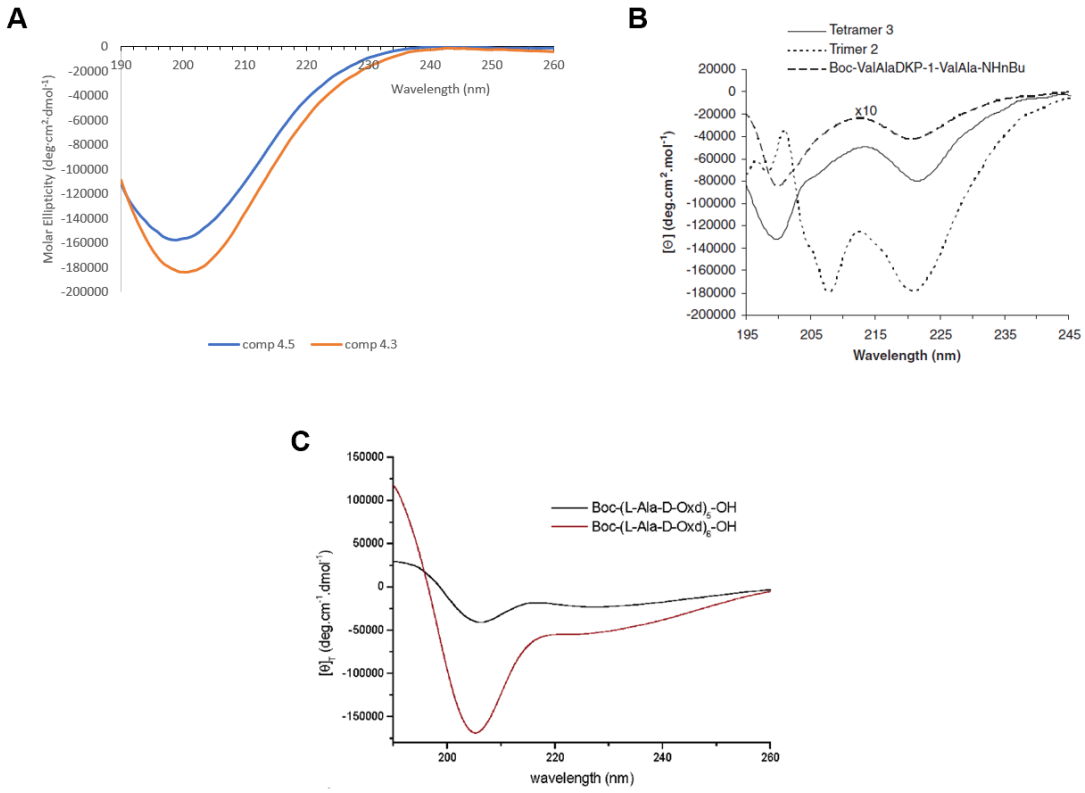

Figure 4.21: A) The CD spectra of Ac-(aza-DKP)$_3$-NH$_2$ **4.3** and Ac-(aza-DKP)$_4$-NH$_2$ **4.5** (PB solution); B) The CD spectra of DKP trimer and tetramer reported by Piarulli's group (0.2 mM in MeOH)[4]; C) The CD spectra of two peptidomimetics showing β-bend ribbon conformation (3 mM in MeOH)[17]

4.5.3 NMR

NMR can help to obtain information about the conformation of foldamers in solution. A first preliminary analysis has been performed on the Ac-(aza-DKP)$_3$-NH$_2$ **4.3** in water. However, ^{1}H NMR spectrum of **4.3** in D_2O/H_2O (10%/90%) showed a bad dispersion of the signals, thus not allowing a complete residue assignment and unambiguous attribution of all signals pertinent for conformational analysis by using standard 1D and 2D NMR sequences. However, we noticed that we have more than one conformer in solution. In order to get better resolution and less broadening of proton signals of **4.3**, CD_3OH was used as solvent to do NMR assay. However, the low solubility of **4.3** could not afford a sufficient concentration of **4.3** in CD_3OH to get spectra of high quality. All of these make the difficult to assign protons of aza-DKPs and prevent further conformational studies

by NMR parameters. Due to lack of time, we have not performed other trials with other solvents and with the other aza-DKPamers.

4.6 Conclusion

In this chapter, we could demonstrate the possibility to employ a side reaction we found during the synthesis of diaza-tripeptides (see chapter 2) to synthesize 2,5-disubstituted aza-DKPs which could not be synthesized efficiently before. These aza-DKPs have the same substituted mode as the DKP monomer which has been used in the synthesis of the DKP foldamer showing a β-bend ribbon structure.[4] Based on the structural similarity between DKP and aza-DKP, we designed and efficiently synthesized an aza-DKP monomer bearing amine and carboxylic acid functions compatible for a solid phase synthesis of foldamers constituted by this aza-DKP monomer. The designed synthetic approach allowed to obtain foldamers, different in length of foldamers (trimer or tetramer) and N-terminal substitution (free amine, acetyl group or 4-bromobenzoyl group) with satisfactory yields. We tried to investigate their conformations by X-ray diffraction, CD and NMR analyses. We attempted different crystallization conditions but, unfortunately, their low solubility in various organic solvents made the process challenging. From CD analysis, both trimer and tetramer showed similar CD spectra in PB solution (pH 7.4) suggesting a similar conformation which does not change with the length of the foldamers. However, we could not speculate their exact conformation due to very few comparable CD signals in literature. The β-bend ribbon is the most possible conformation for the aza-DKPamers because of the structural similarity with the DKP based foldamer. However, they have different CD spectra. Nevertheless, β-bend ribbon conformation is not excluded however other concentration and solvents such MeOH should be tested in CD experiments. The detailed information could be provided by NMR but overlap of signals of the protons for **4.3** in water and the bad solubility of **4.3** in other deuterated solvents prevented its conformational studies by NMR. Further assays should be performed to improve the NMR analysis, such as using a different pH of the buffer in order to improve the resolutions of peaks. Further attempts for crystallization are in progress thanks to the collaboration with Dr. Baptiste Legrand in IBMM at the University of Montpellier.

References

(1) Borthwick, A. D. 2,5-Diketopiperazines: Synthesis, Reactions, Medicinal Chemistry, and Bioactive Natural Products. *Chem. Rev.* **2012**, *112* (7), 3641–3716.

(2) Maujean, T.; Girard, N.; Ganesan, A.; Gulea, M.; Bonnet, D. Three Cheers for Nitrogen: Aza-DKPs, the Aza Analogues of 2,5-Diketopiperazines. *RSC Adv.* **2020**, *10* (71), 43358–43370.

(3) Regenass, P.; Bosc, D.; Riché, S.; Gizzi, P.; Hibert, M.; Karmazin, L.; Ganesan, A.; Bonnet, D. Comparative Study of the Synthesis and Structural and Physicochemical Properties of Diketopiperazines vs Aza-Diketopiperazines. *J. Org. Chem.* **2017**, *82* (6), 3239–3244.

(4) Delatouche, R.; Durini, M.; Civera, M.; Belvisi, L.; Piarulli, U. Foldamers of Bifunctional Diketopiperazines Displaying a β-Bend Ribbon Structure. *Tetrahedron Lett.* **2010**, *32* (51), 4278–4280.

(5) Sharma, G. V. M.; Jadhav, V. B.; Ramakrishna, K. V. S.; Jayaprakash, P.; Narsimulu, K.; Subash, V.; Kunwar, A. C. 12/10- and 11/13-Mixed Helices in α/γ- and β/γ-Hybrid Peptides Containing C-Linked Carbo-γ-Amino Acids with Alternating α- and β-Amino Acids. *J. Am. Chem. Soc.* **2006**, *128* (45), 14657–14668.

(6) Guo, L.; Almeida, A. M.; Zhang, W.; Reidenbach, A. G.; Choi, S. H.; Guzei, I. A.; Gellman, S. H. Helix Formation in Preorganized β/γ-Peptide Foldamers: Hydrogen-Bond Analogy to the α-Helix without α-Amino Acid Residues. *J. Am. Chem. Soc.* **2010**, *132* (23), 7868–7869.

(7) Legrand, B.; André, C.; Wenger, E.; Didierjean, C.; Averlant-Petit, M. C.; Martinez, J.; Calmes, M.; Amblard, M. Robust Helix Formation in a New Family of Oligoureas Based on a Constrained Bicyclic Building Block. *Angew. Chem. Int. Ed.* **2012**, *51* (45), 11267–11270.

(8) Pinnen, F.; Luisi, G.; Lucente, G.; Gavuzzo, E.; Cerrini, S. Approaches to Pseudopeptidic Ergopeptines. Synthesis and Molecular Structure of an α-Aza-Phenylalanine-Containing Oxa-Cyclol. *J. Chem. Soc., Perkin trans. 1* **1993**, *0* (7), 819–824.

(9) Obreza, A.; Urleb, U. A Two-Step Synthesis of Hexahydropyrrolo-[1,2-d][1,2,4]Triazine-1,4-Dione and Related Compounds. *Synth. Commun.* **2003**, *33* (6), 1011–1018.

(10) Bourguet, C. B.; Proulx, C.; Klocek, S.; Sabatino, D.; Lubell, W. D. Solution-Phase Submonomer Diversification of Aza-Dipeptide Building Blocks and Their Application in Aza-Peptide and Aza-DKP Synthesis. *J. Pept. Sci.* **2010**, *16* (6), 284–296.

(11) Bonnet, D.; Margathe, J.-F.; Radford, S.; Pflimlin, E.; Riché, S.; Doman, P.; Hibert, M.; Ganesan, A. Combinatorial Aid for Underprivileged Scaffolds: Solution and Solid-Phase Strategies for a Rapid and Efficient Access To Novel Aza-Diketopiperazines (Aza-DKP). *ACS Comb. Sci.* **2012**, *14* (5), 323–334.

(12) Regenass, P.; Margathe, J.-F.; Mann, A.; Suffert, J.; Hibert, M.; Girard, N.; Bonnet, D. Diastereoselective Synthesis of Novel Aza-Diketopiperazines via a Domino Cyclohydrocarbonylation/Addition Process. *Chem. Commun.* **2014**, *50* (68), 9657–9660.

(13) Hoffman, R. V.; Reddy, M. M.; Klumas, C. M.; Cervantes-Lee, F. The Reactions of

Hydrazines with α-Lactams. Regiochemistry of Hydrazine Addition and Subsequent Ring Closure to N-Aminohydantoins or 1,2,4-Triazine-3,6-Diones. *J. Org. Chem.* **1998**, *63* (24), 9128–9130.

(14) Hamuro, Y.; Marshall, W. J.; Scialdone, M. A. Solid-Phase Synthesis of Acyclic and Cyclic Amino Acid Derived Urea Peptidomimetics Using Phoxime Resin. *J. Comb. Chem.* **1999**, *1* (2), 163–172.

(15) Ivanovich, R. A.; Vincent-Rocan, J.-F.; Elkaeed, E. B.; Beauchemin, A. M. One-Pot Synthesis of Aza-Diketopiperazines Enabled by Controlled Reactivity of N-Isocyanate Precursors. *Org. Lett.* **2015**, *17* (19), 4898–4901.

(16) Ségalas, I.; Prigent, Y.; Davoust, D.; Bodo, B.; Rebuffat, S. Characterization of a Type of β-Bend Ribbon Spiral Generated by the Repeating (Xaa–Yaa–Aib–Pro) Motif: The Solution Structure of Harzianin HC IX, a 14-Residue Peptaibol Forming Voltage-Dependent Ion Channels. *Biopolymers* **1999**, *50* (1), 71–85.

(17) Tomasini, C.; Luppi, G.; Monari, M. Oxazolidin-2-One-Containing Pseudopeptides That Fold into β-Bend Ribbon Spirals. *J. Am. Chem. Soc.* **2006**, *128* (7), 2410–2420.

Conclusion and perspectives

In my PhD project, on the basis of the amyloid positive cross–interaction between Aβ and TTR reported in literature and the β-turn propensity of diaza-tripeptides previously found in our laboratory, we sought to design and synthesize novel peptidomimetic foldamers containing diaza-peptide units based on the sequence of the EF-helix of TTR and to investigate their conformations and activity against $A\beta_{42}$ aggregation, involved in AD.

The work in the chapter 2 aimed to investigate the conformational propensity of diaza-tripeptides in water and the effect of the side chains of aza-residues on the conformation. This work was very important and instructive for the next work in the chapter 3 associated with the design and synthesis of diaza-nonapeptides. Three aqueous soluble diaza-tripeptides were designed and synthesized. Several synthetic instructions for diaza-tripeptides were proposed to help to efficiently prepare diaza-tripeptides. The conformational studies of the three diaza-tripeptides demonstrated that stable Type I and type I′ β-turn structures were induced by diaza-peptide units even in the most challenging solvent water.

The ability of the diaza-peptide unit to induce β-turn structures of tripeptides encouraged us to introduce one or more diaza-peptide units into longer peptides and investigate their conformations. This is a part of work in the chapter 3. It was reported that the EF-helix is a possible binding site of TTR to Aβ but a peptide excised from the EF-helix showed no obvious interaction with Aβ probably due to the loss of its helical structure. Ten diaza-nonapeptides possessing different numbers of diaza-peptide units at the different positions of the EF-helix sequence were designed. The synthesis of these aza-nonapeptides was developed on solid phase. Preliminary conformational studies by CD helped us to choose some peptides with a specific positive band near 225 nm to do further conformation studies (NMR, FTIR and MD simulations). The results from these experiments indicated that the introduction of diaza-peptide units at the N- and C-termini of the sequence induces helical structures (peptides **6** and **10**), which in aprotic polar solvent have more intramolecular hydrogen bond, whereas in water have less intramolecular hydrogen bond. These diaza-peptides based foldamers can mimic the EF-helix as demonstrated by low RMSD values and a similar orientation of the side chains in the MD simulations. When a single diaza-peptide unit was introduced at the N-terminus, peptide **9** showed a 3_{10}-helix conformation in methanol at 258 K. This

suggests that the N-terminal diaza-peptide unit can serve as a helical nucleation template to induce 3_{10}-helix structure of the peptides.

In ThT assays, our designed peptides showed different activity against Aβ aggregation and the activity was correlated with the conformation. Peptide **10** which showed the strongest positive band near 225 nm in CD and was demonstrated to mimic the EF-helix in the MD simulations showed the best activity, which is better than the activity of the natural counterpart **11**. Thus, we can say that by introducing two diaza-peptide units in the sequence of the EF-helix to induce helical structures similar to the EF-helix, the peptide has similar effects on Aβ as TRR shows. The kinetic analysis of the experimental data using AmyloFit platform suggested that peptide **10** targets the primary nucleation of the aggregation whereas the natural peptide **11** and TTR target the secondary nucleation of the aggregation. The activity was further confirmed by CD analysis of $A\beta_{42}$ and $A\beta_{1\text{-}28}$ in the absence or the presence of peptide **10**. The results also indicated that peptide **10** inhibits Aβ aggregation through stablizing the α-helical content of Aβ. We speculated that the helical structures of peptide **10** may interact with the N-terminal helical content of Aβ, thereby preventing its further misfolding and aggregation in toxic species. Further work will be done to try to crystallize $A\beta_{1\text{-}28}$ in the presence of peptide **10**, in collaboration with Lidia Ciccone (Pisa University, Italy).

In addition, due to the problem of reproducibility of the *in vitro* aggregation assays according to the source of $A\beta_{42}$, several conditions were tried to pretreat $A\beta_{42}$ but no satisfactory results could be got so far. Further work on it needs to be performed in the future to get reproducible ThT curves of $A\beta_{42}$. If a general protocol could be established for starting from homogenous monomeric states of $A\beta_{42,}$ this would help to compare the results of all groups working on this tricky amyloid protein.

To verify the proteolytic stability of our aza-peptides, peptide **10** was tested for its stability in human plasma. It showed to be very stable in human plasma whereas the natural peptide **11** degraded very rapidly under the same condition. Thus, using diaza-peptide units to replace natural residues in peptides is a feasible way to improve the proteolytic stability of peptides (two diaza-peptide units in nonapeptides is sufficient). In a MTT assay, peptide **10** demonstrated no toxicity to rat brain endothelial cells, which further proves its potential to be a drug candidate. Unfortunately, peptide **10** displayed only limited BBB permeability in an *in vitro* rat BBB model. The experiment suggested that peptide **10** is a potential substrate of the efflux transporters located at the rat BBB. Further

structural modification should be performed to increase its passive diffusion and reduce its affinity to efflux transporters.

Finally, during the synthesis of the diaza-tripeptides designed in the chapter 2, an interesting side reaction which can give 2,5-disubstituted aza-DKP attracted our attention. In the chapter 4, we used this side reaction to design and synthesize a new aza-DKP monomer. Based on this monomer, we further designed four novel foldamers which we termed aza-DKPamers. The SPPS of these foldamers was developed. As these foldamers were analogous to DKP oligomers, we could expect their potential folding in β-bend ribbon conformation. CD analysis of two of these foldamers was performed and the spectra showed a similar shape with a negative minimum near 200 nm. However, we could not speculate their exact conformation due to very few comparable CD signals in literature. We also tried to get single-crystals of them to do X-ray diffractions but their low solubility in organic solvents makes the task difficult. Further attempts for crystallization are in progress thanks to the collaboration with Dr. Baptiste Legrand in IBMM at the University of Montpellier. The overlap of the ^{1}H-resonance signals of one foldamer made impossible its conformational studies by NMR. Due to lack of time, we have not performed other trials with other solvents and with the other aza-DKPamers. This work will be done in the future.

Overall, my PhD thesis further proves the value of this new strategy of designing peptide amyloid aggregation inhibitors based on positive amyloid protein cross-interactions. Furthermore, it demonstrates that the introduction of diaza-peptide units in peptides is a novel method to induce flexible and adaptative helical structures of peptides and to increase the proteolytic stability of peptide without obvious toxicity to cells. In some cases, the helical structures of peptides are quite important for the activity of peptides, especially for the peptides targeting PPIs. Thus, this method can also be used in the design of other peptide PPI inhibitors that require mimics of helical structures.

Experimental part

Usual solvents were purchased from commercial sources and DCM was dried and distilled over CaH_2. Thin-layer chromatography (TLC) analyses were performed on silica gel 60 F250 (0.26 mm thickness) plates. The plates were visualized with UV light (λ = 254 nm) or stained by a 4 % solution of phosphomolybdic acid or ninhydrin in EtOH. NMR spectra were recorded on an ultrafield Bruker AVANCE 300 (^{1}H, 300 MHz, ^{13}C, 75 MHz) or on a Bruker AVANCE 400 (^{1}H, 400 MHz, ^{13}C, 100 MHz). Chemical shifts δ are in ppm with the solvent resonance as the internal standard (^{1}H NMR, $CDCl_3$: δ = 7.26 ppm, DMSO: δ = 2.50 ppm, CD_3OD and CD_3OH: δ = 3.31 ppm; ^{13}C NMR, $CDCl_3$: δ = 77.16 ppm, DMSO: δ = 39.52 ppm, CD_3OD and CD_3OH: δ = 49.00 ppm), and the following abbreviations are used: singlet (s), doublet (d), doublet of doublet (dd), triplet (t), quintuplet (qt), multiplet (m), broad multiplet (brm), and broad singlet (brs), broad doublet (brd). Mass spectra were obtained using a Bruker Esquire electrospray ionization apparatus. HRMS were obtained using a TOF LCT Premier apparatus (Waters) with an electrospray ionization source. The purity of compounds was determined by HPLC-MS on Agilent 1260 Infinity. Column: ATLANTIS T3 column (C18, 2.1 x 150mm-3μm), mobile phase: ACN/H_2O + 0.1% TFA (gradient 1-30% in 15 or 20 min). Preparative HPLC were performed on Agilent 1260 Infinity II. Column: Pursuit (C18 10 x 250μm-5μm), mobile phase: ACN/H_2O + 0.1% formic acid.

Circular Dichroism Spectroscopy

Peptides was dissolved in MQ water to a concentration of 750 μM as stock solutions. For the measurement in PB solution, 50 μL of stock solution was taken into a cuvette with a pathlength of 1 mm, then the solution was diluted by 250 μL PB solution to a final concentration of 125 μM. The CD spectra were measured by J-810 spectropolarimeter (JASCO, Tokyo, Japan) from 190 to 260 nm at corresponding temperatures. For the measurement in methanol, 50 μL of stock solution in a cuvette was diluted by 250 μL methanol to a final concentration of 125 μM. The CD spectra were recorded from 195 to 260 nm at corresponding temperatures. For the measurement in $CaCl_2$ aqueous solution or urea aqueous solution, 50 μL of stock solution in a cuvette was diluted by 250 μL 1 M $CaCl_2$ aqueous solution or 6 M urea aqueous solution to a final concentration of 125 μM. The CD spectra were recorded from 210 to 260 nm at corresponding temperature. Each CD spectrum was

corrected by subtracting the corresponding baseline (50 µL MQ water + 250 µL corresponding diluent).

FT-IR Spectroscopy

Infrared spectra were recorded using a Shimadzu IRAffinity-1S spectrometer in the range 600–4000 cm^{-1} with a resolution of 2 cm^{-1}. A sample for measurements in the solid state was prepared by dissolving the peptidomimetic in H_2O and MeOH, placing the solution on the crystal plate, and evaporating the solvent (64 scans were averaged). The ATR FT-IR experiment were measured from a solution at 2 mM compound concentration. Transmittance has been recorded and transformed into absorbance (A = 2-log(T)). Data processing was performed using Solver in Excel software (Microsoft). Deconvolution of the spectra was done in the spectral range 1500 - 1800 cm^{-1}. The deconvoluted spectra were fitted with Gaussian band profiles. The positions, and number of the components, which were used as an input file for the curve-fitting function, were obtained from the deconvoluted spectra. The quality of the fitting was estimated by standard deviation and error squared. The assignment of absorption bands of the secondary structure was made as described in literature.

Fluorescence-Detected ThT Binding Assay ($A\beta_{42}$)

$A\beta_{42}$ was purchased from Bachem and ThT was obtained from Sigma. The peptide was dissolved in an aqueous 1% ammonia solution to a concentration of 1 mM and then, just prior to use, was diluted to 0.2 mM with 10 mM Tris-HCl and 100 mM NaCl buffer (pH 7.4). Stock solutions of compounds to test were dissolved in water. ThT fluorescence was measured to evaluate the development of $A\beta_{42}$ fibrils over time using a fluorescence plate reader (Fluostar Optima, BMG labtech) with standard 96-well black microtiter plates (final volume in the wells of 200 µL). Experiments were started by adding the peptide (final $A\beta_{42}$ concentration equal to 10 µM) into a mixture containing 40 µM ThT in 10 mM Tris-HCl and 100 mM NaCl buffer (pH 7.4) with and without the inhibitors at different concentrations (100 and 10 µM) at room temperature. The ThT fluorescence intensity of each sample (performed in triplicate) was recorded with 440/480 nm excitation/emission filters set for 42 h performing a double orbital shaking of 10 s before the first

cycle. The ability of compounds to inhibit $A\beta_{42}$ aggregation was assessed considering the time of the half-aggregation ($t_{1/2}$) and the intensity of the experimental fluorescence plateau (F). The relative extension/reduction of $t_{1/2}$ ($\Delta t_{1/2}$) is defined as the experimental $t_{1/2}$ in the presence of the tested compound relative to the one obtained without the compound and is evaluated as the following percentage: $[t_{1/2}\ (A\beta + \text{compound}) - t_{1/2}\ (A\beta)]/t_{1/2}\ (A\beta) \times 100$. The relative extension/reduction of the experimental plateau is defined as the intensity of experimental fluorescence plateau observed with the tested compound relative to the value obtained without the compound and is evaluated as the following percentage: $(FA\beta + \text{compound} - FA\beta) / FA\beta \times 100$.

CD analysis of $A\beta_{42}$ with and without inhibitors

CD spectra (195-250 nm) were acquired on Jasco J-810 using 0.1 cm quartz cells. The spectra were recorded with 0.1 nm resolution at 25°C and a scan rate of 50 nm/min. Five scans were acquired and averaged for each sample ($A\beta_{42}$ at 25 µM concentration and inhibitor at 100 µM). The data are given as CD intensity in mdeg. Raw data were processed by background subtraction (or inhibitor subtraction when required), followed by smoothing. Secondary structure percentages were calculated from these spectra over the range 200-250 nm using the freely accessible algorithm BeStSel (best-sel.elte.hu) which includes independent basis spectra for both parallel and anti-parallel β-sheet. The deconvolution was performed on the CD measurement, after subtraction of the corresponding buffer or the solution containing the 100 µM concentration of inhibitor.

Human Plasmatic Stability Study

Human plasma was obtained from Etablissement Français du Sang (EFS, Les Ulis, France). Compounds were incubated in duplicate at 1 µM in plasma at 37°C from 0 to 120 minutes (T0, 15, 30, 45, 60 and 120 min). At each time points, 200 µL of acetonitrile was added to 50 µL of incubated plasma. After vortexing 10 seconds and centrifugation 10 minutes at 20000g, supernatant was evaporated to dryness under nitrogen stream 1 hour at 40°C and the dry extract was reconstituted with 50 µL water/acetonitrile (90/10; v/v). After centrifugation 5 minutes at 20000g supernatant was transferred into a vial placed at 4°C in the autosampler before injection into the analytical system.

Compounds quantitation was carried out using an UPLC−MS/MS system consisted of a Waters ACQUITY UPLC® System coupled to a Waters XEVO™ TQ-S Mass Spectrometer operating in positive ion electrospray MRM mode. Reversed phase analysis was performed with an Acquity UPLC BEH C18 1.7 µm, 2.1x50 mm column maintained at 40°C and a gradient over a run time of 4 minutes. All solvents and chemicals were of LC/MS grade and were purchased from VWR International. Mobile phase A was 0.1% formic acid in water and mobile phase B 0.1% formic acid in acetonitrile.

Blood-Brain Barrier (BBB) Permeability Measurement

The study consisted of measuring the passage of peptide **10** through *in vitro* rat blood-brain barrier (BBB) model. The integrity and functionality of *in vitro* rat BBB model were assessed by monitoring the transport of 3 molecules: Lucifer Yellow (LY), propanolol and vinblastine. In addition, peptide **10** was co-incubated with LY, which served as the internal integrity standard. Peptide **10** was tested at 2 and 5 µM and 10 µM. The solutions were prepared in low-binding Eppendorf tubes to limit the loss of peptide **10**. By so doing, the concentrations measured in the T0 solutions were closer the target concentration of 5 and 10 µM. The study was performed on rat BBB model in the apical-to-basal direction (i.e. blood to brain) and from the basal to apical concentration in triplicate. The samples obtained from the apical and basal compartments were then analyzed using a developed analytical LC-MS/MS method, thus making it possible to establish the rate of passage of peptide **10**.

Cell viability assay

MTT (3-(4,5-dimethylthiazol-z-yl)-2,5-diphenyl-tetrazotium bromide) assay was used to determine the non-toxic dose of peptide **10** for transport experiments. Briefly, rat brain endothelial cells were seeded on coated 96-well plates at a density of 37,500 cells.cm^{-2}. After one week, they were exposed to 100 µL per well of peptide **10** suspensions in complete medium, from 0 to 100 µg/mL for 1 h, a time line corresponding to blood-brain barrier exposure to peptide **10**. Cell metabolic activity, reflecting peptide **10** cytotoxicity, was assessed by using MTT. Mitochondrial dehydrogenases of viable cells reduce MTT to water-insoluble blue formazan crystals. At

considered endpoints, exposure medium was replaced by 100 µL of 1 mg/mL MTT solution in phosphate buffer. After 4 h at 37°C, culture medium was replaced by 100 µL of DMSO and mixed to dissolve formazan crystals. Absorbance was measured at 540 nm and metabolic activity was determined as a percentage of the negative controls. To probe the interference of peptide **10** with this test, the absorbance of exposed cells, treated as described above but without MTT, was recorded.

Solid phase peptide Synthesis

All the reaction involved were agitated in plastic syringe tubes equipped with filters on an automated shaker. Each coupling of Fmoc-protected natural amino acids was carried out twice to get satisfactory yields. Removal of Fmoc group was performed in 20%(v/v) piperidine/DMF for 20 min twice. Capping steps were performed by treating with the mixture of acetic anhydride (0.25 M) and NMM (0.25 M) in DMF solution for 20 min. After each reaction, the resin was washed with DMF (3×10mL), MeOH (3×10mL) and DCM (3×10mL) successively. Rink Amide resin (400 mg, 0.4 mmol/g) was swelled by DMF for 1h before using.

The loading of the first amino acid, Fmoc-Gly-OH (2 equiv), was performed in 20%(v/v) NMM/DMF using HCTU (2 equiv) as coupling reagent for 30 min. Couplings between two natural residues (2 equiv) were also performed in 20%(v/v) NMM/DMF using HCTU (2 equiv) as coupling reagents for 20 min each coupling.

To coupling diaza-peptide fragments (building blocks A, B and C) with natural residues, diaza-peptdie fragments (2 equiv) were activated by triphosgene (0.7 equiv) in the presence of DIPEA (2 equiv) in DCM for 15 min (in a flask), then the reactive solutions were transferred to the plastic syringe tubes containing the resin, 3 equiv DIPEA was added and the reactions were agitated at room temperature for 5 h.

To coupling natural amino acids to aza-residues, the natural amino aicds (2 equiv) were firstly activated by DIC (2 equiv) and Oxyma (3.3 equiv) in the mixture of DCM/DMF (1/1) (8 mL) for 10 min (in a flask), then the solutions were transferred to the plastic syringe tubes containing the resin, 15 equiv collidine was added as base. For the coupling Lys to aza-Leu residue, the reaction was agitated at room temperature for 5 h. For the coupling Ser to aza-Tyr residue, the reaction was agitated at 40°C for 5 h.

In the synthesis of aza-DKPamers, to couplings of compound **4.1** to resins, **4.1** (2 equiv) were firstly activated by DIC (2 equiv) and Oxyma (3.3 equiv) in the mixture of DCM/DMF (1/1) (8 mL) for 10 min (in a flask), then the solution was transferred to the plastic syringe tubes containing the resin, 15 equiv collidine was added as base. The reactions were agitated at room temperature for 8 h.

Compounds in chapter 2

(S)-2-(2-acetyl-1-(4-aminobutyl)hydrazine-1-carbonyl)-N-(1-amino-3-hydroxy-1-oxopropan-2-yl)hydrazine-1-carboxamide·HCOOH (compound 2.5)

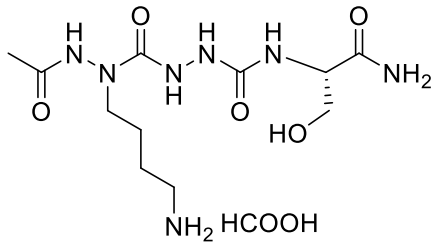

To a solution of **2.23** (39 mg, 0.07 mmol) in 22 mL mixture of AcOH/H_2O (10/1) was added 10% Pd/C (8 mg). The mixture was stirred at room temperature under a hydrogen atmosphere overnight. Then the suspension was filtrated through a pad of celite and the filtrate was lyophilized to give a white solid. The crude was purified by preparative HPLC (Linear gradients of 0.5-10 % ACN in H_2O containing 0.1% formic acid in 10 min) to give **2.5** as a white solid (17 mg, 0.04 mmol, yield: 64%).

HRMS (ESI): Calcd for $[C_{11}H_{23}N_7O_5 + H]^+$: 334.1833, found: 334.1834.

NMR data for compound **2.5** (The detailed spectra can be accessible in the supporting information of this article: DOI: 10.1039/D2OB01225A)

Table S1. ^{1}H NMR chemical shifts of diaza-tripeptide **2.5** in water (11 mM) at 278 K

Residue	δ NH (ppm)	δ H_α (ppm)	δ H_β (ppm)	δ Other protons (ppm)
Ac				CH_3 2.09
aLys[1]	n.d.		3.70, 3.38	γ CH_2 1.62, δ CH_2 1.67, ε CH_2 3.00 NH_3^+ n.d.
aGly[2]	n.d.	n.d.		
Ser[3]	6.65	4.32	3.90, 3.86	OH n.d.
$NH_{2\ Z,\ E}$	n.d.			

n.d. not detected

Table S2. ^{13}C NMR chemical shifts of diaza-tripeptide **2.5** in water (11 mM) at 308 K

Residue	δ CO (ppm)	δ C_α (ppm)	δ CH_β (ppm)	δ Other carbons (ppm)
Ac	176.5			CH_3 22.9
aLys[1]	161.8		50.5	γ CH_2 26.2, δ CH_2 26.7, ε CH_2 42.1
aGly[2]	162.7			
Ser[3]	179.5	60.1	65.5	

Table S3. NMR conformational parameters for **2.5** in water

Residue	Δδ NH/ΔT (ppb/K)	$^{3}J_{HN\text{-}H\alpha}$ (Hz)[a]	$^{3}J_{H\alpha\text{-}H\beta(\beta')}$ (Hz)[a]
aLys[1]	n.d.		
aGly[2]	n.d.		
Ser[3]	–3.4	7.7	5.5, 3.6
$NH_{2\ Z,\ E}$	n.d.		

[a] measured at 309 K; n.d. not detected

Table S4. ^{1}H NMR chemical shifts of diaza-tripeptide **2.5** in methanol (19.4 mM) at 298 K

Residue	δ NH (ppm)	δ H_α (ppm)	δ H_β (ppm)	δ Other protons (ppm)
Ac				CH_3 2.04
aLys[1]	n.d.		3.59, 3.53	γ CH_2 1.57, δ CH_2 1.72, ε CH_2 2.93, 2.85 NH_3^+ n.d.
aGly[2]	9.06	7.73		
Ser[3]	6.51	4.10	3.84	OH n.d.
$NH_{2\ Z,\ E}$	n.d.			

n.d. not detected

Table S5. ^{13}C NMR chemical shifts of diaza-tripeptide **2.5** in methanol (19.4 mM) at 298 K

Residue	δ CO (ppm)	δ C_α (ppm)	δ CH_β (ppm)	δ Other carbons (ppm)
Ac	172.8			CH_3 21.1
aLys[1]	159.7		49.1	γ CH_2 25.0, δ CH_2 25.5, ε CH_2 40.7
aGly[2]	161.2			
Ser[3]	177.0	58.4	64.8	

Table S6. NMR conformational parameters for **2.5** in methanol

Residue	δ NH [a]	Δδ NH/ΔT (ppb/K)	$^{3}J_{HN\text{-}H\alpha}$ (Hz) [b]	$^{3}J_{H\alpha\text{-}H\beta(\beta')}$ (Hz) [b]
aLys[1]	10.71	–5.8		
aGly[2]	9.50, 8.28 (α)	–4.6, –7.9 (α)		
Ser[3]	6.60	–1.4	7.0	5.3, 4.5

[a] signal at 228 K

[b] average value, measured at 298 K

HPLC purity: ATLANTIS T3 column (C18, 2.1 x 150mm-3µm); ACN /H_2O + 0.1 % TFA, gradient 1–30 % in 15 min; R_t = 1.90 min, 100 %.

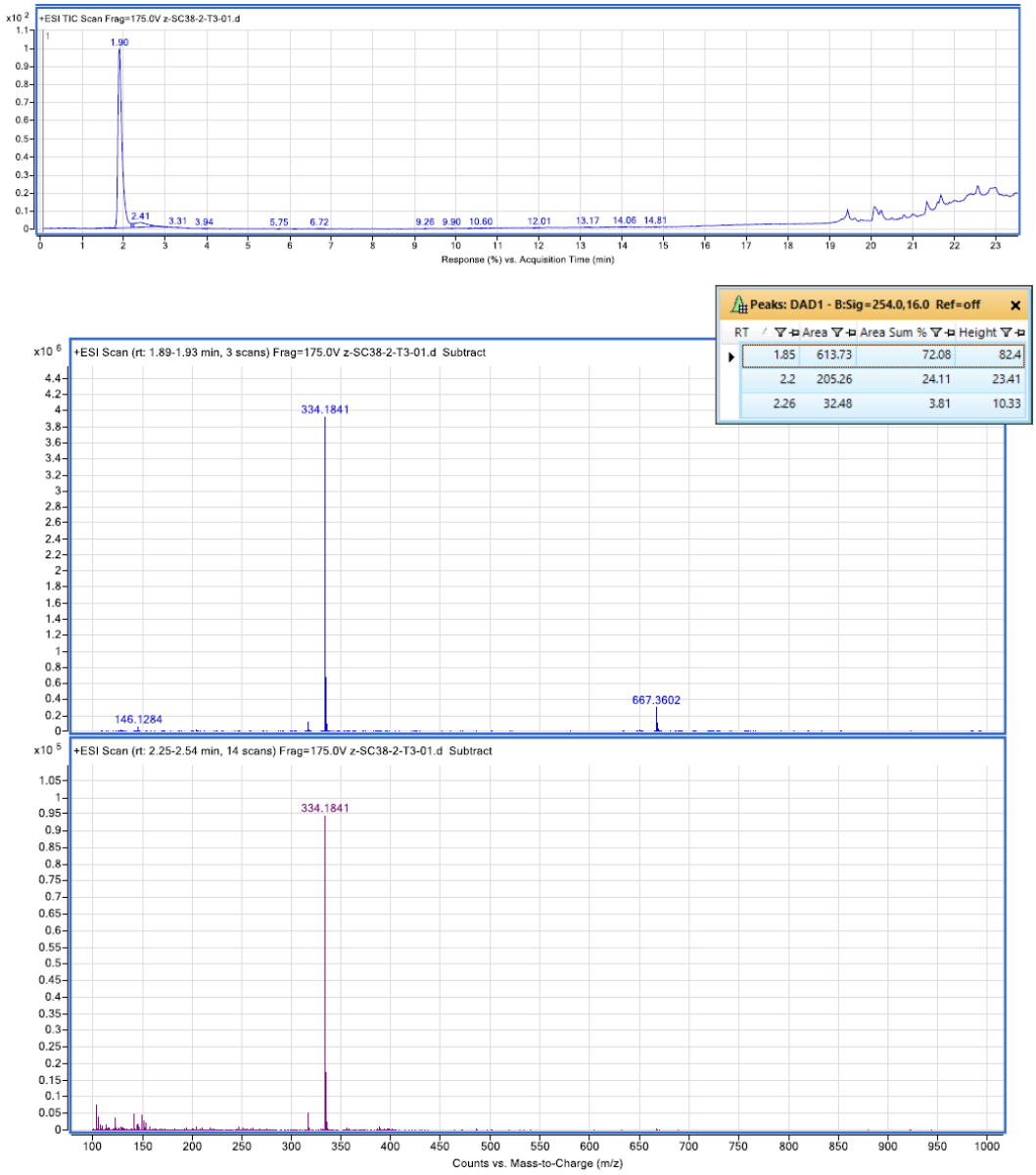

(S)-2-(2-acetyl-1-(4-aminobutyl)hydrazine-1-carbonyl)-N-(1-amino-3-hydroxy-1-oxopropan-2-yl)-1-methylhydrazine-1-carboxamide·HCOOH (compound 2.6)

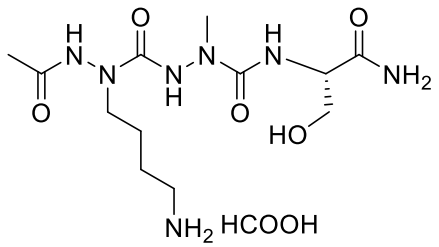

Compound **2.6** was synthesized from **2.33a** (50 mg, 0.09 mmol) as a white solid (20 mg, 0.05 mmol, yield: 58%) by following the synthesis procedure of **2.5** (Preparative HPLC of **2.6** was performed using linear gradients of 0.5-15 % ACN in H_2O containing 0.1% formic acid in 12 min).

HRMS (ESI): Calcd for $[C_{12}H_{25}N_7O_5 + Na]^+$: 370.1809, found: 370.1812.

NMR data for compound **2.6** (The detailed spectra can be accessible in the supporting information of this article: DOI: 10.1039/D2OB01225A)

Table S7. ^{1}H NMR chemical shifts of diaza-tripeptide **2.6** in water (11 mM) at 278 K

Residue	δ NH (ppm)	δ H_α (ppm)	δ H_β (ppm)	δ Other protons (ppm)
Ac				CH_3 2.10
aLys[1]	10.55, 10.48		3.70, 3.38	γ CH_2 1.63, δ CH_2 1.68, ε CH_2 3.00 NH_3^+ 7.62
aAla[2]	9.51, 9.45, 9.04		3.06	
Ser[3]	6.97, 6.89, 6.75	4.27	3.86	OH n.d.
$NH_{2\ Z,\ E}$	7.30, 7.24 7.86,7.78,7.75,7.66			

Table S8. ^{13}C NMR chemical shifts of diaza-tripeptide **2.6** in water (11 mM) at 308 K

Residue	δ CO (ppm)	δ C_α (ppm)	δ CH_β (ppm)	δ Other carbons (ppm)
Ac	176.6			CH_3 22.9
aLys[1]	160.8		50.9	γ CH_2 26.2, δ CH_2 26.8, ε CH_2 42.1
aAla[2]	162.5		38.8	
Ser[3]	178.4	59.2	64.4	

Table S9. ^{1}H NMR chemical shifts of diaza-tripeptide **2.6** in methanol (27.9 mM) at 298 K

Residue	δ NH (ppm)	δ H_α (ppm)	δ H_β (ppm)	δ Other protons (ppm)
Ac				CH_3 2.06
aLys[1]	n.d.		3.74, 3.39	γ CH_2 1.59 δ CH_2 1.73, ε CH_2 2.94 NH_3^+ n.d.
aAla[2]	9.37		3.07	
Ser[3]	6.67	4.24	3.86	OH n.d.
$NH_{2\ Z,\ E}$	7.17, 7.57			

Table S10. ^{13}C NMR chemical shifts of diaza-tripeptide **2.6** in methanol (27.9 mM) at 298 K

Residue	δ CO (ppm)	δ C_α (ppm)	δ CH_β (ppm)	δ Other carbons (ppm)
Ac	173.6			CH_3 21.0
aLys[1]	158.8		49.0	γ CH_2 25.1, δ CH_2 25.8, ε CH_2 40.6
aAla[2]	160.4		36.6	
Ser[3]	176.1	57.8	63.6	

Table S11. Amide proton chemical shifts and NMR conformational parameters for compound **2.6** in methanol. A, B, C and D letters correspond to the four observed conformers, with respective populations of 42%, 27%, 19%, 12%.

Residue	δ NH (ppm) [a]	ΔδNH/ΔT (ppb/K)	$^3J_{HN-H\alpha}$ (Hz) [a]	$^3J_{H\alpha-H\beta(\beta')}$ (Hz) [b]
aLys[1]	10.71 (A), 10.69 (B) 10.76 (C), 10.67 (D)	–4.8 (A), –5.4 (B) –5.0 (C), –5.5 (D)	-	
aAla[2]	9.82 (A), 9.71 (B) 9.68 (C), 9.58 (D)	–4.4 (A), –4.8 (B) –4.0 (C), –4.2 (D)	-	
Ser[3]	6.98 (A), 6.83 (B) 6.81 (C), 6.69 (D)	–3.3 (A), –2.6 (B) –3.0 (C), –2.2 (D)	8.2 (A), 8.0 (B) 7.6 (C), br (D)	5.0, 4.8
$NH_{2\ Z}$ $NH_{2\ E}$	7.70 (A), 7.78 (B) 7.64 (C), 7.70 (D)	–7.1 (A), –7.8 (B) –6.8 (C), –7.1 (D)		
OH	7.83 (A), 7.94 (B) 8.07 (C), 8.11 (D)	–4.9 (A), –5.6 (B) –5.8 (C), –5.4 (D)		
	5.95 (A), 6.19 (B) 5.93 (C), 6.09 (D)	–8.1 (A), –7.0 (B) –12.2 (C), –7.3 (D)		

[a] measured at 228 K; br, broad peak

[b] average value, measured at 298 K

HPLC purity: ATLANTIS T3 column (C18, 2.1 x 150mm-3µm); ACN /H_2O + 0.1 % TFA, gradient 1–30 % in 15 min; R_t = 1.96 min, 100 %.

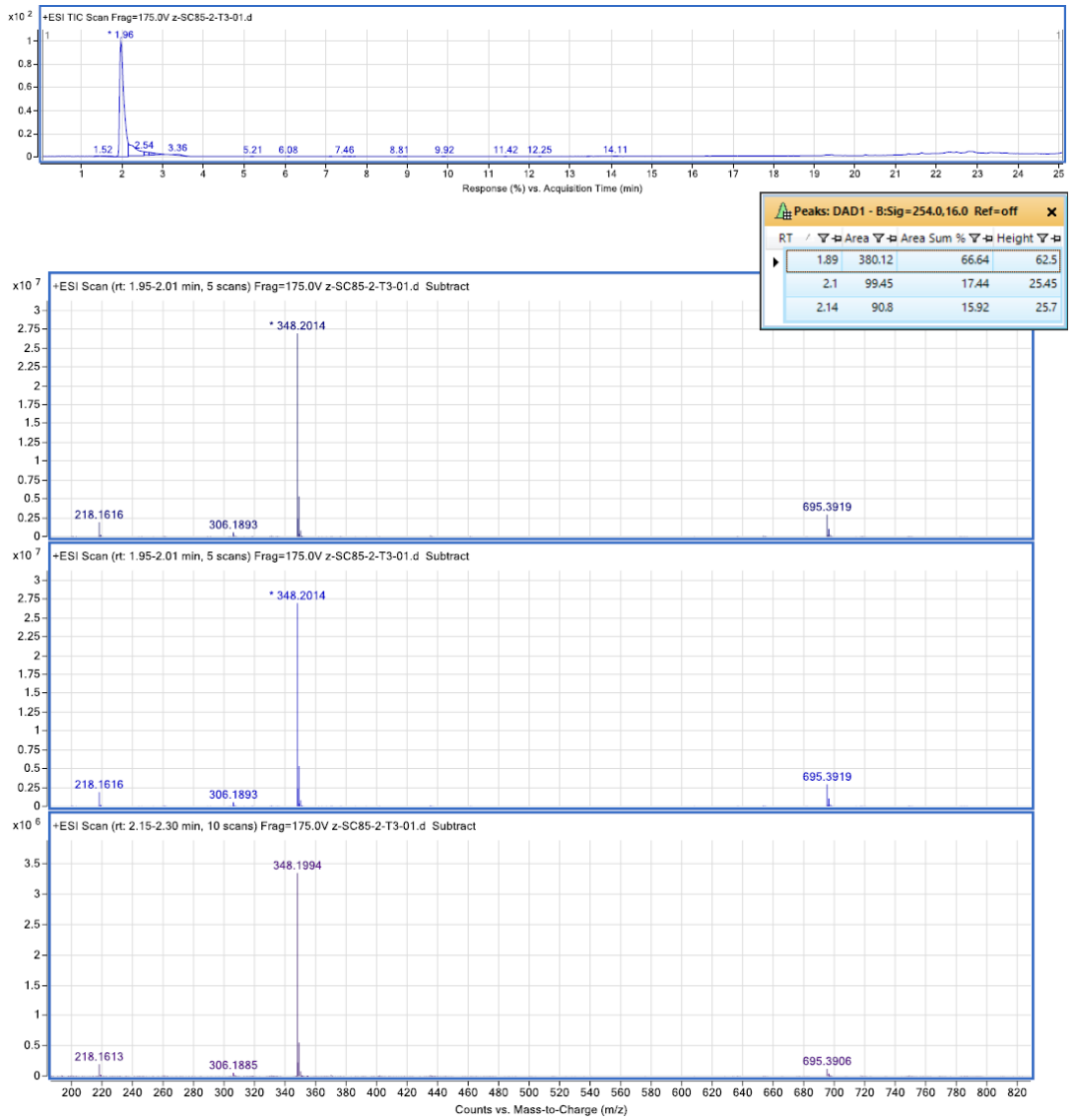

(S)-2-(2-acetyl-1-(4-aminobutyl)hydrazine-1-carbonyl)-N-(1-amino-3-hydroxy-1-oxopropan-2-yl)-1-isobutylhydrazine-1-carboxamide·HCOOH (compound 2.7)

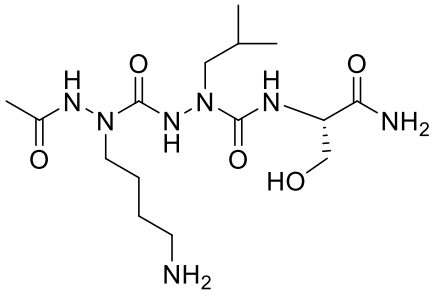

Compound **2.7** was synthesized from **2.33b** (60 mg, 0.10 mmol) as a white solid (25 mg, 0.06 mmol, yield: 59%) by following the synthesis procedure of **2.5** (Preparative HPLC of **2.7** was performed using linear gradients of 0.5-20 % ACN in H_2O containing 0.1% formic acid in 10 min).

HRMS (ESI): Calcd for $[C_{15}H_{31}N_7O_5 + H]^+$: 390.2459, found: 390.2460.

NMR data for compound **2.7** (The detailed spectra can be accessible in the supporting information of this article: DOI: 10.1039/D2OB01225A)

Table S12. ^{1}H NMR chemical shifts of diaza-tripeptide **2.7** in water (10 mM) at 278 K. A, B, C and D letters correspond to the four observed conformers.

Residue	δ NH (ppm)	δ H_α (ppm)	δ H_β (ppm)	δ Other protons (ppm)
Ac				CH_3 2.09
aLys[1]	10.61, 10.41		3.72, 3.36	γ CH_2 1.62, δ CH_2 1.66, ε CH_2 3.00 NH_3^+ 7.62
aLeu[2]	9.52 (A, B) 9.48 (C, D)		3.47, 2.97	γ CH 1.76, δδ CH_3 0.89
Ser[3]	6.96 (A, B) (6.89, 6.80) (C, D)	4.28	3.87	OH 6.06, 5.93
$NH_{2\ Z}$	7.31 (A, B) (7.24, 7.23) (C, D)			
$NH_{2\ E}$	(7.88, 7.76) (C, D) 7.74 (B), 7.66 (A)			

Table S13. ^{13}C NMR chemical shifts of diaza-tripeptide **2.7** in water (10 mM) at 308 K

Residue	δ CO (ppm)	δ C_α (ppm)	δ CH_β (ppm)	δ Other carbons (ppm)
Ac	176.3			CH_3 23.0
aLys[1]	160.5	-	50.9	γ CH_2 26.3, δ CH_2 26.8, ε CH_2 42.1
aLeu[2]	162.5	-	58.6	γ CH 28.7, δ,δ CH_3 22.1
Ser[3]	178.4	59.2	64.4	

Table S14. ^{1}H NMR chemical shifts of diaza-tripeptide **2.7** in methanol (25.6 mM) at 298 K

Residue	δ NH (ppm)	δ H_α (ppm)	δ H_β (ppm)	δ Other protons (ppm)
Ac				CH_3 2.06
aLys[1]	n.d.		3.73, 3.37	γ CH_2 1.58, δ CH_2 1.71, ε CH_2 2.93, 2.88
			3.62, 3.43	$NH3^+$ n.d.
aLeu[2]	n.d.		3.57, 3.00	γ CH 1.84, δ,δ CH_3 0.90
Ser[3]	6.70, 6.52	4.24	3.87, 3.83	OH n.d.
$NH_{2\ Z,\ E}$	7.17, 7.55			

Table S15. ^{13}C NMR chemical shifts of diaza-tripeptide **2.7** in methanol (25.6 mM) at 298 K

Residue	δ CO (ppm)	δ C_α (ppm)	δ CH_β (ppm)	δ Other carbons (ppm)
Ac	173.9[a]			CH_3 21.1
aLys[1]	158.8	-	49.2	γ CH_2 25.1, δ CH_2 26.2, ε CH_2 40.8
aLeu[2]	160.5	-	57.3	γ CH 27.9, δ,δ CH_3 20.6
Ser[3]	176.5	58.1	63.6	

[a] Not observed on 1D ^{13}C spectrum, assigned via $^{2}J_{CH3\text{-}CO}$ correlation peak on HMBC

Table S16. Amide proton chemical shifts and NMR conformational parameters for compound **2.7** in methanol. A, B, C and D letters correspond to the four observed conformers, with respective populations of 55%, 22%, 17%, 6%.

Residue	δ NH (ppm) [a]	ΔδNH/ΔT (ppb/K)	$^3J_{HN-H\alpha}$ (Hz) [a]	$^3J_{H\alpha-H\beta(\beta')}$ (Hz) [b]
aLys[1]	n.d.	-		
aLeu[2]	9.82 (A), 9.74 (B) 9.70 (C), 9.62 (D)	–4.3 (A), –5.0 (B) –4.6 (C), –5.0 (D)		
Ser[3]	6.94 (A), 6.79 (B) 6.71 (C), 6.58 (D)	–2.7 (A), –2.9 (B) –2.4 (C), –2.2 (D)	8.2 (A), 7.7 (B) 7.2 (C), 6.8 (D)	5.0
$NH_{2\ Z}$	7.69 (A), 7.76 (B) 7.59 (C), 7.69 (D)	–6.9 (A), –7.4 (B) –6.4 (C), –6.9 (D)		
$NH_{2\ E}$	7.76 (A), 8.03 (B) 7.97 (C), 8.13 (D)	–4.8 (A), –5.3 (B) –6.1 (C), –5.3 (D)		

[a] measured at 228 K; n.d. not detected

[b] average value, measured at 298 K.

HPLC purity: ATLANTIS T3 column (C18, 2.1 x 150mm-3µm); ACN /H_2O + 0.1 % TFA, gradient 1–30 % in 15 min; R_t = 9.74 and 10.24 min, 100 %.

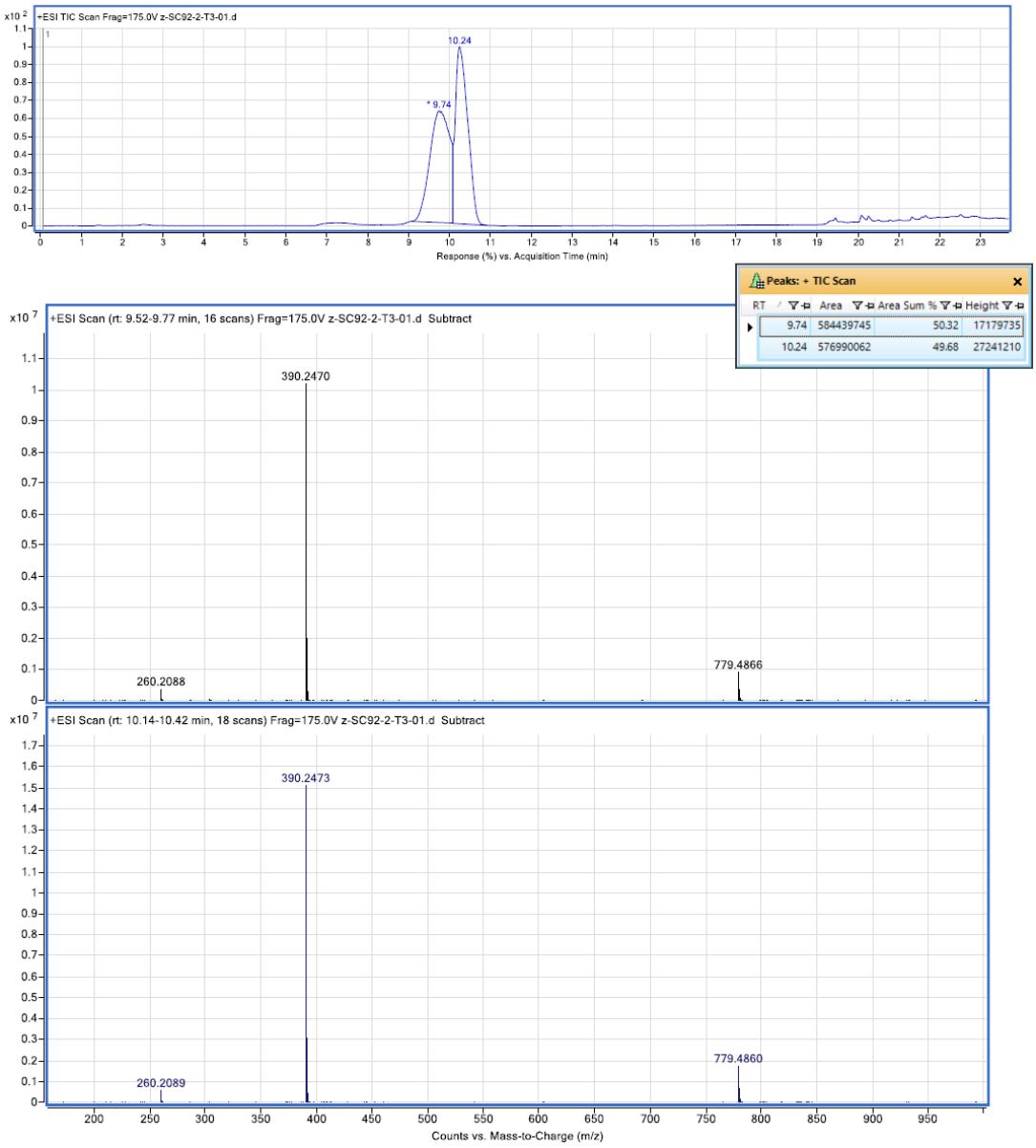

Cbz-protected 4-aminobutyraldehyde diethylacetal (compound 2.8)

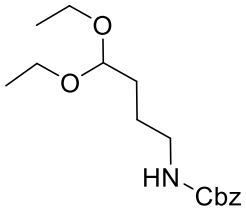

To a mixture of 4-aminobutyraldehyde diethylacetal (1.50 g, 9.30 mmol) and TEA (2.58 mL, 18.61 mmol) in DCM (30 mL) was added benzyl chloroformate (2.12 mL, 18.61 mmol) dropwise at 0°C. The mixture was stirred at room temperature overnight. The volatiles were removed under reduced pressure and the residue was dissolved in EtOAc and H_2O to do extraction. Organic layer was washed with brine, dried over Na_2SO_4, filtrated, concentrated and purified by chromatography on silica gel (elution with cyclohexane/EtOAc 3:1) to give 2.42 g (8.20 mmol, 88%) of **2.8** as a colourless oil. ^{1}H NMR (300 MHz, $CDCl_3$) δ 7.41 – 7.28 (m, 5H, aromatic H), 5.10 (s, 2H, Ph$\underline{CH_2}$), 4.87 (brs, 1H, CONH), 4.47 (t, J = 5.1 Hz, 1H, NHCH$_2$CH$_2$CH$_2\underline{CH}$), 3.71 – 3.57 (m, 2H, O$\underline{CH_2}$CH$_3$), 3.48 (q, 7.0 Hz, 2H, O$\underline{CH_2}$CH$_3$), 3.28 – 3.14 (m, 2H, NH$\underline{CH_2}$CH$_2$CH$_2$CH), 1.72 – 1.50 (m, 4H, NHCH$_2\underline{CH_2}\underline{CH_2}$CH), 1.19 (t, J = 7.0 Hz, 6H, OCH$_2\underline{CH_3}$).

benzyl 2-hydroxypyrrolidine-1-carboxylate (compound 2.9)

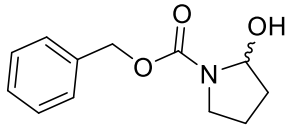

Compound **2.8** (400 mg, 1.36 mmol) was dissolved in AcOH/H_2O (2 mL/1 mL) and the mixture was stirred at room temperature overnight. The volatiles were removed under reduced pressure to give 300 mg (1.36 mmol, 100%) of **2.9** as a colourless oil. ^{1}H NMR (300 MHz, $CDCl_3$) δ 7.41 – 7.28 (m, 5H, aromatic H), 5.51 (m, 1H, NCH), 5.22 – 5.09 (m, 2H, Ph$\underline{CH_2}$), 3.59 (m, 1H, N$\underline{CH_2}$CH$_2$CH$_2$), 3.36 (m, 1H, N$\underline{CH_2}$CH$_2$CH$_2$), 2.16 – 1.75 (m, 4H, NCH$_2\underline{CH_2}\underline{CH_2}$).

benzyl 2-acetylhydrazine-1-carboxylate (compound 2.10)

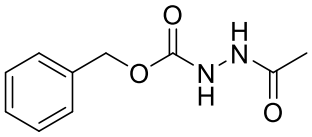

Benzyl carbazate (3.00 g, 18.05 mmol) and collidine (2.17 mL, 21.66 mmol) were dissolved in DCM (60 mL). Acetic anhydride (2.07 mL, 21.66 mmol) was added to the solution dropwise at 0°C under an argon atmosphere. The mixture was stirred at room temperature for 2 h. 10% citric acid aqueous solution (40 mL) was added to do extraction. Organic layer was washed with brine, dried over Na_2SO_4, filtrated, concentrated and purified by chromatography on silica gel (elution with 3% MeOH in DCM) to give 2.60 g (12.50 mmol, 69%) of **2.10** as a white solid. ^{1}H NMR (300 MHz, $CDCl_3$) δ 7.47 – 7.30 (m, 6H, aromatic H and CONH), 6.84 (s, 1H, CONH), 5.22 (s, 2H, Ph$\underline{CH_2}$), 2.44 (s, 3H, $\underline{CH_3}$CO).

acetylhydrazide (compound 2.11)

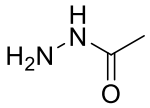

To a solution of **2.10** (683 mg, 3.28 mmol) in MeOH (10 mL) was added 10% Pd/C (136 mg). The mixture was stirred at room temperature under a hydrogen atmosphere overnight. Then the suspension was filtrated through a pad of celite and concentrated under reduced pressure to give 240 mg (3.24 mmol, 99%) of **2.11** as a white solid. ^{1}H NMR (300 MHz, DMSO-d_6) δ 8.90 (s, 1H, CONH), 4.12 (s, 2H, NH_2), 2.51 (s, 3H, CH_3).

tert-butyl 2-(4-(((benzyloxy)carbonyl)amino)butyl)hydrazine-1-carboxylate (compound 2.12a)

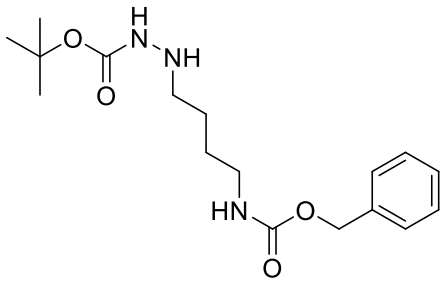

To a solution of *t*-butyl carbazate (358 mg, 2.71 mmol) in dry THF (14 mL) were added **2.9** (599 mg, 2.71 mmol) and APTS (464 mg, 2.44 mmol). The mixture was stirred at room temperature for 5 h. Then $NaBH_3CN$ (255 mg, 4.07 mmol) and AcOH (310 μL, 5.42 mmol) were added to the solution successively. The suspension was stirred at room temperature overnight and then the volatiles were removed under reduced pressure. The residue was dissolved in EtOAc and H_2O to do extraction. The organic layer was dried over Na_2SO_4, filtrated and concentrated under reduced

pressure. The residue was dissolved in EtOH, heated at reflux for 1 h and concentrated under reduced pressure. The crude was purified by chromatography on silica gel (elution with cyclohexane/EtOAc 1:1) to give 378 mg (1.12 mmol, 41%) of **2.12a** as a white solid. ^{1}H NMR (300 MHz, $CDCl_3$) δ 7.44 – 7.20 (m, 5H, aromatic H), 6.10 (brs, 1H, CONH), 5.09 (s, 2H, Ph$\underline{CH_2}$), 4.98 (brs, 1H, CONH), 3.90 (brs, 1H, NH), 3.29 – 3.05 (m, *J* = 6.4 Hz, 2H, NHNH$\underline{CH_2}CH_2$), 2.91 – 2.69 (m, *J* = 6.7 Hz, 2H, NH$\underline{CH_2}CH_2$), 1.63 – 1.27 (m, 13H, $CH_2\underline{CH_2}\underline{CH_2}CH_2$ and C($\underline{CH_3}$)$_3$); ^{13}C NMR (75 MHz, $CDCl_3$) δ 157.0(CO), 156.6(CO), 136.8(aromatic), 128.6(2C, aromatic), 128.2(3C, aromatic), 80.6($\underline{C}(CH_3)_3$), 66.7(Ph$\underline{C}H_2$), 51.7(NHNH$\underline{C}H_2CH_2$), 41.1(NH$\underline{C}H_2CH_2$), 28.5(3C, C($\underline{C}H_3$)$_3$), 27.6(NHCH$_2\underline{C}H_2$), 25.1(NHNHCH$_2\underline{C}H_2$).

Fmoc-protected-1-methylhydrazine (compound 2.13)

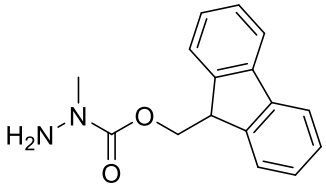

Methylhydrazine (300 mg, 6.51 mmol) and TEA (996 µL, 7.16 mmol) were dissolved in DCM (12 mL) under an argon atmosphere. A solution of 9-fluorenylmethyl chloroformate (1.35 g, 5.21 mmol) in dry DCM (6 mL) was added dropwise to the solution at -78°C. The mixture was stirred at -78°C for 10 min and then at room temperature for 1 h. After that, DCM and H_2O was added to do extraction. Organic layer was washed with brine, dried over Na_2SO_4, filtrated, concentrated and purified by chromatography on silica gel (elution with cyclohexane/EtOAc 1:1) to give 1.28 g (4.78 mmol, 92%) of **2.13** as a white solid. ^{1}H NMR (200 MHz, $CDCl_3$) δ 7.78 (d, *J* = 7.3 Hz, 2H, aromatic H), 7.60 (d, *J* = 7.3 Hz, 2H, aromatic H), 7.48 – 7.23 (m, 4H, aromatic H), 4.45 (d, *J* = 6.9 Hz, 2H, CH$\underline{CH_2}$O), 4.28 (t, *J* = 6.9 Hz, 1H, $\underline{CH}CH_2O$), 3.14 (s, 3H, NCH_3), 0.87 (brs, 2H, NH_2).

Boc-protected-2-isobutylhydrazine (compound 2.14)

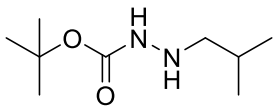

To a solution of *t*-butyl carbazate (2.00 g, 15.1 mmol) in dry THF (20 mL) was added isobutyraldehyde (4.13 mL, 45.3 mmol) and AcOH (0.78 mL, 13.6 mmol). The mixture was stirred

at room temperature overnight. Then the volatiles were removed under reduced pressure and the residue was dissolved in dry THF (30 mL) again. $NaBH_3CN$ (1.42g, 22.7 mmol) and AcOH (1.73 mL, 30.2 mmol) were added to the solution. The suspension was stirred at room temperature for 2 h and then the solvent was removed under reduced pressure. The residue was dissolved in a mixture of EtOAc/10% K_2CO_3 aqueous solution and extracted with EtOAc. The organic layer was washed with brine and concentrated under reduced pressure. The residue was dissolved in MeOH (18 mL) and treated with 1M NaOH aqueous solution (15.1 mmol). The suspension was stirred at room temperature for 1 h. The solvent was removed under reduced pressure and the residue was dissolved in a mixture of EtOAc/brine. Organic layer was dried over Na_2SO_4, filtrated, concentrated and purified by chromatography on silica gel (elution with cyclohexane/EtOAc 2:1) to give 2.24 g (11.91 mmol, 79%) of **2.14** as a colourless oil. ^{1}H NMR (300 MHz, $CDCl_3$) δ 6.00 (brs, 1H, CONH), 3.43 (brs, 1H, NH), 2.65 (d, *J* = 6.8 Hz, 2H, $\underline{CH_2}CH(CH_3)_2$), 1.72 (m, 1H, $CH_2\underline{CH}(CH_3)_2$), 1.45 (s, 9H, $C(\underline{CH_3})_3$), 0.92 (d, *J* = 6.6 Hz, 6H, $CH_2CH(\underline{CH_3})_2$).

1-((9H-fluoren-9-yl)methyl) 2-(tert-butyl) 1-isobutylhydrazine-1,2-dicarboxylate (compound 2.15)

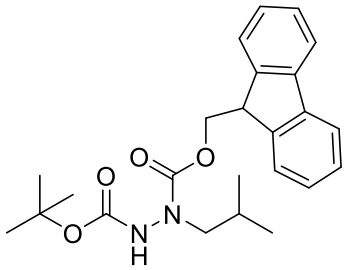

1-Boc-2-isobutylhydrazine **2.14** (400 mg, 2.12 mmol) and collidine (415 µL, 3.19 mmol) were dissolved in dry DCM (20 mL) under an argon atmosphere. Then a solution of 9-fluorenylmethyl chloroformate (550 mg, 2.12 mmol) in dry DCM (9 mL) was added dropwise under ice-cooling. The mixture was stirred at room temperature for 4 h. DCM (20 mL) was added and the mixture was successively washed with 10 % aqueous citric acid and brine, dried over anhydrous Na_2SO_4, filtrated and concentrated under reduced pressure. The residue was purified by chromatography on silica gel (elution with 10% EtOAc in cyclohexane) to give compound **2.15** as a white solid (680 mg, 1.66 mmol, yield: 78%). ^{1}H NMR (300 MHz, $CDCl_3$): δ 7.64 (dd, *J* = 7.4 Hz, 2H, aromatic H), 7.50 (d, *J* = 7.4 Hz, 2H, aromatic H), 7.33 – 7.12 (m, 4H, aromatic H), 6.45 (s, 1H, CONH), 4.35 (brd, 2H, $CH\underline{CH_2}O$), 4.12 (t, *J* = 6.8 Hz, 1H, $\underline{CH}CH_2O$), 3.18 (brd, 2H, NCH_2), 1.73 (brs, 1H, $\underline{CH}(CH_3)_2$),

1.35 (s, 9H, C($\underline{CH_3}$)$_3$), 0.76 (brd, 6H, CH($\underline{CH_3}$)$_2$); ^{13}C NMR (75 MHz, $CDCl_3$): δ 156.7(CO), 155.5(CO), 154.8(CO from rotamer), 143.9(2C, aromatic), 141.4(2C, aromatic), 127.8(2C, aromatic), 127.2(2C, aromatic), 125.2(2C, aromatic), 120.0(2C, aromatic), 81.6($\underline{C}(CH_3)_3$), 68.3(CH$\underline{C}H_2O$), 58.0(NCH_2), 57.6(NCH_2 from rotamer), 47.3($\underline{C}HCH_2O$), 28.3(3C, C($\underline{C}H_3$)$_3$), 26.8($\underline{C}H(CH_3)_2$), 20.0(2C, CH($\underline{C}H_3$)$_2$); HRMS (ESI): Calcd for $[C_{24}H_{30}N_2O_4 + Na]^+$: 433.2103, found: 433.2090.

Fmoc-protected-1-isobutylhydrazine·HCl (compound 2.16)

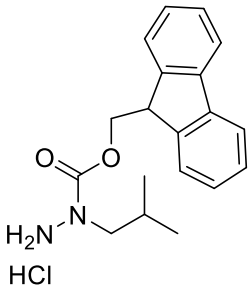

To a solution of **2.15** (550 mg, 1.34 mmol) in MeOH (10 mL) was added HCl 4M in dioxane (6.7 mL, 26.81 mmol) under ice-cooling. The mixture was stirred at room temperature overnight. Then the volatiles were evaporated under reduced pressure to give a white solid. The solid was washed with cyclohexane (10 ml), filtered and dried under reduced pressure to give compound **2.16** as a white solid (437 mg, 1.26 mmol, yield: 94%). ^{1}H NMR (300 MHz, Methanol-d_4): δ 7.81 (d, J = 7.4 Hz, 2H, aromatic H), 7.62 (d, J = 7.4 Hz, 2H, aromatic H), 7.46 – 7.27 (m, 4H, aromatic H), 4.82 (d, J = 4.4 Hz, 2H, CH$\underline{CH_2}$O), 4.30 (t, J = 4.4 Hz, 1H, $\underline{CH}CH_2O$), 2.92 (d, J = 7.5 Hz, 2H, NCH_2), 1.55 (m, 1H, $\underline{CH}(CH_3)_2$), 0.60 (d, J = 6.6 Hz, 6H, CH($\underline{CH_3}$)$_2$); ^{13}C NMR (75 MHz, Methanol-d_4): δ 156.1(CO), 144.8(2C, aromatic), 142.9(2C, aromatic), 128.9(2C, aromatic), 128.3(2C, aromatic), 125.6(2C, aromatic), 121.0(2C, aromatic), 69.4(CH$\underline{C}H_2O$), 57.2(NCH_2), 48.4($\underline{C}HCH_2O$), 27.7($\underline{C}H(CH_3)_2$), 19.5(2C, CH($\underline{C}H_3$)$_2$); HRMS (ESI): Calcd for $[C_{19}H_{22}N_2O_2 + H]^+$: 311.1760, found: 311.1759.

Boc-Ser(Bn)-NH$_2$ (compound 2.17)

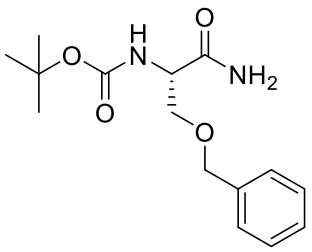

Boc-Ser(Bn)-OH (2.00 g, 6.77 mmol) was dissolved in 12 mL DCM/DMF. EDC (2.81 g, 10.16 mmol) and HOBt (1.56 g, 10.16 mmol) were added at room temperature. The mixture was stirred for 30 min and then 7M NH_3 in MeOH (2.9 mL, 20.32 mmol) were added. The reaction was stirred at room temperature for 4 h and then evaporated under reduced pressure. The residue was dissolved in EtOAc (30 mL) and washed with 10% $NaHCO_3$ aqueous solution and brine successively, dried over anhydrous Na_2SO_4 and concentrated under reduced pressure. The crude product was purified by silica column chromatography using (elution with 10% MeOH in DCM) as eluent to give **2.17** as a white solid (1.56 g, 5.30 mmol, yield: 78%). ^{1}H NMR (300 MHz, $CDCl_3$) δ 7.35 – 7.06 (m, 5H, aromatic H), 6.43 (brs, 1H, CONH), 6.04 (brs, 1H, CONH), 5.43 (d, *J* = 7.2 Hz, 1H, CONH), 4.55 – 4.39 (m, 2H, Ph$\underline{CH_2}$), 4.23 (m, 1H, $\underline{CH}CH_2O$), 3.79 (dd, *J* = 9.4, 4.2 Hz, 1H, $CH\underline{CH_2}O$), 3.51 (dd, *J* = 9.4, 6.4 Hz, 1H, $CH\underline{CH_2}O$), 1.37 (s, 9H, $C(\underline{CH_3})_3$); ^{13}C NMR (75 MHz, $CDCl_3$) δ 173.1(CO), 155.6(CO), 137.5(aromatic), 128.6(2C, aromatic), 128.0(aromatic), 127.9(2C, aromatic), 80.3($\underline{C}(CH_3)_3$), 73.5(Ph$\underline{C}H_2$), 70.0($CH\underline{C}H_2O$), 53.8($\underline{C}HCH_2O$), 28.4(3C, $C(\underline{C}H_3)_3$); HRMS (ESI): Calcd for $[C_{15}H_{22}N_2O_4 + Na]^+$: 317.1477, found: 317.1473.

Ser(Bn)-NH_2·HCl (compound 2.18)

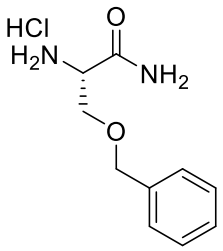

To a solution of **2.17** (1.60 g, 5.44 mmol) in dioxane (20 mL) was add HCl 4M in dioxane (27 mL, 108.78 mmol) under ice-cooling. The mixture was stirred at room temperature for 5 h. Then the volatiles were evaporated under reduced pressure to give a white solid. The solid was washed with Et_2O (20 ml), filtered and dried under reduced pressure to give compound **2.18** as a white solid (1.06

g, 4.6 mmol, yield: 85%). ^{1}H NMR (300 MHz, Methanol-d_4): δ 7.42 – 7.24 (m, 5H, aromatic H), 4.70 – 4.54 (m, 2H, Ph<u>C</u>H$_2$), 4.13 (dd, J = 6.2, 3.9 Hz, 1H, <u>C</u>HCH$_2$O), 3.95 – 3.76 (m, 2H, CH<u>C</u>H$_2$O); ^{13}C NMR (75 MHz, Methanol-d_4): δ 169.9(CO), 138.5(aromatic), 129.5(2C, aromatic), 129.1(3C, aromatic), 74.6(Ph<u>C</u>H$_2$), 69.1(CH<u>C</u>H$_2$O), 54.5(<u>C</u>HCH$_2$O); HRMS (ESI): Calcd for [$C_{10}H_{14}N_2O_2$ + H]$^+$: 195.1128, found: 195.1126.

2-(tert-butyl) 1-(4-nitrophenyl) 1-(4-(((benzyloxy)carbonyl)amino)butyl)hydrazine-1,2-dicarboxylate (compound 2.19)

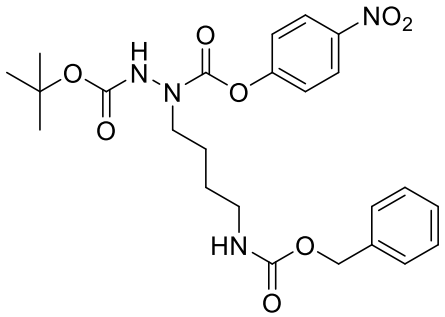

To a solution of **2.12a** (220 mg, 0.65 mmol) in dry DCM (8 mL) were added 4-nitrophenylchloroformate (197 mg, 0.98 mmol) and pyridine (115 µL, 1.43 mmol). The mixture was stirred at room temperature for 5 h. Then the solvent was removed under reduced pressure and the residue was dissolved in EtOAc, washed with 10% K_2CO_3 aqueous solution, 10% citric acid aqueous solution and brine successively. The organic layer was dried over Na_2SO_4, filtrated, concentrated and purified by chromatography on silica gel (elution with cyclohexane/EtOAc 2.5:1) to give 242 mg (0.48 mmol, 74%) of **2.19** as a colourless oil. ^{1}H NMR (300 MHz, $CDCl_3$) δ 8.22 (d, J = 9.0 Hz, 2H, aromatic H), 7.40 – 6.98 (m, 8H, aromatic H and CONH), 5.20 (brs, 1H, CONH), 5.11 (s, 2H, Ph<u>C</u>H$_2$), 3.76 – 3.48 (m, 2H, NHN<u>C</u>H$_2$CH$_2$), 3.32 – 3.08 (m, 2H, NH<u>C</u>H$_2$CH$_2$), 1.81 – 1.55 (m, 4H, CH$_2$<u>C</u>H$_2$<u>C</u>H$_2$CH$_2$), 1.49 (s, 9H, C(<u>C</u>H$_3$)$_3$); ^{13}C NMR (75 MHz, $CDCl_3$) δ 156.7(CO), 156.0(CO), 155.0(CO), 153.8(aromatic), 145.1(aromatic), 136.6(aromatic), 128.5(2C, aromatic), 128.1(2C, aromatic), 128.0(aromatic), 125.1(2C, aromatic), 122.3(aromatic), 122.1(aromatic), 82.1(<u>C</u>(CH$_3$)$_3$), 66.6(Ph<u>C</u>H$_2$), 50.3(NHN<u>C</u>H$_2$CH$_2$), 40.6(NH<u>C</u>H$_2$CH$_2$), 28.2(3C, C(<u>C</u>H$_3$)$_3$), 27.0(NHCH$_2$<u>C</u>H$_2$), 24.1(NHNCH$_2$<u>C</u>H$_2$).

tert-butyl 2-(4-(((benzyloxy)carbonyl)amino)butyl)-2-(hydrazinecarbonyl)hydrazine-1-carboxylate (compound 2.20)

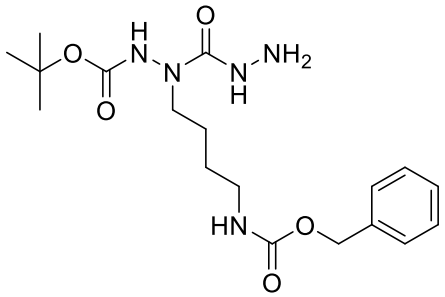

To a solution of **2.19** (242 mg, 0.48 mmol) in dry MeOH (6 mL) was added hydrazine hydrate (141 mg, 2.89 mmol). The mixture was stirred at room temperature overnight. Then the volatiles were removed under reduced pressure and the residue was purified by chromatography on silica gel (elution with 2.5-5% MeOH in DCM) to give 148 mg (0.37 mmol, 78%) of **2.20** as a white solid. ^{1}H NMR (300 MHz, $CDCl_3$) δ 7.59 (brs, 1H, CONH), 7.34 – 7.06 (m, 5H, aromatic H), 6.95 (brs, 1H, CONH), 5.49 (brs, 1H, CONH), 4.98 (s, 2H, Ph$\underline{CH_2}$), 3.64 (brs, 2H, NH_2), 3.50 – 3.24 (m, 2H, NHN$\underline{CH_2}CH_2$), 3.15 – 2.92 (m, 2H, NH$\underline{CH_2}CH_2$), 1.51 – 1.24 (m, 13H, $CH_2\underline{CH_2}\underline{CH_2}CH_2$ and C($\underline{CH_3}$)$_3$); ^{13}C NMR (75 MHz, $CDCl_3$) δ 160.2(CO), 156.8(CO), 154.8(CO), 136.7(aromatic), 128.4(2C, aromatic), 127.9(3C, aromatic), 81.8($\underline{C}(CH_3)_3$), 66.5(Ph$\underline{C}H_2$), 48.1(NHN$\underline{C}H_2CH_2$), 40.6(NH$\underline{C}H_2CH_2$), 28.1(3C, C($\underline{C}H_3$)$_3$), 26.9(NHCH$_2\underline{C}H_2$), 24.3(NHNCH$_2\underline{C}H_2$).

phenyl 5-((tert-butoxycarbonyl)amino)-4,11-dioxo-13-phenyl-12-oxa-2,3,5,10-tetraazatridecanoate (compound 2.21)

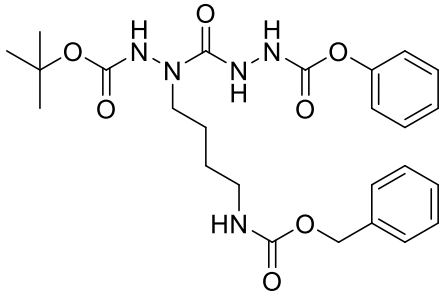

To a solution of **2.20** (340 mg, 0.86 mmol) in dry DCM (8 mL) were added phenyl chloroformate (126 μL, 1.00 mmol) and pyridine (168 μL, 2.09 mmol). The mixture was stirred at room temperature for 2 h. Then DCM and 10% citric acid aqueous solution were added to do extraction. Organic layer was washed with brine, dried over Na_2SO_4, filtrated, concentrated and purified by

chromatography on silica gel (elution with EtOAc/cyclohexane 1.5: 1) to give 435 mg (0.84 mmol, 98%) of **2.21** as a white solid. ^{1}H NMR (300 MHz, $CDCl_3$) δ 7.66 (brm, 3H, CONH), 7.39 – 7.21 (m, 7H, aromatic H), 7.20 – 6.99 (m, 3H, aromatic H), 5.29 (brs, 1H, CONH), 5.07 (s, 2H, Ph$\underline{CH_2}$), 3.80 – 3.27 (m, 2H, NHN$\underline{CH_2}CH_2$), 3.21 – 2.94 (m, 2H, NH$\underline{CH_2}CH_2$), 1.59 – 1.31 (m, 13H, $CH_2\underline{CH_2}\underline{CH_2}CH_2$ and C($\underline{CH_3}$)$_3$); ^{13}C NMR (75 MHz, $CDCl_3$) δ 158.1(CO), 156.9(CO), 155.8(CO), 155.0(CO), 150.8(aromatic), 136.8(aromatic), 129.4(2C, aromatic), 128.5(2C, aromatic), 128.1(3C, aromatic), 125.7(aromatic), 121.5(2C, aromatic), 82.4($\underline{C}(CH_3)_3$), 66.6(Ph$\underline{C}H_2$), 48.4(NHN$\underline{C}H_2CH_2$), 40.7(NH$\underline{C}H_2CH_2$), 28.2(3C, C($\underline{C}H_3$)$_3$), 27.0(NHCH$_2\underline{C}H_2$), 24.1(NHNCH$_2\underline{C}H_2$).

tert-butyl (S)-3-(4-(((benzyloxy)carbonyl)amino)butyl)-9-carbamoyl-4,7-dioxo-12-phenyl-11-oxa-2,3,5,6,8-pentaazadodecanoate (compound 2.22)

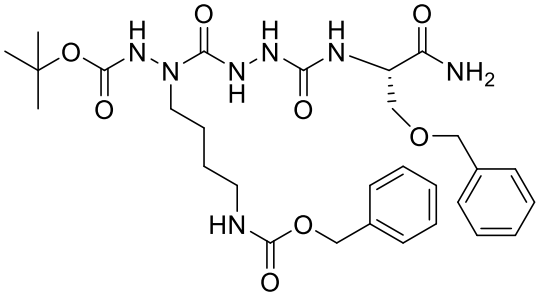

To a solution of **2.21** (433 mg, 0.84 mmol) in acetonitrile (30 mL) were successively added Ser(Bzl)-NH_2·HCl **2.18** (213 mg, 0.92 mmol) and TEA (584 μL, 4.20 mmol) at room temperature. The mixture was stirred at room temperature for 24 h. After removing the volatiles under reduced pressure, the crude was purified by chromatography on silica gel (elution with 3% MeOH in EtOAc) to give **2.22** as a colorless oil (365 mg, 0.59 mmol, yield: 71%). ^{1}H NMR (400 MHz, $CDCl_3$): δ 7.97 (brs, 2H, CONH), 7.49 – 7.19 (m, 11H, aromatic H and CONH), 7.08 (brs, 1H, CONH), 6.54 (brs, 1H, CONH), 6.29 (brs, 1H, CONH), 5.46 (brs, 1H, CONH), 5.04 (s, 2H, Ph$\underline{CH_2}$ from Cbz), 4.53 – 4.38 (m, 3H, $\underline{CH}CH_2O$ and Ph$\underline{CH_2}$ from Bn), 3.81 (m, 1H, CH$\underline{CH_2}$O), 3.71 – 3.24 (m, 3H, CH$\underline{CH_2}$O and NHN$\underline{CH_2}CH_2$), 3.17 – 2.99 (m, 2H, NH$\underline{CH_2}CH_2$), 1.52 – 1.34 (m, 13H, $CH_2\underline{CH_2}\underline{CH_2}CH_2$ and C($\underline{CH_3}$)$_3$); ^{13}C NMR (100 MHz, $CDCl_3$): δ 174.2(CO), 159.7(CO), 158.8(CO), 156.8(CO), 154.9(CO), 137.5(aromatic), 136.7(aromatic), 128.5(2C, aromatic), 128.4(2C, aromatic), 128.1(aromatic), 128.0(aromatic), 127.7 (4C, aromatic), 82.3($\underline{C}(CH_3)_3$), 73.3(Ph$\underline{C}H_2$ from Bn), 69.6(CH$\underline{C}H_2$O), 66.5(Ph$\underline{C}H_2$ from Cbz), 53.9($\underline{C}HCH_2O$), 48.4(NHN$\underline{C}H_2CH_2$),

40.6(NH<u>C</u>H$_2$CH$_2$), 28.2(3C, C(<u>C</u>H$_3$)$_3$), 26.8(NHCH$_2$<u>C</u>H$_2$), 23.9(NHNCH$_2$<u>C</u>H$_2$); HRMS (ESI): Calcd for [$C_{29}H_{41}N_7O_8$ + Na]$^+$: 638.2914, found: 638.2914.

benzyl (S)-(10-acetamido-4-carbamoyl-6,9-dioxo-1-phenyl-2-oxa-5,7,8,10-tetraazatetradecan-14-yl)carbamate (compound 2.23)

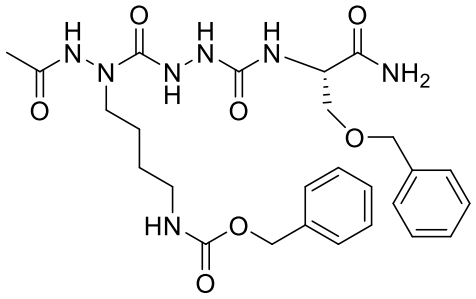

To a solution of **2.22** (100 mg, 0.16 mmol) in dioxane (2 mL) was added HCl 4M in dioxane (2.44 mL, 9.75 mmol) under ice-cooling. The mixture was stirred at room temperature for 3 h. The volatiles were evaporated under reduced pressure to give a white solid. The solid was dissolved in DCM (6 mL) followed by the addition of acetic anhydride (20 µL, 0,21 mmol) and pyridine (43 µL, 0.41 mmol) at room temperature. The mixture was stirred overnight. The volatiles were evaporated under reduced pressure to give a crude, which was purified by chromatography on silica gel (elution with 5-10% MeOH in DCM) to give **2.23** as a white solid (68 mg, 0.12 mmol, yield: 75%). ^{1}H NMR (400 MHz, DMSO-d_6) δ 9.97 (brs, 1H, CONH), 8.66 (brs, 1H, CONH), 7.81 (s, 1H, CONH), 7.42 – 7.07 (m, 13H, aromatic H and CONH), 6.33 (d, J = 8.1 Hz, 1H, CONH), 5.00 (s, 2H, Ph<u>C</u>H$_2$ from Cbz), 4.49 (s, 2H, Ph<u>C</u>H$_2$ from Bn), 4.26 (dt, J = 8.3, 5.2 Hz, 1H, <u>C</u>HCH$_2$O), 3.67 (dd, J = 9.7, 5.7 Hz, 1H, CH<u>C</u>H$_2$O), 3.57 (dd, J = 9.7, 4.6 Hz, 1H, CH<u>C</u>H$_2$O), 3.36 – 3.20 (m, 2H, overlap with H$_2$O, NHN<u>C</u>H$_2$CH$_2$), 2.98 (q, J = 6.3 Hz, 2H, NH<u>C</u>H$_2$CH$_2$), 1.86 (s, 3H, <u>C</u>H$_3$CO), 1.48 – 1.32 (m, 4H, C(<u>C</u>H$_3$)$_3$); ^{13}C NMR (100 MHz, DMSO-d_6) δ 172.2(CO), 169.2(CO), 158.2(CO), 157.6(CO), 156.0(CO), 138.2(aromatic), 137.2(aromatic), 128.3(2C, aromatic), 128.1(2C, aromatic), 127.7(2C, aromatic), 127.4(2C, aromatic), 127.3(2C, aromatic), 72.1(Ph<u>C</u>H$_2$ from Bn), 70.3(CH<u>C</u>H$_2$O), 65.1(Ph<u>C</u>H$_2$ from Cbz), 53.2(<u>C</u>HCH$_2$O), 47.4(NHN<u>C</u>H$_2$CH$_2$), 45.5(NH<u>C</u>H$_2$CH$_2$), 26.5(NHCH$_2$<u>C</u>H$_2$), 24.1(NHNCH$_2$<u>C</u>H$_2$), 21.0(<u>C</u>H$_3$CO); HRMS (ESI): Calcd for [$C_{26}H_{35}N_7O_7$ + H]$^+$: 558.2676, found: 558.2674.

1-((9H-fluoren-9-yl)methyl) 2-(4-nitrophenyl) 1-methylhydrazine-1,2-dicarboxylate (compound 2.29a)

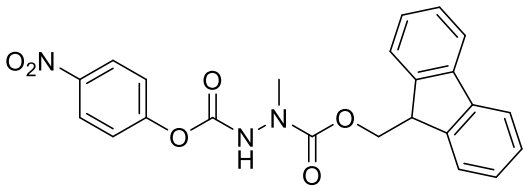

To a solution of 1-Fmoc-1-methylhydrazine **2.13** (300 mg, 1.12 mmol) in dry DCM (20 mL) was added pyridine (0.27 ml, 3.36 mmol) at room temperature under an argon atmosphere. Then a solution of 4-nitrophenylchloroformate (338 mg, 1.68 mmol) in dry DCM (10 mL) was added dropwise under ice-cooling. The mixture was stirred at room temperature overnight. The reaction mixture was successively washed with 10 % aqueous citric acid, 10 % aqueous K_2CO_3, and brine, dried over anhydrous Na_2SO_4 and concentrated under reduced pressure. The crude product (solid) was added to DCM (5 mL) and stirred under ice-cooling for 5 min. The precipitate was filtered and dried under reduced pressure to give **2.29a** as a white solid (370 mg, 0.85 mmol, yield: 76%). ^{1}H NMR (300 MHz, $CDCl_3$): δ 8.18 (d, *J* = 8.8 Hz, 2H, aromatic H), 7.69 (d, *J* = 7.6 Hz, 2H, aromatic H), 7.51 (d, *J* = 7.5 Hz, 2H, aromatic H), 7.38 – 6.96 (m, 7H, aromatic H and CONH), 4.45 (d, *J* = 6.7 Hz, 2H, CH$\underline{CH_2}$O), 4.19 (t, *J* = 6.7 Hz, 1H, $\underline{CH}CH_2O$), 3.21 (s, 3H, NCH_3); HRMS (ESI): Calcd for $[C_{23}H_{19}N_3O_6 + Na]^+$: 456.1172, found: 456.1182.

1-((9H-fluoren-9-yl)methyl) 2-(4-nitrophenyl) 1-isobutylhydrazine-1,2-dicarboxylate (compound 2.29b)

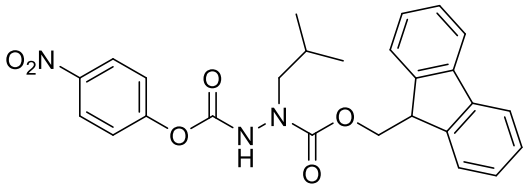

To a suspension of 1-Fmoc-1-isobutylhydrazine·HCl **2.16** (430 mg, 1.24 mmol) in dry DCM (20 mL) was added pyridine (1 mL, 12.42 mmol) at room temperature under an argon atmosphere. Then a solution of 4-nitrophenylchloroformate (626 mg, 3.11 mmol) in dry DCM (20 mL) was added dropwise under ice-cooling. The mixture was stirred at room temperature overnight. The reaction mixture was successively washed with 10 % aqueous citric acid, 10 % aqueous K_2CO_3, and brine, dried over anhydrous Na_2SO_4, filtrated and concentrated under reduced pressure. The residue was

purified by chromatography on silica gel (elution with 10-15% EtOAc in cyclohexane) to give **2.29b** as a white solid (350 mg, 0.74 mmol, yield: 59%). ^{1}H NMR (300 MHz, $CDCl_3$): δ 8.09 (d, *J* = 8.6 Hz, 2H, aromatic H), 7.64 (d, *J* = 7.6 Hz, 2H, aromatic H), 7.46 (d, *J* = 7.6 Hz, 2H, aromatic H), 7.39 – 6.97 (m, 7H, aromatic H and CONH), 4.46 (d, *J* = 6.3 Hz, 2H, CH$\underline{C}H_2$O), 4.14 (t, *J* = 6.3 Hz, 1H, $\underline{CH}CH_2O$), 3.44 – 2.99 (m, 2H, NCH_2), 1.77 (m, 1H, $\underline{CH}(CH_3)_2$), 1.01 – 0.50 (m, 6H, CH($\underline{C}H_3)_2$); ^{13}C NMR (75 MHz, $CDCl_3$): δ 156.4(CO), 155.2(CO), 153.0(aromatic), 145.2(aromatic), 143.6(2C, aromatic), 141.5(2C, aromatic), 128.0(2C, aromatic), 127.2(2C, aromatic), 125.2(2C, aromatic), 124.9(2C, aromatic), 121.9 (2C, aromatic), 120.1(2C, aromatic), 68.5(CH$\underline{C}H_2$O), 57.9(NCH_2), 47.2($\underline{C}HCH_2O$), 26.8($\underline{C}H(CH_3)_2$), 19.9(2C, CH($\underline{C}H_3)_2$); HRMS (ESI): Calcd for [$C_{26}H_{25}N_3O_6$ + Na]$^+$: 498.1636, found: 498.1637.

(9H-fluoren-9-yl)methyl 5-((tert-butoxycarbonyl)amino)-2-methyl-4,11-dioxo-13-phenyl-12-oxa-2,3,5,10-tetraazatridecanoate (compound 2.30a)

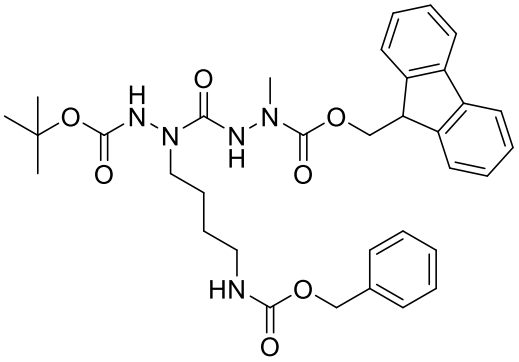

To a solution of **2.29a** (370 mg, 0.85 mmol) in acetonitrile (30 mL) were successively added **2.12a** (259 mg, 0.77 mmol) and DIPEA (0.18 ml, 1.03 mmol) at room temperature. The mixture was stirred at room temperature for 5 h. After removing the volatiles under reduced pressure, the residue was dissolved in EtOAc (40 mL). The solution was successively washed with 10 % aqueous K_2CO_3, 10 % aqueous citric acid, and brine, dried over anhydrous Na_2SO_4 and concentrated under reduced pressure. The crude product was purified by chromatography on silica gel (elution with 1-2% MeOH in DCM) to give **2.30a** as a white solid (382 mg, 0.61 mmol, yield: 79%). ^{1}H NMR (300 MHz, $CDCl_3$): δ 7.68 (d, *J* = 7.5 Hz, 2H, aromatic H), 7.51 (d, *J* = 7.5 Hz, 2H, aromatic H), 7.37 – 7.12 (m, 9H, aromatic H), 7.01 (brs, 2H, CONH), 4.99 (s, 2H, Ph$\underline{C}H_2$), 4.80 (s, 1H, CONH), 4.49 – 4.24 (brm, 2H, CH$\underline{C}H_2$O), 4.16 (t, *J* = 6.6 Hz, 1H, $\underline{CH}CH_2O$), 3.63 – 3.27 (m, 2H, NHN$\underline{C}H_2CH_2$), 3.26

– 2.97 (m, 5H, NH$\underline{CH_2}CH_2$ and NCH_3), 1.46 (s, 4H, $CH_2\underline{CH_2}\underline{CH_2}CH_2$), 1.39 (s, 9H, $C(\underline{CH_3})_3$); ^{13}C NMR (75 MHz, $CDCl_3$) δ 157.5(CO), 157.1(from rotamer, CO), 156.8(2C, CO), 154.6(CO), 143.8(2C, aromatic), 141.3(2C, aromatic), 136.8(aromatic), 128.5(2C, aromatic), 128.0 (3C, aromatic), 127.8(2C, aromatic), 127.2(2C, aromatic), 125.2(2C, aromatic), 120.0(2C, aromatic), 82.1($\underline{C}(CH_3)_3$), 68.5(CH$\underline{C}H_2O$), 66.6(Ph$\underline{C}H_2$), 48.3(NHN$\underline{C}H_2CH_2$), 47.1($\underline{C}HCH_2O$), 40.7(NH$\underline{C}H_2CH_2$), 38.7(NCH_3), 38.1(from rotamer, NCH_3), 28.2(3C, $C(\underline{C}H_3)_3$), 27.1($NHCH_2\underline{C}H_2$), 24.1($NHNCH_2\underline{C}H_2$); HRMS (ESI): Calcd for $[C_{34}H_{41}N_5O_7 + H]^+$: 632.3084, found: 632.3091.

(9H-fluoren-9-yl)methyl 5-((tert-butoxycarbonyl)amino)-2-isobutyl-4,11-dioxo-13-phenyl-12-oxa-2,3,5,10-tetraazatridecanoate (compound 2.30b)

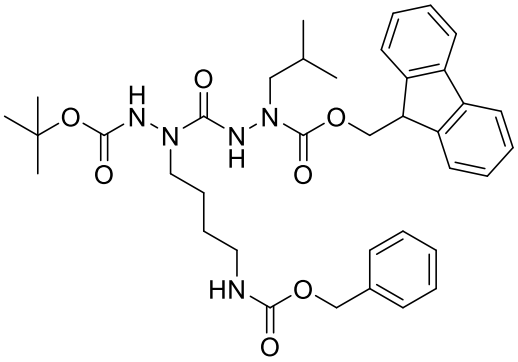

Compound **2.30b** was synthesized from **2.29b** (350 mg, 0.74 mmol) and **2.12a** (236 mg, 0.70 mmol) as a white solid (374 mg, 0.56 mmol, yield: 79%) by following the synthesis procedure of **2.30a**. ^{1}H NMR (400 MHz, $CDCl_3$): δ 7.76 (d, J = 7.5 Hz, 2H, aromatic H), 7.58 (d, J = 7. 5 Hz, 2H, aromatic H), 7.44 – 7.27 (m, 10H, aromatic H and CONH), 7.11 (brs, 1H, CONH), 5.08 (s, 3H, Ph$\underline{CH_2}$ and CONH), 4.63 – 4.41 (m, 2H, CH$\underline{CH_2}$O), 4.23 (t, J = 6.1 Hz, 1H, $\underline{CH}CH_2O$), 3.76 – 3.36 (m, 2H, NHN$\underline{CH_2}CH_2$), 3.35 – 3.05 (m, 4H, NH$\underline{CH_2}CH_2$ and N$\underline{CH_2}$CH), 1.78 (m, 1H, $\underline{CH}(CH_3)_2$), 1.63 – 1.39 (m, 13H, $CH_2\underline{CH_2}\underline{CH_2}CH_2$ and $C(\underline{CH_3})_3$), 0.94 – 0.71 (m, 6H, $CH(\underline{CH_3})_2$); ^{13}C NMR (75 MHz, $CDCl_3$): δ 157.3(CO), 157.2(from rotamer, CO), 156.7(CO), 156.5(CO), 154.3(CO), 143.8(2C, aromatic), 141.3(2C, aromatic), 136.7(aromatic), 128.5(2C, aromatic), 128.0(3C, aromatic), 127.7(2C, aromatic), 127.1(2C, aromatic), 124.9(2C, aromatic), 119.9(2C, aromatic), 81.9($\underline{C}(CH_3)_3$), 68.1(CH$\underline{C}H_2O$), 67.3(from rotamer, CH$\underline{C}H_2O$), 66.6(Ph$\underline{C}H_2$), 58.0(N$\underline{C}H_2$CH), 57.4(from rotamer, N$\underline{C}H_2$CH), 48.2(NHN$\underline{C}H_2CH_2$), 47.5(from rotamer, $\underline{C}HCH_2O$), 47.1($\underline{C}HCH_2O$), 40.6(NH$\underline{C}H_2CH_2$), 28.1(3C, $C(\underline{C}H_3)_3$), 27.1($NHCH_2\underline{C}H_2$), 26.7($\underline{C}H(CH_3)_2$), 24.1($NHNCH_2\underline{C}H_2$), 20.0(2C, $CH(\underline{C}H_3)_2$); HRMS (ESI): Calcd for $[C_{37}H_{47}N_5O_7 + Na]^+$: 696.3373, found: 696.3367.

tert-butyl 2-(4-(((benzyloxy)carbonyl)amino)butyl)-2-(2-methylhydrazine-1-carbonyl)hydrazine-1-carboxylate (compound 2.31a)

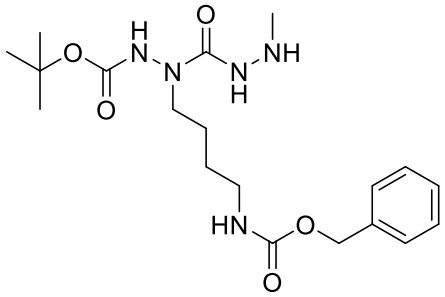

2.30a (390 mg, 0.62 mmol) was treated with 20%(v/v) piperidine/DMF (10 mL). The mixture was stirred at room temperature for 30 min. After removing the volatiles, the residue was dissolved in EtOAc (40 mL). The solution was washed with brine, dried over anhydrous Na_2SO_4, filtrated and concentrated under reduced pressure. The crude product was purified by chromatography on silica gel (elution with 3-5% MeOH in DCM) to give compound **2.31a** as a colorless gel (230 mg, 0.56 mmol, yield: 91%). ^{1}H NMR (300 MHz, $CDCl_3$): δ 7.49 – 7.27 (m, 5H, aromatic H), 6.82 (brs, 2H, CONH), 5.17 – 4.96 (m, 3H, Ph$\underline{CH_2}$ and CONH), 3.75 – 3.38 (m, 2H, NHN$\underline{CH_2}CH_2$), 3.30 – 2.84 (m, 3H, NH$\underline{CH_2}CH_2$ and $\underline{NH}CH_3$), 2.59(s, 3H, NH$\underline{CH_3}$), 1.55 (s, 4H, $CH_2\underline{CH_2}\underline{CH_2}CH_2$), 1.46 (s, 9H, C($\underline{CH_3}$)$_3$); ^{13}C NMR (75 MHz, $CDCl_3$): δ 158.8(CO), 156.9(CO), 154.6(CO), 136.8(aromatic), 128.6(2C, aromatic), 128.2(3C, aromatic), 82.4($\underline{C}(CH_3)_3$), 66.8(Ph$\underline{C}H_2$), 48.2(NHN$\underline{C}H_2CH_2$), 40.8(NH$\underline{C}H_2CH_2$), 39.8(NH$\underline{C}H_3$), 28.3(3C, C($\underline{C}H_3$)$_3$), 27.3(NHCH$_2\underline{C}H_2$), 24.3(NHNCH$_2\underline{C}H_2$); HRMS (ESI): Calcd for $[C_{19}H_{31}N_5O_5 + H]^+$: 410.2398, found: 410.2411.

tert-butyl 2-(4-(((benzyloxy)carbonyl)amino)butyl)-2-(2-isobutylhydrazine-1-carbonyl)hydrazine-1-carboxylate (compound 2.31b)

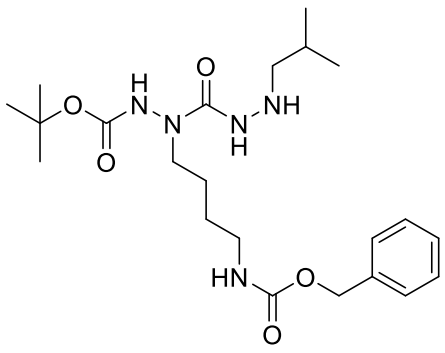

Compound **2.31b** was synthesized from **2.30b** (363 mg, 0.54 mmol) as a white solid (221 mg, 0.49 mmol, yield: 91%) by following the synthesis procedure of **2.31a**. ^{1}H NMR (300 MHz, $CDCl_3$): δ 7.31 (brs, 1H, CONH), 7.29 – 7.15 (m, 5H, aromatic H), 6.96 (brs, 1H, CONH), 5.33 (brs, 1H, CONH), 4.99 (s, 2H, Ph$\underline{CH_2}$), 3.43 (brs, 3H, NHN$\underline{CH_2}CH_2$ and $\underline{NH}CH_2CH$), 3.19 – 2.95 (m, 2H, NH$\underline{CH_2}CH_2$), 2.53 (d, J = 6.8 Hz, 2H, NH$\underline{CH_2}$CH), 1.64 (m, 1H, $\underline{CH}(CH_3)_2$), 1.44 (brs, 4H, $CH_2\underline{CH_2}\underline{CH_2}CH_2$), 1.37 (s, 9H, C($\underline{CH_3}$)$_3$), 0.83 (d, J = 6.7 Hz, 6H, CH($\underline{CH_3}$)$_2$); ^{13}C NMR (75 MHz, $CDCl_3$): δ 159.0(CO), 156.8(CO), 154.8(CO), 136.7(aromatic), 128.5(2C, aromatic), 128.0(3C, aromatic), 81.9($\underline{C}(CH_3)_3$), 66.6(Ph$\underline{CH_2}$), 60.3(NH$\underline{C}H_2$CH), 48.1(NHN$\underline{C}H_2CH_2$), 40.7(NH$\underline{C}H_2CH_2$), 28.2(3C, C($\underline{C}H_3$)$_3$), 27.1(NHCH$_2\underline{C}H_2$), 26.8($\underline{C}H(CH_3)_2$), 24.3(NHNCH$_2\underline{C}H_2$), 20.6(2C, CH($\underline{C}H_3$)$_2$); HRMS (ESI): Calcd for $[C_{22}H_{37}N_5O_5 + H]^+$: 452.2873, found: 452.2867.

tert-butyl (S)-3-(4-(((benzyloxy)carbonyl)amino)butyl)-9-carbamoyl-6-methyl-4,7-dioxo-12-phenyl-11-oxa-2,3,5,6,8-pentaazadodecanoate (compound 2.32a)

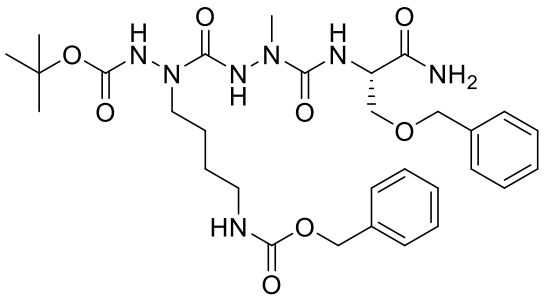

Triphosgene (41 mg, 0.14 mmol) was dissolved in dry DCM (2 mL) under an argon atmosphere. A solution of **2.31a** (143 mg, 0.35 mmol) and DIPEA (60 μL, 0.35 mmol) in dry DCM (4 mL) was added dropwise under ice-cooling. The mixture was stirred at room temperature for 20 min, then Ser(Bn)-NH_2·HCl **2.18** (76 mg, 0.33 mmol) and DIPEA (122 μL, 0.70 mmol) were added successively. The mixture was stirred at room temperature overnight. DCM (30 mL) was added to the reaction and the solution was washed with brine, dried over anhydrous Na_2SO_4, filtrated and concentrated under reduced pressure. The residue was purified by chromatography on silica gel (elution with 4-5% MeOH in DCM) to give compound **2.32a** as a white solid (100 mg, 0.16 mmol, yield: 46%). ^{1}H NMR (300 MHz, $CDCl_3$): δ 7.78 (brs, 1H, CONH), 7.57 (brs, 1H, CONH), 7.38 – 7.14 (m, 10H, aromatic H), 6.99 (brs, 1H, CONH), 6.33 (brs, 1H, CONH), 5.76 (brs, 1H, CONH), 5.17 (brs, 1H, CONH), 4.99 (s, 2H, Ph$\underline{CH_2}$ from Cbz), 4.54 – 4.34 (m, 3H, $\underline{CH}CH_2O$ and Ph$\underline{CH_2}$

from Bn), 3.82 (m, 1H, CHC<u>H</u>$_2$O), 3.71 – 3.24 (m, 3H, CHC<u>H</u>$_2$O and NHNC<u>H</u>$_2$CH$_2$), 3.16 – 3.02 (m, 2H, NHC<u>H</u>$_2$CH$_2$), 2.99 (s, 3H, NC<u>H</u>$_3$), 1.60 – 1.29 (m, 13H, CH$_2$C<u>H</u>$_2$C<u>H</u>$_2$CH$_2$ and C(C<u>H</u>$_3$)$_3$); ^{13}C NMR (75 MHz, $CDCl_3$): δ 174.7(CO), 158.8(CO), 157.5(CO), 157.0(CO), 155.0(CO), 137.7(aromatic), 136.7(aromatic), 128.6(2C, aromatic), 128.5(2C, aromatic), 128.1(3C, aromatic), 127.8(aromatic), 127.8(2C, aromatic), 82.4(<u>C</u>(CH$_3$)$_3$), 73.3(Ph<u>C</u>H$_2$ from Bn), 69.8(CH<u>C</u>H$_2$O), 66.7(Ph<u>C</u>H$_2$ from Cbz), 54.8(<u>C</u>HCH$_2$O), 48.5(NHN<u>C</u>H$_2$CH$_2$), 40.7(NH<u>C</u>H$_2$CH$_2$), 36.4(N<u>C</u>H$_3$), 28.3(3C, C(<u>C</u>H$_3$)$_3$), 27.0(NHCH$_2$<u>C</u>H$_2$), 24.0(NHNCH$_2$<u>C</u>H$_2$); HRMS (ESI): Calcd for [$C_{30}H_{43}N_7O_8$ + Na]$^+$: 652.3071, found: 652.3066.

tert-butyl (S)-3-(4-(((benzyloxy)carbonyl)amino)butyl)-9-carbamoyl-6-isobutyl-4,7-dioxo-12-phenyl-11-oxa-2,3,5,6,8-pentaazadodecanoate (compound 2.32b)

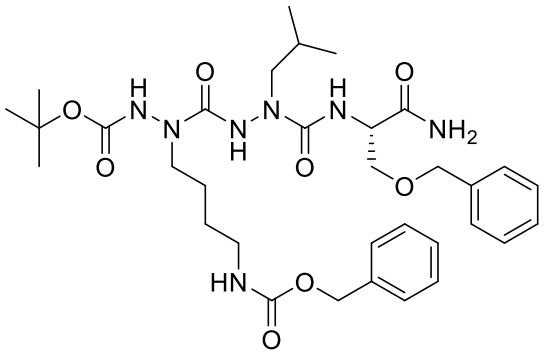

Compound **2.32b** was synthesized from **2.31b** (198 mg, 0.44 mmol) as a white solid (160 mg, 0.24 mmol, yield: 54%) by following the synthesis procedure of **2.32a**. ^{1}H NMR (300 MHz, $CDCl_3$): δ 7.40 (brs, 2H, CONH), 7.34 – 7.11 (m, 10H, aromatic H), 6.96 (brs, 1H, CONH), 6.23 (brs, 1H, CONH), 5.61 (brs, 1H, CONH), 5.06 (brs, 1H, CONH), 5.00 (s, 2H, Ph<u>C</u>H$_2$ from Cbz), 4.51 – 4.36 (m, 3H, <u>C</u>HCH$_2$O and Ph<u>C</u>H$_2$ from Bn), 3.97 – 3.80 (m, 1H, CHC<u>H</u>$_2$O), 3.74 – 3.35 (m, 3H, CHC<u>H</u>$_2$O and NHNC<u>H</u>$_2$CH$_2$), 3.29 – 2.80 (m, 4H NHC<u>H</u>$_2$CH and NHC<u>H</u>$_2$CH$_2$), 1.75 (m, 1H, <u>C</u>H(CH$_3$)$_2$), 1.51 – 1.34 (m, 13H, CH$_2$C<u>H</u>$_2$C<u>H</u>$_2$CH$_2$ and C(C<u>H</u>$_3$)$_3$), 0.91 – 0.74 (m, 6H, CH(C<u>H</u>$_3$)$_2$); ^{13}C NMR (75 MHz, $CDCl_3$): δ 174.6(CO), 158.6(CO), 157.3(CO), 156.9(CO), 154.9(CO), 137.6(aromatic), 136.6(aromatic), 128.5(2C, aromatic), 128.4(2C, aromatic), 128.1(3C, aromatic), 127.7(aromatic), 127.7(2C, aromatic), 82.4(<u>C</u>(CH$_3$)$_3$), 73.1(Ph<u>C</u>H$_2$ from Bn), 69.7(CH<u>C</u>H$_2$O), 66.6(Ph<u>C</u>H$_2$ from Cbz), 56.1(NH<u>C</u>H$_2$CH), 54.5(<u>C</u>HCH$_2$O), 48.4(NHN<u>C</u>H$_2$CH$_2$), 40.5(NH<u>C</u>H$_2$CH$_2$), 28.1(3C, C(<u>C</u>H$_3$)$_3$), 27.0(NHCH$_2$<u>C</u>H$_2$), 26.5(<u>C</u>H(CH$_3$)$_2$), 23.8(NHNCH$_2$<u>C</u>H$_2$), 20.2(CH(<u>C</u>H$_3$)$_2$),

20.1(CH($\underline{C}H_3$)$_2$); HRMS (ESI): Calcd for [$C_{33}H_{49}N_7O_8$ + Na]$^+$: 694.3540, found: 694.3532.

benzyl (S)-(10-acetamido-4-carbamoyl-7-methyl-6,9-dioxo-1-phenyl-2-oxa-5,7,8,10-tetraazatetradecan-14-yl)carbamate (compound 2.33a)

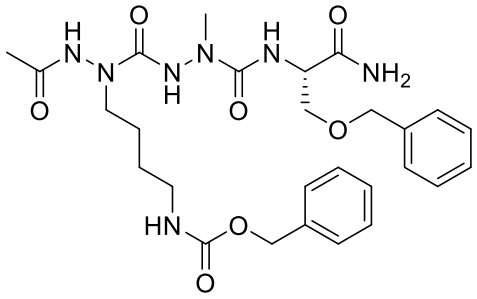

To a solution of **2.32a** (100 mg, 0.16 mmol) in dioxane (1 mL) was added HCl 4M in dioxane (2 mL, 8.00 mmol) under ice-cooling. The mixture was stirred at room temperature for 3 h. Then the reaction was evaporated under reduced pressure to give a white solid. The solid was dissolved in DCM (8 mL) with pyridine (129 µL, 1.60 mmol). Acetic anhydride (45 µL, 0.48 mmol) was added and the mixture was stirred at room temperature overnight. DCM (10 mL) was added and the mixture was successively washed water and brine, dried over anhydrous Na_2SO_4, filtrated and concentrated under reduced pressure. The residue was purified by chromatography on silica gel (elution with 4-10% MeOH in DCM) to give compound **2.33a** as a white solid (69 mg, 0.12 mmol, yield: 75%). ^{1}H NMR (300 MHz, $CDCl_3$): δ 9.58 (brs, 1H, CONH), 8.63 (brs, 1H, CONH), 7.56 – 6.88 (m, 11H, aromatic H and CONH), 6.62 (brs, 1H, CONH), 6.26 (brs, 1H, CONH), 5.49 (brs, 1H, CONH), 4.94 (s, 2H, Ph$\underline{C}H_2$ from Cbz), 4.39 (s, 2H, Ph$\underline{C}H_2$ from Bn), 4.22 (d, *J* = 6.5 Hz, 1H, $\underline{C}HCH_2O$), 3.84 – 2.52 (m, 9H, CH$\underline{C}H_2$O, NHN$\underline{C}H_2CH_2$, NH$\underline{C}H_2CH_2$, NCH_3), 1.84 (s, 3H, CH_3CO), 1.50 – 1.22 (m, 4H, $CH_2\underline{C}H_2\underline{C}H_2CH_2$); ^{13}C NMR (75 MHz, $CDCl_3$): δ 174.7(CO), 171.0(CO), 159.1(CO), 157.5(CO), 157.0(CO), 137.6(aromatic), 136.6(aromatic), 128.5(2C, aromatic), 128.4(2C, aromatic), 128.1(aromatic), 127.9(aromatic), 127.8(4C, aromatic), 73.3(Ph$\underline{C}H_2$ from Bn), 69.6(CH$\underline{C}H_2$O), 66.6(Ph$\underline{C}H_2$ from Cbz), 55.4($\underline{C}HCH_2O$), 48.5(NHN$\underline{C}H_2CH_2$), 40.6(NH$\underline{C}H_2CH_2$), 36.3(NCH_3), 26.9(NHCH$_2\underline{C}H_2$), 24.0(NHNCH$_2\underline{C}H_2$), 20.9($\underline{C}H_3CO$); HRMS (ESI): Calcd for [$C_{27}H_{37}N_7O_7$ + H]$^+$: 572.2827, found: 572.2829.

benzyl (S)-(10-acetamido-4-carbamoyl-7-isobutyl-6,9-dioxo-1-phenyl-2-oxa-5,7,8,10-

tetraazatetradecan-14-yl)carbamate (compound 2.33b)

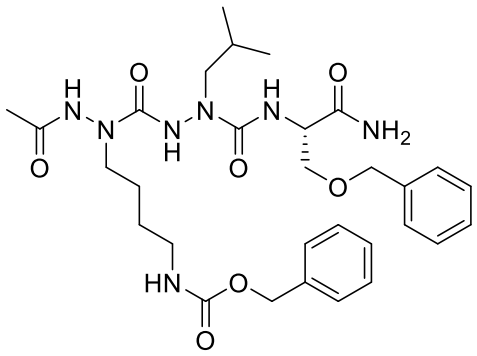

Compound **2.33b** was synthesized from **2.32b** (130 mg, 0.19 mmol) as a white solid (90 mg, 0.15 mmol, yield: 76%) by following the synthesis procedure of **2.33a**. ^{1}H NMR (300 MHz, $CDCl_3$): δ 9.62 (brs, 1H, CONH), 8.44 (brs, 1H, CONH), 7.74 – 7.00 (m, 11H, aromatic H and CONH), 6.74 (brs, 1H, CONH), 5.91 (brs, 1H, CONH), 5.38 (brs, 1H, CONH), 4.97 (s, 2H, Ph$\underline{CH_2}$ from Cbz), 4.43 (s, 2H, Ph$\underline{CH_2}$ from Bn), 4.25 (m, 1H, $\underline{CH}CH_2O$), 3.89 – 2.65 (m, 8H, $CH\underline{CH_2}O$, NHN$\underline{CH_2}CH_2$, NH$\underline{CH_2}CH_2$, N$\underline{CH_2}CH$), 1.87 (s, 3H, CH_3CO), 1.75 (m, 1H, $\underline{CH}(CH_3)_2$), 1.51 – 1.12 (m, 4H, $CH_2\underline{CH_2}\underline{CH_2}CH_2$), 0.88 – 0.54 (m, 6H, $CH(\underline{CH_3})_2$); ^{13}C NMR (75 MHz, $CDCl_3$): δ 174.7(CO), 171.1(CO), 159.1(CO), 157.5(CO), 157.0(CO), 137.6(aromatic), 136.6(aromatic), 128.5(2C, aromatic), 128.4(2C, aromatic), 128.1(aromatic), 127.9(aromatic), 127.8(4C, aromatic), 73.3(Ph$\underline{C}H_2$ from Bn), 69.6($CH\underline{C}H_2O$), 66.6(Ph$\underline{C}H_2$ from Cbz), 56.4(2C, $\underline{C}HCH_2O$ and N$\underline{C}H_2CH$), 48.8(NHN$\underline{C}H_2CH_2$), 40.6(NH$\underline{C}H_2CH_2$), 27.1(NHCH$_2\underline{C}H_2$), 26.6($\underline{C}H(CH_3)_2$), 23.9(NHNCH$_2\underline{C}H_2$), 20.9($\underline{C}H_3CO$), 20.2(CH($\underline{C}H_3)_2$), 20.1(CH($\underline{C}H_3)_2$); HRMS (ESI): Calcd for $[C_{30}H_{43}N_7O_7 + H]^+$: 614.3297, found: 614.3305.

tert-butyl 2-(4-(((benzyloxy)carbonyl)amino)butyl)-5-methyl-3,6-dioxo-1,2,4,5-tetrazinane-1-carboxylate (compound 2.34)

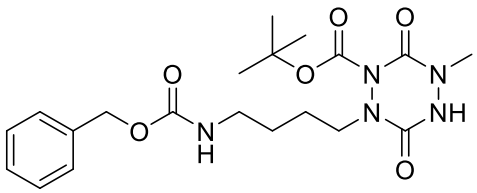

Compound **2.34** was an impurity during the synthesis of **2.32a**.^{1}H NMR (300 MHz, $CDCl_3$) δ 7.45 – 7.27 (m, 5H, aromatic H), 6.76 (brs, 1H, CONH), 5.08 (s, 2H, Ph$\underline{CH_2}$), 4.95 (brs, 1H, CONH),

3.50 – 3.35 (m, 2H, NN$\underline{C}H_2CH_2$), 3.27 (s, 3H, CH_3), 3.25 – 3.15 (m, 2H, NH$\underline{C}H_2CH_2$), 1.71 – 1.50 (m, 4H, $CH_2\underline{CH_2CH_2}CH_2$), 1.45 (s, 9H, $C(CH_3)_3$). ^{13}C NMR (75 MHz, $CDCl_3$) δ 156.7(CO), 154.7(CO), 153.9(CO), 152.3(CO), 136.7(aromatic), 128.7(2C, aromatic), 128.3(3C, aromatic), 82.6($\underline{C}(CH_3)_3$), 66.9(Ph$\underline{C}H_2$), 50.8(NN$\underline{C}H_2CH_2$), 40.7(NH$\underline{C}H_2CH_2$), 32.6(NCH_3), 28.3(3C, $C(\underline{C}H_3)_3$), 27.2($NHCH_2\underline{C}H_2$), 23.8($NNCH_2\underline{C}H_2$). HRMS (ESI): Calcd for $[C_{20}H_{29}N_5O_6 + H]^+$: 436.2196, found: 436.2193.

tert-butyl 2-(4-(((benzyloxy)carbonyl)amino)butyl)-5-isobutyl-3,6-dioxo-1,2,4,5-tetrazinane-1-carboxylate (compound 2.35)

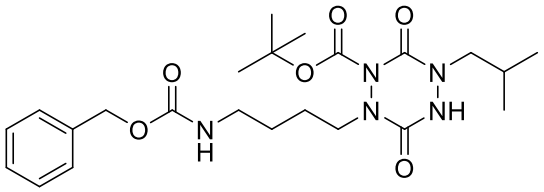

Compound **2.35** was an impurity during the synthesis of **2.32b**.^{1}H NMR (300 MHz, $CDCl_3$) δ 7.44 – 7.25 (m, 5H, aromatic H), 6.57 (brs, H, CONH), 5.09 (s, 2H, Ph$\underline{CH_2}$), 4.89 (brs, 1H, CONH), 3.56 – 3.36 (m, 4H, NN$\underline{CH_2}CH_2$ and N$\underline{CH_2}CH(CH_3)_2$), 3.31 – 3.15 (m, 2H, NH$\underline{CH_2}CH_2$), 2.05 (m, 1H, $NCH_2\underline{CH}(CH_3)_2$), 1.77 – 1.54 (m, 4H, $CH_2\underline{CH_2CH_2}CH_2$), 1.46 (m, 9H, $C(CH_3)_3$), 1.00 – 0.89 (m, 6H, $NCH_2CH(\underline{CH_3})_2$). HRMS (ESI): Calcd for $[C_{20}H_{29}N_5O_6 + Na]^+$: 500.2485, found: 500.2480.

Cbz-protected-1-methylhydrazine (compound 2.36)

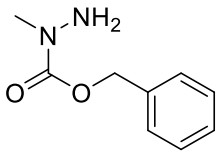

To a solution of methylhydrazine (1.0 mL, 18.99 mmol) in DCM (10 mL) was added 1 M NaOH aqueous solution (15.19 mL). Then benzyl chloroformate (2.15 mL, 15.19 mmol) was added dropwise under ice-cooling. The reaction was stirred at room temperature overnight. After that, DCM and brine was added to do extraction. Organic layer was washed with brine, dried over Na_2SO_4, filtrated, concentrated and purified by chromatography on silica gel (elution with 15-50% EtOAc in cyclohexane) to give 1.33 g (7.39 mmol, 39%) of **2.36** as a colourless oil. ^{1}H NMR (300 MHz, $CDCl_3$) δ 7.46 – 7.28 (m, 5H, aromatic H), 5.15 (s, 2H, Ph$\underline{CH_2}$), 3.43 (brs, 2H, NH_2), 3.14 (s, 3H,

CH_3).

1-benzyl 2-(tert-butyl) 1-methylhydrazine-1,2-dicarboxylate (compound 2.37)

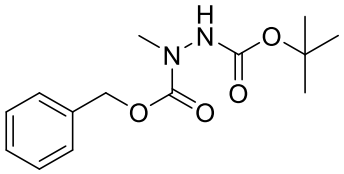

2.36 (1.33 g, 7.39 mmol) was dissolved in a mixture of ACN/H_2O (30 mL/30 mL). Di-*tert*-butyl dicarbonate (4.84 g, 22.16 mmol) and K_2CO_3 (4.08 g, 29.54 mmol) were added to the solution. The mixture was stirred at room temperature overnight. Then the volatiles were removed under reduced pressure and the residue was dissolved in EtOAc and H_2O to do extraction. Organic layer was washed with brine, dried over anhydrous Na_2SO_4, filtrated and concentrated under reduced pressure. The residue was purified by chromatography on silica gel (elution with 10-20% EtOAc in cyclohexane) to give 1.84 g (6.57 mmol, 89%) of **2.37** as a colourless oil. ^{1}H NMR (300 MHz, $CDCl_3$) δ 7.48 – 7.27 (m, 5H, aromatic H), 6.49 (brs, 1H, CONH), 5.16 (s, 2H, Ph$\underline{CH_2}$), 3.19 (s, 3H, CH_3), 1.43 (s, 9H, $C(CH_3)_3$). HRMS (ESI): Calcd for $[C_{14}H_{20}N_2O_4 + Na]^+$: 303.1321, found: 303.1315.

Boc-protected-2-methylhydrazine (compound 2.38)

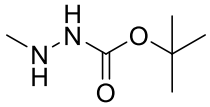

To a solution of **2.37** (940 mg, 3.36 mmol) in MeOH (40 mL) was added 10% Pd/C (200 mg). The mixture was stirred at room temperature under a hydrogen atmosphere for 6 h. Then the suspension was filtrated through a pad of celite and concentrated under reduced pressure to give 415 mg (2.84 mmol, 85%) of **2.38** as a colourless oil. ^{1}H NMR (300 MHz, $CDCl_3$) δ 2.66 (s, 4H, CH_3 and NH), 1.47 (s, 9H, $C(CH_3)_3$). HRMS (ESI): Calcd for $[C_6H_{14}N_2O_2 + Na]^+$: 169.0953, found: 169.0948.

2-(tert-butyl) 1-phenyl 1-methylhydrazine-1,2-dicarboxylate (compound 2.39)

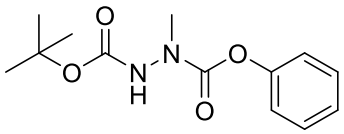

To a suspension of **2.38** (100 mg, 0.68 mmol) in THF (10 mL) was add pyridine (138 µL, 1.71 mmol). The phenyl chloroformate (94 µL, 0.75 mmol) was added dropwise at 0°C under an argon atmosphere. The mixture was stirred at room temperature for 30 min. After removing the THF under reduced pressure, the residue was dissolved in ethyl acetate (40 mL). The solution was washed with 10% citric aqueous solution and brine successively, dried over anhydrous Na_2SO_4, filtrated and concentrated under reduced pressure. The residue was purified by chromatography on silica gel (elution with cyclohexane/EtOAc 10:1) to give 124 mg (0.47 mmol, 69%) of **2.39** as a white solid. ^{1}H NMR (300 MHz, $CDCl_3$) δ 7.4 – 17.31 (m, 2H, aromatic H), 7.25 – 7.06 (m, 3H, aromatic H), 6.62 (brs, 1H, CONH), 3.31 (brd, 3H, NCH_3), 1.50 (s, 9H, $C(CH_3)_3$).

phenyl (S)-(1-amino-3-(benzyloxy)-1-oxopropan-2-yl)carbamate (compound 2.40a)

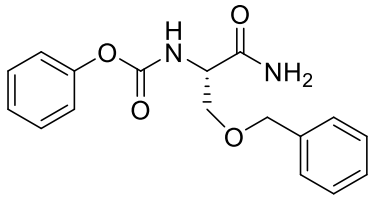

To a suspension of **2.18** (100 mg, 0.52 mmol) in THF (10 mL) was add pyridine (104 µL, 1.23 mmol). The mixture was stirred at room temperature for 5 min and then phenyl chloroformate (71 µL, 0.57 mmol) was added dropwise under ice-cooling. After adding, the mixture was stirred at room temperature for 40 min. After removing the THF under reduced pressure, the residue was dissolved in ethyl acetate (40 mL). The solution was washed with brine, dried over anhydrous Na_2SO_4, filtrated and concentrated under reduced pressure. The residue was purified by chromatography on silica gel (elution with 30-50% EtOAc in cyclohexane) to give 115 mg (0.37 mmol, 71%) of **2.40a** as a white solid. ^{1}H NMR (200 MHz, $CDCl_3$) δ 7.53 – 7.05 (m, 10H, aromatic H), 6.48 (brs, 1H, CONH), 6.02 (brs, 1H, CONH), 5.56 (brs, 1H, CONH), 4.72 – 4.52 (m, 2H, Ph$\underline{CH_2}$), 4.42 (m, 1H, αH), 3.99 (m, 1H, βH), 3.67 (m, 1H, βH). HRMS (ESI): Calcd for $[C_{17}H_{18}N_2O_4 + H]^+$: 315.1345, found: 315.1341.

tert-butyl (S)-2-((1-amino-3-(benzyloxy)-1-oxopropan-2-yl)carbamoyl)-2-methylhydrazine-1-carboxylate (compound 2.41a)

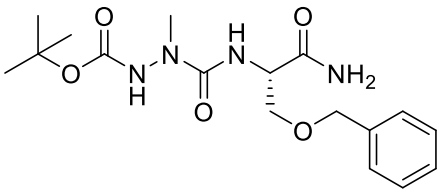

2.40a (200 mg, 0.64 mmol) and **2.38** (112 mg, 0.76 mmol) were dissolved in dry DMF (10 mL). TEA (266 µL, 1.91 mmol) was added to the solution. The mixture was stirred at room temperature overnight. After removing the DMF under reduced pressure, the residue was dissolved in EtOAc (30 mL). The solution was washed with brine, dried over anhydrous Na_2SO_4, filtrated and concentrated under reduced pressure. The residue was purified by chromatography on silica gel (elution with 50-95% EtOAc in cyclohexane) to give 124 mg (0.34 mmol, 53%) of **2.41a** as a colourless oil. ^{1}H NMR (300 MHz, $CDCl_3$) δ 7.43 – 7.24 (m, 5H, aromatic H), 6.81 (brs, 2H, CONH), 6.23 (d, *J* = 7.4 Hz, 1H, CONH), 5.84 (brs, 1H, CONH), 4.65 – 4.42 (m, 3H, Ph$\underline{CH_2}$ and αH), 4.01 (m, 1H, βH), 3.62 (dd, *J* = 9.4, 5.5 Hz, 1H, βH), 3.12 (s, 3H, NCH_3), 1.45 (s, 9H, $C(CH_3)_3$). HRMS (ESI): Calcd for $[C_{17}H_{26}N_4O_5 + Na]^+$: 389.1801, found: 389.1812.

(S)-N-(1-amino-3-(benzyloxy)-1-oxopropan-2-yl)-1-methylhydrazine-1-carboxamide (compound 2.42a)

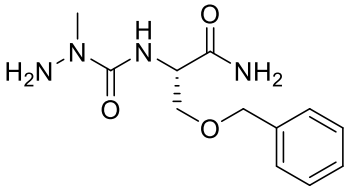

To a solution of **2.41a** (130 mg, 0.36 mmol) in dioxane (3 mL) was add HCl 4M in dioxane (1.8 mL, 7.20 mmol) under ice-cooling. The mixture was stirred at room temperature for 3 h. Then the volatiles were evaporated under reduced pressure to give a crude which was purified by chromatography on silica gel (elution with DCM/MeOH 20:1 with 0.1% ammonia) to give 64 mg (0.24 mmol, 68%) of **2.42a** as a colourless oil. ^{1}H NMR (300 MHz, $CDCl_3$) δ 7.47 – 7.24 (m, 5H, aromatic H), 7.10 (d, *J* = 7.2 Hz, 1H, CONH), 6.71 (brs, 1H, CONH), 5.81 (brs, 1H, CONH), 4.68 – 4.50 (m, 2H, Ph$\underline{CH_2}$), 4.45 (m, 1H, αH), 3.93 (m, 1H, βH), 3.85 – 3.44 (m, 3H, βH and NH_2), 3.13 (s, 3H, NCH_3). HRMS (ESI): Calcd for $[C_{12}H_{19}N_4O_3 + H]^+$: 267.1457, found: 267.1459.

tert-butyl (S)-2-((1-amino-3-(benzyloxy)-1-oxopropan-2-yl)carbamoyl)-2-isobutylhydrazine-1-carboxylate (compound 2.41b)

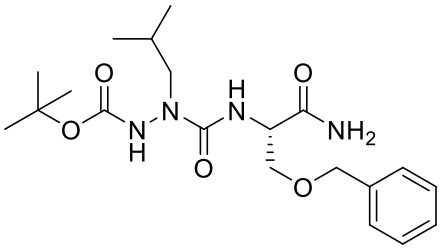

Triphosgene (32 mg, 0.11 mmol) was dissolved in dry DCM (2.5 mL) under an argon atmosphere. A solution of **2.14** (50 mg, 0.27 mmol) and DIPEA (92 µL, 0.53 mmol) in dry DCM (3 mL) was added dropwise under ice-cooling. The mixture was stirred at room temperature for 30 min, then **2.18** (61 mg, 0.27 mmol) and DIPEA (46 µL, 0.27 mmol) were added successively. The mixture was stirred at room temperature overnight. DCM (20 mL) was added to the reaction and the solution was washed with brine, dried over anhydrous Na_2SO_4 and evaporated under reduced pressure. The residue was purified by chromatography on silica gel (elution with cyclohexane/EA 1:2) to give **2.41b** as a white solid (62 mg, 0.15 mmol, yield: 57%). ^{1}H NMR (300 MHz, $CDCl_3$) δ 7.52 – 7.17 (m, 5H, aromatic H), 6.92 (brs, 1H, CONH), 6.48 (s, 1H, CONH), 6.16 (s, 1H, CONH), 5.69 (s, 1H, CONH), 4.65 – 4.38 (m, 3H, Ph$\underline{CH_2}$ and αH), 4.10 (m, 1H, βH), 3.73 – 3.41 (d, J = 9.6 Hz, 2H, βH and N$\underline{CH_2}$CH$(CH_3)_2$), 3.12 (m, 1H, N$\underline{CH_2}$CH$(CH_3)_2$), 1.83 (m, 1H, NCH$_2\underline{CH}(CH_3)_2$), 1.42 (s, 9H, C$(\underline{CH_3})_3$), 1.02 – 0.76 (m, 6H, NCH$_2$CH$(\underline{CH_3})_2$). HRMS (ESI): Calcd for $[C_{20}H_{32}N_4O_5 + H]^+$: 409.2451, found: 409.2461.

(S)-5-((benzyloxy)methyl)-2-methyl-1,2,4-triazinane-3,6-dione (compound 2.44)

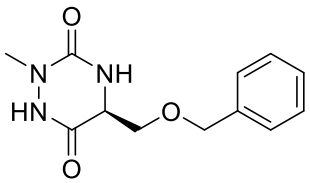

Compound **2.44** (7 mg, 0.03 mmol, 8%) was obtained as an impurity during the synthesis of **2.42a**. ^{1}H NMR (300 MHz, $CDCl_3$) δ 10.49 (brs, 1H, CONH), 7.62 – 7.07 (m, 5H, aromatic H), 5.95 (s,

1H, CONH), 4.54 (s, 2H, Ph$\underline{CH_2}$), 4.11 (m, 1H, αH), 3.84 – 3.62 (m, 2H, βH), 3.10 (s, 1H, CH_3). HRMS (ESI): Calcd for $[C_{12}H_{15}N_3O_3 + H]^+$: 250.1191, found: 250.1178.

(S)-5-((benzyloxy)methyl)-2-isobutyl-1,2,4-triazinane-3,6-dione (compound 2.47)

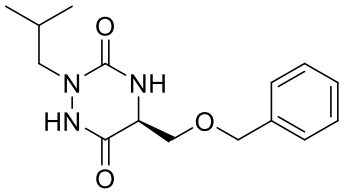

To a solution of **2.41b** (50 mg, 0.12 mmol) in DCM (2 mL) was added TFA (2 mL) under ice-cooling. The mixture was stirred at room temperature for 6 h. The volatiles were evaporated under reduced pressure to give a crude. The crude was purified by chromatography on silica gel (elution with 65-90% EtOAc in cyclohexane) to give compound **2.47** as a white solid (22 mg, 0.08 mmol, yield: 63%). ^{1}H NMR (300 MHz, $CDCl_3$) δ 9.99 (brs, 1H, CONH), 7.67 – 7.12 (m, 5H, aromatic H), 5.73 (d, *J* = 5.2 Hz, 1H, CONH), 4.57 (s, 2H, Ph$\underline{CH_2}$), 4.14 (m, 1H, αH), 3.90 – 3.63 (m, 2H, βH), 3.42 (dd, *J* = 14.4, 7.8 Hz, 1H, N$\underline{CH_2}$CH(CH_3)$_2$), 3.25 (dd, *J* = 14.4, 6.9 Hz, 1H, N$\underline{CH_2}$CH(CH_3)$_2$), 1.99 (m, 1H, NCH$_2\underline{CH}$(CH_3)$_2$), 0.93 (d, *J* = 4.6 Hz, 6H, NCH$_2$CH($\underline{CH_3}$)$_2$). HRMS (ESI): Calcd for $[C_{15}H_{21}N_3O_3 + H]^+$: 292.1661, found: 292.1656.

Compounds in chapter 3

(9H-fluoren-9-yl)methyl 2-(2-isobutylhydrazine-1-carbonyl)-2-methylhydrazine-1-carboxylate·HCl (compound 3.1)

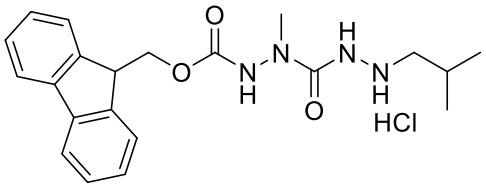

To a solution of **3.10** (1.02 g, 2.12 mmol) in dioxane (8 mL) was added 4 M HCl in dioxane (8 mL). The mixture was stirred at room temperature overnight. The volatiles were removed under reduced pressure. The residue was washed with Et_2O and filtrated to give 800 mg (1.91 mmol, 90%) of **3.1** as a white solid. ^{1}H NMR (300 MHz, $CDCl_3$) δ 9.94 (brs, 2H, $\underline{NH}CH_2$), 8.97 (brs, 1H, CONH), 7.74

(d, *J* = 7.4 Hz, 2H, aromatic H), 7.70 – 7.45 (m, 2H, aromatic H), 7.43 – 7.12 (m, 5H, aromatic H and CONH), 4.43 (s, 2H, CH$\underline{CH_2}$O), 4.22 (s, 1H, $\underline{CH}CH_2O$), 3.14 (s, 5H, NH$\underline{CH_2}$ and N$\underline{CH_3}$), 2.20 (m, 1H, $\underline{CH}(CH_3)_2$), 1.03 (s, 6H, CH($\underline{CH_3}$)$_2$); ^{13}C NMR (75 MHz, $CDCl_3$): δ 157.4(CO), 155.6(CO), 143.6(2C, aromatic), 141.4(2C, aromatic), 128.0(2C, aromatic), 127.3(2C, aromatic), 125.4(2C, aromatic), 120.1 (2C, aromatic), 68.3(CH$\underline{C}H_2O$), 59.1($NHCH_2$), 47.1($\underline{C}HCH_2O$), 36.9(NCH_3), 24.3($\underline{C}H(CH_3)_2$), 20.3(2C, CH($\underline{C}H_3$)$_2$); HRMS (ESI): Calcd for $[C_{21}H_{26}N_4O_3 + H]^+$: 383.2078, found: 383.2081.

tert-butyl 3-(2-(2-(2-(((9H-fluoren-9-yl)methoxy)carbonyl)-1-(4-(tert-butoxy)benzyl)hydrazine-1-carbonyl)hydrazineyl)ethyl)-1H-indole-1-carboxylate (compound 3.3)

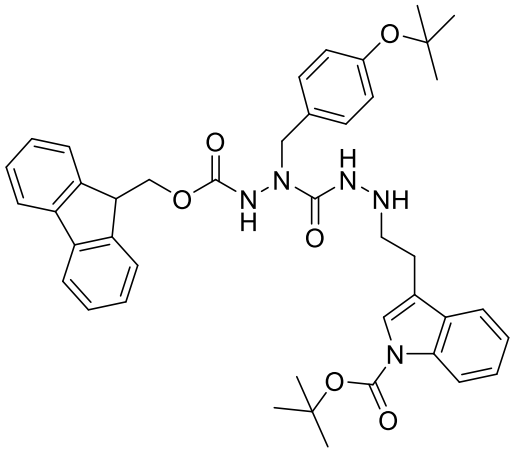

To a solution of **3.27** (1050 mg, 1.31 mmol) in DCM (20 mL) was added N, N-dimethylbarbituric acid (614 mg, 3.93 mmol) and Tetrakis (76 mg, 0.07 mmol). The mixture was stirred at 35°C for 2 h. Then the solution was washed with 10% Na_2CO_3 aqueous solution twice, dried over Na_2SO_4, filtrated, concentrated and purified by chromatography on silica gel (elution with 40-50% EtOAc/cyclohexane) to give 699 mg (0.97 mmol, 74%) of **3.3** as a yellowish solid. ^{1}H NMR (300 MHz, $CDCl_3$): δ 8.01 (d, *J* = 8.2 Hz, 1H, aromatic H), 7.61 (d, *J* = 7.4 Hz, 2H, aromatic H), 7.42 – 7.32 (m, 4H, aromatic H), 7.29 – 7.20 (m, 2H, aromatic H), 7.19 – 7.09 (m, 3H, aromatic H), 7.04 (m, 1H, aromatic H), 6.92 (d, *J* = 8.5 Hz, 2H, aromatic H), 6.77 (d, *J* = 8.5 Hz, 2H, aromatic H), 6.71 (brs, 1H, CONH), 6.54 (brs, 1H, CONH), 4.65 – 4.16 (m, 4H, CH$\underline{CH_2}$O and N$\underline{CH_2}$), 4.01 (t, *J* = 6.0 Hz, 1H, $\underline{CH}CH_2O$), 3.03 (t, *J* = 7.2 Hz, 2H, NH$\underline{CH_2}CH_2$), 2.69 (t, *J* = 7.1 Hz, 2H, $NHCH_2\underline{CH_2}$), 1.54 (s, 9H, C($\underline{CH_3}$)$_3$ from Boc), 1.19 (s, 9H, C($\underline{CH_3}$)$_3$ from *t*Bu); ^{13}C NMR (75 MHz, $CDCl_3$): δ 158.3(CO), 155.3(2C, CO and aromatic), 149.8(CO), 143.3(2C, aromatic), 141.5(2C, aromatic),

135.6(aromatic), 130.7(aromatic), 130.5(aromatic), 129.7(2C, aromatic), 127.9(2C, aromatic), 127.2(2C, aromatic), 124.9(2C, aromatic), 124.3(aromatic), 124.2(2C, aromatic), 123.0(aromatic), 122.4(aromatic), 120.1(2C, aromatic), 119.0(aromatic), 118.4(aromatic), 115.3(aromatic), 83.4($\underline{C}(CH_3)_3$ from Boc), 78.7($\underline{C}(CH_3)_3$ from *t*Bu), 67.4(CH$\underline{C}H_2$O), 51.6(N$\underline{C}H_2$), 50.6(NH$\underline{C}H_2CH_2$), 47.2($\underline{C}HCH_2O$), 28.9(3C, C($\underline{C}H_3)_3$ from Boc), 28.3(3C, C($\underline{C}H_3)_3$ from *t*Bu), 23.7($NCH_2\underline{C}H_2$); HRMS (ESI): Calcd for $[C_{42}H_{47}N_5O_6 + H]^+$: 718.3599, found: 718.3601.

(9H-fluoren-9-yl)methyl (S)-3-(2-((tert-butyldimethylsilyl)oxy)propyl)-14,14-dimethyl-4,12-dioxo-13-oxa-2,3,5,6,11-pentaazapentadecanoate (compound 3.4a)

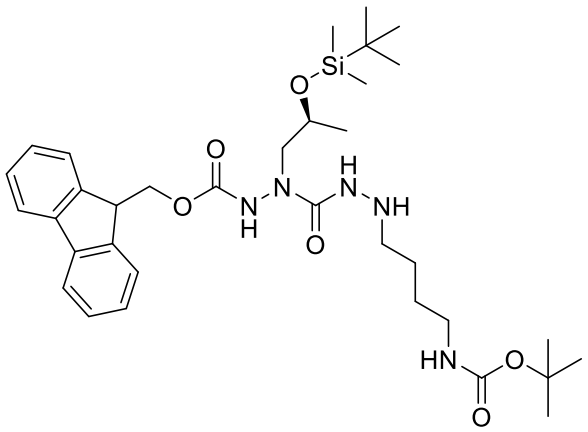

To a solution of **3.37a** (1010 mg, 1.37 mmol) in DCM (20 mL) was added N, N-dimethylbarbituric acid (640 mg, 4.10 mmol) and Tetrakis (79 mg, 0.07 mmol). The mixture was stirred at 35°C for 2 h. Then the solution was washed with 10% Na_2CO_3 aqueous solution twice, dried over Na_2SO_4, filtrated, concentrated and purified by chromatography on silica gel (elution with 50-70% EtOAc/cyclohexane) to give 630 mg (0.96 mmol, 70%) of **3.4a** as a yellowish solid. ^{1}H NMR (300 MHz, $CDCl_3$): δ 7.78 (d, *J* = 7.5 Hz, 2H, aromatic H), 7.59 (d, *J* = 6.9 Hz, 2H, aromatic H), 7.48 – 7.27 (m, 4H, aromatic H), 7.16 (brs, 1H, CONH), 7.07 (brs, 1H, CONH), 4.86 (brs, 1H, CONH), 4.64 – 4.44 (m, 2H, CH$\underline{CH_2}$O), 4.28 – 4.06 (brm, 3H, $\underline{CH}CH_2O$, $CH_2\underline{CH}CH_3$ and NH), 3.63 (m, 1H, $\underline{CH_2}CHCH_3$), 3.42 – 2.94 (m, 3H, $\underline{CH_2}CHCH_3$ and NHNH$\underline{CH_2}$), 2.89 – 2.70 (m, 2H, NH$\underline{CH_2}$), 1.61 – 1.34 (m, 13H, $CH_2\underline{CH_2}\underline{CH_2}CH_2$ and $C(CH_3)_3$ from Boc), 1.13 (d, *J* = 6.1 Hz, 3H, OCH$\underline{CH_3}$), 0.90 (s, 9H, $SiC(CH_3)_3$), 0.10 (s, 3H, $SiCH_3$), 0.06 (s, 3H, $SiCH_3$); ^{13}C NMR (75 MHz, $CDCl_3$): δ 158.5(CO), 156.0(2C, CO), 143.4(aromatic), 143.2(aromatic), 141.4(2C, aromatic), 127.8(2C, aromatic), 127.1(2C, aromatic), 124.9(2C, aromatic), 120.1(2C, aromatic), 78.9($\underline{C}(CH_3)_3$ from Boc),

68.6($CH_2\underline{C}HCH_3$), 67.7($CH\underline{C}H_2O$), 55.7($\underline{C}H_2CHCH_3$), 51.9($NHNH\underline{C}H_2CH_2$), 47.1($\underline{C}HCH_2O$), 40.4($NH\underline{C}H_2CH_2$), 28.4(3C, $C(\underline{C}H_3)_3$ from Boc), 27.6($NHCH_2\underline{C}H_2$), 25.8(3C, $SiC(\underline{C}H_3)_3$), 25.1($NHNHCH_2\underline{C}H_2$), 21.0($CH_2CH\underline{C}H_3$), 17.8($Si\underline{C}(CH_3)_3$), -4.6($SiCH_3$), -4.9($SiCH_3$); HRMS (ESI): Calcd for $[C_{34}H_{53}N_5O_6Si + H]^+$: 656.3838, found: 656.3840.

tert-butyl (S)-(7-acetamido-2,2,3,3,5-pentamethyl-8-oxo-4-oxa-7,9,10-triaza-3-silatetradecan-14-yl)carbamate (compound 3.4b)

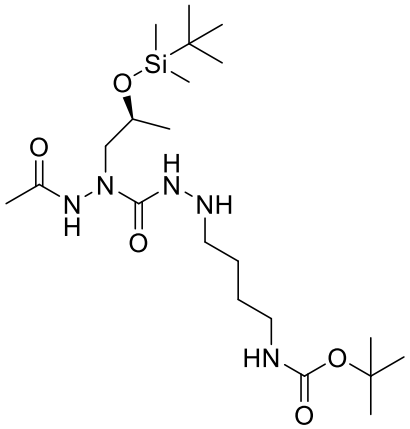

To a solution of **3.37b** (1150 mg, 2.05 mmol) in DCM (30 mL) was added N, N-dimethylbarbituric acid (962 mg, 6.16 mmol) and Tetrakis (119 mg, 0.10 mmol). The mixture was stirred at 35°C for 2 h. Then the solution was washed with 10% Na_2CO_3 aqueous solution twice, dried over Na_2SO_4, filtrated, concentrated and purified by chromatography on silica gel (elution with 50-70% EtOAc/cyclohexane) to give 772 mg (1.62 mmol, 79%) of **3.4b** as a yellowish solid. ^{1}H NMR (300 MHz, $CDCl_3$, 3:1 mixture of rotamer A and rotamer B, * represents the signal of rotamer B): δ 7.65 (brs, 0.75H, CONH), 7.29* (brs, 0.25H, CONH), 7.04* (brs, 0.25H, CONH), 6.79 (brs, 0.75H, CONH), 4.67 (brs, 1H, CONH), 4.37 – 3.98 (m, 2H, NH and $NCH_2\underline{C}HCH_3$), 3.63 (m, 1H, $N\underline{C}H_2CHCH_3$), 3.30 (m, 1H, $N\underline{C}H_2CHCH_3$), 3.17 – 2.97 (m, 2H, $NHNH\underline{C}H_2$), 2.90 – 2.68 (m, 2H, $NH\underline{C}H_2$), 1.99 (s, 3H, $\underline{C}H_3CO$), 1.60 – 1.33 (m, 13H, $CH_2\underline{C}H_2\underline{C}H_2CH_2$ and $C(CH_3)_3$ from Boc), 1.12 (d, J = 6.1 Hz, 3H, $NCH_2CH\underline{C}H_3$), 0.90 (s, 9H, $SiC(CH_3)_3$), 0.09 (s, 3H, $SiCH_3$), 0.07 (s, 3H, $SiCH_3$); ^{13}C NMR (75 MHz, $CDCl_3$, 3:1 mixture of rotamer A and rotamer B, * represents the signal of rotamer B): δ 175.9*(CO), 169.6(CO), 158.7(CO), 158.2*(CO), 156.1(CO), 78.9($\underline{C}(CH_3)_3$ from Boc), 68.6($NCH_2\underline{C}HCH_3$), 67.8*($NCH_2\underline{C}HCH_3$), 57.9*($N\underline{C}H_2CHCH_3$), 56.3($N\underline{C}H_2CHCH_3$), 52.0*($NHNH\underline{C}H_2CH_2$), 51. ($NHNH\underline{C}H_2CH_2$)7, 40.4($NH\underline{C}H_2CH_2$), 28.4(3C, $C(\underline{C}H_3)_3$ from Boc),

27.5($NHCH_2\underline{C}H_2$), 25.8(3C, $SiC(\underline{C}H_3)_3$), 25.0($NHNHCH_2\underline{C}H_2$), 21.1*($\underline{C}H_3CO$), 21.0(2C, $\underline{C}H_3CO$ and $CH_2CH\underline{C}H_3$), 17.9($Si\underline{C}(CH_3)_3$), -4.7($SiCH_3$), -4.8($SiCH_3$); HRMS (ESI): Calcd for $[C_{21}H_{45}N_5O_5Si + H]^+$: 476.3263, found: 476.3267.

Cbz-protected-2-isobutylhydrazine (compound 3.5)

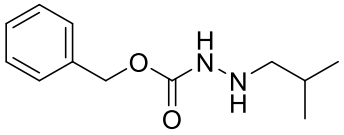

To a solution of benzyl carbazate (2 g, 12.0 mmol) in dry THF (20 mL) was added isobutyraldehyde (3.3 mL, 36.1 mmol) and acetic acid (619 µL, 10.8 mmol). The mixture was stirred at room temperature overnight. Then the volatiles were removed under reduced pressure and the residue was dissolved in dry THF (30 mL) again. $NaBH_3CN$ (1.14 g, 18.1 mmol) and *p*-toluenesulfonic acid monohydrate (3.44 g, 18.1 mmol) were added to the solution successively. The suspension was stirred at room temperature for 2 h and then the solvent was removed under reduced pressure. The residue was dissolved in a mixture of EtOAc/10% K_2CO_3 aqueous solution and extracted with EtOAc. The organic layer was washed with brine and concentrated under reduced pressure. The residue was dissolved in MeOH (18 mL) and treated with 1M NaOH aqueous solution (18.1 mmol). The suspension was stirred at room temperature for 1 h. The solvent was removed under reduced pressure and the residue was dissolved in a mixture of EtOAc/brine. Organic layer was dried over Na_2SO_4, filtrated, concentrated and purified by chromatography on silica gel (elution with 15-25% EtOAc/cyclohexane) to give 2.51 g (11.29 mmol, 94%) of **3.5** as a colourless oil. ^{1}H NMR (300 MHz, $CDCl_3$): δ 7.42 – 7.21 (m, 5H, aromatic H), 6.75 (brs, 1H, CONH), 5.12 (s, 2H, $Ph\underline{C}H_2$), 3.94 (brs, 1H, $\underline{NH}CH_2$), 2.67 (d, J = 6.9 Hz, 2H, $NH\underline{C}H_2$), 1.72 (m, 1H, $\underline{C}H(CH_3)_2$), 0.91 (d, 6H, J = 6.7 Hz, $CH(\underline{C}H_3)_2$); ^{13}C NMR (75 MHz, $CDCl_3$): δ 157.4(CO), 136.2(aromatic), 128.5(2C, aromatic), 128.2(aromatic), 128.1(2C, aromatic), 67.0($Ph\underline{C}H_2$), 59.8($NHCH_2$), 26.8($\underline{C}H(CH_3)_2$), 20.5(2C, $CH(\underline{C}H_3)_2$).

2-benzyl 1-(tert-butyl) 1-isobutylhydrazine-1,2-dicarboxylate (compound 3.6)

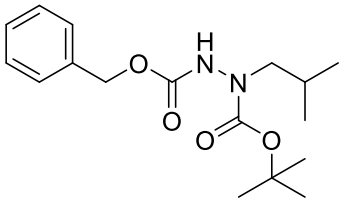

To a solution of **3.5** (1.98 g, 8.9 mmol) in DCM (60 mL) was added di-*tert*-butyl dicarbonate (1.0 mL, 10.7 mmol) and $NaHCO_3$ (2.25 g, 26.7 mmol). The mixture was stirred at room temperature overnight. Water (20 mL) was added and the mixture was extracted with DCM. The organic layer was dried over Na_2SO_4, filtrated, concentrated and purified by chromatography on silica gel (elution with 5-15% EtOAc/cyclohexane) to give 2.34 g (7.26 mmol, 82%) of **3.6** as a colourless oil. ^{1}H NMR (300 MHz, $CDCl_3$): δ 7.61 – 7.24 (m, 5H, aromatic H), 6.67 (brs, 1H, CONH), 5.16 (s, 2H, Ph$\underline{CH_2}$), 3.27 (d, J = 7.0 Hz, 2H, NH$\underline{CH_2}$), 1.89 (m, 1H, $\underline{CH}(CH_3)_2$), 1.43 (s, 9H, C($\underline{CH_3}$)$_3$), 0.89 (d, 6H, J = 6.7 Hz, CH($\underline{CH_3}$)$_2$); ^{13}C NMR (75 MHz, $CDCl_3$): δ 156.3(CO), 155.6(CO), 135.9(aromatic), 128.6(2C, aromatic), 128.4(3C, aromatic), 81.3($\underline{C}(CH_3)_3$), 67.6(Ph$\underline{C}H_2$), δ 57.5(brd, $NHCH_2$), 28.2(3C, C($\underline{C}H_3$)$_3$), 27.0($\underline{C}H(CH_3)_2$), 20.1(2C, CH($\underline{C}H_3$)$_2$); HRMS (ESI): Calcd for [$C_{17}H_{26}N_2O_4$ + Na]$^+$: 345.1785, found: 345.1786.

Boc-protected-1-isobutylhydrazine (compound 3.7)

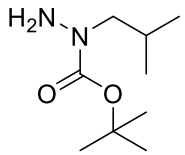

To a solution of **3.6** (2.2 g, 6.8 mmol) in MeOH (40 mL) was added 10% Pd/C (220 mg). The mixture was stirred at room temperature under a hydrogen atmosphere overnight. Then the suspension was filtrated through a pad of celite and concentrated under reduced pressure to give 1.16 g (6.16 mmol, 90%) of **3.7** as a colourless oil. ^{1}H NMR (300 MHz, $CDCl_3$): δ 3.94 (s, 2H, NH_2), 3.12 (d, J = 7.4Hz, 2H, NCH_2), 1.95 (m, 1H, $\underline{CH}(CH_3)_2$), 1.41 (s, 9H, C($\underline{CH_3}$)$_3$), 0.82 (d, J = 6.8 Hz, 6H, CH($\underline{CH_3}$)$_2$); ^{13}C NMR (75 MHz, $CDCl_3$): δ 157.1(CO), 80.0($\underline{C}(CH_3)_3$), 57.7(NCH_2), 28.3(3C, C($\underline{C}H_3$)$_3$), 26.9($\underline{C}H(CH_3)_2$), 19.8(2C, CH($\underline{C}H_3$)$_2$); MS (ESI): Calcd for [$C_9H_{20}N_2O_2$ + Na]$^+$: 211.15, found: 211.15.

1-(tert-butyl) 2-(4-nitrophenyl) 1-isobutylhydrazine-1,2-dicarboxylate (compound 3.8)

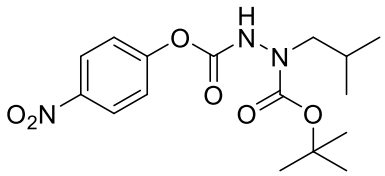

To a mixture of **3.7** (1.16 g, 6.16 mmol) and pyridine (1.49 mL, 18.45 mmol) in dry DCM (40 mL) was added 4-nitrophenylchloroformate (2.11 g, 10.47 mmol). The mixture was stirred at room temperature overnight. Then the volatiles were removed under reduced pressure and the residue was dissolved in EtOAc, washed with 10% K_2CO_3 aqueous solution, 10% citric acid aqueous solution and brine successively. The organic layer was dried over Na_2SO_4, filtrated, concentrated and purified by chromatography on silica gel (elution with 30-90% DCM/cyclohexane) to give 1.66 g (4.70 mmol, 76%) of **3.8** as a white solid. ^{1}H NMR (300 MHz, $CDCl_3$): δ 8.22 (d, J = 8.5 Hz, 2H, aromatic H), 7.70 (brs, 1H, CONH), 7.34 (d, J = 8.7 Hz, 2H, aromatic H), 3.34 (d, J = 7.2 Hz, 2H, NCH_2), 1.96 (m, 1H, $\underline{CH}(CH_3)_2$), 1.48 (s, 9H, $C(\underline{CH_3})_3$), 0.93 (d, J = 6.7 Hz, 6H, $CH(\underline{CH_3})_2$); ^{13}C NMR (75 MHz, $CDCl_3$): δ 155.4(2C, CO), 153.2(aromatic), 145.0(aromatic), 125.1(2C, aromatic), 121.9(2C, aromatic), 82.0($\underline{C}(CH_3)_3$), 57.9(NCH_2), 28.2(3C, $C(\underline{C}H_3)_3$), 27.0($\underline{C}H(CH_3)_2$), 19.9(2C, $CH(\underline{C}H_3)_2$); HRMS (ESI): Calcd for $[C_{16}H_{23}N_3O_6 + Na]^+$: 376.1479, found: 376.1484.

Fmoc-protected-2-methylhydrazine (compound 3.9)

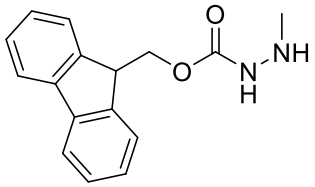

To a solution of di-tert-butyl dicarbonate (886 mg, 8.68 mmol) in DCM (25 mL) was added $NaHCO_3$ (1.04 g, 12.37 mmol). Then methyl hydrazine (500 mg, 10.85 mmol) was added dropwise and the mixture was stirred at room temperature overnight. The reactive solution was filtered through a pad of celite and concentrated under reduced pressure to give the residue, which was dissolved again in THF/H_2O (20 mL/20 mL). To the solution was added $NaHCO_3$ (1.37 g, 16.28 mmol). A THF solution (20 mL) of fluorenylmethyloxycarbonyl chloride (2.25 g, 8.68 mmol) was added dropwise and the mixture was stirred at room temperature for 4 h. The solution was concentrated under reduced pressure and extracted with DCM. The organic layer was washed with brine, dried over Na_2SO_4, filtrated and concentrated. The residue was dissolved in DCM (20 mL). TFA was added

and the mixture was stirred at room temperature for 2 h. Then the volatiles were removed under reduced pressure and the residue was the dissolved in DCM again and washed with 10% $NaHCO_3$ aqueous solution twice, the organic layer was washed with brine, dried over Na_2SO_4, filtrated, concentrated and purified by chromatography on silica gel (elution with EtOAc/cyclohexane 1:1) to give 1.22 g (4.55 mmol, 42%) of **3.9** as a yellow solid. ^{1}H NMR (300 MHz, $CDCl_3$): δ 7.77 (d, *J* = 7.1 Hz, 2H, aromatic H), 7.59 (d, *J* = 6.8 Hz, 2H, aromatic H), 7.48 – 7.27 (m, 4H, aromatic H), 6.32 (brs, 1H, CONH), 4.47 (d, *J* = 6.8 Hz, 2H, CH$\underline{CH_2}$O), 4.25 (t, *J* = 6.8 Hz, 1H, $\underline{CH}CH_2O$), 2.65 (brs, 3H, NH$\underline{CH_3}$), 2.54 (brs, 1H, $\underline{NH}CH_3$).

(9H-fluoren-9-yl)methyl 2-(2-(tert-butoxycarbonyl)-2-isobutylhydrazine-1-carbonyl)-2-methylhydrazine-1-carboxylate (compound 3.10)

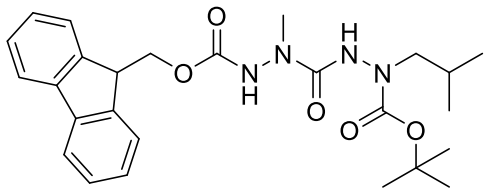

To a solution of **3.9** (690 mg, 2.57 mmol) in DMF (30 mL) was added **3.8** (1.01 g, 2.86 mmol) and DIPEA (1.25 mL, 7.15 mmol). The mixture was stirred at room temperature for 2 h. Water and EtOAc were added to do extraction. Organic layer was washed with brine three times, dried over Na_2SO_4, filtrated, concentrated and purified by chromatography on silica gel (elution with 40-50% EtOAc/cyclohexane) to give 1.02 g (2.11 mmol, 82%) of **3.10** as a white solid. ^{1}H NMR (300 MHz, $CDCl_3$): δ 7.79 (d, *J* = 7.4 Hz, 2H, aromatic H), 7.61 (d, *J* = 7.3 Hz, 2H, aromatic H), 7.48 – 7.30 (m, 5H, aromatic H and CONH), 6.99 (brs, 1H, CONH), 4.56 (brs, 2H, CH$\underline{CH_2}$O), 4.25 (t, *J* = 6.5 Hz, 1H, $\underline{CH}CH_2O$), 3.30 (d, *J* = 7.1 Hz, 2H, N$\underline{CH_2}$), 3.12 (s, 3H, N$\underline{CH_3}$), 1.87 (m, 1H, $\underline{CH}(CH_3)_2$), 1.47 (s, 9H, C($\underline{CH_3}$)$_3$), 0.88 (d, *J* = 6.6 Hz, 6H, CH($\underline{CH_3}$)$_2$); ^{13}C NMR (75 MHz, $CDCl_3$): δ 157.9(CO), 156.5(CO), 155.5(CO), 143.4(2C, aromatic), 141.3(2C, aromatic), 127.9(2C, aromatic), 127.2(2C, aromatic), 125.1(2C, aromatic), 120.1(2C, aromatic), 81.6($\underline{C}(CH_3)_3$), 67.9(CH$\underline{C}H_2O$), 58.2(NCH_2), 47.1($\underline{C}HCH_2O$), 36.2(NCH_3), 28.3(3C, C($\underline{C}H_3)_3$), 26.9($\underline{C}H(CH_3)_2$), 20.1(2C, CH($\underline{C}H_3)_2$); HRMS (ESI): Calcd for $[C_{26}H_{34}N_4O_5 + Na]^+$: 505.2421, found: 505.2422.

(9H-fluoren-9-yl)methyl 2-(4-(tert-butoxy)benzyl)hydrazine-1-carboxylate (compound 3.13)

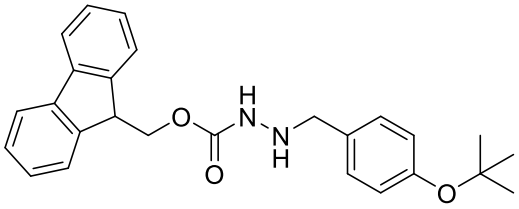

The mixture of 9-fluorenylmethyl carbazate (400 mg, 1.57 mmol) and 4-*tert*-butoxybenzaldehyde (274 μL, 1.57 mmol) in EtOH (15 mL) was stirred at reflux for 2 h. The solvent was removed under reduced pressure and the reside was dissolved in THF (15 mL). $NaBH_3CN$ (168 mg, 2.68 mmol) and acetic acid (207 μL, 3.62 mmol) were added to the solution successively. The suspension was stirred at room temperature overnight and the solvent was removed again under reduced pressure. The residue was dissolved in the mixture of water/EtOAc to do extraction. The organic layer was dried over Na_2SO_4, filtrated and concentrated. Then the residue was dissolved in EtOH, heated at reflux for 1 h and concentrated under reduced pressure. The crude was purified by chromatography on silica gel (elution with EtOAc/cyclohexane 1:3) to give 530 mg (1.27 mmol, 81%) of **3.13** as a colourless oil. ^{1}H NMR (300 MHz, $CDCl_3$) δ 7.78 (d, *J* = 7.8 Hz, 2H, aromatic H), 7.62 (d, *J* = 7.3 Hz, 2H, aromatic H), 7.49 – 7.15 (m, 6H, aromatic H), 7.05 – 6.96 (m, 2H, aromatic H), 6.86 (brs, 1H, CONH), 4.51 (d, *J* = 6.6 Hz, 2H, CH$\underline{CH_2}$O), 4.25 (t, *J* = 6.6 Hz, 1H, $\underline{CH}CH_2O$), 4.16 – 3.55 (m, 3H, $\underline{NHCH_2}$), 1.40 (d, *J* = 2.4 Hz, 9H, C($\underline{CH_3}$)$_3$); ^{13}C NMR (75 MHz, $CDCl_3$) δ 157.3(CO), 155.0(aromatic), 143.8(2C, aromatic), 141.4(2C, aromatic), 132.2(aromatic), 129.7(2C, aromatic), 127.8(2C, aromatic), 127.1(2C, aromatic), 125.1(2C, aromatic), 124.1(2C, aromatic), 120.1(2C, aromatic), 78.5($\underline{C}(CH_3)_3$), 66.9(CH$\underline{C}H_2O$), 55.3($NHCH_2$), 47.3($\underline{C}HCH_2O$), 28.9(3C, C($\underline{C}H_3$)$_3$); HRMS (ESI): Calcd for $[C_{26}H_{28}N_2O_3 + Na]^+$: 439.1992, found: 439.1994.

tert-butyl 3-((2-(((9H-fluoren-9-yl)methoxy)carbonyl)hydrazineyl)methyl)-1H-indole-1-carboxylate (compound 3.14)

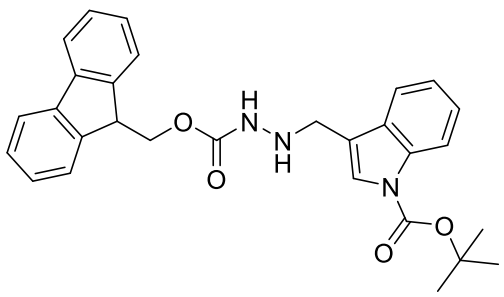

The mixture of 9-fluorenylmethyl carbazate (125 mg, 0.49 mmol) and tert-butyl 3-formyl-1H-indole-1-carboxylate (121 mg, 0.49 mmol) in EtOH (8 mL) was stirred at reflux for 2 h. The solvent was removed under reduced pressure and the reside was dissolved in THF (8 mL). $NaBH_3CN$ (47 mg, 0.74 mmol) and acetic acid (57 μL, 0.99 mmol) were added to the solution successively. The suspension was stirred at room temperature overnight and the solvent was removed again under reduced pressure. The residue was dissolved in the mixture of water/EtOAc to do extraction. The organic layer was dried over Na_2SO_4, filtrated and concentrated. Then the residue was dissolved in EtOH, heated at reflux for 1 h and concentrated under reduced pressure. The crude was purified by chromatography on silica gel (elution with 20-25% EtOAc/cyclohexane) to give 200 mg (0.41 mmol, 84%) of **3.14** as a white solid. ^{1}H NMR (300 MHz, $CDCl_3$) δ 8.19 (d, *J* = 7.7 Hz, 1H, aromatic H), 7.82 – 7.66 (m, 3H, aromatic H), 7.65 – 7.50 (m, 3H, aromatic H), 7.45 – 7.19 (m, 6H, aromatic H), 6.72 (brs, 1H, CONH), 4.46 (d, *J* = 7.0 Hz, 2H, NH$\underline{CH_2}$), 4.36 – 4.03 (m, 4H, CH$\underline{CH_2}$O, $\underline{NH}CH_2$ and $\underline{CH}CH_2O$), 1.66 (s, 9H, C($\underline{CH_3}$)$_3$); HRMS (ESI): Calcd for $[C_{29}H_{29}N_3O_4 + Na]^+$: 506.2050, found: 506.2053.

2-((9H-fluoren-9-yl)methyl) 1-benzyl 1-((1-(tert-butoxycarbonyl)-1H-indol-3-yl)methyl)hydrazine-1,2-dicarboxylate (compound 3.16)

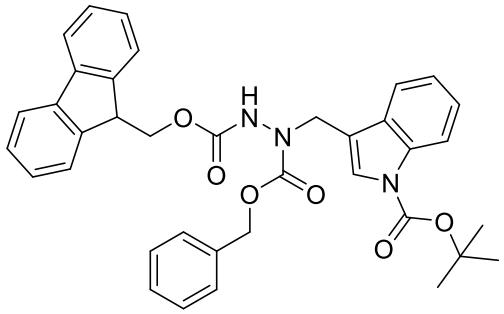

To a solution of **3.15** (170 mg, 0.35 mmol) in DCM (8 mL) was added collidine (56 μL, 0.42 mmol) and CbzCl (59 μL, 0.42 mmol) under an argon atmosphere. The mixture was stirred at room temperature overnight. 10% Citric acid aqueous solution was added to do extraction. Organic layer was washed with brine, dried over Na_2SO_4, filtrated, concentrated and purified by chromatography on silica gel (elution with EtOAc/cyclohexane 1:6) to give 168 mg (0.27 mmol, 78%) of **3.16** as a white solid. ^{1}H NMR (300 MHz, $CDCl_3$) δ 8.13 (d, *J* = 8.3 Hz, 1H, aromatic H), 7.76 (d, *J* = 7.5 Hz, 2H, aromatic H), 7.67 – 7.01 (m, 15H, aromatic H), 6.52 (brs, 1H, CONH), 5.24 (s, 2H, $\underline{CH_2}$Bn),

4.89 (s, 2H, N$\underline{CH_2}$), 4.56 – 4.31 (s, 2H, CH$\underline{CH_2}$O), 4.18 (m, 1H, $\underline{CH}CH_2O$), 1.65 (s, 9H, C($\underline{CH_3}$)$_3$); HRMS (ESI): Calcd for $[C_{37}H_{35}N_3O_6 + NH_4]^+$: 635.2864, found: 635.2865.

tert-butyl 3-((1-((benzyloxy)carbonyl)hydrazineyl)methyl)-1H-indole-1-carboxylate (compound 3.17)

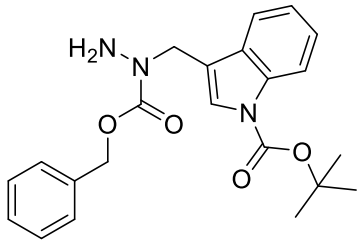

3.16 (164 mg, 0.27 mmol) was dissolved in 20%(v/v) piperidine/DMF (5 mL). The mixture was stirred at room temperature for 20 min. The volatiles were removed under reduced pressure and the residue was taken up to EtOAc. The EtOAc solution was washed with brine, dried over Na_2SO_4, filtrated, concentrated and purified by chromatography on silica gel (elution with EtOAc/cyclohexane 1:4) to give 86 mg (0.22 mmol, 81%) of **3.17** as a colourless oil. ^{1}H NMR (300 MHz, $CDCl_3$) δ 8.19 (d, *J* = 8.2 Hz, 1H, aromatic H), 7.74 – 7.56 (m, 2H, aromatic H), 7.52 – 7.30 (m, 6H, aromatic H), 7.21 (t, *J* = 7.5 Hz, 1H, aromatic H), 5.27 (s, 2H, $\underline{CH_2}$Bn), 4.77 (s, 2H, N$\underline{CH_2}$), 4.09 (brs, 2H, NH_2), 1.71 (s, 9H, C($\underline{CH_3}$)$_3$); HRMS (ESI): Calcd for $[C_{22}H_{26}N_3O_4 + H]^+$: 396.1918, found: 396.1912.

1-benzyl 2-(4-nitrophenyl) 1-((1-(tert-butoxycarbonyl)-1H-indol-3-yl)methyl)hydrazine-1,2-dicarboxylate (compound 3.18)

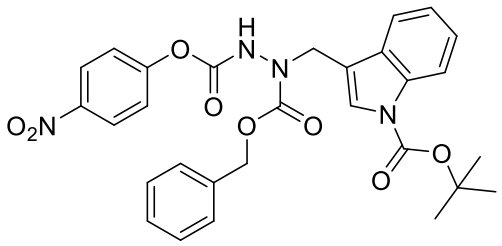

To a mixture of **3.17** (85 mg, 0.22 mmol) and pyridine (52 μL, 0.65 mmol) in dry DCM (4 mL) was added 4-nitrophenylchloroformate (74 mg, 0.37 mmol). The mixture was stirred at room temperature overnight. Then the volatiles were removed under reduced pressure and the residue was dissolved in EtOAc, washed with 10% K_2CO_3 aqueous solution, 10% citric acid aqueous solution

and brine successively. The organic layer was dried over Na_2SO_4, filtrated, concentrated and purified by chromatography on silica gel (elution with 15-20% EtOAc/cyclohexane) to give 86 mg (0.15 mmol, 71%) of **3.18** as a white solid. ^{1}H NMR (300 MHz, $CDCl_3$) δ 8.26 – 7.99 (m, 3H, aromatic H), 7.65 (s, 2H, aromatic H), 7.46 – 7.04 (m, 9H, aromatic H), 6.64 (brs, 1H, CONH), 5.29 (s, 2H, $\underline{CH_2}$Bn), 4.94 (s, 2H, N$\underline{CH_2}$), 1.69 (s, 9H, C($\underline{CH_3}$)$_3$).

tert-butyl 3-((7-(4-(tert-butoxy)benzyl)-11-(9H-fluoren-9-yl)-3,6,9-trioxo-1-phenyl-2,10-dioxa-4,5,7,8-tetraazaundecan-4-yl)methyl)-1H-indole-1-carboxylate (compound 3.19)

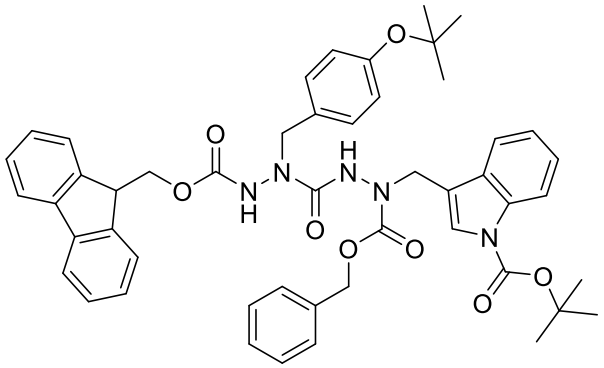

To a solution of **3.13** (69 mg, 0.17 mmol) in DMF (4 mL) was added **3.18** (85 mg, 0.15 mmol) and DIPEA (48 μL, 0.27 mmol). The mixture was stirred at room temperature for 3 h. Water and EtOAc were added to do extraction. Organic layer was washed with brine three times, dried over Na_2SO_4, filtrated, concentrated and purified by chromatography on silica gel (elution with 2-7% EtOAc/DCM) to give 34 mg (0.04 mmol, 27%) of **3.19** as a white solid. ^{1}H NMR (300 MHz, $CDCl_3$) δ 8.12 (d, *J* = 8.0 Hz, 1H, aromatic H), 7.76 (dd, *J* = 14.7, 7.5 Hz, 2H, aromatic H), 7.60 (d, *J* = 7.1 Hz, 2H, aromatic H), 7.53 – 6.80 (m, 18H, aromatic H), 6.32 (brs, 0.5H), 6.11 (brs, 0.5H), 5.24 (s, 2H, $\underline{CH_2}$Bn), 4.91 (s, 2H, N$\underline{CH_2}$), 4.49 (s, 2H, CH$\underline{CH_2}$O), 4.24 (t, *J* = 6.8 Hz, 1H, $\underline{CH}CH_2O$), 4.10 (s, 1H), 3.93 (s, 1H), 1.65 (s, 9H), 1.37 (d, 9H); HRMS (ESI): Calcd for $[C_{49}H_{51}N_5O_8 + Na]^+$: 860.3630, found: 860.3631.

tert-butyl 3-(2-methoxy-2-oxoethyl)-1H-indole-1-carboxylate (compound 3.21)

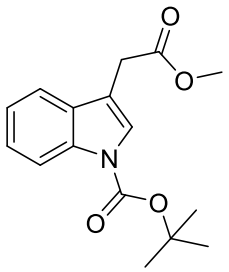

To a solution of indole-3-acetic acid (3 g, 17.13 mmol) in MeOH (110 mL) was added thionyl chloride (6.21 mL, 85.63 mmol) dropwise at 0°C. The mixture was stirred at room temperature for 4 h. The volatiles were removed under reduced pressure. The residue was dissolved in EtOAc, washed with 10% $NaHCO_3$ aqueous solution, dried over Na_2SO_4, filtrated and concentrated. Then the residue was dissolved in DCM (50 mL), di-*tert*-butyl dicarbonate (5.12 mL, 22.27 mmol) and TEA (2.38 mL, 17.13 mmol) were added successively. The resulting solution was stirred at room temperature overnight and then washed with water. The organic layer was dried over Na_2SO_4, filtrated, concentrated and purified by chromatography on silica gel (elution with 5-7% EtOAc/cyclohexane) to give 4.72 g (16.31 mmol, 95%) of **3.21** as a yellowish solid. ^{1}H NMR (300 MHz, $CDCl_3$): δ 8.05 (d, *J* = 8.1 Hz, 1H, aromatic H), 7.50 – 7.37 (m, 2H, aromatic H), 7.26 – 7.09 (m, 2H, aromatic H), 3.62 – 3.57 (m, 5H, CH_2CO and OCH_3), 1.55 (s, 9H, $C(\underline{C}H_3)_3$); ^{13}C NMR (75 MHz, $CDCl_3$): δ 171.4(CO), 149.6(CO), 135.5(aromatic), 130.1(aromatic), 124.5(aromatic), 124.5(aromatic), 122.6(aromatic), 119.0(aromatic), 115.3(aromatic), 113.1(aromatic), 83.6($\underline{C}(CH_3)_3$), 52.1(OCH_3), 30.9($\underline{C}H_2CO$), 28.2(3C, $C(\underline{C}H_3)_3$).

tert-butyl 3-(2-oxoethyl)-1H-indole-1-carboxylate (compound 3.22)

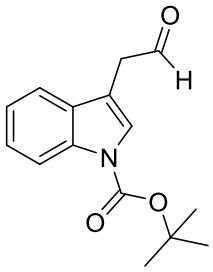

To a solution of **3.21** (4.45 g, 15.39 mmol) in DCM (40 mL) was added 1.5 M DIBAL-H in toluene (15.4 mL, 23.09 mmol) dropwise at -78°C under an argon atmosphere. The mixture was stirred at -78°C for 1 h and quenched with water at 0°C. The mixture was stirred at room temperature for 2 h and extracted with DCM three times. Organic layers were combined and washed with water and

brine, dried over Na_2SO_4, filtrated, concentrated and purified by chromatography on silica gel (elution with EtOAc/cyclohexane 1:9) to give 1.27 g (4.90 mmol, 32%) of **3.22** as a yellow oil. ^{1}H NMR (300 MHz, $CDCl_3$): δ 9.65 (s, 1H, CHO), 8.06 (d, *J* = 8.3 Hz, 1H, aromatic H), 7.47 (s, 1H, aromatic H), 7.33 (d, *J* = 6.8 Hz, 1H, aromatic H), 7.24 (t, *J* = 7.1 Hz, 1H, aromatic H), 7.14 (t, *J* = 7.4 Hz, 1H, aromatic H), 3.64 – 3.59 (m, 2H, CH_2CO), 1.57 (s, 9H, $C(\underline{C}H_3)_3$); ^{13}C NMR (75 MHz, $CDCl_3$): δ 197.4(CO), 148.6(CO), 134.6(aromatic), 129.2(aromatic), 123.9(aromatic), 123.8(aromatic), 121.9(aromatic), 117.8(aromatic), 114.5(aromatic), 110.1(aromatic), 82.9($\underline{C}(CH_3)_3$), 39.0($\underline{C}H_2CO$), 27.2(3C, $C(\underline{C}H_3)_3$).

tert-butyl 3-(2-(2-(((9H-fluoren-9-yl)methoxy)carbonyl)hydrazineyl)ethyl)-1H-indole-1-carboxylate (compound 3.23)

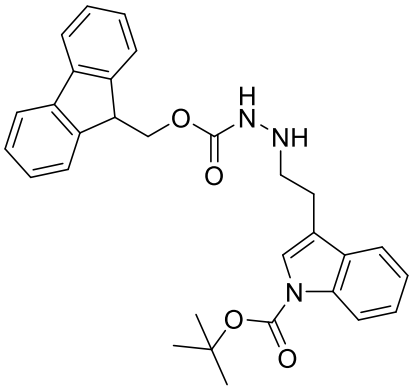

The mixture of 9-fluorenylmethyl carbazate (1.14 g, 4.50 mmol) and **3.22** (1.30 g, 4.50 mmol) in EtOH (65 mL) was stirred at reflux for 1 h. The solvent was removed under reduced pressure and the residue was dissolved in THF (30 mL). $NaBH_3CN$ (481 mg, 7.65 mmol) and acetic acid (592 μL, 10.35 mmol) were added to the solution successively. The suspension was stirred at room temperature overnight and the solvent was removed again under reduced pressure. The residue was dissolved in the mixture of water/EtOAc to do extraction. The organic layer was dried over Na_2SO_4, filtrated and concentrated under reduced pressure. Then the residue was dissolved in EtOH, heated at reflux for 1 h and concentrated under reduced pressure. The crude was purified by chromatography on silica gel (elution with 20-30% EtOAc/cyclohexane) to give 1.79 g (3.60 mmol, 80%) of **3.23** as a white solid. ^{1}H NMR (300 MHz, $CDCl_3$): δ 8.03 (d, *J* = 8.2 Hz, 1H, aromatic H), 7.62 (d, *J* = 7.5 Hz, 2H, aromatic H), 7.48 – 7.32 (m, 4H, aromatic H), 7.31 – 7.06 (m, 6H, aromatic H), 6.32 (brs, 1H, CONH), 4.35 (d, *J* = 6.8 Hz, 2H, $CH\underline{C}H_2O$), 4.08 (t, *J* = 6.8 Hz, 1H, $\underline{C}HCH_2O$),

3.97 (brs, 1H, NHCH$_2$CH$_2$), 3.09 (brs, 2H, NHCH$_2$CH$_2$), 2.73 (brs, 2H, NHCH$_2$CH$_2$), 1.55 (s, 9H, C(CH$_3$)$_3$); ^{13}C NMR (75 MHz, CDCl$_3$): δ 157.4(CO), 149.8(CO), 143.8(2C, aromatic), 141.4(2C, aromatic), 135.7(aromatic), 130.7(aromatic), 127.8(2C, aromatic), 127.2(2C, aromatic), 125.0(2C, aromatic), 124.5(aromatic), 123.1(aromatic), 122.5(aromatic), 120.1(2C, aromatic), 118.9(aromatic), 118.2(aromatic), 115.4(aromatic), 83.5(C(CH$_3$)$_3$), 67.1(CHCH$_2$O), 51.2(NHCH$_2$CH$_2$), 47.3(CHCH$_2$O), 28.3(3C, C(CH$_3$)$_3$), 23.6(NHCH$_2$CH$_2$); HRMS (ESI): Calcd for [C$_{30}$H$_{31}$N$_3$O$_4$ + Na]$^+$: 520.2207, found: 520.2212.

2-((9H-fluoren-9-yl)methyl) 1-allyl 1-(2-(1-(tert-butoxycarbonyl)-1H-indol-3-yl)ethyl)hydrazine-1,2-dicarboxylate (compound 3.24)

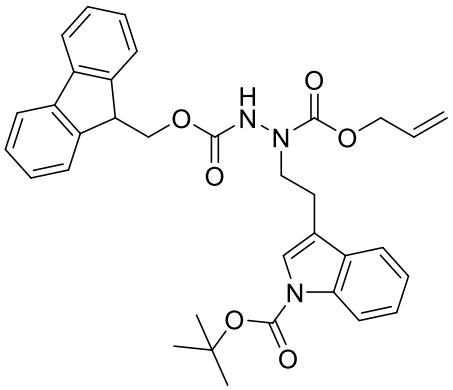

To a solution of **3.23** (1.7 g, 3.42 mmol) in DCM (30 mL) was added NaHCO$_3$ (1.44 g, 17.09 mmol). Then allyl chloroformate (491 µL, 4.62 mmol) was added to the suspension dropwise at 0°C under an argon atmosphere. After adding allyl chloroformate, the mixture was stirred at room temperature for 2 h. Water was added and the mixture was extracted with DCM. The organic layer was dried over Na$_2$SO$_4$, filtrated, concentrated and purified by chromatography on silica gel (elution with EtOAc/cyclohexane 1:5) to give 1.78 g (3.06 mmol, 90%) of **3.24** as a yellowish solid. ^{1}H NMR (300 MHz, CDCl$_3$): δ 8.01 (d, *J* = 8.3 Hz, 1H, aromatic H), 7.55 (d, *J* = 7.5 Hz, 2H, aromatic H), 7.45 – 7.32 (m, 3H, aromatic H), 7.29 (s, 1H, aromatic H), 7.24 – 7.04 (m, 6H, aromatic H), 6.94 (brs, 1H, CONH), 5.66 (brs, 1H, OCH$_2$CHCH$_2$), 5.20 – 4.91 (m, 2H, OCH$_2$CHCH$_2$), 4.53 – 4.21 (m, 4H, CHCH$_2$O and OCH$_2$CHCH$_2$), 4.04 (t, *J* = 6.6 Hz, 1H, CHCH$_2$O), 3.72 (brs, 2H, NCH$_2$CH$_2$), 2.78 (brs, 2H, NCH$_2$CH$_2$), 1.51 (s, 9H, C(CH$_3$)$_3$); ^{13}C NMR (75 MHz, CDCl$_3$): δ 156.3(CO), 155.8(CO), 149.7(CO), 143.5(2C, aromatic), 141.3(2C, aromatic), 135.5(aromatic), 132.1(OCH$_2$CHCH$_2$), 130.4(aromatic), 127.7(2C, aromatic), 127.1(2C, aromatic), 125.0(2C,

aromatic), 124.4(aromatic), 123.1(aromatic), 122.5(aromatic), 120.0(2C, aromatic), 118.8(aromatic), 118.0(aromatic), 117.4($OCH_2CH\underline{C}H_2$), 115.3(aromatic), 83.5($\underline{C}(CH_3)_3$), 67.7($O\underline{C}H_2CHCH_2$), 67.0($CH\underline{C}H_2O$), 50.1($N\underline{C}H_2CH_2$), 47.0($\underline{C}HCH_2O$), 28.2(3C, $C(\underline{C}H_3)_3$), 23.3($NCH_2\underline{C}H_2$); HRMS (ESI): Calcd for $[C_{34}H_{35}N_3O_6 + Na]^+$: 604.2418, found: 604.2425.

tert-butyl 3-(2-(1-((allyloxy)carbonyl)hydrazineyl)ethyl)-1H-indole-1-carboxylate (compound 3.25)

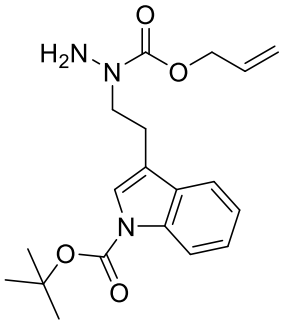

3.24 (1.7 g, 2.92 mmol) was dissolved in 20%(v/v) piperidine/DMF (15 mL). The mixture was stirred at room temperature for 20 min. The volatiles were removed under reduced pressure and the residue was taken up to EtOAc. The EtOAc solution was washed with brine, dried over Na_2SO_4, filtrated, concentrated and purified by chromatography on silica gel (elution with 25-35% EtOAc/cyclohexane) to give 1.0 g (2.69 mmol, 92%) of **3.25** as a yellowish oil. ^{1}H NMR (300 MHz, $CDCl_3$): δ 8.02 (d, *J* = 8.1 Hz, 1H, aromatic H), 7.45 (d, *J* = 7.5 Hz, 1H, aromatic H), 7.31 (s, 1H, aromatic H), 7.24 – 7.07 (m, 2H, aromatic H), 5.71 (brs, 1H, $OCH_2\underline{CH}CH_2$), 5.22 – 5.01 (m, 2H, $OCH_2CH\underline{CH_2}$), 4.42 (brs, 2H, $O\underline{CH_2}CHCH_2$), 3.98 (brs, 2H, NH_2), 3.68 – 3.60 (m, 2H, $N\underline{CH_2}CH_2$), 2.94 – 2.83 (m, 2H, $NCH_2\underline{CH_2}$), 1.55 (s, 9H, $C(\underline{CH_3})_3$); ^{13}C NMR (75 MHz, $CDCl_3$): δ 157.3(CO), 149.6(CO), 135.6(aromatic), 132.7($OCH_2\underline{C}HCH_2$), 130.5(aromatic), 124.3(aromatic), 123.1(aromatic), 122.4(aromatic), 118.8(aromatic), 117.8(aromatic), 117.7($OCH_2CH\underline{C}H_2$), 115.3(aromatic), 83.3($\underline{C}(CH_3)_3$), 66.5($O\underline{C}H_2CHCH_2$), 50.3($N\underline{C}H_2CH_2$), 28.2(3C, $C(\underline{C}H_3)_3$), 23.4($NCH_2\underline{C}H_2$); HRMS (ESI): Calcd for $[C_{19}H_{25}N_3O_4 + Na]^+$: 382.1737, found: 382.1739.

allyl 2-(4-nitrophenyl) 1-(2-(1-(tert-butoxycarbonyl)-1H-indol-3-yl)ethyl)hydrazine-1,2-dicarboxylate (compound 3.26)

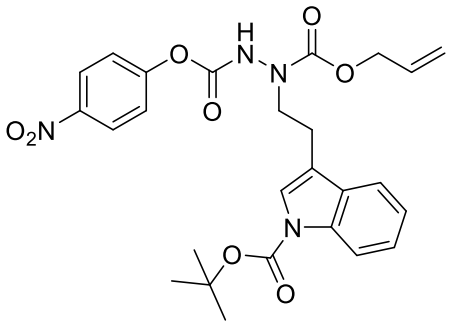

To a mixture of **3.25** (950 mg, 2.64 mmol) and pyridine (638 μL, 7.93 mmol) in dry DCM (15 mL) was added 4-nitrophenylchloroformate (906 mg, 4.50 mmol). The mixture was stirred at room temperature overnight. Then the volatiles were removed under reduced pressure and the residue was taken up to EtOAc. The EtOAc solution was washed with 10% K_2CO_3 aqueous solution, 10% citric acid aqueous solution and brine successively. The organic layer was dried over Na_2SO_4, filtrated, concentrated and purified by chromatography on silica gel (elution with 1-4% EA/DCM) to give 975 mg (1.87 mmol, 70%) of **3.26** as a white solid. ^{1}H NMR (300 MHz, $CDCl_3$): δ 8.13 – 7.97 (m, 3H, aromatic H), 7.70 (brs, 1H, CONH), 7.44 (d, *J* = 7.6 Hz, 1H, aromatic H), 7.37 (s, 1H, aromatic H), 7.27 – 7.07 (m, 4H, aromatic H), 5.76 (brs, 1H, $OCH_2\underline{CH}CH_2$), 5.29 – 5.06 (m, 2H, $OCH_2CH\underline{CH_2}$), 4.54 (d, *J* = 5.6 Hz, 2H, $O\underline{CH_2}CHCH_2$), 3.86 (t, *J* = 7.3 Hz, 2H, $N\underline{CH_2}CH_2$), 2.98 (t, *J* = 7.5 Hz, 2H, $NCH_2\underline{CH_2}$), 1.56 (s, 9H, $C(\underline{CH_3})_3$); ^{13}C NMR (75 MHz, $CDCl_3$): δ 155.8(CO), 155.2(CO), 153.2(aromatic), 149.7(CO), 145.1(aromatic), 135.5(aromatic), 131.8($OCH_2\underline{C}HCH_2$), 130.3(aromatic), 125.1 (2C, aromatic), 124.6(aromatic), 123.2(aromatic), 122.6(aromatic), 121.8 (2C, aromatic), 118.7(aromatic), 118.5(aromatic), 117.2($OCH_2CH\underline{C}H_2$), 115.4(aromatic), 83.8($\underline{C}(CH_3)_3$), 67.4($O\underline{C}H_2CHCH_2$), 50.2($N\underline{C}H_2CH_2$), 28.2(3C, $C(\underline{C}H_3)_3$), 23.5($NCH_2\underline{C}H_2$); HRMS (ESI): Calcd for $[C_{26}H_{28}N_4O_8 + Na]^+$: 547.1799, found: 547.1800.

tert-butyl 3-(2-(5-(4-(tert-butoxy)benzyl)-1-(9H-fluoren-9-yl)-3,6,9-trioxo-2,10-dioxa-4,5,7,8-tetraazatridec-12-en-8-yl)ethyl)-1H-indole-1-carboxylate (compound 3.27)

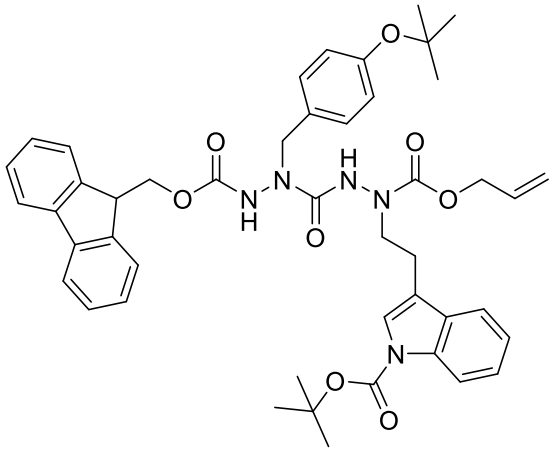

To a solution of **3.26** (720 mg, 1.73 mmol) in DMF (20 mL) was added **3.13** (975 mg, 1.86 mmol) and DIPEA (551 μL, 3.16 mmol). The mixture was stirred at room temperature for 2 h. Water and EtOAc were added to do extraction. Organic layer was washed with brine three times, dried over Na_2SO_4, filtrated, concentrated and purified by chromatography on silica gel (elution with EtOAc/cyclohexane 1:3) to give 1070 mg (1.33 mmol, 77%) of **3.27** as a white solid. ^{1}H NMR (300 MHz, $CDCl_3$): δ 8.00 (d, *J* = 8.6 Hz, 1H, aromatic H), 7.65 (d, *J* = 7.7 Hz, 2H, aromatic H), 7.58 – 7.35 (m, 4H, CONH and aromatic H), 7.34 – 6.86 (m, 9H, aromatic H), 6.80 (d, *J* = 8.4 Hz, 2H, aromatic H), 6.72 (brs, 1H, CONH), 5.75 (m, 1H, $OCH_2\underline{CH}CH_2$), 5.22 – 5.03 (m, 2H, $OCH_2CH\underline{CH_2}$), 4.81 – 4.17 (m, 6H, $CH\underline{CH_2}O$, $N\underline{CH_2}$, $O\underline{CH_2}CHCH_2$), 4.04 (t, *J* = 6.3 Hz, 1H, $\underline{CH}CH_2O$), 3.80 (t, *J* = 7.5 Hz, 2H, $N\underline{CH_2}CH_2$), 2.91 (t, *J* = 7.4 Hz, 2H, $NCH_2\underline{CH_2}$), 1.55 (s, 9H, $C(\underline{CH_3})_3$ from Boc), 1.22 (s, 9H, $C(\underline{CH_3})_3$ from *t*Bu); ^{13}C NMR (75 MHz, $CDCl_3$): δ 157.4(CO), 156.4(CO), 155.5(aromatic), 155.2(CO), 149.8(CO), 143.3(2C, aromatic), 141.5(2C, aromatic), 135.6(aromatic), 132.3($OCH_2\underline{C}HCH_2$), 130.5(aromatic), 129.9(aromatic), 129.8(2C, aromatic), 128.0(2C, aromatic), 127.3(2C, aromatic), 125.0(2C, aromatic), 124.4(aromatic), 124.2(2C, aromatic), 123.2(aromatic), 122.5(aromatic), 120.1(2C, aromatic), 118.9(aromatic), 118.2(aromatic), 117.7($OCH_2CH\underline{C}H_2$), 115.4(aromatic), 83.5($\underline{C}(CH_3)_3$ from Boc), 78.6($\underline{C}(CH_3)_3$ from *t*Bu), 67.7($O\underline{C}H_2CHCH_2$), 67.1($CH\underline{C}H_2O$), 50.7($N\underline{C}H_2$), 50.3($N\underline{C}H_2CH_2$), 47.2($\underline{C}HCH_2O$), 28.9(3C, $C(\underline{C}H_3)_3$ from Boc), 28.3(3C, $C(\underline{C}H_3)_3$ from *t*Bu), 23.6($NCH_2\underline{C}H_2$); HRMS (ESI): Calcd for $[C_{46}H_{51}N_5O_8 + Na]^+$: 824.3630, found: 824.3633.

ethyl (S)-2-((tert-butyldimethylsilyl)oxy)propanoate (compound 3.28)

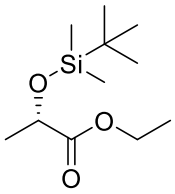

To a solution of (*S*)-ethyl lactate (2.00 g, 16.93 mmol) and imidazole (1.61 g, 23.70 mmol) in dry DCM (40 mL) was added TBDMSCl (3.57 g, 23.70 mmol). The mixture was stirred at room temperature for 5 h. Water and DCM were added to do extraction. Organic layer was washed with brine, dried over Na_2SO_4, filtrated, concentrated and purified by chromatography on silica gel (elution with EtOAc/cyclohexane 1:15) to give 3.90 g (16.78 mmol, 99%) of **3.28** as a colourless oil. ^{1}H NMR (300 MHz, $CDCl_3$): δ 4.30 (q, *J* = 6.7 Hz, 1H, O<u>C</u>HCH_3), 4.25 – 4.09 (m, 2H, CH_3<u>CH_2</u>O), 1.41 (d, *J* = 6.7 Hz, 3H, OCH<u>CH_3</u>), 1.27 (t, *J* = 7.1 Hz, 3H, <u>CH_3</u>CH_2O), 0.90 (s, 9H, $C(CH_3)_3$), 0.10 (s, 3H, $SiCH_3$), 0.07 (s, 3H, $SiCH_3$); ^{13}C NMR (75 MHz, $CDCl_3$) δ 173.2(CO), 67.6(O<u>C</u>HCH_3), 59.8(CH_3<u>C</u>H_2O), 24.9(3C, C(<u>C</u>H_3)$_3$), 20.4(OCH<u>C</u>H_3), 17.4(<u>C</u>$(CH_3)_3$), 13.3(<u>C</u>H_3CH_2O), -5.8($SiCH_3$), -6.1($SiCH_3$).

(S)-2-((tert-Butyldimethylsilyl)oxy)propanal (compound 3.29)

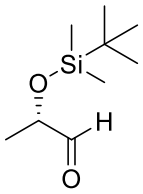

To a solution of **3.28** (3.23 g, 13.90 mmol) in dry DCM (25 mL) was added DIBAL-H (1.5 M in toluene, 11.12 mL, 16.68 mmol) at -78°C dropwise under an argon atmosphere. The mixture was stirred at -78°C for 1 h. A saturated solution of Rochelle salt (30 mL) was added to quench the reaction. The mixture was stirred at room temperature for 3 h. Water (50 mL) and DCM (50 mL) were added to do extraction. Organic layer was washed with brine three times, dried over Na_2SO_4, filtrated, concentrated and purified by chromatography on silica gel (elution with EtOAc/cyclohexane 1:20) to give 1.54 g (8.18 mmol, 59%) of **3.29** as a yellow oil. ^{1}H NMR (300 MHz, $CDCl_3$): δ 9.58 (d, *J* = 1.3 Hz, 1H, CHO), 4.06 (qd, *J* = 6.9, 1.3 Hz, 1H, O<u>C</u>HCH_3), 1.24 (d, *J* = 6.8 Hz, 3H, OCH<u>CH_3</u>), 0.90 (s, 9H, $C(CH_3)_3$), 0.08 (s, 3H, $SiCH_3$), 0.07 (s, 3H, $SiCH_3$); ^{13}C NMR (75 MHz, $CDCl_3$): δ 203.9(CHO), 74.0(O<u>C</u>HCH_3), 25.8(3C, C(<u>C</u>H_3)$_3$), 18.6(OCH<u>C</u>H_3), 18.3(<u>C</u>$(CH_3)_3$), -4.6($SiCH_3$), -4.7($SiCH_3$).

(9H-fluoren-9-yl)methyl (S)-2-(2-((tert-butyldimethylsilyl)oxy)propyl)hydrazine-1-carboxylate (compound 3.30a)

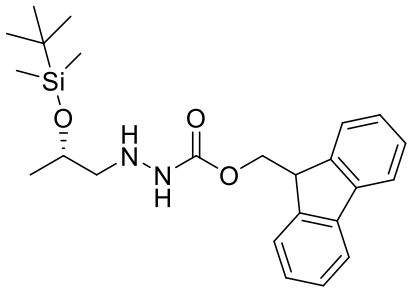

The mixture of 9-fluorenylmethyl carbazate (2.54 g, 10.0 mmol) and **3.29** (1.88 g, 10.0 mmol) in EtOH (60 mL) was stirred at reflux for 2 h. The solvent was removed under reduced pressure and the reside was dissolved in THF (30 mL). $NaBH_3CN$ (943 mg, 15.0 mmol) and acetic acid (1.14 mL, 20 mmol) were added to the solution successively. The suspension was stirred at room temperature overnight and the solvent was removed again under reduced pressure. The residue was dissolved in the mixture of water/EtOAc to do extraction. The organic layer was dried over Na_2SO_4, filtrated and concentrated. Then the residue was dissolved in EtOH, heated at reflux for 1 h and concentrated under reduced pressure. The crude was purified by chromatography on silica gel (elution with EtOAc/cyclohexane 1:5) to give 2.25 g (5.27 mmol, 53%) of **3.30a** as a colourless oil. ^{1}H NMR (300 MHz, $CDCl_3$): δ 7.76 (d, *J* = 7.4 Hz, 2H, aromatic H), 7.60 (d, *J* = 6.9 Hz, 2H, aromatic H), 7.45 – 7.26 (m, 4H, aromatic H), 6.68 (brs, 1H, CONH), 4.46 (d, *J* = 6.3 Hz, 2H, CH$\underline{CH_2}$O), 4.23 (t, *J* = 6.4 Hz, 1H, $\underline{CH}CH_2O$), 4.13 (brs, 1H, $\underline{NH}CH_2$), 3.97 (m, 1H, O$\underline{CH}CH_3$), 2.98 – 2.72 (m, 2H, NH$\underline{CH_2}$), 1.19 (d, *J* = 6.2 Hz, 3H, OCH$\underline{CH_3}$), 0.95 (s, 9H, $C(CH_3)_3$), 0.13 (s, 3H, $SiCH_3$), 0.12 (s, 3H, $SiCH_3$); ^{13}C NMR (75 MHz, $CDCl_3$): δ 157.1(CO), 143.8(aromatic), 143.8(aromatic), 141.3(2C, aromatic), 127.7(2C, aromatic), 127.0(2C, aromatic), 125.1(aromatic), 125.0(aromatic), 112.0(2C, aromatic), 67.4(CH$\underline{C}H_2O$), 67.0(O$\underline{C}HCH_3$), 59.3(NH$\underline{C}H_2$), 47.2($\underline{C}HCH_2O$), 25.9(3C, C($\underline{C}H_3)_3$), 21.6(OCH$\underline{C}H_3$), 18.0($\underline{C}(CH_3)_3$), -4.4($SiCH_3$), -4.8($SiCH_3$); HRMS (ESI): Calcd for $[C_{24}H_{34}N_2O_3Si + H]^+$: 427.2411, found: 427.2416.

(S)-N'-(2-((tert-Butyldimethylsilyl)oxy)propyl)acetohydrazide (compound 3.30b)

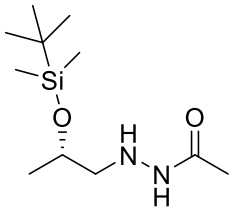

The mixture of acetyl hydrazide (1.1 g, 14.85 mmol) and **3.29** (1.88 g, 14.85 mmol) in EtOH (40 mL) was stirred at reflux for 2 h. The solvent was removed under reduced pressure and the residue was dissolved in THF (30 mL). $NaBH_3CN$ (1.59 g, 25.25 mmol) and acetic acid (1.87 mL, 32.67 mmol) were added to the solution successively. The suspension was stirred at room temperature overnight and the solvent was removed again under reduced pressure. The residue was dissolved in the mixture of water/EtOAc to do extraction. The organic layer was dried over Na_2SO_4, filtrated and concentrated. Then the residue was dissolved in EtOH, heated at reflux for 1 h and concentrated under reduced pressure. The crude was purified by chromatography on silica gel (elution with EtOAc/cyclohexane 2:1) to give 3.3 g (13.39 mmol, 90%) of **3.30b** as a colourless oil. ^{1}H NMR (300 MHz, $CDCl_3$, 5:1 mixture of rotamer A and rotamer B, * represents the signal of rotamer B): δ 7.69 (brs, 0.83H, CONH), 7.15* (brs, 0.17H, CONH), 4.64 (brs, 1H, $\underline{NH}CH_2$), 3.91 (m, 1H, $O\underline{CH}CH_3$), 2.81 – 2.67 (m, 2H, $NH\underline{CH_2}$), 2.05* (s, 0.5H, $\underline{CH_3}CO$), 1.87 (s, 2.5H, $\underline{CH_3}CO$), 1.12* (d, J = 6.2 Hz, 0.5H, $OCH\underline{CH_3}$), 1.11(d, J = 6.2 Hz, 2.5H, $OCH\underline{CH_3}$), 0.85 (s, 7.5H, $C(CH_3)_3$), 0.84* (s, 1.5H, $C(CH_3)_3$), 0.04 (s, 3H, $SiCH_3$), 0.03 (s, 3H, $SiCH_3$); ^{13}C NMR (75 MHz, $CDCl_3$, 5:1 mixture of rotamer A and rotamer B, * represents the signal of rotamer B): δ 175.9*(CONH), 168.9(CONH), 67.9($O\underline{C}HCH_3$), 66.6*($O\underline{C}HCH_3$), 60.0*($NHCH_2$), 59.2($NHCH_2$), 25.9(3C, $C(\underline{C}H_3)_3$), 21.6($OCH\underline{C}H_3$), 21.1($\underline{C}H_3CO$), 19.4*($\underline{C}H_3CO$), 18.1($\underline{C}(CH_3)_3$), 18.0*($\underline{C}(CH_3)_3$), -4.4($SiCH_3$), -4.8($SiCH_3$); HRMS (ESI): Calcd for $[C_{11}H_{26}N_2O_2Si + H]^+$: 247.1836, found: 247.1838.

tert-butyl (4,4-diethoxybutyl)carbamate (compound 3.31)

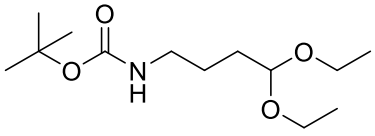

To a solution of 4-aminobutyraldehyde diethylacetal (2.00 g, 11.41 mmol) in THF (50 mL) was added di-*tert*-butyl dicarbonate (2.49 g, 11.41 mmol) and TEA (2.59 mL, 18.61 mmol). The mixture was stirred at room temperature overnight. The volatiles were removed under reduced pressure and

the residue was dissolved in EtOAc and H_2O to do extraction. Organic layer was washed with brine, dried over Na_2SO_4, filtrated, concentrated and purified by chromatography on silica gel (elution with 10-35% EtOAc/cyclohexane) to give 3.08 g (11.18 mmol, 98%) of **3.31** as a colourless oil. ^{1}H NMR (300 MHz, $CDCl_3$) δ 4.70 (brs, 1H, CONH), 4.42 (t, *J* = 5.3 Hz, 1H, $NHCH_2CH_2CH_2\underline{CH}$), 3.65 – 3.51 (m, 2H, $O\underline{CH_2}CH_3$), 3.49 – 3.35 (m, 2H, $O\underline{CH_2}CH_3$), 3.12 – 2.97 (m, 2H, $NH\underline{CH_2}CH_2CH_2CH$), 1.64 – 1.44 (m, 4H, $NHCH_2\underline{CH_2}\underline{CH_2}CH$), 1.38 (s, 9H, $C(\underline{CH_3})_3$), 1.14 (t, *J* = 7.0 Hz, 6H, $OCH_2\underline{CH_3}$); ^{13}C NMR (75 MHz, $CDCl_3$) δ 156.0(CO), 102.8($NHCH_2CH_2CH_2\underline{C}H$), 79.0($\underline{C}(CH_3)_3$), 61.3(2C, $O\underline{C}H_2CH_3$), 40.4($NH\underline{C}H_2CH_2CH_2CH$), 31.1($NHCH_2CH_2\underline{C}H_2CH$), 28.5(3C, $C(\underline{C}H_3)_3$), 25.2($NHCH_2\underline{C}H_2CH_2CH$), 15.3(2C, $OCH_2\underline{C}H_3$).

tert-butyl 2-hydroxypyrrolidine-1-carboxylate (compound 3.32)

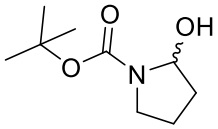

Compound **3.31** (300 mg, 1.15 mmol) was dissolved in acetic acid/H_2O (2 mL/1 mL) and the mixture was stirred at room temperature overnight. The volatiles were removed under reduced pressure to give 210 mg (1.12 mmol, 98%) of **3.32** as a colourless oil. ^{1}H NMR (300 MHz, $CDCl_3$) δ 5.42 (m, 1H, $\underline{CH}OH$), 3.48 (m, 1H, $NH\underline{CH_2}CH_2CH_2$), 3.25 (m, 1H, $NH\underline{CH_2}CH_2CH_2$), 2.06 – 1.70 (m, 4H, $NHCH_2\underline{CH_2}\underline{CH_2}$), 1.47 (s, 9H, $C(\underline{CH_3})_3$).

(9H-fluoren-9-yl)methyl 2-(4-((tert-butoxycarbonyl)amino)butyl)hydrazine-1-carboxylate (compound 3.33)

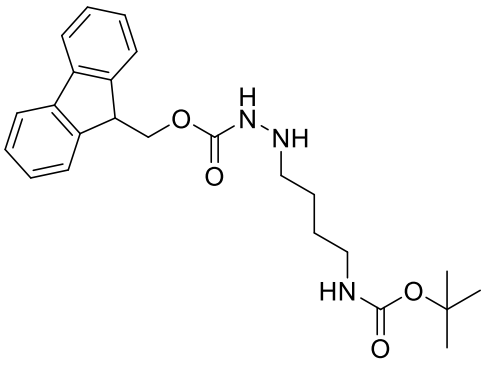

The mixture of 9-fluorenylmethyl carbazate (699 mg, 2.75 mmol) and **3.32** (617 mg, 3.30 mmol) in EtOH (25 mL) was stirred at reflux for 2 h. The solvent was removed under reduced pressure and

the residue was dissolved in THF (20 mL). $NaBH_3CN$ (294 mg, 4.68 mmol) and acetic acid (346 µL, 6.05 mmol) were added to the solution successively. The suspension was stirred at room temperature for 2h and the solvent was removed again under reduced pressure. The residue was dissolved in the mixture of water/EtOAc to do extraction. The organic layer was dried over Na_2SO_4, filtrated and concentrated under reduced pressure. Then the residue was dissolved in EtOH, heated at reflux for 1 h and concentrated under reduced pressure. The crude was purified by chromatography on silica gel (elution with 30-40% EtOAc/cyclohexane) to give 454 mg (1.07 mmol, 39%) of **3.33** as a white solid. ^{1}H NMR (300 MHz, $CDCl_3$) δ 7.77 (d, *J* = 7.6 Hz, 2H, aromatic H), 7.58 (d, *J* = 7.5 Hz, 2H, aromatic H), 7.46 – 7.37 (m, 2H, aromatic H), 7.36 – 7.28 (m, 2H, aromatic H), 6.37 (brs, 1H, CONH), 4.60 (brs, 1H, CONH), 4.47 (s, 2H, CH$\underline{CH_2}$O), 4.22 (t, *J* = 6.4 Hz, 1H, $\underline{CH}CH_2O$), 3.30 – 3.02 (m, 2H, NHNH$\underline{CH_2}$), 3.00 – 2.69 (m, 2H, NH$\underline{CH_2}$), 1.70 – 1.33 (m, 13H, $CH_2\underline{CH_2}\underline{CH_2}CH_2$ and C($\underline{CH_3}$)$_3$).

2-((9H-fluoren-9-yl)methyl) 1-allyl 1-(4-((tert-butoxycarbonyl)amino)butyl)hydrazine-1,2-dicarboxylate (compound 3.34)

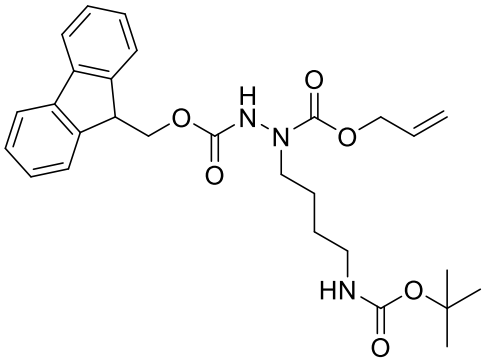

To a solution of **3.33** (1.23 g, 2.89 mmol) in DCM (30 mL) was added $NaHCO_3$ (1.22 g, 14.46 mmol). Then allyl chloroformate (461 µL, 4.34 mmol) was added to the suspension dropwise at 0°C under an argon atmosphere. After adding allyl chloroformate, the mixture was stirred at room temperature for 2 h. Water was added and the mixture was extracted with DCM. The organic layer was dried over Na_2SO_4, filtrated, concentrated and purified by chromatography on silica gel (elution with EtOAc/cyclohexane 1:2) to give 1.27 g (2.49 mmol, 86%) of **3.34** as a white solid. ^{1}H NMR (300 MHz, $CDCl_3$): δ 7.63 (d, *J* = 7.5 Hz, 2H, aromatic H), 7.58 – 7.34 (m, 3H, aromatic H and CONH), 7.32 – 7.12 (m, 4H, aromatic H), 5.75 (m, 1H, $OCH_2\underline{CH}CH_2$), 5.31 – 4.90 (m, 2H,

$OCH_2CH\underline{CH_2}$), 4.72 (brs, 1H, CONH), 4.60 – 4.22 (m, 4H, $CH\underline{CH_2}O$ and $O\underline{CH_2}CHCH_2$), 4.11 (t, *J* = 7.0 Hz, 1H, $\underline{CH}CH_2O$), 3.61 – 3.16 (m, 2H, $NHN\underline{CH_2}$), 3.13 – 2.84 (m, 2H, $NH\underline{CH_2}$), 1.61 – 1.26 (m, 13H, $CH_2\underline{CH_2}\underline{CH_2}CH_2$ and $C(CH_3)_3$). ^{13}C NMR: (75 MHz, $CDCl_3$) δ 156.2(3C, CO), 143.6(2C, aromatic), 141.3(2C, aromatic), 132.3, 127.8(2C, aromatic), 127.1(2C, aromatic), 125.1(2C, aromatic), 120.0(2C, aromatic), 117.9($OCH_2CH\underline{C}H_2$), 79.1($\underline{C}(CH_3)_3$), 67.7($O\underline{C}H_2CHCH_2$), 66.9($CH\underline{C}H_2O$), 49.9($NHN\underline{C}H_2CH_2$), 47.1($\underline{C}HCH_2O$), 40.2($NH\underline{C}H_2CH_2$), 28.4(3C, $C(\underline{C}H_3)_3$), 27.1($NHCH_2\underline{C}H_2$), 24.4($NHNCH_2\underline{C}H_2$); HRMS (ESI): Calcd for $[C_{28}H_{35}N_3O_6 + Na]^+$: 532.2418, found: 532.2423.

allyl 1-(4-((tert-butoxycarbonyl)amino)butyl)hydrazine-1-carboxylate (compound 3.35)

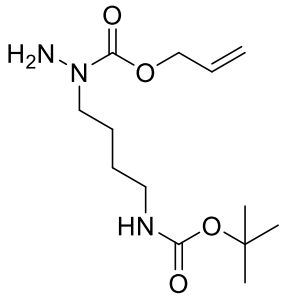

3.34 (1.27 g, 2.49 mmol) was dissolved in 20%(v/v) piperidine/DMF (10 mL). The mixture was stirred at room temperature for 20 min. The volatiles were removed under reduced pressure and the residue was taken up to EtOAc. The EtOAc solution was washed with brine, dried over Na_2SO_4, filtrated, concentrated and purified by chromatography on silica gel (elution with EtOAc/cyclohexane 1:1) to give 600 mg (2.09 mmol, 84%) of **3.35** as a colourless oil. ^{1}H NMR (300 MHz, $CDCl_3$): δ 5.87 (m, 1H, $OCH_2\underline{CH}CH_2$), 5.36 – 5.09 (m, 2H, $OCH_2CH\underline{CH_2}$), 4.90 (brs, 1H, CONH), 4.57 – 4.49 (m, 2H, $O\underline{CH_2}CHCH_2$), 4.03 (s, 2H, NH_2), 3.36 (t, *J* = 6.9 Hz, 2H, $NH_2N\underline{CH_2}CH_2$), 3.16 – 2.95 (m, 2H, $NH\underline{CH_2}CH_2$), 1.66 –1.49 (m, 2H, $NH_2NCH_2\underline{CH_2}$), 1.48 – 1.31 (m, 11H, $NHCH_2\underline{CH_2}$ and $C(CH_3)_3$); ^{13}C NMR (75 MHz, $CDCl_3$): δ 157.2(CO), 155.9(CO), 132.7($OCH_2\underline{C}HCH_2$), 117.6($OCH_2CH\underline{C}H_2$), 78.7($\underline{C}(CH_3)_3$), 66.3($O\underline{C}H_2CHCH_2$), 49.9($NH_2N\underline{C}H_2CH_2$), 40.1($NH\underline{C}H_2CH_2$), 28.3(3C, $C(\underline{C}H_3)_3$), 27.0($NHCH_2\underline{C}H_2$), 24.7($NH_2NCH_2\underline{C}H_2$); HRMS (ESI): Calcd for $[C_{13}H_{25}N_3O_4 + H]^+$: 288.1918, found: 288.1926.

allyl 2-(4-nitrophenyl) 1-(4-((tert-butoxycarbonyl)amino)butyl)hydrazine-1,2-dicarboxylate (compound 3.36)

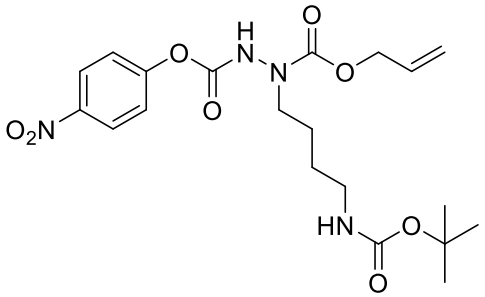

To a mixture of **3.35** (600 mg, 2.09 mmol) and pyridine (504 mL, 6.27 mmol) in dry DCM was added 4-nitrophenylchloroformate (716 mg, 3.55 mmol). The mixture was stirred at room temperature overnight. Then the volatiles were removed under reduced pressure and the residue was taken up to EtOAc. The EtOAc solution was washed with 10% K_2CO_3 aqueous solution, 10% citric acid aqueous solution and brine successively. The organic layer was dried over Na_2SO_4, filtrated, concentrated and purified by chromatography on silica gel (elution with 30-90% DCM/cyclohexane) to give 910 mg (2.01 mmol, 96%) of **3.36** as a white solid. ^{1}H NMR (300 MHz, $CDCl_3$): δ 8.25 (brs, 1H, CONH), 8.15 (d, *J* = 9.1 Hz, 2H, aromatic H), 7.26 (d, *J* = 8.9 Hz, 2H, aromatic H), 5.84 (m, 1H, $OCH_2\underline{CH}CH_2$), 5.31 – 5.10 (m, 2H, $OCH_2CH\underline{CH_2}$), 4.73 (brs, 1H, CONH), 4.62 – 4.54 (m, 2H, $O\underline{CH_2}CHCH_2$), 3.61 – 3.49 (m, 2H, $NHN\underline{CH_2}CH_2$), 3.13 – 3.00 (m, 2H, $NH\underline{CH_2}CH_2$), 1.69 – 1.54 (m, 2H, $NHNCH_2\underline{CH_2}$), 1.53 – 1.44 (m, 2H, $NHCH_2\underline{CH_2}$), 1.35 (s, 9H, $C(\underline{C}H_3)_3$); ^{13}C NMR (75 MHz, $CDCl_3$): δ 156.4(CO), 155.9(CO), 155.5(CO), 153.2(aromatic), 145.1(aromatic), 132.1($OCH_2\underline{C}HCH_2$), 125.2(2C, aromatic), 121.9(2C, aromatic), 118.3($OCH_2CH\underline{C}H_2$), 79.4($\underline{C}(CH_3)_3$), 67.2($O\underline{C}H_2CHCH_2$), 50.1($NHN\underline{C}H_2CH_2$), 40.2($NH\underline{C}H_2CH_2$), 28.4(3C, $C(\underline{C}H_3)_3$), 27.3($NHCH_2\underline{C}H_2$), 24.4($NHNCH_2\underline{C}H_2$); HRMS (ESI): Calcd for $[C_{20}H_{28}N_4O_8 + Na]^+$: 475.1799, found: 475.1803.

(9H-fluoren-9-yl)methyl (S)-6-((allyloxy)carbonyl)-3-(2-((tert-butyldimethylsilyl)oxy)propyl)-14,14-dimethyl-4,12-dioxo-13-oxa-2,3,5,6,11-pentaazapentadecanoate (compound 3.37a)

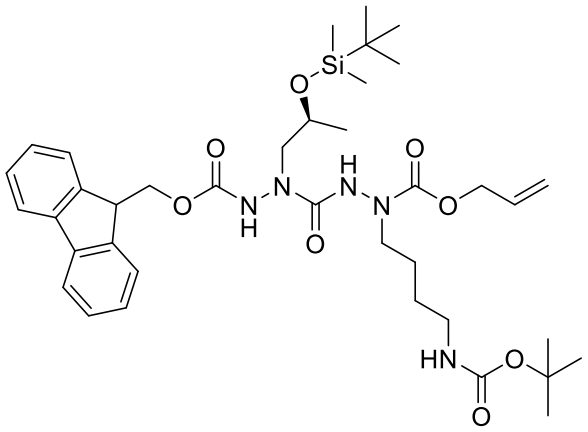

To a solution of **3.30a** (944 mg, 2.21 mmol) in DMF (20 mL) was added **3.36** (910 mg, 2.01 mmol) and DIPEA (876 μL, 5.03 mmol). The mixture was stirred at room temperature for 2 h. Water and EtOAc were added to do extraction. Organic layer was washed with brine three times, dried over Na_2SO_4, filtrated, concentrated and purified by chromatography on silica gel (elution with 10-30% EtOAc/DCM) to give 1010 mg (1.36 mmol, 68%) of **3.37a** as a colourless gel. ^{1}H NMR (400 MHz, Acetone-d_6): δ 8.83 – 8.10 (brm, 2H, CONH), 7.88 (d, J = 7.6 Hz, 2H, aromatic H), 7.72 (d, J = 6.1 Hz, 2H, aromatic H), 7.44 (t, J = 7.4 Hz, 2H, aromatic H), 7.34 (td, J = 7.5, 1.2 Hz, 2H, aromatic H), 5.86 (brs, 2H, CONH and $OCH_2\underline{CH}CH_2$), 5.32 (d, J = 17.3 Hz, 1H, $OCH_2CH\underline{CH_2}$), 5.13 (m, 1H, $OCH_2CH\underline{CH_2}$), 4.66 – 4.38 (m, 4H, $O\underline{CH_2}CHCH_2$ and $CH\underline{CH_2}O$), 4.27 (t, J = 6.8 Hz, 1H, $\underline{CH}CH_2O$), 4.13 (m, 1H, $NCH_2\underline{CH}CH_3$), 3.50 (brs, 4H, $N\underline{CH_2}CHCH_3$ and $NHN\underline{CH_2}CH_2$), 3.05 (q, J = 6.5 Hz, 2H, $NH\underline{CH_2}CH_2$), 1.67 – 1.45 (m, 4H, $CH_2\underline{CH_2}\underline{CH_2}CH_2$), 1.39 (s, 9H, $C(CH_3)_3$ from Boc), 1.17 (d, J = 5.9 Hz, 3H, $NCH_2CH\underline{CH_3}$), 0.90 (s, 9H, $SiC(CH_3)_3$), 0.09 (s, 6H, $Si(CH_3)_2$); ^{13}C NMR (101 MHz, Acetone-d_6): δ 157.6(CO), 157.1(CO), 156.7(CO), 156.2(CO), 144.8(aromatic), 144.7(aromatic), 142.2(2C, aromatic), 134.1($OCH_2\underline{C}HCH_2$), 128.7(2C, aromatic), 128.0(2C, aromatic), 126.1(2C, aromatic), 120.9(2C, aromatic), 116.9($OCH_2CH\underline{C}H_2$), 78.3($\underline{C}(CH_3)_3$ from Boc), 68.1($NCH_2\underline{C}HCH_3$), 68.0($CH\underline{C}H_2O$), 66.5($O\underline{C}H_2CHCH_2$), 56.6($N\underline{C}H_2CHCH_3$), 50.3($NHN\underline{C}H_2CH_2$), 48.0($\underline{C}HCH_2O$), 40.9($NH\underline{C}H_2CH_2$), 28.7(3C, $C(\underline{C}H_3)_3$ from Boc), 27.9($NHCH_2\underline{C}H_2$), 26.3(3C, $SiC(\underline{C}H_3)_3$), 25.4($NHNCH_2\underline{C}H_2$), 21.9($NCH_2CH\underline{C}H_3$), 18.6($Si\underline{C}(CH_3)_3$), -4.4($SiCH_3$), -4.5($SiCH_3$); HRMS (ESI): Calcd for $[C_{38}H_{57}N_5O_8Si + Na]^+$: 762.3869, found: 762.3874.

allyl (S)-5-acetamido-2-(4-((tert-butoxycarbonyl)amino)butyl)-7,9,9,10,10-pentamethyl-4-oxo-8-oxa-2,3,5-triaza-9-silaundecanoate (compound 3.37b)

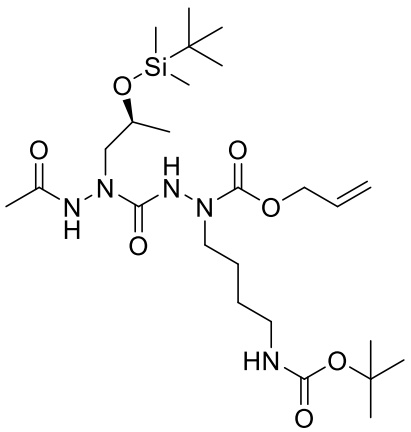

To a solution of **3.30b** (670 mg, 2.72 mmol) in DMF (20 mL) was added **3.36** (1.23 g, 2.72 mmol) and DIPEA (1184 µL, 6.80 mmol). The mixture was stirred at room temperature for 5 h. The volatiles were removed under reduced pressure and the residue was taken up to EtOAc. The EtOAc solution was washed with brine, dried over Na_2SO_4, filtrated, concentrated and purified by chromatography on silica gel (elution with EtOAc/cyclohexane 2:1) to give 1.19 g (2.13 mmol, 78%) of **3.37b** as a white solid. ^{1}H NMR (300 MHz, Acetone-d_6) δ 9.07 (brs, 1H, CONH), 8.56 (brs, 1H, CONH), 6.03 – 5.72 (m, 2H, CONH and $OCH_2\underline{CH}CH_2$), 5.31 (dd, J = 17.3, 1.8 Hz, 1H, $OCH_2CH\underline{CH_2}$), 5.11 (m, 1H, $OCH_2CH\underline{CH_2}$), 4.64 – 4.43 (s, 2H, $O\underline{CH_2}CHCH_2$), 4.02 (m, 1H, $NCH_2\underline{CH}CH_3$), 3.74 – 3.18 (m, 4H, $N\underline{CH_2}CHCH_3$ and $NHN\underline{CH_2}CH_2$), 3.15 – 2.98 (m, 2H, $NH\underline{CH_2}CH_2$), 1.95 (s, 3H, CH_3CO), 1.66 – 1.43 (m, 4H, $CH_2\underline{CH_2}\underline{CH_2}CH_2$), 1.40 (s, 9H, $C(CH_3)_3$ from Boc), 1.15 (d, J = 6.1 Hz, 3H, $NCH_2CH\underline{CH_3}$), 0.89 (s, 9H, $SiC(CH_3)_3$), 0.08 (s, 3H, $SiCH_3$), 0.07 (s, 3H, $SiCH_3$); ^{13}C NMR (75 MHz, Acetone-d_6) δ 169.5(CO), 157.6(CO), 157.1(CO), 156.7(CO), 133.9($OCH_2\underline{C}HCH_2$), 117.2(brd)($OCH_2CH\underline{C}H_2$), 78.3($\underline{C}(CH_3)_3$ from Boc), 67.7($NCH_2\underline{C}HCH_3$), 66.5($O\underline{C}H_2CHCH_2$), 56.6($N\underline{C}H_2CHCH_3$), 50.1($NHN\underline{C}H_2CH_2$), 40.7($NH\underline{C}H_2CH_2$), 28.7(3C, $C(\underline{C}H_3)_3$ from Boc), 27.7($NHCH_2\underline{C}H_2$), 26.2(3C, $SiC(\underline{C}H_3)_3$), 25.1($NHNCH_2\underline{C}H_2$), 21.9($\underline{C}H_3CO$), 21.1($CH_2CH\underline{C}H_3$), 18.5($Si\underline{C}(CH_3)_3$), -4.6(2C, $Si(CH_3)_2$); HRMS (ESI): Calcd for $[C_{25}H_{49}N_5O_7Si + Na]^+$: 582.3293, found: 582.3297.

The NMR data of peptides 6, 9 and 10

Table S17. ^{1}H NMR chemical shifts for the peptide **6** in water at 310 K

Residue	δ NH (ppm)	δ H_α (ppm)	δ H_β (ppm)	δ (ppm)
Ac	/	/	/	CH_3 2.11
ahThr[1]	ND[a]	/	3.53	γ CH 4.02; δ CH_3 1.17
aLys[2]	ND	/	3.33/3.63	γ CH_2 1.55, δ CH_2 1.60, ε CH_2 2.94
Ser[3]	ND	4.22	3.72	
Tyr[4]	ND	4.44	2.91	2,6H 6.92; 3,5H 6.72
Trp[5]	ND	4.61	3.15/3.30	2H 7.24; 4H 7.61; 5H 7.20; 6H 7.28; 7H 7.53
Lys[6]	ND	4.14	1.63/1.79	γ CH_2 1.25; δ CH_2 1.62; ε CH_2 2.94
aAla[7]	ND /	/	3.04	
aLeu[8]	ND	/	2.98/3.50	γ CH 1.81; δ CH_3 0.86
Gly[9]	ND	3.79	/	/
$NH_{2\ Z,\ E}$	ND	/	/	/

[a] : No detected.

Table S18. ^{13}C NMR chemical shifts for the peptide **6** in water at 310 K

Residue	δ CO (ppm)	δ C_α (ppm)	δ C_β (ppm)	δ (ppm)
Ac	174.1	/	/	CH_3 20.5
ahThr[1]	159.9	/	48.3	γ CH 65.3; δ CH_3 19.7
aLys[2]	FA[a]	/	48.3	γ CH_2 23.7, δ CH_2 24.4, ε CH_2 39.7
Ser[3]	173.3	57.1	61.4	/
Tyr[4]	173.4	56.0	36.2	1C 127.4; 2,6CH 130.6; 3,5CH 116.0; 4C 155.4
Trp[5]	FA	54.7	27.0	2CH 124.6; 3C 109.1; 4CH 118.5; 5CH 119.8; 6CH 122.3; 7CH 112.3; 8C 136.6; 9C 127.0
Lys[6]	173.2	53.3	29.8	γ CH_2 22.1; δ CH_2 26.8; ε CH_2 39.7
aAla[7]	FA	/	36.3	/
aLeu[8]	FA	/	56.1	γ CH 26.2; δ CH_3 19.6
Gly[9]	FA	43.4	/	/

[a] : Fail to assignment.

Table S19. ^{1}H NMR chemical shifts for the peptide **10** in water at 310 K

Residue	δ NH (ppm)	δ H_α (ppm)	δ H_β (ppm)	δ (ppm)
ahThr[1]	FA[a]	/	3.49	γ CH 4.13; δ CH_3 1.18
aLys[2]	FA	/	3.29/3.65	γ CH_2 1.62; δ CH_2 1.62; ε CH_2 FA
Ser[3]	6.92	4.23	3.73	/
Tyr[4]	8.08	4.44	2.92	2,6H 6.94; 3,5H 6.75
Trp[5]	7.89	4.55	3.19/3.29	2H 7.24; 4H 7.63; 5H 7.21; 6H 7.28; 7H 7.53
Lys[6]	8.02	4.15	1.65/1.80	γ CH_2 1.26; δ CH_2 1.64; ε CH_2 2.97
aAla[7]	FA	/	3.04	/
aLeu[8]	FA	/	3.00/3.49	γ CH 1.79; δ CH_3 0.86
Gly[9]	7.03	3.79	/	/
$NH_{2\ Z,\ E}$	6.98, 7.42	/	/	/

[a] : Fail to assignment.

Table S20. ^{13}C NMR chemical shifts for the peptide **10** in water at 310 K

Residue	δ CO (ppm)	δ C_α (ppm)	δ C_β (ppm)	δ (ppm)
ahThr[1]	159.9	/	56.8	γ CH 65.5; δ CH_3 19.6
aLys[2]	FA[a]	/	48.2	γ CH_2 24.2; δ CH_2 24.2; ε CH_2 FA[a]
Ser[3]	173.3	56.9	61.4	/
Tyr[4]	173.4	55.9	35.9	1C 128.1; 2,6CH 130.4; 3,5CH 115.7; 4C 154.8
Trp[5]	FA	54.7	26.8	2CH 124.6; 3C 109.2; 4CH 118.4; 5CH 119.6; 6CH 122.2; 7CH 112.1; 8C 136.7; 9C 127.0
Lys[6]	173.2	53.1	29.6	γ CH_2 22.0; δ CH_2 26.5; ε CH_2 39.5
aAla[7]	FA	/	36.3	/
aLeu[8]	FA	/	55.9	γ CH 26.1; δ CH_3 19.6
Gly[9]	FA	43.3	/	/

[a] : Fail to assignment.

Table S21. ^{1}H NMR chemical shifts for the peptide **10** in DMF at 333 K

Residue	δ NH (ppm)	δ H_α (ppm)	δ H_β (ppm)	δ (ppm)
ahThr[1]	FA[a]	/	3.45/3.58	γ CH 4.13; δ CH_3 1.10
aLys[2]	FA	/	3.27/3.81	γ CH_2 1.62/1.67, δ CH_2 1.71, ε CH_2 2.98
Ser[3]	7.17	4.18	3.75/3.77	/
Tyr[4]	8.20	4.33	2.90/2.98	2,6H 6.92; 3,5H 6.64
Trp[5]	7.91	4.59	3.17/3.44	2H 7.33; 4H 7.61; 5H 7.05; 6H 7.11; 7H 7.42
Lys[6]	7.82	4.25	1.86/1.93	γ CH_2 1.57; δ CH_2 1.74; ε CH_2 3.02
aAla[7]	FA	/	3.04	/
aLeu[8]	FA	/	FA	γ CH 1.88; δ CH_3 0.87
Gly[9]	6.70	3.70	/	/
$NH_{2\ Z,\ E}$	6.79, 7.03	/	/	/

[a] : Fail to assignment.

Table S22. ^{13}C NMR chemical shifts for the peptide **10** in DMF at 333 K

Residue	δ CO (ppm)	δ C_α (ppm)	δ C_β (ppm)	δ (ppm)
ahThr[1]	158.8	/	57.1	γ CH 65.5; δ CH_3 20.6
aLys[2]	FA[a]	/	47.9	γ CH_2 24.0, δ CH_2 25.8, ε CH_2 39.9
Ser[3]	173.3	58.7	61.4	/
Tyr[4]	172.7	57.0	35.9	1C 128.1; 2,6CH 130.0; 3,5CH 115.2; 4C 156.4
Trp[5]	173.1	55.0	26.9	2CH 123.8; 3C 110.7; 4CH 118.2; 5CH 118.6; 6CH 121.1; 7CH 111.4; 8C 137.0; 9C 127.5
Lys[6]	171.8	53.2	29.8	γ CH_2 22.5; δ CH_2 27.8; ε CH_2 39.9
aAla[7]	157.4	/	35.6	/
aLeu[8]	FA	/	55.9	γ CH 26.3; δ CH_3 19.8
Gly[9]	FA	43.6	/	/

[a] : Fail to assignment.

Table S23. ^{1}H NMR chemical shifts for the peptide **9** in methanol at 258 K

Residue	δ NH (ppm)	δ H_α (ppm)	δ H_β (ppm)	δ (ppm)
ahThr[1]	FA[a]	/	3.45/3.51	γ CH 4.12; δ CH_3 1.14/1.17
aLys[2]	9.54	/	3.22/3.81	γ CH_2 1.59; δ CH_2 1.59; ε CH_2 2.86
Ser[3]	7.25	4.14	3.78	/
Tyr[4]	8.36	4.31	2.92, 2.95	2,6H 6.79/6.83; 3,5H 6.50/6.57
Trp[5]	7.99	4.38	3.21, 3.35	2H 7.24; 4H 7.54/7.56; 5H 7.04; 6H 7.14; 7H 7.37
Lys[6]	8.09	3.98	1.73, 1.81	γ CH_2 1.30/1.35; δ CH_2 1.62; ε CH_2 2.88
Ala[7]	8.11	4.15	1.42	/
Leu[8]	7.88	4.22	1.59, 1.71	γ CH 1.66; δ CH_3 0.84
Gly[9]	8.13/8.20	3.70, 3.88	/	/
$NH_{2\ Z,\ E}$	6.95, 7.44	/	/	/

[a] : Fail to assignment.

Table S24. ^{13}C NMR chemical shifts for the peptide **9** in methanol at 258 K

Residue	δ CO (ppm)	δ C_α (ppm)	δ C_β (ppm)	δ (ppm)
ahThr[1]	160.7	/	57.9	γ CH 66.6; δ CH_3 21.1
aLys[2]	FA[a]	/	49.0	γ CH_2 25.9; δ CH_2 25.9; ε CH_2 40.4
Ser[3]	174.7	60.0	62.1	/
Tyr[4]	174.8	58.4	36.7	1C 128.1; 2,6CH 130.4; 3,5CH 115.7; 4C 154.8
Trp[5]	175.7	57.2	27.6	2CH 124.6; 3C 109.2; 4CH 118.4; 5CH 119.6; 6CH 122.2; 7CH 112.1; 8C 136.7; 9C 127.0
Lys[6]	175.7	56.5	31.2	γ CH_2 23.6; δ CH_2 28.1; ε CH_2 40.5
Ala[7]	176.2	52.0	17.0	/
Leu[8]	175.3	53.6	40.8	γ CH 25.5; δ CH_3 21.3/23.6
Gly[9]	174.8	43.3	/	/

[a] : Fail to assignment.

Mass and LC-MS spectra of peptides 1-11

Peptide **1**

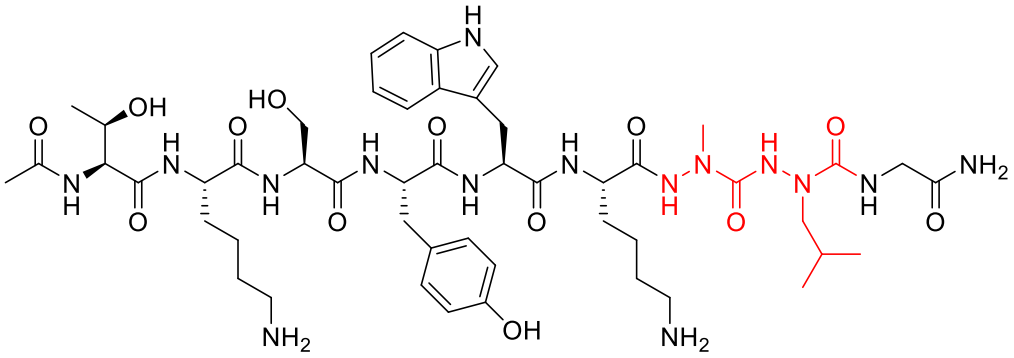

The peptide was purified by semi-preparative HPLC (Linear gradients of 5-47 % ACN in H_2O containing 0.1% formic acid in 13 min, yield: 15%).

HRMS (ESI): Calcd for $[C_{50}H_{77}N_{15}O_{13} + Na]^+$: 1119.5746, found: 1119.5743.

HPLC purity: XSELECT column (C18, 2.1 x 75mm-2.5µm); ACN /H_2O + 0.1 % TFA, gradient 5–100 % in 20 min; R_t = 4.78 min, 100 %.

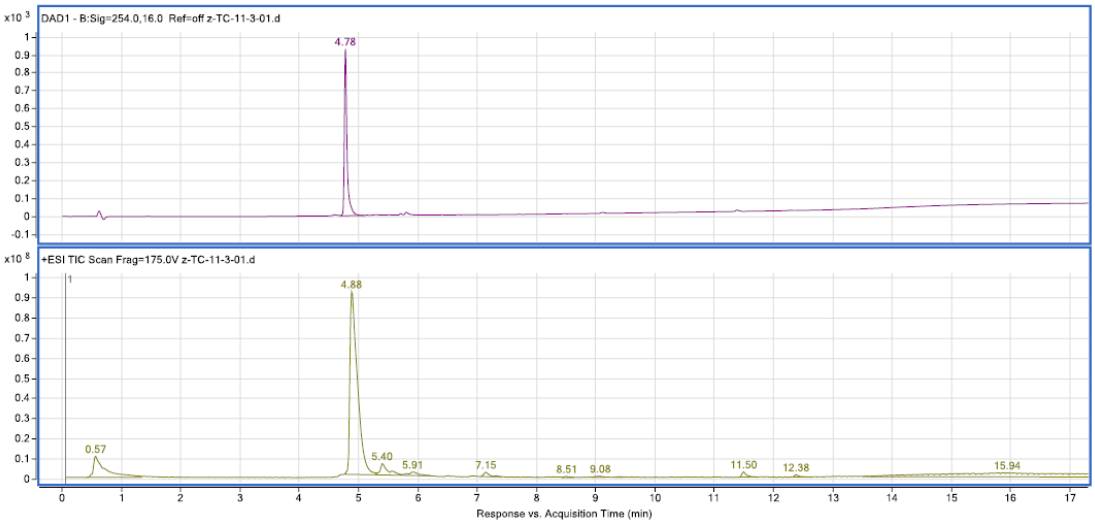

Peptide **2**

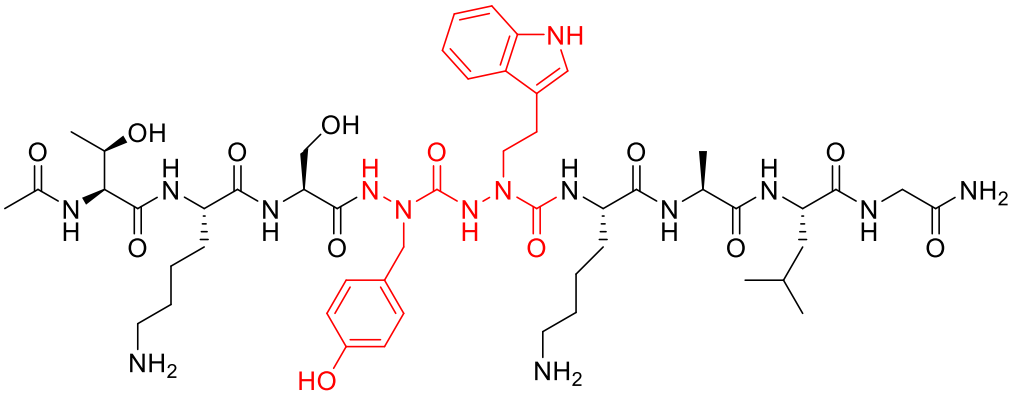

The peptide was purified by semi-preparative HPLC (Linear gradients of 5-47 % ACN in H_2O containing 0.1% formic acid in 13 min, yield: 10%).

HRMS (ESI): Calcd for $[C_{51}H_{79}N_{15}O_{13} + Na]^+$: 1111.6083, found: 1111.6089.

HPLC purity: ECLIPSE PLUS column (C18, 2.1 x 50mm-1.8µm); ACN /H_2O + 0.1 % TFA, gradient 5–100 % in 12 min; R_t = 2.08 min, 100 %.

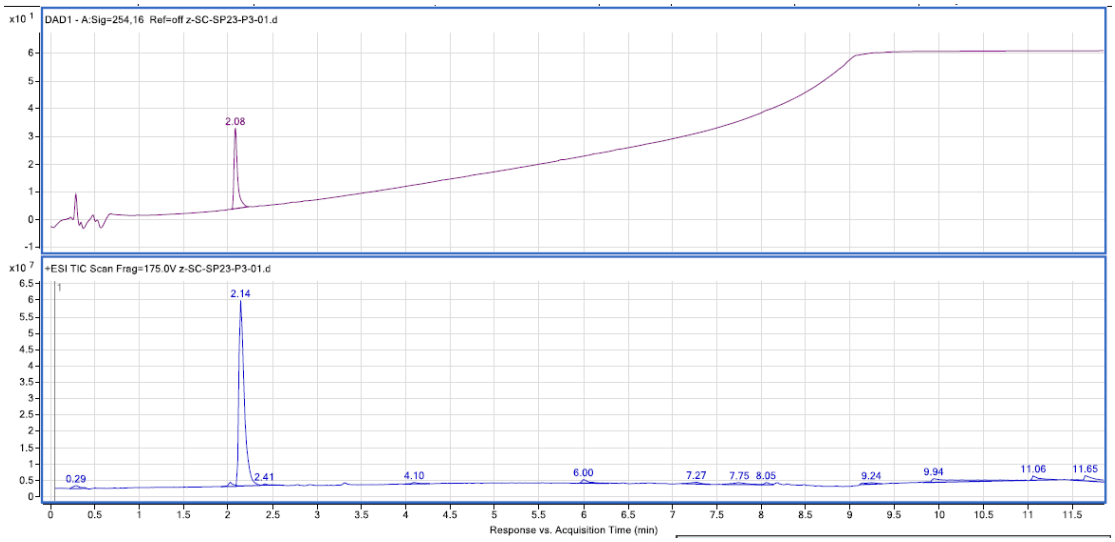

Peptide **3**

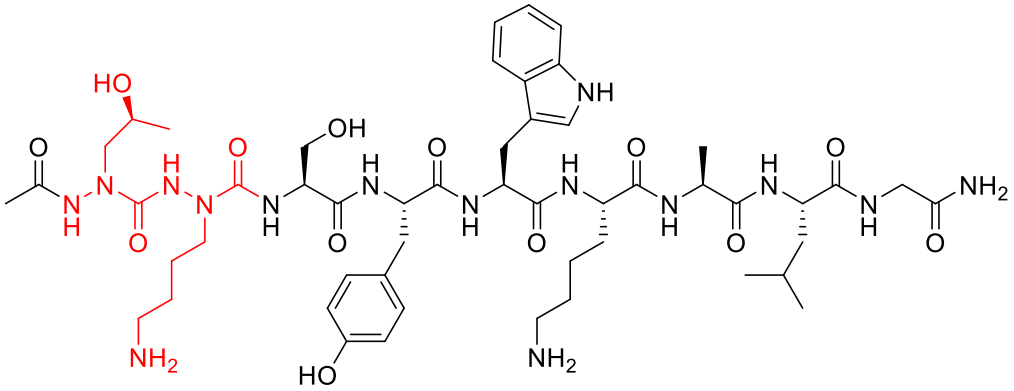

The peptide was purified by semi-preparative HPLC (Linear gradients of 5-47 % ACN in H_2O containing 0.1% formic acid in 13 min, yield: 12%).

HRMS (ESI): Calcd for $[C_{51}H_{79}N_{15}O_{13} + H]^+$: 1110.6055, found: 1110.6049.

HPLC purity: XSELECT column (C18, 2.1 x 75mm-2.5µm); ACN /H_2O + 0.1 % TFA, gradient 5–100 % in 20 min; R_t = 4.89 min, 100 %.

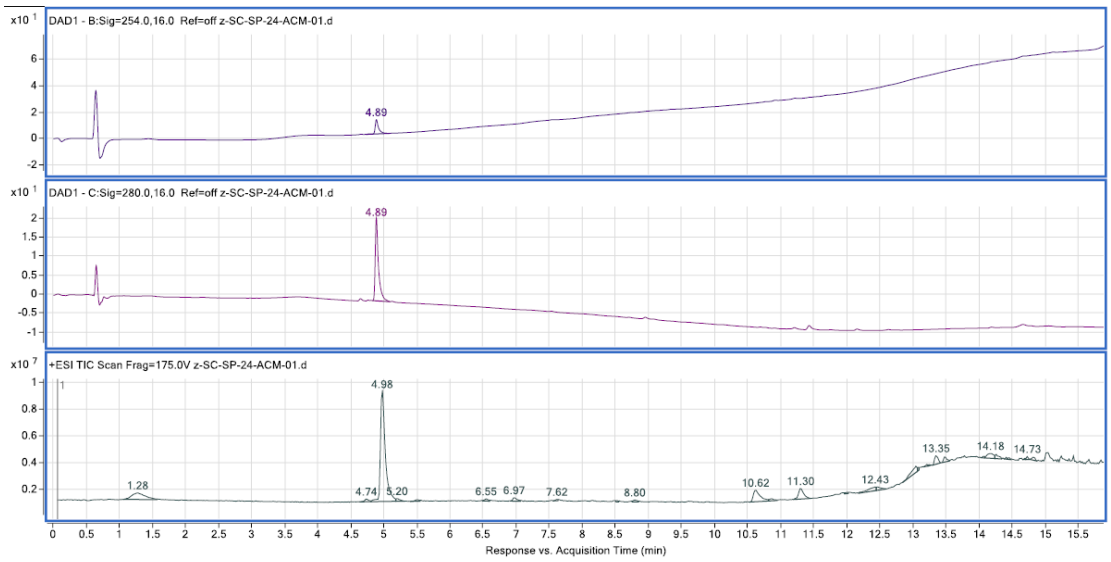

Peptide **4**

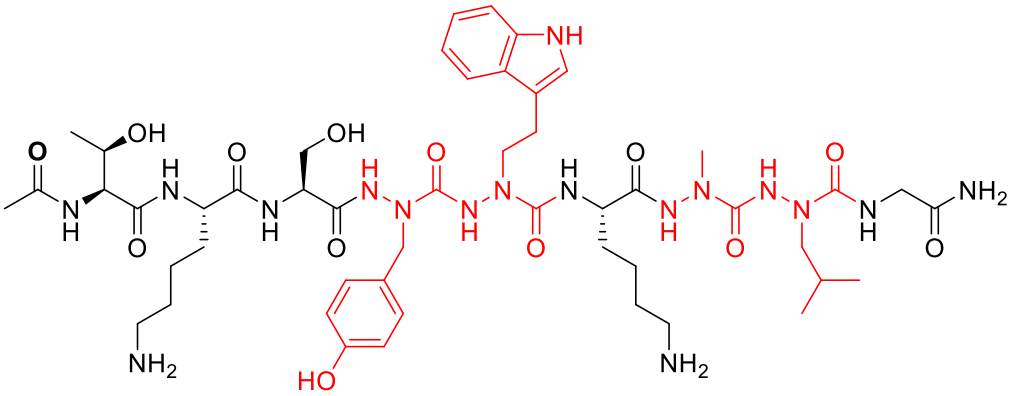

The peptide was purified by semi-preparative HPLC (Linear gradients of 5-47 % ACN in H_2O containing 0.1% formic acid in 13 min, yield: 13%).

HRMS (ESI): Calcd for $[C_{49}H_{77}N_{17}O_{13} + Na]^+$: 1134.5779, found: 1134.5775.

HPLC purity: XSELECT column (C18, 2.1 x 75mm-2.5µm); ACN /H_2O + 0.1 % TFA, gradient 5–100 % in 20 min; R_t = 5.00 min, 100 %.

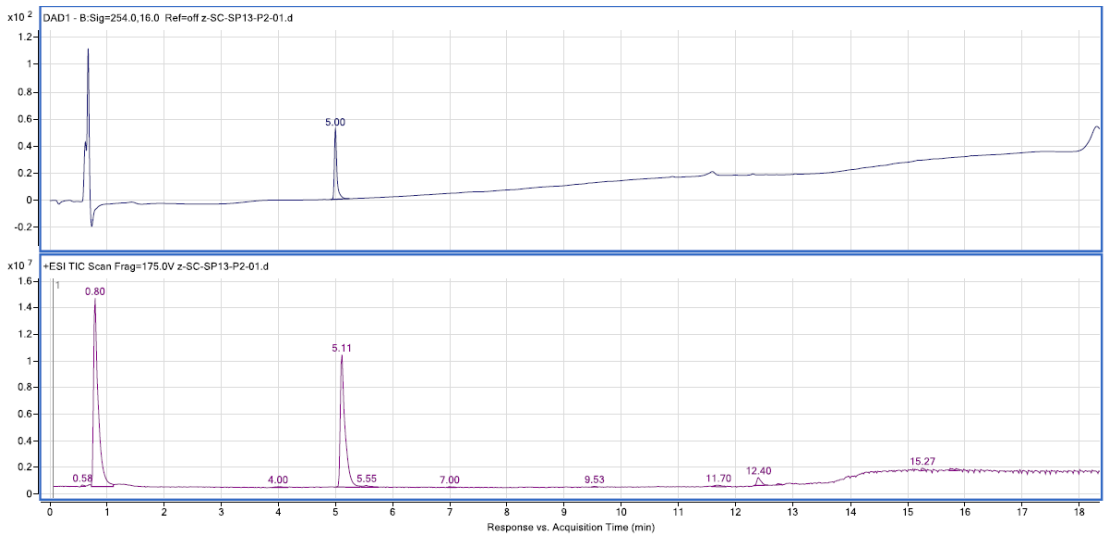

Peptide **5**

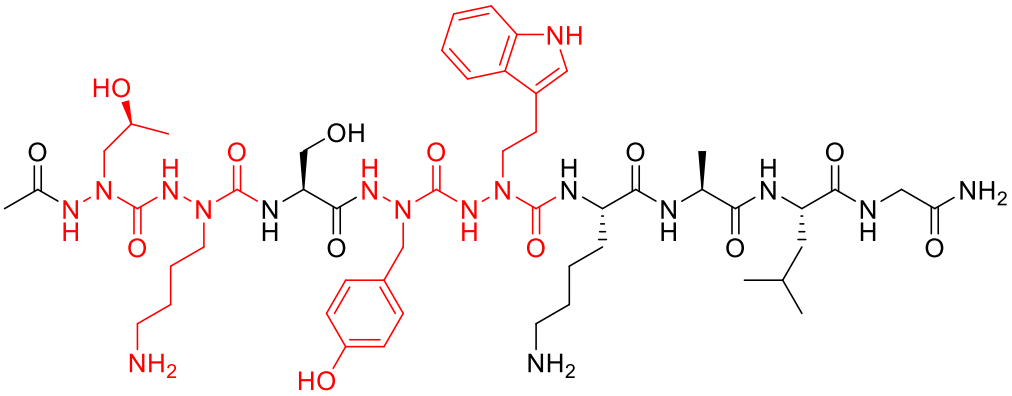

The peptide was purified by semi-preparative HPLC (Linear gradients of 5-47 % ACN in H_2O containing 0.1% formic acid in 13 min, yield: 8%).

HRMS (ESI): Calcd for $[C_{50}H_{79}N_{17}O_{13} + H]^+$: 1126.6116, found: 1126.6112.

HPLC purity: XSELECT column (C18, 2.1 x 75mm-2.5µm); ACN /H_2O + 0.1 % TFA, gradient 5–100 % in 20 min; R_t = 5.09 min, 100 %.

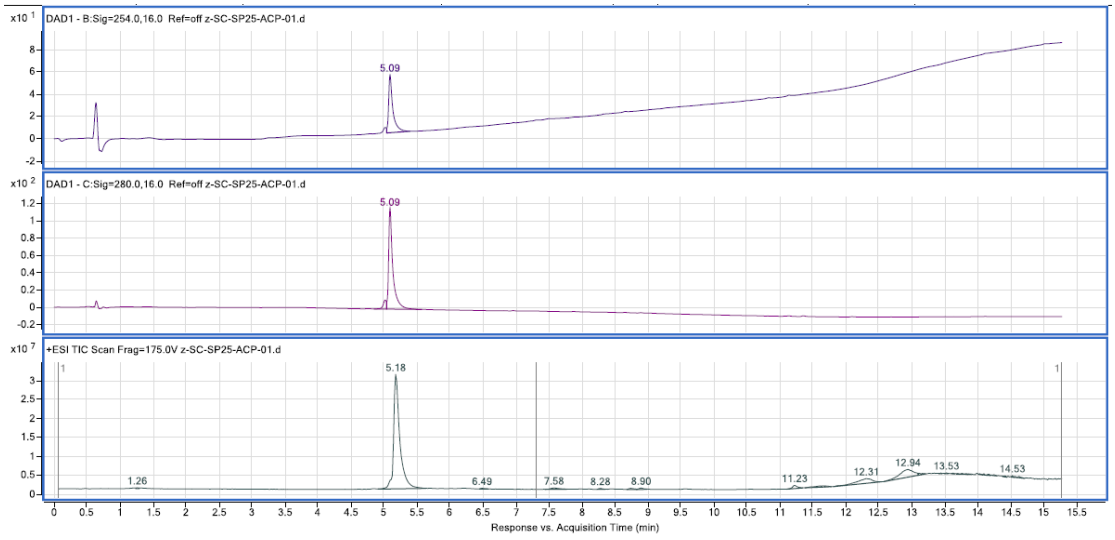

Peptide **6**

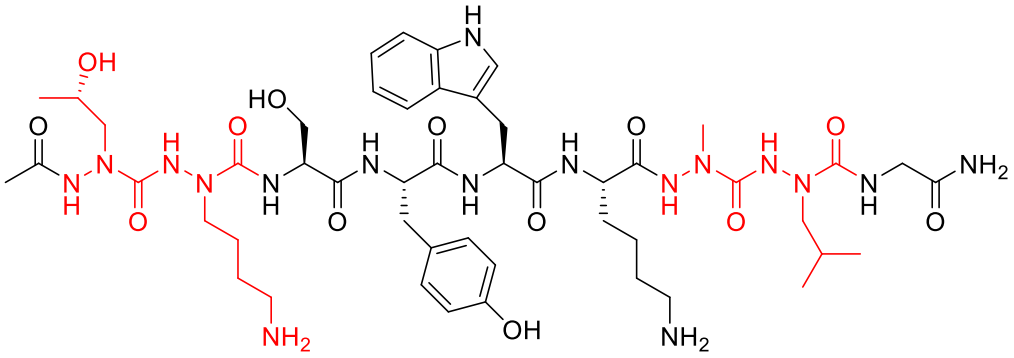

The peptide was purified by semi-preparative HPLC (Linear gradients of 5-47 % ACN in H_2O containing 0.1% formic acid in 13 min, yield: 14%).

HRMS (ESI): Calcd for $[C_{49}H_{77}N_{17}O_{13} + Na]^+$: 1134.5779, found: 1134.5776.

HPLC purity: XSELECT column (C18, 2.1 x 75mm-2.5µm); ACN /H_2O + 0.1 % TFA, gradient 5–100 % in 20 min; R_t = 4.75 min, 100 %.

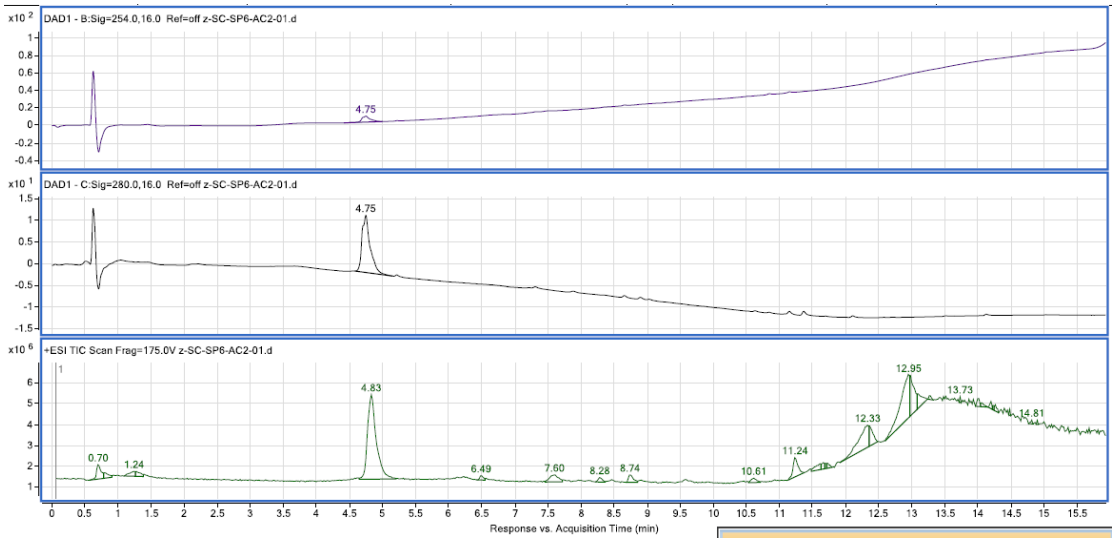

Peptide **7**

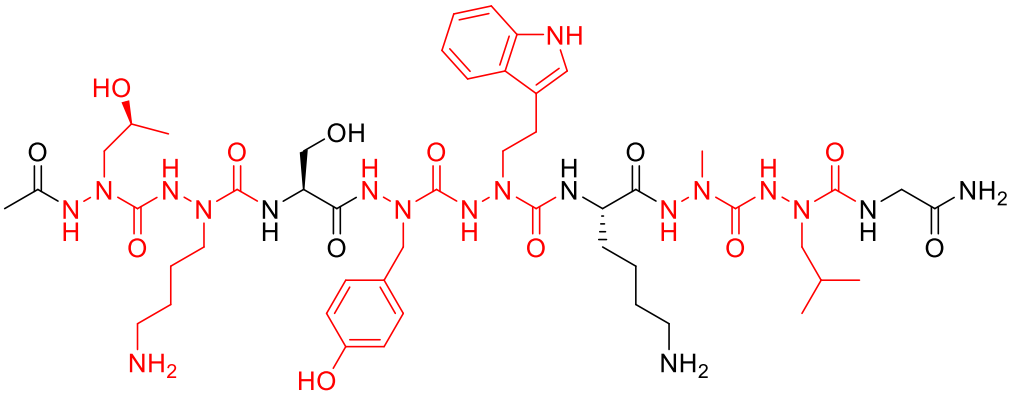

The peptide was purified by semi-preparative HPLC (Linear gradients of 5-47 % ACN in H_2O containing 0.1% formic acid in 13 min, yield: 10%).

HRMS (ESI): Calcd for $[C_{48}H_{77}N_{19}O_{13} + H]^+$: 1128.6021, found: 1128.6018.

HPLC purity: ECLIPSE PLUS column (C18, 2.1 x 50mm-1.8µm); ACN /H_2O + 0.1 % TFA, gradient 5–100 % in 12 min; R_t = 1.98 min, 100 %.

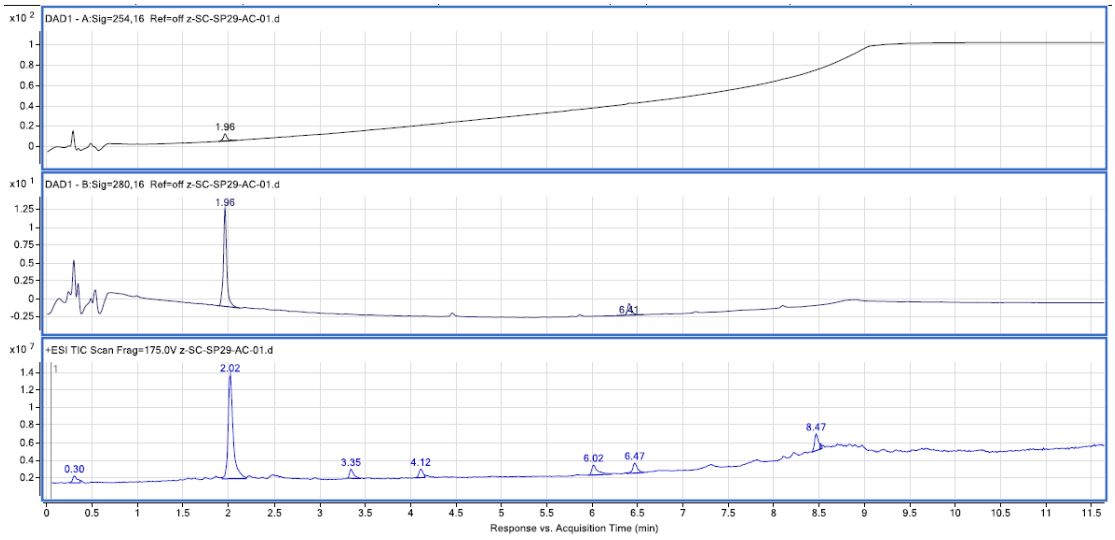

Peptide **8**

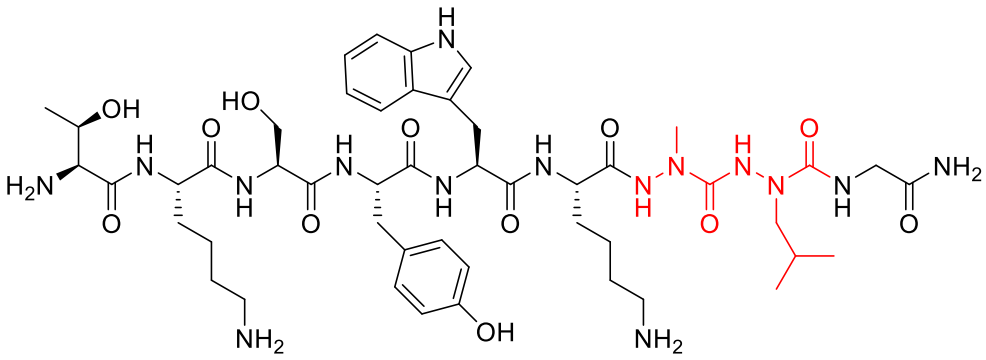

The peptide was purified by semi-preparative HPLC (Linear gradients of 5-47 % ACN in H_2O containing 0.1% formic acid in 13 min, yield: 13%).

HRMS (ESI): Calcd for $[C_{48}H_{75}N_{15}O_{12} + Na]^+$: 1076.5612, found: 1076.5605.

HPLC purity: XSELECT column (C18, 2.1 x 75mm-2.5µm); ACN /H_2O + 0.1 % TFA, gradient 5–100 % in 20 min; R_t = 4.07 min, 100 %.

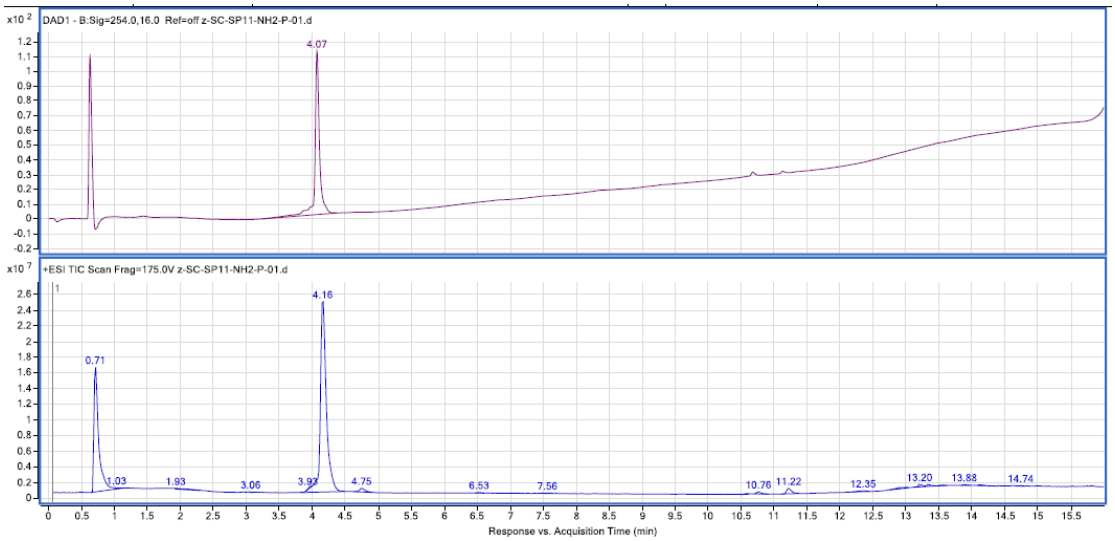

Peptide **9**

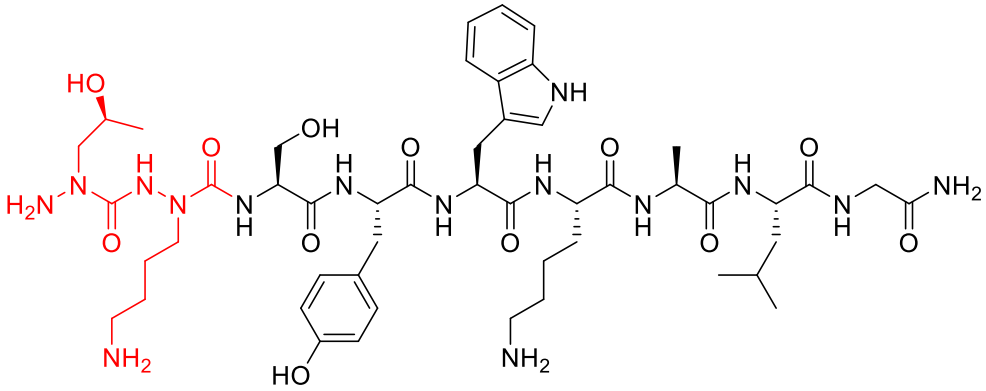

The peptide was purified by semi-preparative HPLC (Linear gradients of 5-47 % ACN in H_2O containing 0.1% formic acid in 13 min, yield: 14%).

HRMS (ESI): Calcd for $[C_{49}H_{77}N_{15}O_{12} + H]^+$: 1068.5949, found: 1068.5945.

HPLC purity: POROSHELL column (C18, 2.1 x 100mm-2.7µm); ACN /H_2O + 0.1 % TFA, gradient 5–100 % in 20 min; R_t = 5.54 min, 100 %.

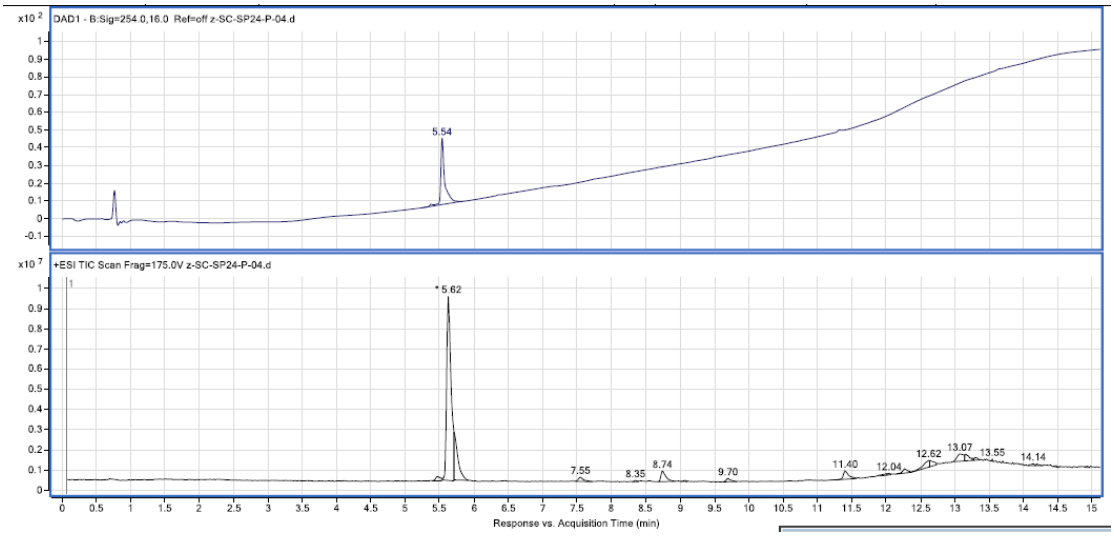

Peptide **10**

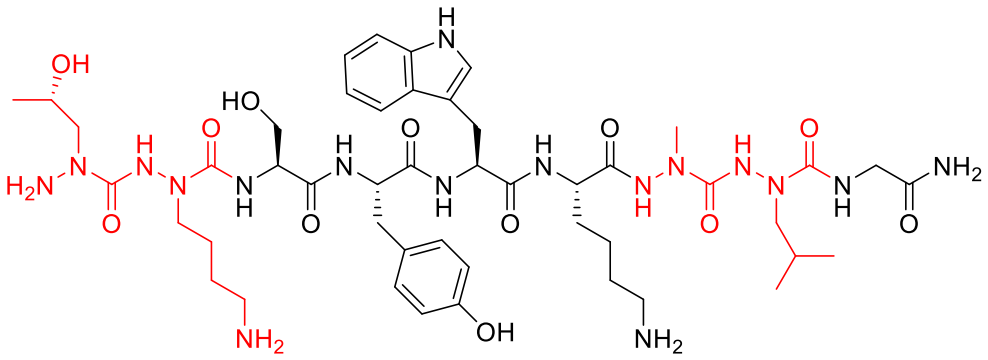

The peptide was purified by semi-preparative HPLC (Linear gradients of 5-47 % ACN in H_2O containing 0.1% formic acid or TFA in 13 min, yield: 7%).

HRMS (ESI): Calcd for $[C_{47}H_{75}N_{17}O_{12} + Na]^+$: 1092.5673, found: 1092.5668.

HPLC purity: XSELECT column (C18, 2.1 x 75mm-2.5µm); ACN /H_2O + 0.1 % TFA, gradient 5–100 % in 20 min; R_t = 4.64 min, 100 %.

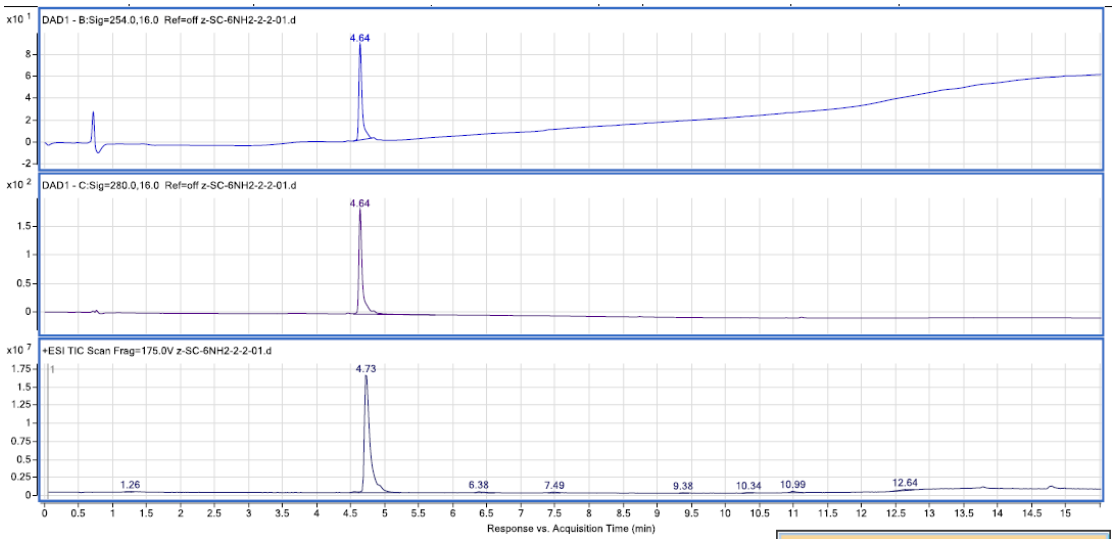

Peptide **11**

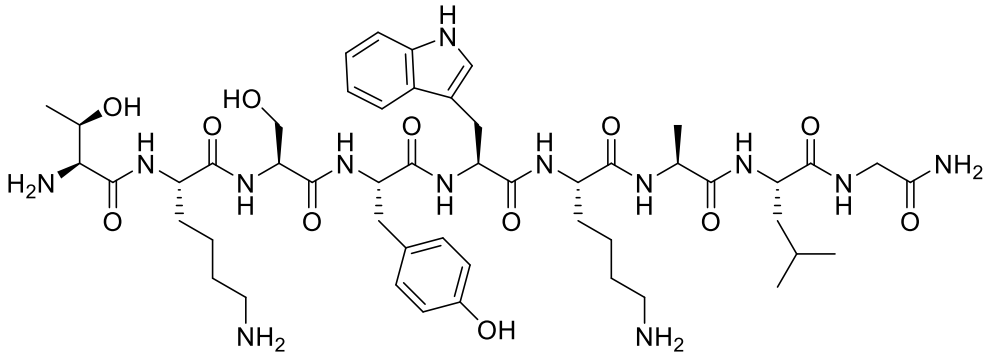

The peptide was purified by semi-preparative HPLC (Linear gradients of 5-47 % ACN in H_2O containing 0.1% formic acid or TFA in 13 min, yield: 32%).

HRMS (ESI): Calcd for $[C_{50}H_{77}N_{13}O_{12} + H]^+$: 1052.5887, found: 1052.5880.

HPLC purity: XSELECT column (C18, 2.1 x 75mm-2.5µm); ACN /H_2O + 0.1 % TFA, gradient 5–100 % in 20 min; R_t = 4.20 min, 100 %.

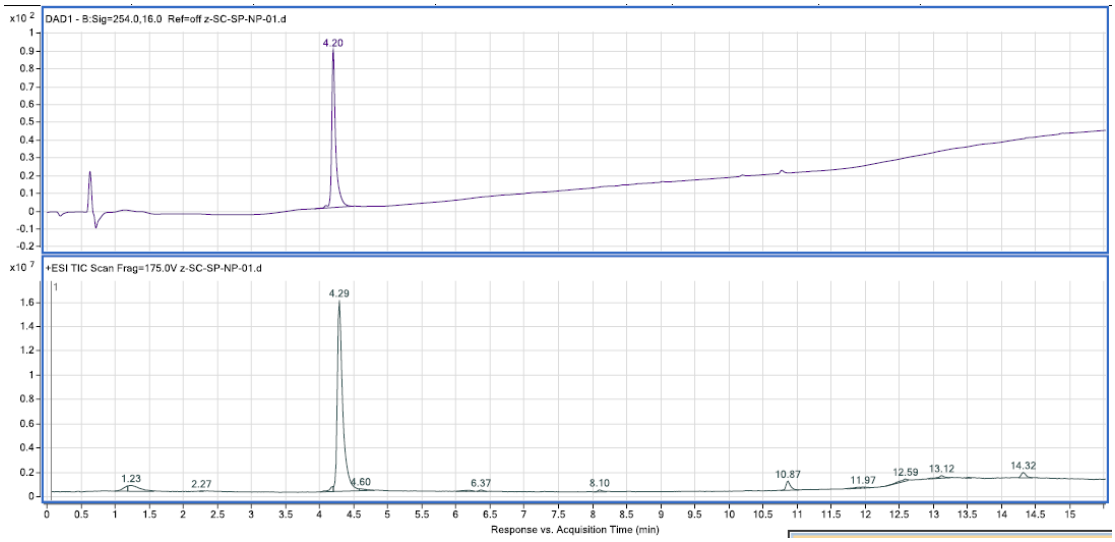

Compounds in chapter 4

(S)-2-(2-(2-((((9H-fluoren-9-yl)methoxy)carbonyl)amino)ethyl)-3,6-dioxo-1,2,4-triazinan-5-yl)acetic acid (compound 4.1)

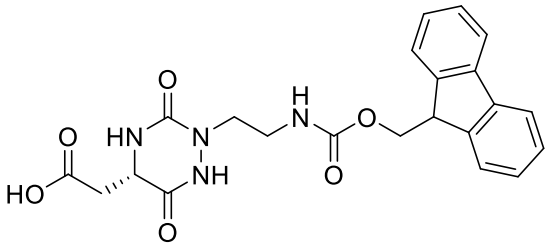

To a solution of **4.6** (3.90 g, 7.38 mmol) in MeOH/EtOAc (120 mL/30 mL) was added 10% Pd/C (975 mg) and triethylsilane (2.35 mL, 14.77 mmol). The mixture was stirred at room temperature under argon and triethylsilane (2.35 mL, 14.77 mmol) was added every 10 min (the total addition of triethylsilane was 7.05 mL during the reaction). The mixture was stirred at room temperature for 30 min and then was filtrated through a pad of celite. The filtrate was concentrated under reduced pressure and purified by chromatography on silica gel (5-10 % MeOH in DCM) to give 2.50 g (5.70 mmol, 77%) of **4.1** as a white solid. ^{1}H NMR (300 MHz, Methanol-d_4) δ 7.78 (d, J = 7.4 Hz, 2H, aromatic H), 7.64 (d, J = 7.4 Hz, 2H, aromatic H), 7.41 – 7.25 (m, 4H, aromatic H), 4.39 – 4.24 (m, 3H, CH$\underline{CH_2}$O and αH), 4.20 (t, J = 7.0 Hz, 1H, $\underline{CH}CH_2O$), 3.76 – 3.51 (m, 2H, NHN$\underline{CH_2}$), 3.43 – 3.32 (m, 2H, $NHCH_2$), 2.89 – 2.65 (m, 2H, βH); ^{13}C NMR (75 MHz, Methanol-d_4) δ 173.6(CO), 165.5(CO), 159.0(CO), 155.8(CO), 145.4(2C, aromatic), 142.6(2C, aromatic), 128.7(2C, aromatic), 128.2(2C, aromatic), 126.3(2C, aromatic), 120.9(2C, aromatic), 68.0(CH$\underline{C}H_2O$), 52.1(αC), 48.4($\underline{C}HCH_2O$), 47.5(NHN$\underline{C}H_2$), 39.3($NHCH_2$), 36.6(βC); HRMS (ESI): Calcd for [$C_{22}H_{22}N_4O_6$ + Na]$^+$: 461.1432, found: 461.1437.

benzyl (S)-2-(2-(2-((((9H-fluoren-9-yl)methoxy)carbonyl)amino)ethyl)-3,6-dioxo-1,2,4-triazinan-5-yl)acetate (compound 4.6)

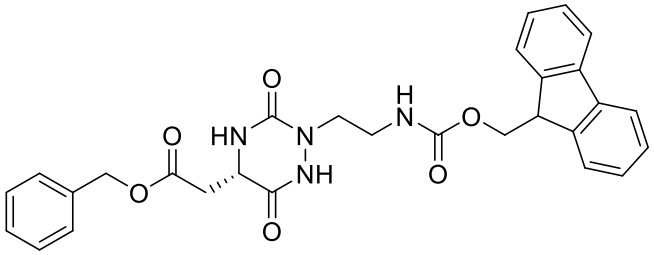

To a solution of **4.7** (2.61 g, 4.04 mmol) in DCM (20 mL) was added 20 mL trifluoroacetic acid. The mixture was stirred at room temperature for 5 h. The volatiles were removed under reduced pressure to give crude product which was purified by chromatography on silica gel (2.5 % MeOH in DCM) to give 2.02 g (3.82 mmol, 95%) of **4.6** as a white solid. ^{1}H NMR (300 MHz, $CDCl_3$) δ 10.04 (brs, 1H, CONH), 7.72 (d, *J* = 7.5 Hz, 2H, aromatic H), 7.53 (d, *J* = 7.4 Hz, 2H, aromatic H), 7.45 – 7.16 (m, 9H, aromatic H), 6.63 (s, 1H, CONH), 5.89 (s, 1H, CONH), 5.10 (s, 2H, Ph$\underline{CH_2}$), 4.41 – 4.23 (m, 3H, CH$\underline{CH_2}$O and αH), 4.14 (m, 1H, $\underline{CH}CH_2O$), 3.81 – 3.55 (m, 2H, NHN$\underline{CH_2}$), 3.53 – 3.29 (m, 2H, $NHCH_2$), 2.95 (dd, *J* = 17.2, 4.0 Hz, 1H, βH), 2.77 (dd, *J* = 17.2, 8.1 Hz, 1H, βH); ^{13}C NMR (75 MHz, $CDCl_3$) δ 170.3(CO), 164.0(CO), 157.2(CO), 154.0(CO), 143.9(aromatic), 143.9(aromatic), 141.4(2C, aromatic), 135.3(aromatic), 128.7(2C, aromatic), 128.6(aromatic), 128.4(2C, aromatic), 127.8(2C, aromatic), 127.2(2C, aromatic), 125.1(2C, aromatic), 120.1(2C, aromatic), 67.2(2C, CH$\underline{C}H_2O$ and Ph$\underline{C}H_2$), 51.0(αC), 47.2($\underline{C}HCH_2O$), 46.9(NHN$\underline{C}H_2$), 38.6($NHCH_2$), 36.2(βC); HRMS (ESI): Calcd for $[C_{29}H_{28}N_4O_6 + H]^+$: 529.2082, found: 529.2085.

benzyl (S)-7-((tert-butoxycarbonyl)amino)-10-carbamoyl-1-(9H-fluoren-9-yl)-3,8-dioxo-2-oxa-4,7,9-triazadodecan-12-oate (compound 4.7)

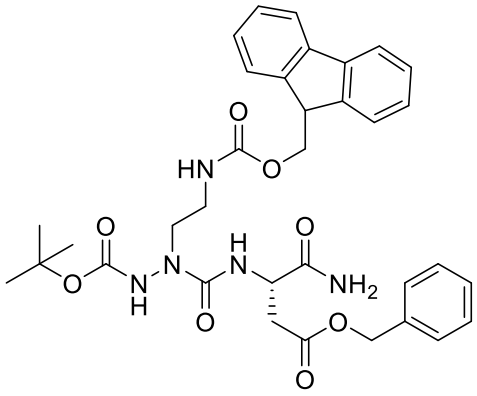

Triphosgene (299 mg, 1.01 mmol) was dissolved in dry DCM (8 mL) under an argon atmosphere. A solution of **4.11** (1.00 g, 2.52 mmol) and DIPEA (526 μL, 3.02 mmol) in dry DCM (50 mL) was added dropwise under ice-cooling. The mixture was stirred at room temperature for 15 min, then **4.13** (520 mg, 2.01 mmol) and DIPEA (965 uL, 5.54 mmol) were added successively. The mixture was stirred at room temperature overnight. DCM (30 mL) and water (50 mL) was added to do extraction, the organic phase was washed with brine, dried over anhydrous Na_2SO_4, filtrated and concentrated under reduced pressure. The residue was purified by chromatography on silica gel (1-

3% MeOH in DCM) to give 790 mg (1.22 mmol, 61%) of **4.7** as a white solid. ^{1}H NMR (300 MHz, $CDCl_3$) δ 7.86 (s, 1H, CONH), 7.75 (d, *J* = 7.5 Hz, 2H, aromatic H), 7.59 (dd, *J* = 7.4, 3.3 Hz, 2H, aromatic H), 7.44 – 7.20 (m, 9H, aromatic H), 6.85 (brs, 1H, CONH), 6.76 (d, *J* = 8.9 Hz, 1H, CONH), 5.99 (brs, 1H, CONH), 5.86 (brs, 1H, CONH), 5.14 – 4.90 (m, 2H, Ph$\underline{CH_2}$), 4.71 – 4.57 (m, 1H, αH), 4.48 – 4.13 (m, 3H, $\underline{CHCH_2}$O), 4.05 – 2.67 (m, 5H, N$\underline{CH_2CH_2}$NH and βH), 2.64 – 2.26 (m, 1H, βH), 1.50 (s, 9H, C($\underline{CH_3}$)$_3$); ^{13}C NMR (75 MHz, $CDCl_3$) δ 174.0(CO), 171.9(CO), 158.0(CO), 157.8(CO), 155.1(CO), 143.9(2C, aromatic), 141.3(2C, aromatic), 135.4(aromatic), 128.6(2C, aromatic), 128.3(aromatic), 128.1(2C, aromatic), 127.8(2C, aromatic), 127.1(2C, aromatic), 125.3(aromatic), 125.2(aromatic), 120.0(2C, aromatic), 82.6($\underline{C}$(CH$_3$)$_3$), 67.2(CH$\underline{C}$H$_2$O), 66.6(Ph$\underline{C}$H$_2$), 50.3(αC), 47.5($\underline{C}$HCH$_2$O), 47.1(NHN$\underline{C}$H$_2$), 38.0(NHCH$_2$), 35.4(βC), 28.2(3C, C($\underline{C}$H$_3$)$_3$); HRMS (ESI): Calcd for [$C_{34}H_{39}N_5O_8$ + H]$^+$: 646.2871, found: 646.2889.

4-benzyl 1-methyl ((1-(9H-fluoren-9-yl)-11,11-dimethyl-3,9-dioxo-2,10-dioxa-4,7,8-triazadodecan-7-yl)carbonyl)-L-aspartate (compound 4.8)

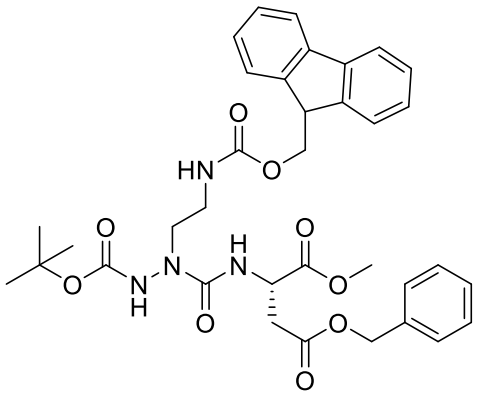

Triphosgene (22 mg, 0.07 mmol) was dissolved in dry DCM (2 mL) under an argon atmosphere. A solution of **4.15** (50 mg, 0.18 mmol) and DIPEA (67 μL, 0.38 mmol) in dry DCM (4 mL) was added dropwise under ice-cooling. The mixture was stirred at room temperature for 15 min, then **4.11** (72 mg, 0.18 mmol) and DIPEA (35 uL, 0.20 mmol) were added successively. The mixture was stirred at room temperature overnight. DCM (10 mL) and water (10 mL) was added to do extraction, the organic phase was washed with brine, dried over anhydrous Na_2SO_4, filtrated and concentrated under reduced pressure. The residue was purified by chromatography on silica gel (EtOAc /cyclohexane 1.5:1) to give 37 mg (0.06 mmol, 31%) of **4.8** as a white solid. ^{1}H NMR (300 MHz, $CDCl_3$) δ 7.74 (d, *J* = 7.4, 2H, aromatic H), 7.64 – 7.53 (m, 2H, aromatic H), 7.42 – 7.21 (m, 10H,

aromatic H and CONH), 6.36 (d, *J* = 8.3 Hz, 1H, CONH), 5.53 (m, 1H, CONH), 5.12 – 4.93 (m, 2H, Ph$\underline{CH_2}$), 4.64 (m, 1H, αH), 4.46 – 4.18 (m, 3H, $\underline{CHCH_2}O$), 3.93 – 3.18 (m, 7H, $N\underline{CH_2CH_2}NH$ and $O\underline{CH_3}$), 3.04 – 2.66 (m, 2H, βH), 1.48 (s, 9H, $C(\underline{CH_3})_3$); ^{13}C NMR (75 MHz, $CDCl_3$) δ 171.5(CO), 170.9(CO), 157.7(2C, (CO)), 154.5(CO), 144.2(aromatic), 144.0(aromatic), 141.4(2C, aromatic), 135.6(aromatic), 128.7(2C, aromatic), 128.4(aromatic), 128.3(2C, aromatic), 127.8(2C, aromatic), 127.2(2C, aromatic), 125.4(aromatic), 125.4(aromatic), 120.0(2C, aromatic), 82.2($\underline{C}(CH_3)_3$), 67.4($PhCH_2$), 66.7($CH\underline{C}H_2O$), 52.6(αC), 50.0(OCH_3), 47.2(2C, $\underline{C}HCH_2O$ and $NHN\underline{C}H_2$), 38.2($NHCH_2$), 37.0(βC), 28.3(3C, $C(\underline{C}H_3)_3$); HRMS (ESI): Calcd for $[C_{35}H_{40}N_4O_9 + Na]^+$: 683.2687, found: 683.2693.

(9H-fluoren-9-yl)methyl (2-hydroxyethyl)carbamate (compound 4.9)

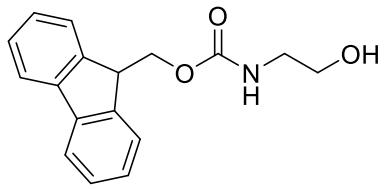

To a solution of ethanolamine (1.00 g, 16.37 mmol) in DCM (100 mL) was added $NaHCO_3$ (6.88 g, 81.85 mmol). A solution of Fmoc-Cl (3.81 g, 14.73 mmol) in dry DCM (100 mL) was added to the mixture dropwise under ice-cooling. The reaction was stirred at room temperature overnight. Then water (100 mL) was added to do extraction. The organic phase was washed with brine, dried over Na_2SO_4, filtrated and concentrated to get crude white solid. The solid was stirred with 60 mL mixed solvent of EtOAc and cyclohexene (1:3) at room temperature for 10 min. The suspension was filtered and the solid was washed with cyclohexene and dried under vacuum to give 3.82 g (13.48 mmol, 92%) of **4.9** as a white solid. ^1H NMR (300 MHz, $CDCl_3$) δ 7.77 (dt, *J* = 7.5 Hz, 2H, aromatic H), 7.60 (d, *J* = 7.4 Hz, 2H, aromatic H), 7.41 (tdd, *J* = 7.5, 1.2, 0.7 Hz, 2H, aromatic H), 7.32 (td, *J* = 7.4, 1.2 Hz, 2H, aromatic H), 5.17 (s, 1H, CONH), 4.44 (d, *J* = 6.7 Hz, 2H, $CH\underline{CH_2}O$), 4.22 (t, *J* = 6.7 Hz, 1H, $\underline{CH}CH_2O$), 3.78 – 3.62 (m, 2H, $\underline{CH_2}OH$), 3.45 – 3.16 (m, 2H, $NH\underline{CH_2}$), 2.14 (s, 1H, $CH_2\underline{OH}$); ^{13}C NMR (75 MHz, $CDCl_3$) δ 157.3(CO), 144.1(2C, aromatic), 141.5(2C, aromatic), 127.9(2C, aromatic), 127.2(2C, aromatic), 125.1(2C, aromatic), 120.1(2C, aromatic), 66.9($CH\underline{C}H_2O$), 62.4($\underline{C}H_2OH$), 47.5($\underline{C}HCH_2O$), 43.7($NH\underline{C}H_2$).

(9H-fluoren-9-yl)methyl (2-oxoethyl)carbamate (compound 4.10)

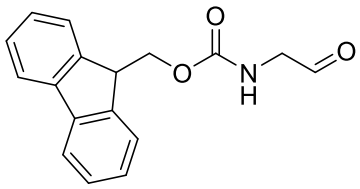

To a solution of **4.9** (3.90 g, 13.78 mmol) in DCM (120 mL) was added Dess-Martin periodinane (9.6 g, 22.63 mmol). The mixture was stirred at room temperature for 2 h. Then 30 mL saturated $Na_2S_2O_3$ aqueous solution was added and the mixture was further stirred at room temperature for 1 h. 50 mL saturated $NaHCO_3$ aqueous solution was added to do extraction. The organic phase was washed with $NaHCO_3$ aqueous solution and brine successively, dried over Na_2SO_4, filtrated, concentrated and purified by chromatography on silica gel (elution with EtOAc /cyclohexane 1:1) to give 2.52 g (8.96 mmol, 65%) of **4.10** as a white solid. ^{1}H NMR (300 MHz, $CDCl_3$) δ 9.52 (s, 1H, CHO), 7.67 (d, *J* = 7.5 Hz, 2H, aromatic H), 7.49 (d, *J* = 7.5 Hz, 2H, aromatic H), 7.36 – 7.13 (m, 4H, aromatic H), 5.39 (s, 1H, CONH), 4.34 (d, *J* = 7.0 Hz, 2H, CH$\underline{CH_2}$O), 4.13 (t, *J* = 6.8 Hz, 1H, $\underline{CH}CH_2O$), 4.07 – 3.92 (m, 2H, NH$\underline{CH_2}$); ^{13}C NMR (75 MHz, $CDCl_3$) δ 196.6(CHO), 156.4(CO), 143.9(2C, aromatic), 141.4(2C, aromatic), 127.9(2C, aromatic), 127.2(2C, aromatic), 125.1(2C, aromatic), 120.1(2C, aromatic), 67.3(CH$\underline{C}H_2O$), 51.7(NH$\underline{C}H_2$), 47.3($\underline{C}HCH_2O$).

tert-butyl 2-(2-((((9H-fluoren-9-yl)methoxy)carbonyl)amino)ethyl)hydrazine-1-carboxylate (compound 4.11)

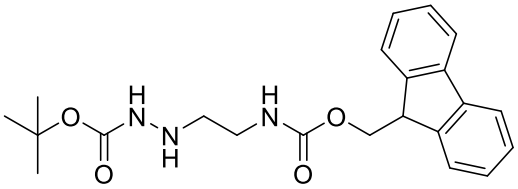

The mixture of *tert*-butyl carbazate (1.18 g, 8.89 mmol) and **4.10** (2.5 g, 8.89 mmol) in EtOH (60 mL) was stirred at reflux for 2 h. The solvent was removed under reduced pressure and the residue was dissolved in THF (60 mL). $NaBH_3CN$ (838 mg, 13.34 mmol) and acetic acid (1018 μL, 17.78 mmol) were added to the solution successively. The suspension was stirred at room temperature for 3 h and the solvent was removed again under reduced pressure. The residue was dissolved in the mixture of water/EtOAc to do extraction. The organic layer was dried over Na_2SO_4, filtrated and concentrated under reduced pressure. Then the residue was dissolved in EtOH, heated at reflux for

1 h and concentrated under reduced pressure. The crude was purified by chromatography on silica gel (elution with EtOAc /cyclohexane 4:6) to give 3.21 g (8.08 mmol, 91%) of **4.11** as a white solid. ^{1}H NMR (300 MHz, $CDCl_3$) δ 7.76 (dt, *J* = 7.6, 1.0 Hz, 2H, aromatic H), 7.61 (d, *J* = 7.4 Hz, 2H, aromatic H), 7.45 – 7.25 (m, 4H, aromatic H), 6.42 (brs, 1H, CONH), 5.67 (brs, 1H, CONH), 4.42 (d, *J* = 7.0 Hz, 2H, CH$\underline{CH_2}$O), 4.23 (t, *J* = 6.9 Hz, 1H, $\underline{CH}CH_2O$), 4.08 (brs, 1H, CONH$\underline{NH}$), 3.37 – 3.14 (m, 2H, NHN$\underline{CH_2}$), 2.96 – 2.72 (m, 2H, NH$\underline{CH_2}$), 1.47 (s, 9H, C($\underline{CH_3}$)$_3$); ^{13}C NMR (75 MHz, $CDCl_3$) δ 157.2, 156.9, 144.1(2C, aromatic), 141.4(2C, aromatic), 127.7(2C, aromatic), 127.1(2C, aromatic), 125.1(2C, aromatic), 120.0(2C, aromatic), 80.7($\underline{C}(CH_3)_3$), 66.7(CH$\underline{C}H_2$O), 51.4(NHN$\underline{C}H_2$), 47.4($\underline{C}HCH_2O$), 38.6($NHCH_2$), 28.4(3C, C($\underline{C}H_3$)$_3$); HRMS (ESI): Calcd for $[C_{22}H_{27}N_3O_4 + Na]^+$: 420.1894, found: 420.1879.

benzyl (S)-4-amino-3-((tert-butoxycarbonyl)amino)-4-oxobutanoate (compound 4.12)

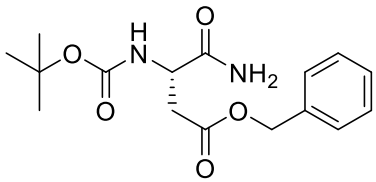

To a solution of Boc-Asp(OBzl)-OH (4.50 g, 13.92 mmol) in DCM/DMF (40 mL/10 mL) was added HOBt (2.93 g, 15.31 mmol) and EDC-HCl (2.93 g, 15.31 mmol). The mixture was stirred at room temperature for 30 min. Then 20% ammonia aqueous solution (1.47 mL, 15.31 mmol) was added to the mixture and the reaction was stirred at room temperature for 2 h. Water was added to do extraction and the organic phase was washed with brine twice, dried over Na_2SO_4, filtrated, concentrated to give a crude solid. The solid was treated with 15 mL EtOAc to get suspension. The suspension was stirred at room temperature for 10 min and then filtrated to get a white solid which was further washed with 5 mL EtOAc. The white solid was dried under reduced pressure to give 4.20 g (13.03 mmol, 94%) of **4.12** as a white solid. ^{1}H NMR (300 MHz, $CDCl_3$) δ 7.42 – 7.29 (m, 5H, aromatic H), 6.46 (brs, 1H, CONH), 5.69 (brs, 2H, $CONH_2$), 5.15 (s, 2H, Ph$\underline{CH_2}$), 4.62 – 4.46 (m, 1H, αH), 3.05 (dd, *J* = 17.1, 4.7 Hz, 1H, βH), 2.75 (dd, *J* = 17.1, 6.2 Hz, 1H, βH), 1.46 (s, 9H, C($\underline{CH_3}$)$_3$); ^{13}C NMR (75 MHz, $CDCl_3$) δ 173.3(CO), 171.9(CO), 155.6(CO), 135.5(aromatic), 128.8(2C, aromatic), 128.5(aromatic), 128.4(2C, aromatic), 80.7($\underline{C}(CH_3)_3$), 67.0(Ph$\underline{C}H_2$), 50.5(αC), 36.2(βC), 28.4(3C, C($\underline{C}H_3$)$_3$); HRMS (ESI): Calcd for $[C_{16}H_{22}N_2O_5 + Na]^+$: 345.1421, found:

345.1430.

benzyl (S)-3,4-diamino-4-oxobutanoate·HCl (compound 4.13)

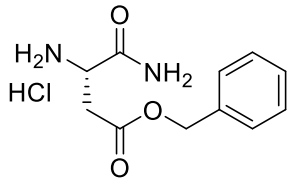

To a solution of **4.12** (4.16 g, 12.91 mmol) in 1,4-dioxane (100 mL) was added 4 M HCl in dioxane (48 mL). The mixture was stirred at room temperature overnight. The volatiles were removed under reduced pressure to give 3.33 g (12.91 mmol, 100%) of **4.13** as a white solid. ^{1}H NMR (300 MHz, Methanol-d_4) δ 7.45 – 7.24 (m, 5H, aromatic H), 5.24 (s, 2H, Ph$\underline{CH_2}$), 4.26 (dd, J = 8.3, 4.3 Hz, 1H, αH), 3.18 – 2.85 (m, 2H, βH); HRMS (ESI): Calcd for $[C_{11}H_{14}N_2O_3 + H]^+$: 223.1077, found: 223.1079.

4-benzyl 1-methyl L-aspartate·HCl (compound 4.15)

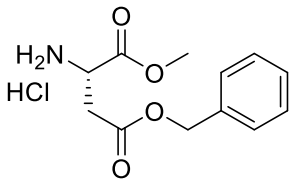

To a solution of **4.16** (1030 mg, 3.06 mmol) in MeOH (10 mL) was added 4 M HCl in dioxane (11.5 mL). The mixture was stirred at room for 2 h. The volatiles were removed under reduced pressure to give 836 mg (2.99 mmol, 98%) of **4.15** as a yellow solid. ^{1}H NMR (300 MHz, $CDCl_3$) δ 8.86 (brs, 3H, NH_3), 7.41 – 7.20 (m, 5H, aromatic H), 5.17 (s, 2H, Ph$\underline{CH_2}$), 4.60 (m, 1H, αH), 3.69 (s, 3H, O$\underline{CH_3}$), 3.45 – 3.14 (m, 2H, βH); HRMS (ESI): Calcd for $[C_{12}H_{15}N_3O_4 + H]^+$: 238.1074, found: 238.1075.

4-benzyl 1-methyl (tert-butoxycarbonyl)-L-aspartate (compound 4.16)

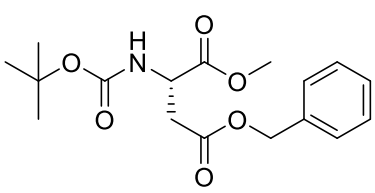

To a solution of Boc-Asp(OBzl)-OH (1.00 g, 3.09 mmol) in DMF (7 mL) was added K_2CO_3 (641 mg, 4.64 mmol). Then iodomethane (385 μL, 6.19 mmol) was added dropwise at 0°C under an argon atmosphere. The mixture was stirred at room temperature for 3 h. H_2O and EtOAc were added to do extraction and the organic phase was washed with brine twice, dried over Na_2SO_4, filtrated, and concentrated to give 1.04 g (3.09 mmol, 100%) of **4.16** as a yellowish solid. ^{1}H NMR (300 MHz, $CDCl_3$) δ 7.41 – 7.27 (m, 5H, aromatic H), 5.53 (d, J = 8.7 Hz, 1H, CONH), 5.20 – 5.06 (m, 2H, Ph$\underline{CH_2}$), 4.60 (m, 1H, αH), 3.69 (s, 3H, O$\underline{CH_3}$), 3.11 – 2.80 (m, 2H, βH), 1.45 (s, 9H, C($\underline{CH_3}$)$_3$); ^{13}C NMR (75 MHz, $CDCl_3$) δ 171.5(CO), 170.7(CO), 155.4(CO), 135.5(aromatic), 128.6(2C, aromatic), 128.4(aromatic), 128.3(2C, aromatic), 80.1($\underline{C}(CH_3)_3$), 66.8(Ph$\underline{C}H_2$), 52.6(αC), 50.1(OCH_3), 36.9(βC), 28.3(3C, C($\underline{C}H_3$)$_3$).

Compound **4.2**

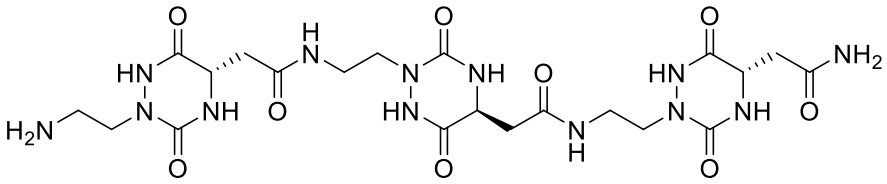

The compound was purified by semi-preparative HPLC (Linear gradients of 2-20 % ACN in H_2O containing 0.1% formic acid in 13 min, yield: 49%)

HRMS (ESI): Calcd for $[C_{21}H_{33}N_{13}O_9 + H]^+$: 612.2597, found: 612.2603.

HPLC purity: XSELECT column (C18, 2.1 x 75mm-2.5µm); ACN /H_2O + 0.1 % TFA, gradient 5–100 % in 20 min; R_t = 0.44 min, 100 %.

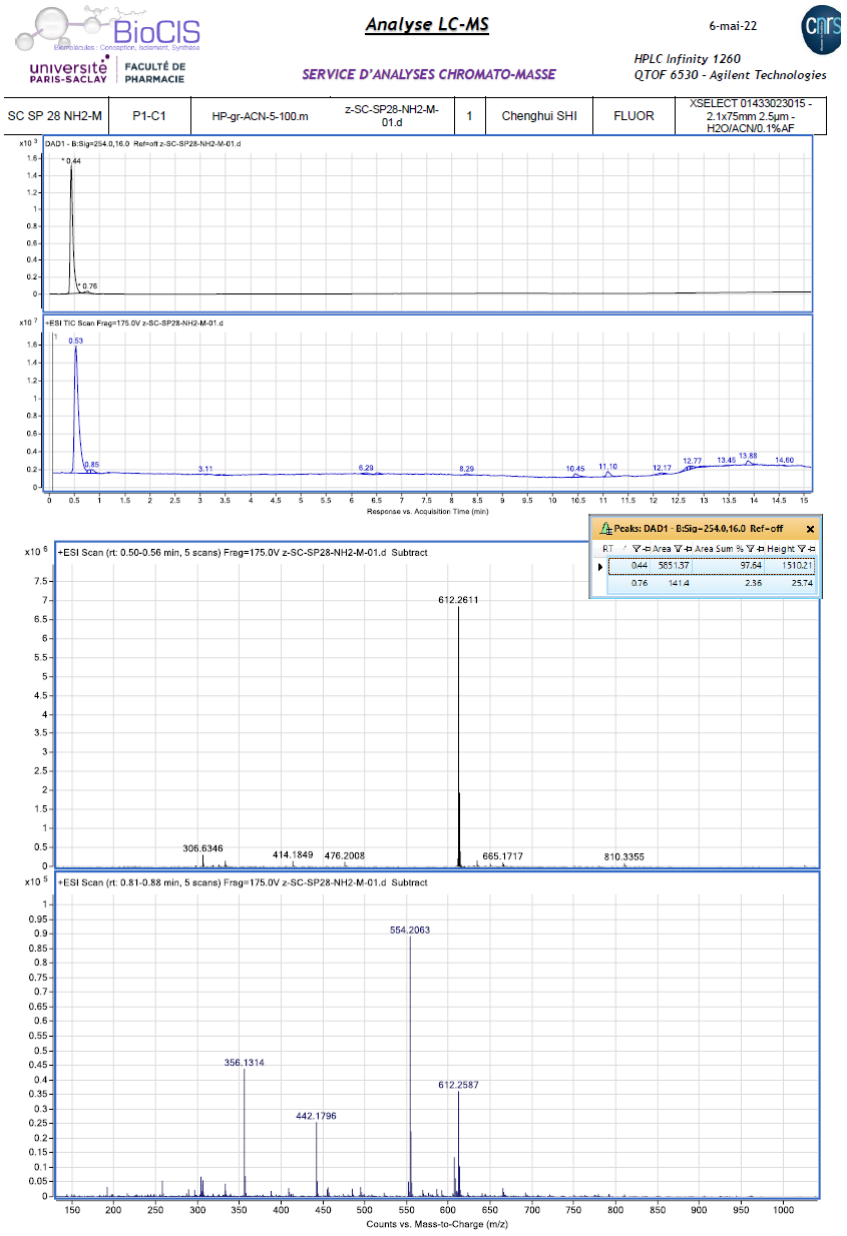

Compound **4.3**

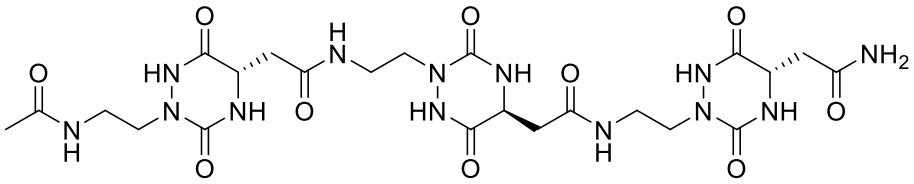

The compound was purified by semi-preparative HPLC (Linear gradients of 1-20 % ACN in H_2O containing 0.1% formic acid in 15 min, yield: 34%)

HRMS (ESI): Calcd for $[C_{23}H_{35}N_{13}O_{10} + Na]^+$: 676.2522, found: 676.2537.

HPLC purity: XSELECT column (C18, 2.1 x 75mm-2.5µm); ACN /H_2O + 0.1 % TFA, gradient 5–100 % in 20 min; R_t = 0.69 and 0.88 min (two conformers), 100 %.

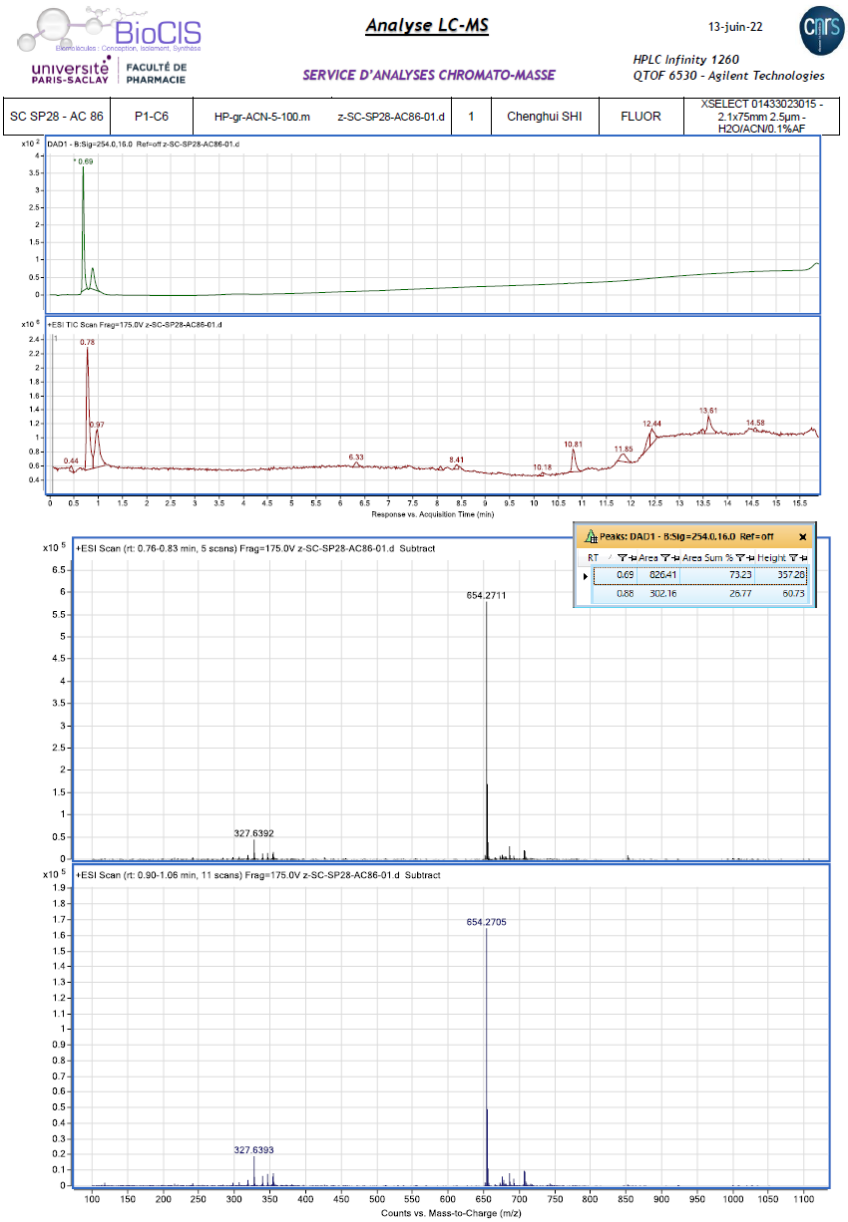

Compound **4.4**

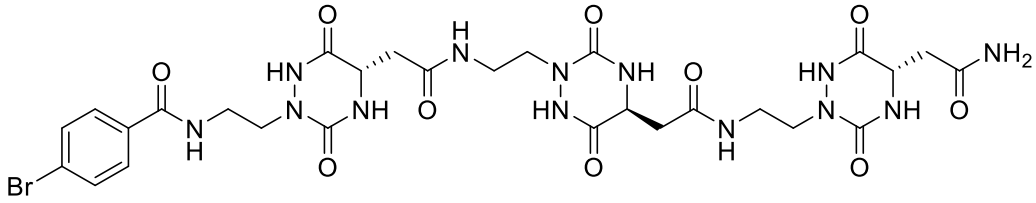

The compound was purified by washing with 5 mL ACN/H_2O (1/1) twice (yield: 19%).

HRMS (ESI): Calcd for $[C_{28}H_{36}BrN_{13}O_{10} + H]^+$: 794.1964, found: 794.1946.

HPLC purity: XSELECT column (C18, 2.1 x 75mm-2.5µm); ACN /H_2O + 0.1 % TFA, gradient 5–100 % in 20 min; R_t = 5.16 min, 100 %.

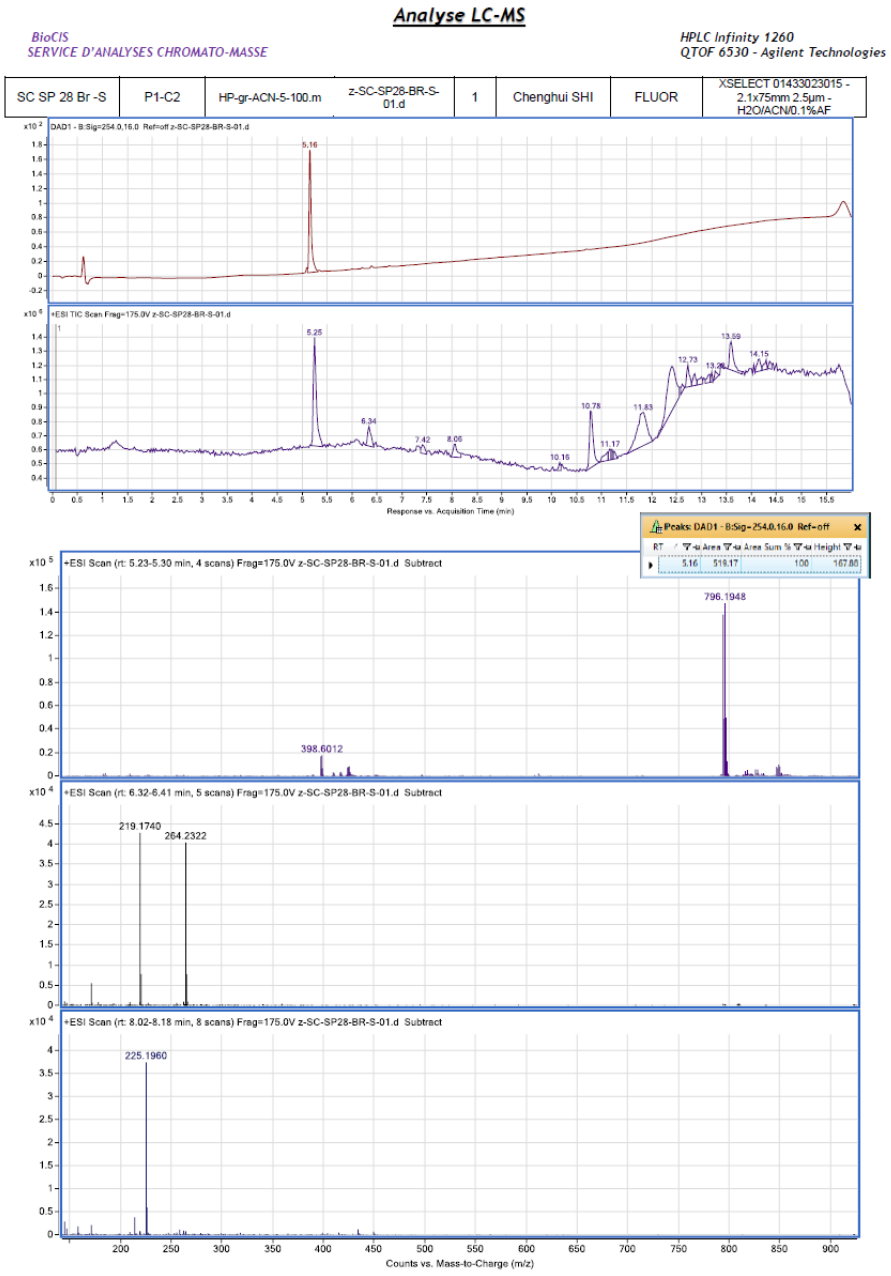

Compound **4.5**

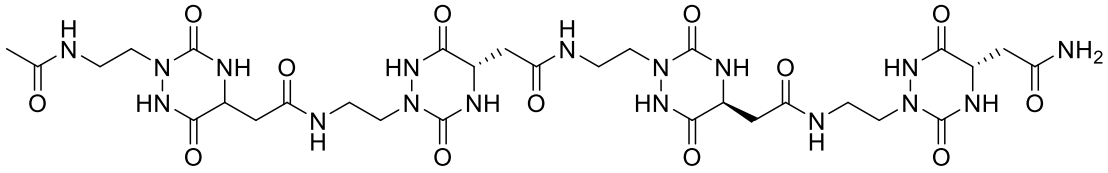

The compound was purified by semi-preparative HPLC (Linear gradients of 1-20 % ACN in H_2O containing 0.1% formic acid in 15 min, yield: 27%)

HRMS (ESI): Calcd for $[C_{30}H_{45}N_{17}O_{13} + H]^+$: 852.3461, found: 852.3457.

HPLC purity: XSELECT column (C18, 2.1 x 75mm-2.5µm); ACN /H_2O + 0.1 % TFA, gradient 5–100 % in 20 min; R_t = 10.68 and 11.11 min (two conformers), 100 %.

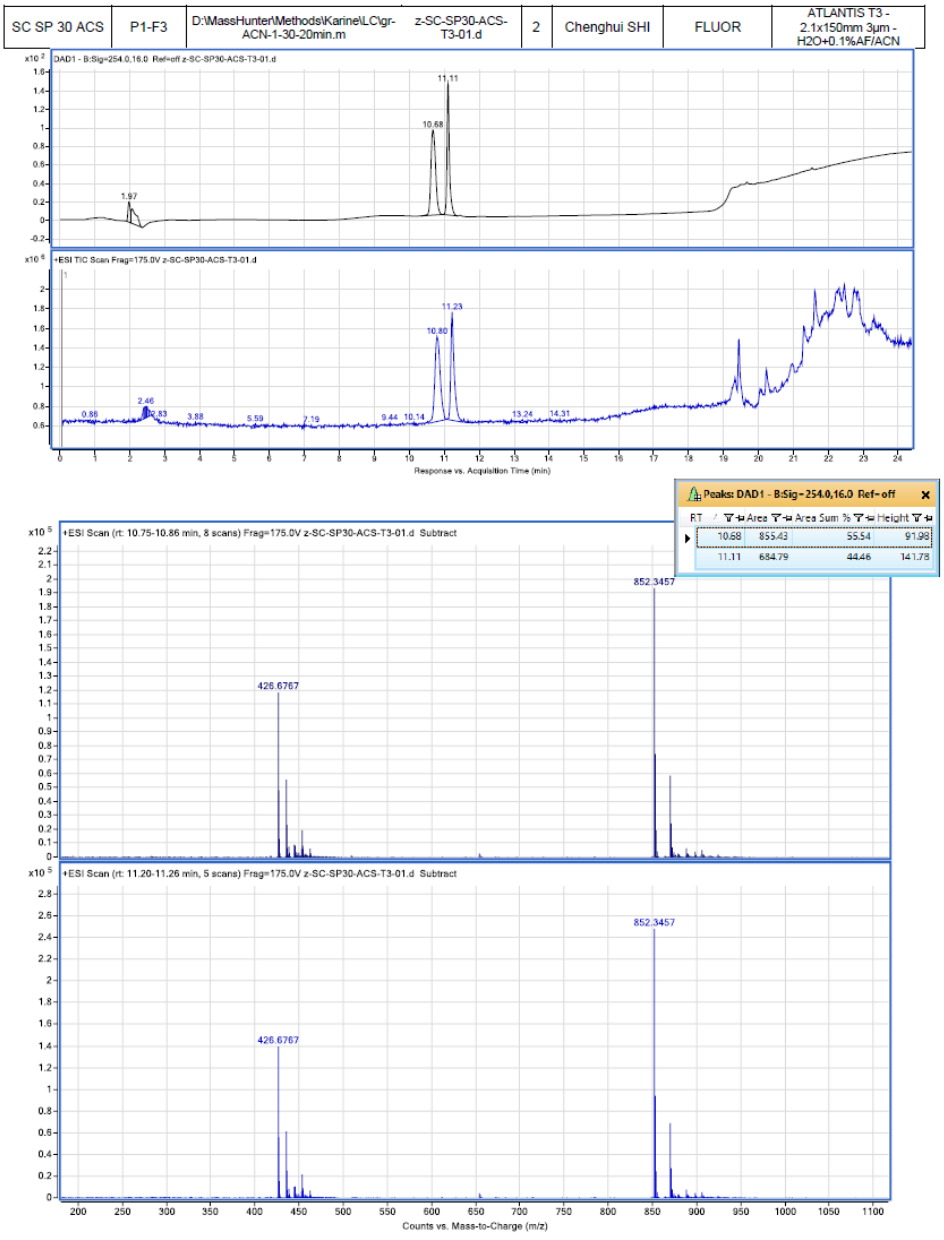

université PARIS-SACLAY
ÉCOLE DOCTORALE
Innovation thérapeutique
du fondamental à l'appliqué
(ITFA)

Titre : Synthèse et analyse conformationnelle de foldamères peptidomimétiques contenant des unités diaza-peptides: application aux interactions protéine-protéine

Mots clés : agrégation amyloide, amyloide β, transthyrétine, azapeptide, peptidpmimétiques, foldamères

Résumé : Les amyloses constituent un groupe de maladies impliquant le dépôt de protéines amyloïdes, des interactions protéine-protéine aberrantes, dans les tissus et les organes. La maladie d'Alzheimer (MA) est l'amylose la plus fréquente avec une mortalité élevée. Le dépôt de plaques β-amyloïdes (Aβ) et d'enchevêtrements neurofibrillaires de Tau (NFT) dans le cerveau sont deux caractéristiques pathologiques des patients atteints de MA. Concevoir de nouveaux peptides ou peptidomimétiques basés sur les protéines capables d'interagir de manière croisée avec Aβ est une stratégie prometteuse pour découvrir de nouvelles molécules inhibant l'agrégation de Aβ. La transthyrétine (TTR) a été décrite comme une protéine chaperon de Aβ qui peut inhiber l'agrégation de Aβ *in vitro*. Un site de liaison possible de TTR à Aß est son hélice EF mais un peptide dérivé de l'hélice EF n'a pas montré d'interaction évidente avec Aß. La perte de structure secondaire du peptide excisé a été proposée pour expliquer la perte de l'interaction. Ainsi, la conception et la synthèse de foldamères peptidiques, qui peuvent imiter la structure hélicoïdale, basée sur l'hélice EF, pourraient être un moyen de trouver de nouveaux inhibiteurs d'agrégation Aβ.

Notre laboratoire a rapporté que les unités diaza-peptides dans les tripeptides (diaza-tripeptides) sont capables d'induire une structure en coude β unique ou une structure de coudes β répétés des tripeptides dans le méthanol. Cette propension conformationnelle intrigante nous a amenés à nous demander si l'introduction d'unités diaza-peptidiques dans la séquence de l'hélice EF peut induire une structure hélicoïdale des peptides, augmentant ainsi l'interaction avec Aβ. Nous avons d'abord étudié le comportement conformationnel des diaza-tripeptides en solution aqueuse. Trois diaza-tripeptides solubles dans l'eau avec différentes chaînes latérales au niveau du résidu central ont été conçus et synthétisés pour étudier les effets des chaînes latérales sur leur conformation. L'étude conformationnelle de ces peptides dans l'eau a été réalisée par RMN. Ensuite, plusieurs aza-nonapeptides possédant des unités diaza-peptides ont été conçus et synthétisés sur la base de l'hélice EF. Des études conformationnelles de ces peptides par CD, RMN, FTIR et simulation par dynamique moléculaire ont montré que l'introduction de différents nombres d'unités diaza-peptides à différentes positions de la séquence a de grands impacts sur la conformation des peptides. L'activité d'inhibition de l'agrégation Aß a été testée par spectroscopie de fluorescence à la thioflavine-T (ThT) et par CD. Le peptide le plus actif a également été testé pour sa stabilité protéolytique, sa perméabilité de la BHE et sa toxicité cellulaire, ce qui prouve que les foldamères peptidiques contenant des unités diaza-peptide sont des foldamères potentiellement utilisables comme médicaments. De plus, nous avons utilisé une réaction secondaire que nous avons trouvée lors de la synthèse des diaza-tripeptides pour concevoir et synthétiser un monomère aza-DKP (aza-dicétopipérazine), qui s'inspire des travaux du groupe de Piarulli sur les foldamères à base de DKP. En utilisant ce monomère aza-DKP, quatre oligomères aza-DKP ont été conçus et synthétisés. Les études conformationnelles sont en cours.

En résumé, le travail présenté dans la thèse confirme la stratégie selon laquelle il est possible de concevoir des inhibiteurs peptidiques de l'agrégation Aβ capables d'imiter la structure hélicoïdale basée sur l'hélice EF du TTR. De plus, il fournit une preuve de concept que l'utilisation d'unités diaza-peptide dans la conception et la synthèse de foldamères peptidiques est une stratégie prometteuse pour cibler les interactions protéine-protéine impliquant des structures hélicoïdales.

Title : Synthesis and conformational analysis of peptidomimetic foldamers containing diaza-peptide units: application in protein-protein interactions

Keywords : amyloid aggregation, β-amyloid, transthyretin, azapeptide, peptidomimetics, foldamers

Abstract : Amyloidosis is a group of diseases involving amyloid protein deposition, an aberrant protein–protein interaction (PPI), in tissues and organs. Alzheimer's disease (AD) is the most common amyloidosis with high mortality. The deposition of β-amyloid (Aβ) plaques and Tau neurofibrillary tangles (NFTs) in the brain are two pathological hallmarks for AD patients. Designing new peptides or peptidomimetics based on the proteins capable of cross-interacting with Aβ is a promising strategy for discovering new molecules inhibiting Aβ aggregation. Transthyretin (TTR) has been reported as a chaperone protein of Aβ which can inhibit Aβ aggregation *in vivo* and *in vitro*. One possible binding site of TTR to Aβ is its EF-helix but a peptide derived from the EF-helix did not show obvious interaction with Aβ. The loss of secondary structure of the excised peptide was proposed for explaining the loss of the interaction. Thus, the design and synthesis of peptidic foldamers, which can mimic helical structure, based on the EF-helix might be a feasible way to find novel Aβ aggregation inhibitors.

Our laboratory has reported that diaza-peptide units in tripeptides (diaza-tripeptides) are able to induce single β-turn structure or repeated β-turn structure of the tripeptides in methanol. This intriguing conformationl propensity led us to wonder if the introduction of diaza-peptide units in the sequence of the EF-helix can induce a helical structure of the peptides, thereby increasing the interaction with Aβ. We first investigated the conformational behavior of diaza-tripeptides in aqueous solution. Three water-soluble diaza-tripeptides with different side chains in the central residue were designed and synthesized to study the effects of the side chains on their conformation. The conformational study of these peptides in water was performed by NMR. Then, several aza-nonapeptides possessing diaza-peptide units were designed and synthesized based on the EF-helix. Conformational studies of these peptides by CD, NMR, FTIR and MD simulation showed that introducing different numbers of diaza-peptide units at the different positions of the sequence has great impacts on the conformation of the peptides. The activity to inhibit Aβ aggregation was tested by thioflavin-T (ThT) fluorescence spectroscopy and CD assays. The most active peptide was also tested for proteolytic stability, BBB permeability and toxicity, which give evidences that peptidic foldamers containing diaza-peptide units are druggable foldamers. In addition, we used a side reaction we found during the synthesis of the diaza-tripeptides to design and synthesize an aza-DKP (aza-diketopiperazine) monomer, which is inspired by the work from Piarulli' group on DKP-based foldamers. Using this aza-DKP monomer, four aza-DKP oligomers were designed and synthesized. The conformational studies are in progress.

In summary, the work presented in the thesis confirms the strategy that designing peptidic Aβ aggregation inhibitors capable of mimicking helical structure based on the EF-helix of TTR is feasible. Moreover, it provides a proof of concept that the use of diaza-peptide units in the design and synthesis of peptide foldamers is a promising strategy for targeting PPIs involving helical structures.